

UNCLASSIFIED

AD NUMBER
AD782258
NEW LIMITATION CHANGE
TO Approved for public release, distribution unlimited
FROM Distribution authorized to U.S. Gov't. agencies only; Test and Evaluation; JUN 1973. Other requests shall be referred to Air Force Flight Dynamics Laboratory, Attn: FBA, Wright-Patterson AFB, OH 45433.
AUTHORITY
AFFDL ltr dtd 13 Oct 1975

THIS PAGE IS UNCLASSIFIED

AFFDL-TR-73-51

AD-782 258

**ADVANCED METALLIC STRUCTURES:  
CARGO WING DESIGN FOR IMPROVED  
COST, WEIGHT, AND INTEGRITY**

*C. R. BIGHAM, ET AL  
LOCKHEED-GEORGIA COMPANY*

TECHNICAL REPORT AFFDL-TR-73-51

JUNE 1973

Distribution limited to U. S. Government agencies only; test and evaluation; statement applied June 1973. Other requests for this document must be referred to AF Flight Dynamics Laboratory (FBA), Wright-Patterson AFB, Ohio 45433.

AIR FORCE FLIGHT DYNAMICS LABORATORY  
AIR FORCE MATERIALS LABORATORY  
AIR FORCE SYSTEMS COMMAND  
WRIGHT-PATTERSON AIR FORCE BASE, OHIO 45433

20070921336

Best Available Copy



## NOTICE

When Government drawings, specifications, or other data are used for any purpose other than in connection with a definitely related Government procurement operation, the United States Government thereby incurs no responsibility nor any obligation whatsoever; and the fact that the government may have formulated, furnished, or in any way supplied the said drawings, specifications, or other data, is not to be regarded by implication or otherwise as in any manner licensing the holder or any other person or corporation, or conveying any rights or permission to manufacture, use, or sell any patented invention that may in any way be related thereto.

Copies of this report should not be returned unless return is required by security considerations, contractual obligations, or notice on a specific document.

## ERRATA

### PAGE

### ITEM

- 69 Clarification of the Tapered Shingle Concept: The spanwise tapering mentioned in the first paragraph does not require machining of either skin or stiffener thickness. The notable feature of this design lies in the fact that only simple width profiling is required to obtain finished panels.
- 77 In Table XII, units for the thermal expansion coefficient,  $\alpha$ , are  $10^{-6}$  inches/inch/ $^{\circ}$ F.
- 78 In Table XII, units for the thermal expansion coefficient,  $\alpha$ , are  $10^{-6}$  inches/inch/ $^{\circ}$ F.
- 236 In Figure 114, the  $1.000 \pm .010$  thickness dimension is limited by material availability. Add note "unless limited by material stock thickness."
- 238 In Table XXXIV, thicknesses associated with  $K_c$  values are not listed. These are as follows (thicknesses given in parentheses):
- |             |             |             |              |              |             |
|-------------|-------------|-------------|--------------|--------------|-------------|
| 55.4(.1530) | 64.8(.2512) | 95.0(.2511) | 110.1(.1490) | 126.6(.1520) | 90.9(.1540) |
| 59.5(.1490) | 57.3(.1540) | 88.3(.1477) | 111.1(.1550) | 123.5(.1530) | 72.1(.2510) |
|             |             | 94.8(.1552) | 125.6(.2532) | 159.1(.2480) |             |
|             |             | 80.4(.0981) |              |              |             |

Units are: ksi  $\sqrt{\text{in.}}$  for  $K_c$ , inches for thickness.

**ADVANCED METALLIC STRUCTURES:  
CARGO WING DESIGN FOR IMPROVED  
COST, WEIGHT, AND INTEGRITY**

*C. R. BIGHAM, ET AL*

Distribution limited to U. S. Government agencies only; test and evaluation; statement applied June 1973. Other requests for this document must be referred to AF Flight Dynamics Laboratory (FBA), Wright-Patterson AFB, Ohio 45433.

**Best Available Copy**



## FOREWORD

This report presents the results of preliminary design studies using advanced technologies to develop wing box structure for an advanced metallic cargo/tanker air vehicle. The latest Air Force structural requirements, including MIL-STD-1530(USAF) and the "Proposed USAF Damage Tolerance Criteria," dated 18 August 1972, were used in the studies.

This program is one of two related programs involving cargo/tanker air vehicle structure. The other program is reported in AFFDL-TR-73-53. Work reported herein was sponsored by the Advanced Metallic Structures-Advanced Development Project Office (AMS-ADPO), Air Force Flight Dynamics Laboratory (AFFDL), under the joint management and technical direction of AFFDL and the Air Force Materials Laboratory, Air Force Systems Command, Wright-Patterson Air Force Base, Ohio 45433. The work was performed under Contract F33615-72-C-2165, Flight Dynamics Laboratory Project Number 486U, "Advanced Cargo/Tanker Structures."

Mr. Jamie Florence is the Air Force Project Engineer.

The preliminary design studies were performed by the Advanced Structures Department Lockheed-Georgia Company, under the direction of W. A. Pitman, Advanced Development Programs Group Engineer. C. R. Bigham was the Project Leader. Other principal participants in the program were as follows: R. E. Barrie, Design; L. M. Atkinson, Stress and Weights; O. L. Freyre, Fatigue/Fracture/Damage Tolerance; H. W. Stemme, Materials; V. W. Masoner, Manufacturing; H. V. Davis, Cost and Producibility; W. H. Sproat/E. J. Siracusa, NDI/Quality Assurance; and W. M. McGee, Test.

The work was performed from July, 1972, to May, 1973, and was released for publication in June, 1973. This report is also identified as LG73ER0126 for Lockheed internal control purposes. This technical report has been reviewed and is approved.

---

JOHN C. FRISHETT, Major, USAF  
Program Manager, AMS Program Office  
Structures Division  
Air Force Flight Dynamics Laboratory

## ABSTRACT

With the current Air Force medium transport and tanker fleets rapidly approaching the end of their useful life, a requirement for their replacement is inevitable. Demonstration of innovative advanced structures concepts is required prior to production design decisions in order to qualify these advances for new system acceptance. The long lead times required for the development and demonstration of advanced structures dictates that advanced development programs be initiated now to insure the availability of the various technologies when needed for anticipated future systems. This requirement has led to this advanced development program to develop improved aircraft structural designs for a cargo/tanker category aircraft. The C-141 inner wing box was used as the baseline for the preliminary design study phase of this development program. The major objective of this study was to develop advanced designs which would double the fatigue life endurance of the baseline, and which could be produced at lower cost and weight. The objective was achieved through an iterative process of integrating, evaluating, and exploiting new and improved technology in design concepts, fracture mechanics, analysis methods, design criteria, materials, tests, manufacturing methods, and nondestructive inspection methods. From the study of a comprehensive matrix of cover and substructure concepts, eight configurations were formulated for analysis. Upon completion of the analysis, the configurations were evaluated using a merit rating system which recognized the important performance characteristics of a structural design. This evaluation resulted in the selection of three recommended configurations which met the objective for further study in the planned follow-on program. Also, a comprehensive damage tolerance criteria sensitivity analysis was performed as a part of this study to evaluate the effects of variations in critical criteria parameters on selected design control functions.

## TABLE OF CONTENTS

<u>Section</u>	<u>Title</u>	<u>Page</u>
I	INTRODUCTION	1
II	SUMMARY	3
III	BASELINE COMPONENT AND STRUCTURAL REQUIREMENTS	9
	3.1 Baseline Component Selection	9
	3.2 Baseline Structure Configuration	9
	3.3 Baseline Design Criteria	15
	3.4 ADP Program Criteria	15
	3.5 Baseline Update to 1972 Technology	16
IV	TECHNICAL APPROACH	21
	4.1 Scope	21
	4.2 Study Procedure	21
V	NEW STRUCTURAL CONCEPTS/CONFIGURATIONS	25
	5.1 Design Approach	25
	5.2 Material Selection	26
	5.3 Structural Optimization	29
	5.4 Cover and Substructure	31
	5.5 Configuration Concepts	36
VI	MATERIALS AND PROCESSES	75
	6.1 Materials	75
	6.2 Procurement Specifications	88
	6.3 Finishes and Processes	89
	6.4 Joining Methods	92
VII	STRESS AND WEIGHTS ANALYSIS	95
	7.1 Stress Analysis	95
	7.2 Weight Analysis	119



## TABLE OF CONTENTS (Continued)

<u>Section</u>	<u>Title</u>	<u>Page</u>
VIII	FATIGUE AND DAMAGE TOLERANCE ANALYSIS	130
	8.1 Fatigue Analysis	130
	8.2 Damage Tolerance Analysis	144
IX	MANUFACTURING	163
	9.1 Evaluation of Baseline	163
	9.2 Evaluation of ADP Designs	163
	9.3 Manufacturing Plan	164
	9.4 Assembly Sequence	164
	9.5 Manufacturing Cost Effectiveness	172
	9.6 Manufacturing Development Items	172
X	QUALITY ASSURANCE/NDI	178
	10.1 Evaluation of Baseline Design	178
	10.2 Evaluation of ADP Design	178
	10.3 Reliability of NDI Methods	181
XI	COST/PRODUCIBILITY	185
	11.1 Baseline Costs	185
	11.2 Costs of ADP Candidate Designs	186
	11.3 Costs of Recommended ADP Designs	189
XII	CONCEPT EVALUATION	197
	12.1 Merit Rating System	197
	12.2 Evaluation Criteria	197
	12.3 Configuration Subjected to ADP Evaluation Criteria	200
	12.4 Concept Scoring and Selection of Three Recommended Designs	200
	12.5 Concept Test Verification	203

## TABLE OF CONTENTS (Concluded)

<u>Section</u>	<u>Title</u>	<u>Page</u>
XIII	CONCLUSIONS AND RECOMMENDATIONS	205
	13.1 Conclusions	205
	13.2 Recommendations	205
Appendix I	PRELIMINARY DESIGN DRAWINGS	207
Appendix II	SUMMARY OF TEST RESULTS	225
	Materials Properties Tests	225
	Static Component Tests	255
	Fatigue Component Tests	277
	Damage Tolerance Component Tests	291
Appendix III	CRITERIA SENSITIVITY AND TRADE STUDIES	303
	Statistical Variation in Fracture Properties	303
	Spectrum Severity	310
	Initial Flaw Size	315
	Thermal and Chemical Environment	320
	Proof Testing	322
	NDT Demonstration Program	326
	Fracture and Fatigue Control Plan	333
	In-Service Inspectability Factors	350
	Residual Strength Load Requirement	386
	REFERENCES	389

## LIST OF ILLUSTRATIONS

<u>Figure</u>	<u>Title</u>	<u>Page</u>
1	Baseline Selection Criteria	10
2	Baseline Structure - C-141 Inner Wing	11
3	Basic Geometry	13
4	Design Approach	22
5	Study Procedure	23
6	Attainable Stress to Density Ratio	30
7	Panel Structural Optimization - Aluminum	32
8	Panel Structural Optimization - Titanium	33
9	Weldbond Configuration	38
10	Spar - Weldbond Configuration	39
11	Typical Rib - Weldbond Configuration	40
12	Hat Stringer Configuration	42
13	Rib to Cover Attachment - Hat Stringer Configuration	43
14	Bonded Spanwise Splice (Formed)	44
15	Substructure - Hat Stringer Configuration	45
16	Lockskin Configuration	47
17	Rib to Cover Attachment - Lockskin Configuration	48
18	Substructure - Lockskin Configuration	49
19	Monolithic Configuration	51
20	Rib to Cover Attachment - Monolithic Configuration	52
21	Substructure - Monolithic Configuration	53
22	Cover Design - Non-Penetrating Clip	54
23	Sandwich Configuration	56
24	Rib to Cover Attachment - Sandwich Configuration	57
25	Substructure - Sandwich Configuration	58
26	Composite Hat Configuration	60
27	Rib to Cover Attachment - Composite Hat Configuration	61
28	Substructure - Composite Hat Configuration	62
29	Virgin Plank Configuration	64



## LIST OF ILLUSTRATIONS (Continued)

<u>Figure</u>	<u>Title</u>	<u>Page</u>
30	Non-penetrating Clip	65
31	Bonded/Clamped Spanwise Splice	66
32	Spar-Virgin Plank Configuration	67
33	Typical Rib - Virgin Plank Configuration	68
34	Tapered Shingle Configuration	70
35	Upper Surface - Tapered Shingle Configuration	71
36	Spar - Tapered Shingle Configuration	72
37	Typical Rib - Tapered Shingle Configuration	73
38	Critical Stress Intensity Factor	81
39	Material Crack Growth Data	82
40	S-N Data - 7050-T76511, Aluminum, Built-Up	84
41	S-N Data - 7050-T76511, Aluminum, Coupon	85
42	Finite Element Model: Cargo/Tanker Study	99
43	Detail Cutout Analysis Model Geometry	102
44	Typical Rib Geometry and Internal Loads	104
45	Typical Rib Element Internal Loads and Stresses	105
46	Governing Design Criteria	109
47	Spanwise Stress Levels - Baseline Update	111
48	Spanwise Stress Levels - Weldbond Configuration	112
49	Spanwise Stress Levels - Virgin Plank Configuration	113
50	Spanwise Stress Levels - Tapered Shingle Configuration	114
51	Typical Chordwise Stress Distribution	115
52	Surface T-Bar Distribution-Weldbond Configuration	116
53	Surface T-Bar Distribution-Virgin Plank Configuration	117
54	Surface T-Bar Distribution - Tapered Shingle Configuration	118
55	Weight-Ratio Comparison of Configurations	123
56	Weight Effects of Advanced Technology - 'A' Stringer Weldbond Design	124
57	Weight Effects of Advanced Technology - Virgin Plank Design	125

# LIST OF ILLUSTRATIONS (Continued)

<u>Figure</u>	<u>Title</u>	<u>Page</u>
58	Weight Effects of Advanced Technology - Tapered Shingle Design	126
59	Weight Comparison - 'A' Stringer Weldbond Design	127
60	Weight Comparison - Virgin Plank Design	128
61	Weight Comparison - Tapered Shingle Design	129
62	Parametric Wing Surface Fatigue Analysis	132
63	Wing Surface Fatigue Analysis, Built-Up Structure S-N Data, 7075-T76511 Extrusion, W.S. 77.7	134
64	Wing Surface Fatigue Analysis, Built-Up Structure S-N Data, 7075-T76511, W.S. 285.3	134
65	Wing Surface Fatigue Analysis, Built-Up Structure S-N Data, 7075-T76511, W.S. 415.4	135
66	Wing Surface Fatigue Analysis, Coupon S-N Data, 7075-T76511 Extrusion, W.S. 77.7	135
67	Wing Surface Fatigue Analysis, Coupon S-N Data, 7050-T76511, W.S. 285.3	136
68	Wing Surface Fatigue Analysis, Coupon S-N Data, 7050-T76511, W.S. 415.4	136
69	Wing Surface Fatigue Analysis, Built-Up Structure S-N Data, 7475-T76 Sheet, W.S. 77.7	137
70	Wing Surface Fatigue Analysis, Built-Up Structure S-N Data, 7475-T76 Sheet, W.S. 285.3	137
71	Wing Surface Fatigue Analysis, Built-Up Structure S-N Data, 7475-T76 Sheet, W.S. 415.4	138
72	Wing Surface Fatigue Analysis, Built-Up Structure S-N Data, 7050-T76511 Extrusion, W.S. 77.7	138
73	Wing Surface Fatigue Analysis, Built-Up Structure S-N Data, 7050-T76511 Extrusion, W.S. 285.3	139
74	Wing Surface Fatigue Analysis, Built-Up Structure S-N Data, 7050-T76511 Extrusion, W.S. 415.4	139
75	Wing Surface Fatigue Analysis, Built-Up Structure S-N Data, 7075-T7651 Plate, W.S. 77.7	140
76	Wing Surface Fatigue Analysis, Built-Up Structure S-N Data, 7075-T7651 Plate, W.S. 415.4	140

## LIST OF ILLUSTRATIONS (Continued)

<u>Figure</u>	<u>Title</u>	<u>Page</u>
77	Wing Surface Fatigue Analysis, Built-Up Structure S-N Data, 7050-T7651 Plate, W.S. 77.7	141
78	Wing Surface Fatigue Analysis, Built-Up Structure S-N Data, 7050-T7651 Plate, W.S. 415.4	141
79	Wing Spar Fatigue Analysis, Coupon S-N Data, 2219-T87 Sheet, W.S. 77.7	142
80	Wing Spar Fatigue Analysis, Coupon S-N Data, 2219-T87 Sheet, W.S. 285.3	142
81	Wing Spar Fatigue Analysis, Coupon S-N Data, 2219-T87 Sheet, W.S. 415.4	143
82	Fatigue Analysis Stress Concentration Factors	144
83	Wing Surface Damage Tolerance Analysis, Crack Growth Curves, Virgin Plank Configuration	149
84	Wing Surface Damage Tolerance Analysis, Design Tension Stress vs. Flights to Failure, Virgin Plank Configuration	150
85	Wing Surface Damage Tolerance Analysis, Crack Lengths At $F_{DM}$ , Virgin Plank Configuration	152
86	Wing Surface Damage Tolerance Analysis, Residual Strength Effect, Virgin Plank Configuration	153
87	Wing Surface Design Stress Threshold, Hole Cold- Working Effect, Virgin Plank Configuration	159
88	Wing Chordwise Splice Damage Tolerance Analysis, Stress Intensity Coefficient	161
89	Wing Chordwise Splice Damage Tolerance Analysis, Design Tension Stress & Critical Crack Lengths	162
90	Manufacturing Plan - Weldbond Configuration	166
91	Manufacturing Plan - Virgin Plank Configuration	167
92	Manufacturing Plan - Tapered Shingle Configuration	168
93	Manufacturing Sequence - Weldbond Configuration	169
94	Manufacturing Sequence - Virgin Plank Configuration	170
95	Manufacturing Sequence - Tapered Shingle Configuration	171
96	Manufacturing Cost Effectiveness-Weldbond Configuration	173



## LIST OF ILLUSTRATIONS (Continued)

<u>Figure</u>	<u>Title</u>	<u>Page</u>
97	Manufacturing Cost Effectiveness - Virgin Plank Configuration	174
98	Manufacturing Cost Effectiveness - Tapered Shingle Configuration	175
99	Crack Detection Probability	182
100	Ultrasonic NDI Repeat Inspections	183
101	Cost Comparison of Configurations	187
102	Cost Development Procedure	188
103	Cost Comparison - Weldbond Design	192
104	Cost Comparison - Virgin Plank Design	193
105	Cost Comparison - Tapered Shingle Design	194
106	Tensile Specimen	230
107	Compression Specimen	230
108	Shear Specimen	231
109	Bearing Specimen	231
110	Axial Load Fatigue Specimen	233
111	Rectangular Fatigue Specimen	233
112	Crack Growth-Compact Tension Specimen	234
113	Spectrum Crack Growth Specimen	234
114	Compact Tension Specimen	236
115	General Configuration Specimen For $K_{Ic}$ Tests	237
116	Specimen Configuration for $K_{Isc}$ Tests	237
117	Crack Growth of 7050-T7351 Aluminum Plate - 95% RH	241
118	Crack Growth of 7050-T7351 Aluminum Plate - 3.5% NaCl	242
119	Crack Growth of 7050-T7651 Aluminum Plate - 95% RH	243
120	Crack Growth of 7050-T7651 Aluminum Plate - 3.5% NaCl	244
121	Crack Growth of 7050-T7351 Aluminum Extrusion - 95% RH	245

# LIST OF ILLUSTRATIONS (Continued)

<u>Figure</u>	<u>Title</u>	<u>Page</u>
122	Crack Growth of 7050-T76511 Aluminum Extrusion - 95% RH	246
123	Crack Growth of 7050-T76511 Aluminum Extrusion - 3.5% NaCl	247
124	Crack Growth of Ti 6-6-2 STOA Plate - 95% RH	248
125	Crack Growth of Ti 6-6-2 STOA Plate - 3.5% NaCl	249
126	Crack Growth of Ti 6-2-2-2-2 ST Plate - 95% RH	250
127	Crack Growth of Ti 6-2-2-2-2 ST Plate - 3.5% NaCl	251
128	Crack Growth of Ti 6-2-2-2-2 STA Plate - 95% RH	252
129	Crack Growth of Ti 6-2-2-2-2 STA Plate - 3.5% NaCl	353
130	Spectrum Crack Growth - 7050-T73 & T76 Extrusion - 95% RH	254
131	Spectrum Crack Growth - 7050-T73 & T76 Plate - 95% RH	254
132	Rib Cap Shear Specimen (N-P Clips)	257
133	Rib Cap Shear Specimen (Weldbond "A" Stringer)	258
134	Rib Cap Shear Specimen (Weldbond "Hat" Stringer)	259
135	Clamped W.S. 77 Chordwise Joint Specimen	260
136	Test Arrangement, Rib Cap to Cover Shear Test, (N-P Clip Configuration, ADP 1006)	263
137	Non-Penetrating Clip Rib Cap/Cover Test Specimen	264
138	Close-up Of N-P Clip Attachment Between Rib Cap and Cover	264
139	Test Arrangement, Rib Cap to Cover Shear Test, (Weldbond "A" Stringer Configuration, ADP 1003-103)	265
140	Front and Side Views of "A" Stringer Shear Test Specimen Before Loading	266
141	"A" Stringer Shear Test Specimen Under Load and After Failure	267
142	Test Arrangement, Front and Side Views, Rib Cap to Cover Shear Test (Weldbond "Hat" Stringer Configuration, ADP1003-101)	268

## LIST OF ILLUSTRATIONS (Continued)

<u>Figure</u>	<u>Title</u>	<u>Page</u>
143	Weldbond "Hat" Test Panel After Failure (Weldbond Between Hat Crown and Rib Cap Pulled Apart)	269
144	Weldbond "Hat" Specimen Modification (Hiloks Used For Attaching Rib Cap to Hat Crown)	270
145	Failure of Modified Test Panel (Weldbond Connection at Skin Line Failed)	270
146	Clamped Chordwise Splice Tension Test Specimen (ADP 1005)	271
147	Chordwise Splice Specimen After Failure (Clamping Bolts Failed In Tension)	271
148	Test Arrangement, Spanwise Splice Fail Safe Shear Test (ADP 1008)	272
149	Plan and End Views of Bonded/Clamped Spanwise Splice Shear Specimen (ADP 1008)	273
150	Test Arrangement, Spanwise Splice Fail Safe Tension Test (ADP 1009)	274
151	Inside Surface, Spanwise Splice Tension Specimen (ADP 1009)	275
152	Edge View, Spanwise Splice Tension Specimen (ADP 1009)	276
153	Stringer to Skin $K_T$ Specimen	279
154	N-P Rib Attachment Clip Fatigue Test Specimen	280
155	W.S. 77 Chordwise Joint Specimen	281
156	Simulated Stringer/Skin Weldbond Fatigue Specimen (ADP 1001-101)	284
157	Simulated Stringer/Skin Taperlok Fatigue Specimen (ADP 1001-103)	284
158	Compression Stability Plates Used in Stringer/Skin Specimen Fatigue Tests	285
159	Test Arrangement, N-P Clip Fatigue Test (ADP 1007)	286
160	Close-Up of Test Panel Showing N-P Clip Arrangement	287
161	Non-Penetrating Clips and Panel After Disassembly	288
162	Contact Surface of N-P Clip Indicating no Significant Fretting Effect	288

## LIST OF ILLUSTRATIONS (Continued)

<u>Figure</u>	<u>Title</u>	<u>Page</u>
163	Test Arrangement, Chordwise Joint Fatigue Test (ADP 1002)	289
164	Compression Stability Plates Used in Chordwise Joint Fatigue Test	290
165	Damage Tolerance Spanwise Splice Shear Specimen	293
166	Damage Tolerance Spanwise Splice Tension Specimen	294
167	Damage Tolerance Weldbonded "A" Stringer Specimen	295
168	Damage Tolerance Retardation Test Specimen	296
169	Test Arrangement, Damage Tolerance Weldbond, "A" Stringer Specimen	298
170	Crack Growth Data - Crack No. 1	299
171	Crack Growth Data - Crack No. 2	300
172	Residual Strength Test Specimen	301
173	Retardation Test Evaluation - 7075-T6511 Aluminum	304
174	$K_c$ Variation	306
175	$da/dN$ Variation Data	307
176	Effect of Scatter In $da/dN$ Data	308
177	Effect of Scatter In $da/dN$ Data For Constant Life	309
178	Variation In Fatigue Damage Based On Flight Hours	311
179	Variation In Fatigue Damage Based On Full Stop Landings	312
180	Effect of Spectrum Severity On Life	314
181	Effect of Initial $a/Q$ On Life, Surface Flaw	317
182	Effect of Initial Crack Size On Life - Through Crack Emanating From A Hole	318
183	Effect of Initial Crack Size On Life - Corner Crack Emanating From A Hole	319
184	Proof Load Variation	324
185	Hypothetical Detection Probability Surface	328
186	Program Organization	336
187	Fracture & Fatigue Control Plan Milestones	339
188	Fuel Probe Hole Configuration	353



## LIST OF ILLUSTRATIONS (Concluded)

<u>Figure</u>	<u>Title</u>	<u>Page</u>
189	Crack Growth Analysis	354
190	Visually Detected Crack Length Distribution - Fuel Probe Hole, Inner Wing, C-141 Fatigue Specimen 'B'	357
191	Visually "Missed" Crack Length Distribution Using Walker Analysis, Initial Flaw Length $L_o = 0.52$	358
192	Visually "Missed" Crack Length Distribution Using Walker Analysis, Initial Flaw Length $L_o = 0.37$	359
193	Visually "Missed" Crack Length Distribution Using Forman Analysis, Initial Flaw Length $L_o = 0.37$	360
194	Spanwise Splice Joint Specimen	363
195	Effect of Inspection Interval - Design Tension Stress	365
196	Surface Flaw - Effect of Initial $a/Q$ on Design Tension Stress	368
197	Through the Thickness Crack - Effect of Initial Crack Size on Design Tension Stress	369
198	Typical C-141 Baseline Spanwise Splice	371
199	Stress Redistribution Curves	374
200	Safe Crack Growth Period Variation - Design Stress Vs. Time to Load Path Failure	377
201	Safe Crack Growth Period Variation - Design Stress Vs. Safe Crack Growth Period	378
202	Multiple Crack Study, Two Panels - Allowable Design Stress	382
203	Multiple Crack Study, Two Panels - Crack Growth Curves	383
204	Multiple Crack Study, Three Panels - Allowable Design Stress	384
205	Multiple Crack Study, Three Panels - Crack Growth Curves	385

## LIST OF TABLES

<u>Table</u>	<u>Title</u>	<u>Page</u>
I	Configurations Submitted to ADP Evaluation Criteria	5
II	Merit Rating Summary of Candidate Concepts	6
III	Summary of Study Results	7
IV	Damage Tolerance Criteria	17
V	Weight Breakdown - C-141 Inner Wing	18
VI	Cost Breakdown - Baseline Update	19
VII	Aluminum Alloy Material Selection Summary - ADP Designs	27
VIII	Titanium and Composite Material Selection Summary - ADP Designs	28
IX	Cover Configurations	34
X	Rib, Bulkhead & Spar Configurations	35
XI	Splices and Joints	35
XII	Preliminary Design Allowables of Candidate Materials	77
XIII	Summary - Joining Methods	94
XIV	Critical Load Conditions: C-141A Inner Wing	97
XV	FAMAS Finite Element Model Description	100
XVI	Description of ASOP Model of Typical Access Door	103
XVII	Surface Compression Loads	106
XVIII	Weight Summary	121
XIX	Weight Breakdown - ADP Designs	122
XX	Wing Surface Fatigue Analysis, Summary - Allowable Design Tension Stresses	146
XXI	Inspection and Fail Safe Load Data	148
XXII	Initial Flaw Shape ( $a/2c$ ) Study	157
XXIII	Wing Surface Damage Tolerance Analysis, Summary - Allowable Design Tension Stresses	158
XXIV	Tooling Evaluation Parameters	165
XXV	In-Service Inspectability Factors	179
XXVI	C-141 Inner Wing NDI Procedures	180

# LIST OF TABLES (Concluded)

<u>Table</u>	<u>Title</u>	<u>Page</u>
XXVII	Cost Breakdown - Three Selected Designs	190
XXVIII	Itemized Structural Costs - Baseline and Selected Configurations	191
XXIX	Merit Rating System	198
XXX	Configurations Submitted to ADP Evaluation Criteria	201
XXXI	Merit Rating Summary of Candidate Concepts	202
XXXII	Materials Test Plan	227
XXXIII	Summary of Materials Test Parameters	228
XXXIV	Summary of Materials Static Test Results	238
XXXV	Summary of Materials Fatigue Test Results	240
XXXVI	Static Component Tests	256
XXXVII	Static Component Test Results	261
XXXVIII	Fatigue Component Tests	278
XXXIX	Fatigue Component Test Results	282
XL	C-141 Spectrum Loading Schedule for Test ADP1007	283
XLI	Damage Tolerance Component Tests	292
XLII	Damage Tolerance Component Test Results	297
XLIII	Baseline Load Spectrum	313
XLIV	Modified Load Spectrum	316
XLV	NDT Technique/Flaw Geometry Dependence	330
XLVI	Fracture and Fatigue Critical Parts - Inner Wing Box	337
XLVII	Summary of Total Cost Fracture and Fracture Control Plan	340
XLVIII	Summary of C-141 Inner Wing Fatigue Specimen "B" Inspection and Damage	352
XLIX	Analytic Values for Flaws Visually Missed	356
L	Component Spanwise Splice Crack Morphology	362
LI	Summary - Influence of In-service Inspection Interval and Flaw Size Variation on Allowable Design Stress	367
LII	Allowable Design Stress for Residual Strength Variation	387

## LIST OF SYMBOLS

<u>Symbol</u>	<u>Definition</u>
$a$	Crack depth
A/C	Aircraft
$a_{crit}$	Critical Half Crack Length (in.)
$a_o$	Initial Crack Length (in.)
$a/2c$	Surface Flaw Shape
$a/Q$	Flaw Shape Parameter Ratio
BL	Buttline
$2c$	Crack Length
$C_{L MAX}$	Lift Coefficient, Maximum
CPM	Cycles Per Minute
CPS	Cycles Per Second
CU	Distance from Neutral Axis to Outer Fiber
$da/dN$	Crack Growth Rate - (in./cycle)
D.S.	Design Stress
$e/D$	Edge Distance
E	Modulus of Elasticity
EAS	Equivalent Air Speed
E.B.	Electron Beam
$f$	Test Cyclic Frequency
$F_{DM}$	Minimum Unrepaired Service Usage (Depot Level Inspection)
FPS	Feet Per Second
$F_{TU}$ or $F_{tu}$	Ultimate Tension Allowable
FUS STA	Fuselage Station
G	Shear Modulus of Elasticity
GW	Gross Weight
H	Height
HAZ	Heat Affected Zone
HRS	Hot Rolled Steel
Hz	Hertz- Cycles Per Second



## LIST OF SYMBOLS (Continued)

<u>Symbol</u>	<u>Definition</u>
I	Moment of Inertia
IN	Inch
INBD	Inboard
IWBRS or IWBR STA	Inner Wing Box Rib Station
$\Delta K$	Stress Intensity Factor Range
$K_c$	Critical Stress Intensity Factor
$K_{Ic}$	Minimum Critical Stress Intensity Factor
$K_{Isc}$	Stress Corrosion Cracking Threshold
$K_t$ or $K_T$	Stress Concentration Factor
L	Length
LB(S)	Pound(s)
LD	Load
M	Moment
MAX.	Maximum
MIN.	Minimum
N/C	Numerical Controlled
N-P	Non-Penetrating
$N_X$	Chordwise Axial Load Per Inch
OUTBD	Outboard
OWBRS	Outer Wing Box Rib Station
P	Axial Load
$P_{xx}$	Minimum Required Residual Strength
Q	Flaw Shape Parameter
R	Stress Ratio
RFP	Request for Proposal
RH	Relative Humidity
RT	Room Temperature
t, T	Thickness
$\bar{t}$ , t-bar or $T_{BAR}$	Average Panel Thickness Including Stringer Areas

## LIST OF SYMBOLS (Concluded)

<u>Symbol</u>	<u>Definition</u>
V	Shear
W/	With
W/O	Without
WS or WSTA	Wing Station
x, y, z	Direction or Axis when used as subscript
$\mu$	Micro Inches
$\sigma$	Far-Field Stress

## SECTION I

### INTRODUCTION

Structural problems associated with recent aircraft development programs have spotlighted the need for more intensive structural development to reduce program risk and to enhance reliability for future systems. Although there have been various causes of past structural problems, they tend to reflect the quest for ever-higher structural efficiency in which the performance capabilities of materials and configurations were exploited beyond the limits proved feasible by adequate research and development programs.

#### 1.1 ADP PROGRAM OBJECTIVES

The need for advanced structural development led the Air Force to initiate the long-term Advanced Metallic Structures-Advanced Development Program (AMS-ADP) involving several aircraft types. One of these was established for cargo/tanker category aircraft.

The objectives of the ADP are to develop improved aircraft structural designs and to define and implement the development programs required to substantiate them prior to acquisition of new Air Force systems. In addition to the development of new design configurations, and improved materials applications and manufacturing techniques, the program includes a review of design criteria, proposed fatigue and fracture criteria and their effects, analysis methods, and quality assurance measures required to develop reliable structures.

#### 1.2 SPECIFIC OBJECTIVES - ADP CARGO/TANKER WING PROGRAM

The specific objectives established for the cargo/tanker wing program are to:

- (1) Double the fatigue life of baseline structure (60,000 hours in lieu of 30,000 hours).
- (2) Decrease weight by 4 to 8 percent.
- (3) Maintain cost at or below baseline levels.

To achieve these objectives, a study procedure was defined for creating and evaluating new structural concepts. Eight concepts were conceived, analyzed, and evaluated. Three of these concepts were then selected for additional design, analysis, and evaluation.



## SECTION II

### SUMMARY

The objectives of this Cargo/Tanker Structures Program are to develop designs with double the fatigue life of the baseline C-141 inner wing box, with an overall weight saving of 4 to 8% and without increased cost. These objectives, established at the outset, were met and exceeded by two of the three recommended designs, while the latest damage tolerance requirements of the "Proposed USAF Damage Tolerance Criteria," dated 18 August 1972, were also met. As the third design is especially amenable to low-cost production, cost saving was emphasized in this design at the expense of weight saving.

The feasibility of several new and innovative design concepts was demonstrated by component tests of key features of the three configurations.

From the study of a comprehensive matrix of cover and substructure concepts, eight configurations were formulated for analysis. These configurations are described in Table I. Upon completion of the analysis, the configurations were evaluated using a merit rating system which recognizes the important performance characteristics of a structural design, including efficiency (cost and weight), integrity, reliability, and other practical considerations. The merit rating summary is given in Table II. This evaluation resulted in the selection of three recommended configurations for further study in the planned follow-on program.

The three recommended configurations are characterized by the cover concepts, since the upper and lower covers are the dominant features. These three configurations are listed in Table III by names descriptive of the cover concepts. Pertinent results of the studies are given, along with corresponding data for the updated baseline structure. Of course, all of the new configurations give twice the life of the baseline. The Weldbond configuration provides excellent cost and weight savings with a higher technical risk as compared with the other configurations. The Virgin Plank configuration offers very good cost and weight savings with a moderate technical risk. The Tapered

Shingle configuration provides the largest cost saving of all in a design which incurs the lowest technical risk. Collectively, these configurations establish a diverse, challenging medium for accomplishing the Program development and demonstration objectives.

TABLE I  
CONFIGURATIONS SUBMITTED TO ADP EVALUATION CRITERIA

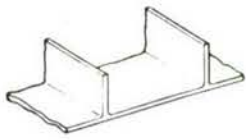
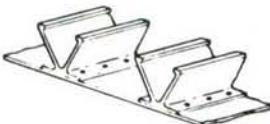
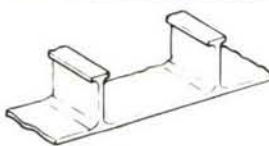
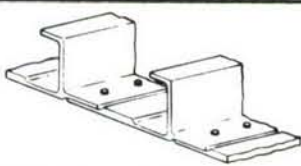
CONFIG. NO.	COVER CONCEPT	SPANWISE SPLICE CONCEPT	SPARS AND SUBSTRUCTURE
1	Weldbond "A" Stringer	Weldbond	<u>Spars</u> - Sine Wave Web, Welded <u>Ribs</u> - Truss Type, Back-to-back Channel Caps, Square Section Braces
2	Weldbond "Hat" Stringer	Adhesive Bonded/Clamped	<u>Spars &amp; Bulkheads</u> - Geodetic Stiffened <u>Ribs</u> - Cross Truss Arrangement
3	Lockskin	Weldbond	<u>Spars</u> - Sine Wave Web (Titanium) <u>Ribs</u> - Web/Stiffener
4	Monolithic Welded	Welded	<u>Spars</u> - Integrally Stiffened (Welded) <u>Ribs</u> - Caps Welded to Covers, "H" Section Braces
5	Honeycomb Sandwich	Mechanical Fasteners, Cold Worked Holes	<u>Spars &amp; Bulkheads</u> - Honeycomb Sandwich (Aluminum) <u>Ribs</u> - "H" Section Braces (No Separate Rib Caps)
6	Composite "Hat" Stringer	Adhesive Bonded	<u>Spars &amp; Bulkheads</u> - Web/Stiffener (Composite Reinforced) <u>Ribs</u> - Post & Cross Strap (Composite Reinforced)
7	Virgin Plank	Adhesive Bonded/Clamped	<u>Spars</u> - One-piece Forging <u>Ribs</u> - Truss Type, Conventional Caps Attached with N-P Clips, "H" Section Braces
8	Tapered Shingle	Stress Wave Rivet	<u>Spars &amp; Bulkheads</u> - Web/Stiffener <u>Ribs</u> - Truss Type, Tubular Braces
Baseline	Integrally Stiffened	Taperlocks	<u>Spars</u> - Built-up Web/Stiffener <u>Ribs</u> - Truss Type, "H" Section Braces <u>Bulkheads</u> - Web/Stiffener and Integrally Stiffened

TABLE II  
MERIT RATING SUMMARY OF CANDIDATE CONCEPTS

CONFIG. NO.	CONCEPT	MERIT RATING					REMARKS
		STRUC. EFF.	TECH. ADVAN.	INTEG. & RELIA.	ABILI- TIES	TOTAL	
1	Weldbond "A" Stringer	4.56	4.09	3.56	1.07	13.28	
2	Weldbond "Hat" Stringer	3.90	4.09	3.63	1.04	12.66	
3	Lockskin	3.03	5.00	4.24	1.00	13.27	Cost Prohibitive
4	Monolithic Welded	3.58	3.76	2.80	0.92	11.06	
5	Honeycomb Sandwich	1.21	4.38	3.31	0.91	9.81	
6	Composite "Hat" Stringer	3.23	4.97	4.01	0.93	13.14	Cost Prohibitive
7	Virgin Plank	4.11	4.11	3.56	1.10	12.88	
8	Tapered Shingle	4.04	4.33	4.17	1.09	13.63	
Baseline	Integrally Stiffened	3.00	3.00	3.00	1.00	10.00	



TABLE III  
SUMMARY OF STUDY RESULTS

CONFIGURATION	WEIGHT LBS. (1)	COST \$ (2)	FATIGUE LIFE HRS. $\times 10^3$	WEIGHT SAVINGS (%)	COST SAVINGS (%) (3)
BASELINE UPDATE 	7,012	376,961	30	-	-
WELDBOND 	6,415	331,120	60	8.5	20
VIRGIN PLANK 	6,536	341,910	60	6.8	16
TAPERED SHINGLE 	6,935	294,287	60	1.1	33

NOTES: (1) Total structural weight, one side only.

(2) Values are total recurring and non-recurring costs per aircraft.

(3) Percentages are based on variable recurring costs only (See Section XI).

## SECTION III

### BASLINE COMPONENT AND STRUCTURAL REQUIREMENTS

#### 3.1 BASELINE COMPONENT SELECTION

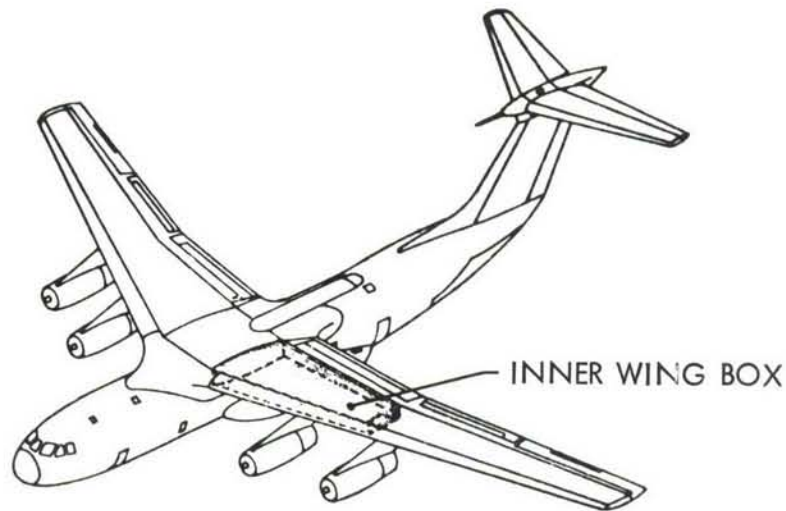
The C-141 Inner Wing was selected as the baseline for the Cargo/Tanker ADP Program because it corresponds closely to the baseline requirements of the Statement of Work (RFP F33615-72-Q-1893, Section 3.0.1). Figure 1 shows the specific ways in which the C-141 Inner Wing complies with these requirements.

The C-141 baseline wing not only satisfies the RFP requirements; it also represents a sound structural design which has encountered only a few relatively minor structural problems during more than three million hours of fleet service. Most of these have been attributable to corrosion.

The C-141 wing closely represents current state of the art design, and improvements in a good modern design through the use of advanced technology are much more meaningful than attempted improvements in an outdated design. Baseline update involves primarily minor changes in material temper, finishes, and processes, and it reflects the more stringent fatigue and damage tolerance requirements now in use as discussed in the following subsections. Thus, the use of this baseline allows an assessment of the effects of criteria changes on a modern wing design, and it provides the opportunity of clearly distinguishing between advanced-technology improvements and those improvements resulting from evolutionary technology which might be the case if an older airplane, such as the C-130 or KC-135, were used as the baseline.

#### 3.2 BASELINE STRUCTURE CONFIGURATION

The baseline structure selected for the advanced cargo/tanker study is the inner wing box of the C-141 aircraft, shown in Figure 2. The two-spar, multi-rib box has a span of 29 feet and extends from WS 77.7 at the center wing joint to IWBR Sta. 374.5 at the outer wing joint. The front spar forms the forward boundary of the box. It is located at 12% chord with a sweep



ADPO RECOMMENDED CRITERIA FOR BASELINE VEHICLE AND COMPONENT SELECTION	REFERENCE	C-141A INNER WING COMPLIES CLOSELY WITH THESE REQUIREMENTS (AS SHOWN BELOW)
<ul style="list-style-type: none"> <li>Should represent the current structures technology for valid "improvement over state-of-the-art" reference.</li> <li>Should meet the requirements of the MIL-A-8860 series specifications and ASIP (ASD TR 66-57).</li> </ul>	<p>SOW Par. 3.0.1(a)</p> <p>SOW Par. 3.0.1(b)</p>	<ul style="list-style-type: none"> <li>Static strength criteria of C-141 were those of MIL-A-8860 series combined with CAR-4b.</li> <li>Fatigue life criteria were based on MIL-A-8860 series.</li> <li>Damage tolerance criteria were those of CAR-4b.</li> <li>Full-scale test programs closely follow those specified in MIL-STD-1530 (ASIP)</li> </ul>
<ul style="list-style-type: none"> <li>Should have service experience available.</li> </ul>	SOW Par. 3.0.1(c)	<ul style="list-style-type: none"> <li>Total fleet cumulative flight time (281 airplanes): 3,145,141 hr.</li> <li>High-time airplane flight time: 19,166 hr.</li> <li>Individual airplane usage is tracked and monitored continuously through ASIP programs implementation.</li> </ul>
<ul style="list-style-type: none"> <li>Should have potential for demonstrating significant advancements in technology.</li> </ul>	SOW Par. 3.0.1(d)	<ul style="list-style-type: none"> <li>Fatigue improvements can be easily demonstrated by comparative component and full scale tests. In addition ADP wing could be flown in future to compare service experience.</li> </ul>
<ul style="list-style-type: none"> <li>The component shall be one which is critical to the safety of the aircraft and is most amenable to technology demonstration.</li> </ul>	SOW Par. 3.0.1(e)	<ul style="list-style-type: none"> <li>The C-141A inner wing is obviously critical to safety of the aircraft. This component is also most amenable to technology demonstration.</li> </ul>

FIGURE 1 BASELINE SELECTION CRITERIA



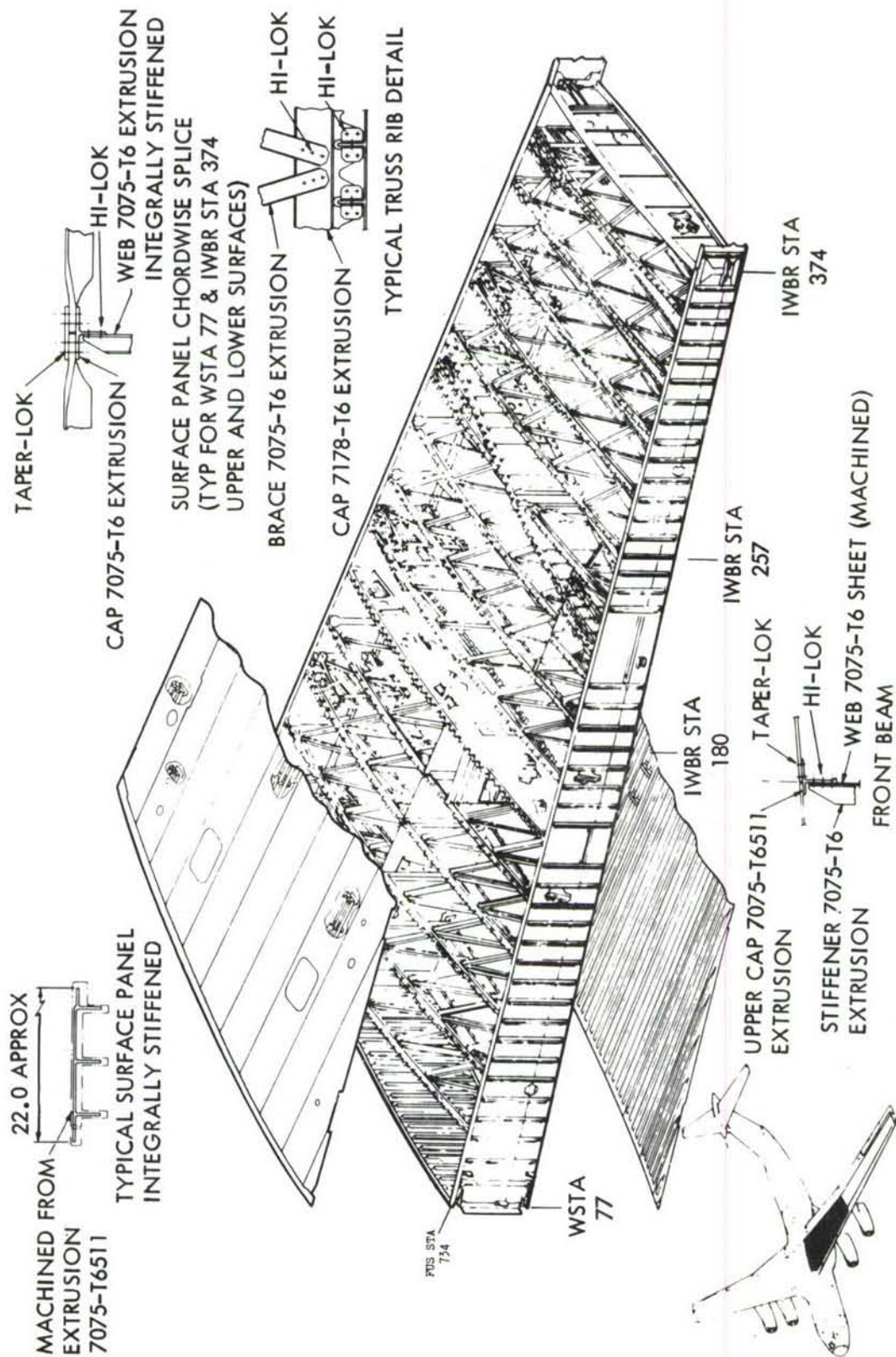


FIGURE 2 BASELINE STRUCTURE - C-141 INNER WING



angle of  $26^{\circ}$ . The rear spar is positioned some 18 1/2 feet aft at WS 77.7 and has a sweep angle of  $11^{\circ}$ . The leading and trailing edges and the pylon structure are not included in the baseline.

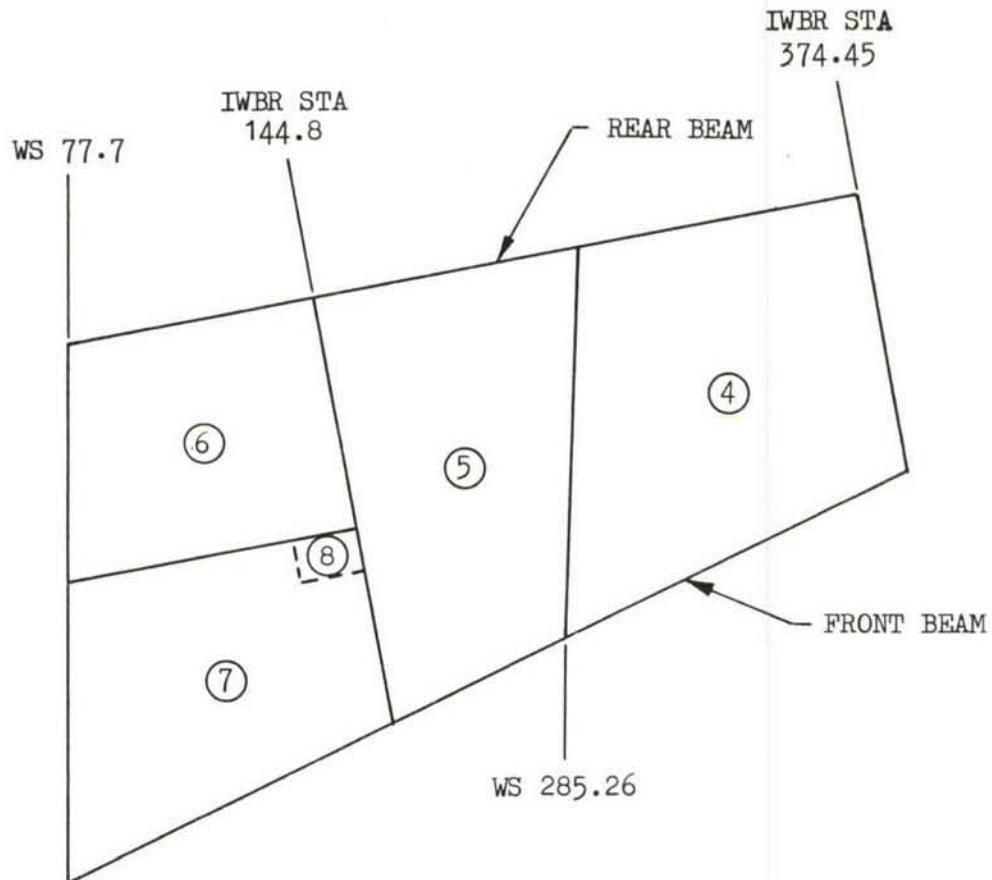
Since chordwise splice plates at the inner and outer wing joints may require changes due to revised panel configurations, they are included in the baseline. The entire inner wing box is an integral fuel tank, divided into four compartments by bulkheads at the pylon rib and IWBR Sta. 144.8, and a partial beam at mid-chord extending from WS 77.7 to IWBR Sta. 144.8. This is illustrated in Figure 3. Pylon attachment fittings mounted on the front beam and lower surface panels are machined from 4340 steel forgings and are included in the baseline structure.

#### 3.2.1 Cover Panels

The integrally stiffened surface panels are made from 7075-T6511 extrusions which are machined to final dimensions. All panels are approximately 21 inches wide, with the spanwise joints running parallel to the rear beam. The integral stiffeners are simple risers spaced at approximately 4.1-inch centers for all panels. The panels are designed to carry axial loads, shear, and normal pressures from air-load, fuel pressures, and other effects. The panels are joined together along spanwise splices by Taper-Lok fasteners, and are supported for compression and bending loads by full-depth ribs at approximately 23-inch intervals.

#### 3.2.2 Spars

The spars are of conventional design, comprising upper and lower caps fabricated from 7075-T6 extrusions and webs machined from 7075-T6 sheet. Web stiffeners, made from 7075-T6 tee extrusions, are located at approximately 8 inches pitch and are attached with Hi-Lok fasteners. The front spar has an intermediate cap and a web splice located at approximately one-third of the beam height from the lower surface. This is a fail-safe design feature which extends the full length of the inner wing. Attachment of spar caps to surface panels is made with Taper-Lok fasteners.

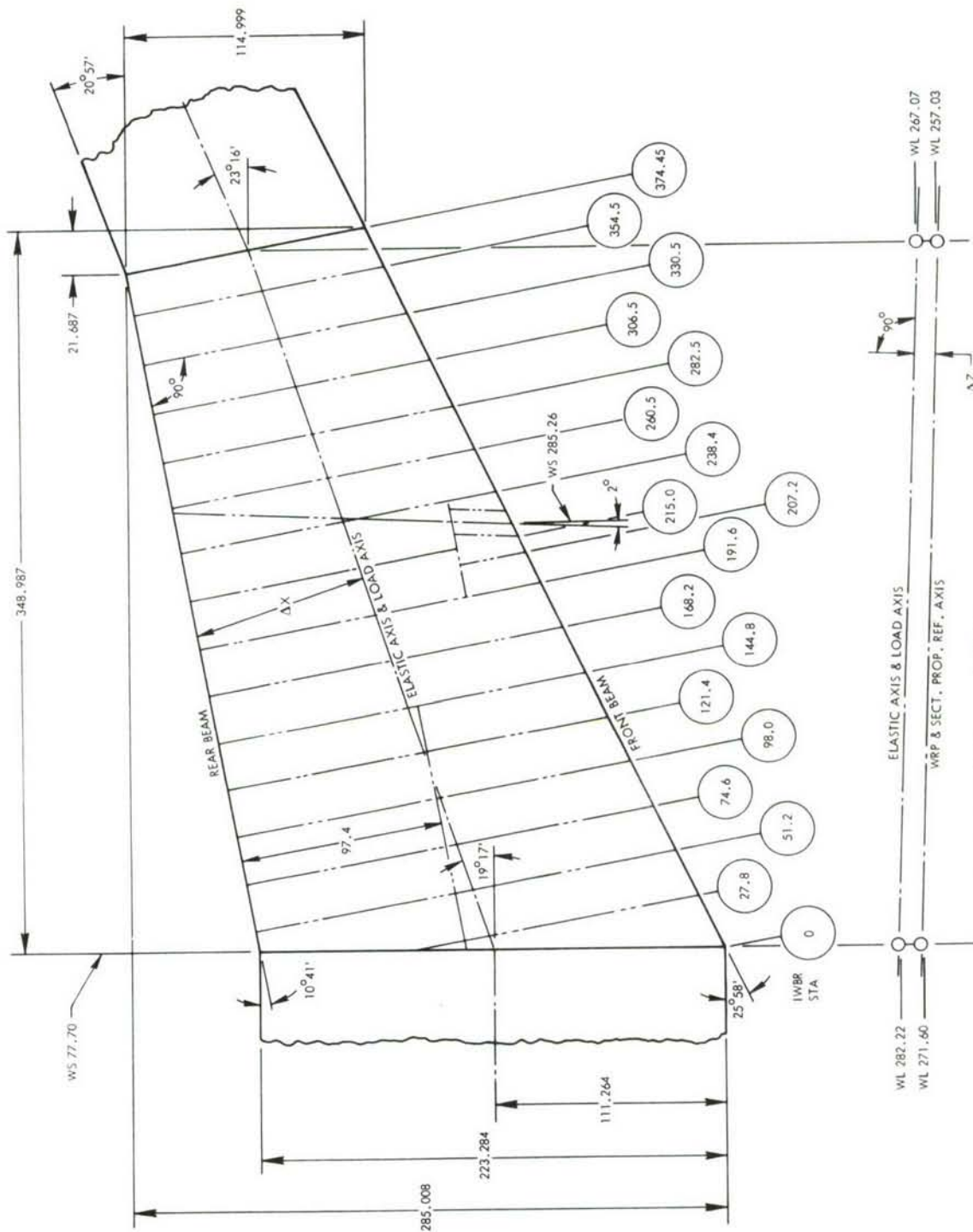


TANK NO.

- 4 OUTBD EXTENDED RANGE TANK
- 5 INBD EXTENDED RANGE TANK
- 6 INBD AUXILIARY TANK
- 7 INBD MAIN TANK
- 8 SUMP - INBD MAIN TANK

(a) Fuel Tank Identification

FIGURE 3 BASIC GEOMETRY



(b) C-141 Inner Wing

FIGURE 3 BASIC GEOMETRY

### 3.2.3 Ribs

Typical wing box ribs are trusses made up of 7178-T6 extruded caps and diagonal braces fabricated from 7075-T6 extrusions. The inboard and outboard closure ribs, the pylon support rib, and the fuel bulkhead at IWBK Sta. 144.8 are all of the web-stiffened type. All ribs, except the pylon support rib and the production joint rib at WS 77.7, are mounted normal to the rear beam.

### 3.3 BASELINE DESIGN CRITERIA

The baseline C-141 inner wing box was designed to meet the applicable requirements of the MIL-A-8860(ASG) series specifications <sup>(1)</sup>, dated 18 May 1960, and CAR-4b through Amendment 4b-11 <sup>(2)</sup>, effective 1 October 1959. The C-141 is basically a 2.5 g transport-category airplane, designed for maneuver loads, specification gust velocities and landing sink rates. The design fatigue life goal was 30,000 flight hours, 12000 landings, and 6500 cycles of fuselage pressurization.

The basic design loads criteria and fatigue spectra have been extracted from applicable reports which have been submitted to the Air Force.

### 3.4 ADP PROGRAM CRITERIA

The baseline design criteria, with minor changes and additions, also apply to the ADP program. Static strength requirements are unchanged, and baseline bending and torsional stiffness were maintained in all ADP designs. Changes in the fatigue area include updating the fatigue load spectrum to reflect operational usage data collected in the C-141 airplane tracking program. Fatigue loads for the ADP program are based on the test loads spectrum developed for the C-141 wing-fuselage fatigue test specimen, with the number of full-stop landings increased to 8187. The safe-life requirement for ADP designs is twice the fatigue life of the baseline. In addition, a peak-to-peak ground-air-ground cycle is used in place of the mean-to-mean cycle description of the baseline airplane.

The primary addition to the structural design criteria pertain to damage tolerance. The ADP inner wing designs comply with the requirements of MIL-STD-1530



(USAF), "Aircraft Structural Integrity Program, Airplane Requirements," dated 1 September 1972, and the "Proposed USAF Damage Tolerance Criteria," dated 18 August 1972. Table IV highlights the principal aspects of the criteria.

### 3.5 BASELINE UPDATE TO 1972 TECHNOLOGY

An analysis of the design and production methods used for the baseline structure was completed, and all areas of change required to meet 1972 technology standards were identified. The purpose of this update was to provide a meaningful basis for comparison and to demonstrate the true contribution of advanced technology beyond the current state of the art.

Technological improvements in design criteria, materials, joining systems, finishes and processes, structural configurations, analysis methods, fabrication methods, and inspection techniques were assessed; and incremental changes in cost, weight, static strength, fatigue life, and corrosion resistance were evaluated. To provide a common base for evaluation, and to minimize the difficulty in quantifying some of these performance parameters, all changes were expressed in terms of weight and cost; if a material change showed an increase in static strength, this was converted to a weight reduction. The results of this update, summarized in Tables V and VI, were used as a basis for comparison with the ADP designs. A detailed explanation of the cost development for the updated baseline is given in Section XI. An explanation of some of the more significant incremental weight changes is noted below.

- (1) Finishes and Processes - Overcoating all fastener heads and a topcoat sealant has been introduced inside the tank for increased reliability and corrosion resistance - + 57 pounds.
- (2) Fasteners - The increase reflects the introduction of high clamp-up fasteners for ribs and spars and a change from Taperloks to high strength bolts at the chordwise splices - + 55 pounds.
- (3) Materials - 7075-T76 in lieu of 7075-T6 aluminum is used for all major components to provide better stress corrosion resistance. The lower-static properties of this material imposes weight and cost penalties due to the required increase in material thickness - + 318 pounds.

TABLE IV

DAMAGE TOLERANCE CRITERIA

DESIGN CRITERIA

DESIGN APPROACHES	CRITERIA ELEMENTS
<ul style="list-style-type: none"> <li>● SLOW CRACK GROWTH STRUCTURE</li> <li>● FAIL-SAFE, CRACK ARREST STRUCTURE</li> <li>● FAIL-SAFE, MULTIPLE LOAD PATH STRUCTURE</li> </ul>	<ul style="list-style-type: none"> <li>● INSPECTABILITY</li> <li>● MIN. ASSUMED INITIAL DAMAGE SIZE               <ul style="list-style-type: none"> <li>- INTACT NEW STRUCTURE</li> <li>- REMAINING FAIL-SAFE STRUCTURE</li> </ul> </li> <li>● MIN. PERIOD OF UNREPAIRED SERVICE USAGE</li> <li>● MIN. ASSUMED IN-SERVICE DAMAGE SIZE</li> <li>● DAMAGE GROWTH LIMITS</li> <li>● MIN. REQUIRED RESIDUAL STRENGTH</li> </ul>

TABLE V

## WEIGHT BREAKDOWN - C-141 INNER WING

	ORIGINAL DESIGN	1972 UPDATE WEIGHTS (LB)					TOTAL 1972 UPDATE	
		FINISHES PROCESSES	FASTENERS	BETTER OPTIMIZATION	MATERIALS	FATIGUE		DAMAGE TOLERANCE
UPPER SKINS	1874			-6	113	87	0	2068
LOWER SKINS	1687				134	78	64	1963
FRONT BEAM	385		6		20	5	5	421
UPPER CAP	50				3	0	0	53
LOWER CAP	137				10	5	5	157
WEB & STIFFENERS	198	6			7	0	0	211
REAR BEAM	379		6		17	4	3	409
UPPER CAP	63				3	0	0	66
LOWER CAP	79				5	4	3	91
WEB & STIFFENERS	237	6			9	0	0	252
JOINTS, SPLICES, FASTENERS - UPPER	56							56
JOINTS, SPLICES, FASTENERS - LOWER	78							78
SPANWISE FUEL BULKHEAD	47				1			48
BL 77.7 RIB	309				2			311
BL77.7 SPLICE PLATES	155		43		11			209
IWBR 374 RIB	110				1			111
RIBS & BULKHEADS	1091				19			1110
SURGE BOX & VENT BOX	20							20
PYLON FITTINGS	61							61
ACCESS DOORS	39					- 10		29
PAINT & SEALANT	61	57						118
TOTAL BOX (ONE SIDE ONLY)	6352	+57	+55	-6	+318	+164	+72	7012

TABLE VI

## COST BREAKDOWN - BASELINE UPDATE

	ORIGINAL DESIGN	1972 UPDATE COST (\$)					TOTAL 1972 UPDATE
		FINISHES & PROCESSES	FASTENERS	MATERIAL	FATIGUE DAMAGE TOLERANCE	Q.A.	
SURFACES	46894			1333	890	345	49462
SPANWISE SPLICE	28950						28950
CHORDWISE SPLICE	446		996				1442
RIBS	75850		2647				78497
SPARS	36685		729	152	37	33	37636
BULKHEAD & CLOSURE RIBS	8716						8716
SURGE & VENT BOX PYLON FITTINGS, DOORS, PAINT & SEALANT	10119	10278					20397
QUALITY ASSURANCE	15829					1398	17227
TOTAL RECURRING COST (CUM. AVG. FOR 100 A/C)	223489	10278	4372	1485	927	378	242327



- (4) Fatigue - Analyses based on combined stresses and a peak-to-peak G-A-G cycle dictate that lower design cutoff stress levels be used which results in both weight and cost increases - + 164 pounds.
- (5) Damage Tolerance - Increases result from the lower stress levels used to satisfy the revised damage tolerance requirements - + 72 pounds.

It should be noted that the above weights attributed to fatigue and damage tolerance are delta weights and do not reflect the total weight effect for fatigue or damage tolerance criteria when considered alone. An explanation of the rationale in determining the delta weights for fatigue and damage tolerance is as follows: first, in updating the baseline, effects of fatigue and damage tolerance criteria were considered significant only for surface panel and spar cap structure. Effects were felt to be negligible in the substructure. Second, effects of material changes, fatigue requirements, and damage tolerance criteria are interrelated; i.e., a weight change and corresponding stress change resulting from any one of the three parameters affects the other two. Since effects of damage tolerance criteria generally overshadow fatigue effects, and fatigue in turn encompasses materials changes, update analysis was conducted considering: first, updated materials; second, fatigue requirements; and, finally, damage tolerance criteria. After each change was evaluated, the delta weight over and above the previous weight change was calculated and recorded.

A numerical explanation of the above is given for clarification. The total weight for changes due to fatigue was 432 pounds. Since 268 pounds had already been included for material changes in the covers and spar caps, which in itself enhanced the fatigue life, this value was subtracted from the 432 pounds, thus leaving 164 pounds for the delta weight for fatigue. Again, a weight increment of 504 pounds was calculated for effects of damage tolerance criteria. Since the previous weights for the material and fatigue changes enhanced the damage tolerance strength, the additional delta weight of 504 pounds minus 268 pounds (materials) minus 164 pounds (fatigue), or 72 pounds, was incorporated for damage tolerance. In this manner, the accumulative delta weights are given such that these can be added together to obtain the overall weight of the updated baseline.

## SECTION IV

### TECHNICAL APPROACH

#### 4.1 SCOPE

Existing rib spacings, fuel tank arrangements, center and outer wing joints, and attachment structure for edges were generally retained throughout the preliminary design study to maintain functional interfaces of the ADP article with the remainder of the baseline aircraft. This provides a direct comparison with the baseline and emphasizes that the basic form of construction of the C-141 inner wing is highly suited for an advanced-technology wing design.

The scope of the preliminary design studies emphasized alternate materials, forms of construction, manufacturing and assembly methods, and geometric changes corresponding to alternate damage tolerance concepts.

#### 4.2 STUDY PROCEDURE

The study procedure adopted for this program involved several distinct phases of successively greater depth and narrower scope, finally converging on the three selected designs: the Weldbond, Virgin Plank, and Tapered Shingle concepts. This approach is illustrated in Figures 4 and 5.

In the initial phase, numerous component concepts were considered, each of which evidenced advantages in weight, cost, damage tolerance, fatigue, or other desirable aspects. These were broadly screened with simplified analytical substantiation to eliminate the least-likely candidates, using the specified selection criteria. In the second phase, compatible cover and substructure concepts were combined to define eight wing box configurations for preliminary assessment. Provisional loads and material strength data, including approximate design cutoff stress levels for fatigue and fracture requirements, were established for this purpose. Several variations were introduced during this phase as suggested by trade studies and a more detailed design analysis, and the resultant configurations were compared with the baseline, using the merit rating system described in Section XII.

In the concluding phase, preliminary designs of the three highest scoring configurations were developed with fully supporting stress, fatigue, damage tolerance, cost, and weight analyses to confirm the merit rankings and to ensure compliance with all design requirements.

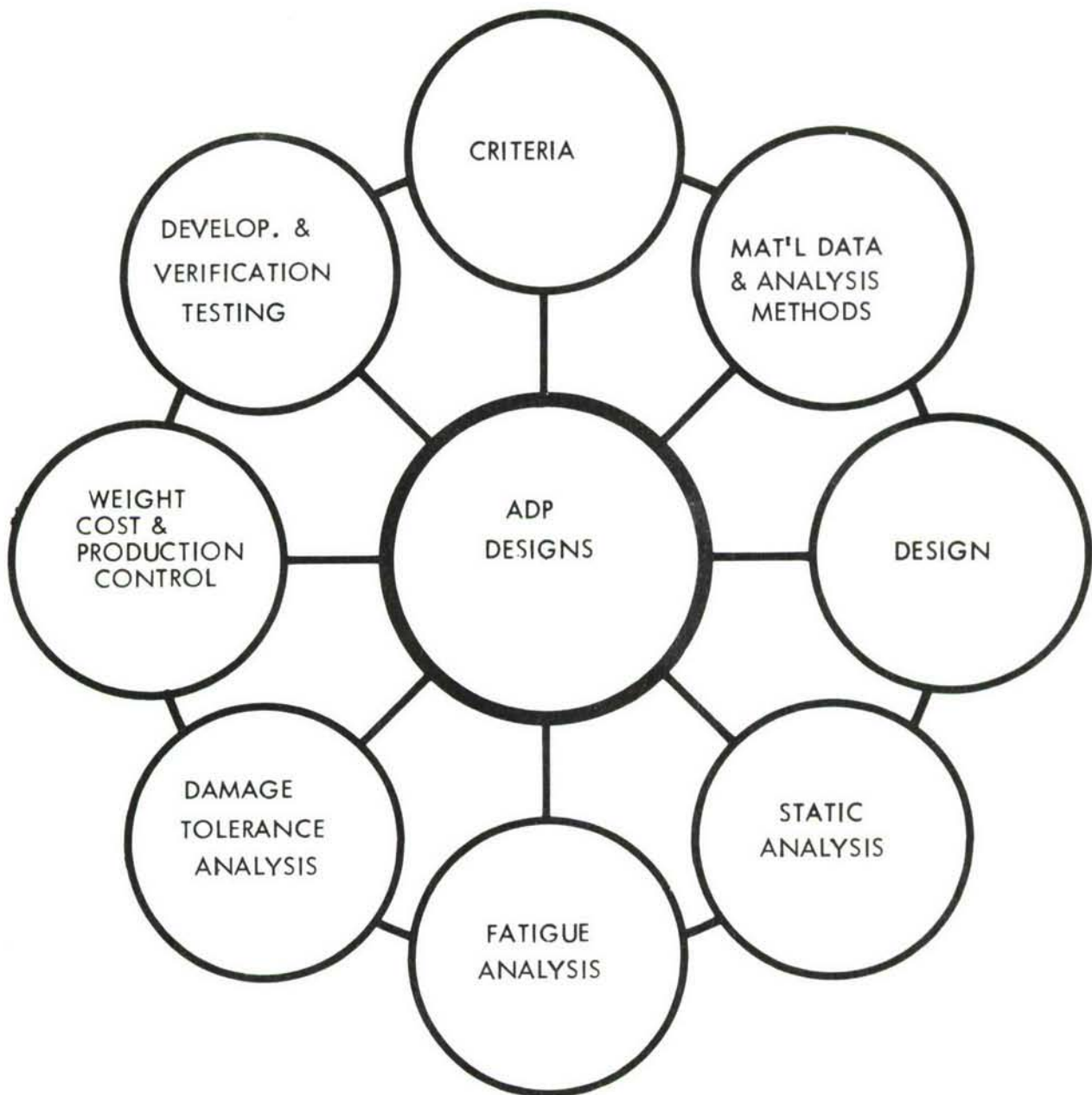


FIGURE 4 DESIGN APPROACH

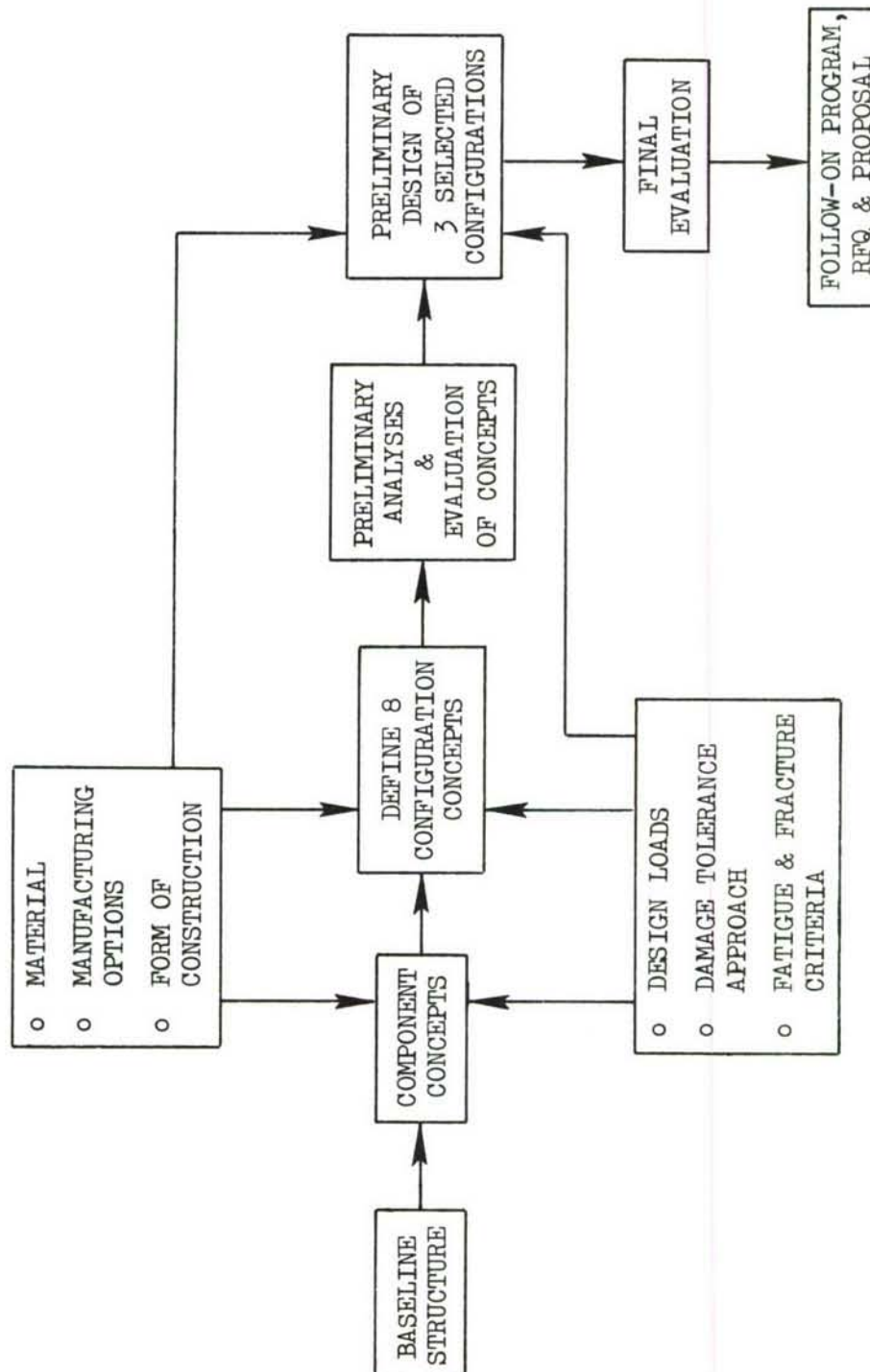


FIGURE 5 STUDY PROCEDURE



## SECTION V

### NEW STRUCTURAL CONCEPTS/CONFIGURATIONS

#### 5.1 DESIGN APPROACH

The structural areas where fatigue cracks usually occur are typically characterized by discontinuities or disruptions, stress risers, or sudden variation in the load paths. Such areas are associated with holes, cutouts, doors, doubler fasteners, sharp radii, and other abrupt changes in cross section. One of the most successful ways of increasing fatigue endurance is to minimize such areas, and major improvements can be made by reducing perforations of the covers.

Major effort during this study was focused on designs which eliminated or substantially minimized conventional fasteners, since fasteners constitute the prime causes of stress concentrations in most areas of the structure. Hence, the predominance of bonded and weldbonded joints, which offer great promise of enhanced fatigue performance, is evident in several designs.

Since more than one-half the baseline wing box weight consists of cover material, the initial emphasis of design work was on the different cover configurations which showed promise for the ADP wing. This is in keeping with program objectives which emphasize minimum-cost designs with substantially improved fatigue performance and reduced weight.

The substructure of the baseline article is not generally fatigue-critical; hence, low cost and weight were the major factors influencing the various substructure designs. Care was also taken to ensure that designs were compatible with the selected cover configurations.

Some of the design features aimed at cost reduction are listed below:

- o Reduced number of parts/fasteners
- o Simplified assembly techniques
- o Maximum use of net extrusions
- o Elimination of complicated machining
- o Low-cost automated fastener systems

## 5.2 MATERIAL SELECTION

The baseline structure selected for this study is subjected to relatively low load intensity. The box structure is tapered, and the load level remains relatively constant spanwise. The upper surface compression loads peak near the mid-chord at a value of 15,000 pounds per inch, while the lower surface compression loads peak near 11,000 pounds per inch. Tension loadings are of the same general magnitude. Consequently, a range of materials of intermediate strengths where local stability could be controlled by minimum-weight construction were tentatively selected. The materials considered were primarily metallic, in consonance with the basic objective of the program to explore innovative advanced metallic structural concepts. Advanced composites were considered as reinforcement materials, although all-composite structural configurations were not considered.

The materials selected above were then subjected to trade studies to determine those materials which had an optimum balance of tensile, fatigue, fracture toughness, and corrosion properties for specific applications. In addition, these materials had to meet processing and manufacturing criteria which considered the structural application and manufacturing technology. Among the trade-offs made were:

- o Fatigue and tensile strength level versus fracture toughness
- o Composition versus fracture properties
- o Weldability versus mechanical and fatigue properties
- o Corrosion resistance versus mechanical properties.

From the above evaluations, a list of candidate materials evolved for the ADP Configurations. These materials, with designated applicable product forms and primary reasons for selection, are listed in Tables VII and VIII.

Low-density materials generally perform better in lightly loaded structures, especially in low shear and compression applications typical of large aircraft wings and fuselages. By equating the various modes of stability failure and solving for the attainable

TABLE VII

## ALUMINUM ALLOY MATERIAL SELECTION SUMMARY - ADP DESIGNS

<u>ALLOY</u>	<u>PRODUCT FORM</u>	<u>REASON FOR SELECTION</u>
<ul style="list-style-type: none"> <li>7050 T76 ALUMINUM</li> </ul>	PLATE, EXTRUSION, FORGING	DEEP HARDENABLE ADVANCED ALLOY PROVIDING HIGH STRENGTH/WEIGHT, EXCELLENT CORROSION RESISTANCE, GOOD FRACTURE TOUGHNESS.
<ul style="list-style-type: none"> <li>7475 T761 ALUMINUM</li> </ul>	SHEET	HIGH PURITY 7075 ALLOY PROVIDING HIGH STRENGTH/WEIGHT, EXCELLENT CORROSION RESISTANCE, SUPERIOR FRACTURE TOUGHNESS.
<ul style="list-style-type: none"> <li>2219 T87 ALUMINUM</li> </ul>	SHEET, PLATE	WELDABLE ALLOY WITH BEST BALANCE OF STATIC, FATIGUE AND FRACTURE PROPERTIES.
<ul style="list-style-type: none"> <li>7075 T76 ALUMINUM (BASELINE UPDATE)</li> </ul>	SHEET, PLATE, EXTRUSION	BEST CURRENTLY AVAILABLE ALLOY, COMPRISING BALANCED MECHANICAL PROPERTIES AND IMPROVED CORROSION RESISTANCE.

TABLE VIII

## TITANIUM AND COMPOSITE MATERIAL SELECTION SUMMARY - ADP DESIGNS

<u>TITANIUM ALLOY</u>	<u>PRODUCT FORM</u>	<u>REASON FOR SELECTION</u>
<ul style="list-style-type: none"> <li>6Al-6V-2Sn STA, STOA</li> </ul>	SHEET, PLATE, EXTRUSION, FORGING	HIGH STRENGTH/WEIGHT, GOOD FATIGUE CHARACTERISTICS, COMMERCIALY AVAILABLE
<ul style="list-style-type: none"> <li>6Al-2Zr-2Sn-2Mo 2Cr - 0.25Si ST, STA</li> </ul>	SHEET, PLATE, EXTRUSION, FORGING	ADVANCED ALLOY WITH HIGH STRENGTH/ WEIGHT, HIGH MODULUS, SUPERIOR FRACTURE TOUGHNESS
<u>COMPOSITES</u>	<u>PRODUCT FORM</u>	<u>REASON FOR SELECTION</u>
<ul style="list-style-type: none"> <li>BORON - EPOXY</li> </ul>	TAPE	HIGH STRENGTH/WEIGHT, THERMAL COMPATIBILITY WITH ALUMINUM
<ul style="list-style-type: none"> <li>GRAPHITE - EPOXY</li> </ul>	HI-STRENGTH TAPE	HIGH STRENGTH/WEIGHT, LOW COST, THERMAL COMPATIBILITY WITH TITANIUM



specific compression stress levels, it can be shown that aluminum alloys can attain higher stress levels per pound of structure than titanium or steel, both of which have higher ultimate stress levels per pound than aluminum. Figure 6 shows a typical comparison of the performance of these materials for application in fuselage-and-wing-type structures.

The relatively low loadings ruled out the efficient use of steel in the cover, spar, and rib designs. However, selective use of high heat treat steel (260 KSI and above) is contemplated for certain critical fittings such as pylon support fittings. For these applications, the 18 Ni-300 maraging steel is selected over currently used 300M steel as the best advanced alloy with proven potential for developing superior fracture toughness as well as the required high static and fatigue properties.

In the less conventional concepts, which used Lockskin and corrugation-stiffened/sandwich configurations, high-strength titanium and combinations of titanium and advanced composite materials offered attractive advantages. The most promising titanium alloys were Ti-6Al-6V-2Sn and Ti-6Al-2Zr-2Sn-2Mo-2Cr-0.25Si. The latter (referred to as 6-2-2-2-2) is a new alloy developed by Reactive Metals which offers high strength and toughness and deep hardenability.

Composite materials considered were boron-epoxy and high-strength graphite-epoxy. The latter offered significant cost advantages over boron-epoxy, but had the disadvantage of a more incompatible coefficient of thermal expansion when used in combination with aluminum and titanium alloys.

### 5.3 STRUCTURAL OPTIMIZATION

In conjunction with the material selection studies, structural optimization analyses and studies were conducted for various forms of construction, geometric shapes, and geometric arrangements. Through a continuation of the iterative process, the candidate materials in various forms, shapes, and arrangements were selected for possible configurations. Analyses and optimization studies were made from these configurations to optimize the detail structural design and meet all design requirements and objectives. Computer programs, verified by experimental results, were extensively used. The programs optimize several design parameters such as riser spacing, height,

$C_s = 1.0$  FOR STIFFENED SHEET (HAT OR BETTER)

$C_s = 0.81$  INTEGRALLY STIFFENED UNFLANGED RISERS

$P_i$  = LOAD PER INCH (AXIAL COMPRESSION)

$a$  = EFFECTIVE COLUMN LENGTH (RIB, RING, FRAME OR BULKHEAD SPACING)

$F_{cr}$  = CRITICAL COMPRESSION STRESS

$\rho$  = MATERIAL DENSITY

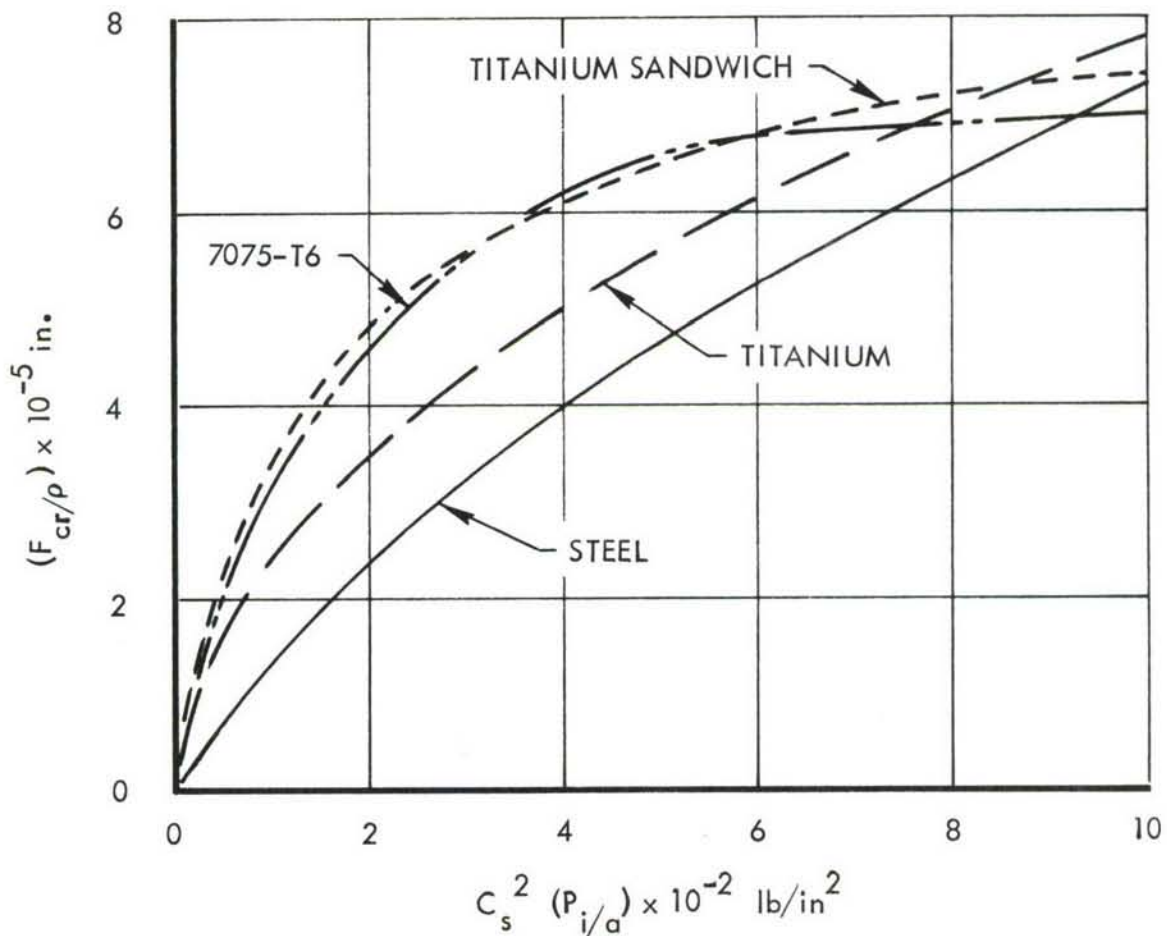


FIGURE 6 ATTAINABLE STRESS TO DENSITY RATIO

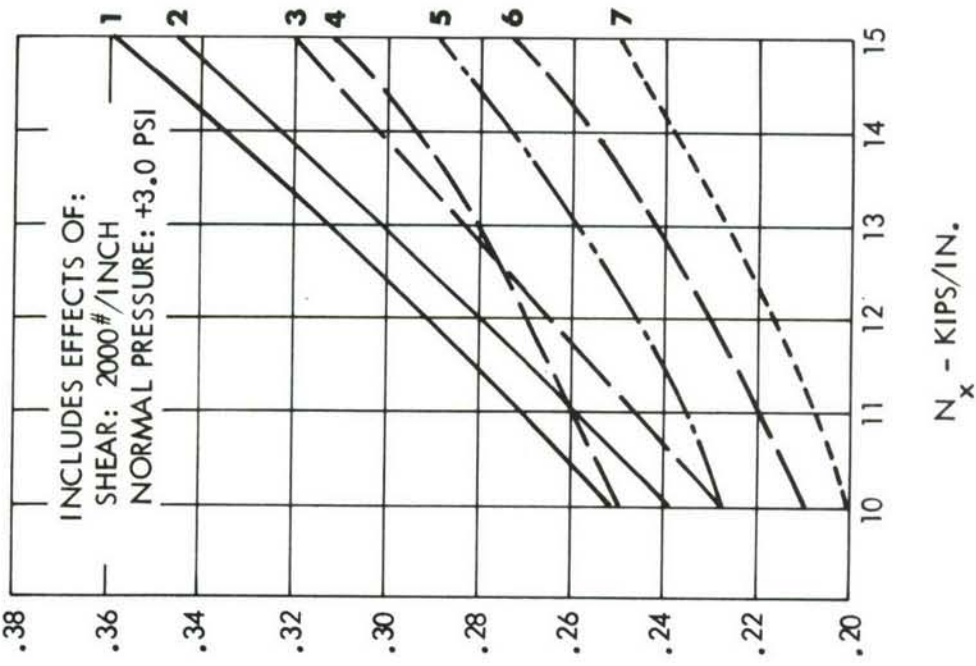
flange widths and thicknesses, and panel thickness. Also, maximum tension stress thresholds for fatigue and damage tolerance are parameters used in the optimization. This optimization ensured efficient minimum weight structural designs for ultimate load conditions and provided for reduced stress levels resulting from fatigue or damage-tolerance requirements.

Various possible configurations were optimized for a load range of 8,000 to 16,000 pounds per inch. The results of the optimization process were plotted for ease in performing weight and cost trade studies. Some typical panel results, t-bar (average panel thickness including stringer areas) versus load range are given in Figures 7 and 8. Figure 7 presents typical aluminum results, and Figure 8 presents typical titanium and titanium/composite results.

#### 5.4 COVER AND SUBSTRUCTURE CONCEPTS

To facilitate the evaluation of cover and substructure concepts, selection matrices were devised which listed promising combinations of design configurations, material alloys and forms, and assembly methods. These are illustrated in Tables IX and X. This process was used to ensure that promising concepts were not omitted from consideration. A similar approach was taken for the major splices and joints: Tables XI shows the principal joining methods that were considered.

These concepts were then subjected to a preliminary screening, using the evaluation criteria outlined in Section XII, and compatible cover and substructure concepts were combined to define eight ADP wing box configurations.



EQUIVALENT  
 $T_{\text{BAR}} - \text{IN.}$

- 1 2219-T85 UNFLANGED INTEGRAL STIFFENED EXTRUSION
- 2 2219-T85 FLANGED INTEGRAL STIFFENED EXTRUSION
- 3 7475-T76 FACE SHEET - 5052-H39 HONEYCOMB CORE
- 4 7475-T76 SKIN - 7050-T76 "A" SECTION EXTRUSION
- 5 2021-T81 UNFLANGED INTEGRAL STIFFENED EXTRUSION
- 6 7475-T76 SKIN - 7050-T76 "HAT" SECTION EXTRUSION
- 7 7050-T76 FLANGED INTEGRAL STIFFENED EXTRUSION

FIGURE 7 PANEL STRUCTURAL OPTIMIZATION - ALUMINUM



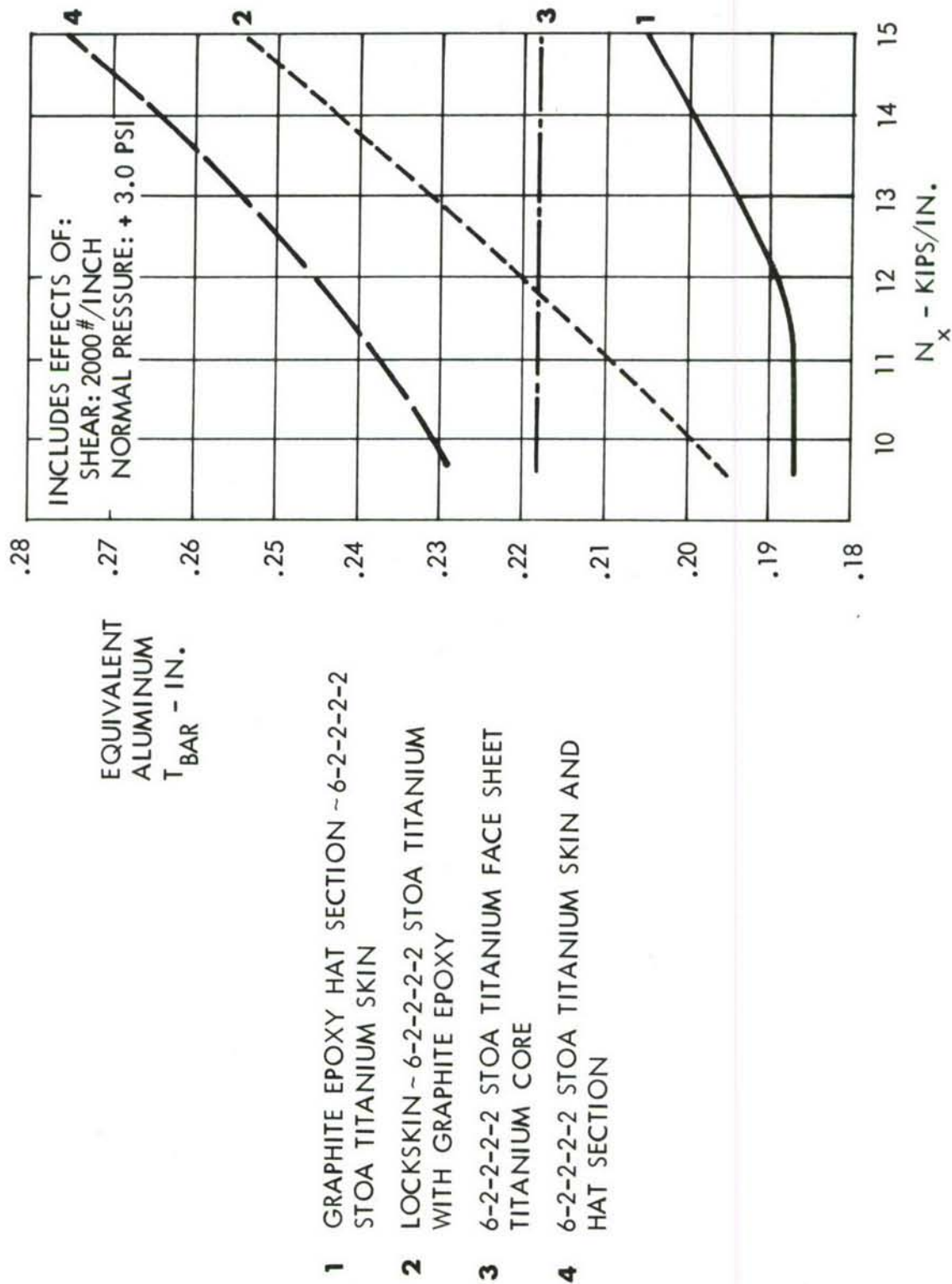



FIGURE 8 PANEL STRUCTURAL OPTIMIZATION-TITANIUM

TABLE IX  
COVER CONFIGURATIONS

OPTION CONCEPT		MATERIAL			FORM			ASSY METHOD						
		ALUM	ST	TI	COM- POSITE	EXTR	SHT/ PLT	HONEY COMB	MECH FAST.	WELD BOND	ADH BOND	WELD	BRAZE	DIFF BOND
CONVENTIONAL														
(A) INTEGRALLY STIFFENED		●				●								
(B) BUILT UP	SKIN	●												
	STRINGER	●				●			● (OR)	●				
(C) SINGLE SKIN		●						●		●				
	CORRUGATION													
SANDWICH														
(A) CORRUGATED CORE		●						●		● (OR)	●			
(B) HONEYCOMB	SKIN	●						●						
	CORE	●								●				
(C) HONEYCOMB	SKIN			●				●						
	CORE			●									● (OR)	●
MONOLITHIC														
(A) WELDED ASSY		●				●		●				●		
(B) BRAZED ASSY				●				●					●	
LAMINATED														
(A) SHEET METAL		●				●		●			●			
(B) LOCKSKIN	SKIN			●		●		●						
	CORE				●						●			
REINFORCED														
(A) COMPOSITE REINF					●						●			
	SKIN	●						●			●			

TABLE X  
RIB, BULKHEAD & SPAR CONFIGURATIONS

CONFIGURATION	MATERIAL			FORM				ASSEMBLY METHOD			
	ALUM	TI	COM- POSITE	SHT/ PLT	EXTR	FORGING/ CASTING	HONEY- COMB	MECH FAST.	WELD BOND	ADH BOND	WELD
<u>PLATE/STIFFENER</u>											
(A) WEB/VERT. STIFFENER	●			●	●			● (OR) ●	● (OR) ●	●	
(B) WEB/TRUSS	●			●	●			● (OR) ●	● (OR) ●	●	
(C) COMPOSITE REINFORCED	● (OR) ●		●	●	●					●	
<u>SANDWICH</u>											
(A) HONEYCOMB	●			●			●			●	
(B) CORRUGATED CORE	●			●						●	
(C) LOCKSKIN		●	●	●						●	
<u>CORRUGATED WEB</u>											
(A) FLAT ELEMENT	● (OR) ●			●							●
(B) CURVED ELEMENT	● (OR) ●			●							●
<u>MONOLITHIC</u>											
(A) WAFFLE PATTERN	●					●					
(B) INTEGRALLY STIFFENED	●				●	●					
(C) WELDED	●			●	●						●
<u>TRUSS</u> 											
(A) CONVENTIONAL RIB	●				●			● (OR) ●	● (OR) ●		
(B) SPACE TRUSS 3 DIM.	●				●			● (OR) ●	● (OR) ●		

 NOT APPLICABLE TO BULKHEADS OR SPARS

TABLE XI  
SPLICES AND JOINTS

TYPE	MECH. FASTENER	RIVET BOND	WELD- BOND	BONDED FIBERGLASS	WELDED	BONDED	NON- PENETRATING CLIP	CLAMP
SPANWISE	●	●	●	●	●	●		
CHORDWISE	●	●				●		●
SPAR CAP TO WEB	●	●	●		●	●		
RIB TO COVER	●	●	●		●	●	●	
RIB TO SPAR	●	●	●		●	●		

## 5.5 CONFIGURATION CONCEPTS

A description of the eight configurations developed during Phase IA of this program is presented here. Illustrations are included to depict the main features of each concept. Design drawings and layouts are presented in Appendix I.

### 5.5.1 Weldbond Configuration

This design has a number of features aimed at substantially improving fatigue life. Extruded 7050-T76 stringers are attached to 7475-T76 skins by the weldbond process as shown in Figure 9. Replacement of conventional fasteners with weldbond minimizes the number of fastener holes, thereby improving fatigue quality. The stringers are shaped to form small 'A' frame trusses, providing an efficient method for transferring shear between the rib cap and covers. This feature eliminates the need for shear clips between the covers and rib caps, again minimizing fastener holes as well as detail parts. The stringers are tabbed out at the rib caps to reduce the stress level at the fastener holes in the stringer.

This configuration relies on slow crack growth to satisfy damage tolerance requirements. Hence, the number of spanwise splices is dictated by practical limitations rather than fail-safe "crack-stopper" requirements. To ensure adequate access for spotwelding equipment, each surface assembly comprises three weldbonded panels with an additional integrally stiffened panel on the upper surface containing the large cutouts required for tank access.

The spar design selected for use with this cover configuration is the welded aluminum assembly depicted conceptually in Figure 10. Spar webs, made from 2219-T87 material, are formed in a "Sine Wave" pattern and are welded to upper and lower caps using an electron beam burn-through weld technique. Development of the burn-through weld has determined the feasibility of this method of construction. However, further development is required in the follow-on program. The "sine wave" corrugation minimizes any tendency of the spar web to pick up axial tension stress near the spar caps, and eliminates the row of fastener holes normally required to join the web to the cap. This should produce significant improvement in fatigue life of the spar caps and webs.



A typical rib (Figure 11) is of conventional truss arrangement with the diagonals fabricated from 7050-T76 square tubes. The rib caps are back-to-back extruded channels of 7050-T76 aluminum and are attached to the stringers with Hilok fasteners. This design is aimed primarily at low cost, and the entire rib assembly is fabricated from net extrusions. Bulkheads and close-out ribs are of the web stiffener type and are constructed from 7050-T76 and 7475-T76 material using the weldbond fastener system.

This design has many attractive features, including projected weight savings of 8.5% and cost savings of 20%, and is one of the three designs selected for further study.

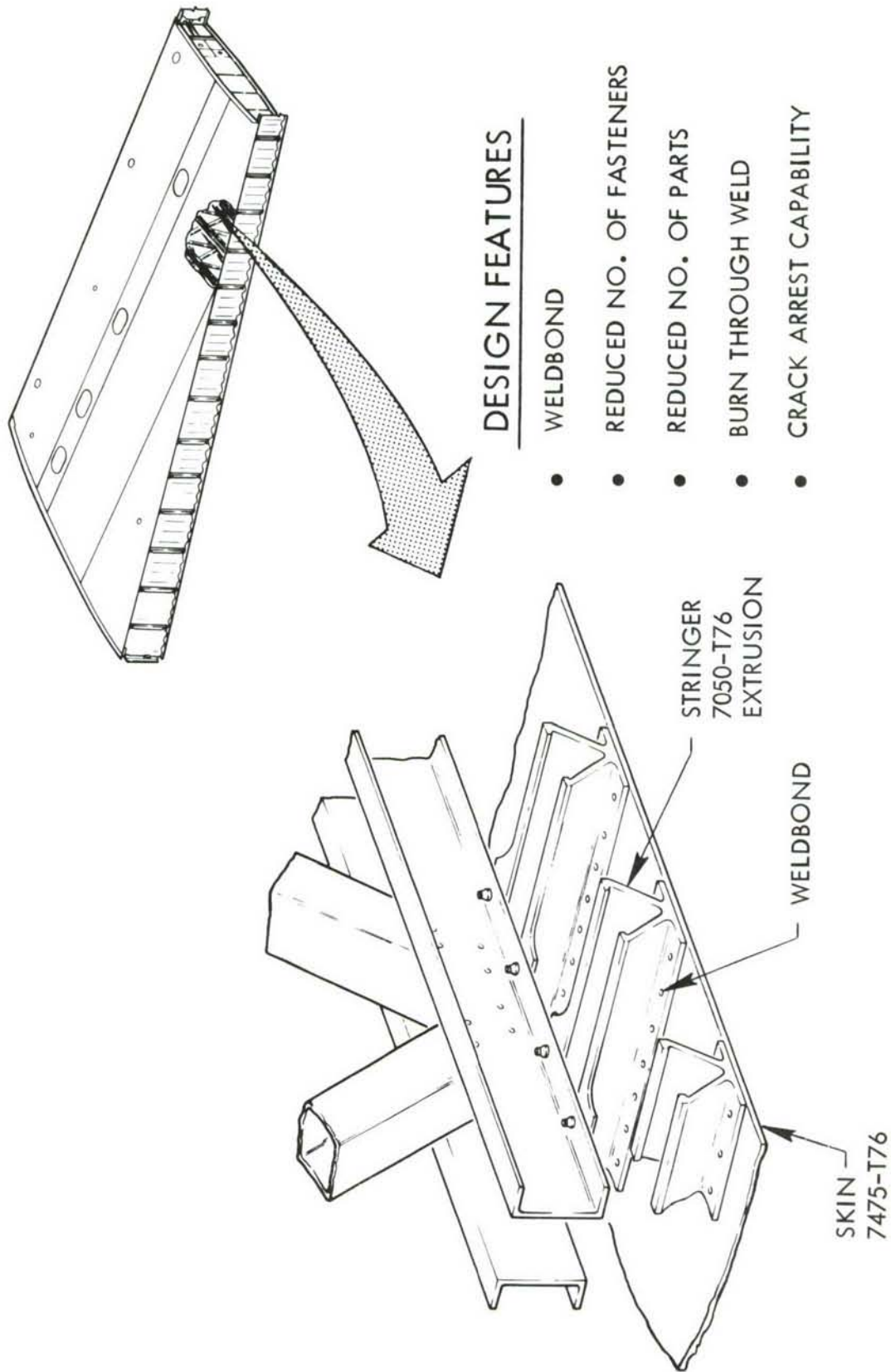


FIGURE 9 WELDBOND CONFIGURATION

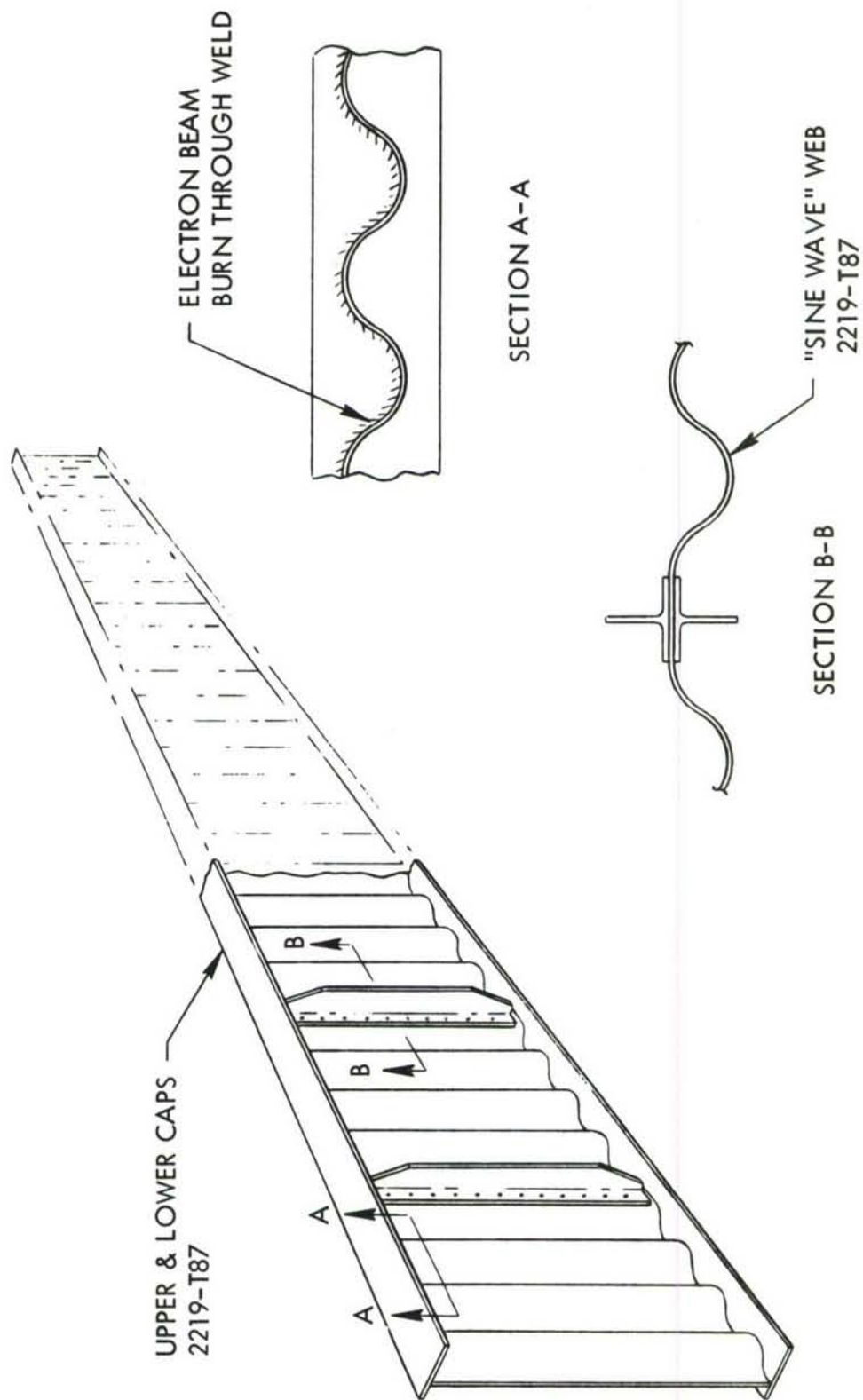


FIGURE 10 SPAR - WELDBOND CONFIGURATION

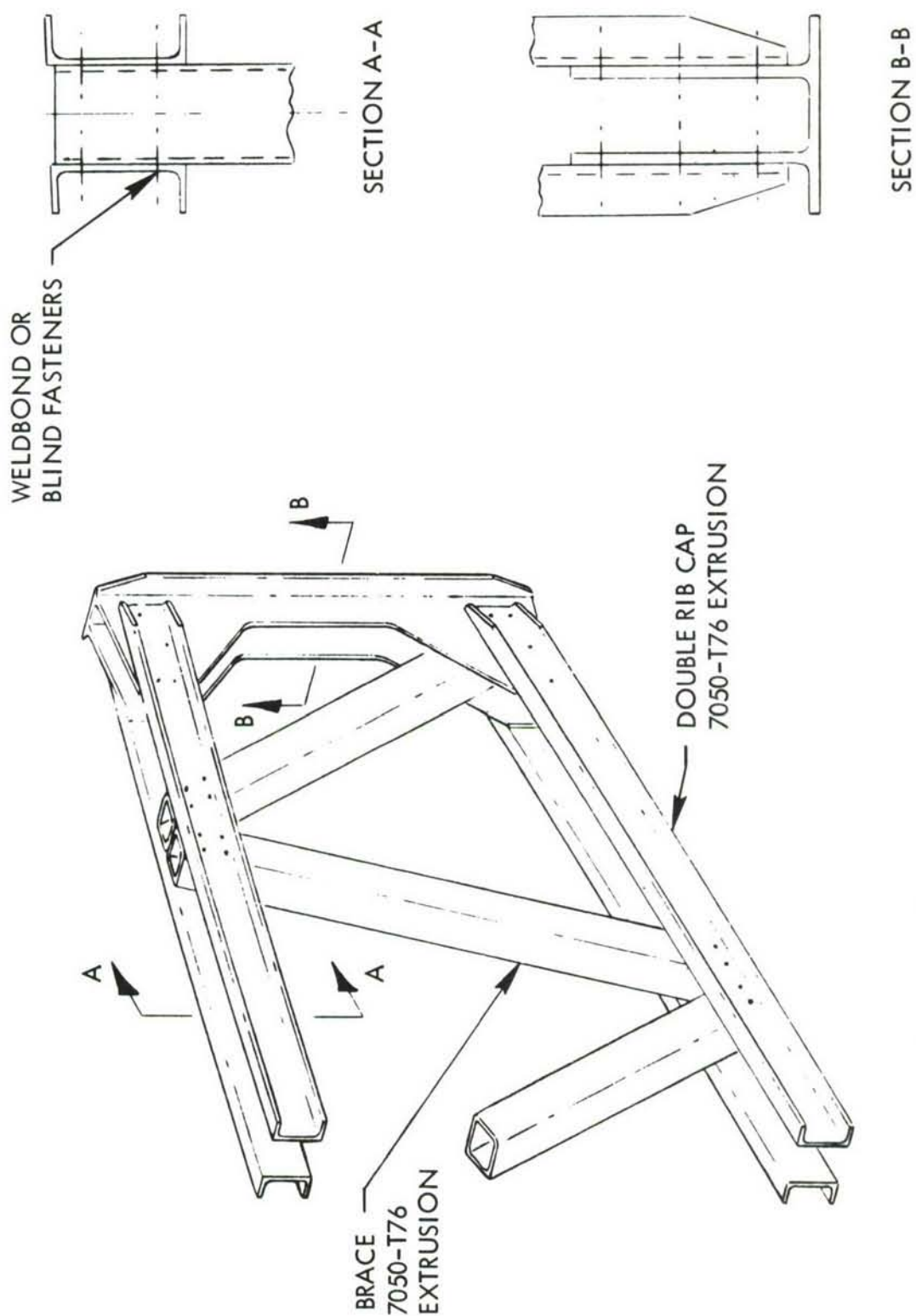


FIGURE 11 TYPICAL RIB - WELDBOND CONFIGURATION



### 5.5.2 Hat Stringer Configuration

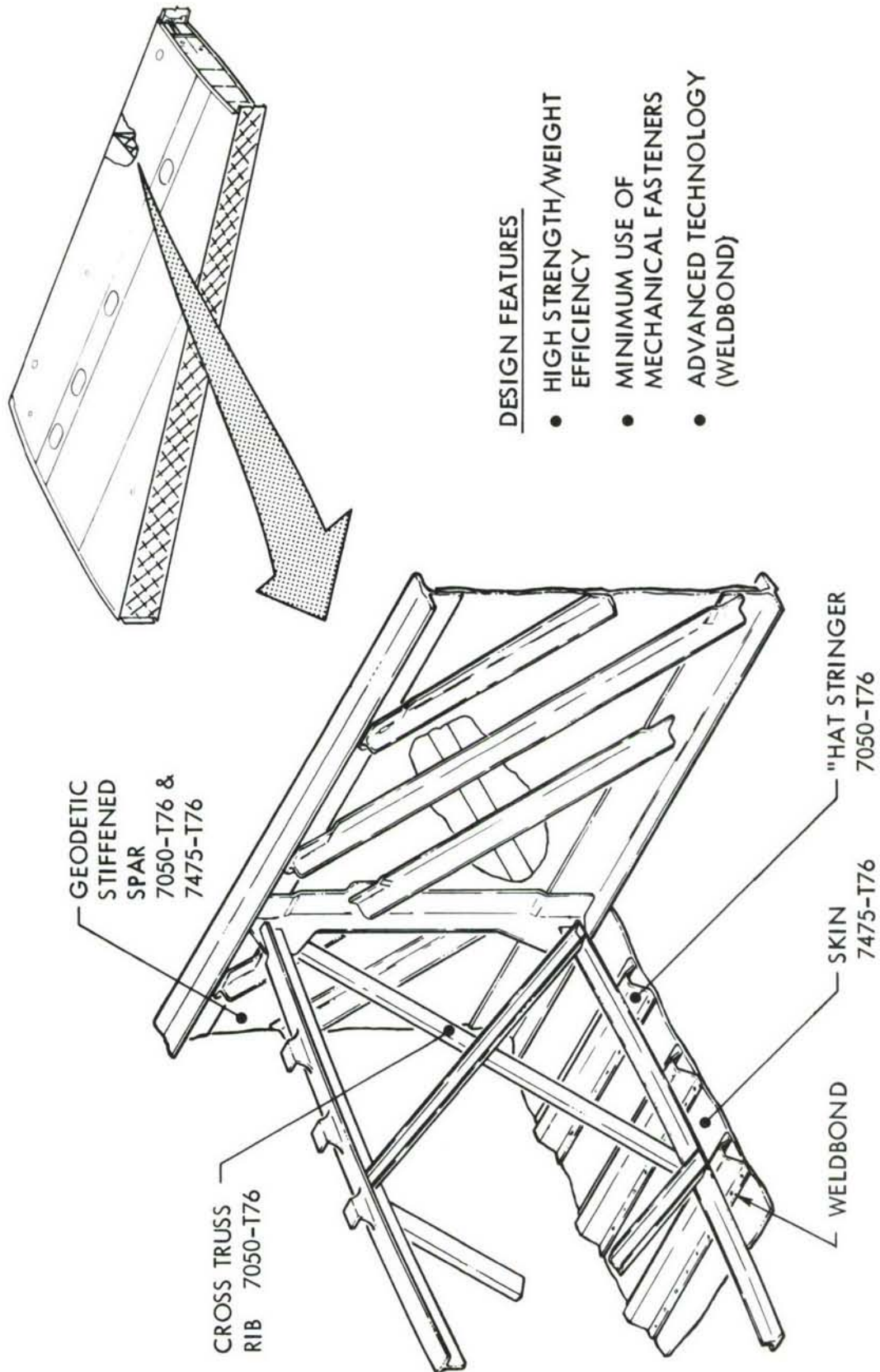
This configuration, shown in Figure 12, features conventional built-up structure fabricated from advanced aluminum alloys. The substructure for this concept includes several features presented by Douglas in the "Quick Look" program<sup>(12)</sup>: a "Cross Truss" design for ribs and a "Geodetic" stiffener arrangement for spars and bulkheads. Considerable effort was directed toward eliminating mechanical fasteners from the cover material and reducing the number of detail parts.

The hat-section stringer selected for upper and lower covers (see Figure 13) is a 7050-T76 net extrusion designed with angled sides to provide capability of transmitting modest rib-cap-to-cover shear loads. In highly loaded areas, such as flap track back-up ribs, shear clips attaching directly to the skin are required. The skin is made from 7475-T76 plate material which is machined to final dimensions. Weldbonding is again proposed as the primary joining method. Mechanical fasteners in conjunction with cold worked holes are used in areas inaccessible for spot welding equipment. With this design, weldbonding is also used for the attachment of rib cap to stringers, and this involves making a rib cap/stringer assembly prior to the attachment of the outer skin.

Each cover consists of three separate skin panels which are joined together with the bonded/clamped spanwise splice shown in Figure 14. This splice is a variation of the joint concept proposed for the Virgin Plank design (Paragraph 5.5.7) but has been adapted for use where the skin panels can be formed in the splice area.

The cross-truss rib design selected for this configuration is shown in Figure 15. The rib cap is made from a 7050-T76 extrusion and is attached directly to the skin in the local areas of high shear transfer. The braces forming the cross-truss arrangement are extruded channels of 7050-T76 material which require no machining other than cutting to length. Spar and bulkhead designs both feature "Geodetic" stiffening, an arrangement in which stiffeners oriented at 45° to the vertical axis are mounted on both sides of the web.

Although this configuration scored high in the merit rating table, it was eliminated primarily because of an estimated cost increase of 10% over baseline and because of potential corrosion problems associated with the interior regions of the hat-section stringer.



#### DESIGN FEATURES

- HIGH STRENGTH/WEIGHT EFFICIENCY
- MINIMUM USE OF MECHANICAL FASTENERS
- ADVANCED TECHNOLOGY (WELDBOND)

FIGURE 12 HAT STRINGER CONFIGURATION

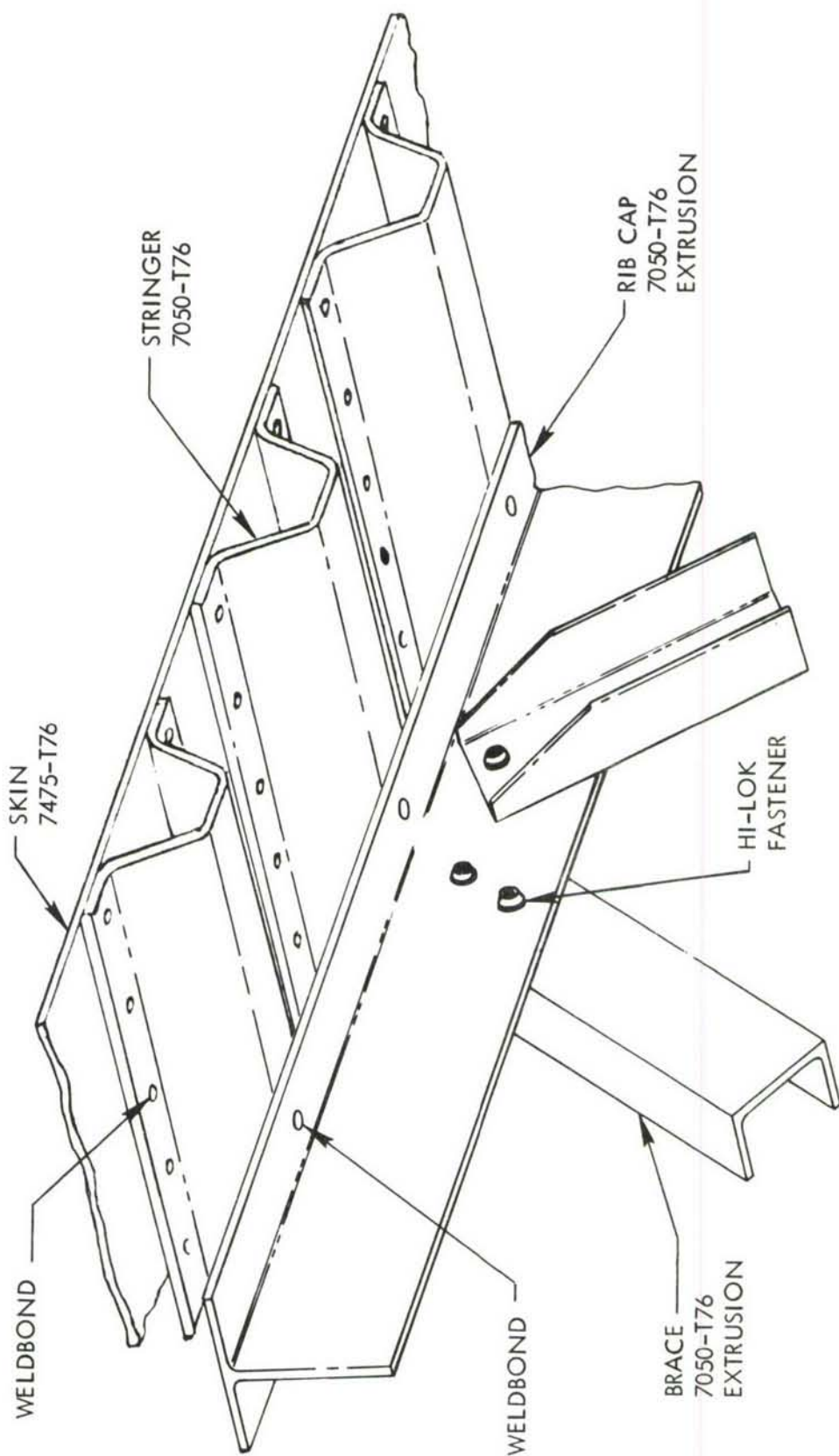


FIGURE 13 RIB TO COVER ATTACHMENT - HAT STRINGER CONFIGURATION

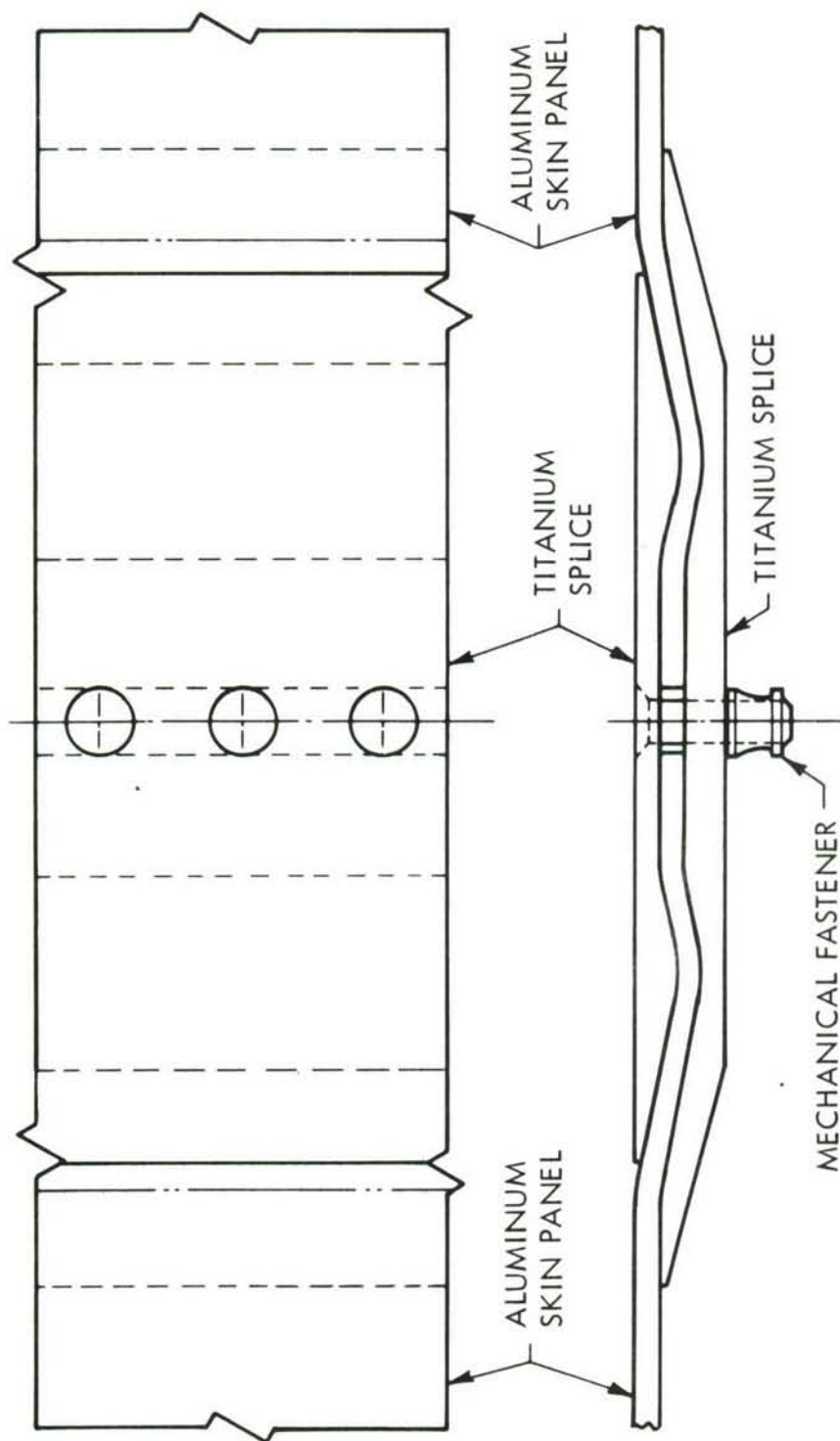


FIGURE 14 BONDED SPANWISE SPLICE (FORMED)



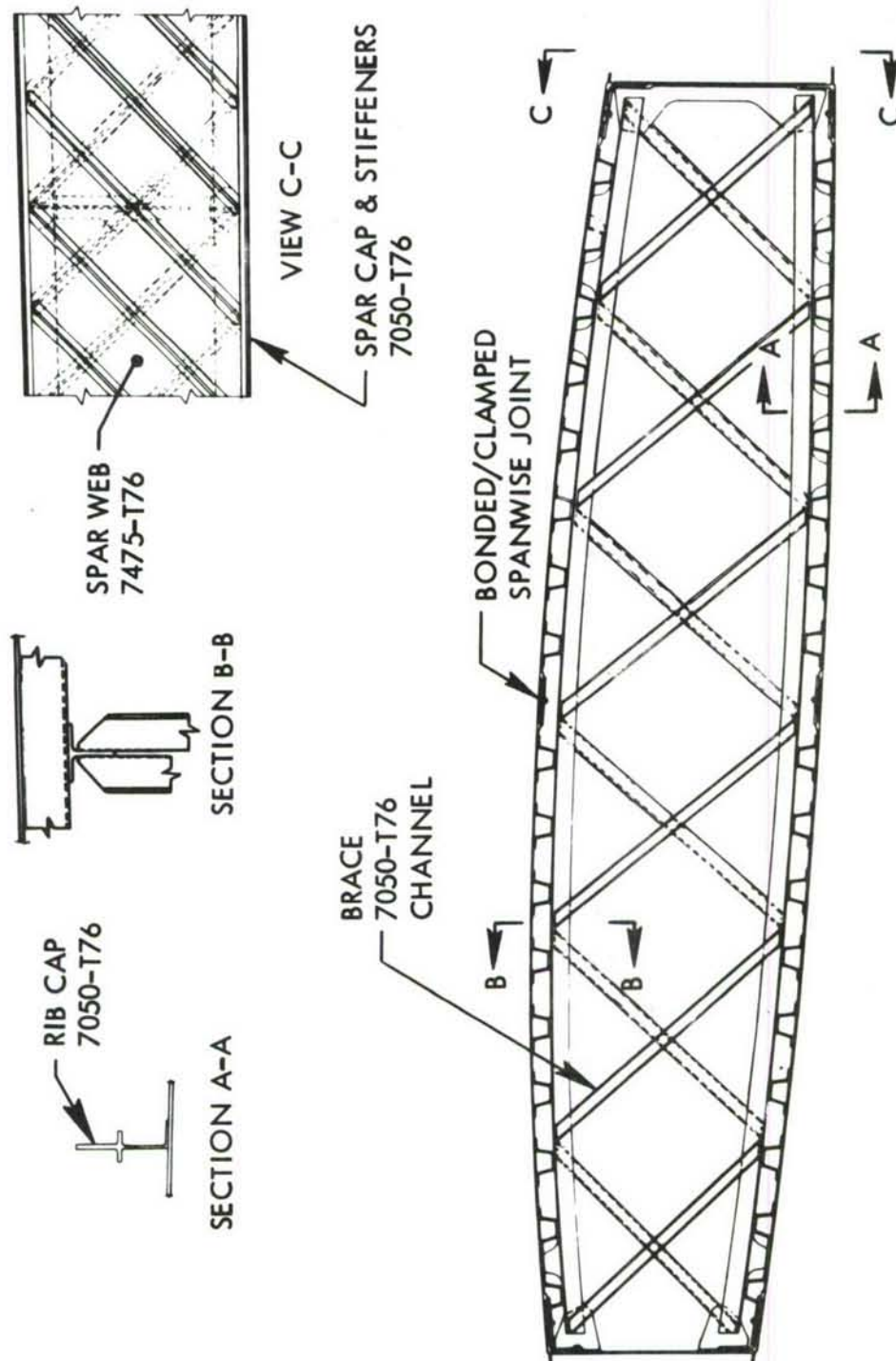


FIGURE 15 SUBSTRUCTURE - HAT STRINGER CONFIGURATION

### 5.5.3 Lockskin Configuration

This configuration is an advanced-technology design featuring a "Lockskin" cover (titanium face sheets sandwiching a graphite core) stiffened by Z-section titanium stringers as shown in Figure 16. A "Sine Wave" spar web was selected for this configuration, with titanium used to make the spar material compatible with the covers. The remaining substructure is fabricated from advanced aluminum alloys selectively reinforced with composites.

This design offers a number of highly desirable features which include the fail-safe capability of a laminated assembly, good fatigue resistance as a result of the composite interlayer, and a high strength-to-weight efficiency.

As with the Weldbond and Hat Stringer configurations, a primary objective in developing this design was to eliminate fasteners from the cover material. To achieve this, a combination of weldbonding and adhesive bonding was used (see Figure 17). In the first assembly stage, titanium (6-2-2-2-2) stringers and shear clips are weldbonded to the inner skin to form an inner skin assembly. The second stage involves the adhesive bonding of this assembly to the graphite core and outer skins. Weldbonding is proposed as the joining system for spanwise splices. Three splices are required due to the width limitations for available titanium sheet.

Rib and bulkhead designs are of the web/stiffener type and are fabricated from 7475-T76 aluminum sheet and 7050-T76 extrusions. Boron-epoxy is planned for use in reinforcing various substructure components such as rib caps and stiffeners wherever a significant improvement in strength-to-weight efficiency is realized. Figure 18 shows a typical rib design, configured with elliptical lightening holes which also provide bay-to-bay access within the wing box integral fuel tank. This design produced the highest score from an advanced-technology aspect, but a predicted cost of 82% over baseline caused it to be eliminated from further consideration.

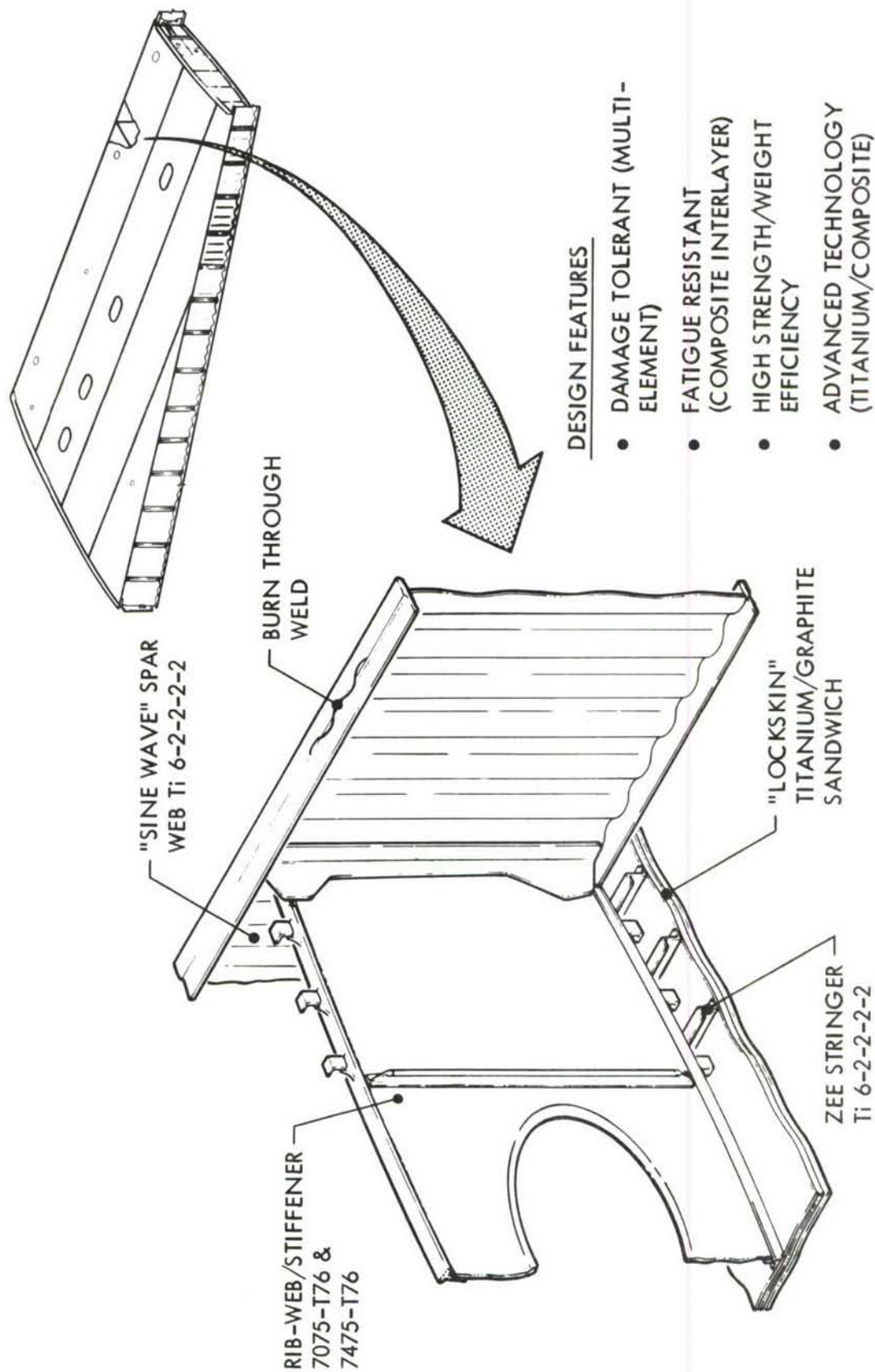


FIGURE 16 LOCKSKIN CONFIGURATION

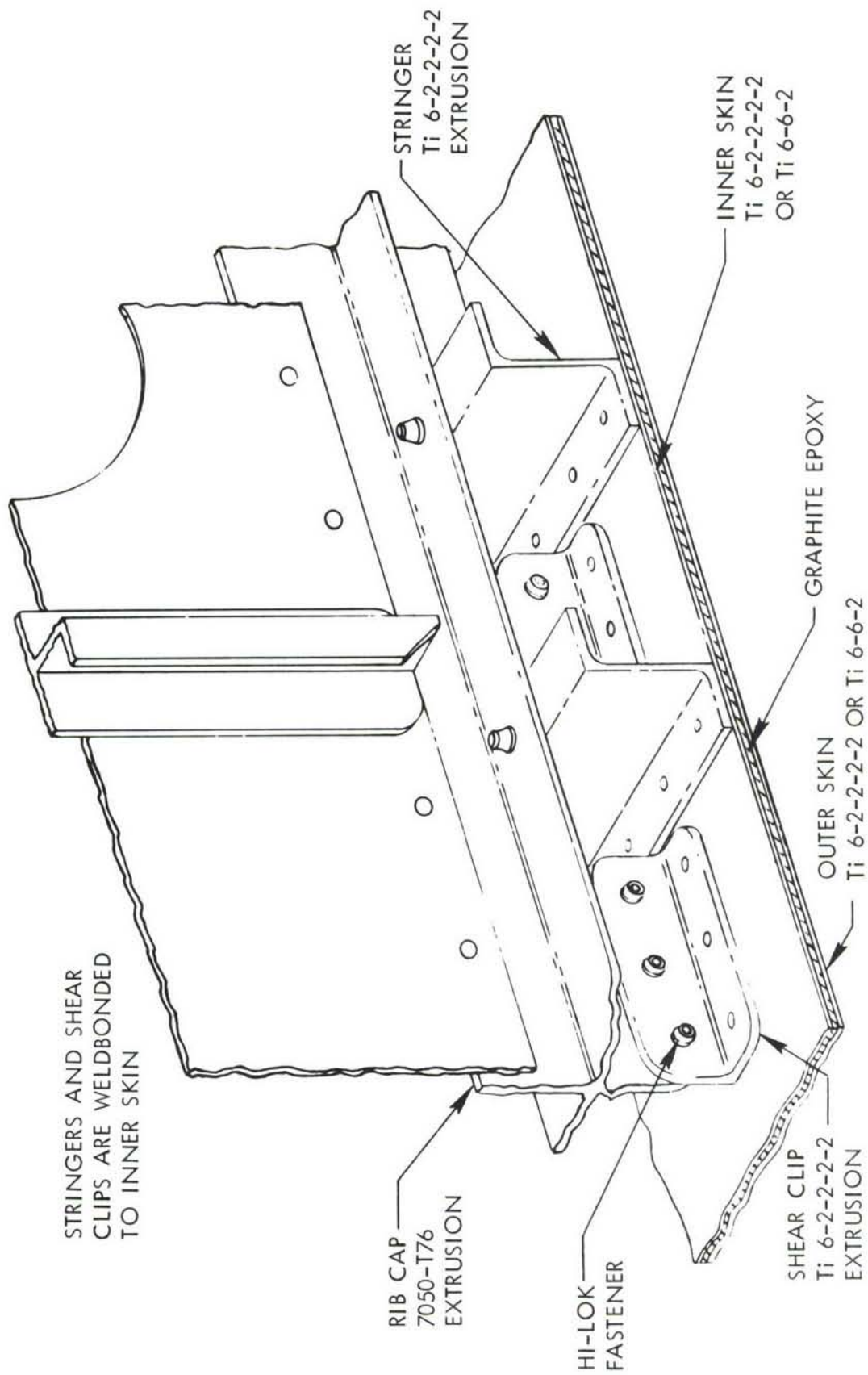


FIGURE 17 RIB TO COVER ATTACHMENT - LOCKSKIN



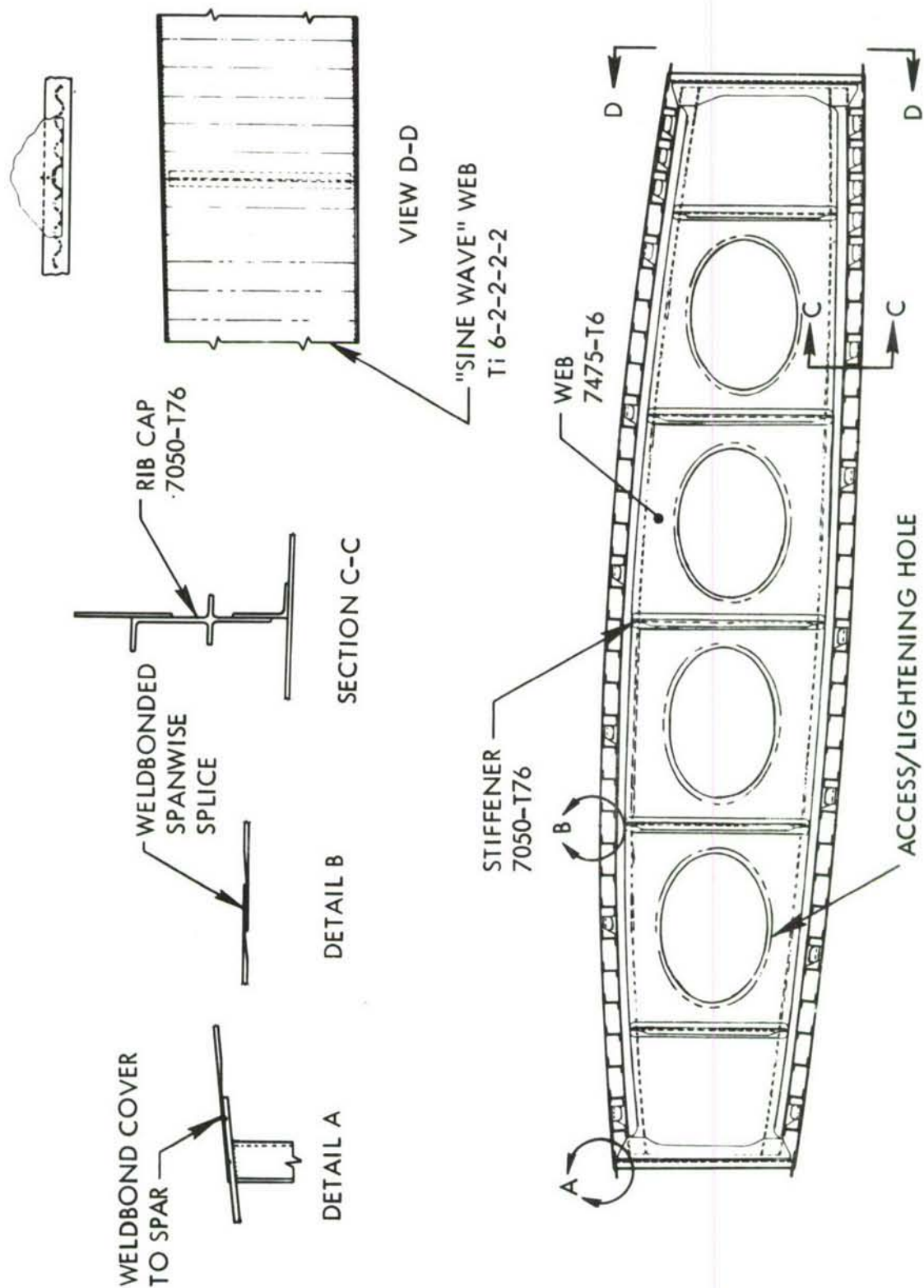


FIGURE 18 SUBSTRUCTURE - LOCKSKIN CONFIGURATION

#### 5.5.4 Monolithic Configuration

In this configuration, a monolithic approach was adopted for all major components with emphasis on integrally stiffened extrusions, one-piece forgings, and large welded-up assemblies as shown in Figure 19. Several aluminum alloys including 2021-T81 were considered for welded assemblies with 2219-T87 being finally selected because of its superior fracture toughness properties.

Upper and lower covers are fabricated from 2219-T87 integrally stiffened extrusions (approximately 23 inches wide) and fusion welded together at the spanwise joints. Rib caps are also 2219-T87 extrusions and, after being formed to contour, are welded to the covers using an electron beam burn through weld technique (see Figure 20). This method of assembly completely eliminates the need for mechanical fasteners through the cover material and greatly reduces the number of detail parts. Another advantage of this form of construction is that skin thicknesses may be increased locally around cutouts and splice areas, thereby eliminating doublers and minimizing stress concentrations.

A typical rib, as shown in Figure 21, features a conventional truss rib arrangement where H-section extruded 7050-T76 braces are attached to the rib caps with mechanical fasteners. The spar design is a welded assembly consisting of an integrally stiffened web welded to the spar cap using a burn-through weld process. An alternative spar design also considered for this configuration was a one-piece forging.

It was recognized that considerable manufacturing development would be required to provide a reliable welded joint for rib cap to cover attachment; therefore, an alternative method of rib cap attachment was devised (see Figure 22). This type of attachment clip provides a positive attachment for rib cap to cover that eliminates the need for fastener holes through the cover material. This is accomplished by wedging the clips between vertical stiffeners and machined knobs in the skin panel and attaching them to the rib cap with mechanical fasteners.

Although attractive from a cost standpoint, further development of this configuration was not pursued due to the large number of development problems associated with the design. Also, a total weight in excess of the baseline was predicted.

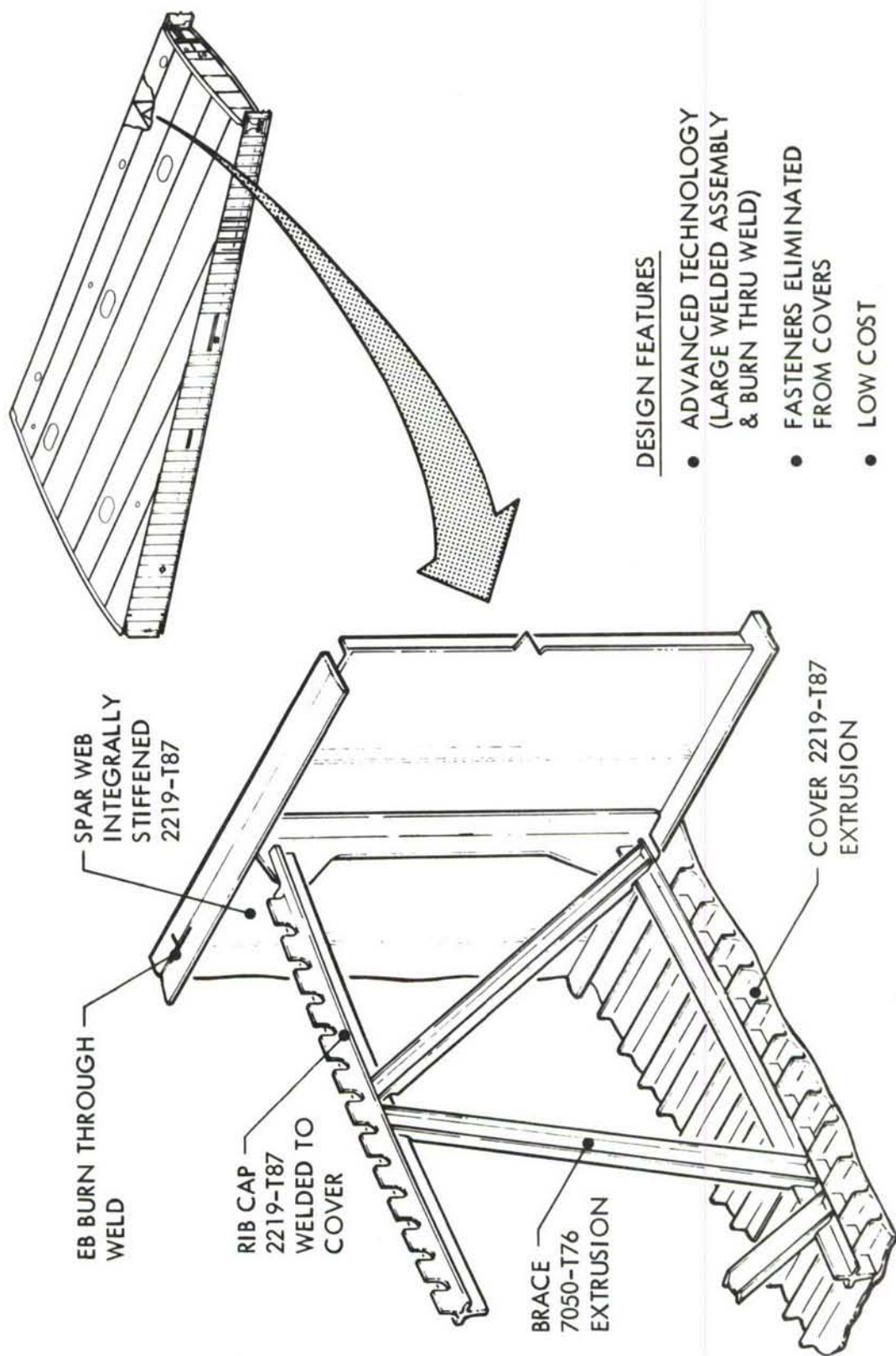


FIGURE 19 MONOLITHIC CONFIGURATION



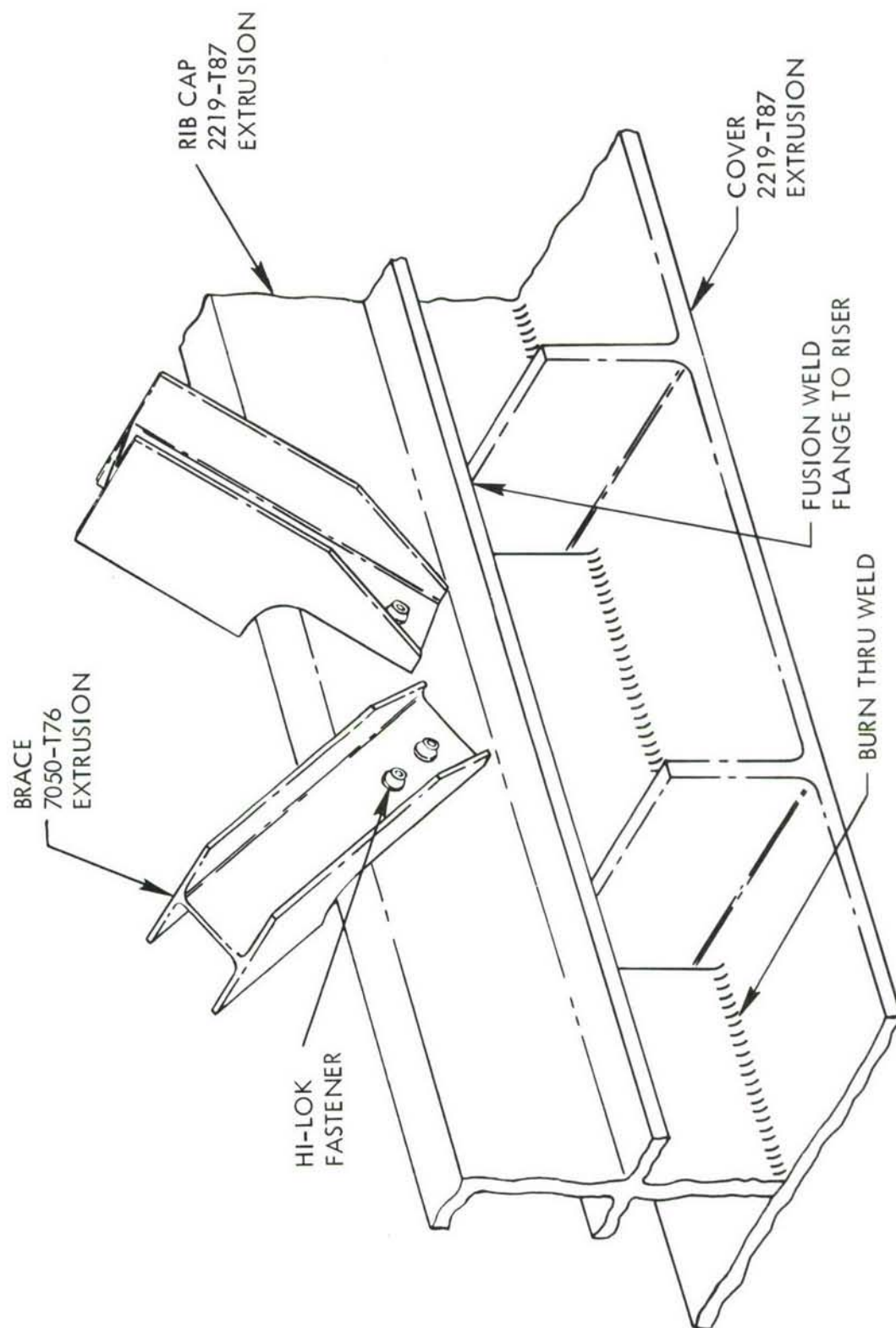


FIGURE 20 RIB TO COVER ATTACHMENT - MONOLITHIC CONFIGURATION



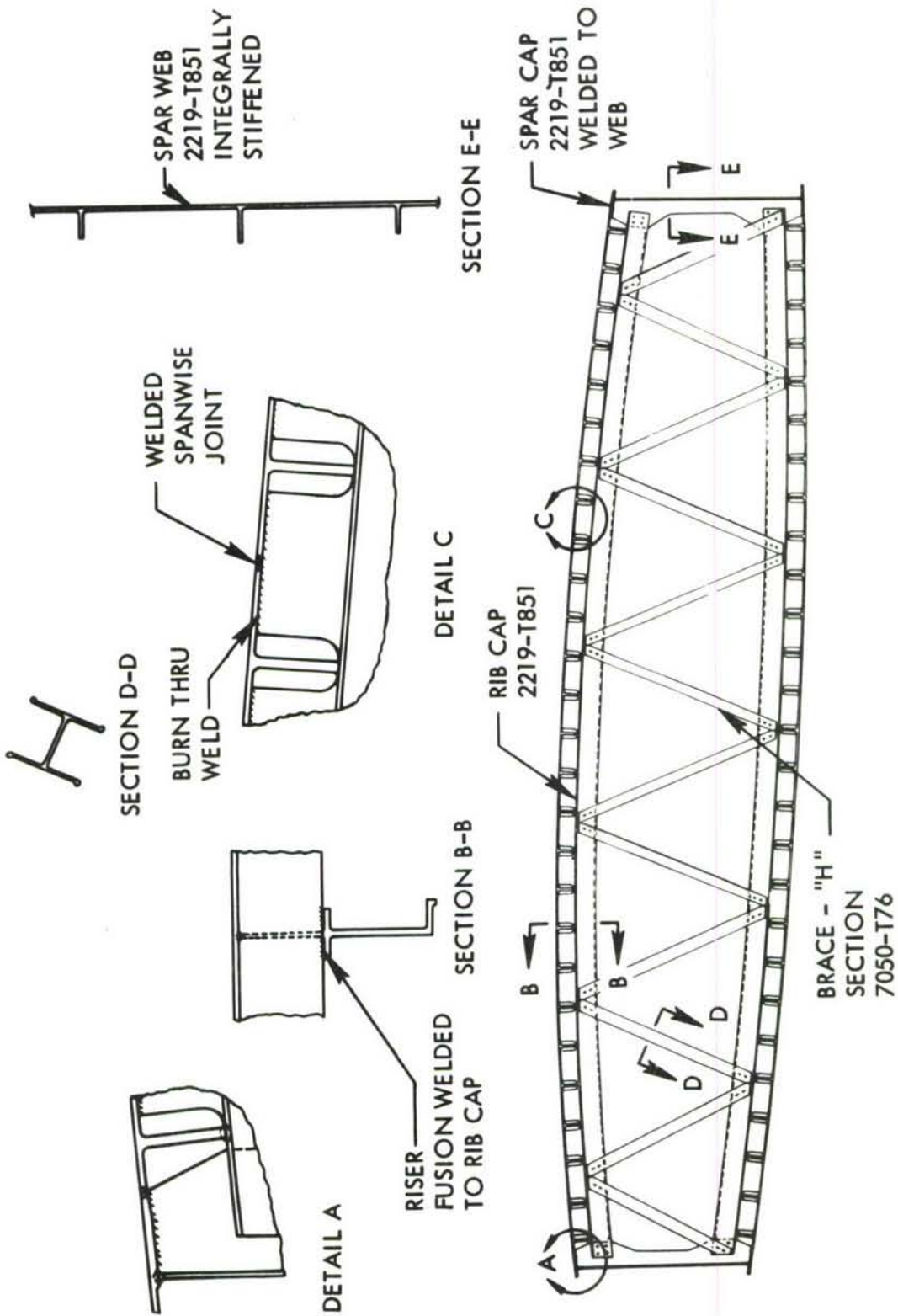


FIGURE 21 SUBSTRUCTURE - MONOLITHIC CONFIGURATION

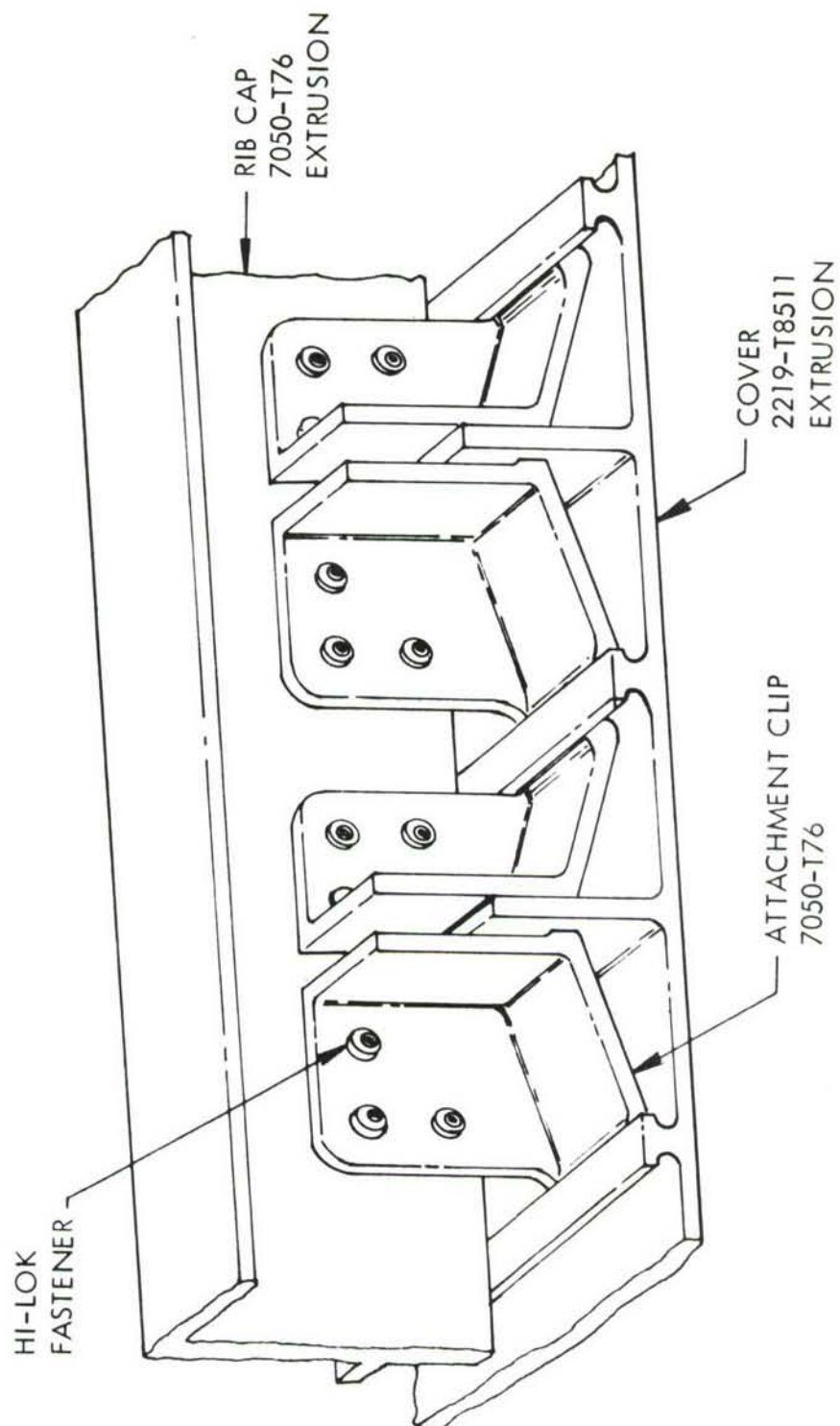


FIGURE 22 COVER DESIGN - NON-PENETRATING CLIP

#### 5.5.5 Sandwich Configuration

This configuration, shown in Figure 23, utilizes honeycomb sandwich structure for all major components with the exception of ribs. The upper and lower covers are titanium designs, and both adhesive bonding and brazing were considered as a means of assembly. Spars and bulkheads are also honeycomb construction, but here the primary material is aluminum. With this design, spanwise joints are located on a percentage chord line and panel runouts at the front beam are eliminated. A feature of the cover design is the use of A-section stringers which serve the dual purpose of spanwise splice plates and attachment members for the truss rib arrangement as illustrated in Figure 24. These stringers are fabricated from titanium 6-2-2-2-2 extrusions and are located at chord increments of approximately 10%. Mechanical fasteners in cold worked holes are used in the two spanwise splice locations on both upper and lower surfaces, and also for the attachment of covers to spar caps. It will be noted that, with this design, rib caps are eliminated, although it is recognized that some chordwise reinforcing at rib locations is required. Spar and bulkhead designs for this configuration are of conventional honeycomb construction and are 7050-T76 and 7475-T76 materials throughout with the exception of spar caps which are titanium 6-2-2-2-2 to match the covers (see Figure 25). The diagonals forming the truss ribs are aluminum 7050-T76 H-section extrusions and attach to the A-stringers with mechanical fasteners.

This configuration was originally conceived as a minimum weight design, but the inclusion of non-optimum factors for honeycomb sandwich constructions resulted in a weight penalty of 10% over baseline. Other factors, including high cost, poor repairability and predictability, made this the lowest scoring design of the eight configurations evaluated.

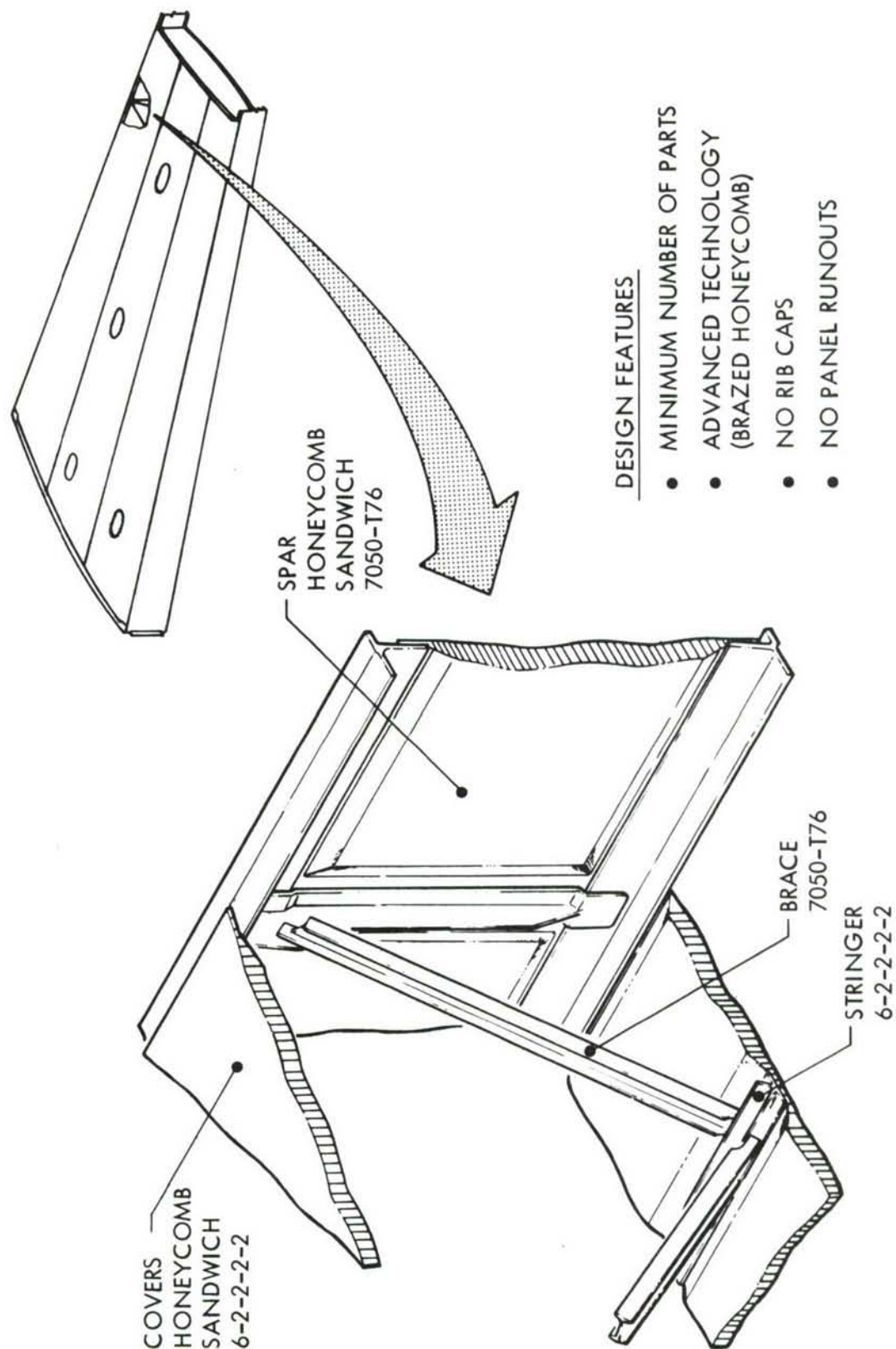


FIGURE 23 SANDWICH CONFIGURATION



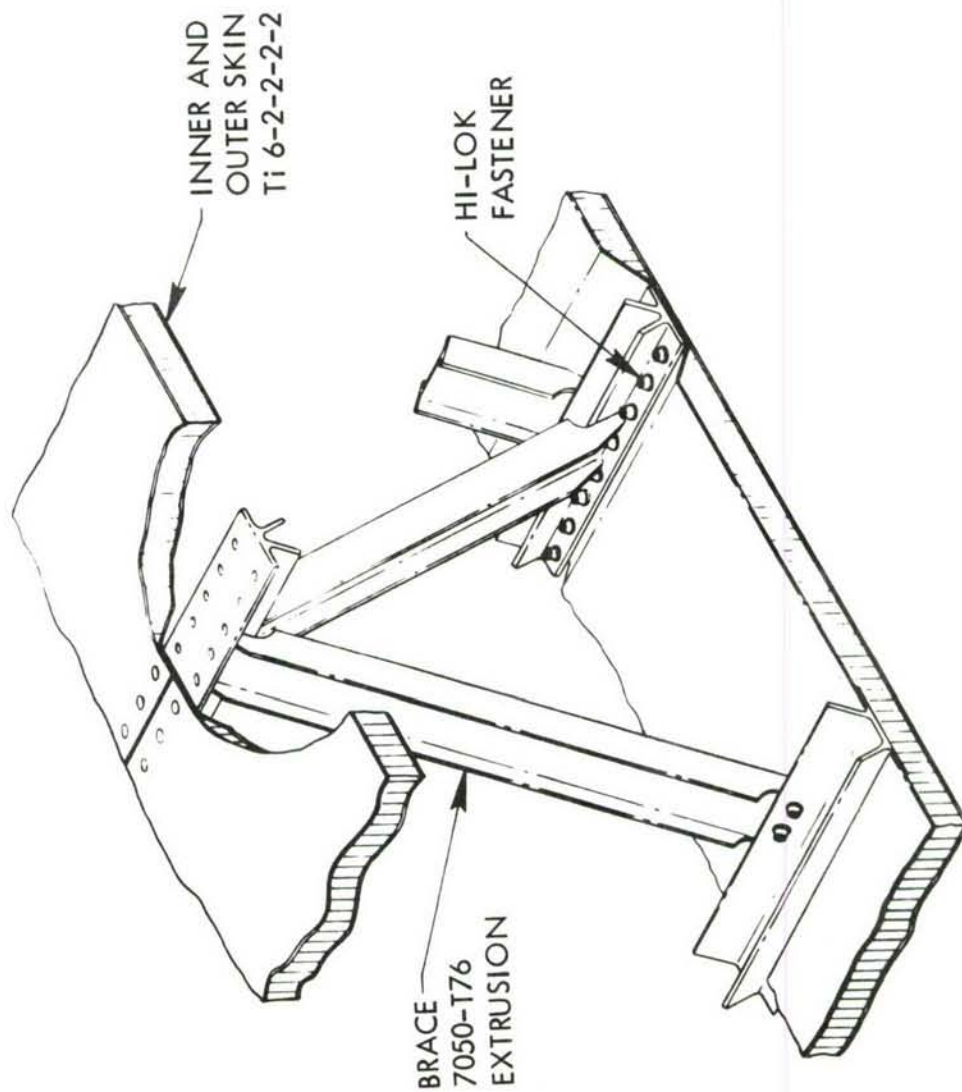


FIGURE 24 RIB TO COVER ATTACHMENT - SANDWICH CONFIGURATION

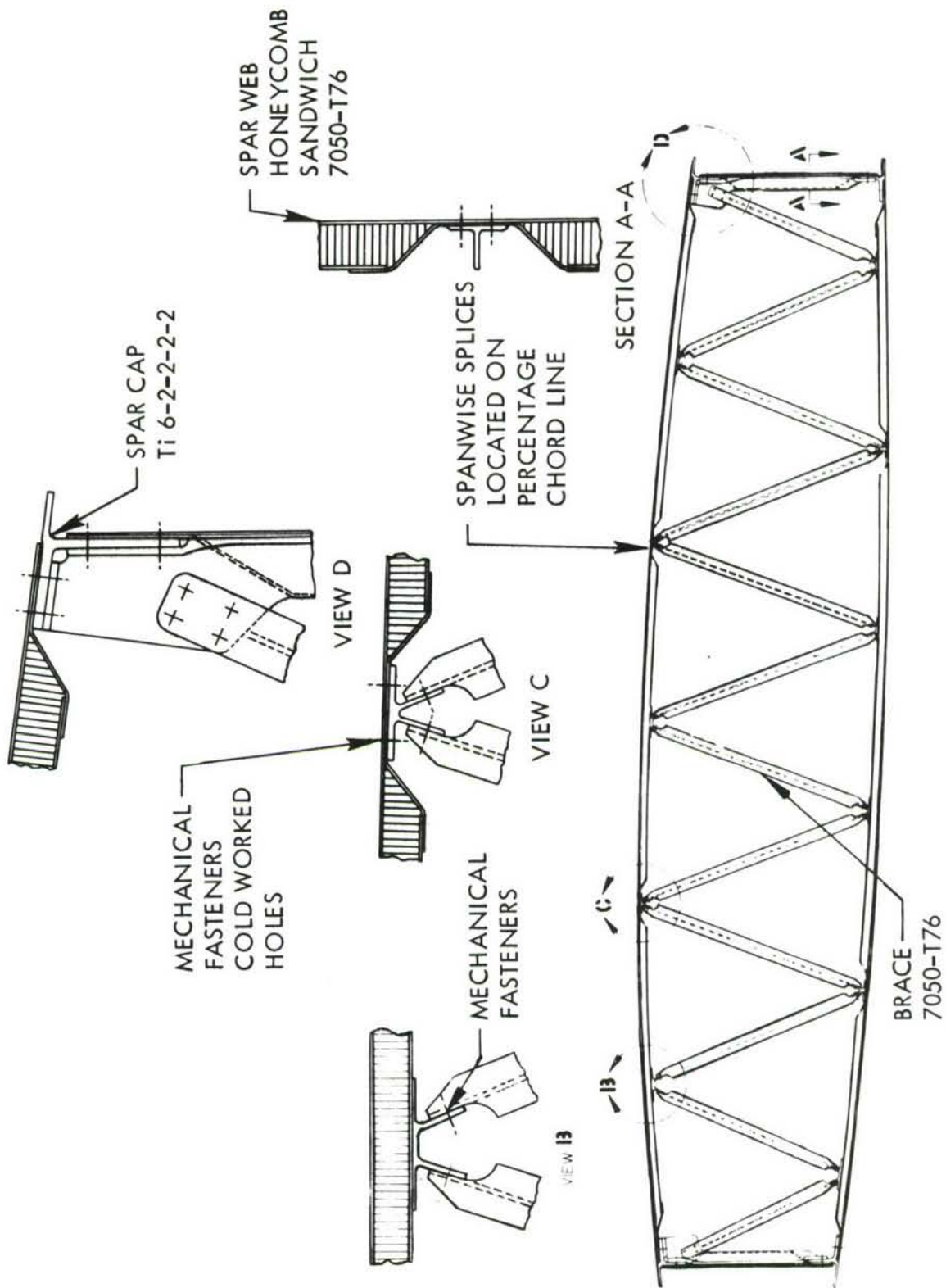


FIGURE 25 SUBSTRUCTURE - SANDWICH CONFIGURATION

#### 5.5.6 Composite Hat Configuration

In this design concept, extensive use is made of composite reinforced metals as shown in Figure 26. Cover designs utilize graphite-epoxy stringers to reinforce titanium skin panels, and the aluminum substructure is selectively reinforced with boron-epoxy laminates.

Figure 27 shows a graphite-epoxy hat-section stringer bonded to a titanium 6-2-2-2-2 skin. Several factors influenced the selection of this combination of materials including compatible coefficients of expansion, reduced cost and weight of graphite compared with boron, and the absence of the corrosion potential that exists with graphite/aluminum assemblies. Upper and lower cover assemblies consist of four separate panels, and the spanwise splices are adhesive bonded butt and splice joints. This form of bonded construction eliminates the need for mechanical fasteners and provides excellent fatigue resistance. Weldbonding is used to attach rib cap shear clips and also for the attachment of covers to spar caps.

The rib design for this configuration, shown in Figure 28, consists of vertical posts designed to withstand crushing and normal loads and a cross strap arrangement to transmit shear. Rib caps are back-to-back channels, and these and all other rib components are made from 7050-T76 aluminum extrusions. Bulkheads and spars are of web/stiffener design and are fabricated from 7475-T76 and 7050-T76 materials selectively reinforced with boron-epoxy.

As with the Lockskin design described previously, the use of titanium and composites imposes a substantial cost penalty on this configuration. A modest weight saving was projected, but the overall design offered little in the way of other attributes and was therefore discontinued.

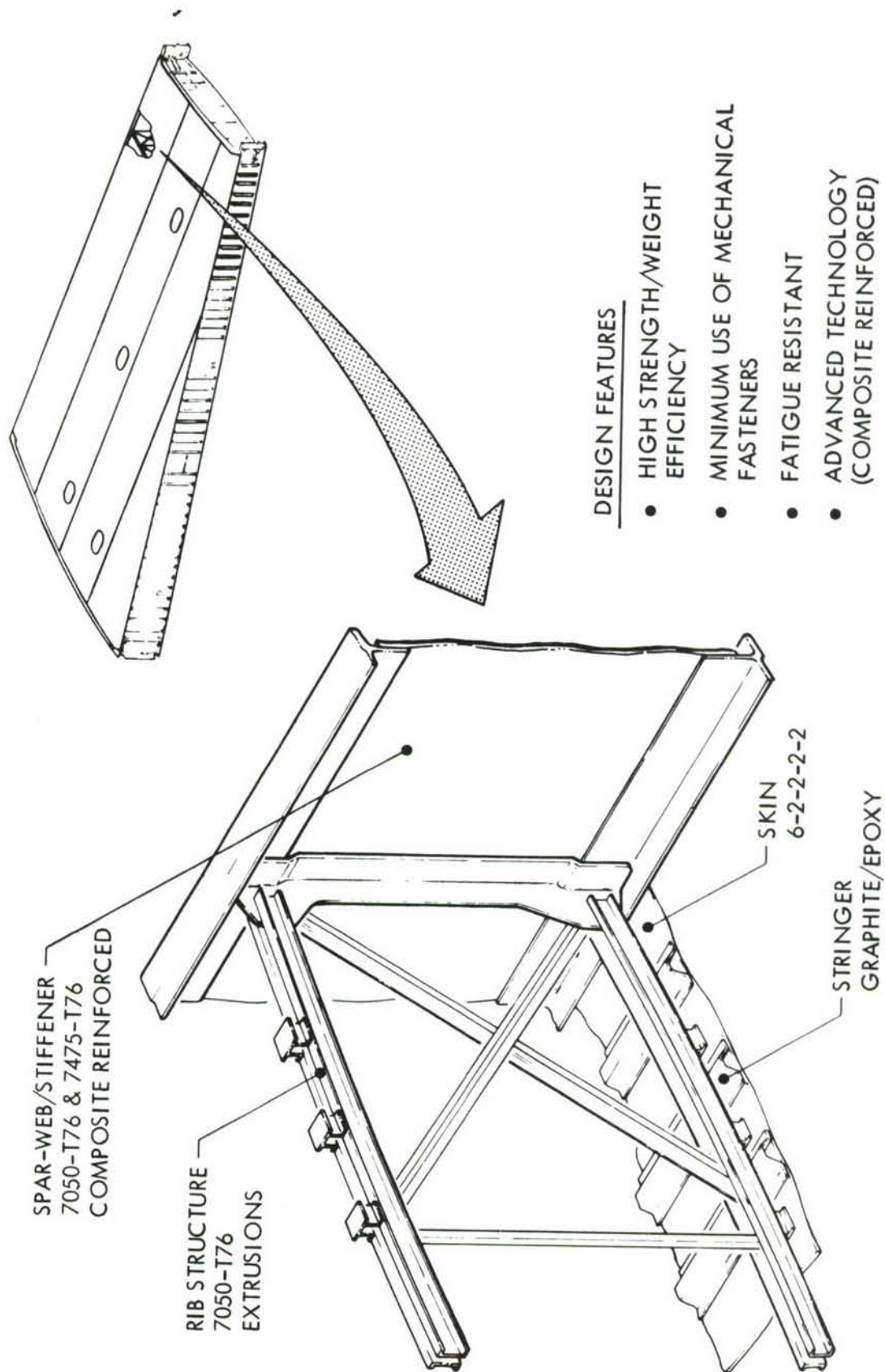


FIGURE 26 COMPOSITE HAT CONFIGURATION



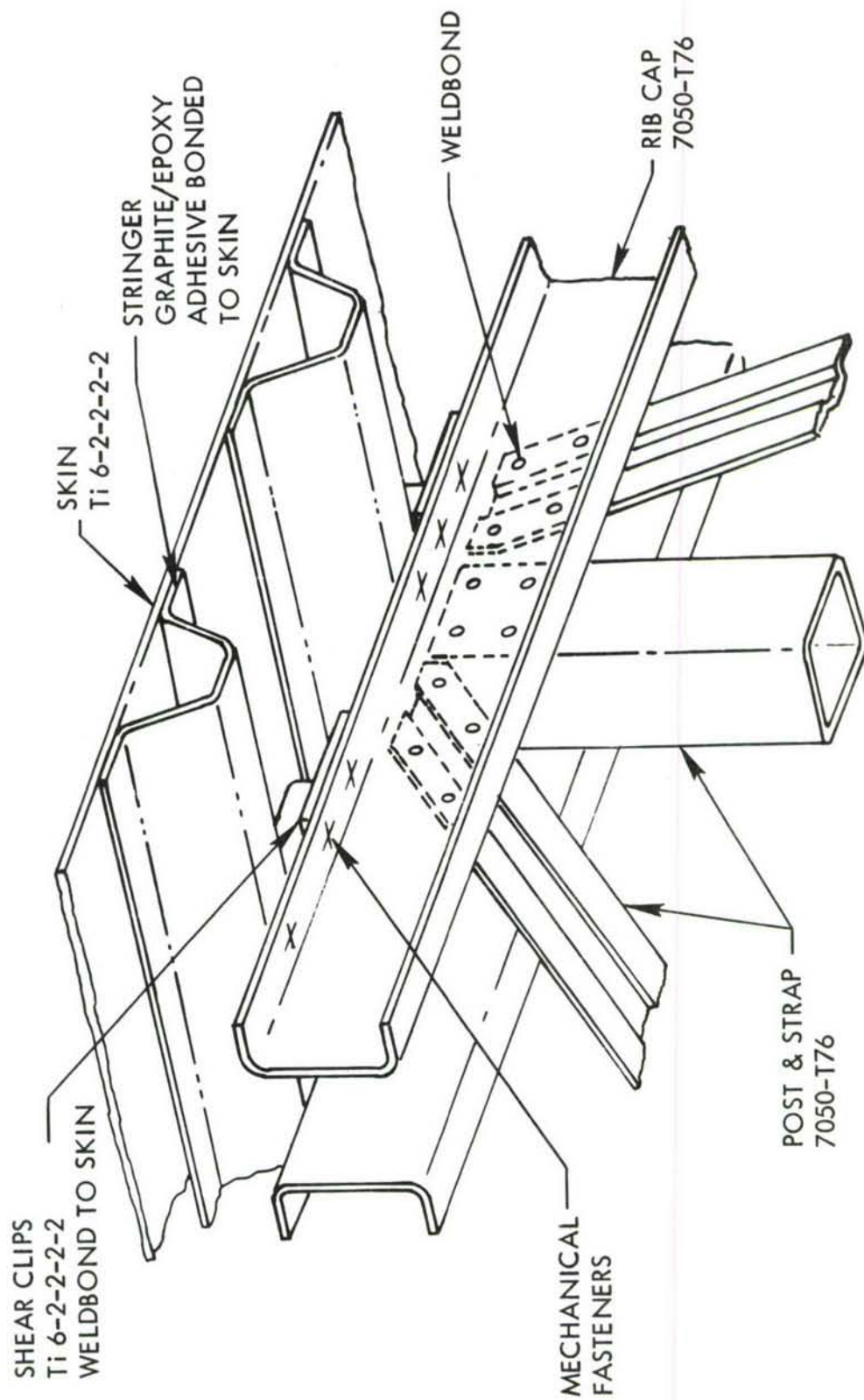


FIGURE 27 RIB TO COVER ATTACHMENT - COMPOSITE HAT CONFIGURATION

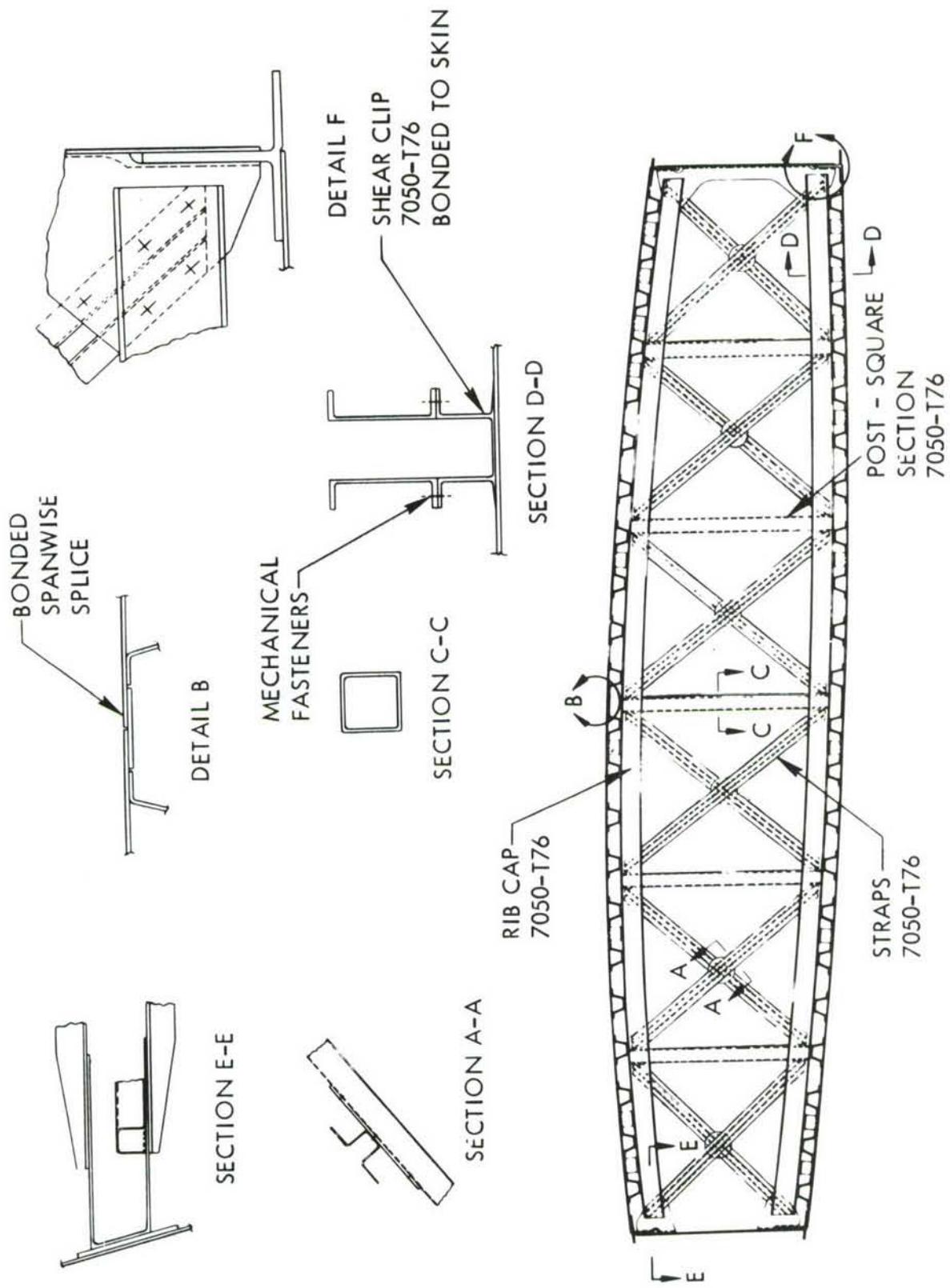


FIGURE 28 SUBSTRUCTURE - COMPOSITE HAT CONFIGURATION

### 5.5.7 Virgin Plank Configuration

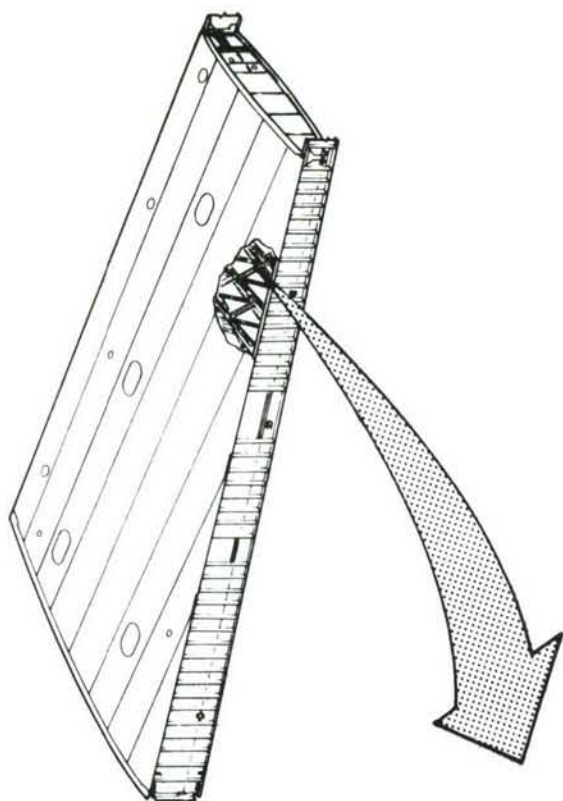
The cover design for this configuration, illustrated in Figure 29, is similar to that of the baseline except that advanced aluminum alloy 7050-T76 is utilized and conventional fastener systems for spanwise joints and rib attachment are eliminated. The 'tee' riser arrangement produces an efficient cover design, and also provides a retaining flange for the non-penetrating clamped rib attachment clip shown in Figure 30. This clip is an outgrowth of the design shown for the Monolithic configuration, but it is considerably lighter and cheaper. Its design also permits a simpler machined skin panel configuration. Individual skin panels are approximately 27 inches wide and are joined together with the bonded/clamped spanwise splice shown in Figure 31. This novel splice concept uses adhesive bonding for primary load transfer with a clamping device capable of withstanding limit loads as a secondary load path in the event of a bond failure. Mechanical fasteners which penetrate only the splice plates run the entire length of the joint. They provide the clamping force required in the event of a bond failure and also apply pressure to the joint during the curing operation. The wave pattern groove in the skin, when mated with a matched land on the splice plate, allows the transfer of shear along the joint, even with a disbanded condition. Thus, a fully mechanical fail-safe feature is provided by this design.

A one-piece spar forging made from 7050-T76 material is used for front and rear spars (see Figure 32). It will be noted that with this configuration the fasteners normally required to join the web to caps and stiffeners are eliminated, producing a significant improvement in fatigue life. Current cost estimates for this forging show it to be somewhat costlier than built-up structure, but the improved fatigue performance and weight savings justify its consideration.

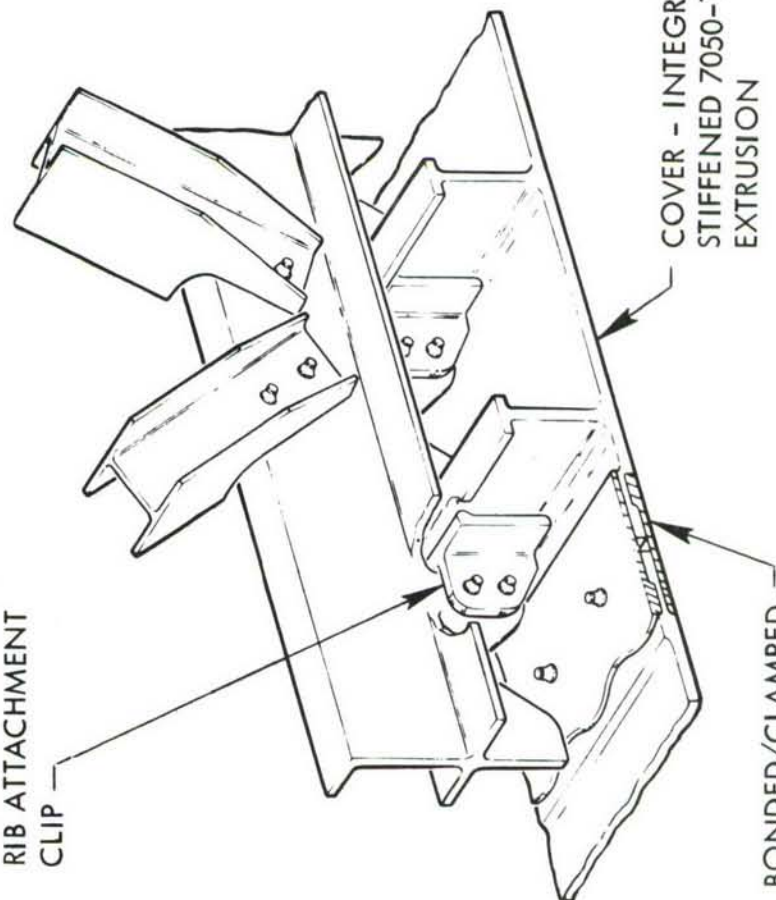
A typical rib, shown in Figure 33, features an 'H' section brace attached to the rib caps with Hilok fasteners. Rib caps and braces are fabricated from 7050-T76 extrusions.

This configuration resulted in a high merit rating score with estimated weight savings of 6.8% and cost savings of 16%. It is recommended for further development in the follow-on phases.





NONPENETRATING  
RIB ATTACHMENT  
CLIP



COVER - INTEGRALLY  
STIFFENED 7050-T76  
EXTRUSION

BONDED/CLAMPED  
SPANWISE SPLICE

## DESIGN FEATURES

- HIGH STRENGTH/WEIGHT EFFICIENCY
- MINIMUM USE OF MECHANICAL FASTENERS
- NONPENETRATING CLIPS
- BONDED/CLAMPED SPLICES
- ONE PIECE FORGED SPARS

FIGURE 29 VIRGIN PLANK CONFIGURATION



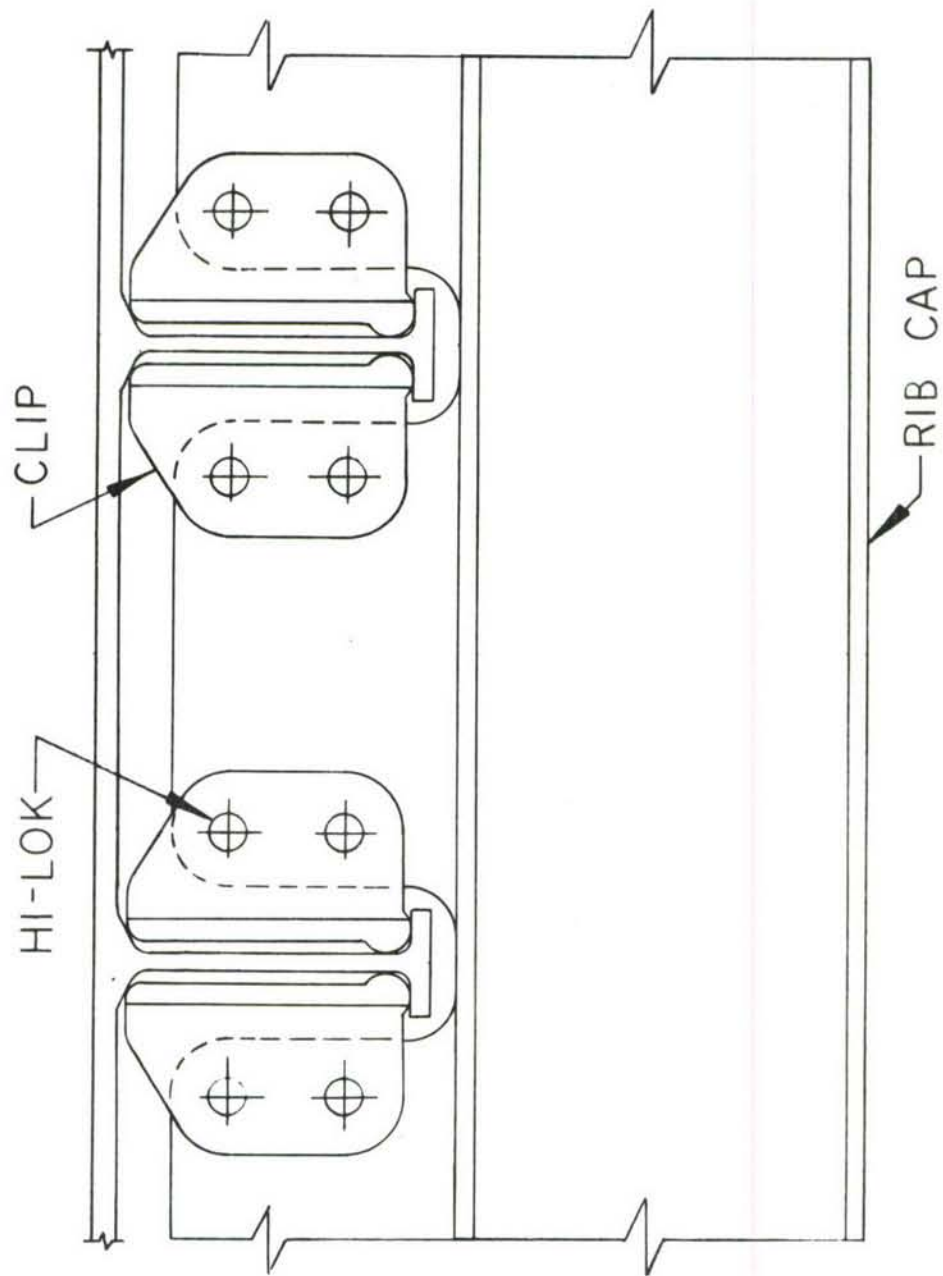


FIGURE 30 NONPENETRATING CLIP

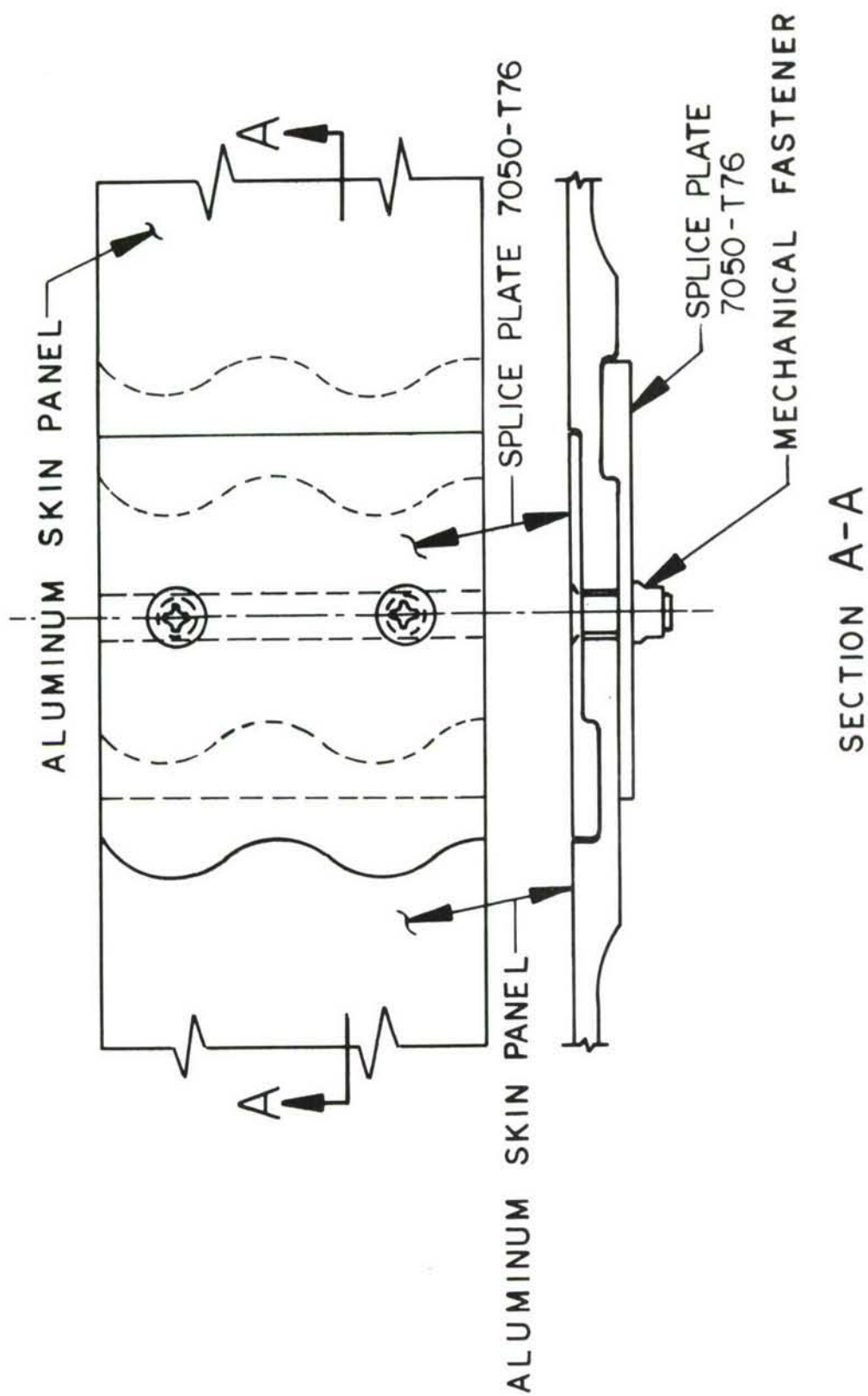


FIGURE 31 BONDED/CLAMPED SPANWISE SPLICE

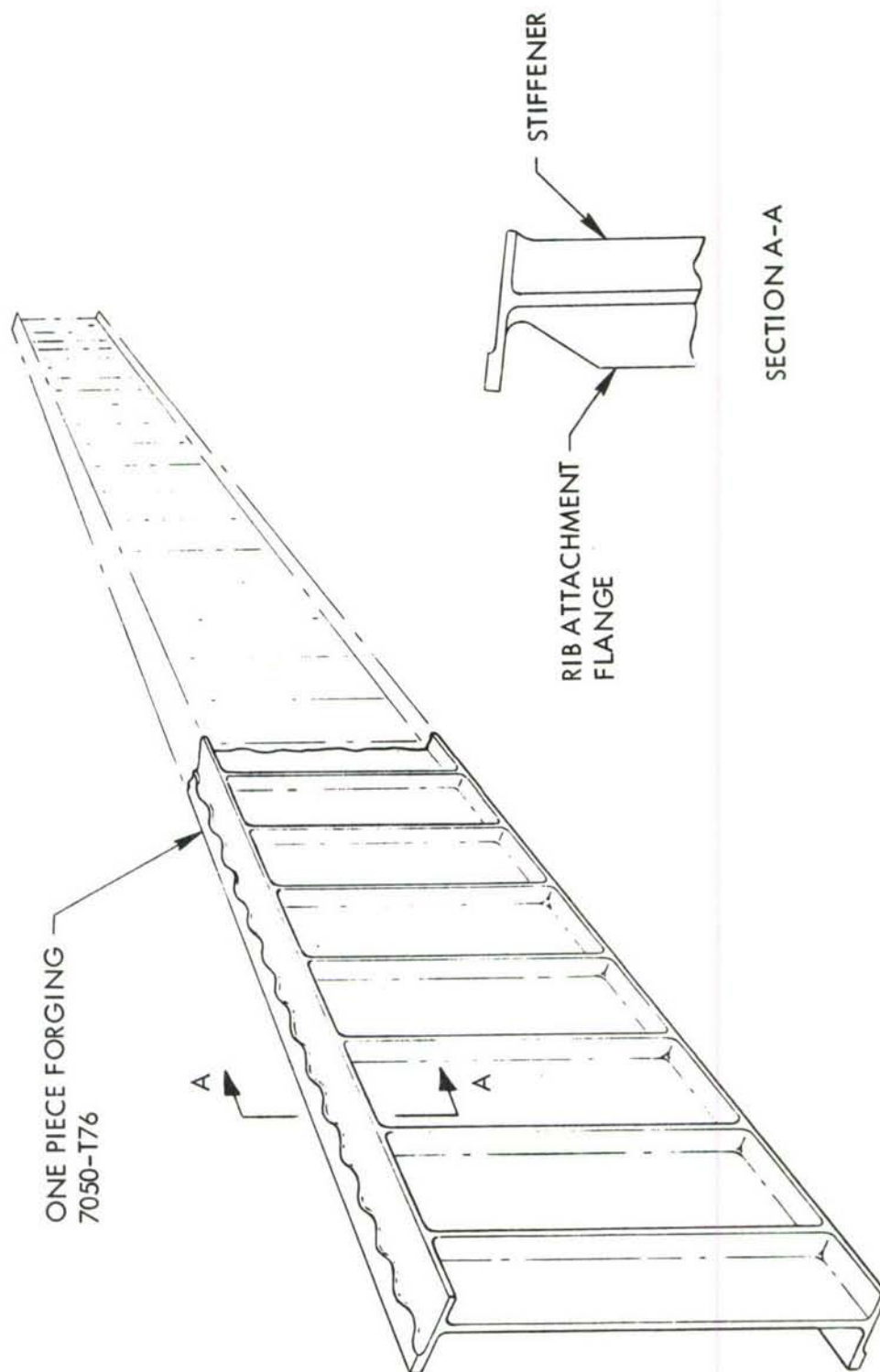


FIGURE 32 SPAR - VIRGIN PLANK CONFIGURATION

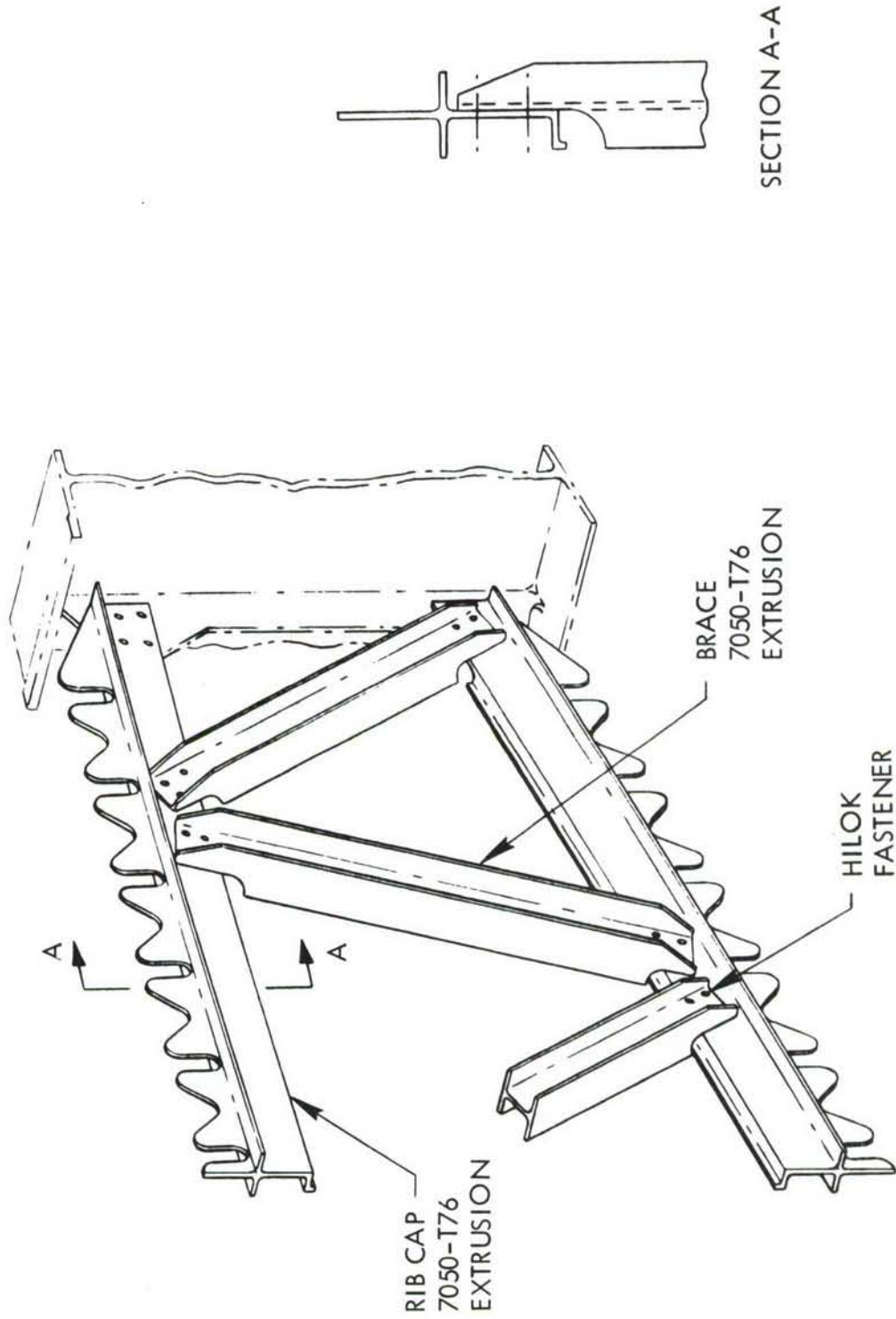


FIGURE 33 TYPICAL RIB - VIRGIN PLANK CONFIGURATION



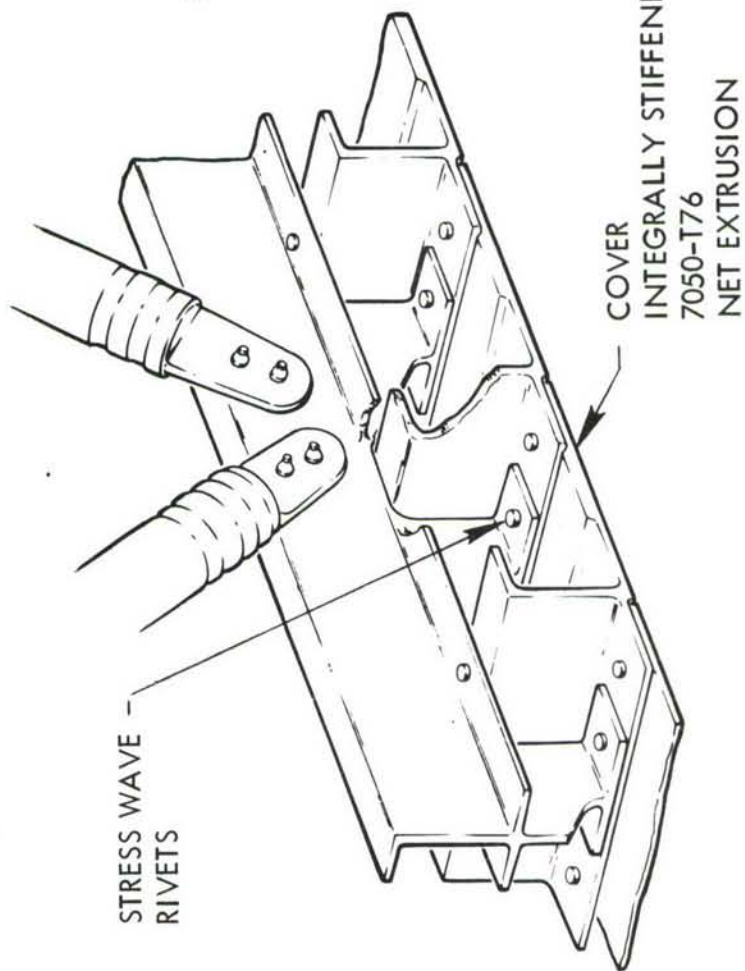
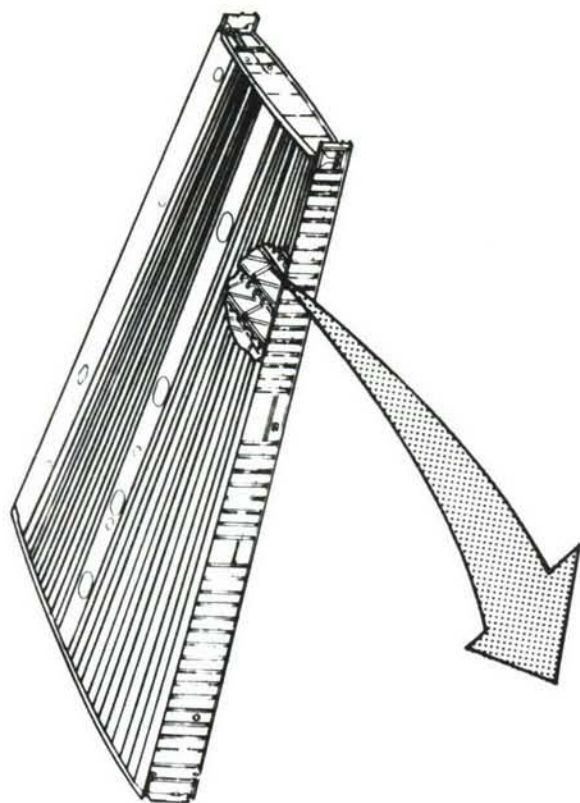
### 5.5.8 Tapered Shingle Configuration

Several unique features are incorporated into the cover design for this configuration to eliminate some of the problems usually associated with an integrally stiffened design. Individual skin panels are 7050-T76 extrusions with a single L-shaped riser as shown in Figure 34. This arrangement allows spanwise tapering of the panels in such a manner that panel runouts at the front beam are eliminated. Two constant width panels, Figure 35, are retained on the upper surface to accommodate the large cutouts required for tank access and fuel pump installation. All other panels are net extrusions and are formed at the inboard and outboard ends to suit the chordwise splice arrangement. The use of net extrusions results in a substantial cost savings, both in the cost of raw material and the elimination of expensive machining operations. The fastener system proposed for this configuration is the Grumman stress wave rivet. This system lends itself more readily to automation than other more sophisticated mechanical fastener systems primarily because elaborate hole preparation is unnecessary. Also, the hole filling property of this fastener results in a reliable interference fit which in turn provides substantial fatigue improvement.

Front and rear spars are of conventional build-up structure and are fabricated from 7050-T76 and 7475-T76 material (see Figure 36). Stress wave rivets are utilized in fatigue critical areas, such as spar cap to web, and conventional aluminum rivets are used in all other locations.

Figure 37 shows the conventional truss rib arrangement proposed for this configuration. The rib cap is made from a 7050-T76 extrusion and is attached directly to the skin by picking up fasteners in the spanwise splice. The braces are fabricated from circular tubes and are attached to the impact-extruded end fittings by a combination of swaging and capillary action bonding.

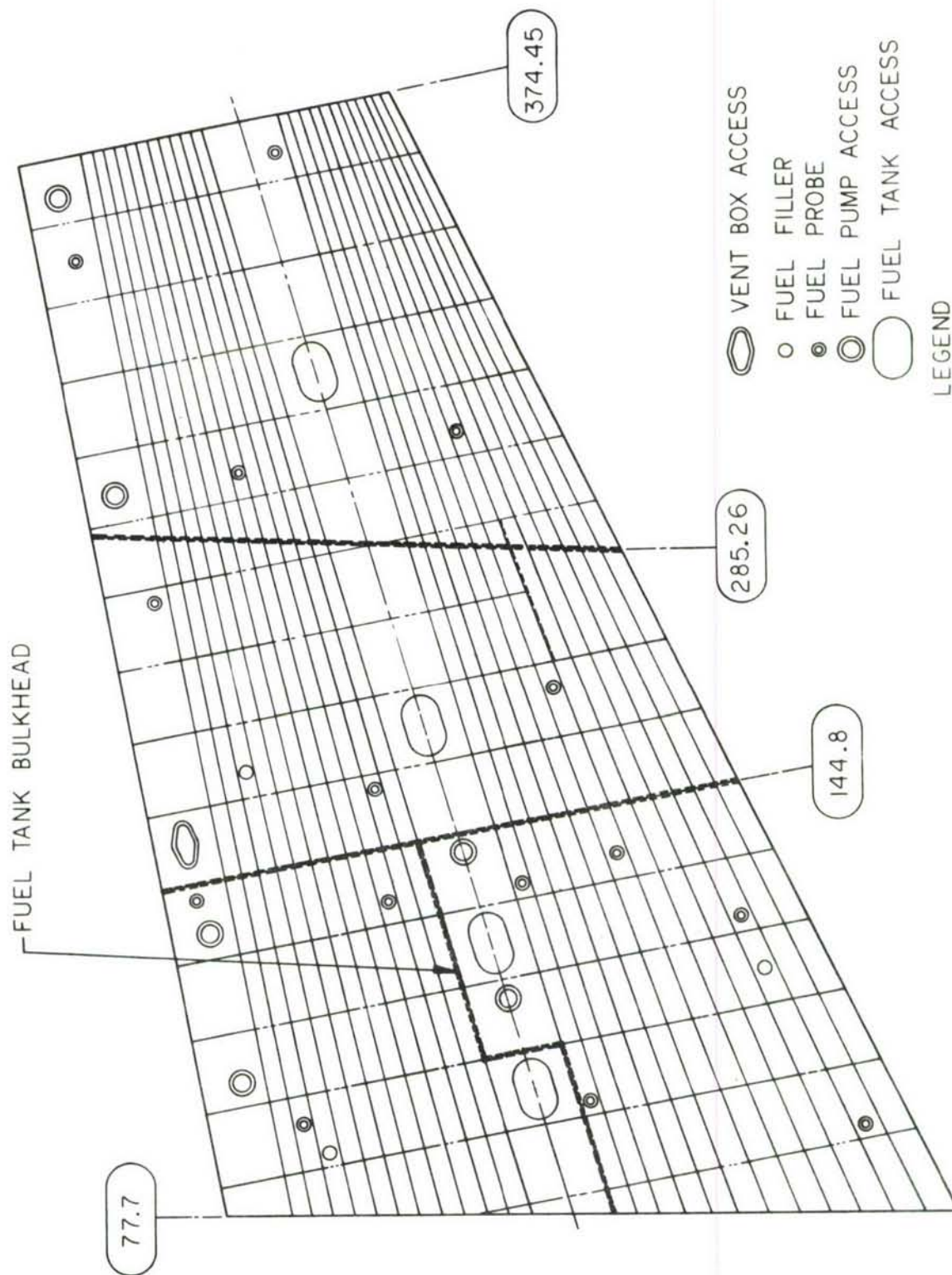
This configuration, with a small weight saving and a cost saving of 33%, scored highest of all the designs evaluated. It is one of the three configurations recommended for further development in Phases IB and II of the follow-on program.



### DESIGN FEATURES

- DAMAGE TOLERANT (MULTI-ELEMENT)
- NO RISER RUNOUTS AT FRONT BEAM
- COVERS - NET EXTRUSIONS
- STRESS WAVE RIVET

FIGURE 34 TAPERED SHINGLE CONFIGURATION





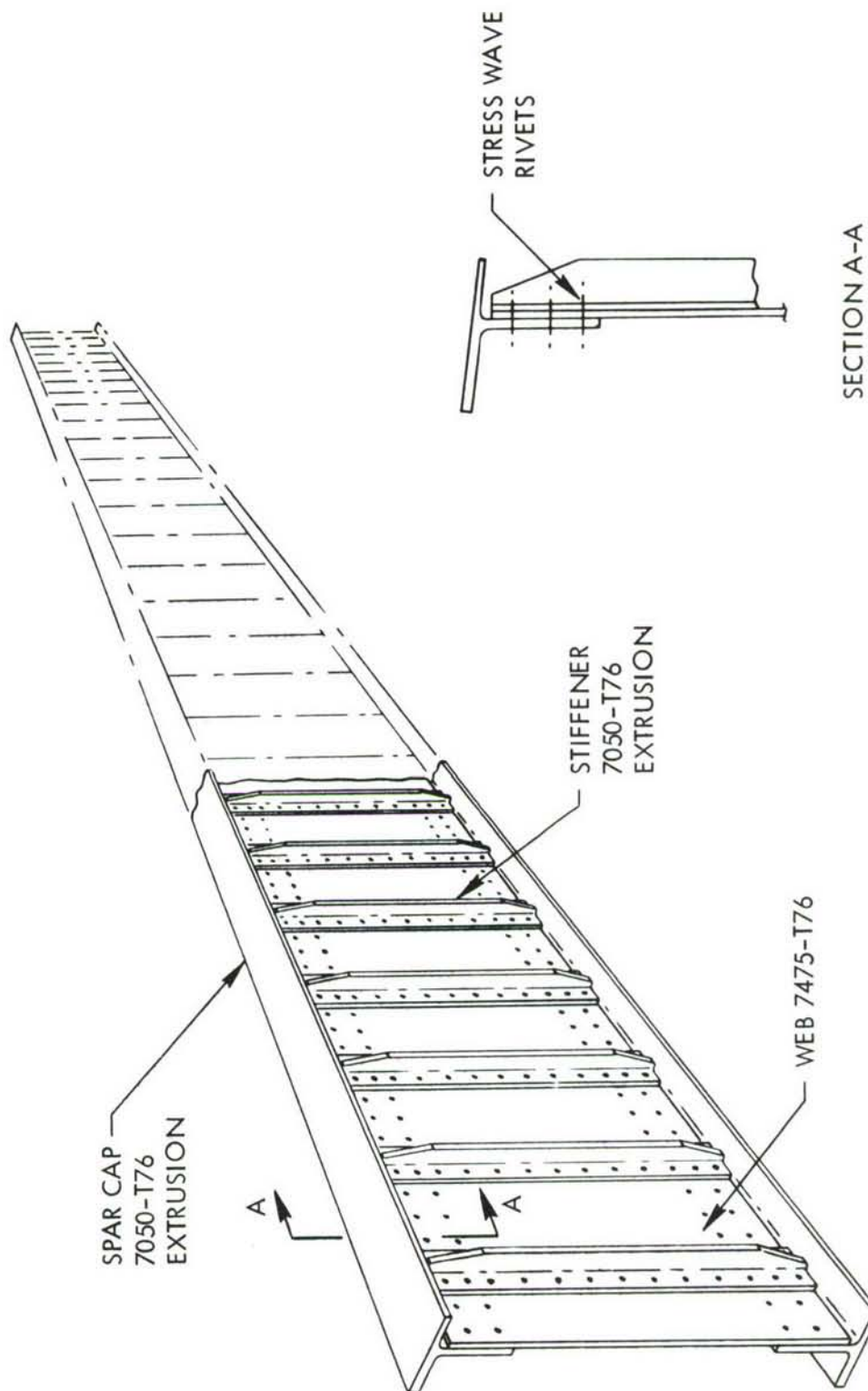


FIGURE 36 SPAR - TAPERED SHINGLE CONFIGURATION



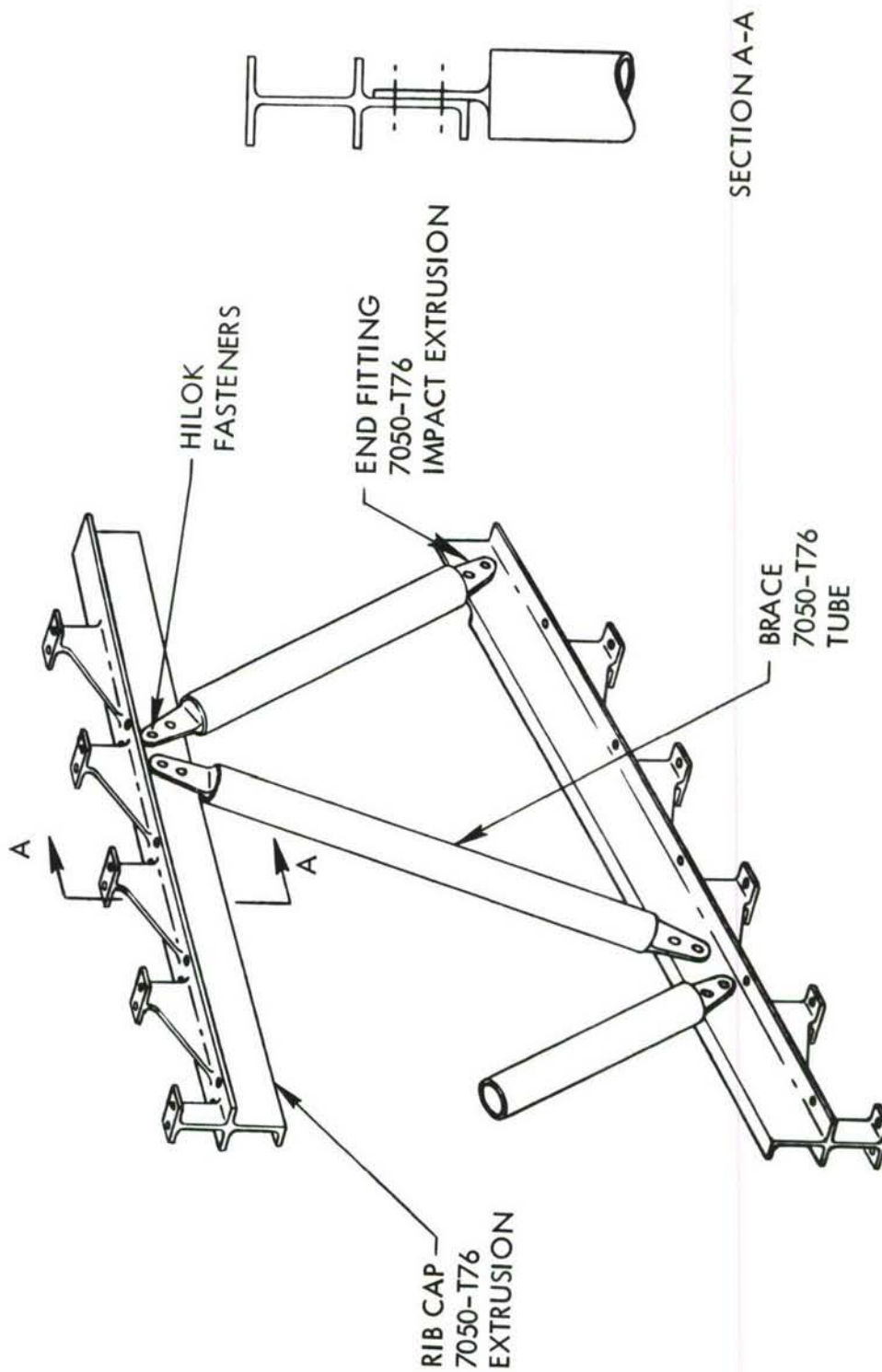


FIGURE 37 TYPICAL RIB - TAPERED SHINGLE CONFIGURATION

## SECTION VI

### MATERIALS AND PROCESSES

Primarily metallic materials were considered for the study since the basic program objective is concerned with advanced metallic structural concepts for cargo/tanker aircraft. Selective use of advanced composites was also considered as reinforcement for basically metallic designs. Due to the low internal loads of 10 to 15 KIPS/inch in the baseline component, a matrix of materials of intermediate strength was tentatively selected. This preliminary materials selection was based on the philosophy of utilizing the best available materials, both new and existing, provided that a demonstrated producibility exists. Thus, those candidate materials in the very early stage of development were eliminated on the basis of high risk. The basic materials selections have been based on property improvements resulting from new heat treating parameters, higher purity alloys, and revised thermomechanical treatments.

#### 6.1 MATERIALS

Candidate materials reviewed for applicability to this study included aluminum, titanium, and steel alloys and boron and graphite epoxy composites for reinforcement of the basic metallic designs. The aluminum and titanium alloys were evaluated for broad usage, (skins, ribs, spars, etc.) whereas the application for the steel alloys were generally limited to critical fittings since the relatively low internal loads prevented their efficient use elsewhere. Preliminary design allowables for those materials evaluated in detail for utilization in the eight structural concepts are included in Table XII.

##### 6.1.1 Aluminum

Various aluminum alloys have been used extensively in the C-141 inner wing baseline update and in the eight advanced design concepts which have been evaluated. The three design configurations proposed for follow-on studies make extensive use of two newly developed, high strength aluminum alloys, 7050 and 7475. Also, the unique welded sine-wave spar design in the

Weldbond configuration utilizes 2219 aluminum which has excellent weldability. These advanced design concepts utilizing the 7050, 7475, and 2219 alloys have been evaluated and compared with the 7075-T6 baseline and 7075-T76 baseline up-date configurations. Design data for these candidate aluminum alloys are discussed in the following paragraphs.

#### 6.1.1.1 Static Design Allowables

The static mechanical properties of the baseline aluminum alloy 7075-T6 and T76 along with the candidate alloys are shown in Table XII. The data basis stipulated in the table indicate the design allowables for candidate alloys 7050 and 7475 are tentative and uncontrolled. These data are based on limited test values and anticipated specification minimums. The final product specifications and the statistically computed and derived minimum guaranteed values are projected to be higher than the design allowables values of Table XII for all forms and tempers.

Current design allowable ultimate tensile strength for 7050-T76511 extruded products are equivalent to the baseline alloy 7075 in the T6 condition and seven percent higher in the updated 76 temper. The computed design values ( $F_{70}$ ,  $n$ ,  $E_c$ , &  $E_t$ ), as shown in Table XII, used in the panel optimization programs are based on an assumed typical, compressive and tensile stress strain curves. These values are substantially higher for 7050-T76511 than the baseline alloy with a minor reduction in the compressive modulus (2%), which makes it more efficient in a compression critical structure.

Alloy 7475 and 2219 were selected for the design concepts due to their excellent properties adaptable to these design configurations.

Alloy 7475-T76 sheet and plate static properties ( $F_{tu}$ ,  $F_{ty}$ ,  $F_{su}$ ) are 10% lower than 7075-T6 but equal to 7050-T76. However, the outstanding fracture properties and superior fatigue strength establishes this alloy as a logical candidate. Alloy 2219 has been available for a number of years, with its major usage confined to designs exposed to extreme temperatures -450 to + 600°F. It was selected in the T87 temper because of its excellent weldability, post-weld response to thermal treatment and retention of parent material static



**TABLE XII**  
**PRELIMINARY DESIGN ALLOWABLES OF CANDIDATE MATERIALS**  
(a) ALUMINUM

MATERIAL	ALUMINUM														
	7075	7075	7475 BARE	7475	2219 BARE	2219	7050	7050	7050	7050	7050	7050	7050	7075	7075
ALLOY	T6511	T76511	T761	T7651	T87	T8511	T7351	T7651	T73511	T76511	T73652	T7652	T6	T76	T76
HEAT TREAT CONDITION/CYCLE	E	E	S	P	S, P	E	P	P	E	E	P	P	S, P	S, P	S, P
MATERIAL FORM (1)	QQ-A-200/11	QQ-A-200/15	-	-	MIL-A-8920	AMS 4162	-	-	-	-	-	-	QQ-A-250/12	QQ-A-250/12	QQ-A-250/12
MATERIAL SPECIFICATION	≤ 3.00	≤ 1.00	≤ 0.25	0.25-0.499	≤ 2.00	≤ 0.499	≤ 3.00	≤ 3.00	≤ 3.00	≤ 3.00	≤ 3.00	≤ 3.00	0.25-0.499	0.25-0.499	0.25-0.499
THICKNESS RANGE (IN)	B	B	S	S	B	S	S	S	S	S	S	S	B	B	B
MIL-HDBK-5B BASIS (2)	L	L	L	L	L	L	L	L	L	L	L	L	L	L	L
GRAIN DIRECTION	-	-	0.101	0.101	0.102	0.102	0.102	0.102	0.102	0.102	0.102	0.102	0.101	0.101	0.101
DENSITY (LB/CI)	85	75	71	70	64	58	71	77	79	81	72	77	80	71	71
DESIGN DATA															
TENSILE STRENGTH, ULT. $F_{tu}$ KSI	76	65	61	60	52	42	63	69	70	72	62	66	73	61	61
TENSILE STRENGTH, YIELD $F_{ty}$ KSI	76	65	60	58	52	42	58	68	65	75	59	66	72	60	60
COMPRESSIVE STR., YIELD $F_{cy}$ KSI	43	40	43	41	38	33	40	46	40	42	40	44	48	41	41
SHEAR STRENGTH, ULT. $F_{su}$ KSI	77	66	61	-	53	42	58	68	65	75	61	-	73	62	62
.7 SECTANT STRESS $F_{.7}$ KSI	20	25	29	-	18	18	19	13	25	31	21	-	15	21	21
SHAPE FACTOR $n$	10.4	10.4	10.0	10.2	10.5	10.5	10.3	10.3	10.3	10.3	10.3	10.3	10.3	10.3	10.3
MODULUS, TENSILE $E_t$ KSI x 10 <sup>3</sup>	10.7	10.7	10.5	10.6	10.8	10.8	10.4	10.5	10.5	10.5	10.5	10.5	10.5	10.5	10.5
MODULUS, COMPRESSIVE $E_c$ KSI x 10 <sup>3</sup>	4.0	4.0	3.8	3.9	4.0	4.0	3.9	3.9	3.9	3.9	3.9	3.9	3.9	3.9	3.9
MODULUS, SHEAR $G$ KSI x 10 <sup>3</sup>	120	109	113	112	101	81	109	120	109	119	109	108	124	110	110
BEARING, ULT. ( $e/d=1.5$ ) $F_{bru}$ KSI	151	138	145	145	128	107	138	148	138	150	138	138	160	139	139
BEARING, ULT. ( $e/d=2.0$ ) $F_{bru}$ KSI	98	87	90	88	84	67	90	105	87	97	90	86	106	92	92
BEARING, YIELD ( $e/d=1.5$ ) $F_{bry}$ KSI	116	104	105	103	97	82	108	122	104	115	108	99	124	109	109
BEARING, YIELD ( $e/d=2.0$ ) $F_{bry}$ KSI	28	29	NA	43	27	36	35	36	-	38	36	34	27	-	-
FRACTURE TOUGHNESS $K_{Ic}$ KSI <sup>1/2</sup> /IN	68/.15	84/.15	120/.15	-	73/.15	56/.15	56/.15	56/.15	56/.15	57/.15	-	-	63	78	78
FRACTURE TOUGHNESS $K_{C/t}$ KSI <sup>1/2</sup> /IN	12.9	12.9	13.1	13.1	12.4	12.4	13.1	13.1	13.1	13.1	13.1	13.1	12.9	12.9	12.9
THERMAL EXP. COEFF. $\alpha$ IN/IN/°F															

- (1) S - Sheet, P - Plate, E - Extrusion, F - Forging  
(2) B - "B" Basis, S - "S" Basis, T - Target  
(3)  $K_{Ic}$  values were typical values in the LT direction.



TABLE XII (Continued)

PRELIMINARY DESIGN ALLOWABLES OF CANDIDATE MATERIALS

(b) TITANIUM AND STEEL

MATERIAL		TITANIUM					STEEL		
ALLOY	HEAT TREAT CONDITION/CYCLE	6-2-2-2-2	6-2-2-2-2	6-6-2	6-4	9Ni-4Co-.30C	PH13-8Mo	18Ni-300 Mar.	
MATERIAL FORM (1)		ST	STA	STOA	HTA	Q&T	H1000	STA	
MATERIAL SPECIFICATION		S,P,E,F	S,P,E,F	S,P,E,F	S,P,E,F	Wrought	Wrought	Wrought	
THICKNESS RANGE (IN)		-	-	-	-	AMS 6541 AMS 6546	AMS 5629	ASTM A538	
MIL-HDBK-5B BASIS (2)		≤ 4.00	≤ 4.00	≤ 1.50	.1875-2.00	≤ 8.5	≤ 12.0	All	
GRAIN DIRECTION		S	S	S	A	S	S	T	
DENSITY (LB/CI)		L	L	L	L	L	L	All	
DESIGN DATA		0.162	0.162	0.164	0.160	0.284	0.279	0.300	
TENSILE STRENGTH, ULT.	F <sub>tu</sub> KSI	160	170	160	130	240	200	280	
TENSILE STRENGTH, YIELD	F <sub>ty</sub> KSI	143	152	150	120	185	185	265	
COMPRESSIVE STRENGTH, YIELD	F <sub>cy</sub> KSI	145	165	160	126	222	202	265	
SHEAR STRENGTH, ULT.	F <sub>su</sub> KSI	110	113	109	76	144	120	154	
.7 SECANT STRESS	F <sub>.7</sub> KSI	156	179	168	-	-	203	287	
SHAPE FACTOR	n	10	9	31	-	-	10	33	
MODULUS, TENSILE	E <sub>t</sub> KSI x 10 <sup>3</sup>	17.0	18.0	16.0	16.0	28.5	29.4	26.5	
MODULUS, COMPRESSIVE	E <sub>c</sub> KSI x 10 <sup>3</sup>	17.0	18.0	16.3	16.4	28.5	29.4	29.0	
MODULUS, SHEAR	G KSI x 10 <sup>3</sup>	6.7	6.7	6.3	6.2	10.8	11.3	10.2	
BEARING, ULT. (e/D=1.5)	F <sub>bru</sub> KSI	-	-	-	191	-	330	392	
BEARING, ULT. (e/D=2.0)	F <sub>bru</sub> KSI	290	302	310	245	-	400	507	
BEARING, YIELD (e/D=1.5)	F <sub>bry</sub> KSI	-	-	-	163	-	270	356	
BEARING, YIELD (e/D=2.0)	F <sub>bry</sub> KSI	241	246	240	198	-	297	432	
FRACTURE TOUGHNESS	K <sub>Ic</sub> KSI√IN	61	55	50	-	100	100	-	
FRACTURE TOUGHNESS	K <sub>IC/t</sub> KSI√IN/IN	117/.15	103/.15	88/.15	-	-	-	65/.15	
THERMAL EXP. COEFF.	α IN/IN/°F	-	-	5.0	-	6.4	-	-	

(1) S - Sheet, P - Plate, E - Extrusion, F - Forging

(2) B - "B" Basis, S - "S" Basis, T - Target

TABLE XII (Concluded)

PRELIMINARY DESIGN ALLOWABLES OF CANDIDATE MATERIALS

(c) COMPOSITE MATERIALS

COMPOSITE MATERIAL	BORON	GRAPHITE
TYPE	EPOXY TAPE	EPOXY HIGH STRENGTH TAPE
DENSITY (LB/CI)	0.073	0.054
DESIGN DATA		
MODULUS, 0°	E <sub>1</sub> 10 <sup>3</sup> KSI	20.0
MODULUS, 90°	E <sub>2</sub> 10 <sup>3</sup> KSI	2.1
SHEAR MODULUS	G 10 <sup>3</sup> KSI	0.85
POISSON'S RATIO	$\nu_{12}$	0.21
TENSILE STRAIN, 0°	$\epsilon_1$ 10 <sup>-6</sup> IN/IN	8,700
TENSILE STRAIN, 90°	$\epsilon_2$ 10 <sup>-6</sup> IN/IN	3,825
COMPRESSIVE STRAIN, 0°	$\epsilon_1$ 10 <sup>-6</sup> IN/IN	9,900
COMPRESSIVE STRAIN, 90°	$\epsilon_2$ 10 <sup>-6</sup> IN/IN	10,000
SHEAR STRAIN	$\gamma_{12}$ 10 <sup>-6</sup> IN/IN	15,000
THERMAL EXPANSION, 0°	$\alpha_1$ 10 <sup>-6</sup> IN/IN/°F	-0.28
THERMAL EXPANSION, 90°	$\alpha_2$ 10 <sup>-6</sup> IN/IN/°F	16.0

properties after weld. It is being specified for welded application.

#### 6.1.1.2 Fracture Design Consideration

The fracture properties of materials have become of paramount importance in selection and application for structural design. Improved damage tolerance design criteria and materials specification requirements prompted industry to develop alloys that exhibited superior fracture toughness to meet these definitions.

Fracture toughness data,  $K_{Ic}$ ,  $K_{Ic}$  for a number of alloys and tempers are shown in Table XII and plotted vs thicknesses in Figure 38. The crack growth data for a number of stress ratios are also presented in Figure 39. The fracture data for the prime alloys, 7050, 7475, and 2219, were derived from the extensive test programs currently in progress, and from limited in-house tests. The data indicate that alloy 7050 plain stress fracture toughness in the 76511 extruded temper is 30% higher than the T76 temper of 7075 baseline alloy. The plain stress fracture toughness of 7475-T76 sheet is 40% higher than 7075-T76 sheet material. Aluminum alloy 2219 in the T87 temper is approximately 8% lower in both plain strain ( $K_{Ic}$ ) and plain stress ( $K_{Ic}$ ) than 7075-T76 alloy. Crack growth rate comparisons show that alloys 2219, 7050, and 7475 have the lowest crack-growth rates with 7075-T6 having the highest rate. In making comparisons of the crack-growth rates in Figure 38, note that the curves are for different stress ratios. Data were not available for comparisons at the same ratios.

#### 6.1.1.3 Fatigue Data

As noted previously, the newly developed, high strength 7050 and 7475 alloys are the prime materials for the majority of the structural concepts which have been studied. In addition, 2219 aluminum is utilized for its excellent weldability and strength after welding for the sine wave spars in the Weldbond Concept and for the skin panels and ribs in the Monolithic configuration. For the fatigue analyses of the various configurations evaluated, two types of fatigue data have been developed and include; (1) coupon S-N data from



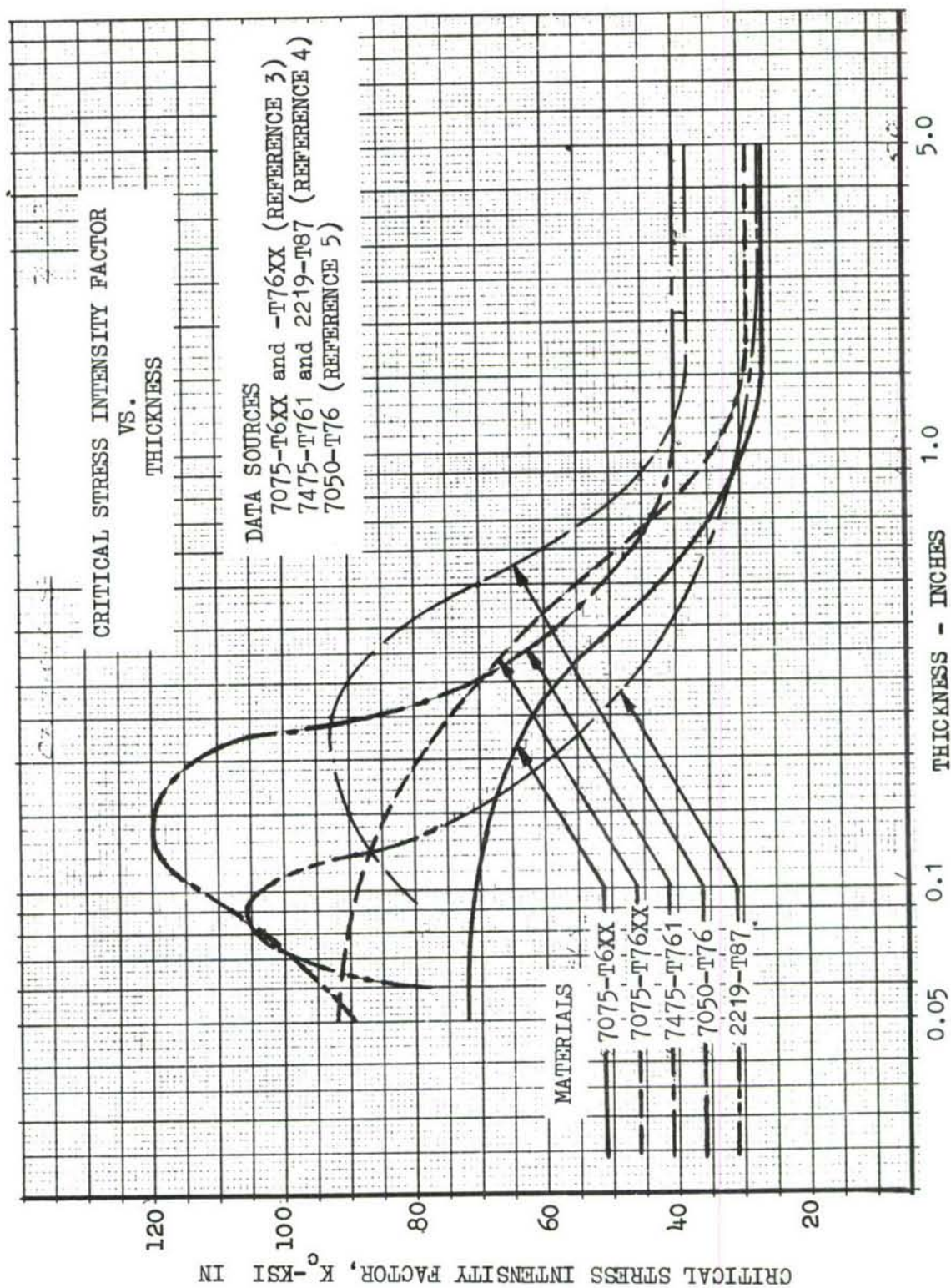


FIGURE 38 - CRITICAL STRESS INTENSITY FACTOR



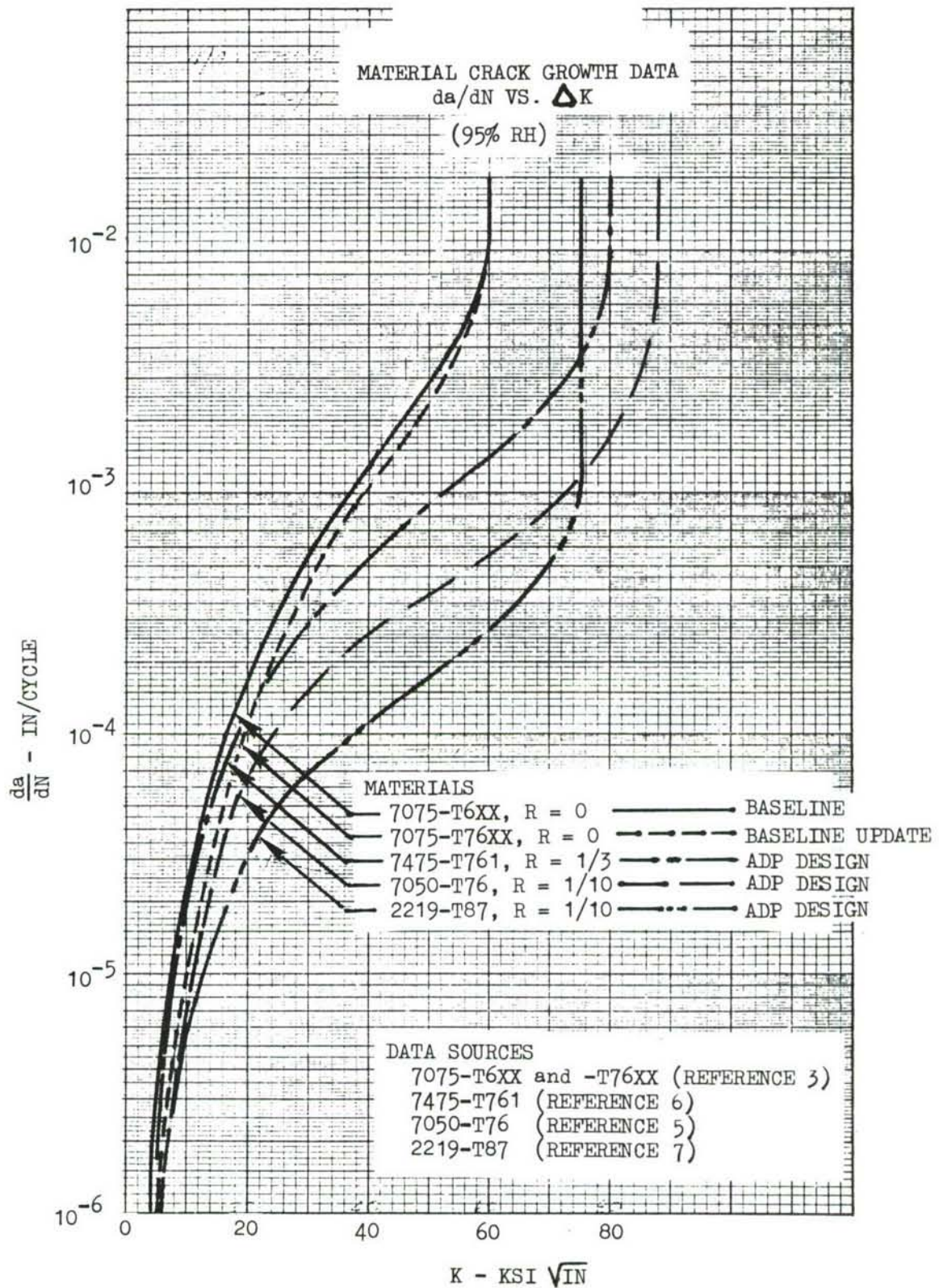


FIGURE 39 - MATERIAL CRACK GROWTH DATA

notched specimens and (2) built-up structures S-N data which have been shown in Lockheed and industry studies to accurately represent actual full scale structures. Typical built-up structures and coupon S-N data are shown in Figures 40 and 41, respectively, for 7050 aluminum for  $K_t = 3.25$ .

Since both the 7050 and 7475 alloys are relatively new and limited fatigue data was available for notched coupons only at the beginning of this program, the basis for all the S-N curves is to present the variable stress in terms of percent of  $F_{tu}$  rather than on an absolute basis. This then allowed for development of families of coupon S-N curves for the various tempers and forms of each material by utilizing to the fullest the very limited amount of available test data. As the program progressed the initial S-N curves were updated to include test data from Lockheed, other ADP programs, and vendor data. It should be noted that when coupon fatigue data became available for 7475-T76 ( $F_{tu} = 70$  KSI), these data indicated a better fatigue endurance than the 7050 alloys which have higher tensile strengths. This has been reflected in the S-N data and analyses. For example, for the 7475-T76 alloy the maximum stress at  $10^6$  cycles is approximately 17.0 KSI, whereas for the 7050-T76 alloys,  $F_{max} = 15.2$  at  $10^6$  cycles. These data are at  $R = +0.10$  and  $K_t = 3.0$ . Comparable stresses for 7075-T6 and -T76 are 14.0 and 12.5 KSI, again at  $10^6$  cycles.

The built-up structures S-N curves (Figure 40) are significantly different from the notched coupon curves with respect to both slope and endurance limit. These curves for the advanced aluminum alloys have characteristics similar to those developed under Lockheed IRAD and transport fleet tracking programs for 7075-T6 aluminum. The stress - cycles to failure relationship, however, represents the improved fatigue performance for these newer alloys. These built-up structures S-N data have been utilized, as appropriate, for mechanically fastened joints where the effects of fretting, load transfer, fastener tilting, etc. have a significant influence on the fatigue endurance, and the actual fatigue endurance is not represented by notched coupon S-N data. The coupon curves are used, however, for the analysis of cut-outs and access holes and for the welded and weldbonded structural configurations.



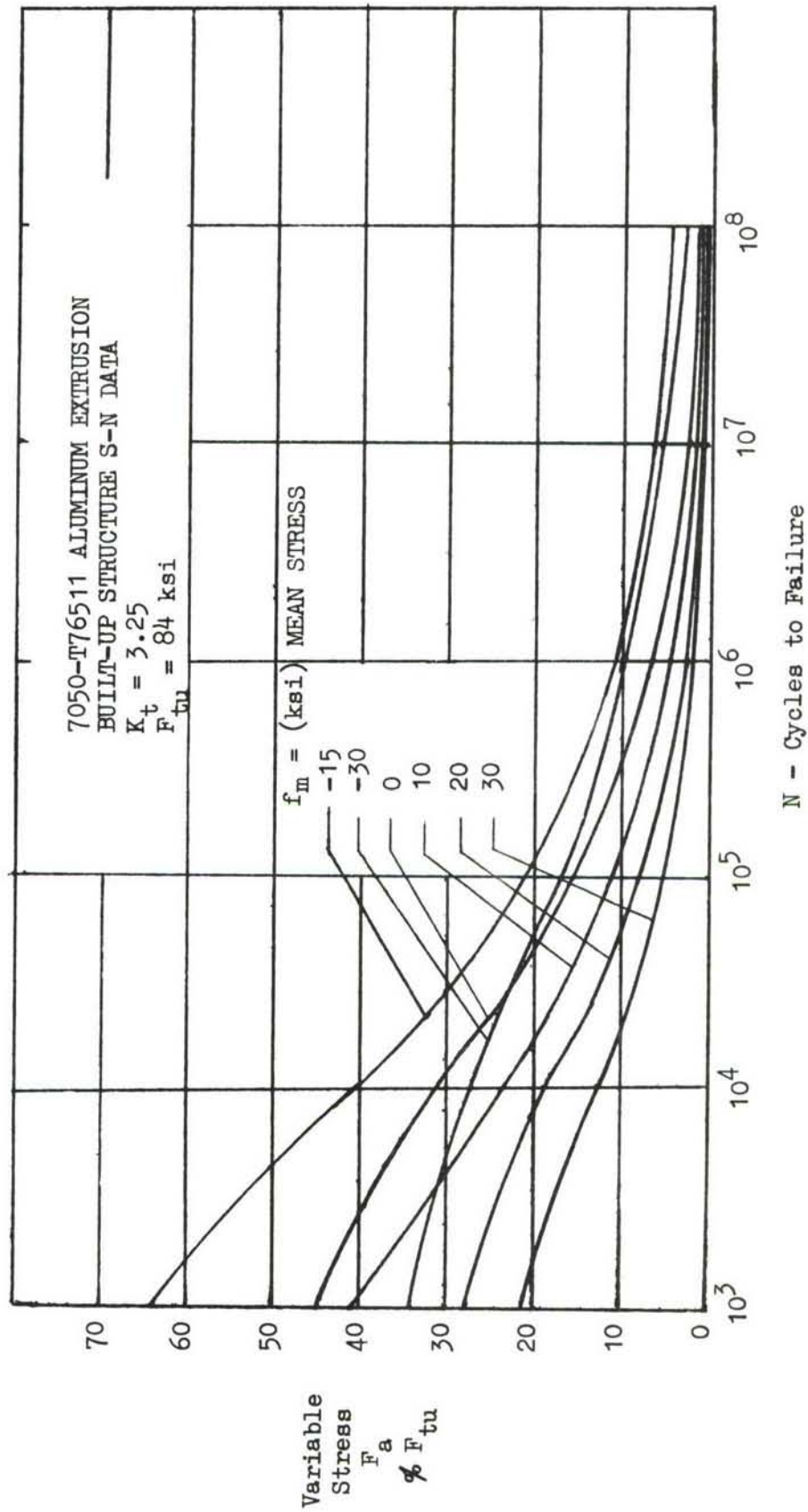


FIGURE 40 S-N DATA - 7050-T76511 ALUMINUM, BUILT-UP

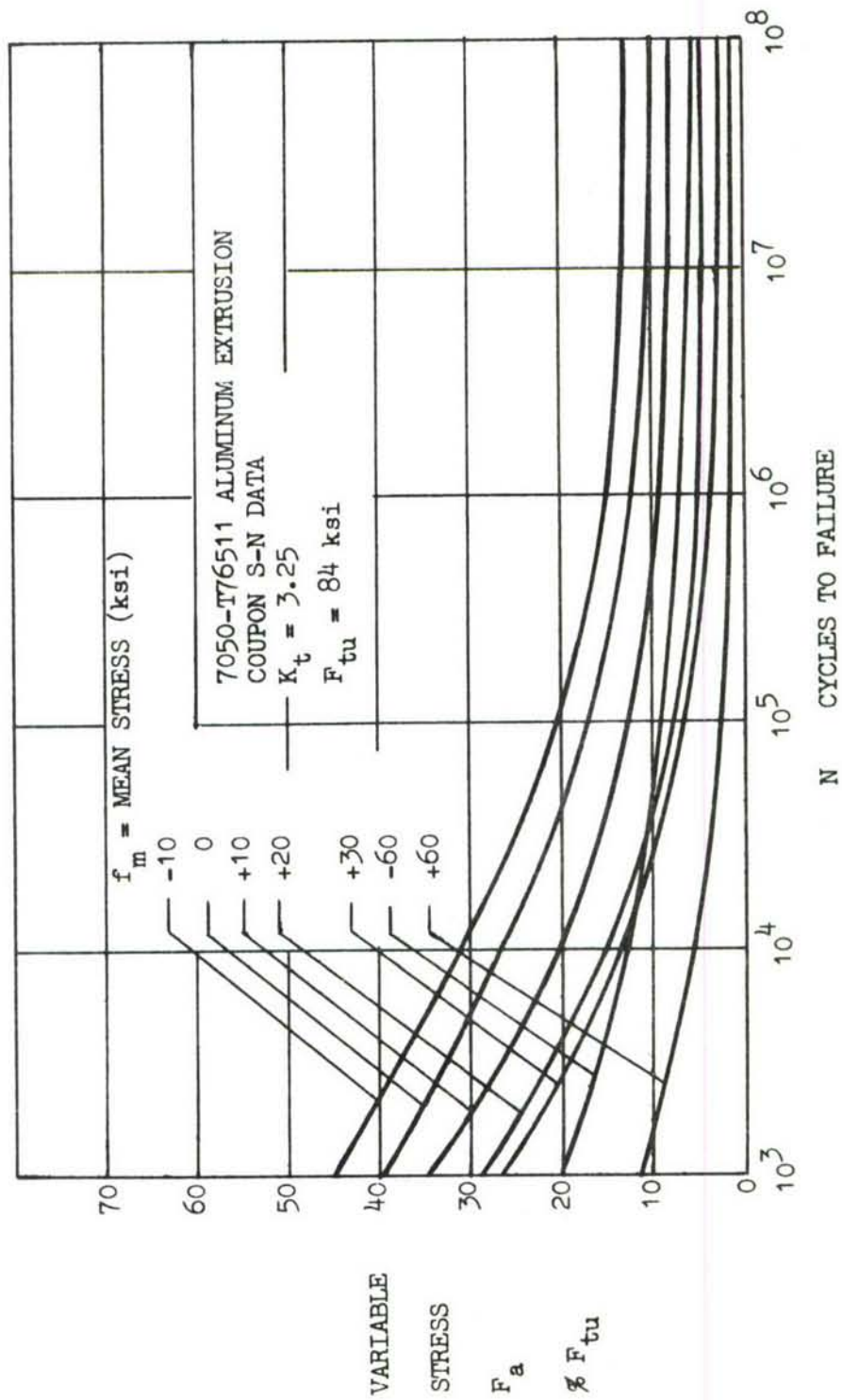


FIGURE 41 - S-N DATA - 7050-T76511 ALUMINUM, COUPON



The latter was justified by an analysis of data for weldbonded joints obtained from full load transfer joint test specimens, the type generally in use by industry to evaluate this type structure. Subsequently, a limited development program was initiated to evaluate the effect of variation in load transfer on fatigue performance. This program has not been completed, but initial test results indicate that coupon S-N data may not best describe fatigue characteristics of low load transfer joints. However, more tests are needed before it can be concluded that some type of built-up structure S-N data should be used. The fact that weldbonding has attractive cost saving potential, and early tests indicate fatigue performance equivalent to steel Taperloks (Reference Table XXXIX), justifies additional fatigue development work on this process in the follow-on program.

#### 6.1.1.4 Environmental Effects

The effect of environment on the various alloys is another parameter to consider in the materials selection process. This effect can be in the form of general corrosion, exfoliation and/or stress corrosion. The resistance of the candidate alloy to the preceding environmental effects is outlined below.

The general corrosion can be minimized by the use of organic finishes, alclad and anodizing. Alloy 7050 with a higher copper content than 7475 & 7075 requires a better finish to minimize the general corrosion attack, possibly a high strength cladding. The use of alloys in the T76 overage intermediate temper results in high resistance to exfoliation corrosion when evaluated per QQ-A-00250/24 specification. The T76 tempers of 7050 & 7475 have shown freedom from exfoliation in the fabricated surface. The stress corrosion properties of alloys in T76 temper do not exhibit the immunity that is available in the T73 temper. The stress corrosion thresholds of the selected alloys are guaranteed at 50% of the yield strength of the material when exposed to a corrosive environment acting on the short transverse direction. This threshold which lies between 25 - 35 KSI is compared with 5KSI for 7075-T6 and 25 KSI for 7075-T76.

### 6.1.2 Titanium

Three new or advanced structural concepts employing extensive use of titanium alloys have been studied during this program. These are discussed in detail in Section V and include; (1) the Lockskin configuration where graphite is sandwiched between two titanium sheets to form the wing cover panels, (2) the Sandwich configuration which utilizes titanium honeycomb sandwich panels, and (3) the Composite Hat configuration with titanium cover panels. The three titanium alloys selected for evaluation include Ti-6Al-2Sn-2Zr-2Mo-2Cr-0.25Si (primary candidate), Ti-6Al-6V-2Sn, and Ti-6Al-4V. The 6-6-2 and 6-4 alloys were selected as back-up for the 6-2-2-2-2 primary candidate since limited design data was available.

Design allowables for the Ti-6Al-2Sn-2Zr-2Mo-2Cr-.25Si and the Ti-6Al-6V-2Sn and Ti-6Al-4V backup alloys are shown in Table XII (b). The 6-2-2-2-2 alloy has a very good strength/weight ratio and excellent fracture toughness as seen from the design allowables data in Table XII. The deep hardenability, fracture toughness modulus, and strength/weight ratio of this new alpha-beta alloy make it most attractive when compared with the high density and low modulus of the metastable beta alloys such as Beta III and Beta C. For example the modulus and density of the 6-2-2-2-2 alloy are  $17 \times 10^3$  KSI and  $0.162 \text{ lb/in}^3$  as compared with  $15 \times 10^3$  KSI and  $0.183 \text{ lb/in}^3$  for Beta III.

### 6.1.3 Steel

As noted previously, the relatively low internal loads in the C-141 inner wing are such that the aluminum and titanium alloys are more efficient in the major structural components than the higher strength steels. There will be a need for utilizing the higher strength and toughness of steel alloys in selected applications, such as pylon fittings, etc. Those steels currently considered as candidate materials include the 9Ni-4Co, 18Ni maraging, and PH13-8Mo stainless steels. Design allowables for these materials are listed in Table XII. The 9Ni-4Co and 18Ni maraging steels have been selected for high strength, deep hardenability, fracture toughness

and ease of fabrication as compared to other commonly used, high strength alloys such as 4340 and 300M. The PH13-8Mo was selected for its corrosion resistance, toughness, and ease of fabrication. The 9Ni-4Co and PH13-8Mo steels have a  $K_{Ic}$  of approximately 100 whereas 300M, for example, is approximately 60 and D6AC may range from 50 - 80. The 18Ni maraging steel has approximately the same ultimate tensile strength as 300M but a higher  $K_{Ic}$  ( $61 \text{ KSI}\sqrt{\text{in}}$  vs  $65 \text{ KSI}\sqrt{\text{in}}$  ).

#### 6.1.4 Advanced Composites

Considerable attention has been focused, recently, on structural concepts which incorporate advanced composite materials as reinforcement for metallic materials. This will then incorporate the stiffness, light weight and fatigue resistance of the composites with the ease of fabrication of say, an aluminum or titanium alloy. This concept has been incorporated in two designs evaluated in this program; i.e., the Lockskin configuration and the Composite Hat configuration. In both designs, graphite-epoxy is bonded to titanium skin panels. Graphite is lower in cost than boron and is used with the titanium rather than aluminum in order to minimize thermal residual stresses after bonding which are most damaging from a fatigue standpoint. Table XII (c) lists the design allowables for the boron and graphite advanced composites.

### 6.2 PROCUREMENT SPECIFICATIONS

Attainment of the cargo/tanker structure design goals, especially those relating to fracture and fatigue performance and corrosion resistance, requires higher quality materials than those presently produced in accordance with existing procurement specification requirements. Closer control of the following items is required for improved quality:

- o Chemical composition
- o Melting practice
- o Thermomechanical treatment



- o Processing
- o Macrostructure
- o Microstructure
- o Heat-treatment
- o Internal defects
- o Quality control requirements
- o Fracture properties as a function of thickness
- o Mechanical testing requirements

Purchase of the material for fracture critical structure will be controlled by newly written and/or revised procurement specifications containing requirements for the aforementioned items. These specifications will ensure that the basic materials and the resulting structure will have as a minimum the static, fracture-toughness, and corrosion resistant properties used in design. Tests will be conducted prior to shipping on all billets, forgings, extrusions, plates, etc., to verify that the specified values are obtained. Portions will also be cut from these items, or integral projections thereof, at receiving inspection, and additional tests performed as required.

### 6.3 FINISHES AND PROCESSES

Finishes and processes reflecting the latest technology were selected for protecting the wing structural components from corrosion and for fuel tank sealing. Where corrosion resistance is not inherent in the materials called for in each of the design configurations, additional measures will be taken to ensure corrosion protection at least commensurate with the best state of the art. In a few areas, developmental work is required to acquire either the know-how or the desired assurance of efficiency of the protection system. In this category, there is one notable case in point: welded bonded assemblies. In order to assure the high level of protection required, a development program is required to attain in one system the combined objectives of high corrosion resistance, reliability of process results, and economy of production. In the



meantime, protection systems are described below which are considered sure of providing a high level of corrosion protection, although the systems described are not as economical as desired.

#### 6.3.1 Finishes

The following were selected as the basic surface finishes for application to components made of the indicated materials:

- o Titanium
  - shot peen
  - passivate
- o Aluminum
  - shot peen
  - sulfuric acid anodize (chromic where bonding)
  - dichromate seal
  - polyurethane coat (MIL-C-27725)
- o Steel
  - shot peen
  - cadmium plate (QQ-P-416, Class 2, Type II)
  - polyurethane coat (MIL-C-27725)

#### 6.3.2 Processes

For corrosion prevention, processes capable of providing the high level of required protection have been selected. Processing of the general type applicable to all design configurations is presented below. Processing pertinent to the particular configuration is then given for each of the three recommended designs.

##### 6.3.2.1 General Processing

The following processing applicable to all design configurations was selected:

- o Coat all aluminum parts located in the bottom of the fuel tanks and one inch up with a second coat of polyurethane (MIL-C-27725) containing a biocidal additive.
- o Seal all faying surfaces, and wet-install all fasteners with a corrosion-inhibitive sealant (MIL-S-81733), except stress wave rivets.
- o Post-assembly fillet seal all joints forming fuel tank boundaries and brush-overcoat all fasteners penetrating fuel tank boundaries with a

sealant (MIL-S-8802).

- o Overcoat all fasteners on the inside of the fuel tank area not coated with a sealant with polyurethane (MIL-C-27725).
- o Overcoat all sealant exposed to fuel with a sealant top coat (MIL-C-83019).

#### 6.3.2.2 Processing: Weldbond Configuration

For this configuration, the structure is to be weldbonded using epoxy adhesive. Any voids are vacuum impregnated with the same adhesive, then cured. The weldbonded assemblies are chromic acid anodized and left unsealed to permit metal bonding in the front and rear beam spanwise splice joints. The intermediate spanwise splice joints, which are subsequently weldbonded after anodizing of the rib to cover subassembly, are masked in the weldbonded areas during the anodizing of that subassembly. Independent development work is currently under way at Lockheed to explore methods of producing a weldbonded joint at least equivalent in corrosion resistance to the best current state of the art metal-bonded joints. Further development to achieve a production-ready process is recommended for the follow-on program. Should simpler processing procedures fall short of the corrosion resistance goal, reliance will be placed on chromic acid anodized bond surfaces with only the spotweld area left bare. Bare spotweld surfaces may be obtained either by masking before anodizing or an automatic wire brushing operation.

MIL-C-27725 polyurethane is applied to all structure (including the interior of the square tube rib diagonals) with the exception of the exterior surface skins. These surfaces are coated with applied epoxy/polyurethane (MIL-P-23377/MIL-C-83286) system.

All sub-structures assembled with mechanical fasteners are sulfuric acid anodized and coated with MIL-C-27725 polyurethane prior to assembly. The faying surfaces of mechanically fastened joints are sealed and fasteners sealed wet installed with corrosion inhibiting sealant.

Since the inverted "A" type stringers on the lower surface will trap fuel and water, provisions are made to drain these locations through use of suction tubes located in each enclosed area.

#### 6.3.2.3 Processing: Virgin Plank Configuration

For this configuration, the structural assembly technique permits detail processing of material components. Due to current industry inability to reliably bond to sulfuric acid anodized adherends, chromic acid anodizing is used in the bond lines of the details which make up the bonded/clamped spanwise splice. The remaining areas of these details, including all exterior surfaces and all other detail components which are mechanically fastened, are sulfuric acid anodized. In order to eliminate the undesirable double anodizing process required in this and other bonded configurations, additional development of the parameters for structural adhesive bonding to sulfuric acid anodized adherends is necessary.

MIL-C-27725 polyurethane is applied to all structure prior to assembly, and mechanical fasteners wet installed with corrosion inhibiting sealant. Joint faying surfaces are sealed with the same sealant in all areas except those which are adhesive bonded. Exterior surfaces are painted with the epoxy/polyurethane (MIL-P-23377/MIL-C-83286) system.

#### 6.3.2.4 Processing: Tapered Shingle Configuration

The conventional built-up structure of this configuration allows detail chemical processing entirely. All components are sulfuric acid anodized and coated with the MIL-C-27725 polyurethane paint prior to assembly. Joint faying surfaces are to be sealed with corrosion inhibiting sealant. The stress wave rivets are to be driven dry. Exterior surfaces are to be painted with the epoxy/polyurethane system (MIL-P-23377/MIL-C-83286).

### 6.4 JOINING METHODS

To maximize the fatigue strength of the structure, emphasis was placed on designs which minimized surface penetration by mechanical fasteners. Consequently, several innovative design concepts were devised to accomplish this. Two examples



are the bonded-clamped joint and the non-penetrating clips. Weldbonding and stress wave riveting, both of which provide potential fatigue improvement through reduction of effective  $K_T$ 's, are also used for fatigue critical applications. HILOKS and aluminum rivets are selected as the mechanical fastener system for non-critical substructure. A summary of joining methods used in the three recommended configurations is given in Table XIII. Component tests and initial manufacturing development were accomplished for several of these during Phase IA to establish conceptual feasibility. Additional investigation and development of some of these systems must be accomplished during a follow-on program. These are listed below.

- o Weldbonding - corrosion resistance, improved fatigue performance, automated spotwelding procedures, and optimum adhesives.
- o Burn-through welding - elimination of undesirable oxides in the weld, improved static and fatigue properties, and out-of-chamber EB welding procedures.
- o Stress wave rivets - stress corrosion resistance and automated riveting procedures.
- o Bonded/Clamped joints - static strength and fatigue allowables, environmental protection, and optimum configuration of Lockmold tooling.
- o Rib cap to surface attachment - static and fatigue allowables for "A" stringer and non-penetrating clip.
- o Adhesive bonding - processes and allowables for bonding to sulfuric acid anodized adherends.

Some of these development items are discussed in more detail in Section 9.6.



TABLE XIII

## SUMMARY - JOINING METHODS

STRUCTURAL SPLICE	CONFIGURATION 1: WELDBOND	CONFIGURATION 7: VIRGIN PLANK	CONFIGURATION 8: TAPERED SHINGLE
SURFACE SPLICES SPANWISE	WELDBOND	BONDED/CLAMPED SPLICES USING HILOKS IN COLD- WORKED HOLES	STRESS WAVE RIVETS
CHORDWISE	STEEL TENSION BOLTS PRELOADED TO PROVIDE HIGH CLAMPUP IN COLD-WORKED HOLES. ALTERNATE: TAPERLOKS - TO BE EVALUATED ON FOLLOW-ON PROGRAM.		
SURFACE TO RIB CAP ATTACHMENT	HILOKS IN TABS OF "A" STRINGERS	NON-PENETRATING CLIPS	STRESS WAVE RIVETS & HILOKS IN COLD-WORKED HOLES
TRUSS RIBS	HILOKS AND ALUM RIVETS	HILOKS	
BULKHEADS	WELDBOND, HILOKS AND ALUMINUM RIVETS	HILOKS AND ALUMINUM RIVETS	
SPAR CAPS TO SPAR WEBS	BURN THROUGH WELD	(INTEGRAL FORGING)	STRESS WAVE RIVETS
SPAR WEBS TO STIFF- NERS	(SINE WAVE WEB)	(INTEGRAL FORGING)	HILOKS AND RIVETS
ACCESS HOLES AND MISCELLANEOUS OPEN- INGS	( NON-STRUCTURAL CLAMPED-IN COVERS )		

## SECTION VII

### STRESS AND WEIGHTS ANALYSIS

To establish the three best designs from a series of candidate configurations, it is essential that the stress and weights analyses be accurate and responsive. Predicted stresses and weights supplied efficiently and clearly permit not only evaluations among proposed designs, but also allow more design concepts and variations to be considered. Effective use of Lockheed-Georgia's computer methods and facilities by the stress and weights analysts working on this ADP effort produced reliable results in very short turn-around times. Stresses (internal loads) for the baseline and proposed designs were predicted by utilizing an automated combination of computer graphics, finite element structural analysis, and computer output scan programs. Weights for the baseline and proposed designs were predicted from C-141 actual weights by comparing stress allowables, material densities, and manufacturing procedures.

In the following sections the basis, methods, and sample results for the static loads and weights analyses are presented.

#### 7.1 STRESS ANALYSIS

All internal static loads analyses relied on finite element methods. The facilities and computer programs, including ASOP (Automated Structural Optimization Program), used to perform these analyses are part of Lockheed-Georgia's production system. In addition to standard batch processing, the system provides interactive graphics capabilities. These capabilities were extensively used to generate and verify input sequence and to reduce and clarify analysis output.

To satisfactorily provide stress results for design evaluations, the analysts were required to:

- A. Construct a finite element model which conformed to the geometric and stiffness criteria of the proposed ADP designs;
- B. Define a set of external static load conditions which conformed to the C-141 design load conditions;

- C. Apply the external load conditions to the finite element model, compute resulting internal loads, and scan these results to identify critical areas; and
- D. Use the computed internal loads acting on model components (ribs, cut-outs, and cover panels) and carry out structural optimization and margin of safety analyses.

The model constructed for the updated baseline in Step A was modified to achieve a good wing cover thickness distribution. Steps C and D were then repeated. The internal loads from this modified model were used for all the ADP designs. Aspects of the analysis sequence are discussed in the following sections.

#### 7.1.1 Stiffness Criteria and External Loads

The ADP inner wing box configurations are designed to the same static loads requirements as the baseline C-141 structure. Baseline bending and torsional stiffnesses are also maintained in ADP designs to ensure no degradation in airplane performance.

The critical external static load conditions were taken from C-141 loads and stress analysis reports. There are fourteen (14) critical conditions, listed in Table XIV, which envelope the inner wing box structure by producing maximum internal element loads. These load conditions have three sources:

- o Original C-141 design conditions,
- o Load conditions resulting from transporting the Minuteman Missile, and
- o Final loads developed from measured C-141 flight test data.

Most of the conditions consist of six component loads, i.e.,  $P_x$ ,  $P_y$ ,  $P_z$ ,  $M_x$ ,  $M_y$ , and  $M_z$  given at regular spanwise intervals along the inner wing box. To be applicable to finite element analysis methods, these beam type loads were converted to grid point loads by a project panel point loads computer program. All the resulting grid loads conditions were found to be balanced.



TABLE XIV

## CRITICAL LOAD CONDITIONS: C-141A INNER WING

STRESS CONDITION NUMBER	EXTERNAL LOADS DATA		N <sub>z</sub> @ C.G.	GROSS WEIGHT (LB.)	V <sub>e</sub> (KTS)	MACH NO.	FUEL WEIGHT (LB.)
	CASE NUMBER	DESCRIPTION					
3NPM15*	3MWM15	SYM. MAN. CLEAN WING	2.5	316,100	355	.825	111,475
3MF104	3MF104	SYM. MAN. $\delta F = 45^\circ$	2.0	213,520	183	.410	8,900
MT0026	MT0026	SYM. MAN. $\delta F = 35^\circ$	2.0	213,520	200	.302	8,900
IAM352*	CASE 5	ABRUPT MANEUVER	0	236,600	390	.90	31,980
IMW992*	IMW992	2.0 G TAXI	2.0	284,640	0	.2	150,020
JACK.*	WING JACK	ANY JACKING CONFIG.	1.33	257,500	0	0	52,880
MIPM33	MIPM33	SYM. MAN. CLEAN WING	2.5	300,600	355	.825	79,300
MIPM35	MIPM35	SYM. MAN. CLEAN WING	2.498	300,600	364	.850	79,300
MST032*	MST032	SYM. MAN. CLEAN WING	2.5	300,600	364	.825	79,300
MIR16R	MIAR16R	POS. ACCEL. ROLL (CLEAN)	2.0	230,198	392	.850	8,900
MIR39R	MIAR39R	POS. ACCEL. ROLL (CLEAN)	2.0	300,600	364	.850	79,300
MPC323	MPC323	SYM. MAN. (CLEAN)	2.5	316,100	392	.850	111,480
MPC324	MPC324	SYM. MAN. (CLEAN)	2.5	316,100	369	.825	111,480
RPC305*	RPC305	NEG. CHECKED ROLL (CLEAN)	2.0	316,100	378	.850	111,480

\* THE C-141 WING WAS STATICALLY TESTED TO ULTIMATE LOADS FOR THESE CONDITIONS.



### 7.1.2 Internal Loads Analysis

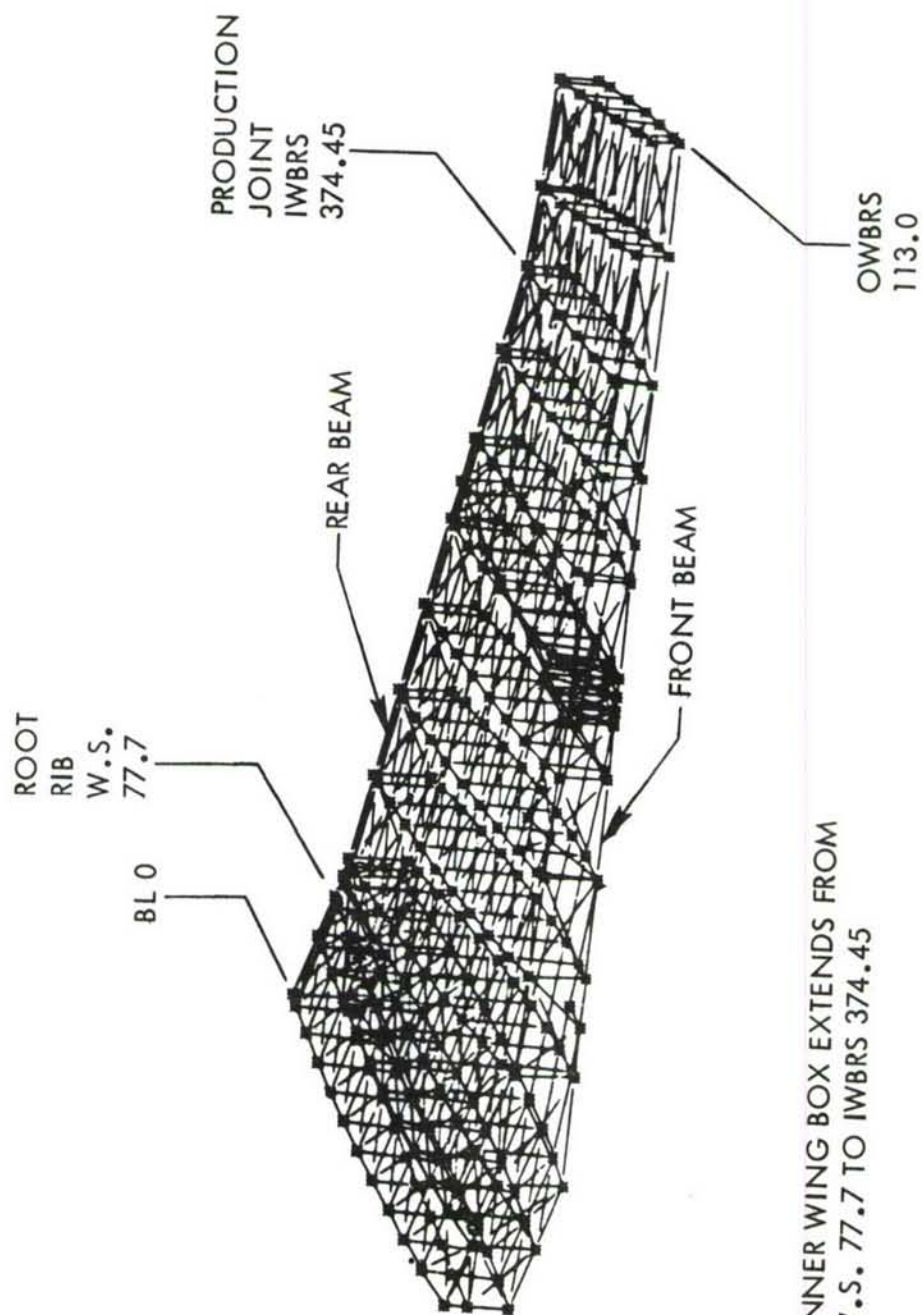
The original C-141 wing internal loads were computed by the unit beam method. This method is essentially a computerized engineering beam theory analysis which uses modified areas to account for sweep effects. Internal loads for the stress analyses of the ADP designs were predicted by finite element methods.

Lockheed-Georgia's general finite element structural analysis and matrix extraction system of computer programs, FAMAS, and the computer graphics facilities were used to construct and analyze the three-dimensional model of the ADP inner wing box.

A computer graphics display and plot of the basic model is shown on Figure 42. This plot is representative of the interactive computer graphics applications which permitted 1) visual identification of model geometry and property errors and 2) immediate correction of these errors on the model's permanent data files. Thus, erroneous analyses were entirely eliminated, and turn-around times were reduced since use of data handling personnel - keypunch and program set-up - was minimized.

As shown in Table XV, the basic model consists of 328 nodes, 1230 structural elements, and has 940 degrees of freedom. It includes a representation of all wing box structure from the centerline of the fuselage to 113 inches outboard of the end of the inner wing box. This basic model was analyzed by FAMAS Program 97 - a large order displacement method program. The chordwise and spanwise stress distributions obtained from the "FAMAS" analysis (based on the baseline box element areas) compared quite well with those of the unit beam analyses for these same load conditions. This comparison supplied confidence in the grid loads conditions and the finite element model description.

Chordwise optimization of surface panel material distribution was accomplished through a modification of the basic model. In essence this second analysis optimized the distribution of the bending areas in the chordwise box cross-section to maximize box stiffness and minimize the chordwise variation in margins of safety from the front to the rear spar. Extreme care was taken to ensure gradual tapering of the spanwise elements to prevent erratic changes in end loads with the resulting large shears and element stresses. The internal loads resulting from this modified model were used for all the subsequent ADP designs.



NOTE: INNER WING BOX EXTENDS FROM W.S. 77.7 TO IWBR 374.45

FIGURE 42 FINITE ELEMENT MODEL: CARGO/TANKER STUDY

TABLE XV  
FAMAS FINITE ELEMENT MODEL DESCRIPTION  
(328 NODES, 940 DEGREES OF FREEDOM)

<u>GROUP</u>	<u>ELEMENT TYPE</u>	<u>NUMBER</u>
STRINGERS	AXIALS	291
RIB CAPS	AXIALS	293
STIFFENERS	AXIALS	199
SPAR WEBS	QUAD SHEAR PANELS & TRIANGULAR MEMBRANES	37
RIB WEBS	QUAD SHEAR PANELS & TRIANGULAR MEMBRANES	152
COVERS	QUAD SHEAR PANELS & TRIANGULAR MEMBRANES	258
		<hr/>
TOTAL		1230



### 7.1.3 Structural Optimization

Structural optimization analyses were conducted throughout the design phase for all of the most promising design configurations. These analyses not only considered design loadings, but also practical geometric limitations such as constant stringer heights and minimum skin gages. Loads for the optimization studies were taken from the internal loads analysis of the basic three dimensional model. For structure non-critical in compression, optimization analyses determined stringer pitch, stringer height, area distribution between skin and stringer, and other variables significant in minimizing cost as well as weight.

ASOP (Automated Structural Optimization Program) was used for the detail analysis of the structure surrounding the nonstructural access doors of the upper surface. "FAMAS" internal loads were used to load the boundary nodes of the ASOP finite element model. Figure 43 shows a typical region of structure and the detail modeling in ASOP to optimize cover material around and immediately adjacent to an upper surface cutout. Some 170 nodes (Reference Table XVI), 240 axial elements, 138 triangular membranes, and 70 quadrilateral membranes define structural members to the detail required for accurate determination of stresses around the cutout. This made possible precise tailoring of material requirements, particularly those resulting from fatigue.

Ribs were optimized by using a two-dimensional graphics finite element analysis. Figures 44 and 45 present results from a typical rib analysis. Figure 44 shows rib scale geometry, element axial loads, and bending moments. Figure 45 presents the internal loads in a typical rib element as well as the rib element flange stresses and shear flows. The graphical displays permit rapid changes in configuration, loads, and stress sizing. Computations are performed in real time and the results are displayed immediately. After the analysis is completed, a printed copy is obtainable.

The optimization of the cover panels is interrelated to the FAMAS analysis. An optimized element was required to not only withstand a certain load level but to do so at a stress level compatible with the FAMAS analysis. This relationship was maintained for all configurations. Table XVII summarizes the design compression



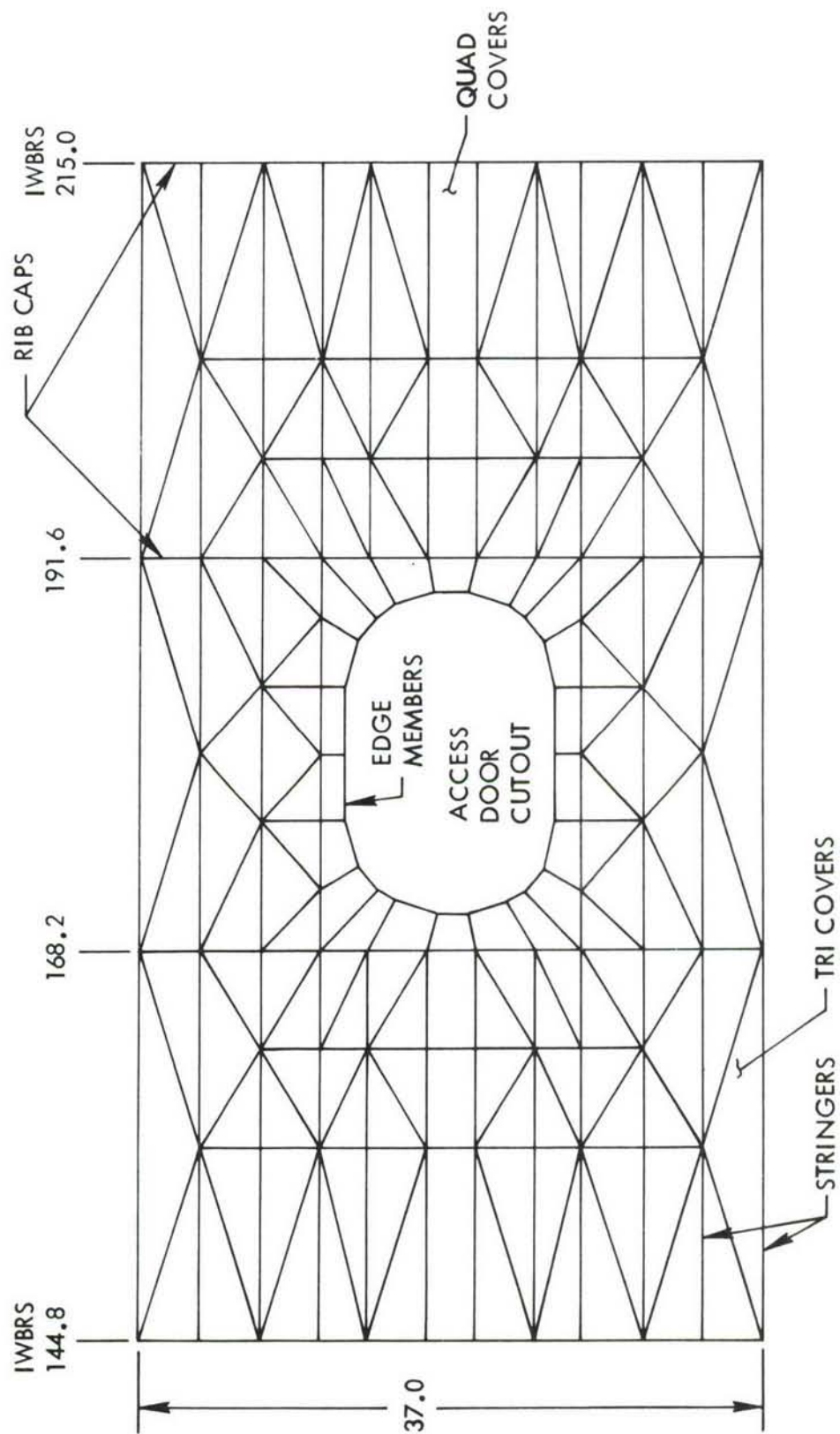
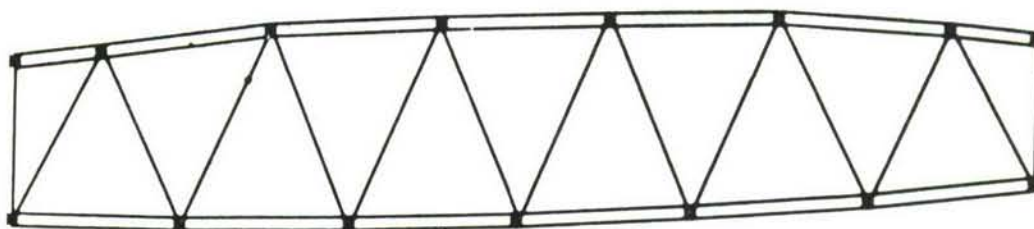


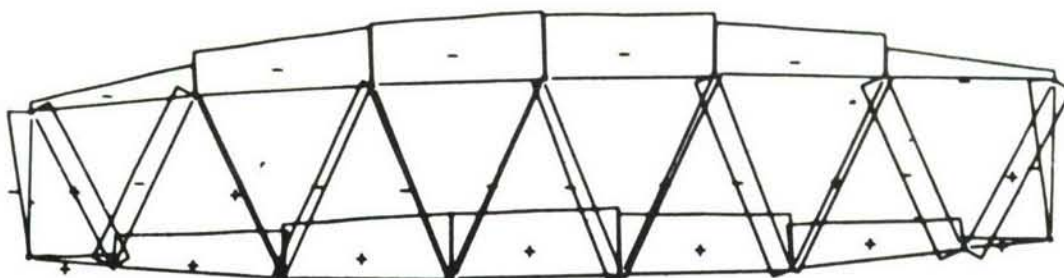
FIGURE 43 DETAIL CUTOUT ANALYSIS MODEL GEOMETRY

TABLE XVI  
DESCRIPTION OF ASOP MODEL OF TYPICAL ACCESS DOOR  
(170 NODES)

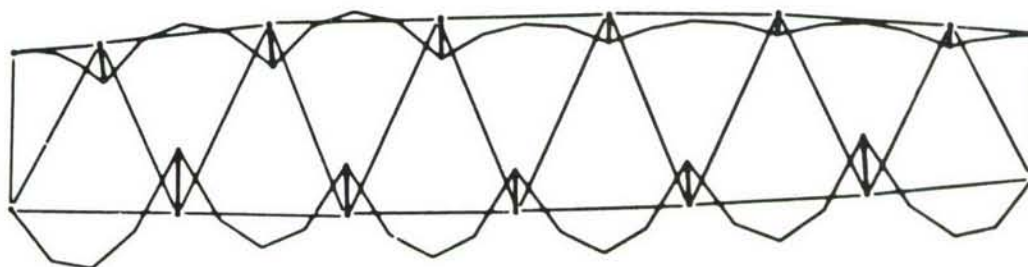
<u>ELEMENT TYPE</u>	<u>NUMBER</u>
AXIAL ELEMENTS	240
TRIANGULAR ELEMENTS	138
QUADRILATERAL MEMBRANES	<u>70</u>
TOTAL	455



MODEL GEOMETRY



AXIAL LOADS



BENDING MOMENTS

FIGURE 44 TYPICAL RIB GEOMETRY AND INTERNAL LOADS

ELEMENT NO. 10

LD. CASE NO. 1

V = -466.4

E = 0.1050+08

V = 571.6

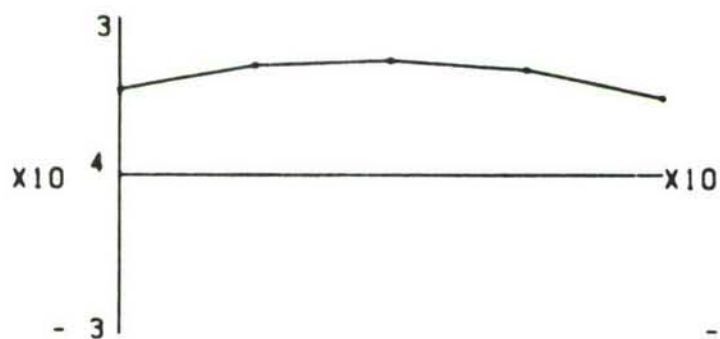
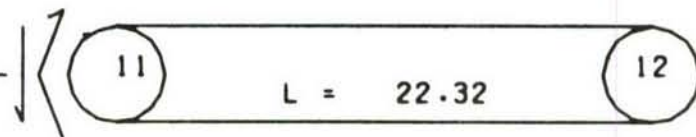
P = 1.4736+04

L = 22.32

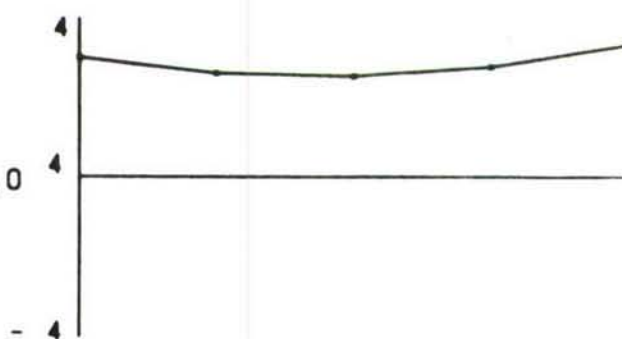
P = 1.5264+04

M = 3141.

M = -4315.

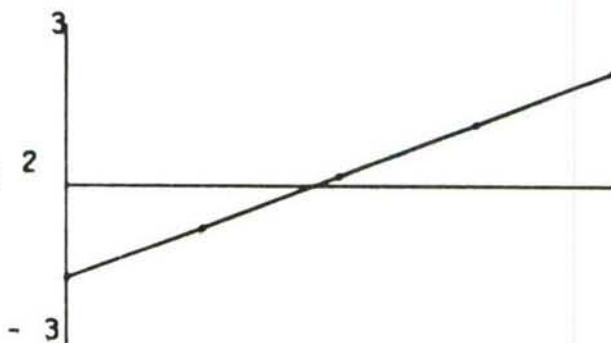


UPPER FLANGE



LOWER FLANGE

AREA = 0.6400 x10<sup>2</sup>  
CU = 1.350  
H = 2.700  
I = 0.6300



SHEAR FLOW , V/H

AREA = 0.6400  
CU = 1.350  
H = 2.700  
I = 0.6300

FIGURE 45 TYPICAL RIB ELEMENT INTERNAL LOADS AND STRESSES



TABLE XVII  
SURFACE COMPRESSION LOADS

	<u>N<sub>x</sub> (KIPS/INCH): ULTIMATE</u>		
	<u>LOW</u>	<u>HIGH</u>	<u>MEAN</u>
<u>UPPER SURFACE</u>			
IWBRS 51	10	15	14
IWBRS 330	12	15	14
<u>LOWER SURFACE</u>			
IWBRS 51	9	12	11
IWBRS 330	8	11	10

load intensities obtained from the internal loads. The range of ultimate compression loads across the chord in KIPS/inch are shown at two representative stations for both upper and lower surfaces. It is seen that design compression load intensities do not vary much in the spanwise direction for either surface. In fact, there is more variation in the chordwise direction at any given station. This table also shows that downbending  $N_x$  values are approximately 70% of the corresponding upbending values. Shears are in the 2000-3000 pound/inch range.

A series of stringer/panel optimization computer programs tailored to consider weldbond hats, "A" section extrusions, and unflanged stiffened skins were used to do the cover optimizations. Figure 7 presents typical results of cover design optimization. The curves represent different materials and configurations including several types of plate/stringer configurations as well as integrally stiffened and sandwich designs. The ordinate of the curves is equivalent thickness, T-Bar, which includes all surface structure (stringers as well as skin). The abscissa is  $N_x$  compression loading in kips per inch. These curves include the effects of representative shear and pressure loadings, as indicated in the upper portion of the graph, as well as some practical design limitations.

#### 7.1.4 Stress Analysis Summary

Stress analyses were performed for all candidate configurations. Structure components were sized to develop the same allowable loads as the baseline while not exceeding the allowable stresses governed by either the static strength or the fatigue and damage tolerance thresholds. With the exception of the upper surface for the Weldbond, Monolithic and Tapered Shingles configurations, all cover structure is critical for either fatigue or damage tolerance requirements. Both surfaces of the Hat Stringer configuration, the lower surface of the Monolithic configuration, and the inboard portion of the lower surface of the Weldbond configuration are fatigue critical while the remainder of the cover configurations are critical for damage tolerance. All chordwise joints are fatigue critical.

Relative to the exception noted above, the upper covers of the Weldbond and Monolithic configurations are compression critical. This results from the lower compression capability of the "A" stringer of the Weldbond configuration and the lower strength of the 2219 aluminum material for the Monolithic configuration. The Weldbond configuration which is one of the recommended designs has a slight weight penalty in the upper cover. However, this penalty is offset by the elimination of the shear clips which attach the rib caps to the surfaces.

The Tapered Shingle configuration utilized single riser net extruded panels tapered such that no risers run out along the front spar. This taper is obtained by routing the skin flange, a much less costly process than machining the entire extrusion. Utilization of tapered net extrusions results in a steadily increasing T-bar thickness in the spanwise direction as the risers converge. This results in final T-bar thicknesses greater than those required for structural requirements. This weight penalty is accepted, however, in order to gain the large cost savings from use of the net extrusion. Consequently, in this design, the root stresses are governed by fracture, but the remainder of the span is credited to cost-controlled design. For the upper surface, the weight penalty is 220 pounds. On the lower surface, the compression load intensity is sufficiently low to allow both a thin and a thick skin dimension in the panel. By routing the thick dimension to obtain the spanwise taper, the increase in T-bar is minimized such that the excess weight in the lower surface is insignificant.

The Weldbond, Virgin Plank and Tapered Shingle configurations are the designs recommended for further study during the follow-on program. Figure 46 presents a pictorial view of the surface for these designs. From these, it can be readily seen which structure of the upper and lower surfaces is critical for compression, fatigue, fracture, and cost design.

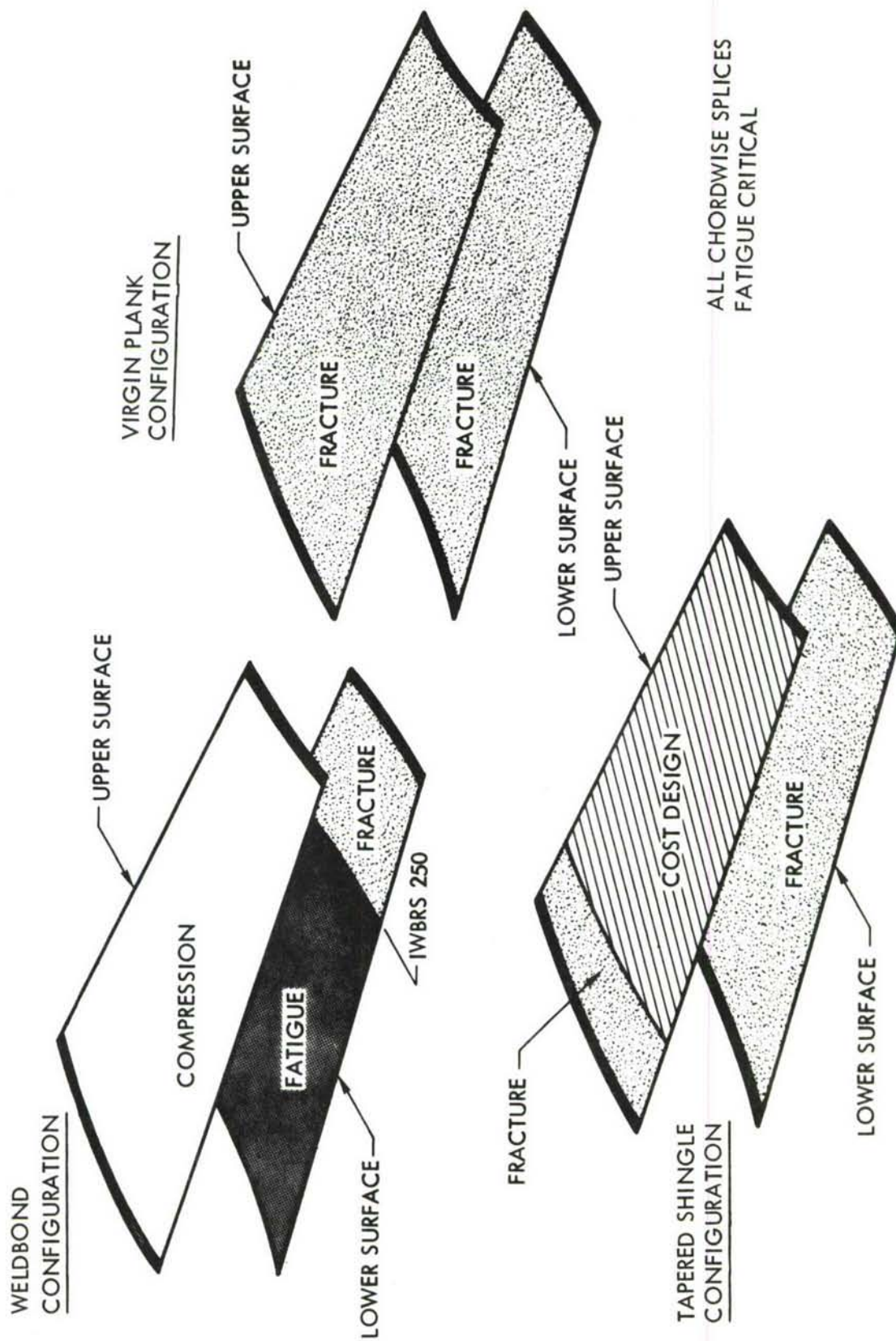


FIGURE 46 GOVERNING DESIGN CRITERIA



Maximum spanwise stress levels for the baseline update and the three recommended configurations are given in Figures 47, 48, 49, and 50. For each configuration, the actual tension and compression stresses are given. For comparison purposes, the fatigue and damage tolerance threshold stresses as well as the compression allowable stresses are presented. By comparing these curves, the relative criticality of each allowable can be visualized for each configuration. Figure 51 presents a typical chord-wise stress distribution at Sta. 168.2 which indicates the variation of stress between the front and rear beam. Figures 52, 53, and 54 give the T-bar distribution of the cover material for each configuration which is compatible with the stress levels previously given.

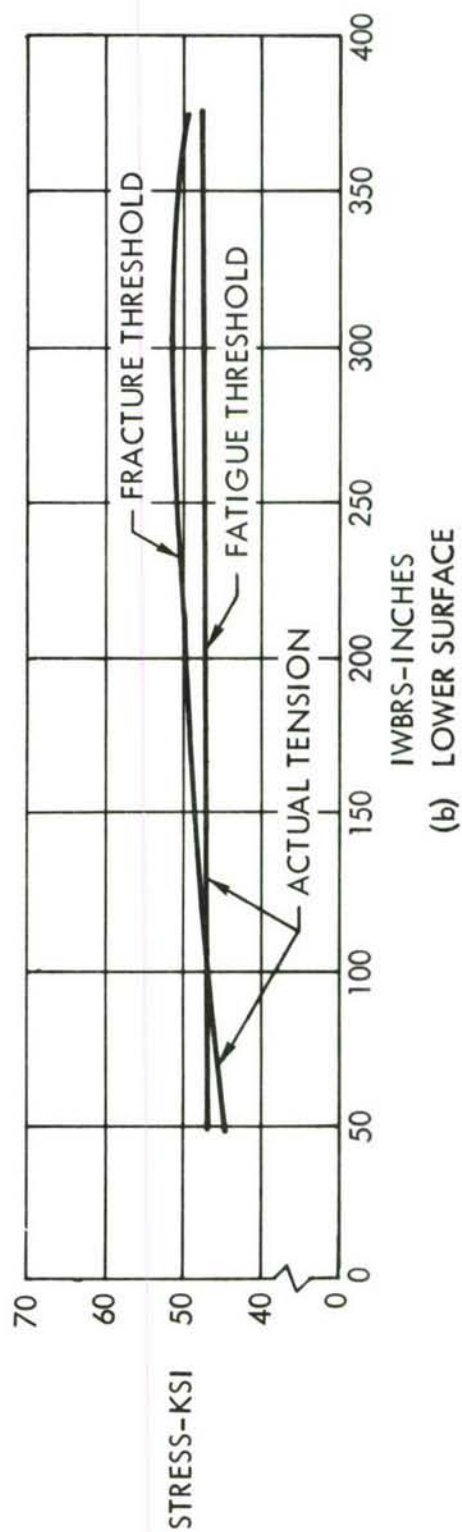
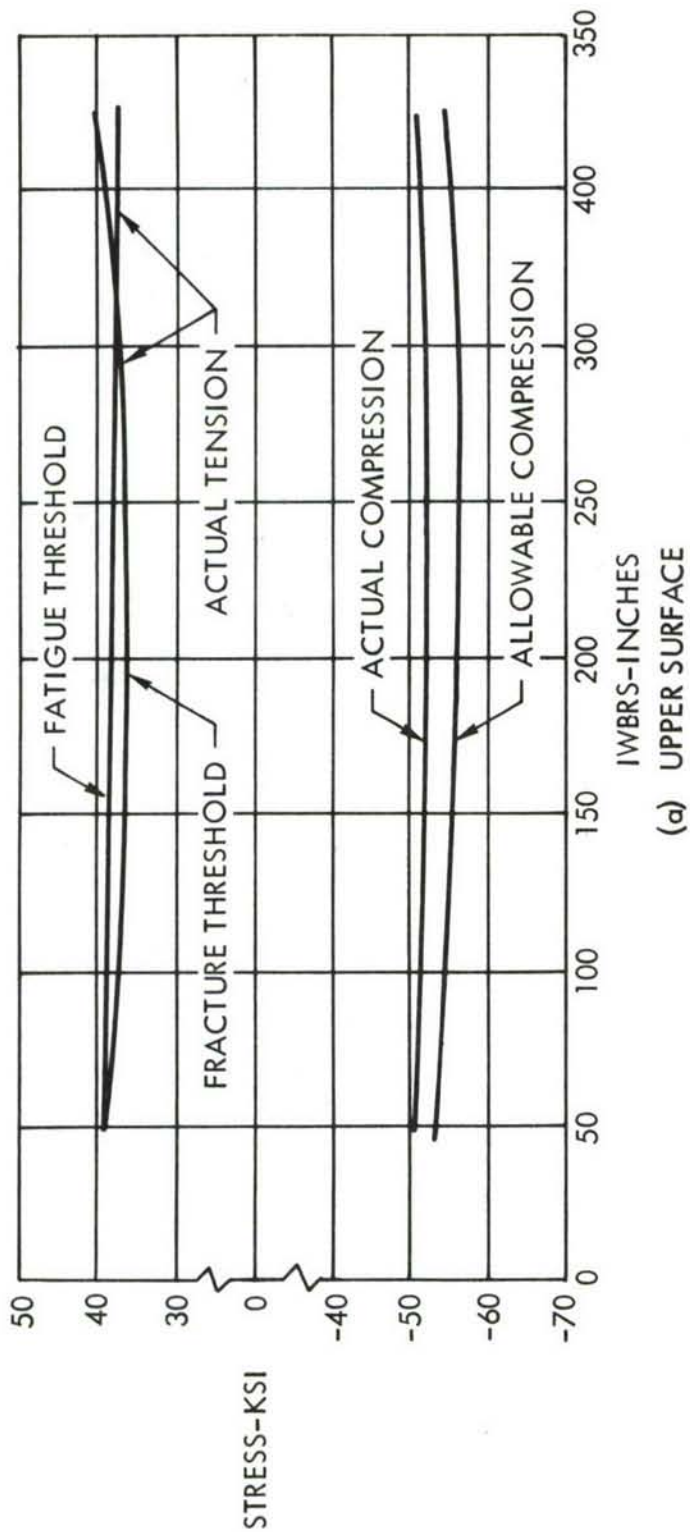


FIGURE 47 SPANWISE STRESS LEVELS - BASELINE UPDATE

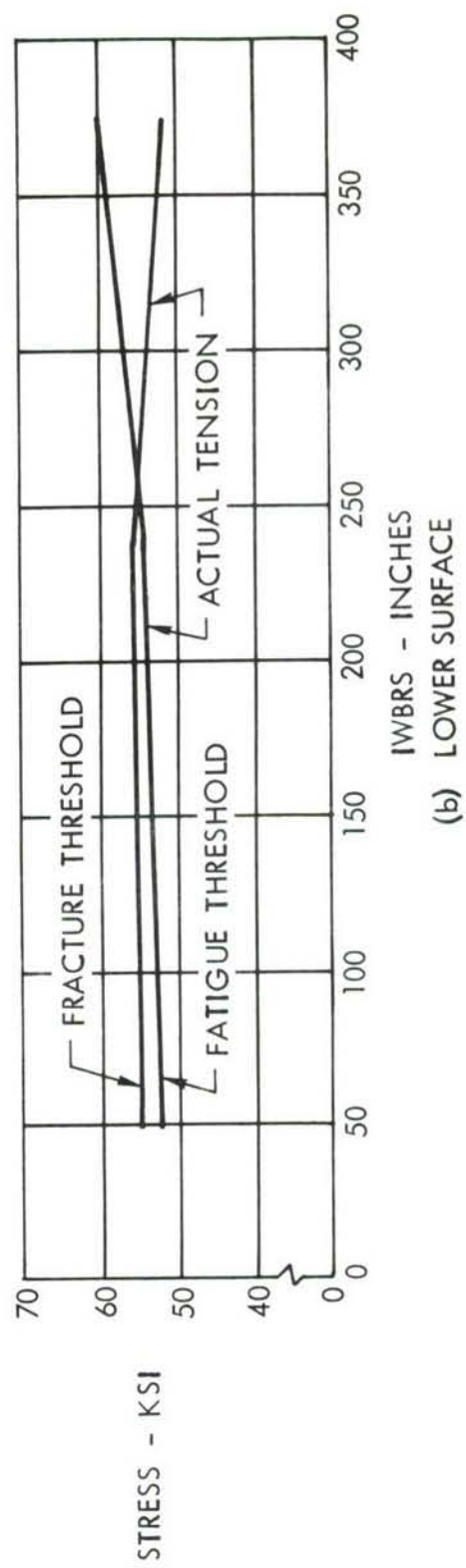
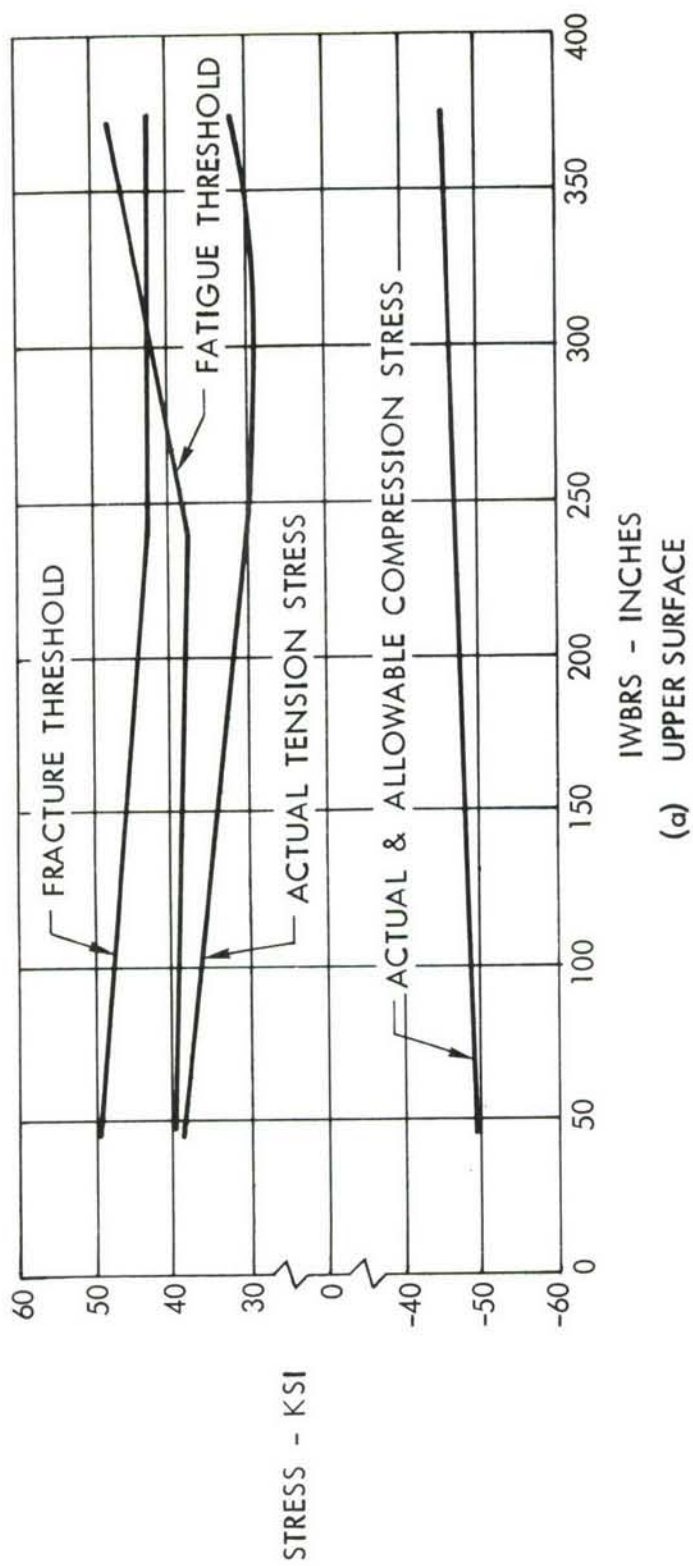


FIGURE 48 SPANWISE STRESS LEVELS - WELDBOND CONFIGURATION

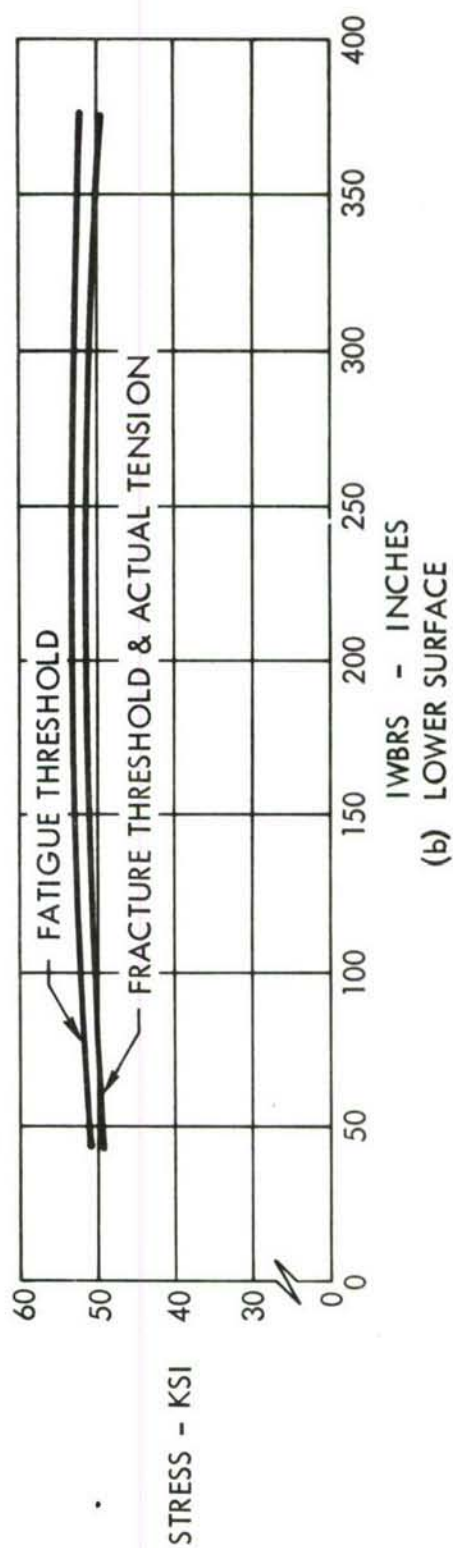
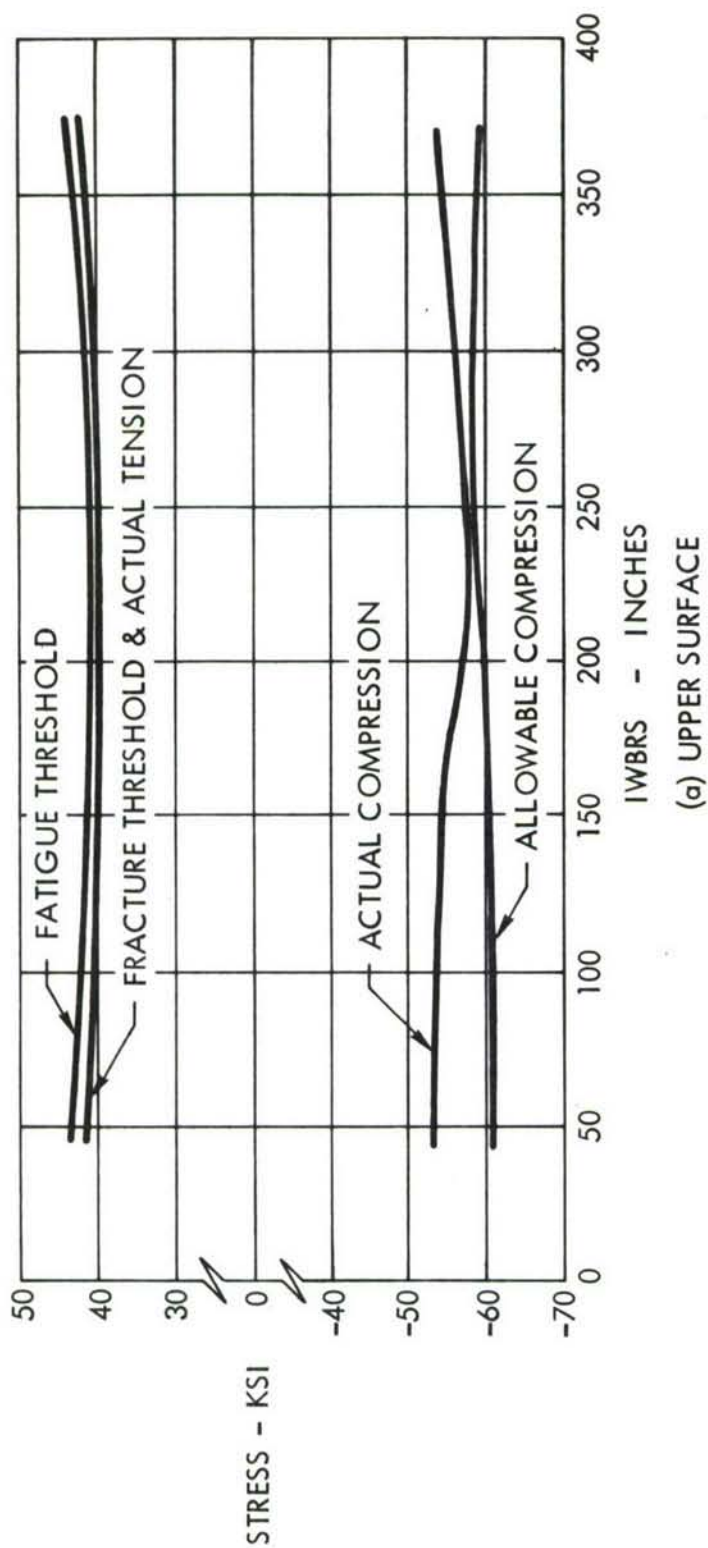


FIGURE 49 SPANWISE STRESS LEVELS - VIRGIN PLANK CONFIGURATION



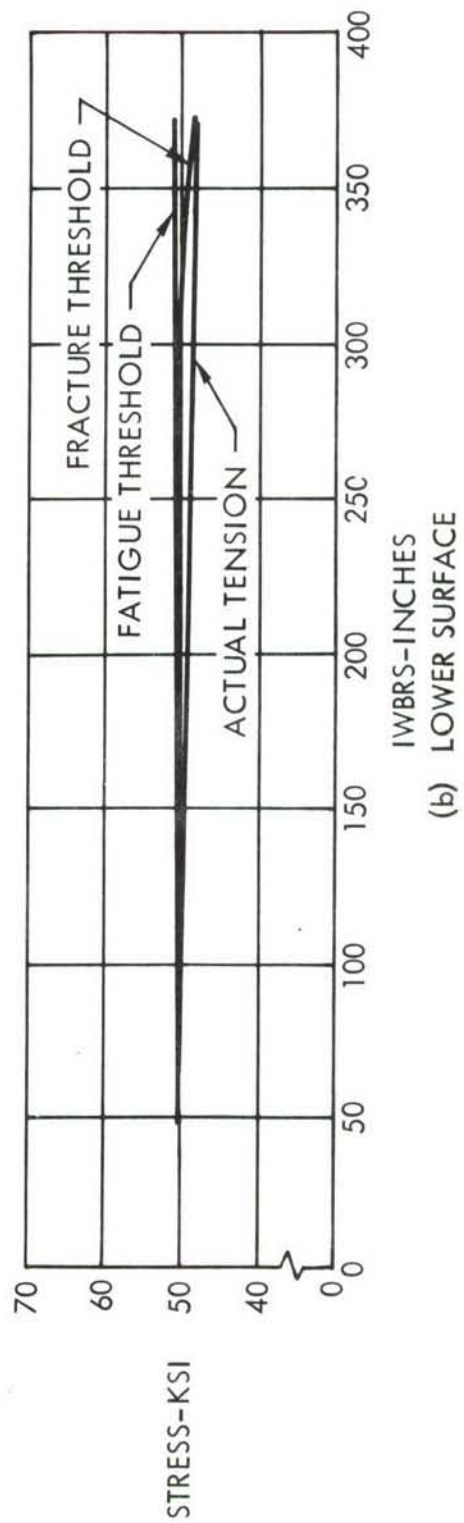
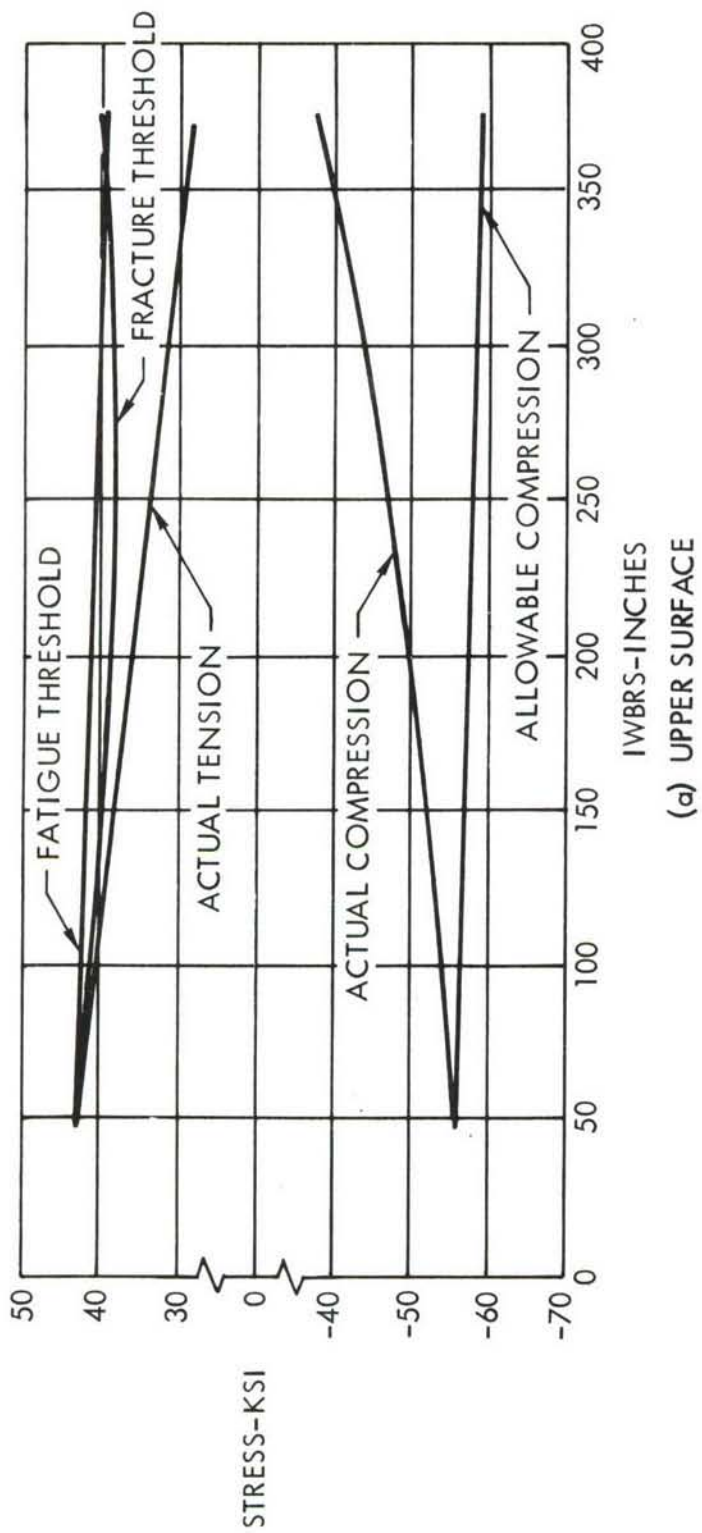
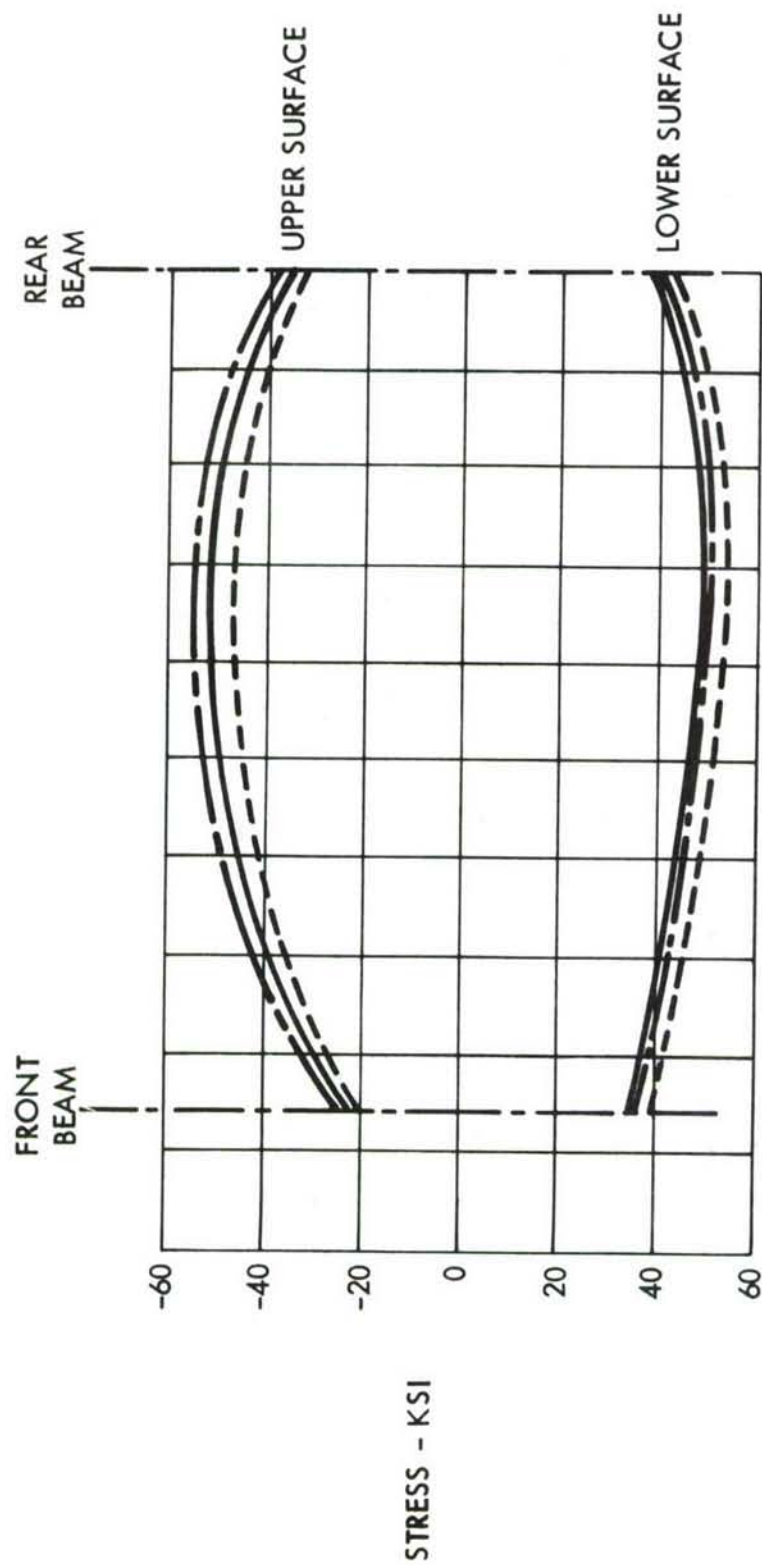


FIGURE 50 SPANWISE STRESS LEVELS - TAPERED SHINGLE CONFIGURATION



STA 168.2, CONDITION M1 PM33

FIGURE 51 TYPICAL CHORDWISE STRESS DISTRIBUTION

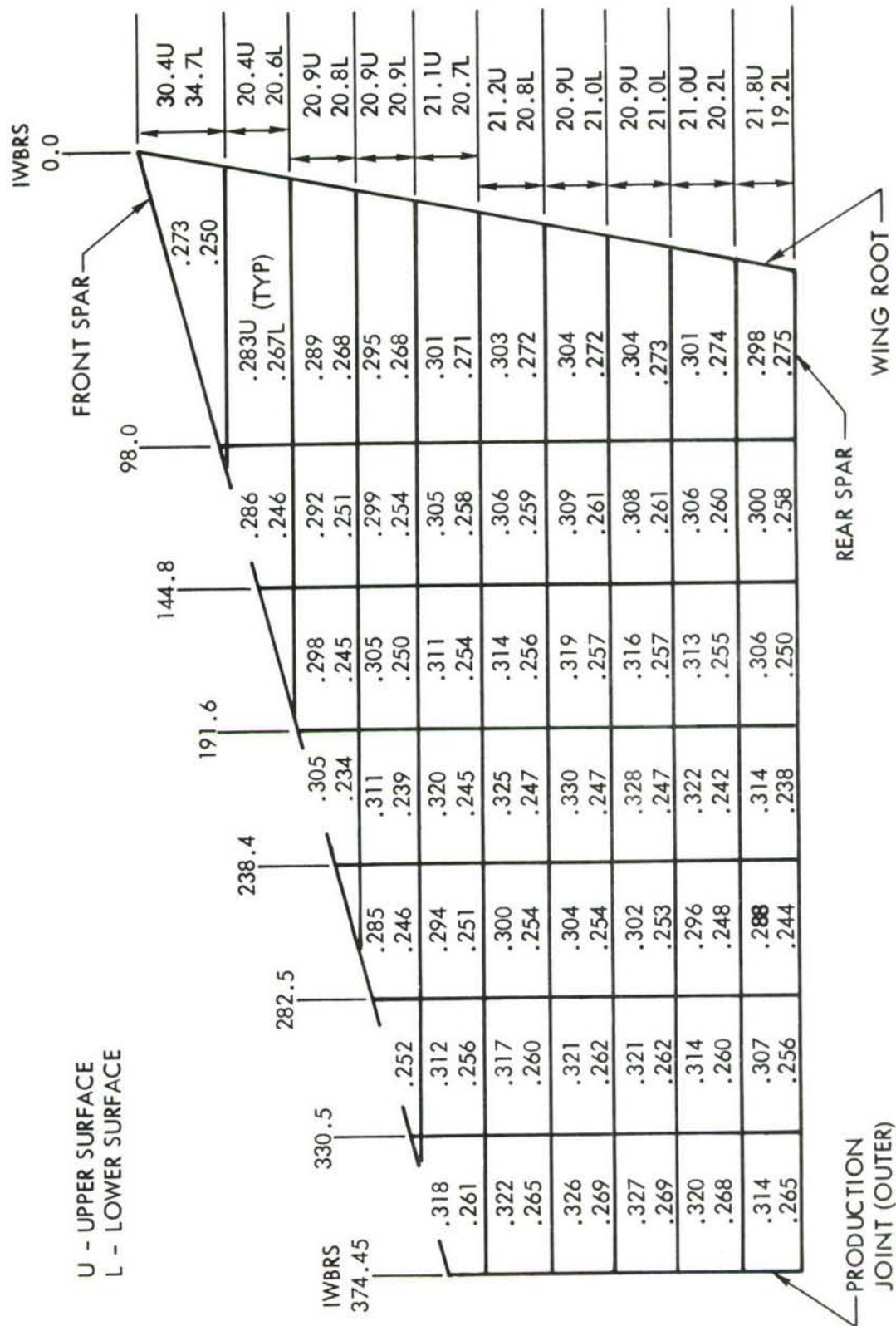


FIGURE 52 SURFACE T-BAR DISTRIBUTION - WELDBOND CONFIGURATION

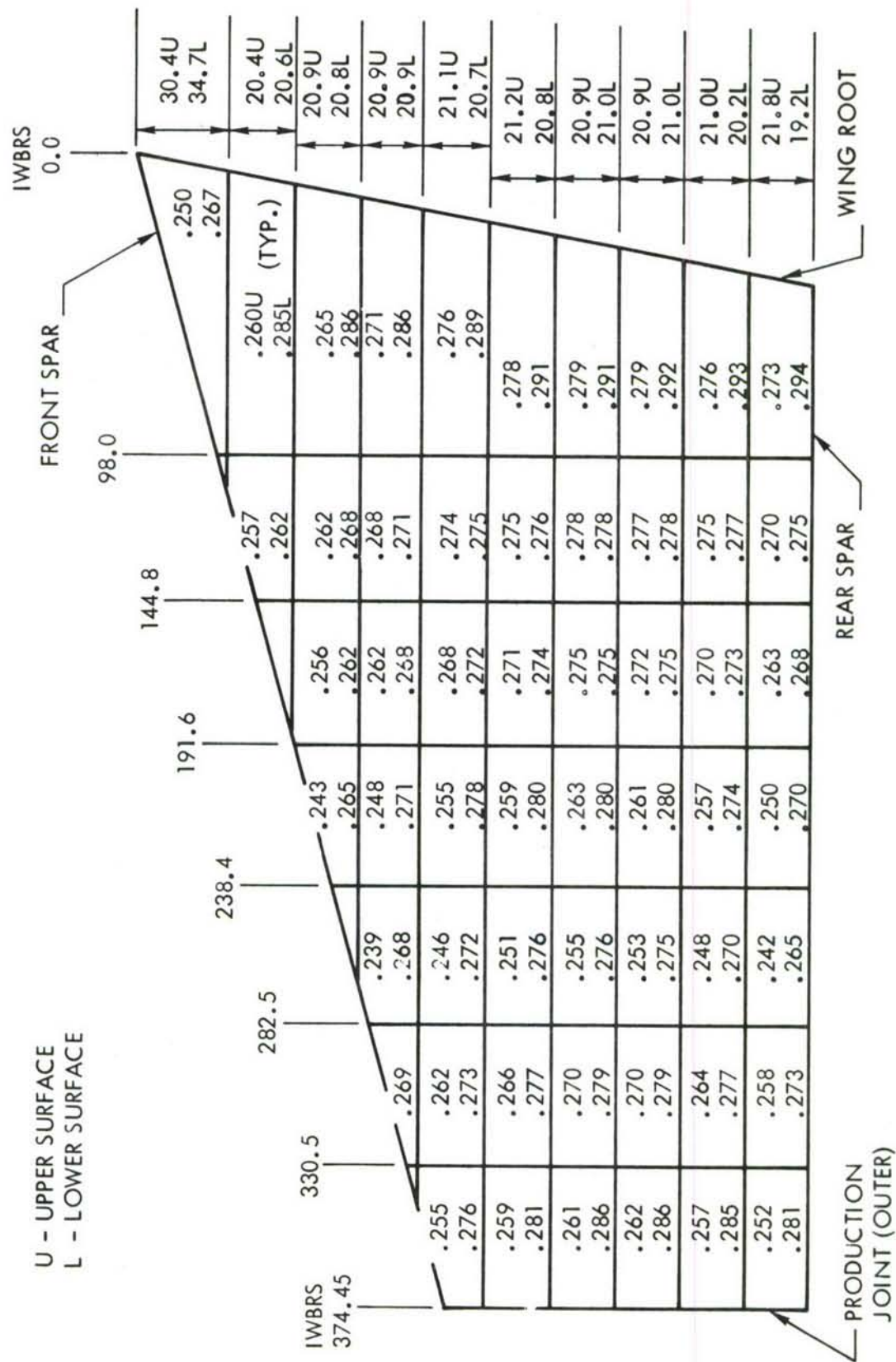


FIGURE 53 SURFACE T-BAR DISTRIBUTION - VIRGIN PLANK CONFIGURATION



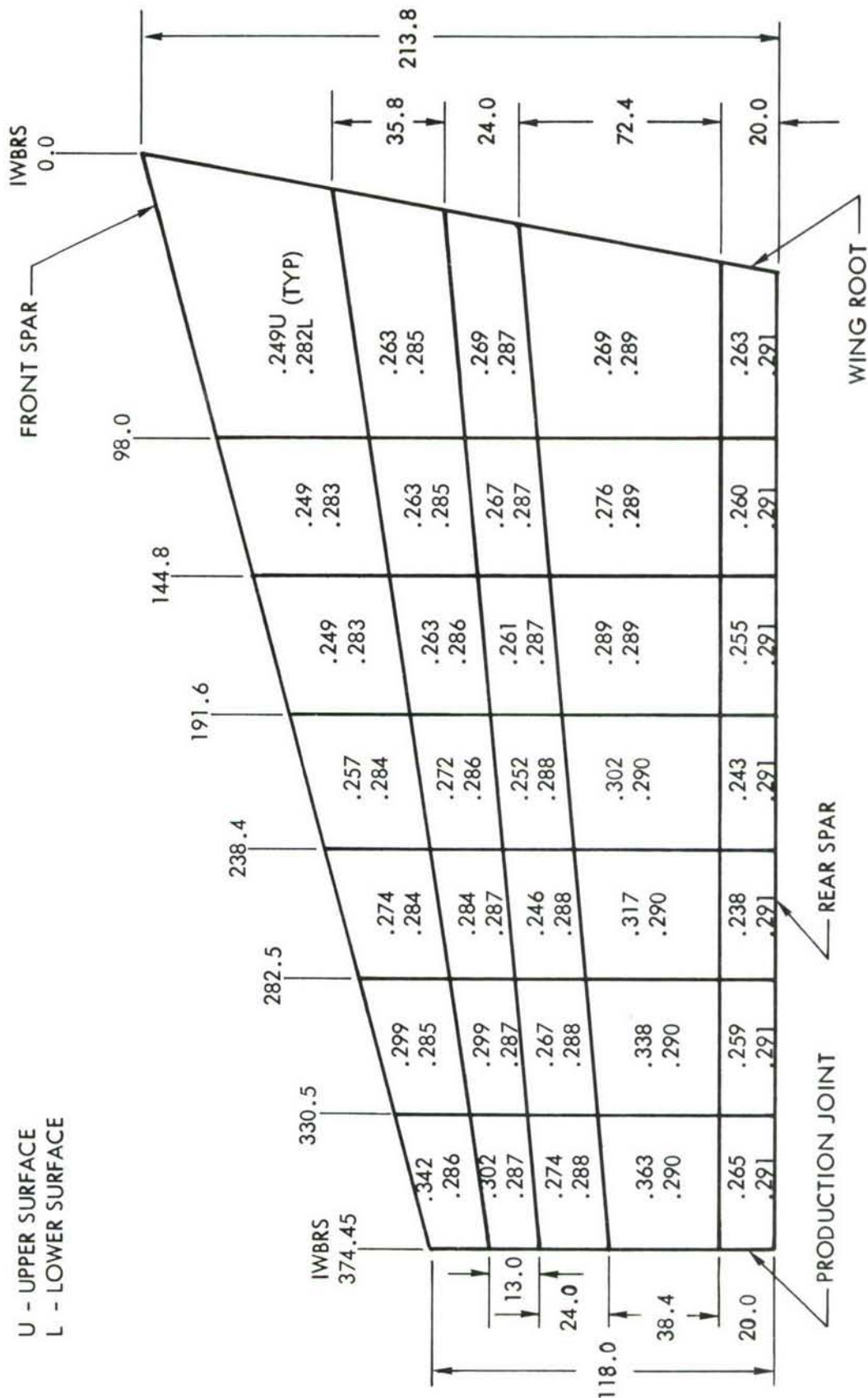


FIGURE 54 SURFACE T-BAR DISTRIBUTION - TAPERED SHINGLE CONFIGURATION

## 7.2 WEIGHT ANALYSIS

The weights predicted for the updated baseline and ADP configurations were based on C-141 actual weights. For those configurations which closely resemble the C-141 construction, i.e. integral stiffener or skin/stringer construction, C-141 known weight factors provided a very reliable method of prediction. For the composite and honeycomb designs, weight factors experienced for similar construction on prior programs were used.

### 7.2.1 Updated Baseline Weights

For convenience and efficiency, the wing box was subdivided into several spanwise segments which coincided with the FAMAS finite element model. The weight of each segment was calculated by multiplying the C-141 actual weight by the ratio of updated tension allowables (governed by fatigue and fracture criteria) to the tension allowables taken from C-141 stress reports. Weight differences which resulted because of material changes were calculated by the ratio of appropriate material allowables.

### 7.2.2 ADP Configuration Weights

To predict weights for the ADP designs it was necessary to calculate non-optimum factors. These were found by taking the required stress areas from C-141 stress reports and integrating them over each segment to find optimum weights. The ratio of C-141 actual weights to these optimum weights are non-optimum factors. These factors account for machine tolerances, splice and hole beef-ups, and other miscellaneous manufacturing characteristics. Since most ADP configurations were similar to the baseline (integral or skin-stringer aluminum) these factors were applied to the optimum weights. Additional non-optimum factors (10%) were applied to Ti-graphite configurations to account for residual stresses. The honeycomb configuration had an additional 25% non-optimum added factor to account for doublers, edge members, potting around holes and core stabilization. Beam caps were analyzed with the

covers as bending material. Beam webs and ribs were done in a similar manner by comparing C-141 actual weights and t-bars with optimized ADP t-bars.

### 7.2.3 Weight Results

Weights for all ADP configurations are given in Table XVIII. Weights for the recommended designs are detailed by component in Table XIX. Bar charts of weight-ratios as compared to the baseline update are given in Figure 55 for ease of visual comparison of weights for all configurations. The weight effects of advanced technology for the three recommended designs are illustrated in Figures 56 through 58. For example, Figure 56 shows the effects on the Weldbond design. Changing the material only from 7050-T76 to 7075-T76 increases the weight of this design 233 pounds. Also, the elimination of the other advanced technology concepts further increases the weight by 1197 pounds. Conversely, the changing of the baseline material to 7050-T76 material, while maintaining all baseline concepts, reduces the weight 273 pounds. Also, the incorporation of the advanced concepts reduces the weight 1157 pounds. The similar effects for the Virgin Plank and Tapered Shingle designs are shown in Figures 57 and 58. Typical main drivers of weight reduction are shown in Figures 59 through 61. On the Weldbond design (Figure 59), for example, the use of weldbond, the "A" section stringer with the resulting elimination of the shear clips, and the advanced aluminum alloys reduces the weight from 4532 pounds to 4093 pounds. A prime contributing factor in this design is the reduction of  $K_T$  from 3.42 to 3.25 with a corresponding increase in allowable tension stresses from 38 KSI to 39.5 KSI. Typical values for the other ADP designs are given in Figures 60 and 61.

TABLE XVIII  
WEIGHT SUMMARY

CONFIGURATION		TOTAL BOX (LB) (ONE SIDE ONLY)
NUMBER	DESCRIPTION	
ORIGINAL DESIGN	INTEGRALLY STIFFENED	6352
BASILINE UPDATE	INTEGRALLY STIFFENED	7012
1	WELDBOND	6415
2	HAT STRINGER	6530
3	LOCKSKIN	6770
4	MONOLITHIC (WELDED)	7120
5	SANDWICH	7700
6	COMPOSITE HAT	6805
7	VIRGIN PLANK	6536
8	TAPERED SHINGLE	6935



TABLE XIX

## WEIGHT BREAKDOWN - ADP DESIGNS

STRUCTURAL COMPONENT	BASELINE		ADP CONFIGURATIONS		
	ORIGINAL DESIGN	1972 UPDATE	#1 WELDBOND	#7 VIRGIN PLANK	#8 TAPERED SHINGLE
UPPER SKINS	1874	2068	1980	1541	1992
LOWER SKINS	1687	1963	1681	1581	1889
FRONT BEAM	385	421	371	367	386
UPPER CAP	50	53	55	46	51
LOWER CAP	137	157	125	134	139
WEB	198	211	191	187	196
REAR BEAM	379	409	399	375	401
UPPER CAP	63	66	76	63	70
LOWER CAP	79	91	82	88	91
WEB	237	252	241	224	240
JOINTS, SPLICES, FASTENERS - UPPER	56	56	46	369	146
JOINTS, SPLICES, FASTENERS - LOWER	78	78	48	386	187
SPANWISE FUEL BULK HEAD	47	48	56	47	56
BL 77.7 RIB	309	311	309	284	309
BL 77.7 SPLICE PLATE & FASTENERS	155	209	198	198	198
IWBR 374 RIB	110	111	123	110	123
RIBS & BULK HEADS	1091	1110	977	1051	1021
SURGE & VENT BOXES	20	20	20	20	20
PYLON FITTINGS	61	61	61	61	61
ACCESS DOORS	39	29	28	28	28
PAINT & SEALANT	61	118	118	118	118
TOTAL BOX (ONE SIDE ONLY)	6352	7012	6415	6536	6935

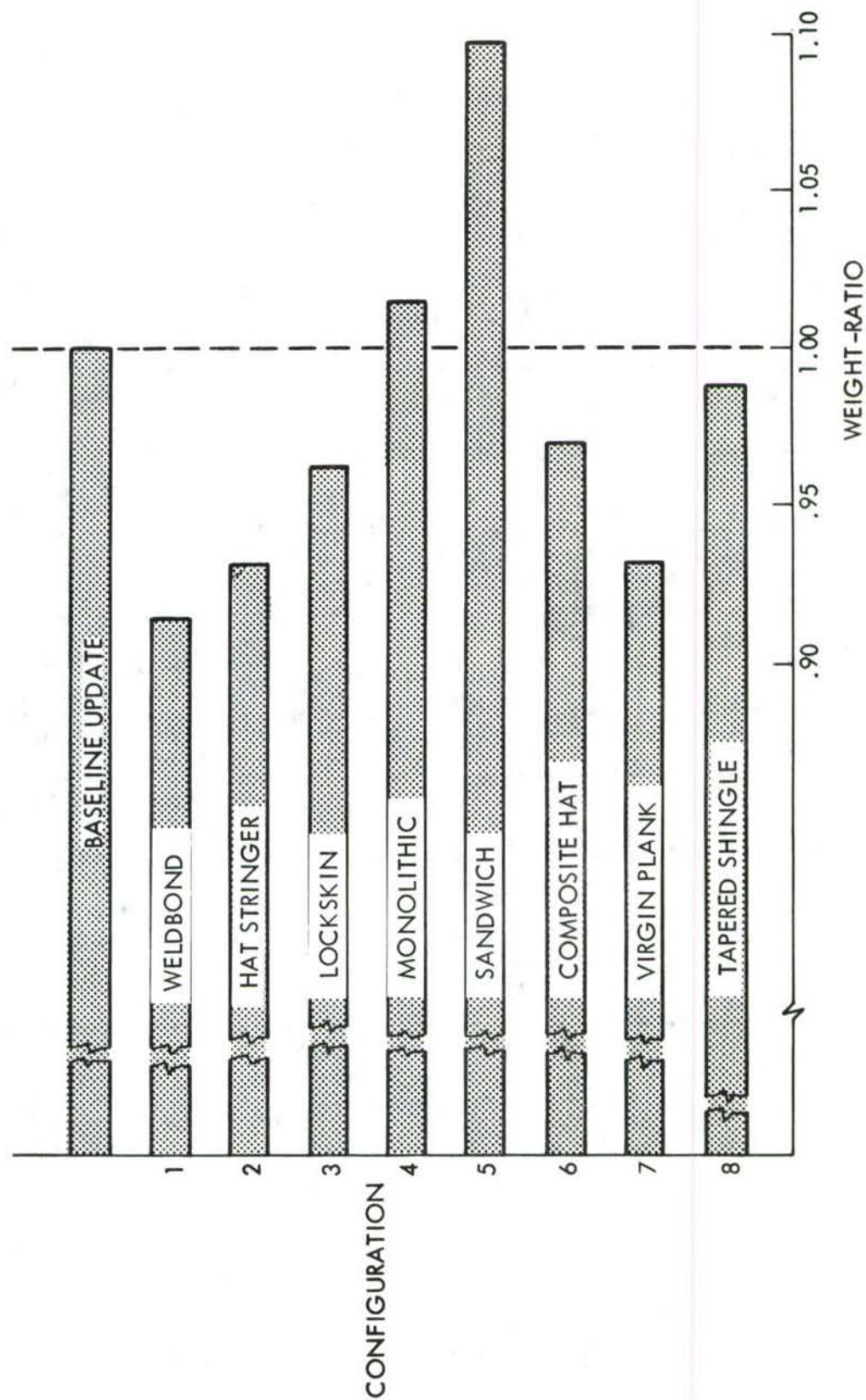


FIGURE 55 WEIGHT-RATIO COMPARISON OF CONFIGURATIONS

# 'A' STRINGER WELDBOND DESIGN

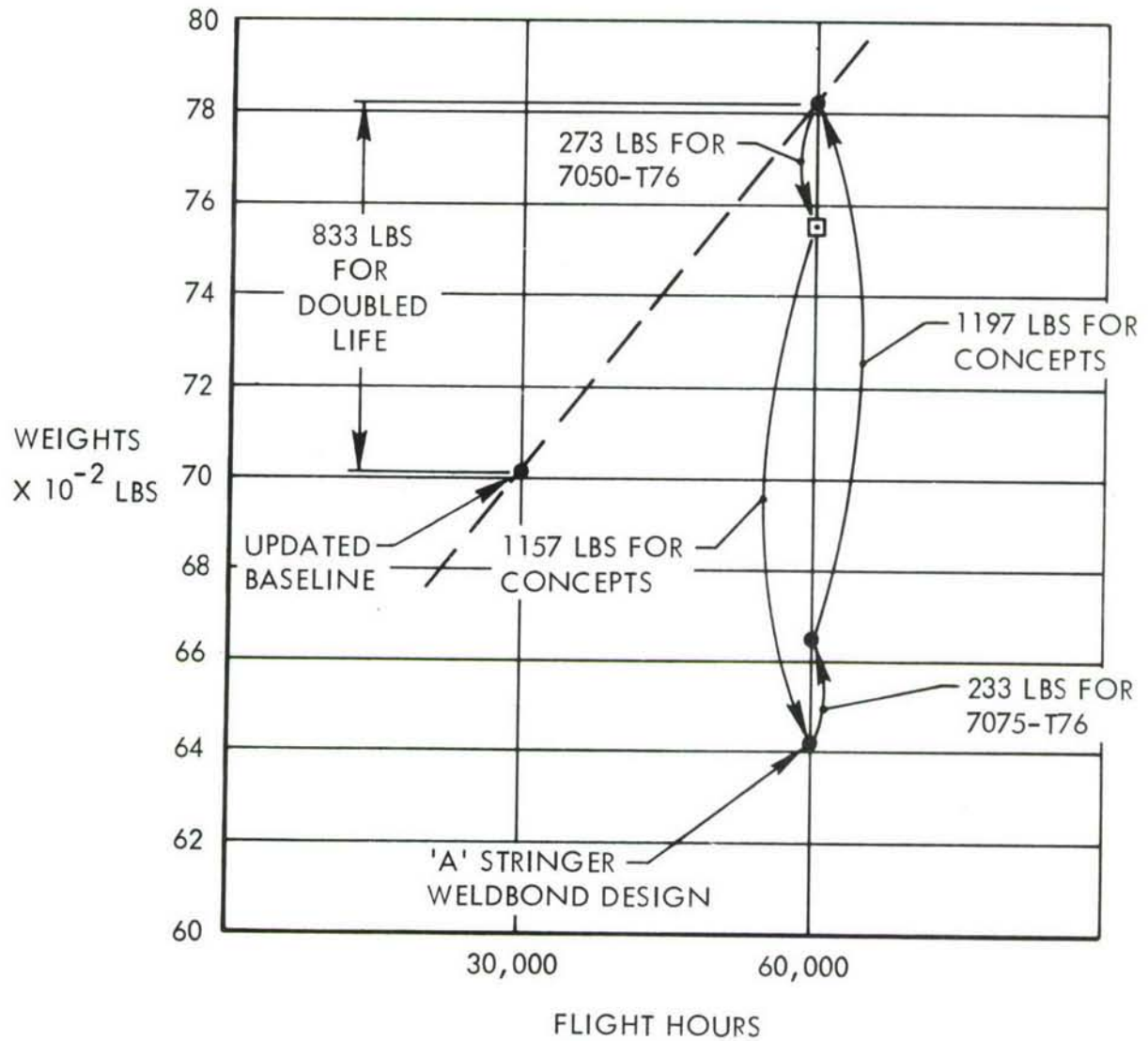


FIGURE 56 WEIGHT EFFECTS OF ADVANCED TECHNOLOGY - 'A' STRINGER WELDBOND DESIGN

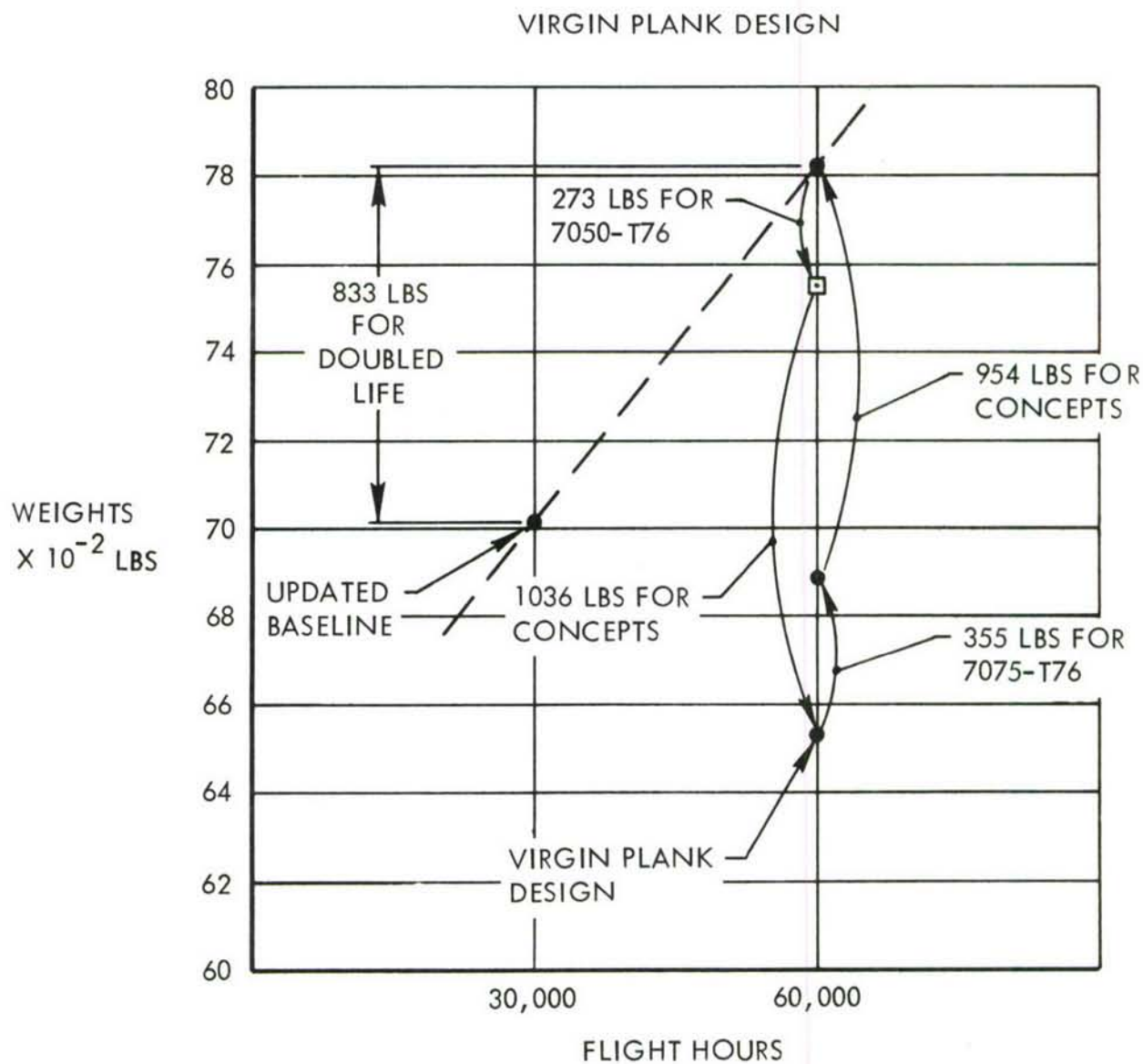


FIGURE 57 WEIGHT EFFECTS OF ADVANCED TECHNOLOGY - VIRGIN PLANK DESIGN



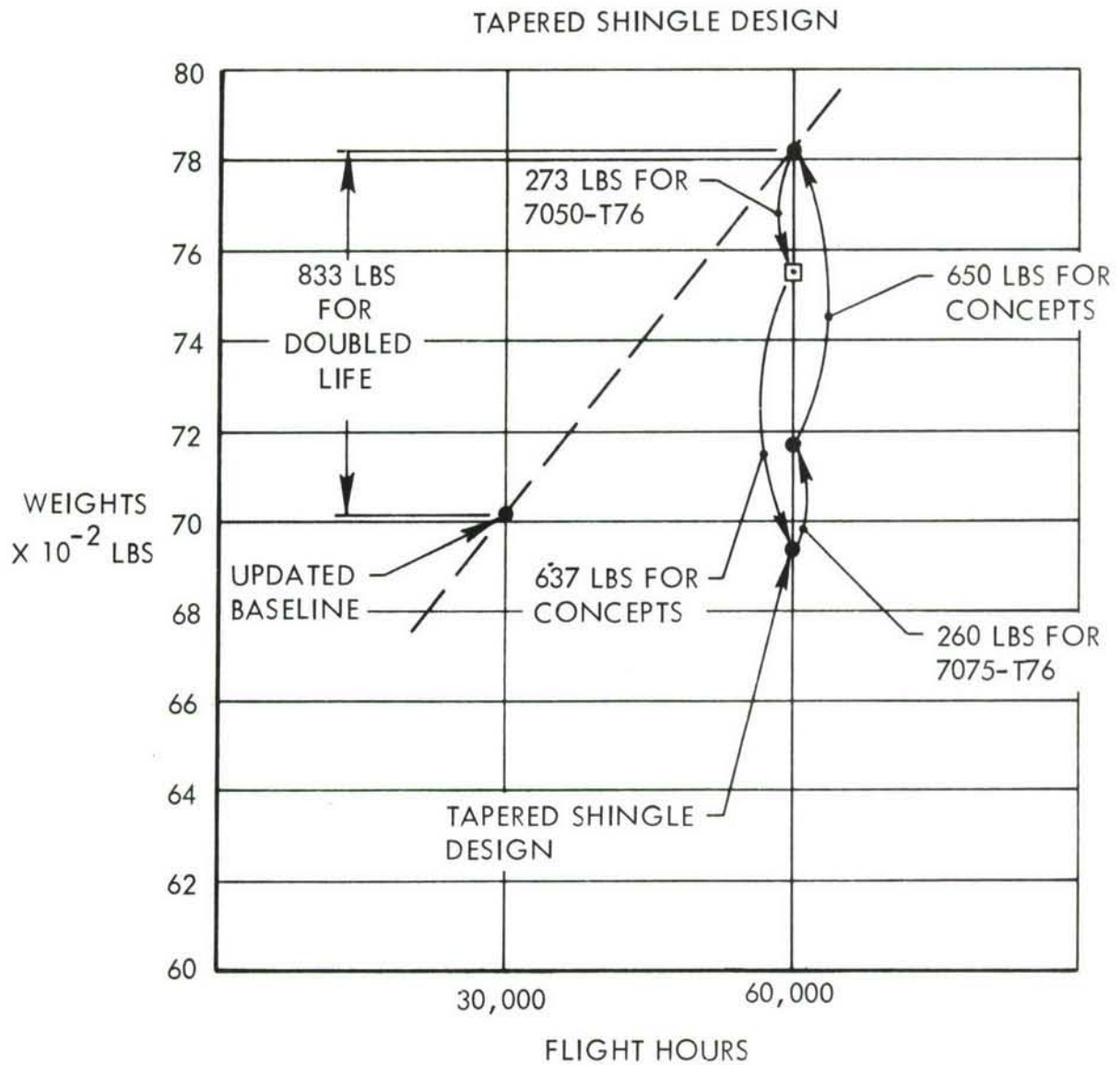
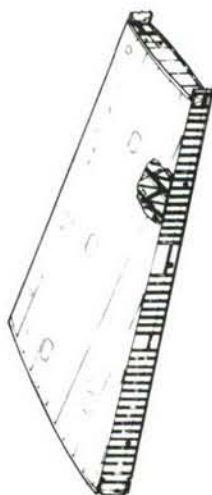


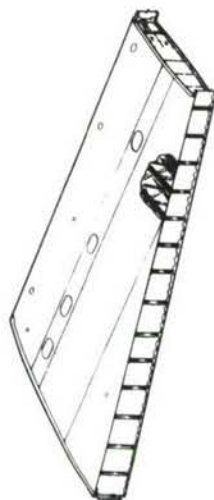
FIGURE 58 WEIGHT EFFECTS OF ADVANCED TECHNOLOGY -  
TAPERED SHINGLE DESIGN

# BASELINE UPDATE



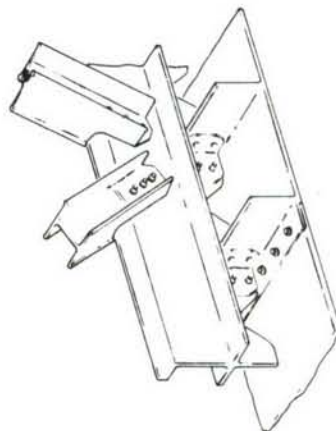
7,012 LBS  
(30,000 HRS)  
7,845 LBS  
(60,000 HRS)

# 'A' STRINGER WELDBOND DESIGN



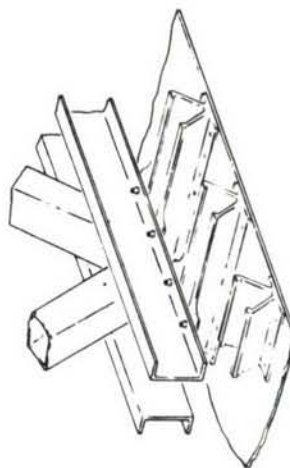
6,415 LBS  
(60,000 HRS)

TOTAL  
WEIGHT



4,532 LBS  
(30,000 HRS)  
5,365 LBS  
(60,000 HRS)

SURFACES  
AND  
SPANWISE  
SPICES



4,093 LBS  
(60,000 HRS)

## CONTRIBUTING FACTORS FOR WEIGHT REDUCTION

$$K_T = 3.42$$

$$F_T \text{ ALLOW} = 38.0 \text{ KSI} \quad (30,000 \text{ HRS})$$

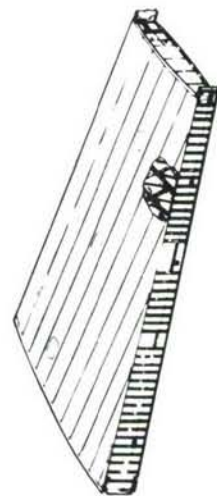
WS 77.7  
UPPER  
SURFACE

$$K_T = 3.25$$

$$F_T \text{ ALLOW} = 39.5 \text{ KSI} \quad (60,000 \text{ HRS})$$

FIGURE 59 WEIGHT COMPARISON - 'A' STRINGER WELDBOND DESIGN

# BASELINE UPDATE

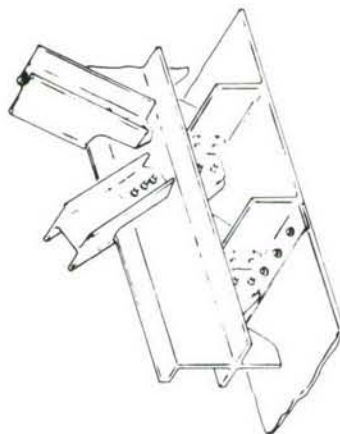
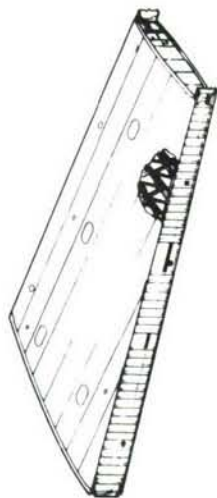


7,012 LBS  
(30,000 HRS)  
7,845 LBS  
(60,000 HRS)

TOTAL  
WEIGHT

6,536 LBS  
(60,000 HRS)

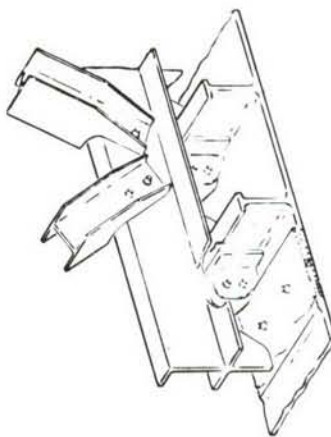
# VIRGIN PLANK DESIGN



4,532 LBS  
(30,000 HRS)  
5,365 LBS  
(60,000 HRS)

SURFACES  
AND  
SPANWISE  
SPICES

4,208 LBS  
(60,000 HRS)

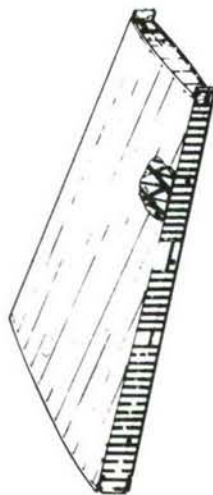


## CONTRIBUTING FACTORS FOR WEIGHT REDUCTION

$K_T = 3.42$	$K_T = 2.55$
$F_{T \text{ ALLOW}} = 38.0 \text{ KSI}$ (30,000 HRS)	$F_{T \text{ ALLOW}} = 42.0 \text{ KSI}$ (60,000 HRS)
WS 77.7 UPPER SURFACE	

FIGURE 60 WEIGHT COMPARISON - VIRGIN PLANK DESIGN

# BASELINE UPDATE

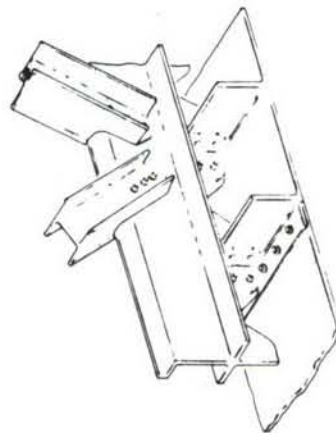
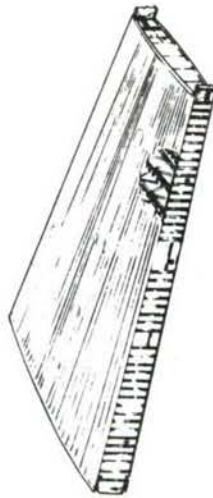


7,012 LBS  
(30,000 HRS)  
7,845 LBS  
(60,000 HRS)

TOTAL  
WEIGHT

6,935 LBS  
(60,000 HRS)

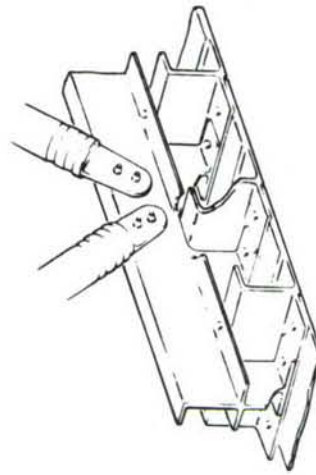
# TAPERED SHINGLE DESIGN



4,532 LBS  
(30,000 HRS)  
5,365 LBS  
(60,000 HRS)

SURFACES  
AND  
SPANWISE  
SPLICES

4,565 LBS  
(60,000 HRS)



## CONTRIBUTING FACTORS FOR WEIGHT REDUCTION

$K_T = 3.42$	$K_T = 2.62$
$F_T \text{ ALLOW} = 38.0 \text{ KSI}$ (30,000 HRS)	$F_T \text{ ALLOW} = 43.0 \text{ KSI}$ (60,000 HRS)
WS 77.7 UPPER SURFACE	

FIGURE 61 WEIGHT COMPARISON - TAPERED SHINGLE DESIGN



## SECTION VIII

### FATIGUE AND DAMAGE TOLERANCE ANALYSIS

The broad range of requirements and interactions which make up the ADP design and analysis approach are depicted on Figure 4. The repeated loads aspects of the criteria form a very significant feature of the general design approach, particularly in this program where an extremely long service life requirement is specified. Considering the addition of damage tolerance requirements to the design iteration cycle, the significance of the repeated loads effects reaches an even higher level of importance. The impact of these expanded requirements must be moderated through technological advances in the fields of materials development, structural analysis, and general as well as detail design. To develop a structure which is efficient and in compliance with the ADP fatigue and damage tolerance criteria, these fields were systematically addressed in various design concepts by way of materials selection and analytical establishment of allowable design stress levels. Development of innovative structural arrangements, which improved the quality of the detail design, permitted a substantial exploitation of the basic strength properties of the materials chosen. The analyses performed in support of this phase of the program are discussed below.

#### 8.1 FATIGUE ANALYSIS

##### 8.1.1 Fatigue Criteria and Loads

The fatigue analyses in the Phase IA program were based on loads corresponding to the test load spectrum applied to the C-141 wing-fuselage airplane fatigue specimen. This spectrum was modified based on operational airplane tracking data to include 8187 full-stop landings and 5595 touch-and-go landings within 30,000 flight hours. In addition, a log average peak-to-peak ground-air-ground cycle was used in the analysis.

All fatigue analyses related to updating the baseline structure to 1972 technology were based on a safe-life requirement of 30,000 flight hours. ADP design concepts were developed for twice the baseline requirement, that is, 60,000 flight hours. A scatter factor of 4 was applied to the design safe life in the fatigue analyses of all structures.

### 8.1.2 Fatigue Analysis Approach

The fatigue analysis computer programs used in the ADP study are suitable for providing the necessary design support for major airplane development programs. These programs can generate complex spectra from mission profiles, basic loads data, and airplane utilization rates for purposes of detail fatigue analyses and for establishing fatigue test requirements. Additionally, a broad range of output options permit close evaluations of the major sources of fatigue damage. One option, for example, indicates damage per mission as a percent of the total fatigue damage caused by each of the missions considered in the analysis, including the mission utilization function. A second option allows utilization rates to be varied to study the effects of a different mission mix, or to evaluate more closely the predicted fatigue response of the structure as a function of different using commands. Damage by source provides a further breakdown of fatigue damage contribution on the basis of elements of each mission in the life of the structure. Fatigue damage contribution due to gust, taxi, ground-air-ground cycle, etc., can be simply addressed within this option.

Special computing capabilities are also available that are particularly suited to preliminary design efforts. Initial analyses can be conducted in parametric form where, for a particular material and load spectrum, a relationship can be established between predicted time to crack initiation, quality of detail design, and design stress level. Such parametric analysis results provide an excellent basis for trade studies in which a variety of design concepts can be assessed. For example, Figure 62 shows results obtained for the upper wing surface at W.S. 77.7. The data include a generalized analysis as well as specific results for the spanwise splice arrangement in the Virgin Plank configuration. In addition, results are shown for the spanwise splice arrangement of the updated baseline. Some interesting points can be observed from these data concerning design criteria, structural concepts and materials selection. For example, the fatigue allowable design tension stress in the upper surface wing root area for the proposed baseline update and the Virgin Plank configuration is 39.4 KSI and 44.2 KSI, respectively. These allowable stresses were based on an effective stress concentration factor of 3.42 and a safe life of 30,000 flight hours for the baseline update, and an effective stress concentration factor of 2.55 with a safe life requirement of 60,000 flight hours for the Virgin Plank design. From the

BUILT-UP STRUCTURE S-N DATA  
 7050-T76511 EXTRUSION  
 W.S. 77.7 UPPER SURFACE

SPANWISE SPLICE:

----- VIRGIN PLANK ( $K_T = 2.55$ ) ----- 7075-T76511 BASELINE  
 ----- BASELINE UPDATE ( $K_T = 3.42$ ) ----- UPDATE ( $K_T = 3.42$ )

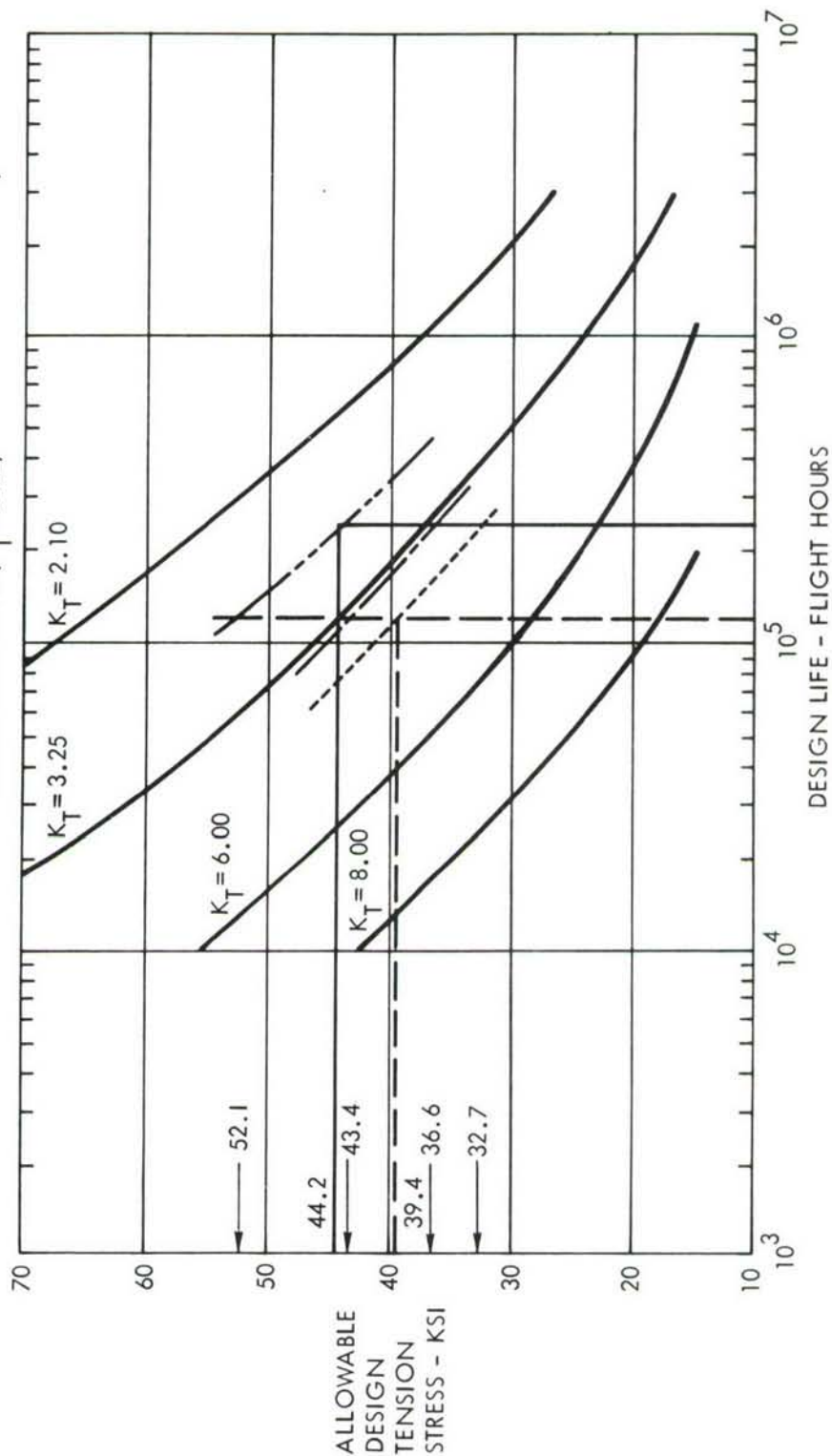


FIGURE 62 PARAMETRIC WING SURFACE FATIGUE ANALYSIS



figure it can be seen that if the material selection for the baseline update was not limited to 1972 technology, the fatigue allowable design stress could be increased from the specified 39.4 KSI to 43.4 KSI by simply fabricating the structure from 7050-T76511 aluminum. If the detail design improvement of the Virgin Plank design is incorporated along with the new material, the fatigue allowable design stress can be further increased to 52.1 KSI. It can also be observed that, if the detail design of the updated baseline were retained in the Virgin Plank structure, the fatigue allowable design stress would be reduced from the specified 44.2 KSI to 36.6 KSI. The most important general conclusion to be drawn from Figure 62 is the relative contribution of design stress level and quality of detail design to the achievement of superior fatigue performance.

#### 8.1.3 Fatigue Analysis Results

The information required for fatigue design control was developed from fatigue analysis data similar to that discussed above. Referring to Figure 62, it can be seen that a cross-plot of the general data at a plane corresponding to the design life specified in the criteria will provide the relationship between design stress level and effective stress concentration factor for the particular life requirement. Results of this type were developed for the upper and lower wing surfaces at 3 stations of the inner wing box. Stations selected include the inboard and outboard chordwise splice areas and the inboard pylon rib station. Figures 63 through 74 show basic analysis data for all wing cover materials used in the baseline update and proposed ADP designs. Configurations are listed on the figures for reference purposes. The chordwise splice plates were made from plate stock and were assessed on the basis of the data shown in Figures 75 through 78. In addition, data were developed for the fatigue analysis of the various spar concepts. The primary area of concern in this case was the web-cap splice arrangement. Figures 79, 80 and 81 show the general analysis data for the Weldbond configuration. Other spar design concepts were assessed on the basis of the appropriate wing cover data.

The general fatigue analysis data were used in preliminary design to establish the allowable design stresses for selected alternative structural arrangements. In each



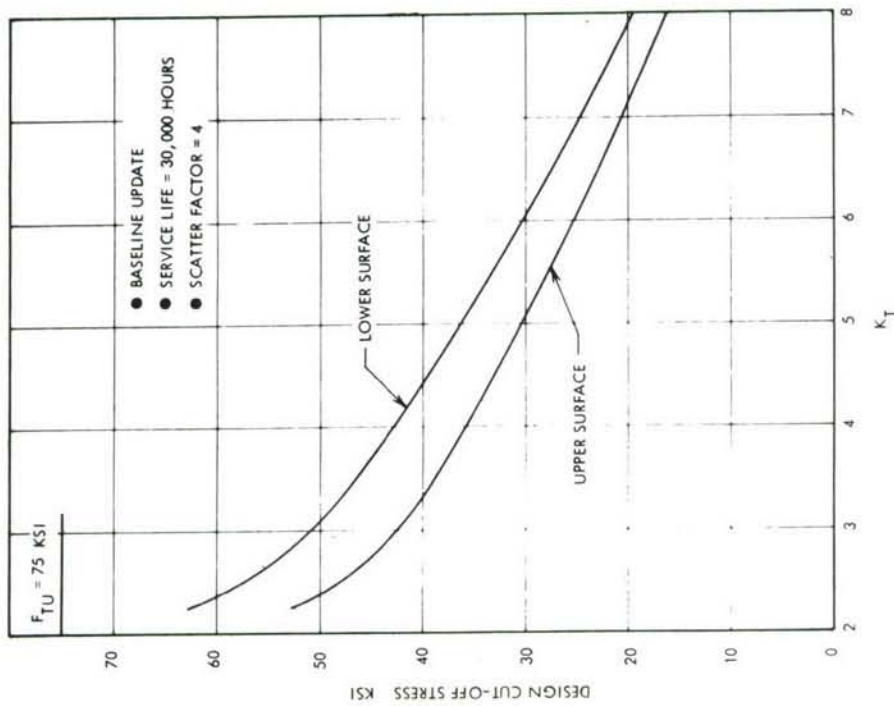


FIGURE 63 WING SURFACE FATIGUE ANALYSIS  
BUILT-UP STRUCTURE S-N DATA  
7075-T76511 EXTRUSION  
W.S. 77.7

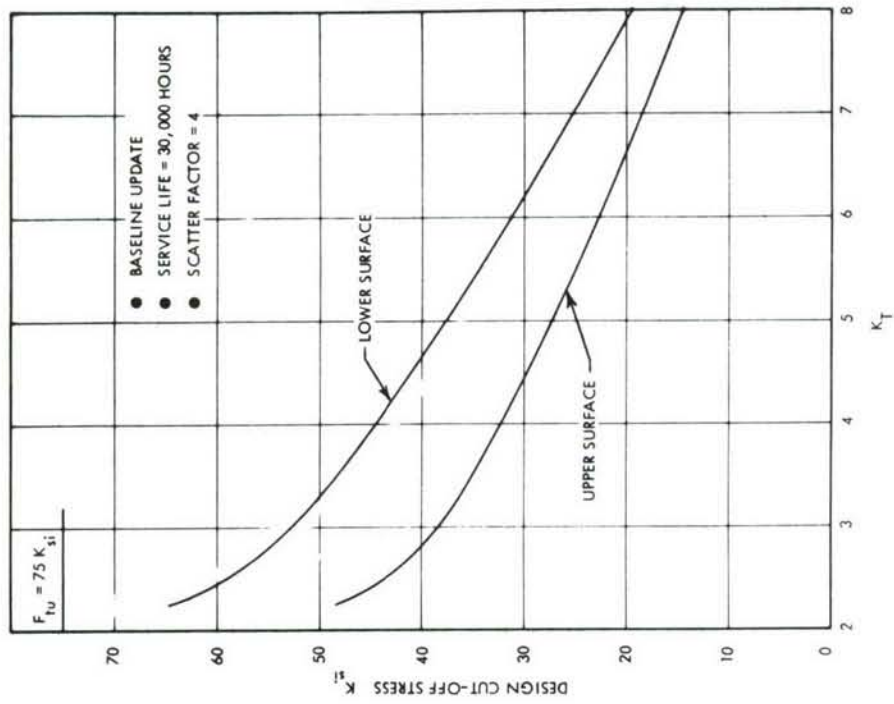


FIGURE 64 WING SURFACE FATIGUE ANALYSIS  
BUILT-UP STRUCTURE S-N DATA  
7075-T76511 EXTRUSION  
W.S. 285.3

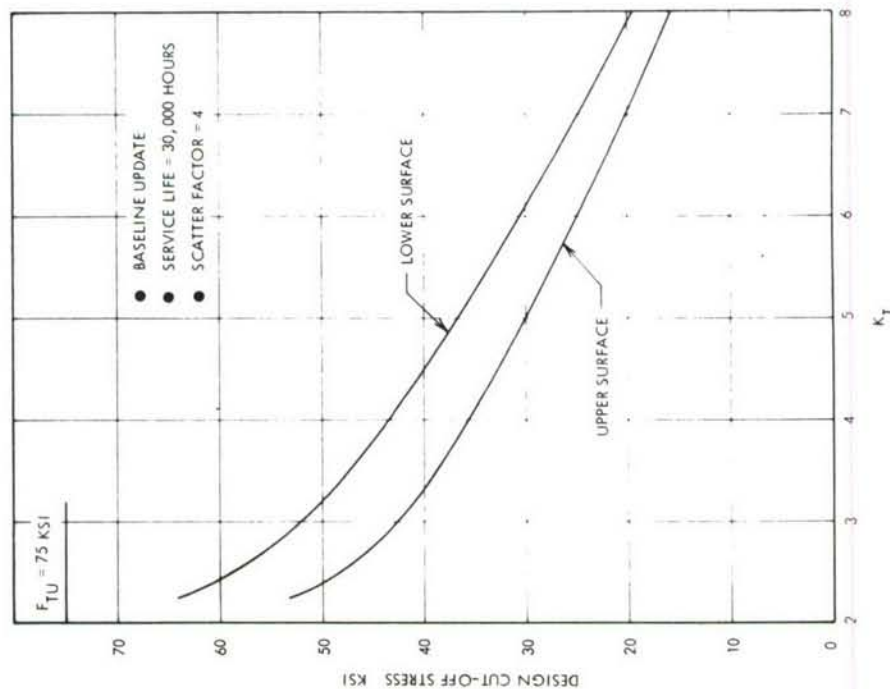


FIGURE 65 WING SURFACE FATIGUE ANALYSIS  
BUILT-UP STRUCTURE S-N DATA  
7075-T76511 EXTRUSION  
W.S. 415.4

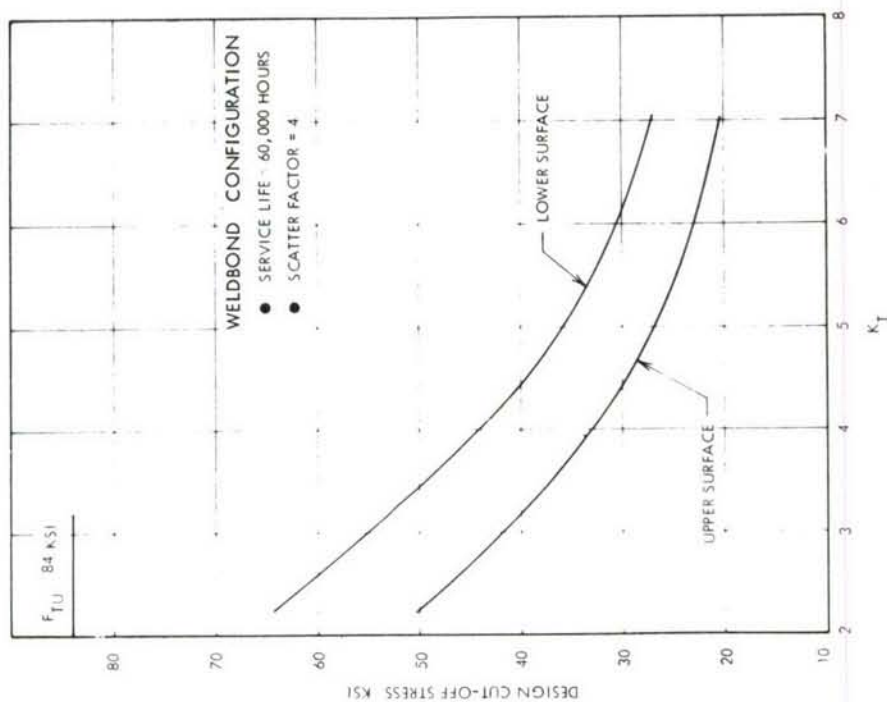


FIGURE 66 WING SURFACE FATIGUE ANALYSIS  
COUPON S-N DATA  
7050-T76511 EXTRUSION  
W.S. 77.7

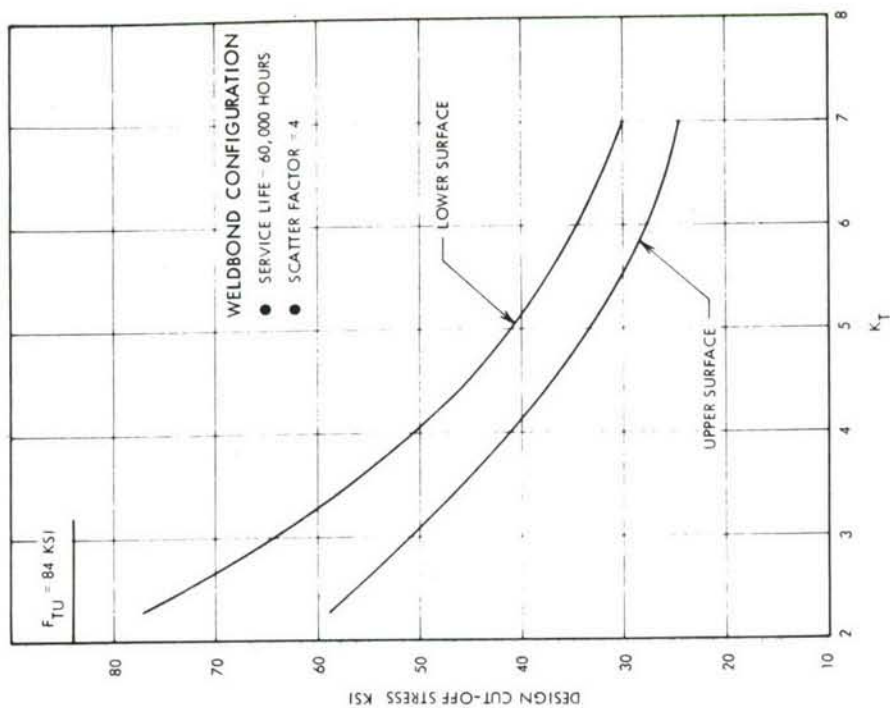


FIGURE 68 WING SURFACE FATIGUE ANALYSIS  
COUPON S-N DATA  
7050-T76511 EXTRUSION  
W.S. 415.4

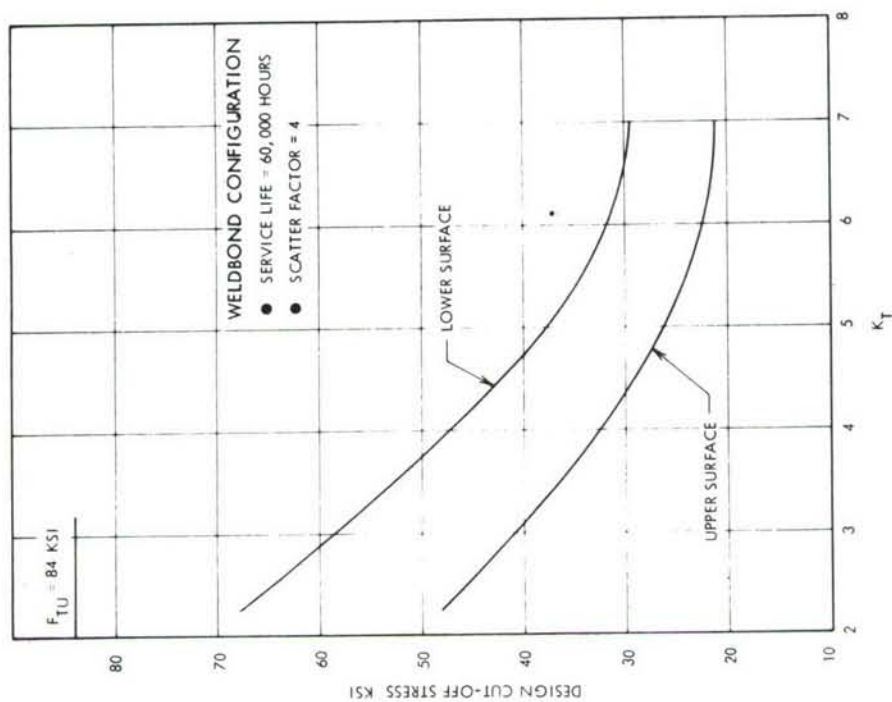


FIGURE 67 WING SURFACE FATIGUE ANALYSIS  
COUPON S-N DATA  
7050-T76511 EXTRUSION  
W.S. 285.3

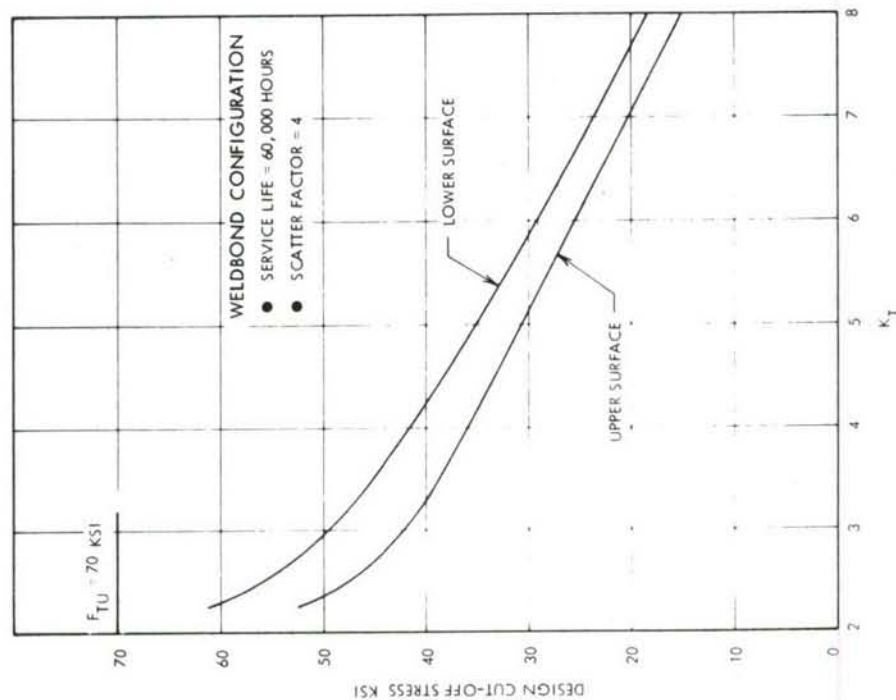


FIGURE 69 WING SURFACE FATIGUE ANALYSIS  
BUILT-UP STRUCTURE S-N DATA  
7475-T76 SHEET  
W.S. 77.7

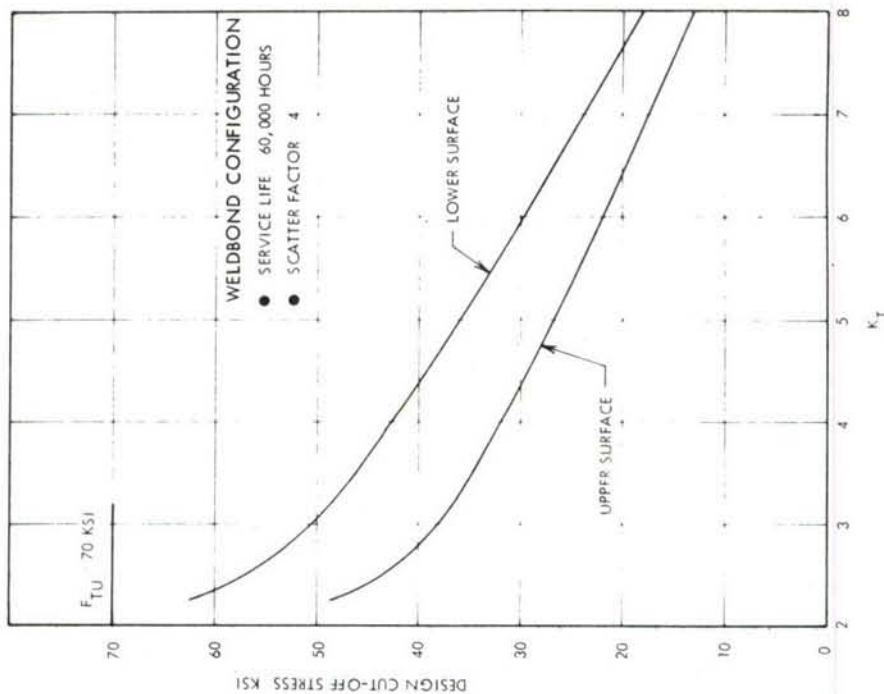


FIGURE 70 WING SURFACE FATIGUE ANALYSIS  
BUILT-UP STRUCTURE S-N DATA  
7475-T76 SHEET  
W.S. 285.3



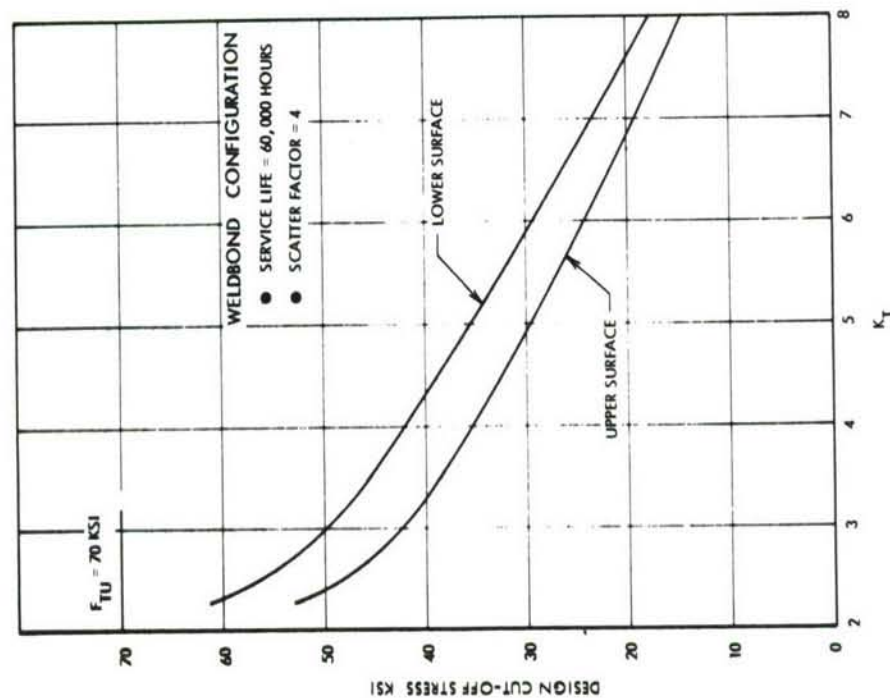


FIGURE 71 WING SURFACE FATIGUE ANALYSIS  
BUILT-UP STRUCTURE S-N DATA  
7475-T76 SHEET  
W.S. 415.4

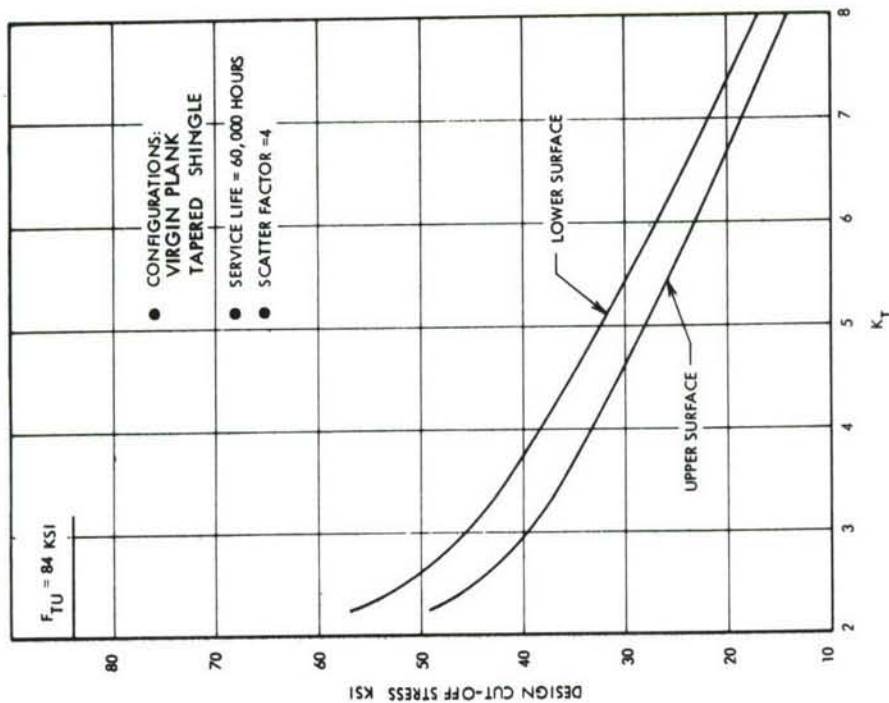


FIGURE 72 WING SURFACE FATIGUE ANALYSIS  
BUILT-UP STRUCTURE S-N DATA  
7050-T76511 EXTRUSION  
W.S. 77.7

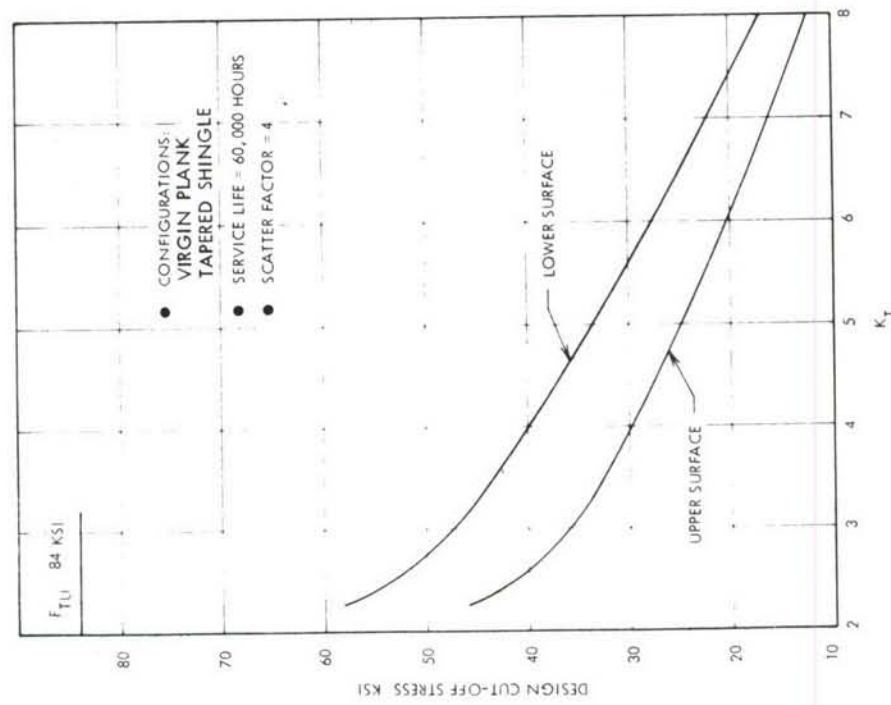


FIGURE 73 WING SURFACE FATIGUE ANALYSIS  
BUILT-UP STRUCTURE S-N DATA  
7050-T76511 EXTRUSION  
W.S. 285.3

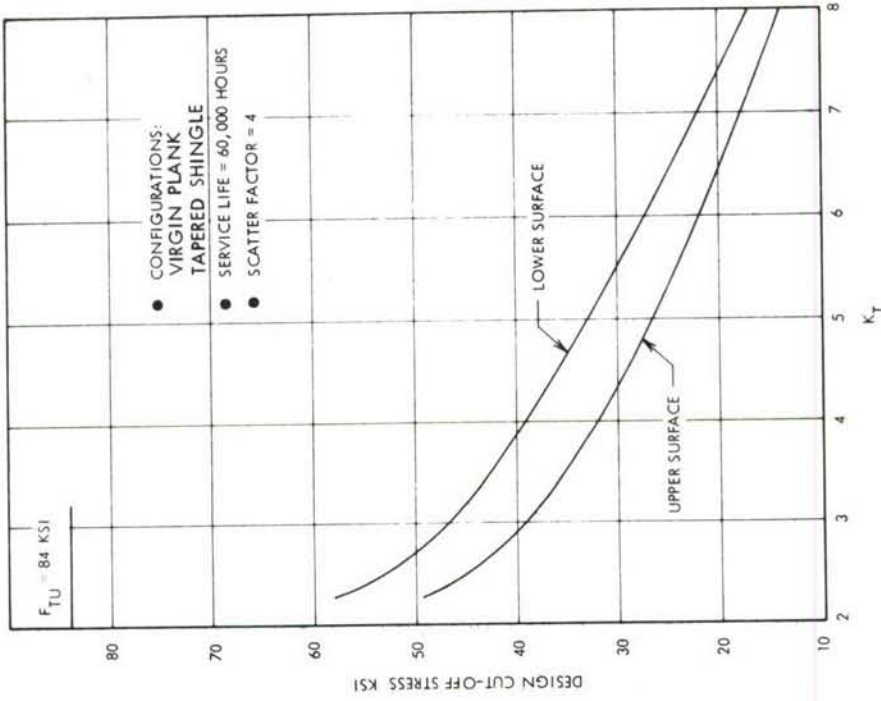


FIGURE 74 WING SURFACE FATIGUE ANALYSIS  
BUILT-UP STRUCTURE S-N DATA  
7050-T76511 EXTRUSION  
W.S. 415.4

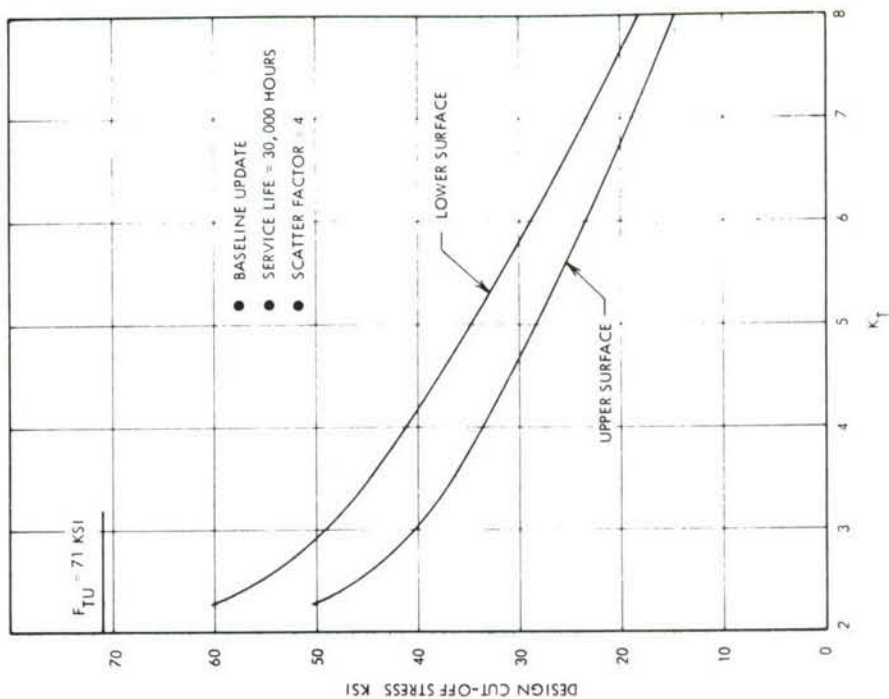


FIGURE 76 WING SURFACE FATIGUE ANALYSIS  
BUILT-UP STRUCTURE S-N DATA  
7075-T7651 PLATE  
W.S. 415.4

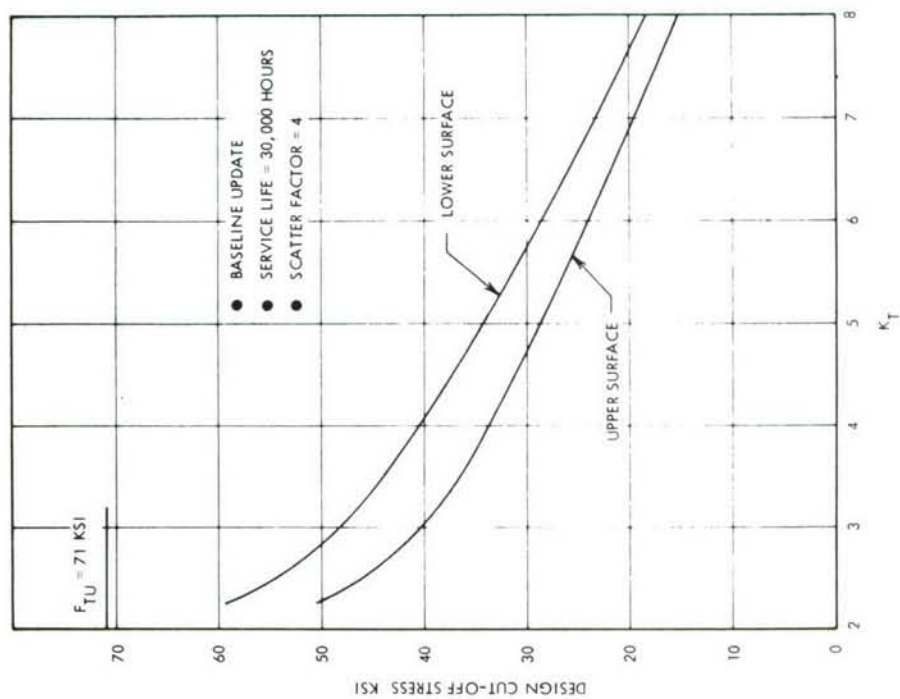


FIGURE 75 WING SURFACE FATIGUE ANALYSIS  
BUILT-UP STRUCTURE S-N DATA  
7075-T7651 PLATE  
W.S. 77.7

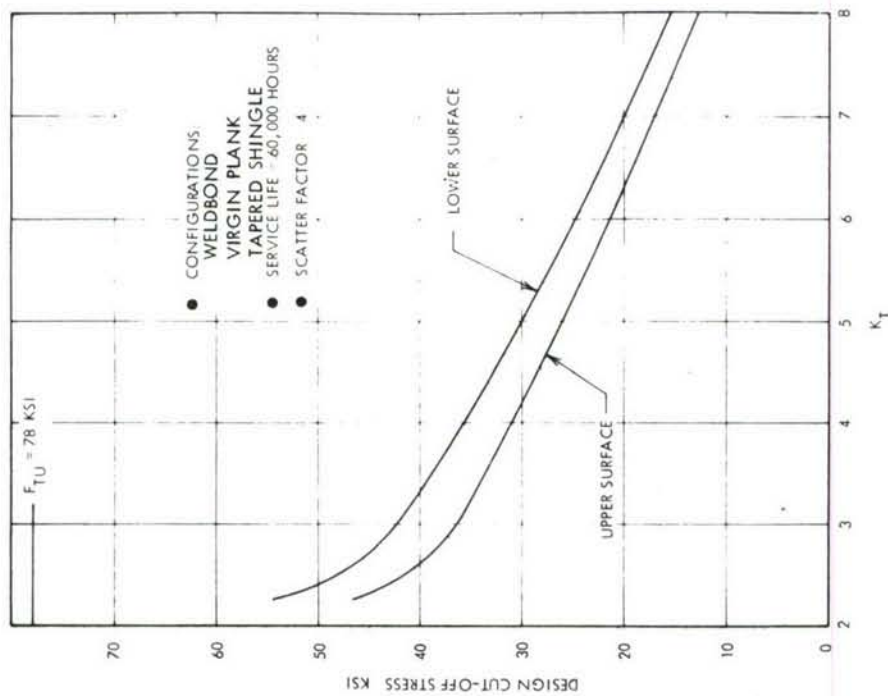


FIGURE 77 WING SURFACE FATIGUE ANALYSIS  
BUILT-UP STRUCTURE S-N DATA  
7050-T7651 PLATE  
W.S. 77.7

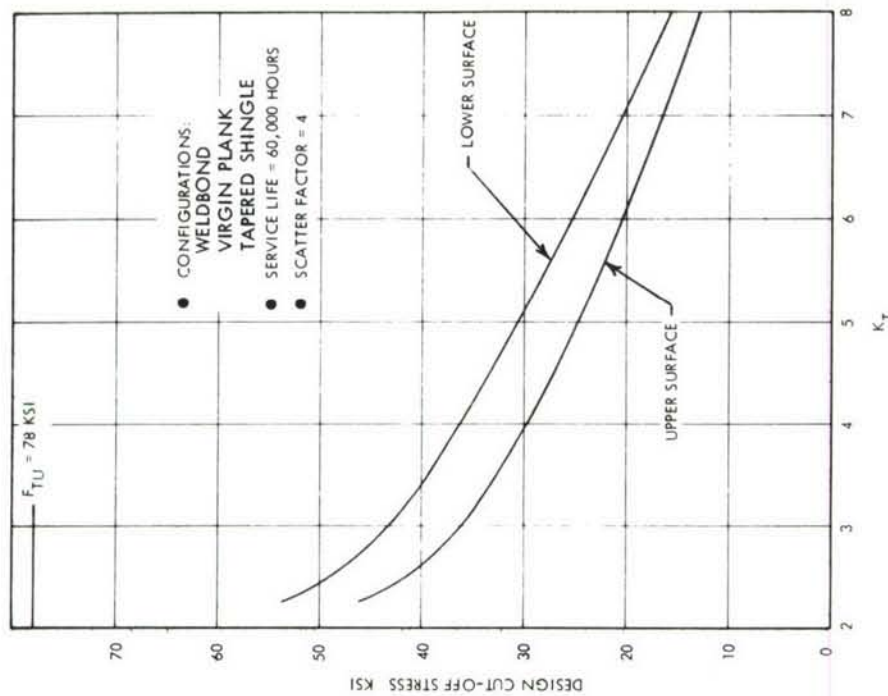


FIGURE 78 WING SURFACE FATIGUE ANALYSIS  
BUILT-UP STRUCTURE S-N DATA  
7050-T7651 PLATE  
W.S. 415.4



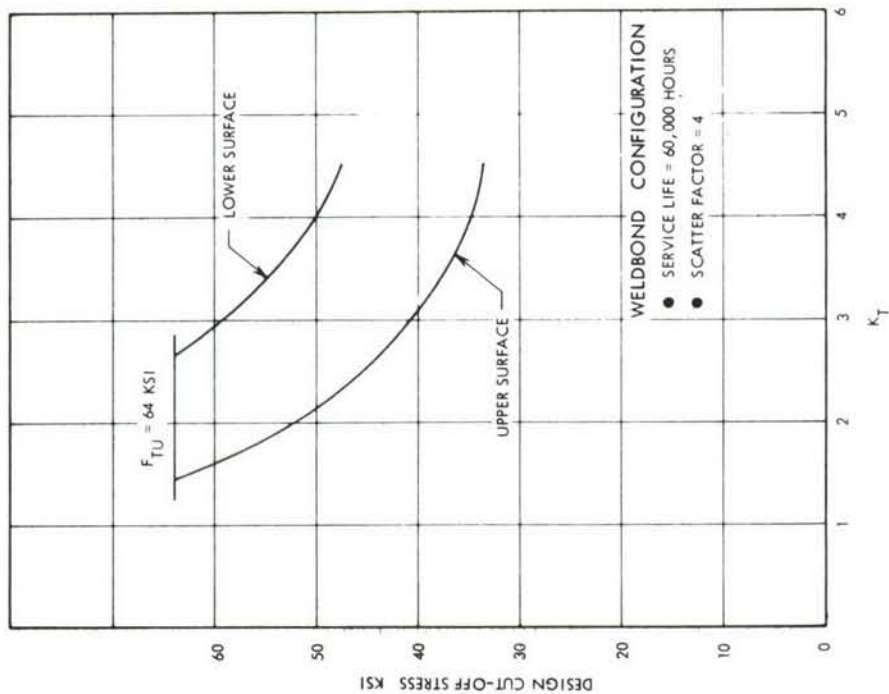


FIGURE 80 WING SPAR FATIGUE ANALYSIS  
COUPON S-N DATA  
2219-T87 SHEET  
W.S. 285.3

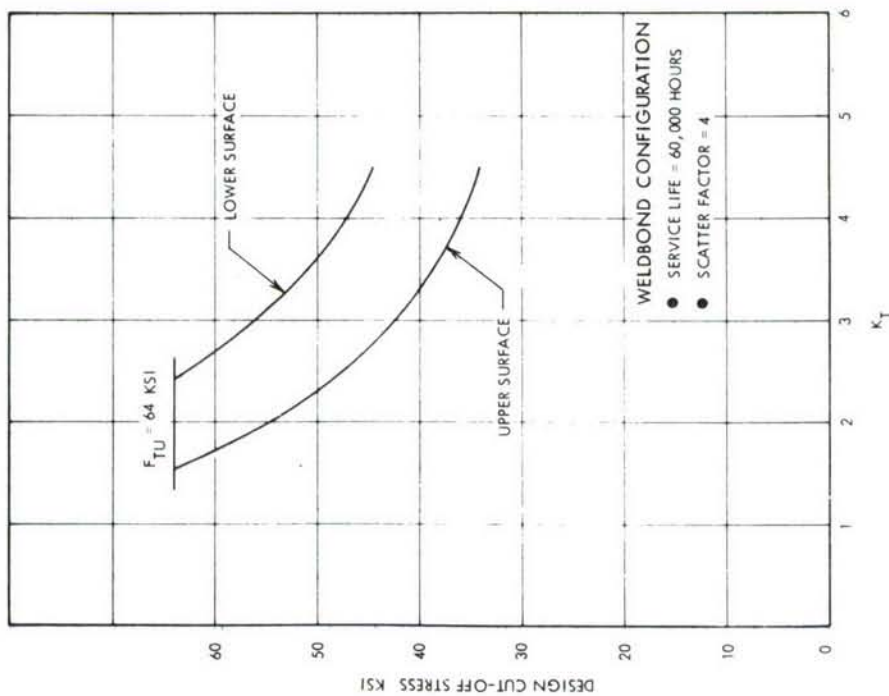


FIGURE 79 WING SPAR FATIGUE ANALYSIS  
COUPON S-N DATA  
2219-T87 SHEET  
W.S. 77.7

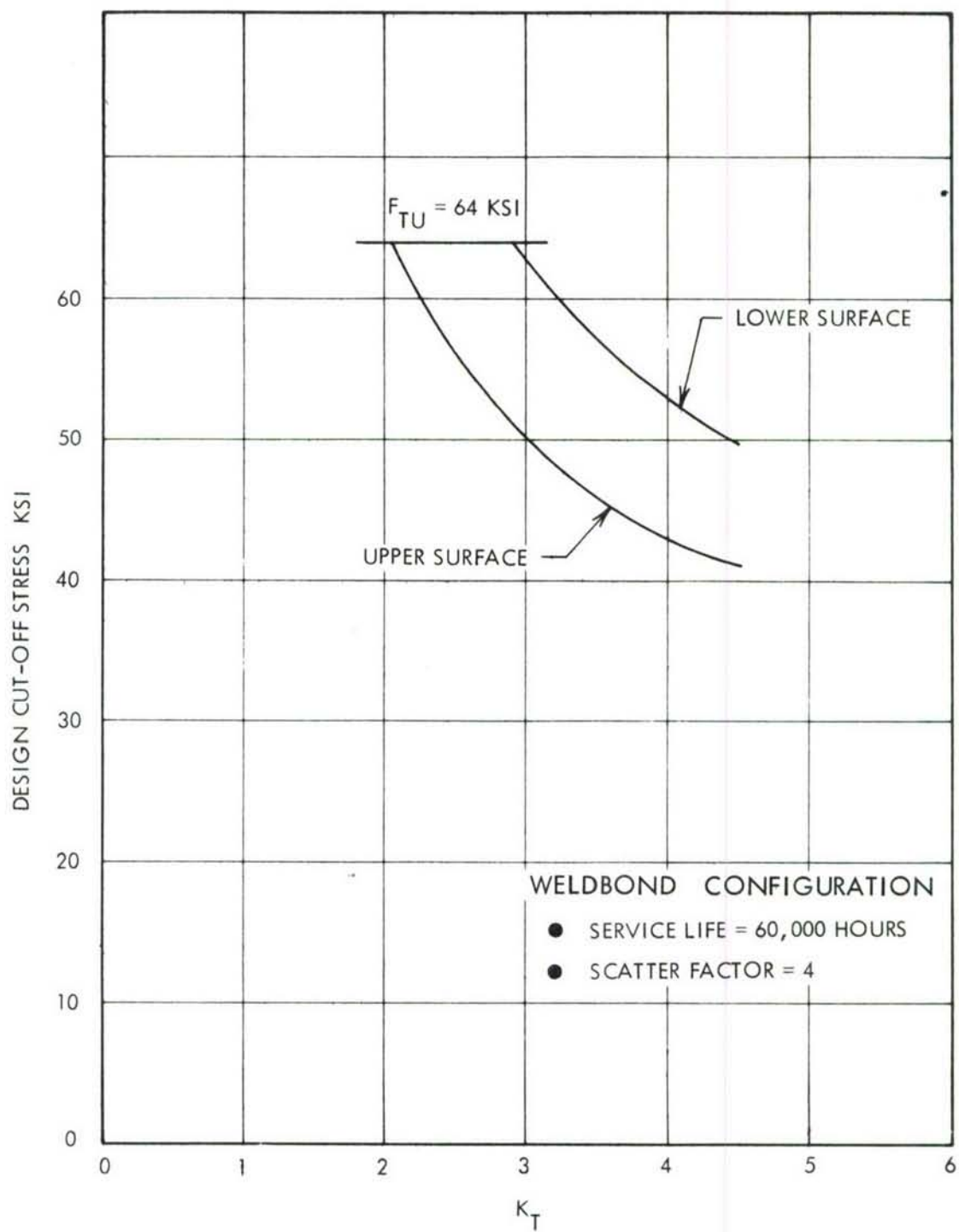


FIGURE 81 WING SPAR FATIGUE ANALYSIS  
COUPON S-N DATA  
2219-T87 SHEET  
W.S. 415.4

case the proposed structural arrangement was assessed in terms of a quality index or effective stress concentration factor. Figure 82 presents a summary of the stress concentration factors corresponding to the detail design found in the proposed structural concepts. Two values of stress concentration are shown: basic values correspond in general to the simple geometric stress concentration factor whereas the design value includes the influence of load transfer, hole preparation, fastener fit, etc. The allowable fatigue design stresses were determined by entering the general fatigue analysis curves with the appropriate value of effective stress concentration. Table XX presents a summary of the more significant design stress control results derived in this manner.

## 8.2 DAMAGE TOLERANCE ANALYSIS

### 8.2.1 Damage Tolerance Criteria and Loads

The criteria for the Cargo/Tanker ADP program establishes safe crack growth and residual strength requirement for 3 basic approaches to the design of damage tolerance in aircraft structures. One approach, the slow crack growth concept, applies to structure where flaws or defects are not permitted to attain the critical size required for unstable crack propagation. The other 2 approaches apply to fail-safe design concepts where the structure is designed and fabricated with the capability to arrest unstable crack propagation. In all cases, the assumed damage and damage growth limits are specified as a function of the design approach and the degree of structural inspectability. Compliance with the criteria requires that the strength and safety of the remaining structure not be degraded below a specified level for a given period of unrepaid service usage.

The repeated loads used in the damage tolerance analysis were the same as those considered in the fatigue analysis. However, since crack growth analyses are influenced by the ordering or sequence of loading, the fatigue load spectrum was converted to an average spectrum by factoring the number of cycles at each load level occurring in 1 lifetime by the number of full-stop landings in 1 lifetime. The resulting average mission load spectrum was used to conduct analyses and tests based on a flight-by-flight loading concept.

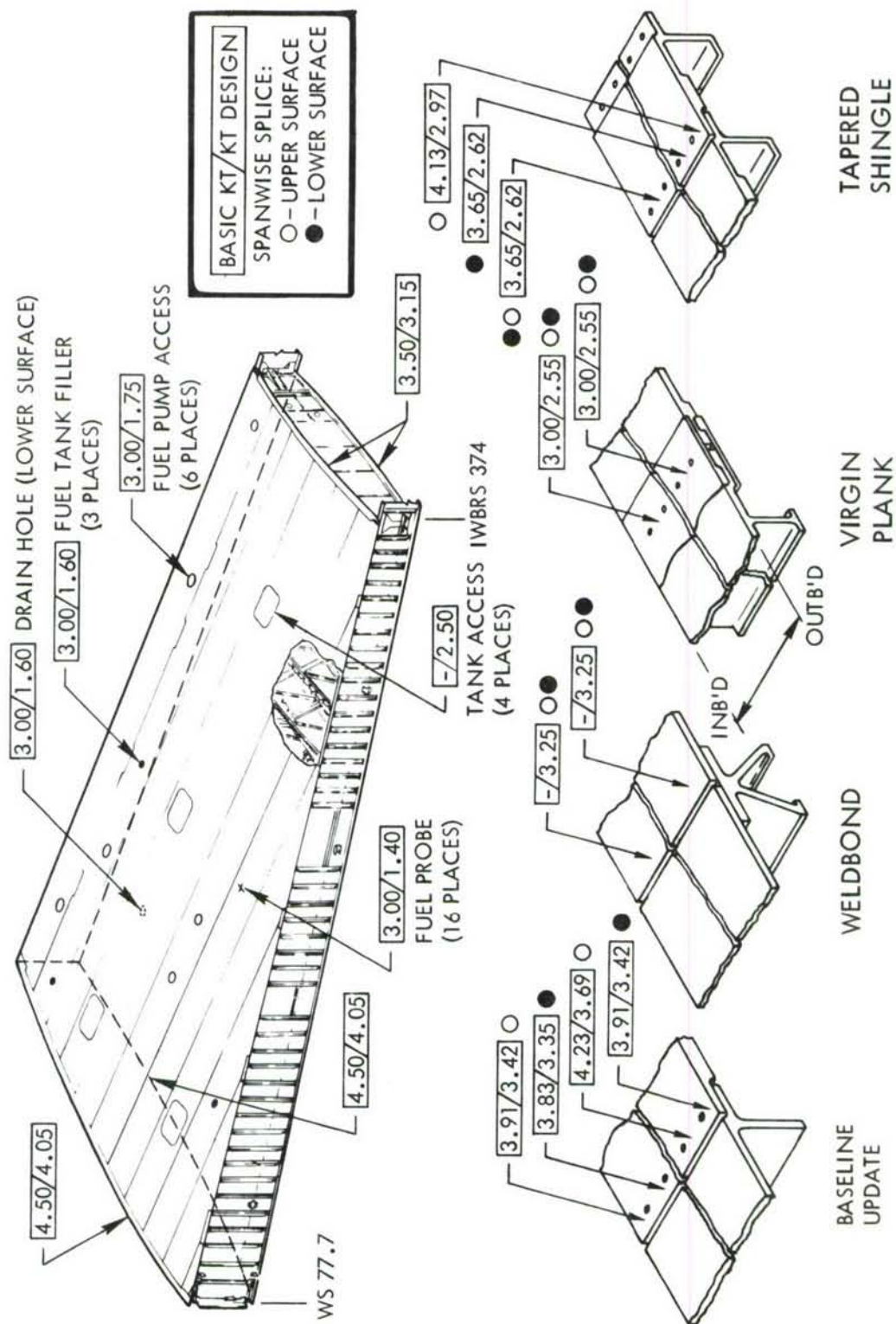


FIGURE 82 FATIGUE ANALYSIS STRESS CONCENTRATION FACTORS



TABLE XX  
WING SURFACE FATIGUE ANALYSIS  
SUMMARY - ALLOWABLE DESIGN TENSION STRESS

COMPONENT	W.S.	DESIGN TENSION STRESS (KSI)			
		BASELINE UPDATE	WELD BOND	VIRGIN PLANK	TAPERED SHINGLE
UPPER SURFACE	77.7	39.4	39.9	44.2	43.2
	285.6		38.7	40.5	
	415.4	37.4	48.0	44.0	39.1
LOWER SURFACE	77.7	47.7	52.6	51.1	50.0
	285.6		55.4	52.5	
	415.4	48.0	60.0	52.1	51.0
CHORDWISE SPLICE					
UPPER SURFACE	77.7	33.6	30.6	30.6	30.6
LOWER SURFACE	77.7	40.3	34.5	34.5	34.5
UPPER SURFACE	415.4	39.0	35.8	35.8	35.8
LOWER SURFACE	415.4	47.8	42.2	42.2	42.2

The inspections and inspection frequency data used in the damage tolerance analyses are listed in Table XXI. C-141 airplane inspections performed on operational airplanes are listed along with the corresponding ADP design criteria inspections. It should be observed that not all of the operational airplane service inspections were used in the damage tolerance analyses. Residual strength load requirements, which are a function of inspection periods, are also shown in the table. The loads are based on average load exceedance data and correspond to the maximum load that could occur once in 100 times the applicable inspection interval. Fail safe structures must sustain the residual strength load with a 1.15 dynamic factor at the time of load path failure.

#### 8.2.2 Damage Tolerance Analysis Approach

Damage tolerance analyses were performed using a Lockheed-developed computer program entitled "CRACK GROWTH/GELAC." This computer program provides the capability for determining crack growth as a function of operational load experience. Flight-by-flight loads based on the average mission spectrum were used in the ADP program analyses.

Allowable design tension stresses in compliance with the damage tolerance criteria were established through detail analyses of the crack growth behavior in design concepts under consideration. Figure 83 shows results for the growth behavior of a surface-flaw initiated crack. A range of stress-load ratios were applied to the load spectrum to determine the behavior as a function of design stress level. In each case, the growth curve was developed to the point where the critical crack length was reached at a loading condition which occurred in the succeeding flight. The number of flights required to reach this point is referred to as the safe crack growth period for a given design stress. Other initial assumed flaw sizes and shapes specified in the criteria were similarly treated.

The above data were replotted to relate the safe crack growth period as a direct function of design stress level. Figure 84 shows the derived data for the lower surface at W.S. 77.7 for the Virgin Plank design. Analysis results plotted in this form provided a simple method for selecting design stresses that were in compliance with the

TABLE XXI  
INSPECTION AND FAIL SAFE LOAD ( $P_{XX}$ ) DATA

(Loads as % of limit)

UPBENDING

BASELINE INSPECTION	EQUIVALENT CRITERIA INSPECTION	INSPECTION FREQUENCY		WS 77.7 LOAD OCCURRING IN 100 INSPECTION INTERVALS	WS 285.26 LOAD OCCURRING IN 100 INSPECTION INTERVALS	WS 415.39 LOAD OCCURRING IN 100 INSPECTION INTERVALS
		TIME	FLIGHTS			
*In-Flight	In-Flight	1.5 Days	1	51.1	52.3	50.6
*Preflight	Walk Around	1.5 Days	1	51.1	52.3	50.6
Home Station	Ground Equivalent	10 Days	15	61.7	61.9	60.0
Minor	Special Visual	70 Days	105	68.2	69.3	66.9
*Major	Special Visual	140 Days	209	70.6	72.1	69.3
Mid-Interval IRAN	Depot Level	18 Mos.	819	75.3	77.4	74.0
*Depot-IRAN	Depot Level	36 Mos.	1637	77.7	80.2	76.9
*Non-Inspectable	Non-Inspectable	-	-	83.5	86.6	83.4

DOWNBENDING

*In-Flight	In-Flight	1.5 Days	1	61.3	67.4	52.1
*Preflight	Walk Around	1.5 Days	1	61.3	67.4	52.1
Home Station	Ground Equivalent	10 Days	15	64.0	71.9	56.5
Minor	Special Visual	70 Days	105	66.4	74.8	59.5
*Major	Special Visual	140 Days	209	67.1	76.0	60.4
Mid-Interval IRAN	Depot Level	18 Mos.	819	68.6	77.9	62.1
*Depot-IRAN	Depot Level	36 Mos.	1637	69.7	79.3	63.5
*Non-Inspectable	Non-Inspectable	-	-	71.5	81.8	66.0

NOTES: Slow Crack Growth Structure - In Flight and Home Station - Not Applicable

Crack Arrest Structure - Non-Inspectable - Not Applicable

For Crack Arrest Structure and Multiple Load Path Structure,  $F_{yy} = 1.15 \times P_{XX}$   
60,000 Hours = 16,374 Flights, Current Usage = 2,000 hours/year

\*Design Criteria Inspections

INITIAL SURFACE FLAW,  $a/Q = 0.10"$   
 WS 77.7 LOWER SURFACE,  $t_s = 0.223"$   
 RETARDATION FACTOR = 1.5 (REFERENCE SECTION 8.2.3)

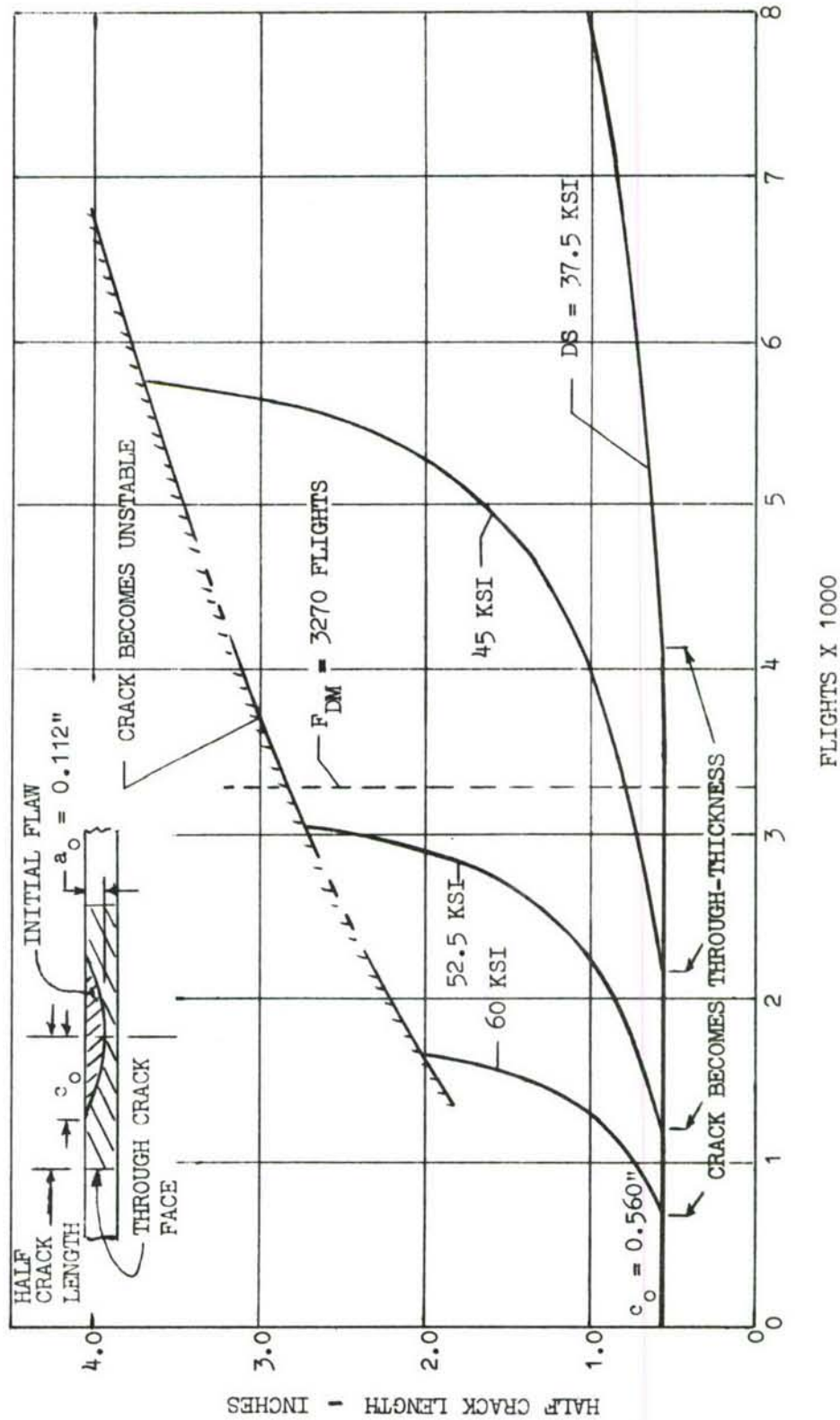


FIGURE 83 - WING SURFACE DAMAGE TOLERANCE ANALYSIS, CRACK GROWTH CURVES,  
 VIRGIN PLANK CONFIGURATION



W.S. 77.7 LOWER SURFACE,  $t = 0.223$ "  
 RETARDATION FACTOR = 1.5" (REFERENCE SECTION 8.2.3)  
 MATERIAL = 7050-T76511 ALUMINUM PANELS

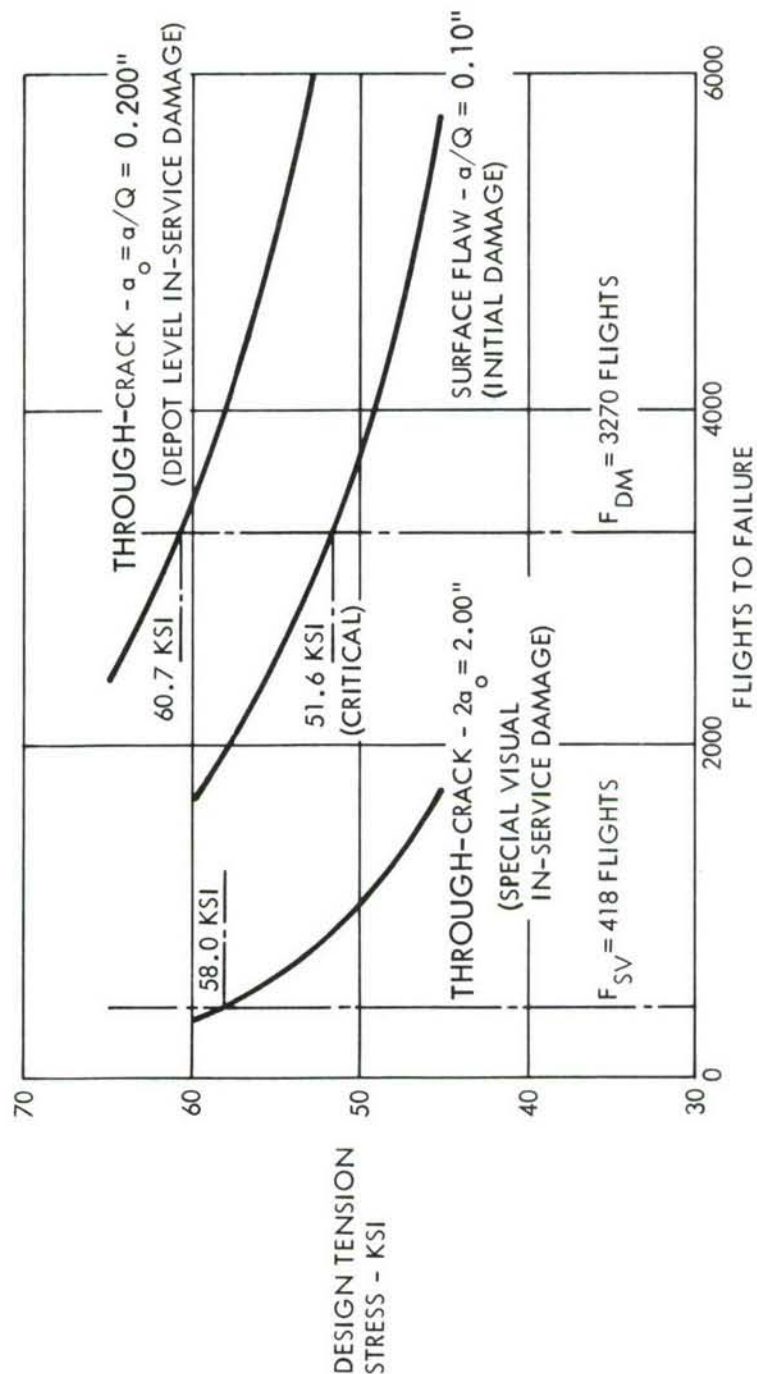


FIGURE 84 WING SURFACE DAMAGE TOLERANCE ANALYSIS  
 DESIGN TENSION STRESS VS. FLIGHTS TO FAILURE  
 VIRGIN PLANK CONFIGURATION

safe crack growth periods required in the damage tolerance criteria. This format also presents a vivid illustration of the influence of the inspection interval on the allowable design stress.

In addition to the safe crack growth requirement, the design stress must also provide for a specified level of residual strength during the stable fatigue crack growth period. Selecting the governing condition from a safe crack growth analysis, further analyses for a carefully selected range of design stress levels were performed to determine the crack length after the minimum period of unrepaired service usage. Results for the example chosen are shown in Figure 85. Crack lengths and corresponding design stresses at  $F_{DM}$  were replotted in Figure 86 along with critical crack length data for the residual strength load condition. Stresses at which the critical crack length is reached are plotted in terms of the related design stress to maintain a uniform strength basis in the analysis. The point where the two curves intersect defines the optimum design stress at which both the safe crack growth and residual strength requirements are met. Other points in the structure are analyzed in a similar manner.

Special consideration was given to the damage tolerance analysis of the chordwise splice at W.S. 77.7. An approach was formulated to support studies for the case of a through-the-thickness crack emanating symmetrically from both sides of a loaded hole. The analysis applies to a double shear splice with a single row of fasteners. Because of the difficulty associated with determining the condition of the panel sandwiched between the splice plates, the crack was assumed to be located in the wing panel instead of the splice plate. External loading consisted of a uniform tensile far-field stress applied in the spanwise direction. Rib stiffnesses were assumed to be sufficient to prevent out-of-plane deformations.

Considering the intact structure and the applied loading, it was concluded that, at the splice for an uncracked panel, the chordwise stress distribution and deformation is periodical with a wave length equal to the fastener spacing. Furthermore, the chordwise displacement and the spanwise shear stresses at points midway between fasteners vanish. Since the introduction of a crack will alter conditions locally, a sufficiently large area was considered around the crack to allow the assumption at the boundaries of zero chordwise displacements and spanwise shear stresses.

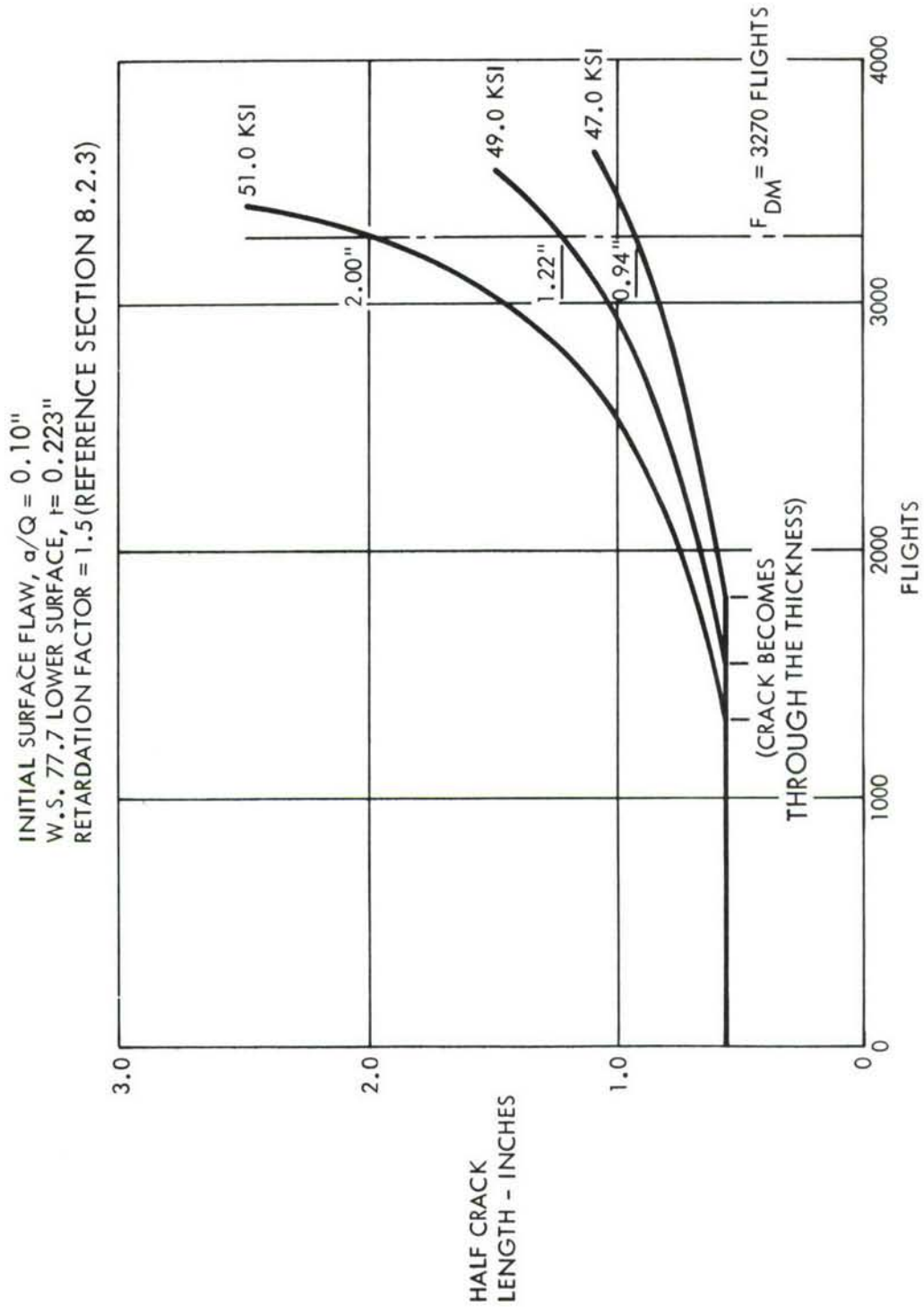


FIGURE 85 WING SURFACE DAMAGE TOLERANCE ANALYSIS  
CRACK LENGTHS AT  $F_{DM}$   
VIRGIN PLANK CONFIGURATION

# DESIGN STRESS REDUCTION DUE TO FAIL-SAFE LOAD

W.S. 77.7 LOWER SURFACE

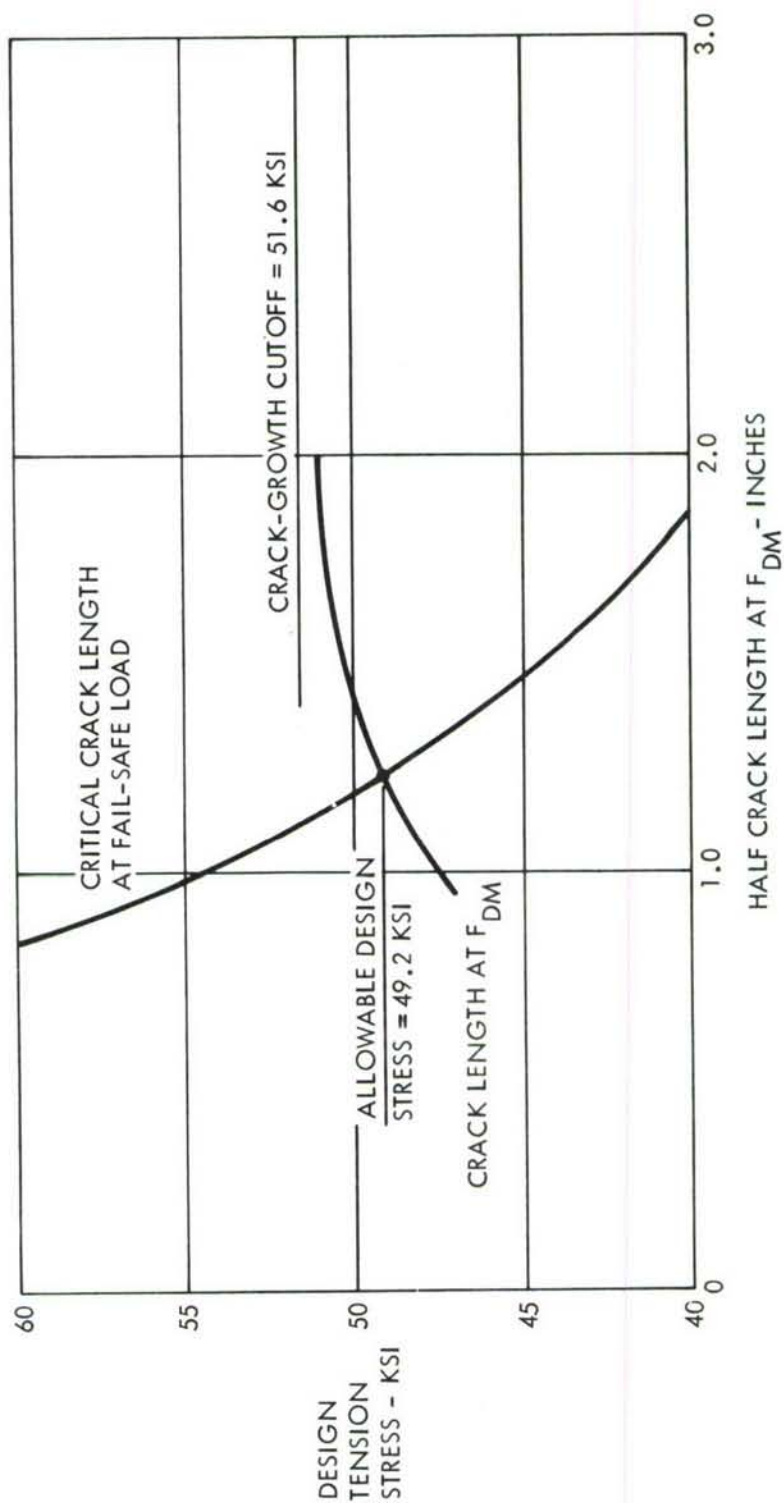


FIGURE 86 WING SURFACE DAMAGE TOLERANCE ANALYSIS  
RESIDUAL STRENGTH EFFECT  
VIRGIN PLANK CONFIGURATION



Such boundary conditions were satisfied by a separable solution for a plane elasticity problem using the well known biharmonic equation. In addition to the edge boundaries, the model was treated as individual regions lying between the fastener line and the chordwise edges of the panel and splice plates. The splice was assumed symmetrical in the analysis and only the outboard half considered. Load components carried by the fasteners at the edges of the regions were represented by singularity functions and the edge surface tractions were represented by Fourier series. General solutions for each region were obtained in terms of the unknown fastener loads and Fourier coefficients. A collocation method with truncated series representations of the normal stress and shear stress along the fastener row containing the crack was used. By satisfying continuity conditions at discrete points along uncracked boundaries and zero stress conditions at discrete points along the cracked faces, together with the continuity conditions at fastener locations, a set of simultaneous equations was obtained. The unknown Fourier coefficients and unknown fastener load components resulted from the solution of these equations. Stresses and deformations could then be determined with reasonable accuracy at all points in the model except in the immediate area of the crack tips where sharp strain gradients are present. In order to accurately define the stress state at the crack tip, the results of the above analysis were used to define the conditions at the boundaries of a cracked finite element. A single cracked finite element was used to determine the level of the crack tip stress intensity for a particular crack length and far field stress level. Development of the Lockheed-Georgia cracked finite element and its applications are described in references 8 and 9.

### 8.2.3 Damage Tolerance Analysis Results

Preliminary studies were performed to determine the trend or influence of the various aspects of the damage tolerance criteria on structural strength requirements. The purpose of these studies was to form a basis for the selection of the approach to be followed in complying with the criteria with the least impact on structural weight. It was concluded that for the proposed design concepts the slow crack growth approach offered the best potential for achieving the desired objective.

Analyses for design stress level control based on the damage tolerance criteria were conducted for the same wing stations considered in the fatigue analyses. Each location was analyzed in a manner similar to that outlined in the analysis approach section of the report for the lower wing surface at W.S. 77.7. Within the scope of a preliminary design effort, the developed results represent a very realistic implementation of the criteria. For example, crack growth retardation effects were included in the determination of allowable design stress levels. The level of retardation used in the analysis was based on panel test data where crack growth was measured as a function of cyclic loads applied on a flight-by-flight basis. The basic load spectrum was converted to two levels of stress spectra severity: one corresponded to the stress level of the baseline airplane and the other to a lower stress level intended to cover the lower range of potential stress levels for the ADP designs. All loads in the spectrum were applied in the tests, including compression-compression load cycles. The results indicated a relatively low level of crack retardation under these test conditions. Crack growth period extension factors were derived and applied to the safe crack growth analyses results developed from constant load amplitude crack growth rate data. Specifically, the crack growth period with retardation was 1.76 times the calculated crack growth period without retardation at the baseline design stress level. The factor for the less severe stress spectrum, which corresponds to the lower design stress level, was 1.50. Fundamentally, the approach followed with regard to including retardation effects was a direct approach based on experimental data specifically applicable to a particular design.

Another refinement concerns the fracture analysis related to the surface flaw data specified in the criteria. Surface flaws are listed in the criteria in terms of  $a/Q$  instead of dimensionalized shapes. Since  $a/2c$  values are not specified, it was mutually agreed by Lockheed and the ADPO that fracture allowable design stresses would be based on the assumption of a variable  $a/2c$  during the crack growth period of surface flaws. Analyses considering a variable  $a/2c$  were accomplished by modifying the computer program to evaluate surface flaw crack growth considering the variation in the stress intensity which occurs along the crack front. Crack growth morphology under these circumstances is characterized by slower crack growth along the surface than in the thickness direction. As a result, when the part-through crack



grows and penetrates the thickness, the  $2c$  dimension is generally smaller with the variable  $a/2c$  assumption than if a constant  $a/2c$  is assumed. In addition, the initial value of  $a/2c$  was taken as the worst case within an  $a/2c$  range of 0.10 to 0.50. There are complex interactions between the initial flaw depth, initial  $a/2c$  and other functions such as thickness, load spectrum and design stress level. Table XXII illustrates some of the influences of initial flaw assumptions along with related crack growth patterns. It should be observed that the flaws tend to become somewhat semi-circular during the safe crack growth period. Of particular importance is the fact that the critical initial  $a/2c$  is dependent on  $a/Q$ . This can be observed by noting that the safe crack growth period decreases as the initial  $a/2c$  increases for an  $a/Q$  of 0.03. The trend in the safe crack growth period is reversed at the higher  $a/Q$ . These complexities were taken into account in the analyses.

Damage tolerance analyses for the wing surface panels were conducted as outlined above. The derived allowable design stresses based on the fracture criteria are shown in Table XXIII. Allowables used for design stress level control include the residual strength requirements. For comparison, values based solely on the safe crack growth requirement are also listed to show the influence of the residual strength requirement on the design cut-off stress. Generally, the residual strength load was more significant at the higher design stresses levels and as a result had a greater influence on the lower wing box surface stresses, particularly for the ADP designs.

The wing surface allowable design stresses for all structural requirements, including fracture requirements, are summarized in Figures 47 through 50 in Section VII. These results indicate that the designs are reasonably well balanced with respect to the structures related functions shown in Figure 4, the Design Approach. An initial review of Figure 46 may suggest that the Virgin Plank design lacks the balance of the other design concepts, and that a more fracture resistant material should have been chosen. However, if cold working of the holes in the spanwise splice plates was omitted, both surfaces of this structure would be designed by a reduced fatigue threshold. The allowable design stress levels would be revised as shown in Figure 87. Final selections on structural arrangements, and materials and processes, were made on the basis of weight and cost effectiveness.

TABLE XXII  
INITIAL FLAW SHAPE ( $a/2c$ ) STUDY

W.S. 77.7 Upper Surface  
7050-T76 Aluminum,  $t = 0.202$   
Design Stress = 45.0 ksi  
Retardation Factor = 1.5

a/Q INCHES	(a/2c) <sub>o</sub>	a <sub>o</sub> INCHES	C <sub>o</sub> INCHES	(a/2c) <sub>t</sub>	C <sub>t</sub> INCHES	FLIGHTS					
						PART-THRU PROPAGATION	THRU-THICKNESS PROPAGATION	TOTAL TO FAILURE			
.03	.10	.033	.165	.43	.235	10,049	↓ DECREASING	4965	↑ INCREASING	15,014	↓ DECREASING
	.25	.044	.088	.46	.220	8,951	↓ DECREASING	5300	↑ INCREASING	14,250	↓ DECREASING
	.33	.052	.079	.46	.219	7,812	↓ DECREASING	5316	↑ INCREASING	13,128	↓ DECREASING
.10	.10	.112	.560	.18	.564	920	↓ DECREASING	1529	↑ INCREASING	2,448	↓ INCREASING
	.25	.146	.292	.33	.304	632	↓ DECREASING	3738	↑ INCREASING	4,370	↓ INCREASING
	.33	.173	.262	.37	.272	335	↓ DECREASING	4244	↑ INCREASING	4,578	↓ INCREASING

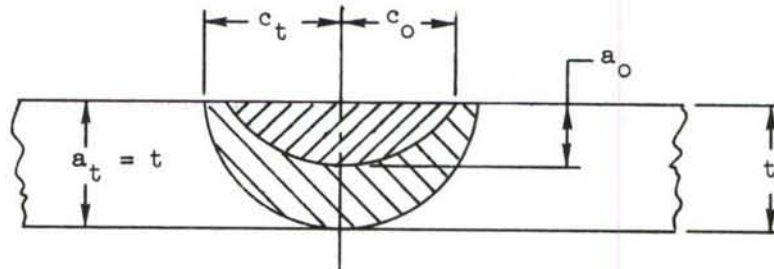




TABLE XXIII

WING SURFACE DAMAGE TOLERANCE ANALYSIS  
SUMMARY - ALLOWABLE DESIGN TENSION STRESSES

CONFIGURATION	W. S.	DESIGN STRESSES (Ksi)				CRITICAL CONDITION								
		LOWER SURFACE		UPPER SURFACE		FLAW TYPE	INITIAL SIZE	MINIMUM UNREPAIRED SERVICE USAGE						
		CRITERIA		CRITERIA										
		CRACK GROWTH ONLY	INCLUDING RESIDUAL STRENGTH	CRACK GROWTH ONLY	INCLUDING RESIDUAL STRENGTH									
Baseline	77.	46.9	45.8	39.6	39.6	Surface	a/Q=.10	(FLIGHTS)						
	285.	51.9	50.4	37.4	37.4			3274						
	415.	49.1	49.1	40.1	40.1									
Weldbond	77.	56.5	54.4	49.5	49.4									
	285.	59.6	56.5	43.0	42.5									
	415.	54.6	52.0	43.1	42.3									
Virgin Plank	77.	51.6	49.2	42.1	41.8									
	285.	55.2	51.2	39.5	39.1									
	415.	51.8	48.8	42.7	42.3									
Tapered Shingle	77.	52.4	50.0	43.3	43.0	↓	↓							
	285.	53.7	49.8	38.9	38.5									
	415.	51.0	48.0	40.5	40.1									

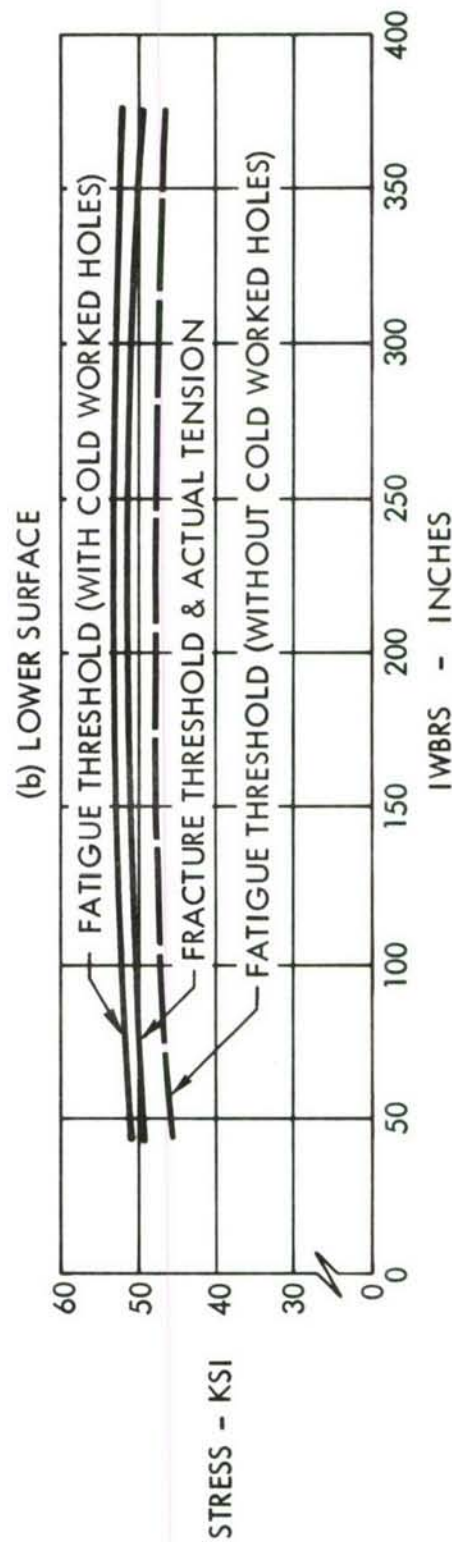
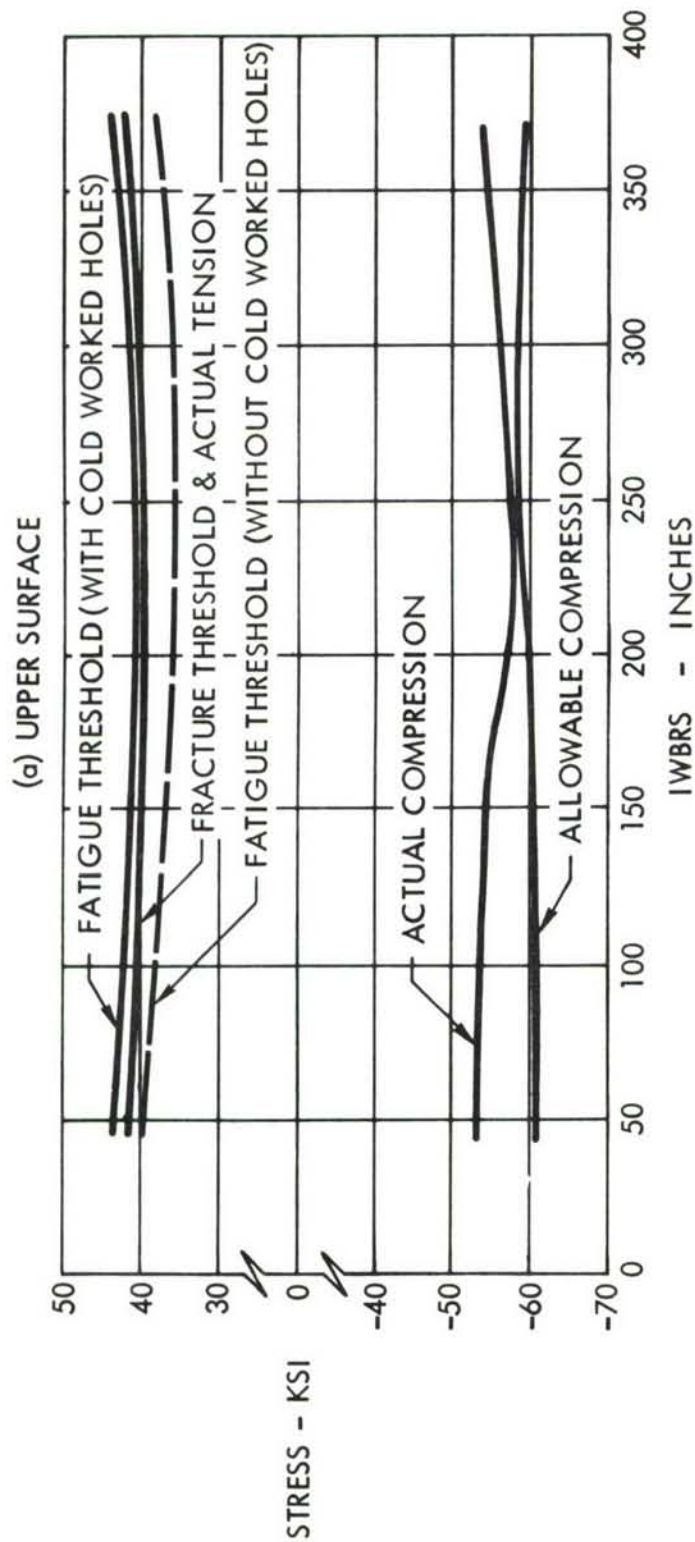


FIGURE 87 WING SURFACE DESIGN STRESS THRESHOLD  
HOLE COLD WORKING EFFECT  
VIRGIN PLANK CONFIGURATION

The fracture analysis of the W.S. 77.7 chordwise splice was based on a two part analysis: a detail internal load and deformation analysis followed by a cracked finite element analysis to determine crack tip stress intensity levels. A description of the general analysis procedure is presented in Section 8.2.2. The analysis was performed by selecting a range of crack lengths located along the row of fasteners in a general area of the splice. As indicated previously the cracks were assumed to be through-the-thickness cracks extending symmetrically from a fastener hole in the panel. For specific crack lengths, within the range selected for study, internal load and deformation analyses and cracked finite element stress intensity determinations were made for a unit external load condition. The resulting stress intensities were normalized on the basis of stress intensities for equivalent center through-cracks in an infinite plate subjected to the same far field tensile stress level. These ratios were further modified to include the Bowie correction factor due to the hole effect. Figure 88 shows the net correction factors which were applied to the nominal load spectrum in the fracture analysis of the baseline update chordwise splice. The calculated allowable design stresses and corresponding critical crack lengths are presented in Figure 89.

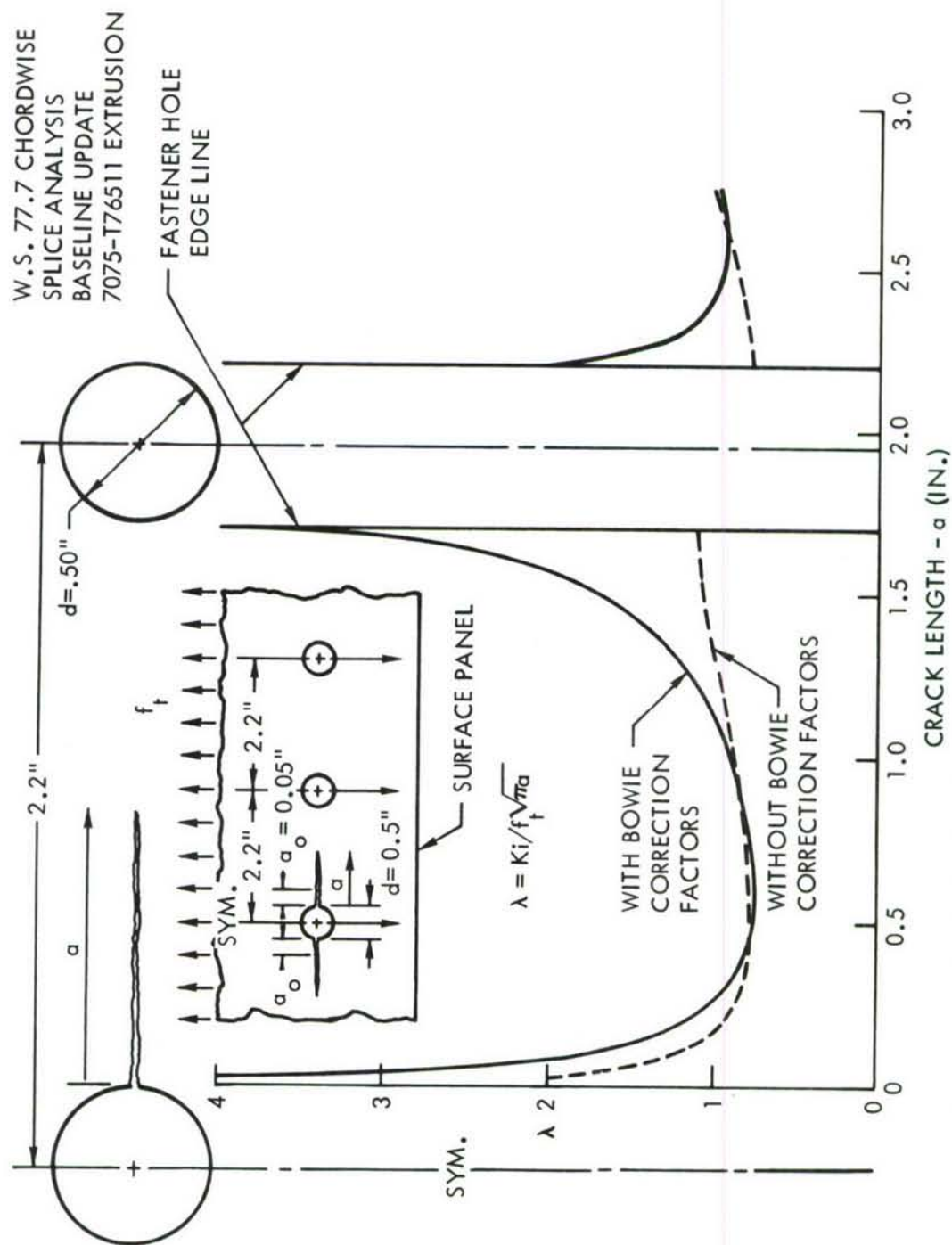


FIGURE 88 WING CHORDWISE SPLICE DAMAGE TOLERANCE ANALYSIS  
STRESS INTENSITY COEFFICIENT



W.S. 77.7 CHORDWISE SPLICE  
7075-T76511 EXTRUSION

— UPPER SURFACE  
- - - LOWER SURFACE

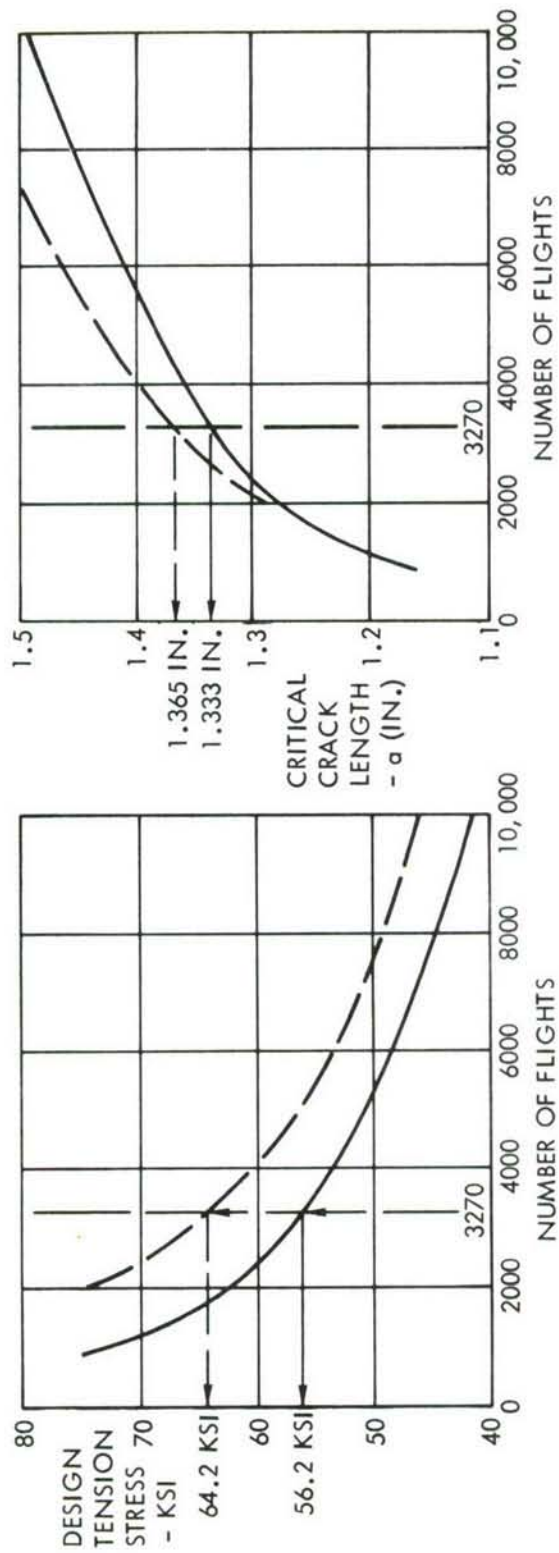


FIGURE 89 WING CHORDWISE SPLICE DAMAGE TOLERANCE ANALYSIS  
DESIGN TENSION STRESSES AND CRITICAL CRACK LENGTHS

## SECTION IX

### MANUFACTURING

Because of the ADP emphasis on advanced technology designs which can be produced for less cost, major effort was spent in developing new and innovative tooling and manufacturing approaches taking full advantage of improved processes either presently under development or proven feasible in recent R&D programs. Some of these are discussed in subsequent paragraphs along with a list of items requiring additional development.

#### 9.1 EVALUATION OF BASELINE

The C-141 inner wing baseline structure was in production until the late 1960's and represents near state-of-the-art manufacturing technology. Only minor changes were required to update the baseline manufacturing/tooling plan to 1972 technology. These changes are reflected in the cost analyses developed during the study.

#### 9.2 EVALUATION OF ADP DESIGNS

##### 9.2.1 Manufacturing

The evaluation criteria shown below formed the basis for the manufacturing ability rating of candidate concepts discussed in Section XII, "Concept Evaluation:"

- o Feasibility, including cost effectiveness
- o Predictability
- o Development of manufacturing process
- o Tooling requirements - fabrication and assembly
- o Facilities availability
- o Personnel requirements - levels of skill
- o Practicality, including cost realism

Technology advancement was considered as a final evaluation parameter which recognized new manufacturing techniques offering potential payoffs in cost, schedule, quality, and other important performance areas. In all cases, emphasis was placed on manufacturing processes which ensured highest reliability of dimensional accuracy and repeatability, material integrity, and overall economy based on minimum rejection/rework of finished parts.

#### 9.2.2 Tooling

The tooling evaluation parameters, shown in Table XXIV, were established concurrently with the above criteria and were used to evaluate candidate concepts. The type of tooling, the tooling material, and the fabrication process were largely dictated by design application and engineering tolerances, but in all cases effort was made to select tooling which would minimize cost and meet engineering requirements.

### 9.3 MANUFACTURING PLAN

Figures 90 through 92 show the three recommended designs and the initial manufacturing plan developed for each design. Each plan was developed to:

- o Establish a cost-effective sequence of major operations. (Detail operations -- e.g., deburring, cold working of holes, cleaning, and thermal treatments -- are not defined but were recognized and considered as a significant part of all evaluations.)
- o Determine development requirements for new or altered manufacturing processes.
- o Outline departmental responsibilities to ensure adequate control. (For example, in the close control of elapsed time between cleaning and application of primer in the metal bonding process.)

### 9.4 ASSEMBLY SEQUENCE

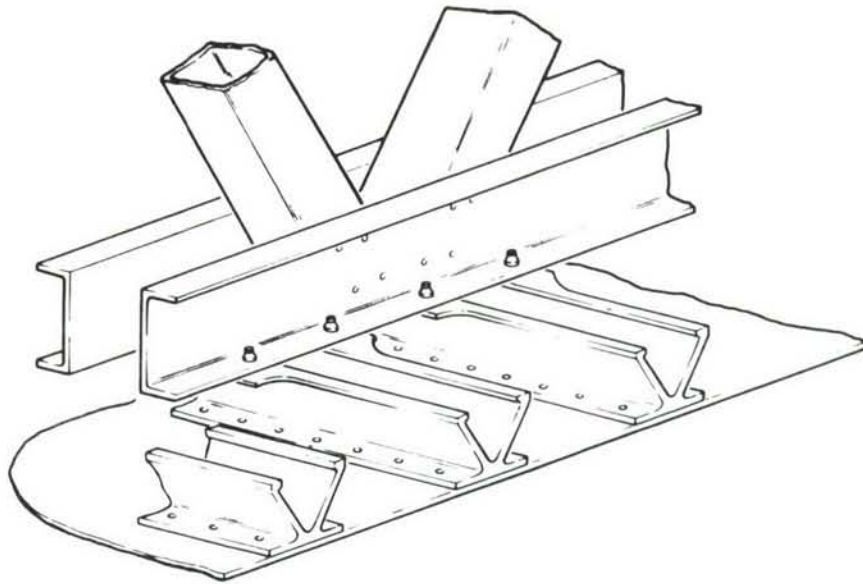
Figures 93 through 95 show the proposed assembly sequence for each configuration. Larger subassemblies lend themselves to cost effective automated processes which

TABLE XXIV  
TOOLING EVALUATION PARAMETERS

POINTS ①	TYPE OF TOOLING	FABRICATION PROCESSES	TOOLING MATERIAL	ENGINEERING TOLERANCES
1	TEMPLATE(S)	SAW AND FILE	AL	$\pm 1/8"$
2	SHOP AID TYPE - VISE JAWS	MILL-DRILL	AL & HOT ROLLED STEEL	$\pm 1/16"$
3	STRAIGHT - SOFT	MACHINED AND/OR CAST	AL-HRS-CAST	$\pm .030"$ & $\pm .060"$
4	STRAIGHT - HARD	MACHINED	HIGH STRENGTH STEELS	$\pm .030"$
5	CONTOUR - SOFT	MACHINED AND/OR CAST	AL-HRS-CAST	$\pm .030"$ & $\pm .060"$
6	CONTOUR - HARD	MACHINED	HIGH STRENGTH STEELS	$\pm .030"$
7	COMPOUND CONTOUR - SOFT	MACHINED AND/OR CAST	AL-HRS-CAST	$\pm .010$ TO $\pm .030"$
8	COMPOUND CONTOUR - HARD	MACHINED - 3 AXIS	HIGH STRENGTH STEELS	$\pm .010$ TO $\pm .015"$
9	COMPOUND CONTOUR - HARD	MACHINED - 4 AXIS	HIGH STRENGTH HI-TEMP STEELS	$\pm .005$ TO $\pm .015"$
10	COMPOUND CONTOUR WITH BLANK CONTROL - MULTIPLE SURFACES	MACHINED - 4 AXIS AND BENCH ASSEMBLY	HI-TEMP - HI- STRENGTH STEELS	$\pm .003$ TO $\pm .010"$

① 1 ————— 10  
DIFFICULTY





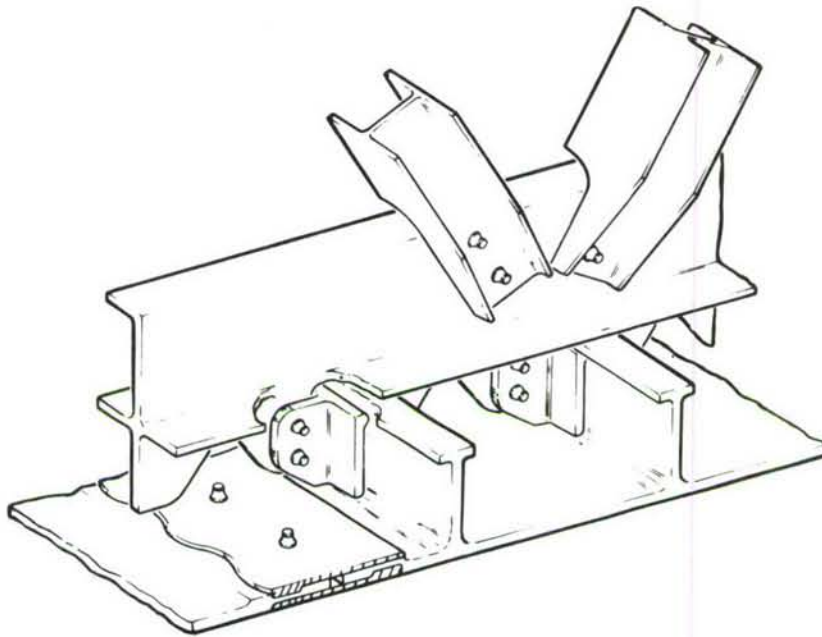
#### MANUFACTURING PLAN

- MACHINE SKIN PANEL
- STRINGERS - USE AS-EXTRUDED EXCEPT FOR ROUTING OF RIB ATTACHMENT FLANGE
- CLEAN & WELDBOND STRINGERS TO SKIN - OVEN CURE AT 250°F
- FORM RIB CAPS AND DRILL
- ASSEMBLE RIB CAPS, BRACES, ETC.
- ASSEMBLE TWO SUBASSEMBLIES
- ELECTRON BEAM WELD SPAR CAPS TO WEB
- ASSEMBLE SPARS TO WING BOX - BOND - OVEN CURE AT 250°F
- COMPLETE ASSEMBLY

#### DEVELOPMENT REQUIREMENTS

- TOOLING FOR SKIN-SPAR BONDING
- BURN THROUGH WELD OF ALUMINUM
- COORDINATED FORMING & ASSEMBLY TOOLS
- CORROSION PREVENTION SYSTEM FOR WELDBOND

FIGURE 90 MANUFACTURING PLAN - WELDBOND CONFIGURATION



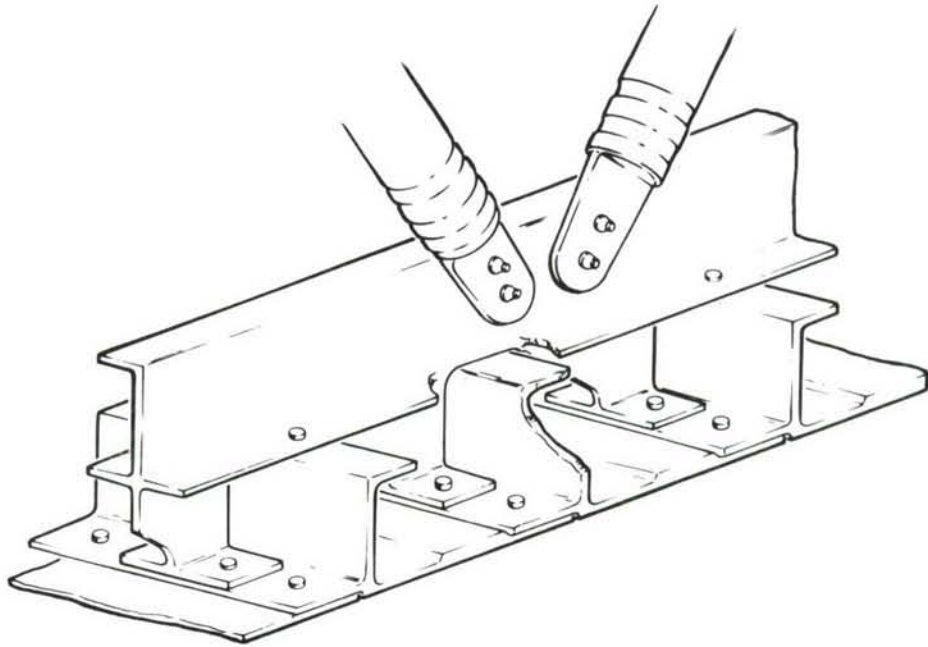
#### MANUFACTURING PLAN

- PLANE SKIN PANELS WITH MULTIPLE TOOL SETUP
- OVEN BOND SKIN SPLICES
- ASSEMBLE PREDRILLED CLIPS, DESTACK, DEBURR, & ASSEMBLE
- ASSEMBLE SPARS
- BOND CLOSE-OUT SPLICE
- ASSEMBLE SUB-STRUCTURE

#### DEVELOPMENT REQUIREMENTS

- NON-PENETRATING CLIP - ASSEMBLY PROCEDURE
- TOOLING FOR SKIN-SPLICE BOND
- MULTIPLE TOOL PLANING OF SKIN PANELS

FIGURE 91 MANUFACTURING PLAN - VIRGIN PLANK CONFIGURATION



#### MANUFACTURING PLAN

- PLANE INTEGRAL STIFFENED PANELS
- ASSEMBLE COVERS (RIVET)
- FORM AND OVERAGE RIB CAPS
- ASSEMBLE RIB CAPS TO COVERS
- ASSEMBLE SPARS
- ASSEMBLE SUB-STRUCTURE

#### DEVELOPMENT REQUIREMENTS

- TUBE AND END FITTING ASSEMBLY PROCESS
- AUTOMATED INSTALLATION OF STRESS WAVE RIVETS
- RIB CAP FORMING AND THERMAL TREATMENT SEQUENCE
- MULTIPLE TOOL PLANING OF SKIN PANELS

FIGURE 92 MANUFACTURING PLAN - TAPERED SHINGLE CONFIGURATION

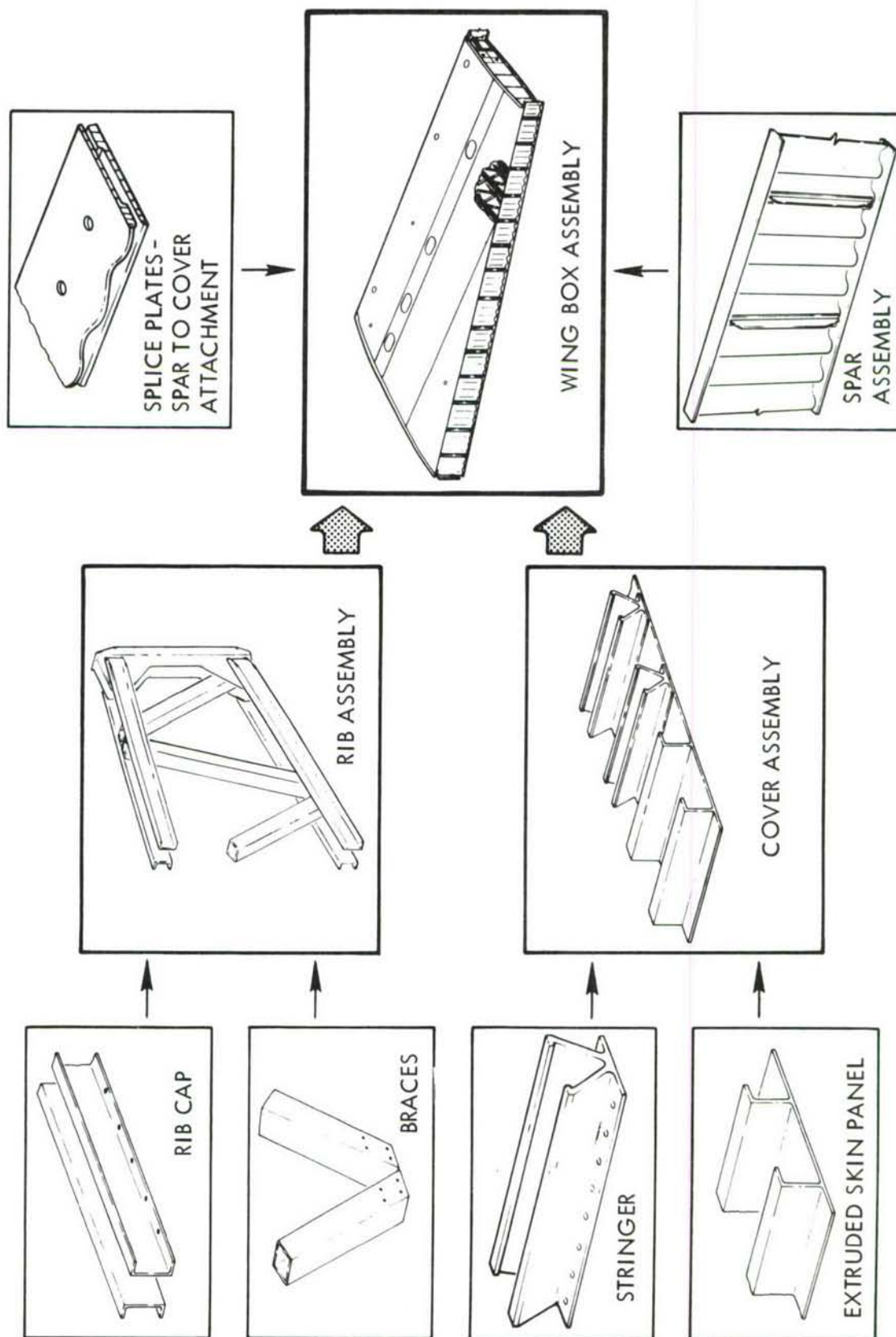


FIGURE 93 MANUFACTURING SEQUENCE - WELDBOND CONFIGURATION



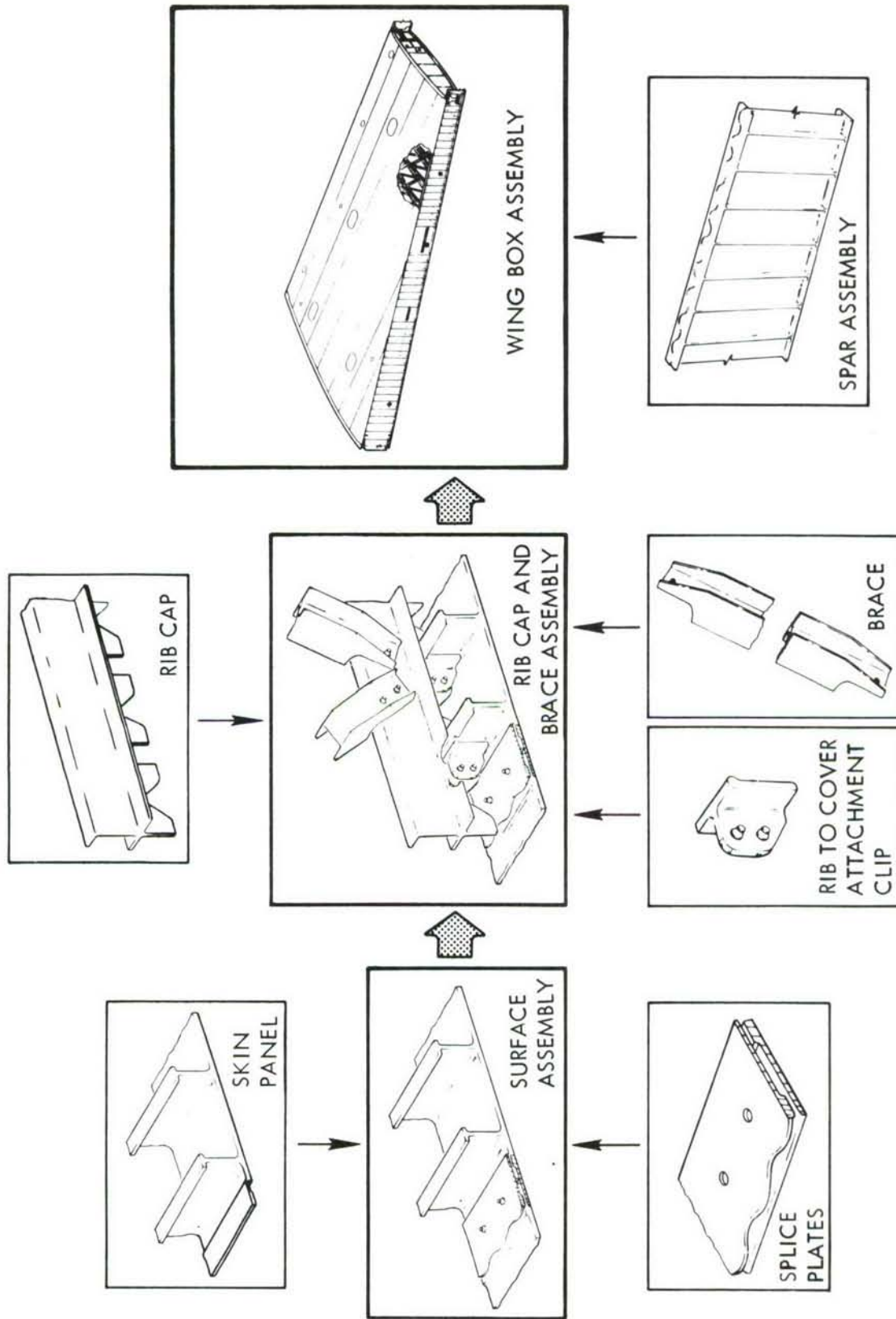


FIGURE 94 MANUFACTURING SEQUENCE - VIRGIN PLANK CONFIGURATION

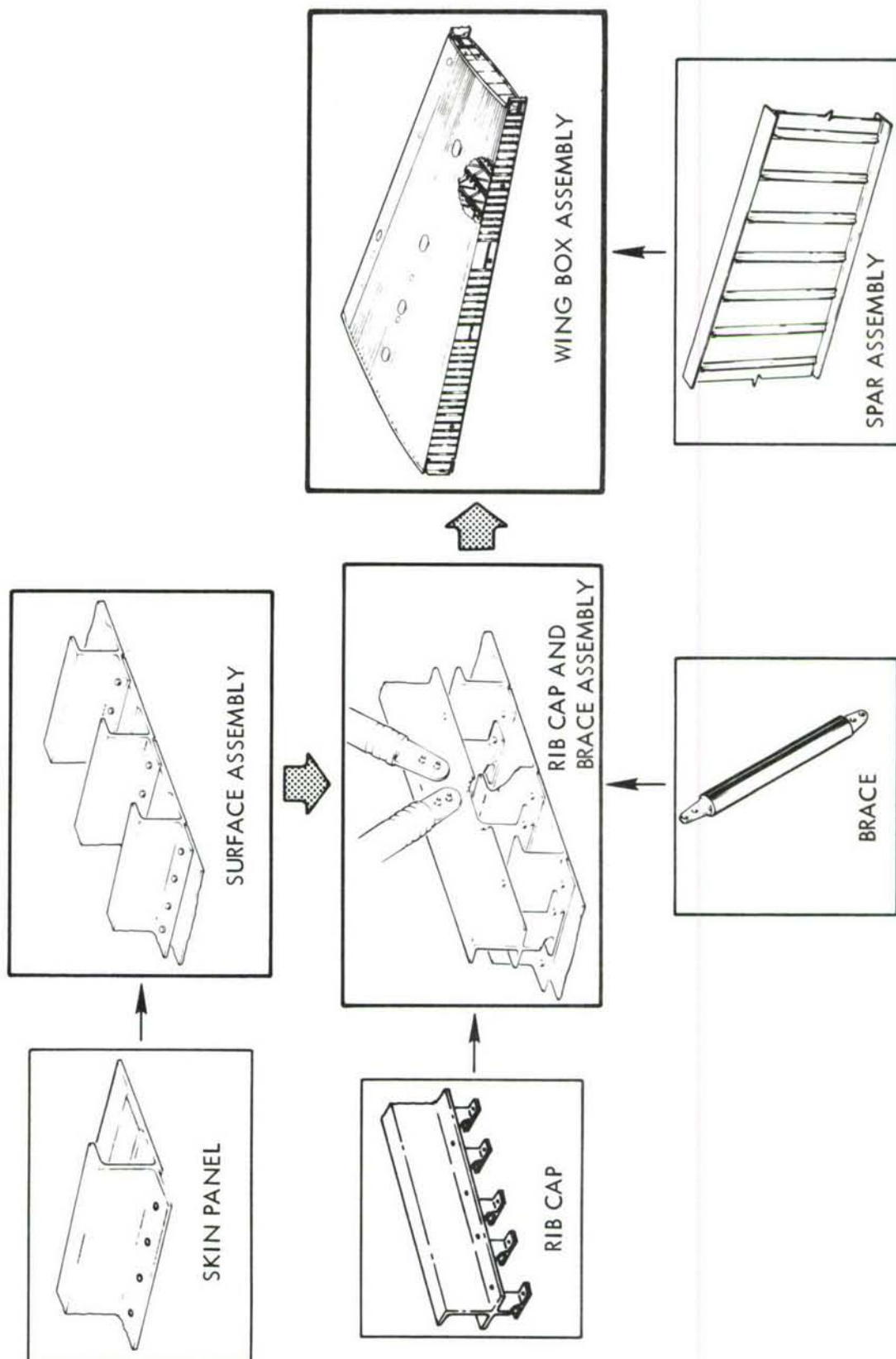


FIGURE 95 MANUFACTURING SEQUENCE - TAPERED SHINGLE CONFIGURATION

provide repeatable dimensional accuracy. The use of coordinated tooling, together with close production control, ensures a minimum tolerance build-up which is necessary for high-quality, low-cost structures.

## 9.5 MANUFACTURING COST EFFECTIVENESS

Figures 96 through 98 show some of the manufacturing processes proposed for each configuration to achieve low cost. Cost effectiveness has been achieved in primary and secondary fabrication processes and in assembly procedures. All facets of manufacturing were investigated for additional cost savings. Some of these include:

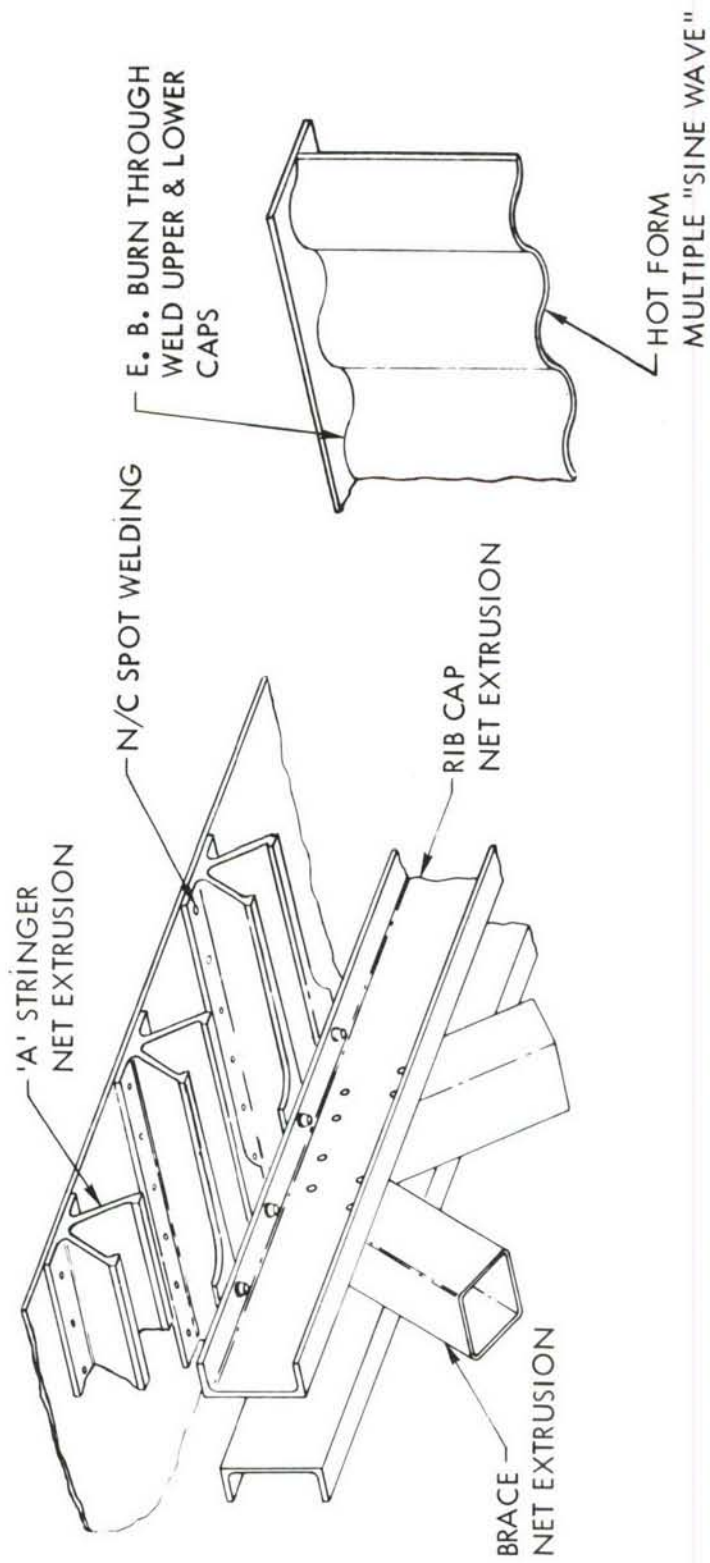
- o Multiple-tool planing of integrally stiffened skins
- o Gang milling using straight and contoured cutters
- o Air actuated drill jigs, lathe chucks, etc.
- o Automated drilling, reaming and deburring
- o Vacuum handling equipment for fabrication and assembly
- o Coordinated tooling through all phases of manufacture
- o Larger sub-assemblies

## 9.6 MANUFACTURING DEVELOPMENT ITEMS

Several manufacturing processes which show large potential payoffs in ADP designs require some additional development before commitment to prototype production. The status of some of the more significant items is presented below.

### 9.6.1 Welded "Sine Wave" Spar

The use of the "Sine Wave" spar concept proposed in the weldbond configuration necessitates the development of a reliable electron beam burn-through weld technique for aluminum alloys. Welding experiments conducted during 1966 utilizing the TIG welding process were discontinued because the oxide on the interface of the aluminum details became entrapped in the weld as large flakes. The oxide flakes exhibited a complete loss of cohesiveness which resulted in a weld efficiency of only ten to twenty percent. However, more recent experiments conducted on both 6061 and 2219 aluminum alloys using the electron beam process indicate that weld efficiencies of 80%



- BONDING PROCESS FOR SPLICE  
AT FRONT BEAM USES  
ELASTOMERIC TOOLING  
(SEE SECTION 9.6.2)

FIGURE 96 MANUFACTURING COST EFFECTIVENESS - WELDBOND CONFIGURATION



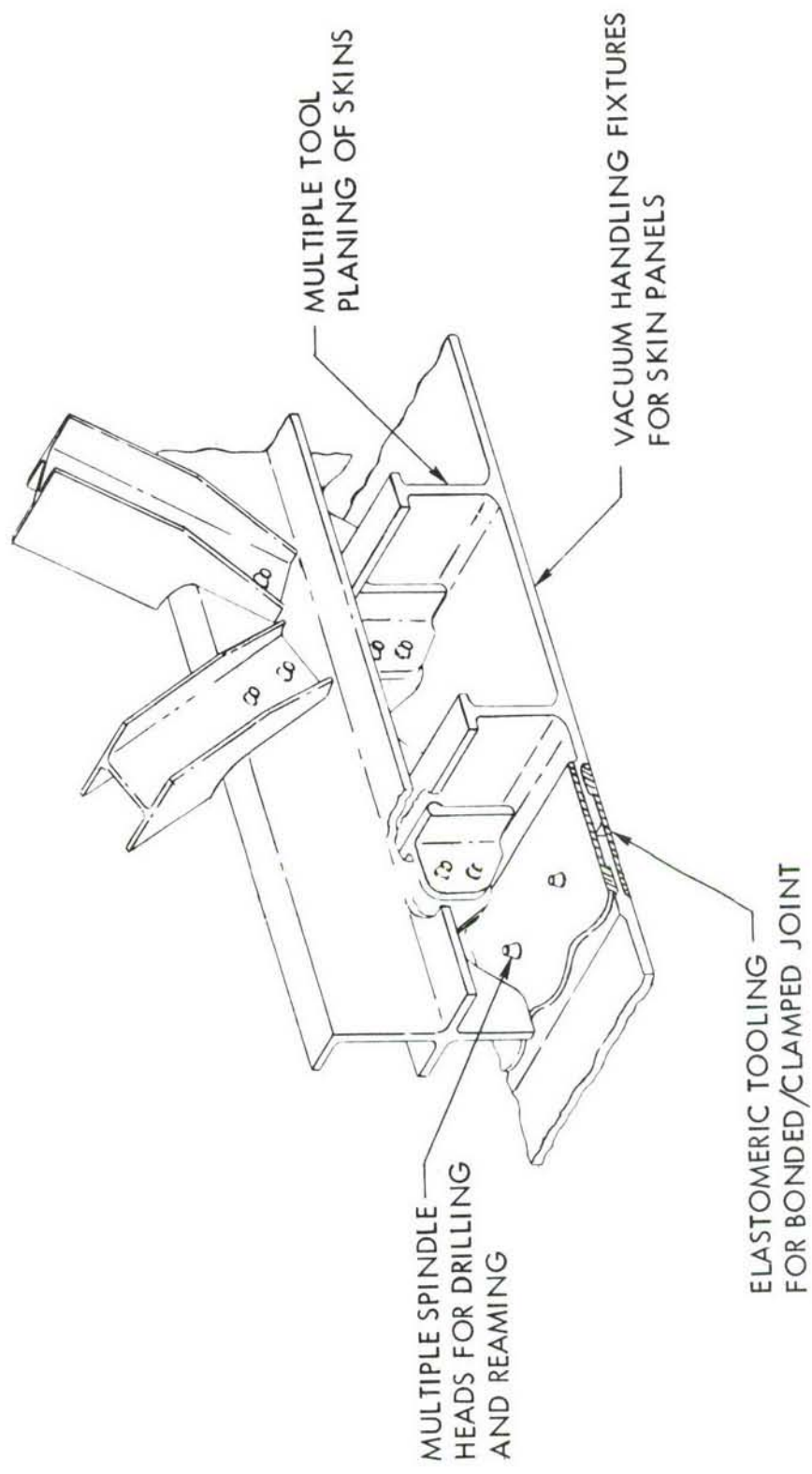


FIGURE 97 MANUFACTURING COST EFFECTIVENESS - VIRGIN PLANK CONFIGURATION

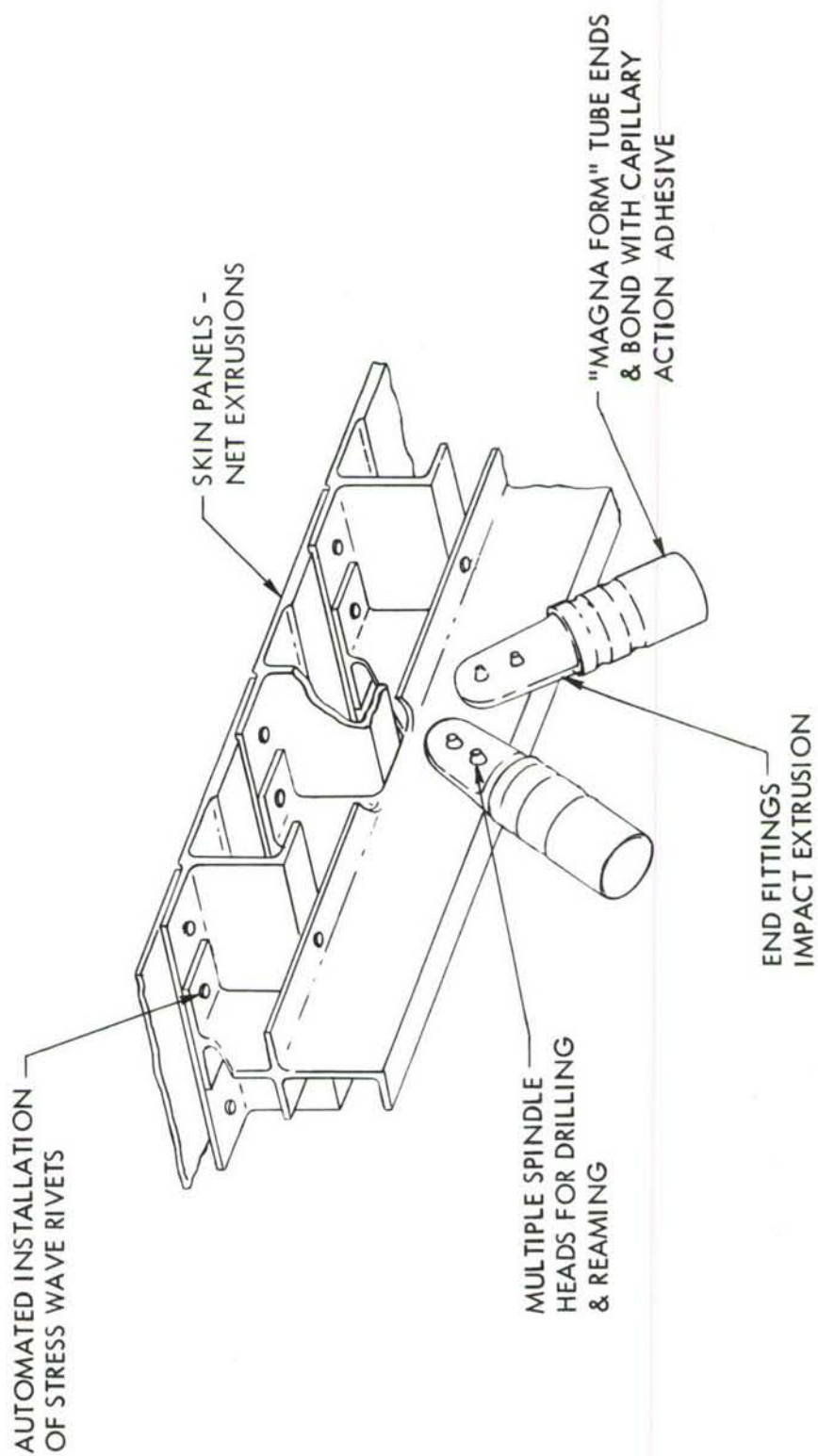


FIGURE 98 MANUFACTURING COST EFFECTIVENESS - TAPERED SHINGLE CONFIGURATION

or higher are attainable. An EB-welded specimen fabricated from 0.160" thick 6061-T4 sheet stock was tested with excellent results. An ultimate allowable in excess of 95% of parent metal  $F_{tu}$  was obtained with good reduction in area across the weld. Similar experiments using 2219-T87 aluminum show efficiencies of 81% when welded joints were aged at 375° for 36 hours, then air cooled. Additional development work is needed to improve weld efficiencies in 2219 to the 90% range for ADP usage.

In addition, for out-of-chamber EB welding desired for ADP designs, a technique to pivot or rotate the welding gun must be developed in order to reduce the oxide film to microscopic particles. This is presently accomplished in the vacuum chamber by a circle generator which oscillates the electron beam to break up the oxide film.

#### 9.6.2 Lockmold Elastomeric Tooling for Bonded/Clamped Splices

This process developed by Lockheed utilizes the thermal expansion of rubber to provide bonding pressure, thereby eliminating the high cost of bagging and autoclaving. This process has been used successfully on development projects for bonding C-140 fuselage panels and close out ribs for the C-141 horizontal stabilizer. The additional development necessary for its use on the bonded splices in the Weldbond configuration and the Virgin Plank configuration is considered to be low risk, and primarily involves the sizing of rubber and restraining tooling to ensure the uniform application of the correct bonding pressure at the 250°F adhesive curing temperature.

#### 9.6.3 Magnaformed/Bonded Joints

The use of the magnaform/bonding process for attachment of end fittings (shown in the Tapered Shingle configuration rib diagonals) has a good potential as a low cost joining method which provides excellent structural performance. There was a spring-back problem associated with early development of the magnaform process, but this problem can be eliminated by use of a post-forming application of capillary action adhesive. Additional development of this process consists primarily of optimizing forming procedures and adhesive cure cycles.

#### 9.6.4 Fatigue Resistant Splices

Several improved spanwise splice design concepts were considered for proposed cargo/tanker designs. One of these was proposed to fulfill the need for a bonded/clamped joint suitable for use with the Virgin Plank configuration. The machining of the matching sine wave patterns shown in the covers and splice plates requires the development of a coordinated numerically controlled machining process to ensure proper fit of the mating parts.

#### 9.6.5 Stress Wave Riveting

The use of stress wave riveting for fabrication of critical cover and spar assemblies will require the development of automated procedures not presently in use. Requirements will dictate the use of integrated tooling with N/C positioning as well as means of absorbing shock of gun recoil while maintaining proper position.

#### 9.6.6 Weldbond Process

The weldbond process is very attractive for ADP designs, and its use is contemplated for several applications including stringer to skin attachment and spanwise splices. Although the basic process has been proven, additional development of the optimum surface preparation and adhesives to be used for the best balance of corrosion resistance and structural performance will be required. Also, additional development of automated spotwelding procedures is necessary. Recent fatigue tests, as discussed in Section 6.1.1.3, have indicated that improvements in the Fatigue Quality Index are desirable for low load transfer weldbonded joints. Currently, indications are that this fatigue improvement may be achieved by controlling process variables during spotwelding and/or improving the metallurgical characteristics of the weld nugget/HAZ (Heat Affected Zone) through a cold working or forging process.



## SECTION X

### QUALITY ASSURANCE/NDI

The basic program philosophy in the Phase IA study was to place heavy emphasis on designing for inspectability. Particular attention was given to critical joints and splices to eliminate potential problem areas and to ensure adequate inspection methods. In addition, the inspectability of designs incorporating new technology such as Weld-bond and Lockskin were evaluated in the light of methods and equipment currently available.

#### 10.1 EVALUATION OF BASELINE DESIGN

Inspectability information was collected for evaluation of baseline structural arrangements. In addition to an analysis of nondestructive inspection requirements for the baseline update, an assessment of baseline inspectability was made for purposes of defining preliminary inspection categories for use in fracture analyses. This inspectability assessment was made on 10 major subdivisions of structure (1. Upper covers, 2. Lower covers, 3. Spars, 4. Special areas, e.g., pylon and flap track fittings, 5. Chordwise splice, 6. Spanwise splice, 7. Structure under fairings, 8. Bulkheads, 9. Major fittings, 10. Truss ribs) for inspection criteria ranging from in-flight-evident to non-inspectable. These results are summarized in Table XXV.

#### 10.2 EVALUATION OF ADP DESIGNS

In support of the concept evaluation described in Section XII, ADP designs were reviewed and scored using a relative merit rating system. Parameters considered in this evaluation were:

- o Cost
- o Accessibility to parts
- o Defect character
- o Part configuration
- o Surface finish
- o Material composition
- o Human factors

TABLE XXV  
IN-SERVICE INSPECTABILITY FACTORS

C-141 INSPECTION	INTERVAL	CORRESPONDING USAF DAMAGE TOLERANCE CRITERIA INSPECTION	ACCESSIBILITY FACTORS	NDI TECHNIQUES USED <sup>(1)</sup>	DAMAGE SIZE DETECTION CAPABILITY (IN.)
In-Flight	Not Applicable	In-Flight	None	None	20.0
Pre-Flight	Before Flight	Walk Around/ Special Visual	None	None	5.0
Thru-Flight	Enroute, Before Flight	Ground Evident	None	None	10.0
Home Station	10 Days 38 Flights	Ground Evident	None	None	10.0
Minor	70 Days 105 Flights	Special Visual	None Required on Inner Wing	None	2.0 (Visual)
Major	140 Days 209 Flights	Special Visual	All Access Doors & Panels	None	2.0 (Visual)
Mid-Interval IRAN	18 Months 819 Flights	Depot Level	All Access Doors, Leading Edges, & Panels	See Table XXVI	
Depot IRAN	36 Months 1637 Flights	Depot Level	All Access Doors, Pylons, Wing Edges at Pylons		
ACI(Analytical Condition Inspection)	36-42 Months on Limited Number of Aircraft	Depot Level	All Access Doors, Pylons, Wing Edges at Pylons		
Special Investigation	After Extreme Conditions	Depot Level on Affected Areas	As Required		

NOTES: (1) Assumed based on experience.  
(2) Data applies to C-141A Inner Wing only.

TABLE XXVI  
C-141 INNER WING NDI PROCEDURES<sup>(1)</sup>

LOCATION CATEGORY	PAGE	PROCEDURE	ASSUMED CRACK LENGTH <sup>(2)</sup> DETECTABILITY (INCHES)
Skin Panels at Flanges, Access Openings, Pump & Probe Holes, Vent Boxes	4.3	E/C Surface Probe U/S Shear Wave E/C Bolt Hole Probe	0.15 0.25 0.08
Wing Attach Fittings at F.S. 734 and 958	4-1	P Inspect Hole Wall	0.30
Access Doors "O" Ring Groove	4-11	P	0.10
Front Beam Upper Cap Splice Fitting, WS 405 and IWBR 374.47	4-28	X/R	1.25
Upper and Lower Chord- wise Splice, IWBR 374	4-38	X/R	1.25
Upper and Lower Chord- wise Splice, WS 77.7	4-50	X/R	1.25
Rear Beam Web Splice and Tee, IWBR 374	4-48	VISUAL P	2.0 0.1

CODE: E/C - Eddy Current  
U/S - Ultrasonic  
P - Penetrant  
X/R - X-ray Radiography

NOTES: (1) From C-141 Inspection Manual T.O. 1C-141A-36  
Procedures (Reference 10)

(2) Based on a consensus of estimates tempered  
with data referenced in Section 10.3



### 10.3 RELIABILITY OF NDI METHODS

Two Lockheed programs on the reliability of nondestructive inspection methods were reviewed for application to ADP designs. Results of one program involved inspections of simulated aircraft structure, using data derived from ultrasonic shear wave scans around fasteners. In these tests, fatigue cracks were known to be present in 10% of fastener locations, with crack lengths ranging from 0.03" to 0.30". The desired 90% detection level at a 95% level of confidence as required by the "Proposed USAF Damage Tolerance Criteria" was not achieved in this effort. Rather, a 70% detection level of 95% confidence for cracks in the 0.20" to 0.25" upper midrange was attained. Redundant inspections, where the second observation was conducted with knowledge of results from the first, yielded significant gains for detection of cracks in the mid-range from 0.10" to 0.20" as shown in Figure 99. Less significant gains at the range extremes from redundant inspection yielded 8% to 10% improvements in detection level.

The second program involved inspection of C-130 wing boxes after fatigue test. Data were acquired on detection of surface fatigue cracks radiating from fastener holes in wing planks. These data were obtained from ultrasonic shear wave and eddy current surface scans. Detection levels of 70%, at 95% confidence levels, for 0.45" cracks were observed for both of these NDI methods with single inspections. Independent repeat inspections, combined to yield composite defect finds, were also conducted. Five inspections were required to attain a 100% find for 0.2" cracks; two inspections were needed to yield a 100% find for 0.4" cracks as shown in Figure 100. Work is currently in progress on this program to measure the influence of human factors on inspection reliability.

It is apparent from the NDI Reliability programs described above that a single inspection will not be adequate for the detection of flaws within a length range from 0 to approximately 0.5". Capabilities of single inspections for detection of cracks from 0.5" to 2.0" lengths are also marginal, yet damage tolerance criteria for the "Slow Crack Growth" model used extensively in this program require reliable detection of 2.0" cracks in service. Additionally, the "Slow Crack Growth" model appears to have the least stringent NDI requirements as compared to the other two models "Fail-Safe Crack Arrest" and "Multiple Load Path, Fail-Safe" defined in the Damage Tolerance Criteria.



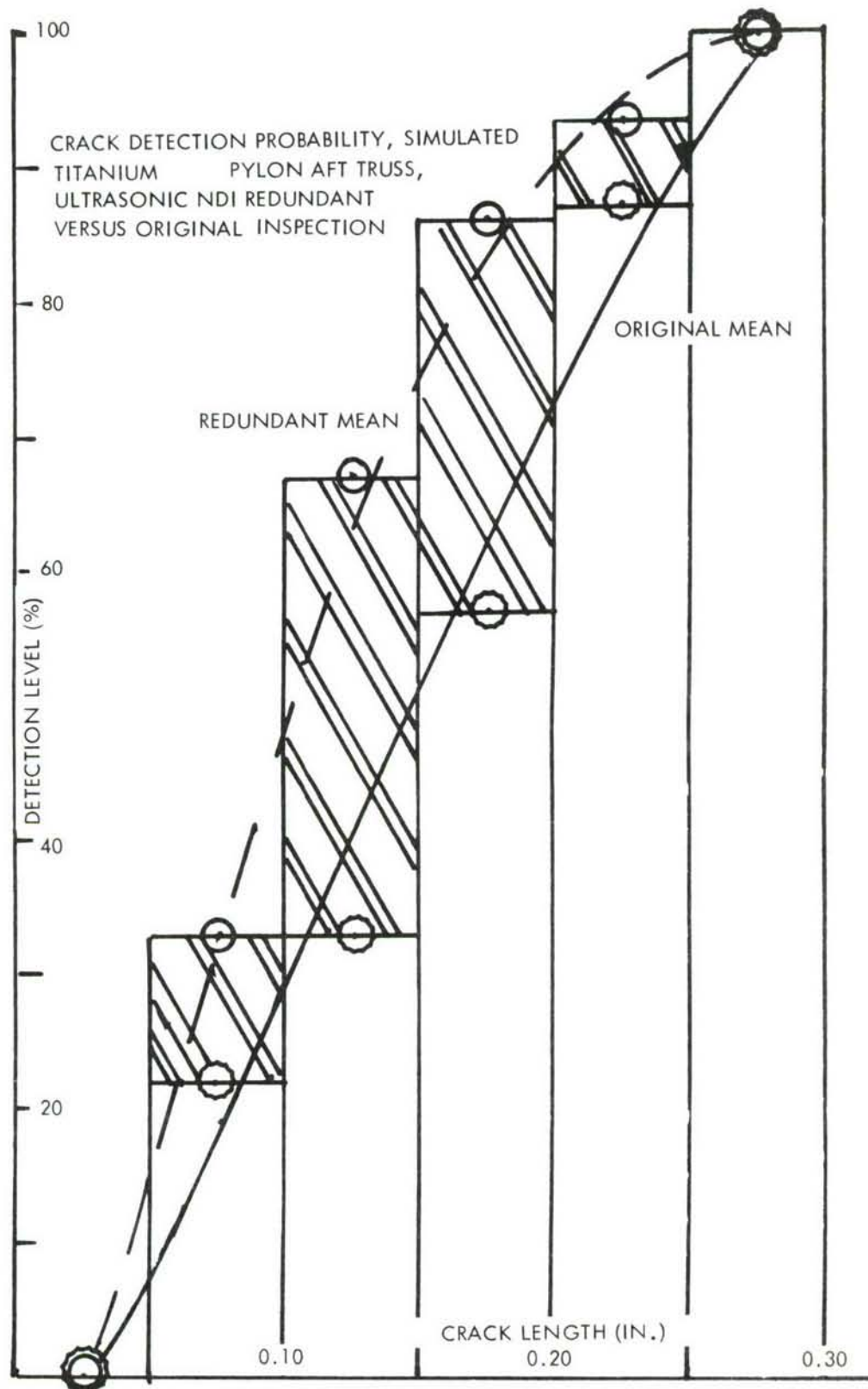


FIGURE 99 CRACK DETECTION PROBABILITY

 INDICATES NUMBER OF INSPECTIONS

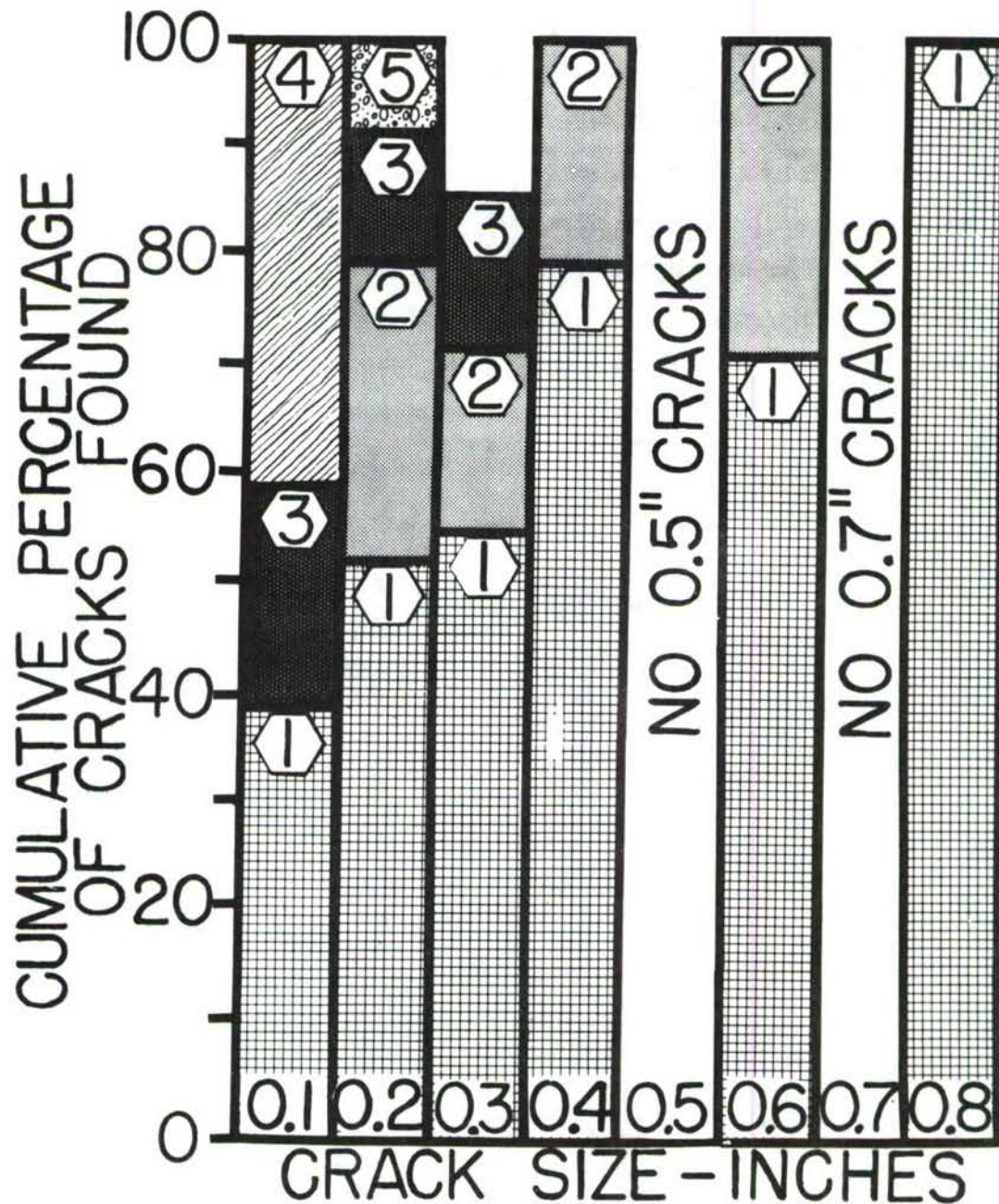


FIGURE 100 ULTRASONIC NDI REPEAT INSPECTIONS

Assurances of structural integrity throughout the life of the aircraft by NDI can be used effectively if the structure is inspectable and the NDI cost is not prohibitive. All candidate designs reviewed in this program rated within a narrow band of index values which fell within the range of good to very good inspectability. This cost can be taken as the dominant selection factor. No NDI cost values were estimated on this program, but an estimate of production NDI cost, as a percent of the total, is indicated by the experience gained on the B-1 Bomber program. The demonstration of production level NDI reliability, which is the first time such a requirement has been implemented, has cost less than 0.005 of the total B-1 design, development, test, and evaluation functions (Reference 13). It is anticipated that a similar cost increment would be added to a cargo/tanker inner wing production inspection cost to fulfill the production NDI demonstration requirement.



## SECTION XI

### COST/PRODUCIBILITY

Cost estimates were developed for the baseline, updated baseline, candidate ADP designs, and recommended designs. Costs for the baseline original C-141 inner wing were developed from actual costs incurred on the C-141 production program. The updated baseline cost was estimated by modifying the original baseline cost by incremental cost values derived from detailed analysis of the design changes to update the baseline to 1972 technology. Cost estimates for the ADP candidate designs were based on a step-by-step detail analysis using actual material requirements and standard labor data. After the recommended ADP designs were selected, more refined cost estimates were made on those designs and these costs were updated to reflect additional optimization.

#### 11.1 BASELINE COSTS

The baseline cost data were derived from actual material and manhour costs incurred on three separate contracts for 5, 145, and 134 aircraft sets of C-141 wings. The detailed breakdown for the inner wing was achieved by proportioning the total wing box cost by the ratio of planform areas. The apportionment was initially made on the basis of weight, but after additional data were studied, apportionment by area was judged more appropriate. Since systems were excluded from the structural study, the fuel system cost was independently estimated and extracted from the baseline cost. To convert these actual costs to "1972 dollars," the manhour rates for 1972 were used, and material costs were increased by the appropriate factor for economic escalation, based on historical experience of industry prices since 1958.

Inner wing costs were developed for 100 aircraft based on a labor learning curve of 84% and a material learning curve of 89%. These percentages were derived from actual experience on the C-141 wing box subcontract and were also used in developing costs for all ADP designs.

An updated baseline cost was obtained by modifying the original cost by incremental cost values derived from analysis of the changes attendant to the original C-141 design



to 1972 technology. This updating included such considerations as material selection, fastener systems, nondestructive inspection, finishes and processes, and damage tolerance criteria for the major structural elements. The more significant incremental changes resulting from this exercise are discussed in Section 3.5.

## 11.2 COSTS OF ADP CANDIDATE DESIGNS

Figure 101 shows cost ratios of all eight candidate configurations relative to the total cost of the updated baseline structure. The Lockskin, Sandwich, and Composite Hat configurations were eliminated primarily because of the high costs shown. Although cost contributed to elimination of the "Hat" stringer configuration, other shortcomings were equally important. The Monolithic configuration was eliminated for weight reasons even though its cost seemed promising. The surviving Weldbond, Virgin Plank, and Tapered Shingle designs were then costed more extensively along the lines discussed below.

Initially, manufacturing plans were formulated for each selected configuration, the baseline, and the updated baseline. Section IX identifies the manufacturing processes and sequence of manufacturing operations. Working within this manufacturing plan cost estimates for each major structural component were developed for the selected configurations, the baseline, and the updated baseline. These estimates were based on a step-by-step detail analysis, using actual material requirements and standard labor data. The total structural cost of each configuration was developed by substituting the cost of the redesigned sub-components. Figure 102 is a typical flow chart of activities required to develop the cost of candidate configurations.

Detailed estimates for the redesigned sub-components were established by analysis of the direct material and labor requirements to produce the designs in accordance with the manufacturing plan developed herein.

Raw material requirements were established from the fabrication requirements. For other material items contributing significantly to cost, such as fasteners, detailed costs were determined by part count. For the most part, material costs were estimated using standard Lockheed pricing practice. In some cases, vendor quotations and Lockheed-Georgia inventory cost reports were used.

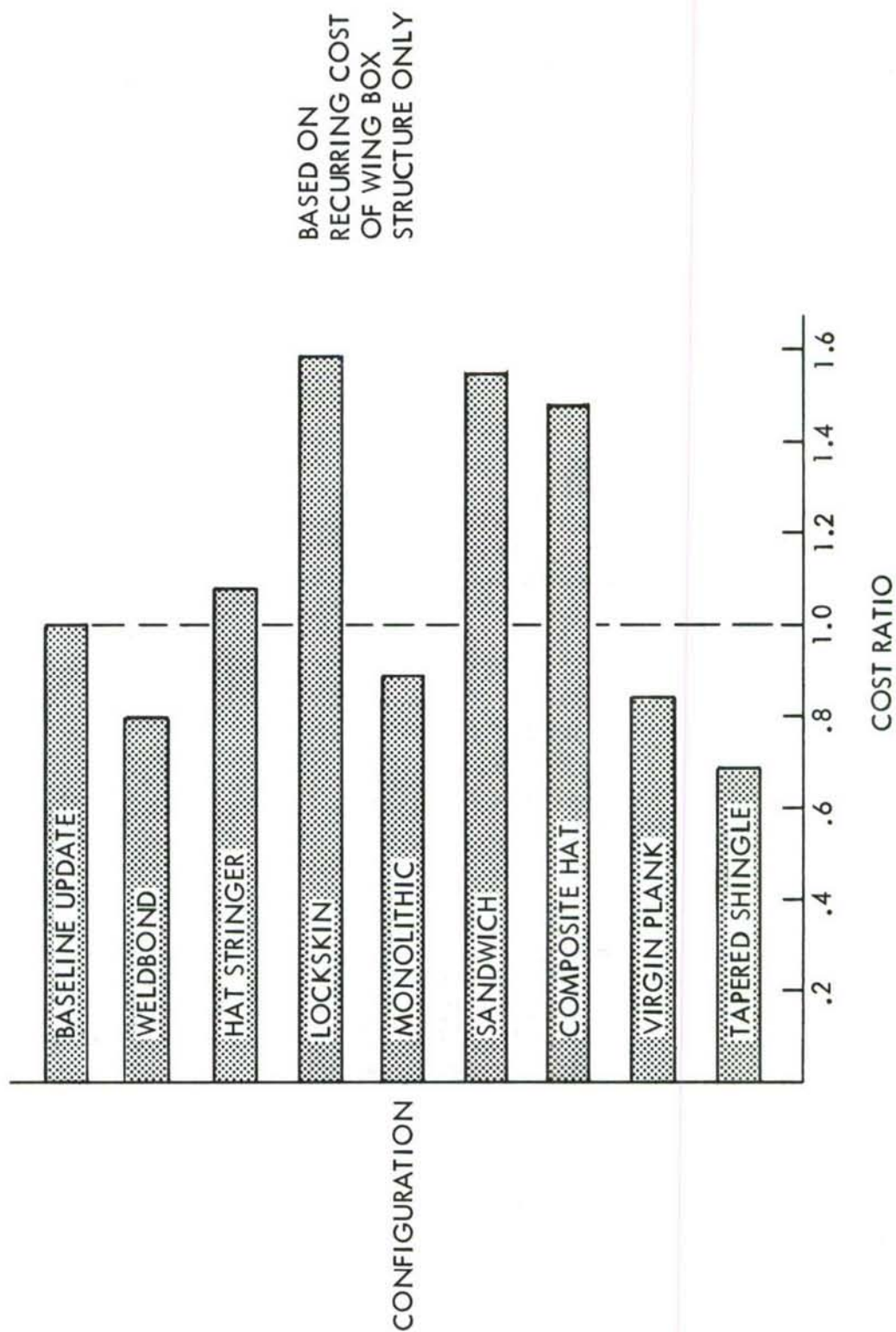


FIGURE 101 COST COMPARISON OF CONFIGURATIONS

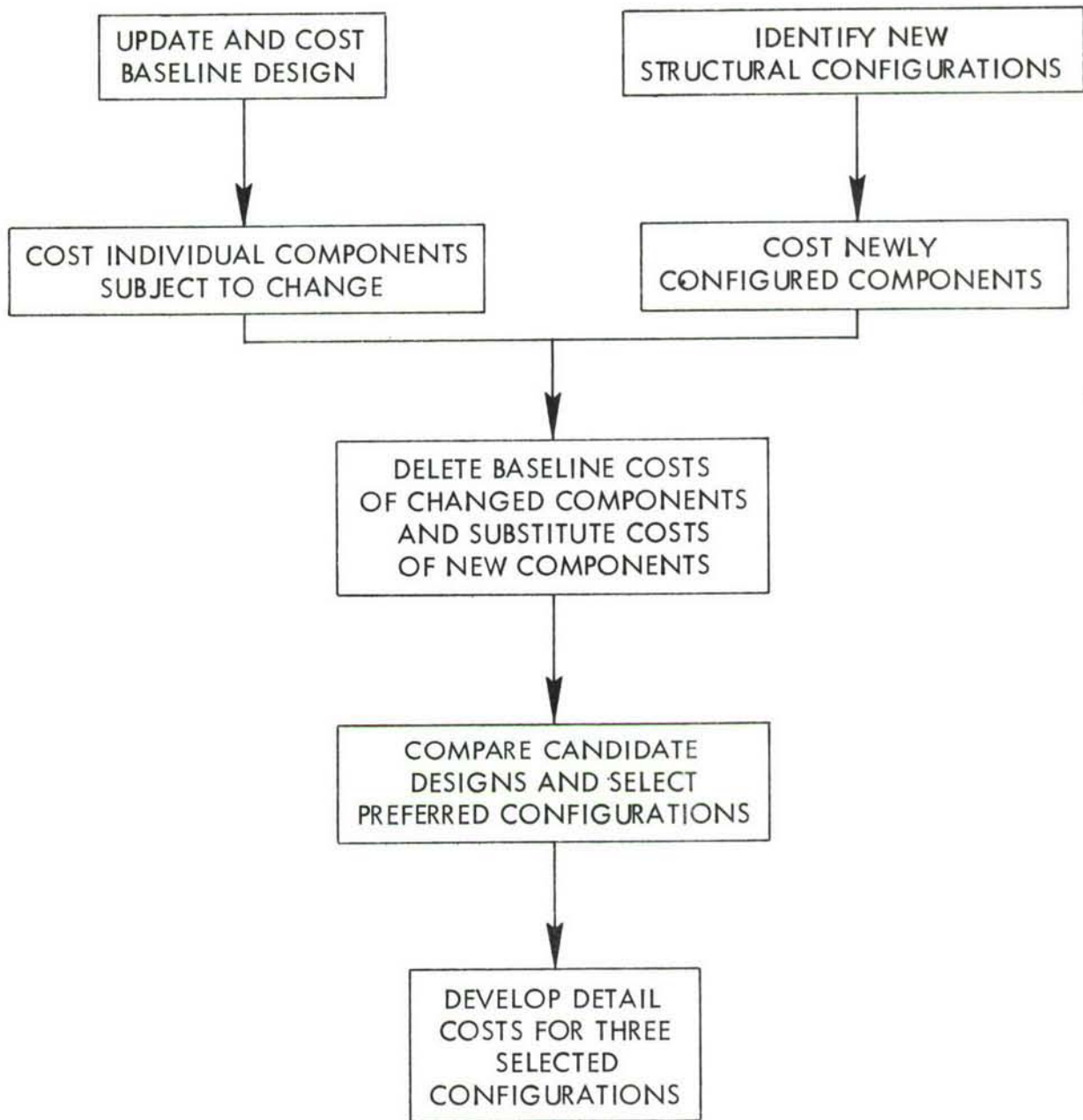


FIGURE 102 COST DEVELOPMENT PROCEDURE



Based on the manufacturing plan, the production labor requirements were developed by using Lockheed estimating standards along with appropriate realization factors and learning curves for quantity consideration. For sheet-metal fabrication, machining, processing, welding, and bonding, Lockheed-Georgia time standards data were used, supplemented by standard cost handbooks from other Lockheed facilities. For the more advanced structures using weldbonding and composites, standard data developed at Lockheed-Georgia for those processes and materials were used.

Tooling estimates for each configuration were made on the basis of those tooling concepts related to the manufacturing plan, number of parts and individual tools required, major assembly tools involved such as bonding fixtures or large machining tools, and degree of tooling development required.

### 11.3 COSTS OF RECOMMENDED ADP DESIGNS

Cost estimates for the baseline, baseline update, and the final three ADP design configurations are summarized in Table XXVII for the complete inner wing box. Costs presented cover initial design engineering, initial tooling, and recurring production labor, material, and quality assurance. Table XXVIII is a further cost breakdown, wherein apportionment of recurring cost is made in accordance with the sub-component breakdown for each of the ADP designs, the baseline, and the baseline update configurations. The non-recurring cost is not broken down; therefore, it is not identified with the sub-components and is only presented in Table XXVII. Costs presented are estimates derived by progressive iterations considering the latest refinements in design details and manufacturing plans. Figures 103, 104, and 105 show for the Weldbond, Virgin Plank, and Tapered Shingle Configurations, respectively, typical examples of the cost savings features associated with the ADP designs. These and other cost features are discussed below.

#### 11.3.1 Weldbond Design

In this design, significant cost savings over the baseline are obtained in the spanwise splices, ribs, rib cap attachment to the covers, and spar cap attachment to the covers.



TABLE XXVII  
COST BREAKDOWN - THREE SELECTED DESIGNS  
INNER WING BOX COMPLETE

CONFIGURATION	BASELINE	UPDATED BASELINE	WELDBOND	VIRGIN PLANK	TAPERED SHINGLE
I RECURRING COST (CUM AVG FOR 100 A/C)					
MATERIAL \$	51,536	57,531	35,923	64,565	41,376
LABOR HRS	12,187	13,080	11,260	9,805	8,605
LABOR \$	156,115	167,564	144,260	125,597	110,232
Q.A. HRS	1,182	1,345	1,092	951	835
Q.A. \$	15,829	17,227	14,625	12,735	11,176
TOTAL \$	223,480	242,322	194,808	202,897	162,784
% OF UPDATED BASELINE			80.5%	83.8%	67.2%
II ADDITIONAL RECURRING COST (CONSTANT VALUE FOR THIS STUDY)					
(CUM AVG FOR 100 A/C)	45,840	45,840	45,840	45,840	45,840
TOTAL \$					
III RECURRING TOTAL \$ FOR 100 A/C	26,932,000	28,816,200	24,064,800	24,873,700	20,862,400
IV NON-RECURRING TOOLING ENGINEERING	2,918,000	2,918,000	3,502,000	3,674,000	3,356,000
TOTAL \$	2,535,000	2,535,000	2,535,000	2,535,000	2,535,000
	5,453,000	5,453,000	6,037,000	6,209,000	5,891,000
V SUMMARY					
TOTAL COST 100 A/C \$	32,385,000	34,269,200	30,101,800	31,082,700	26,753,400
PROFIT @ 10% \$	3,238,500	3,426,920	3,010,180	3,108,270	2,675,340
TOTAL PRICE 100 A/C \$	35,623,500	37,696,120	33,111,980	34,190,970	29,428,740
AVERAGE PRICE \$ (PER A/C)	356,235	376,961	331,120	341,910	294,287

TABLE XXVIII

ITEMIZED STRUCTURAL COSTS - BASELINE AND SELECTED CONFIGURATIONS  
CUMULATIVE AVERAGE FOR 100 AIRCRAFT

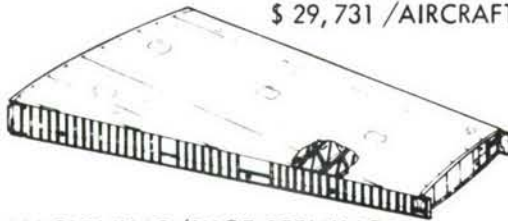
CONFIGURATION	BASELINE	UPDATED BASELINE	WELDBOND	VIRGIN PLANK	TAPERED SHINGLE
SURFACES	46,885	49,462	46,951	50,428	23,423
SPANWISE SPLICES	28,950	28,950	8,892	24,370	17,653
CHORDWISE SPLICES	446	1,440	12,763	1,440	10,137
RIBS	20,336	22,089	16,365	22,089	23,913
RIB ATTACHMENT	55,514	56,409	37,431	24,033	16,863
SPARS	22,655	22,706	18,532	29,663	22,152
SPAR ATTACHMENT	14,030	14,925	8,123	8,123	8,346
BULKHEADS AND CLOSURE RIBS	8,716	8,716	6,685	9,618	6,507
SURGE & VENT BOX, PYL FTGS, ACCESS DOORS, PAINT & SEAL	10,119	20,398	20,398	20,398	20,398
STRINGER RUNOUTS	-	-	(1) 4,043	-	-
SURFACE CUTOUTS	-	-	-	-	(2) 2,216
QUALITY ASSURANCE	15,829	17,227	14,625	12,735	11,176
TOTAL RECURRING COST (\$)	223,480	242,322	194,808	202,897	162,784

(1) Stringer close out member at front beam -- not required with integrally stiffened designs.

(2) Reinforcing pads bonded to net extruded skin panels -- not required where skins are machined.

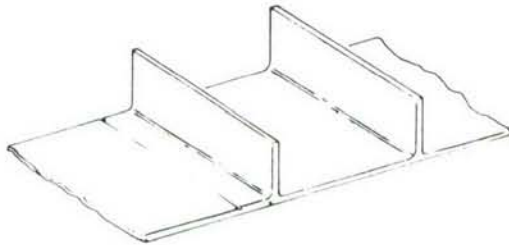
BASELINE (\$ 242, 322)

11 PANELS  
45, 048#/AIRCRAFT  
\$ 29, 731 /AIRCRAFT



MACHINING/SHOT PEENING  
1540 HOURS  
\$ 19, 731/AIRCRAFT

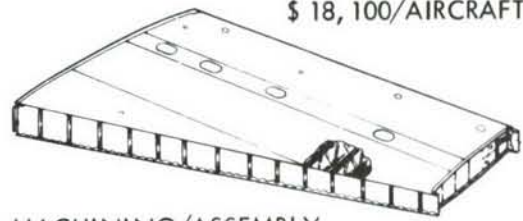
10, 040 TAPERLOKS  
15, 080" SPANWISE JOINT  
\$ 1.92 /IN.  
\$ 28, 950 /AIRCRAFT



RIB ATTACHMENT  
7040 CLIPS  
21, 120 HILOKS  
\$ 56, 409

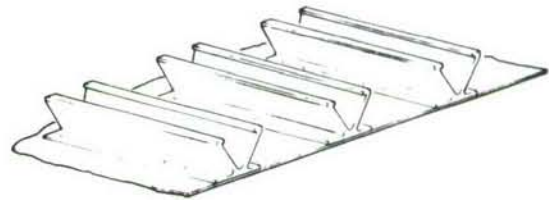
WELDBOND (\$ 194, 808)

4 PANELS  
19, 723#/AIRCRAFT  
\$ 18, 100/AIRCRAFT



MACHINING/ASSEMBLY  
2252 HOURS  
\$ 28, 851/AIRCRAFT

3770 IN.  
\$ 0.09/IN.  
\$ 354/AIRCRAFT

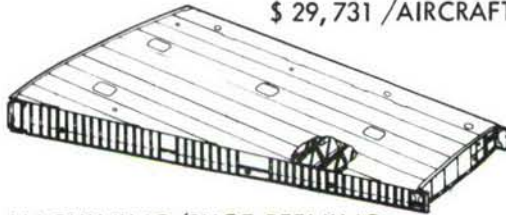


0 CLIPS  
8320 FASTENERS  
4352 SHIMS  
\$ 37, 431/AIRCRAFT

FIGURE 103 COST COMPARISON - WELDBOND DESIGN

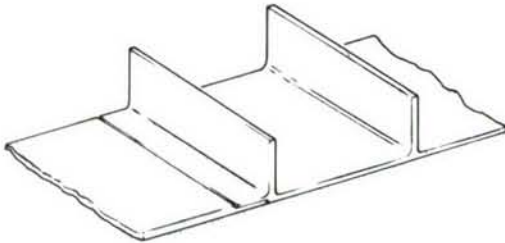
BASELINE (\$ 242, 322)

11 PANELS  
45, 048#/AIRCRAFT  
\$ 29, 731 /AIRCRAFT



MACHINING/SHOT PEENING  
1540 HOURS  
\$ 19, 731/AIRCRAFT

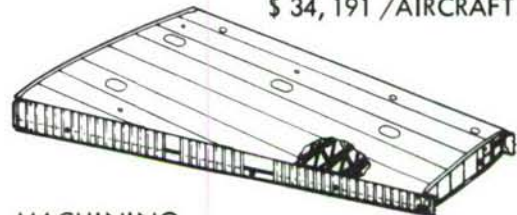
10, 040 TAPERLOKS  
15, 080" SPANWISE JOINT  
\$ 1.92 /IN.  
\$ 28, 950 /AIRCRAFT



RIB ATTACHMENT  
7040 CLIPS  
21, 120 HILOKS  
\$ 56, 409

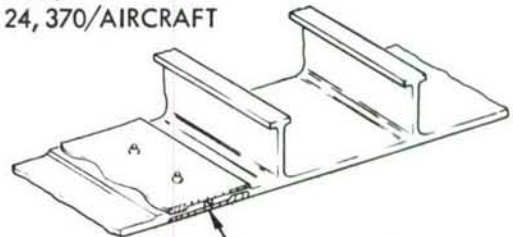
VIRGIN PLANK (\$ 202, 897)

8 PANELS  
45, 048#/AIRCRAFT  
\$ 34, 191 /AIRCRAFT



MACHINING  
1268 HOURS  
\$ 16, 237/AIRCRAFT

6024 HILOKS  
9050"  
\$ 2.69/IN.  
\$ 24, 370/AIRCRAFT



4506 CLIPS  
9012 FASTENERS  
\$ 24, 033

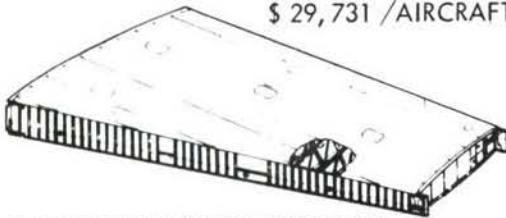
BONDED/CLAMPED

FIGURE 104 COST COMPARISON - VIRGIN PLANK DESIGN



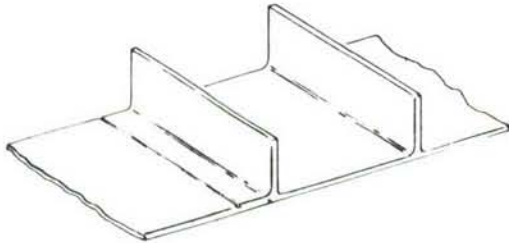
BASELINE (\$ 242,322)

11 PANELS  
45,048#/AIRCRAFT  
\$ 29,731 /AIRCRAFT



MACHINING/SHOT PEENING  
1540 HOURS  
\$ 19,731/AIRCRAFT

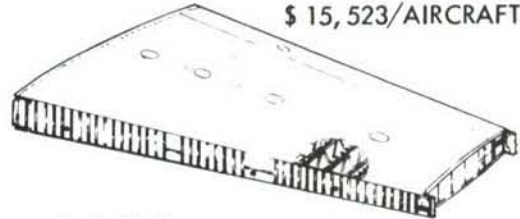
10,040 TAPERLOKS  
15,080" SPANWISE JOINT  
\$ 1.92 /IN.  
\$ 28,950 /AIRCRAFT



RIB ATTACHMENT  
7040 CLIPS  
21,120 HILOKS  
\$ 56,409

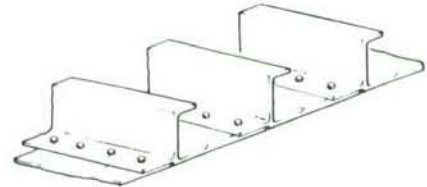
TAPERED SHINGLE (\$ 162,784)

33 PANELS  
12,855#/AIRCRAFT  
\$ 15,523/AIRCRAFT



MACHINING  
601 HOURS  
\$ 7,700/AIRCRAFT

27,747 FASTENERS  
34,684"  
\$ 0.51/IN.  
\$ 17,653/AIRCRAFT



0 CLIPS  
3456 FASTENERS  
\$ 16,863/AIRCRAFT

FIGURE 105 COST COMPARISON - TAPERED SHINGLE DESIGN

The weldbonded spanwise splices show substantial savings over the baseline primarily because of a reduction of 75% in the number of splices. Also, a significant material cost for TaperLok fasteners is eliminated. Rib costs are reduced by building the ribs up in a sub-assembly using multi-drilled tooling for installing aluminum rivets which replace the more costly Hi-Loks of the baseline. Rib cap attachment cost savings accrue from the elimination of clips and a reduction in Hi-Lok fasteners brought about by the decreased number of rib cap/stiffener intersections. Cost savings are realized in the spar cap attachment, since the bonded clamped joint uses only a small percent of the high-cost fasteners used in the mechanically attached baseline joint. However, part of this cost saving is offset by the addition of machined splice plates and metal bonding.

Material cost savings in the covers are offset by the cost of additional labor required to fabricate and attach the separate stringers to the skin. Chordwise splices and stringer run-outs are cost penalties to this configuration primarily because of additional parts required compared to the updated baseline. Other structural elements are essentially the same cost as the baseline.

#### 11.3.2 Virgin Plank Design

In this configuration, significant cost savings result in the rib attachment and spar attachment. The non-penetrating rib cap to cover clip is inherently less expensive than the baseline, since the number of high cost Hi-Lok fasteners in each clip is reduced by one-third. An additional saving results from a reduction in the number of clips and associated Hi-Loks. This comes from the increased panel riser spacing. The spar cap attachment is the same as for the Weldbond design.

Labor savings in fabrication of the covers results from the reduced number of panels, but these savings are offset by increased material costs for the riser shape and alloy change. Cost savings are realized from a decrease in the number of spanwise splices even though the cost per splice is slightly more for the bonded clamped design used here.

Spar cost is greater for the forged spar over the built-up baseline design because 86% of the purchased forging material is subsequently machined away. Advancements

in forging equipment and technology will show dramatic cost benefits in the spar. Other structural elements have essentially the same cost as the baseline.

### 11.3.3 Tapered Shingle Design

This design offers the highest total cost savings of the three recommended designs. Savings result in the covers, spanwise splices, rib attachment, and spar attachment.

Cost savings in the covers come from the Tapered Shingle design, which uses net extrusions to eliminate practically all costly machining operations and replaces them with simple profiling. Material cost is also substantially reduced. Spanwise splices are increased in number, but an overall savings is realized through the use of automated stress-wave riveting.

Two factors contribute to reduced rib cap attachment costs:

- o Elimination of separate clips;
- o Fifty percent reduction in rib cap attachment fasteners (from decreased number of rib cap/stiffener intersections and dual use of some spanwise splice fasteners to attach rib cap flanges).

A savings in spar attachment costs results from the use of stress-wave rivets in lieu of more costly TaperLoks.

Chordwise splices, ribs, and surface cutout areas are cost penalties in this configuration primarily because of additional parts required. Rib truss diagonals are three-piece instead of one-piece, and chordwise splices and cutouts require doublers as well as additional rivets. Other structural elements are essentially the same cost as the baseline.

## SECTION XII

### CONCEPT EVALUATION

#### 12.1 MERIT RATING SYSTEM

The method of concept evaluation considers a merit rating system which recognizes the important performance characteristics of a structural design including efficiency (cost and weight), integrity, reliability, and other practical considerations. Since a prime objective of the ADP programs is technology advancement, this aspect is also evaluated and given considerable weight in the overall concept evaluation process. A complete breakdown of the merit rating system is shown in Table XXIX.

#### 12.2 EVALUATION CRITERIA

Candidate designs were evaluated using the rating system (Table XXIX). Four major components of structure were considered for each design: upper cover, lower cover, ribs, and spars. The different splicing, joining, and assembly methods were handled as sub-variations of the basic configurations such that relative advantages or disadvantages of these methods could be separated in the final evaluation.

The scoring of candidate concepts was conducted by specialists in the respective disciplines. Scores were assigned relative to the updated baseline configuration, which was assumed to have a score of 10.

The evaluation criteria used to score the major performance parameters are discussed below.

##### 12.2.1 Structural Efficiency - Cost and Weight

The costs of ADP designs were derived from considerations of the manufacturing processes involved, materials usage, fastener types and numbers, parts count, and other significant variables. Designs were scored on a relative basis, with those showing the largest savings given a maximum score. Designs whose



TABLE XXIX

## MERIT RATING SYSTEM

for the

CARGO/TANKER C-141 INNER WING PHASE IA PROGRAM

Structural* Efficiency = 0.3	Technology Advancement = 0.3	Integrity & Reliability = 0.3	Abilities = 0.1
Cost = 0.5 Weight = 0.5	Concepts = 0.3 Manufacturing = 0.3 Materials = 0.3 Fracture = 0.1	Static = 0.1 Fatigue = 0.3 Safe Crack = 0.2 Multiple Load Path = 0.4	Inspectability = 0.5 Manufacturability = 0.2 Maintainability = 0.1 Repairability = 0.1 Predictability = 0.1

\*Service life will be maintained at 60,000 hours with 24,000 landings. Any design not maintaining these will be considered unacceptable.

aggregate component costs significantly exceeded baseline costs (by 20% or more) were eliminated.

Similarly, designs with weight savings of 10% were given maximum scores while those weighing more than 1.1 times baseline were considered unacceptable.

#### 12.2.2 Technology Advancement

Ratings for technology advancement considered those aspects of each design which gave substantial promise of advancing the state of the art of structural design. Factors included the use of advanced materials and processes, new and innovative design concepts, new manufacturing and tooling approaches, and unique methods of meeting fracture design requirements.

A high score in this category usually connotes an element of risk when compared with more conventional design approaches.

#### 12.2.3 Integrity and Reliability

Since structural requirements were considered inviolate for all designs, the scoring of integrity and reliability was based largely on the potential of each design to meet these objectives with a high level of confidence. Some of the factors considered were the general design arrangement, design complexity, materials properties and application, reliability of materials processing and fabrication, and fracture concepts.

#### 12.2.4 Abilities

The "abilities" score was derived from a careful review of ADP designs in which a comparison was made with conventional designs whose performance characteristics were proven by service experience. As in the other evaluations, a score of 10 was assumed for the baseline configuration.

Material alloys and finishes, internal structure arrangement, and splicing concepts were some of the important factors which determined accessibility for inspection, practicability of maintenance and repair, and overall manufacturability.

### 12.3 CONFIGURATIONS SUBJECTED TO ADP EVALUATION CRITERIA

A comprehensive matrix of cover and substructure designs was subjected to ADP evaluation criteria. These designs embodied a variety of structural configurations which used advanced aluminum and titanium alloys. Composites were also used but primarily for reinforcement of basic metallic designs. Table XXX summarizes the designs analyzed. A more detailed description of each design is contained in Section V.

### 12.4 CONCEPT SCORING AND SELECTION OF THREE RECOMMENDED DESIGNS

The scoring of designs subjected to ADP evaluation is summarized in Table XXXI. The Sandwich configuration is the only design with an indicated merit rating less than baseline, although the Monolithic design shows only a slight advantage. It should be noted that the Lockskin and Composite "Hat" designs have excellent overall merit ratings but were dropped when it became evident that they would not meet the cost objective established for the program.

The remaining four configurations show roughly equivalent merit ratings and are justifiable recommended designs. The "Hat" stringer configuration, however, is actually quite similar to the A-stringer Weldbond concept and has some disadvantages that are not presented by the A-stringer Weldbond configuration. One of these pertains to corrosion protection and inspection of blind areas within the "hat" section stringer. This led to the selection of the A-stringer Weldbond as the preferred design. This design, together with the Virgin Plank and the Tapered Shingle, comprise the three recommended designs.

TABLE XXX

## CONFIGURATIONS SUBMITTED TO ADP EVALUATION CRITERIA

CONFIG. NO.	COVER CONCEPT	SPANWISE SPLICE CONCEPT	SPARS AND SUBSTRUCTURE
1	Weldbond "A" Stringer	Weldbond	<u>Spars</u> - Sine Wave Web, Welded <u>Ribs</u> - Truss Type, Back-to-back Channel Caps, Square Section Braces
2	Weldbond "Hat" Stringer	Adhesive Bonded/Clamped	<u>Spars &amp; Bulkheads</u> - Geodetic Stiffened <u>Ribs</u> - Cross Truss Arrangement
3	Lockskin	Weldbond	<u>Spars</u> - Sine Wave Web (Titanium) <u>Ribs</u> - Web/Stiffener
4	Monolithic Welded	Welded	<u>Spars</u> - Integrally Stiffened (Welded) <u>Ribs</u> - Caps Welded to Covers, "H" Section Braces
5	Honeycomb Sandwich	Mechanical Fasteners, Cold Worked Holes	<u>Spars &amp; Bulkheads</u> - Honeycomb Sandwich (Aluminum) <u>Ribs</u> - "H" Section Braces (No Separate Rib Caps)
6	Composite "Hat" Stringer	Adhesive Bonded	<u>Spars &amp; Bulkheads</u> - Web/Stiffener (Composite Reinforced) <u>Ribs</u> - Post & Cross Strap (Composite Reinforced)
7	Virgin Plank	Adhesive Bonded/Clamped	<u>Spars</u> - One-piece Forging <u>Ribs</u> - Truss Type, Conventional Caps Attached with N-P Clips, "H" Section Braces
8	Tapered Shingle	Stress Wave Rivet	<u>Spars &amp; Bulkheads</u> - Web/Stiffener <u>Ribs</u> - Truss Type, Tubular Braces
Baseline	Integrally Stiffened	Taperlocks	<u>Spars</u> - Built-up Web/Stiffener <u>Ribs</u> - Truss Type, "H" Section Braces <u>Bulkheads</u> - Web/Stiffener and Integrally Stiffened



TABLE XXXI  
MERIT RATING SUMMARY OF CANDIDATE CONCEPTS

CONFIG. NO.	CONCEPT	MERIT RATING					REMARKS
		STRUC. EFF.	TECH. ADVAN.	INTEG. & RELIA.	ABILI- TIES	TOTAL	
1	Weldbond "A" Stringer	4.56	4.09	3.56	1.07	13.28	
2	Weldbond "Hat" Stringer	3.90	4.09	3.63	1.04	12.66	
3	Lockskin	3.03	5.00	4.24	1.00	13.27	Cost Prohibitive
4	Monolithic Welded	3.58	3.76	2.80	.92	11.06	
5	Honeycomb Sandwich	1.21	4.38	3.31	.91	9.81	
6	Composite "Hat" Stringer	3.23	4.97	4.01	.93	13.14	Cost Prohibitive
7	Virgin Plank	4.11	4.11	3.56	1.10	12.88	
8	Tapered Shingle	4.04	4.33	4.17	1.09	13.63	
Baseline	Integrally Stiffened	3.00	3.00	3.00	1.00	10.00	

## 12.5 CONCEPT TEST VERIFICATION

Several new design concepts embodied in the three recommended designs were verified by component tests during the Phase IA program. The more significant concepts are described below. (For more specific results, see Appendix II.)

### 12.5.1 "A"Stringer Rib/Cover Shear Transfer Capability

A segment of rib cap was directly attached to an "A" stringer stiffened skin panel through tabs provided in the "A" stringer (no shear clips), and a shear load applied between the cap and skin. A shear transfer capability equivalent to the most stringent requirements of the baseline was verified by this test.

### 12.5.2 Non-Penetrating Clip Load Transfer Capability

A test similar to that described in Section 12.5.1 above was conducted using a rib cap/cover panel joined only by non-penetrating clips. Results showed excellent shear load transfer capability through the N-P clips, and the feasibility of this design for all but the most highly loaded ribs was established.

### 12.5.3 Non-Penetrating Clip Fretting Resistance

A simulated rib cap was attached to a segment of skin panel using the N-P clips described above. The panel was subjected to spectrum fatigue loading, while a constant normal load (simulating net air loads and crushing pressures) was applied between the panel and rib cap. At the end of one test lifetime, the panel was disassembled and inspected. No fretting was apparent in either the skin panel or the clips.

### 12.5.4 Bonded/Clamped Spanwise Splice Fatigue Resistance

The bonded/clamped spanwise splice design shown in Figure 31 was developed too late to be included in the concept component fatigue test program, but

tests of similar configurations conducted under other Lockheed R&D programs have proven the feasibility of this concept.

## SECTION XIII

### CONCLUSIONS AND RECOMMENDATIONS

The conclusions and recommendations drawn from the Phase IA study program are presented here.

#### 13.1 CONCLUSIONS

1. Through the use of innovative design concepts, advanced materials, and improved manufacturing technology, it is feasible to obtain substantially improved fatigue performance of primary wing structure while saving both weight and cost.
2. Although the requirements of the new damage tolerance criteria outlined in the "Proposed USAF Damage Tolerance Criteria," dated 18 August 1972, are much more stringent than past requirements, they do not necessarily rule out the development of balanced designs that recognize all structural requirements. However, to avoid penalties, extra care must be given to the design approach used, the materials selected, and the choice of reasonable inspection periods and NDI procedures.
3. The complexity of the new damage tolerance requirements of the "Proposed USAF Damage Tolerance Criteria" presents difficulty in interpreting the intent of the criteria and applying them to a specific design.
4. The state of the art of applied fracture analysis must be substantially developed to provide adequate training of industry and Air Force personnel, computer programs capable of responding to damage tolerance criteria, and a comprehensive test data base including panel test data and basic fracture properties.
5. Some of the new design concepts evolving from the study require considerable additional development before they are applied to production prototype programs. These are listed in the body of the report.

#### 13.2 RECOMMENDATIONS

1. Develop the recommended designs presented herein through further analysis and test in subsequent phases of the ADP program.



2. Provide funding for promising development programs which are complementary to ADP program objectives in order to maximize the benefit to be derived from the ADP effort.
3. To provide for more consistent interpretation of damage tolerance requirements, consider simplifying existing criteria by writing a more condensed general specification applicable to all new airframe systems. Write into this specification a requirement for establishing more specific criteria for each airplane project.
4. Initiate efforts to identify total needs with regard to fracture analysis technology, and proceed to outline a long-range program which will close the gap in the state of the art of this new technology field. Some of the more obvious needs include:
  - o Training - the indoctrination of more people in fundamentals of fracture technology, terminology, and objectives, particularly working level people. At present, there is an industry-wide shortage of personnel qualified to perform fracture work. More effective information transfer would be helpful in this regard.
  - o Analysis methods - the continued development of fundamental concepts to analyze fracture of materials and structures. Finite element analyses, particularly those incorporating the higher order cracked finite elements, should receive heavy emphasis since these methods not only provide solutions to complex classical problems but, more importantly, provide a suitable approach to the analysis of actual hardware designs.
  - o Test data - the development of a sufficient quantity of basic materials fracture data (MIL-HDBK-5, "A" and "B" type values) to adequately account for scatter, and sufficient damage tolerance tests of full scale structure to evaluate effectiveness of analysis technology and the manner by which the technology is implemented in the development of new structure.

APPENDIX I  
PRELIMINARY DESIGN DRAWINGS

This appendix contains general-arrangement drawings of the eight basic configurations developed during this program.

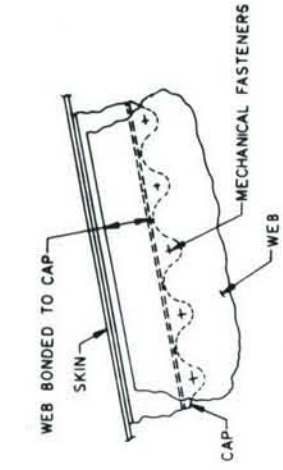
Additional preliminary design layouts were made of the various concepts, but these are not included in this report, as all relevant information has been incorporated into the general arrangement drawings.

<u>Drawing Number</u>	<u>Page</u>	<u>Title</u>
ADP 1020	209	General Arrangement - Inner Wing Structure, "A" Frame Stringer, Configuration 1 - Weldbond
ADP 1021	211	Inner Wing Structure - Hat Section Stringer Design - Configuration 2
ADP 1022	213	General Arrangement - Inner Wing Structure - Lockskin Zee Stringer & Sine Wave Spar - Configuration 3
ADP 1023	215	Inner Wing Structure - Monolithic Design - Configuration 4
ADP 1024	217	Inner Wing Structure - Honeycomb Sandwich Design - Configuration 5
ADP 1025	219	Inner Wing Structure - Composite Hat Design - Configuration 6
ADP 1026	221	General Arrangement - Inner Wing Structure - Integral Stiffened Skin Panels and Non-penetrating Clip - Configuration 7 - Virgin Plank
ADP 1027	223	General Arrangement - Inner Wing Structure - Net Extrusion Skin Panels - Configuration 8 - Tapered Shingle

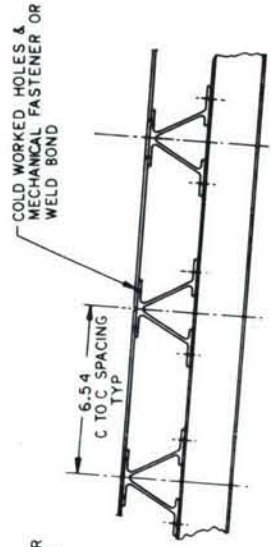




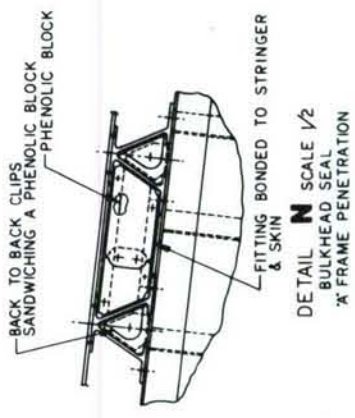




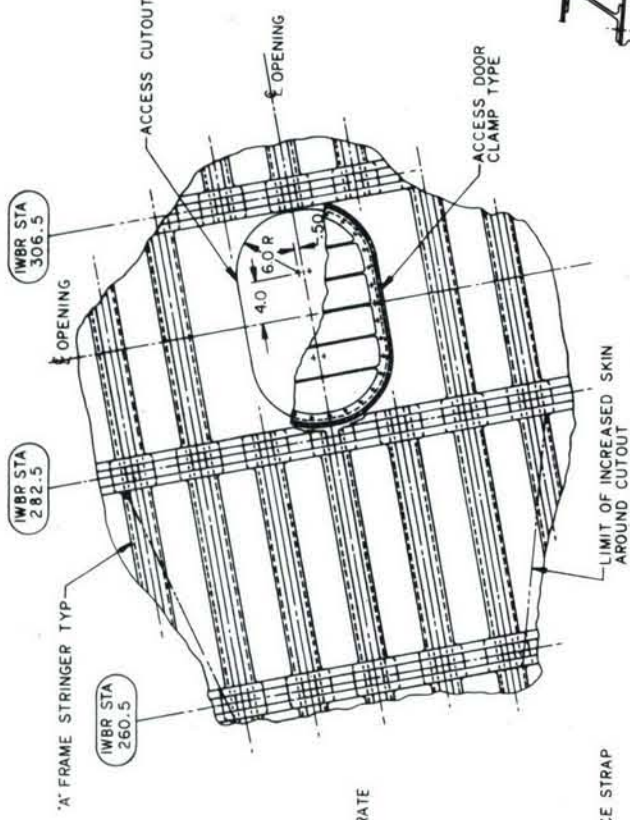
SECTION **P-P** SCALE 1/2  
INTERMEDIATE BEAM



DETAIL **C** SCALE 1/2  
SKIN SPLICE

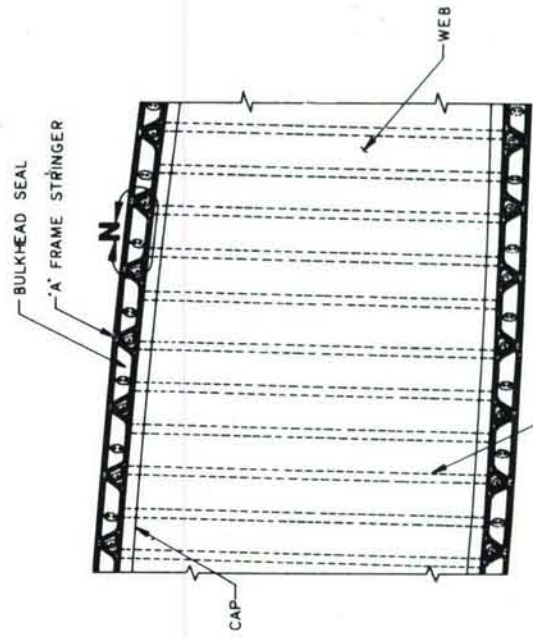


NOTE: IT IS PROPOSED TO HAVE AN INTEGRALLY STIFFENED SKIN PANEL ON THE UPPER SURFACE TO ACCOMMODATE THE TANK ACCESS DOORS. DRAWING WILL BE AMENDED TO REFLECT THIS CHANGE AT A LATER DATE

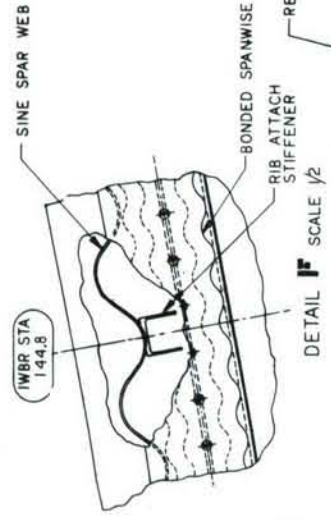


SECTION **M-M** SCALE 1/5  
FUEL TANK BULKHEAD

DETAIL **L-L** SCALE 1/5  
VIEW LOOKING FROM INSIDE OUT  
ACCESS CUTOUT

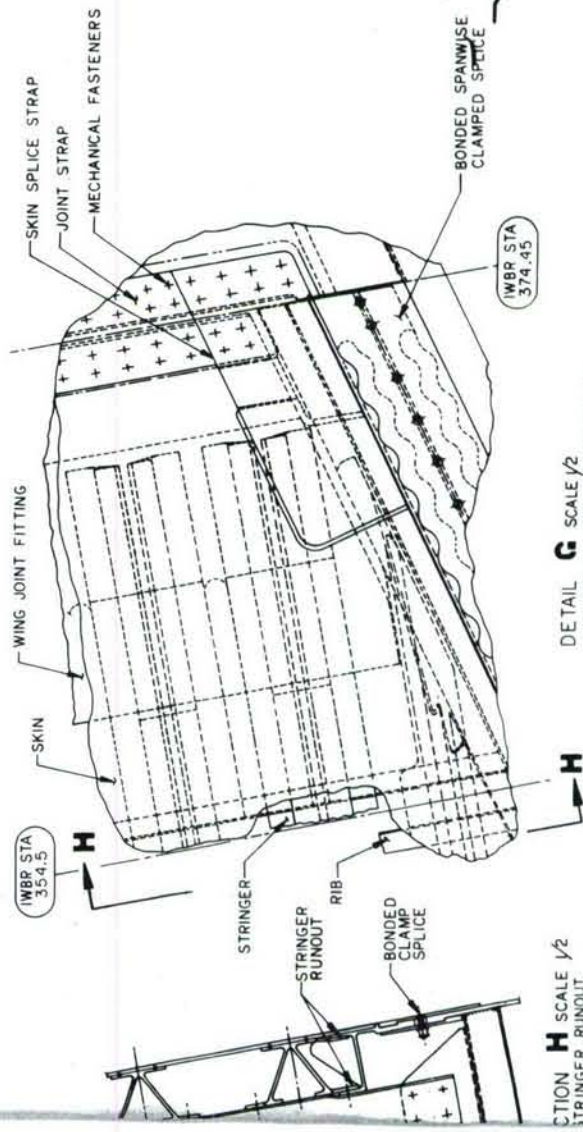
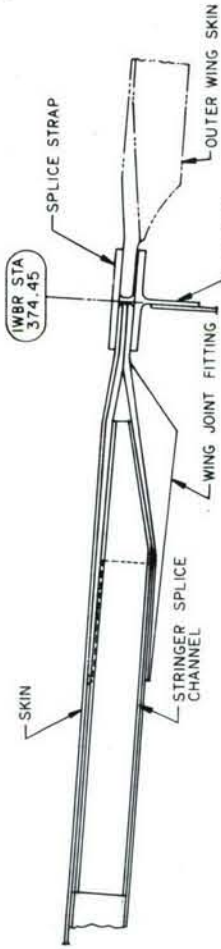


SECTION **K-K** SCALE 1/2  
CHORDWISE WING JOINT



DETAIL **F** SCALE 1/2

SECTION **J-J** SCALE 1/2



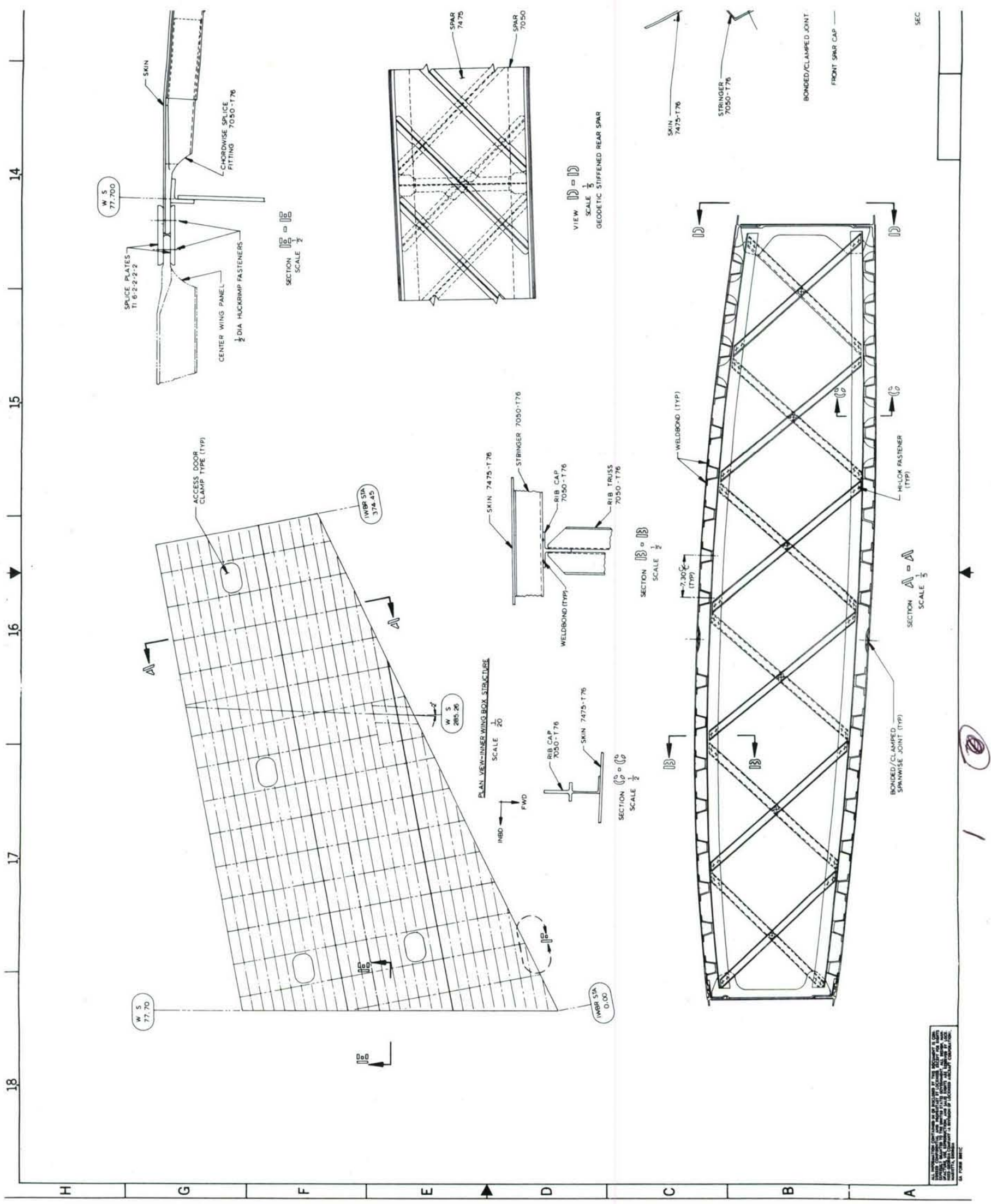
SECTION **H** SCALE 1/2  
STRINGER RUNOUT

DETAIL **G** SCALE 1/2  
SPAR & WING JOINT INTERSECTION

GENERAL ARRANGEMENT INNER WING  
STRUCTURE - 'A' FRAME STRINGER &  
ALUMINUM SKIN - CONFIGURATION 1 - **WELDBOND**

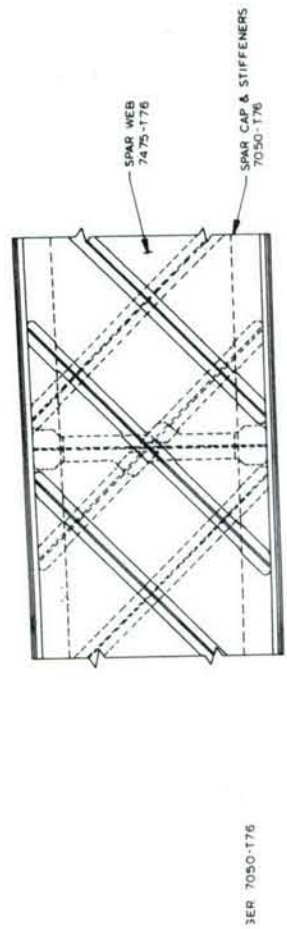
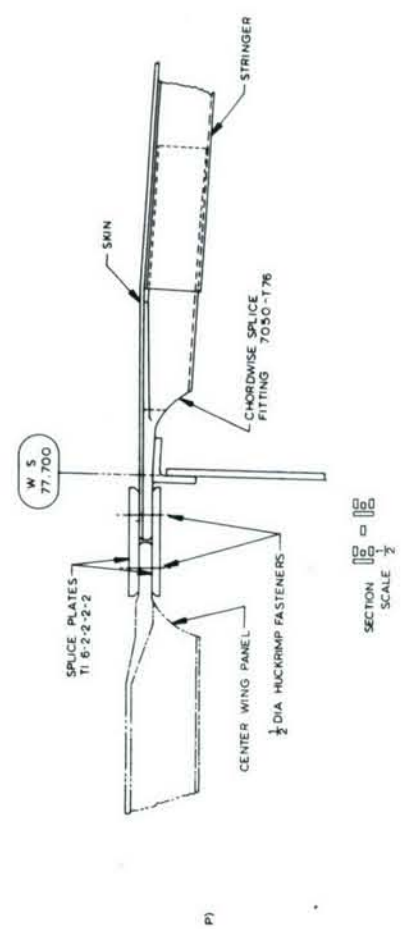
SCALE NOTED	A. ROBERTSON	1-12-73	ADP1020
-------------	--------------	---------	---------



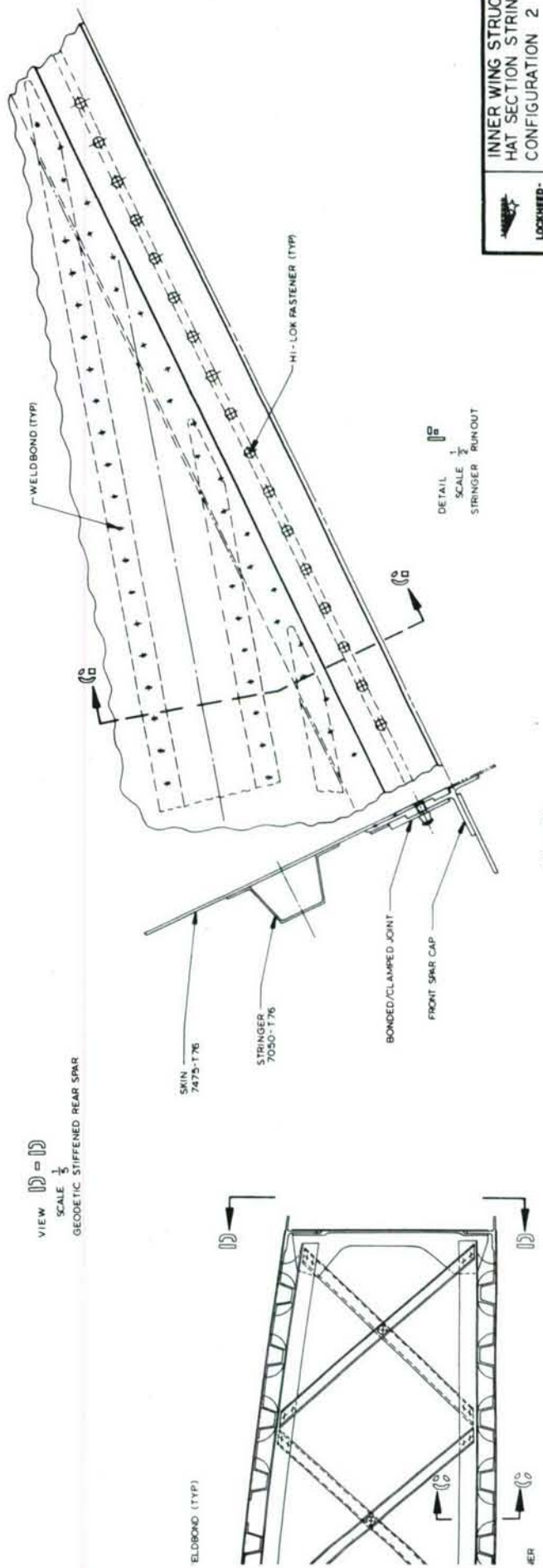


ALL INFORMATION CONTAINED HEREIN IS UNCLASSIFIED EXCEPT WHERE SHOWN OTHERWISE. DATE 05-11-2010 BY 60322 UCBAW/STP

15 14 13 12 11



VIEW D-D  
SCALE 1/2  
GEOMETRIC STIFFENED REAR SPAR



LOCKHEED-GEORGIA COMPANY A member of Lockheed Martin			
INNER WING STRUCTURE - HAT SECTION STRINGER DESIGN - CONFIGURATION 2			
DATE	NOTED	BY	APP'D
1-23-73	J.A. SMITH		
CARGO - PANE 2			ADP 1021

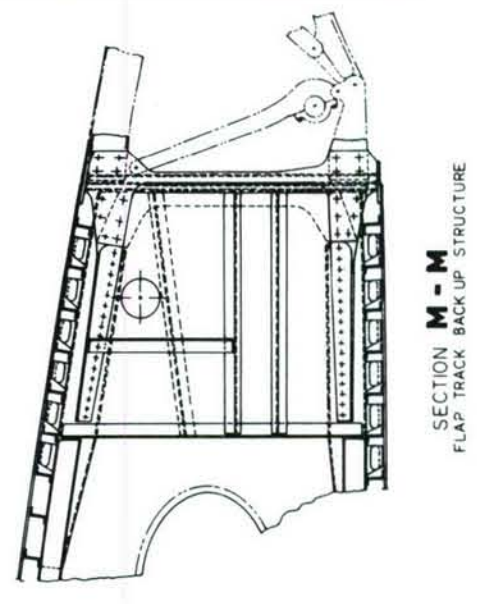
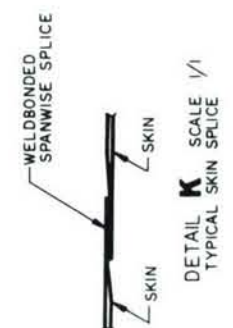
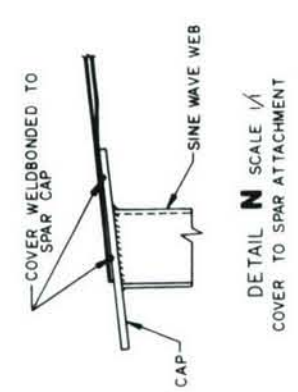
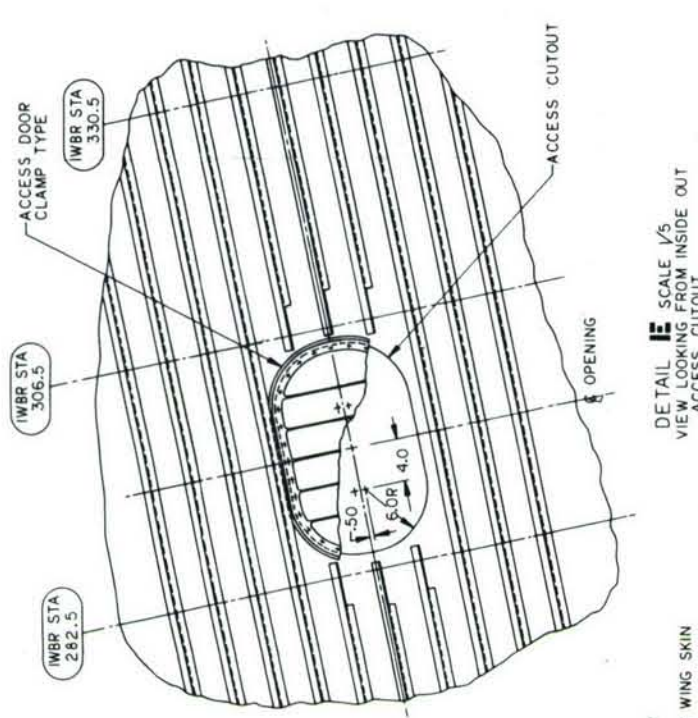
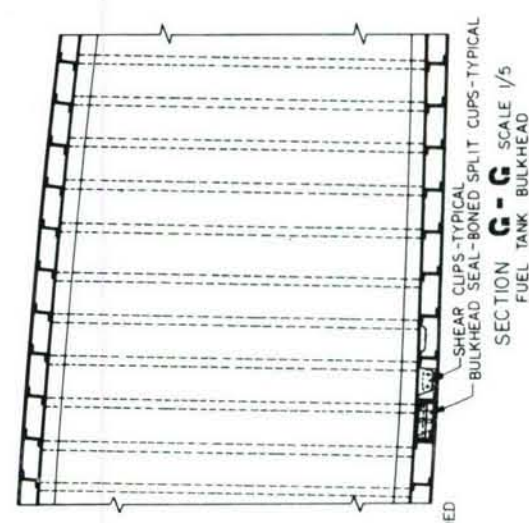
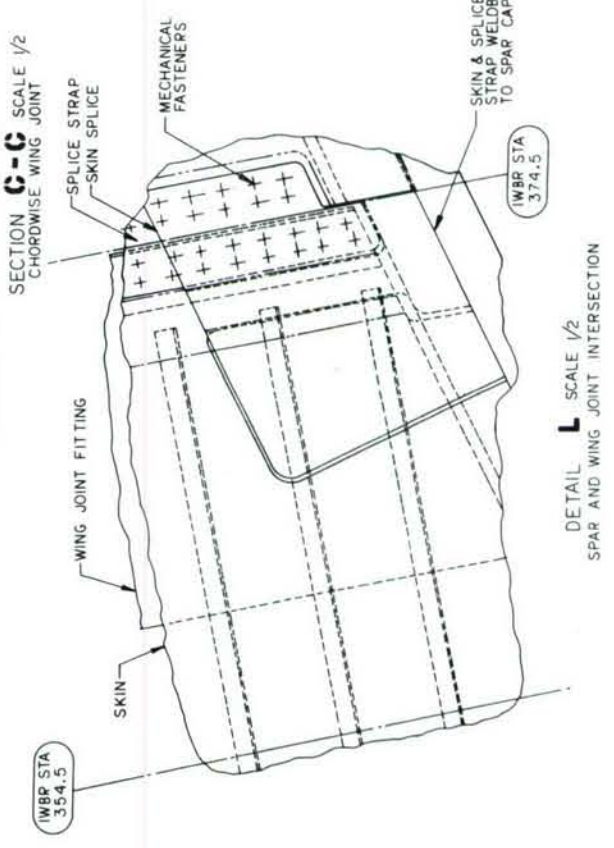
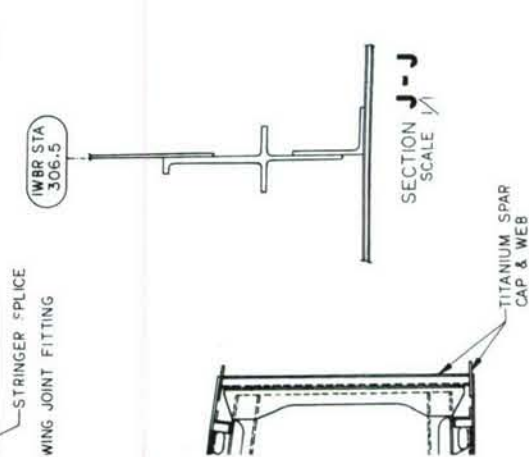
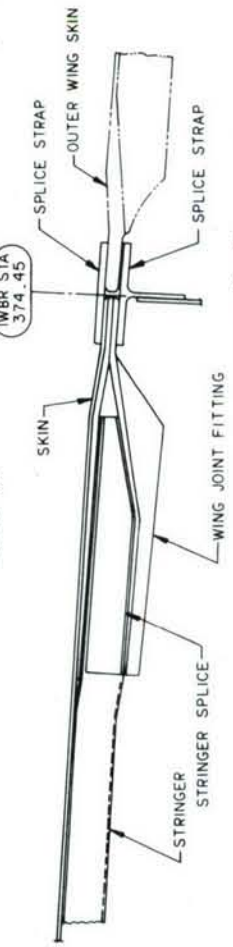
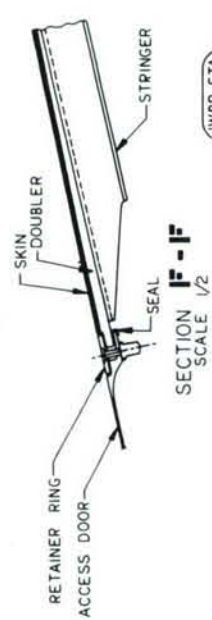
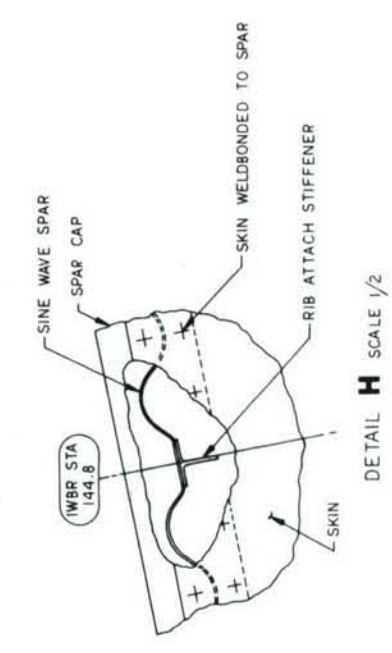
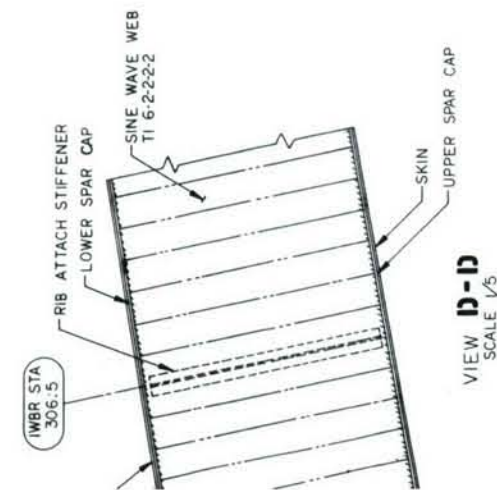
SECTION SCALE 1/2

2





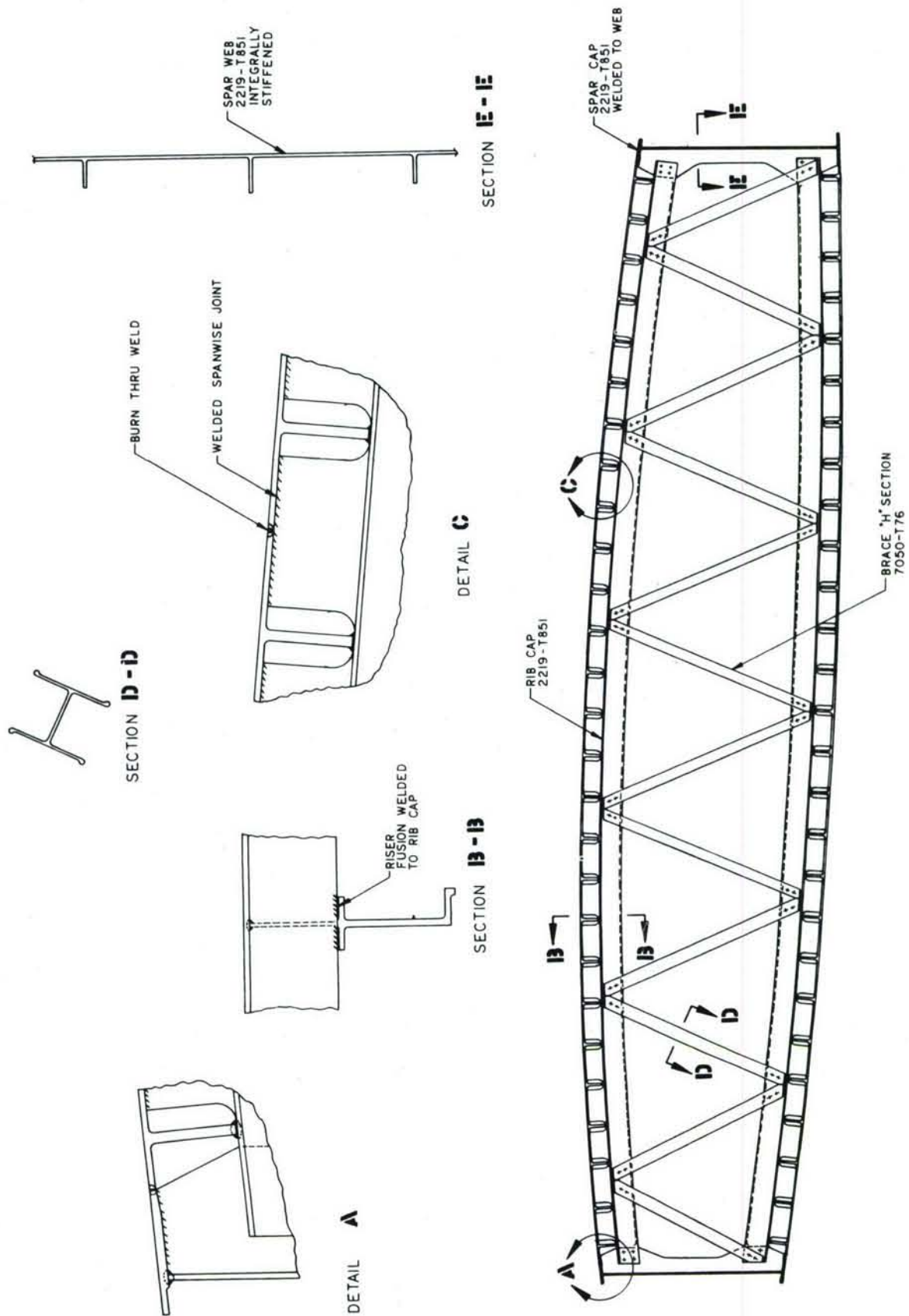




GENERAL ARRANGEMENT INNER WING  
STRUCTURE - LOCKSKIN, ZEE STRINGER  
& SINE WAVE SPAR - CONFIGURATION **3**

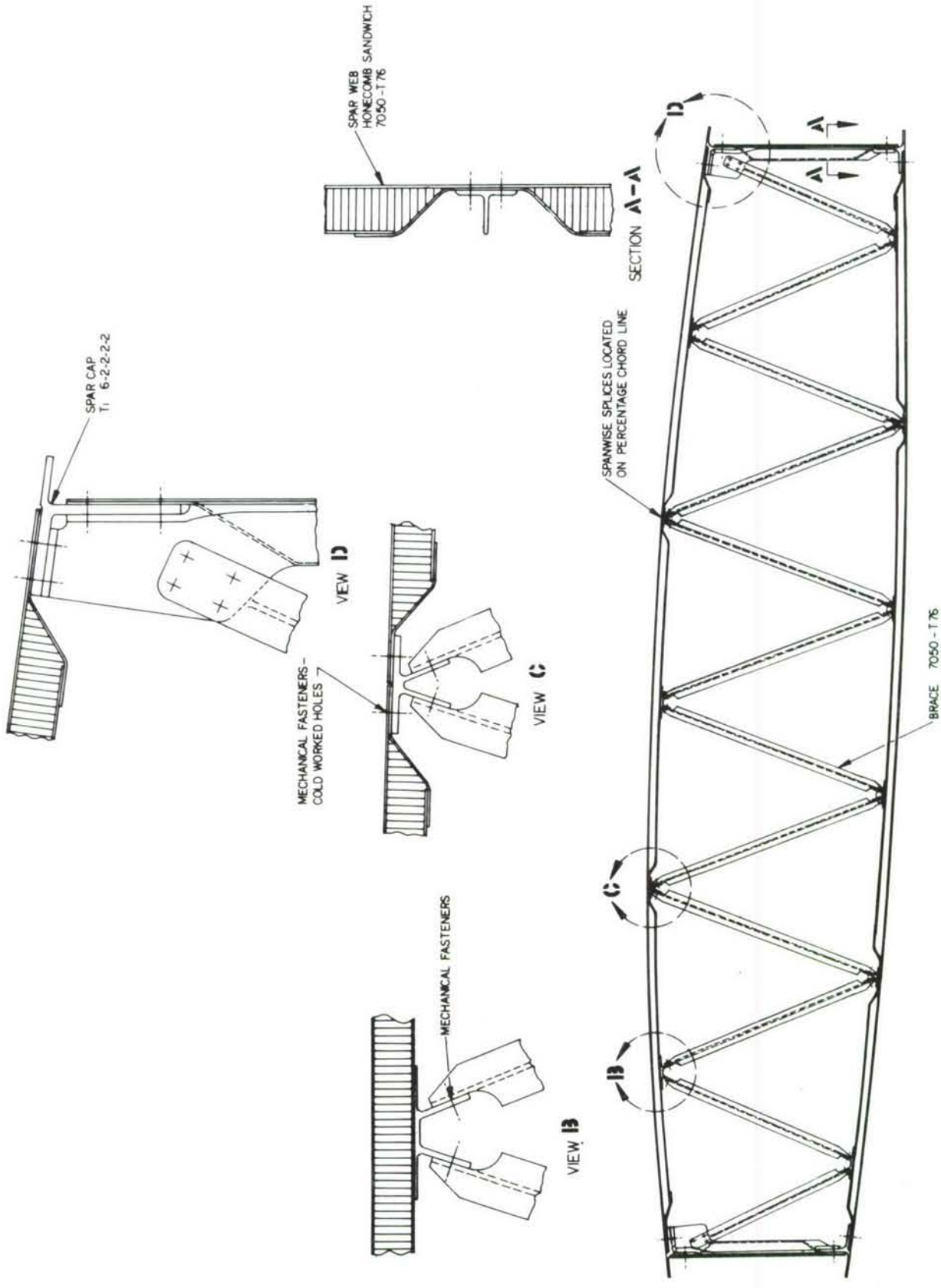
SCALE NOTED A. ROBERTSON 1-22-73 ADP 10 22





INNER WING STRUCTURE  
MONOLITHIC DESIGN  
CONFIGURATION 4

ADPI023

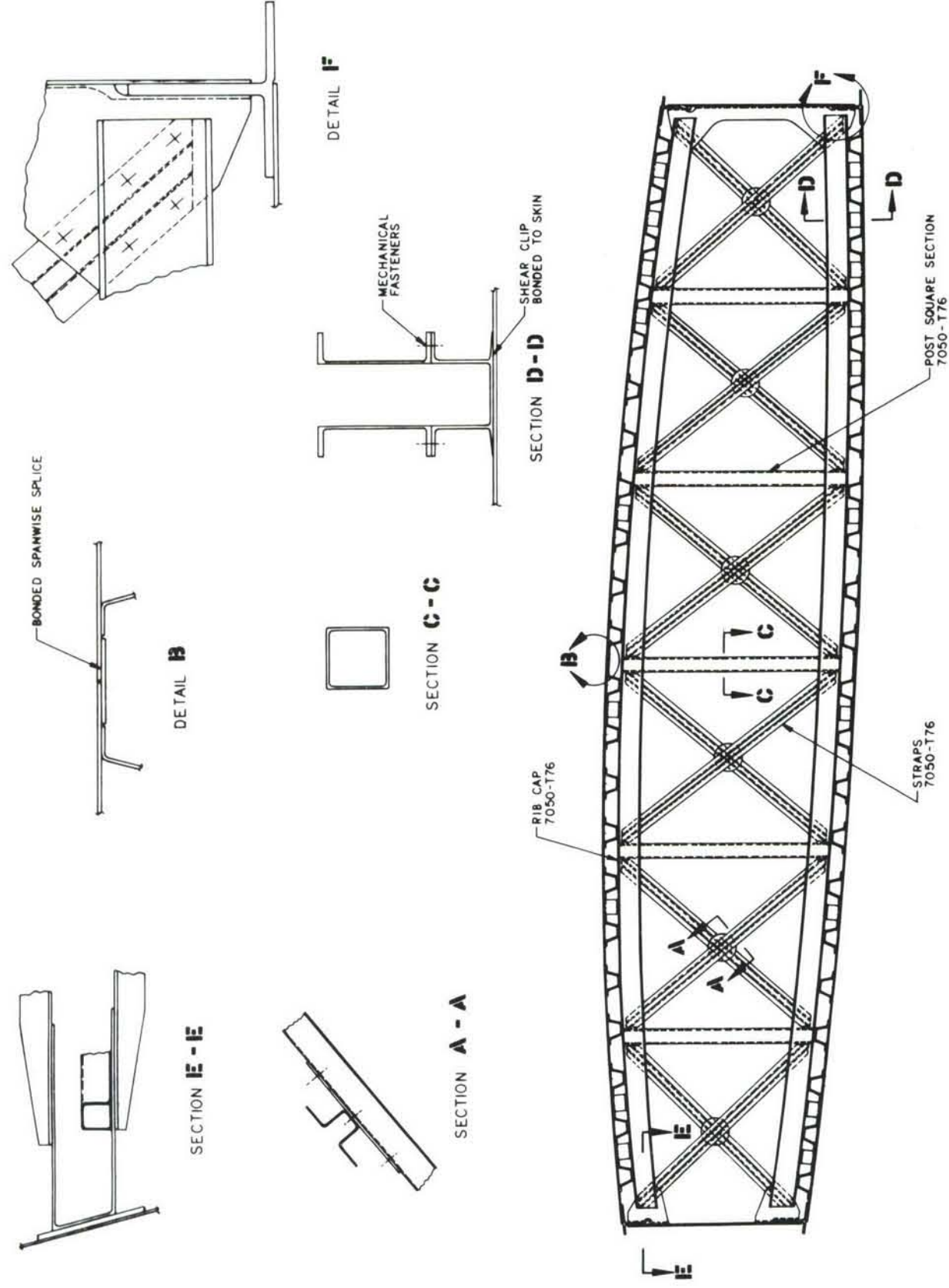


INNER WING STRUCTURE  
HONEYCOMB SANDWICH DESIGN  
CONFIGURATION 5

ADPI024

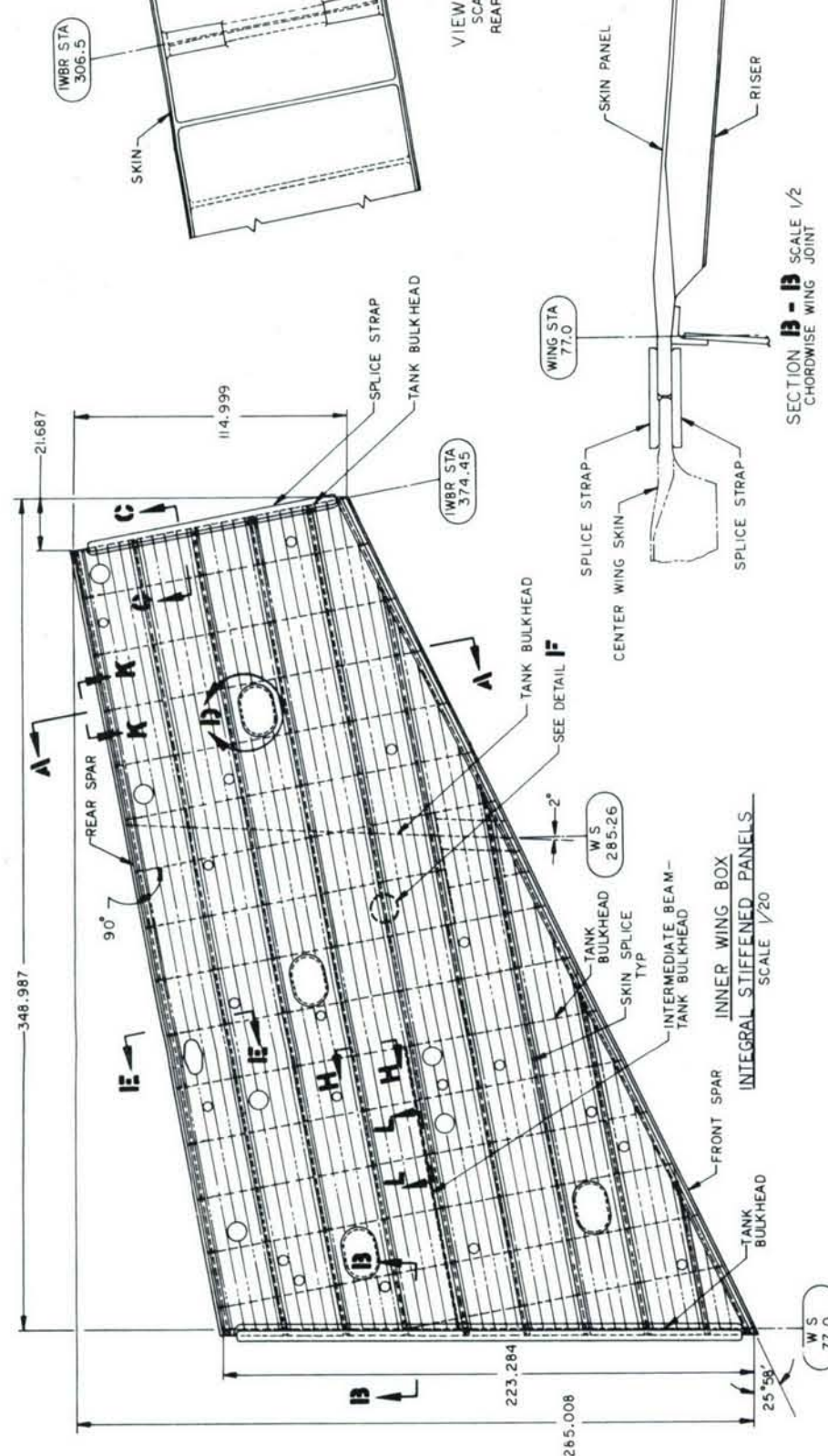
### INNER WING STRUCTURE COMPOSITE HAT DESIGN CONFIGURATION 6

ADPI025

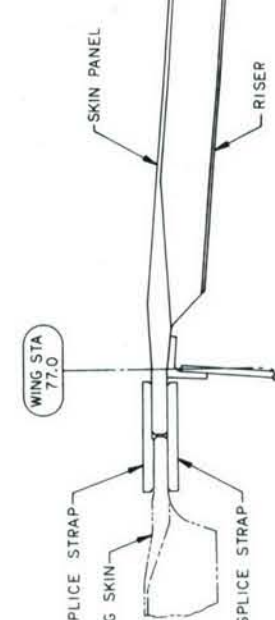




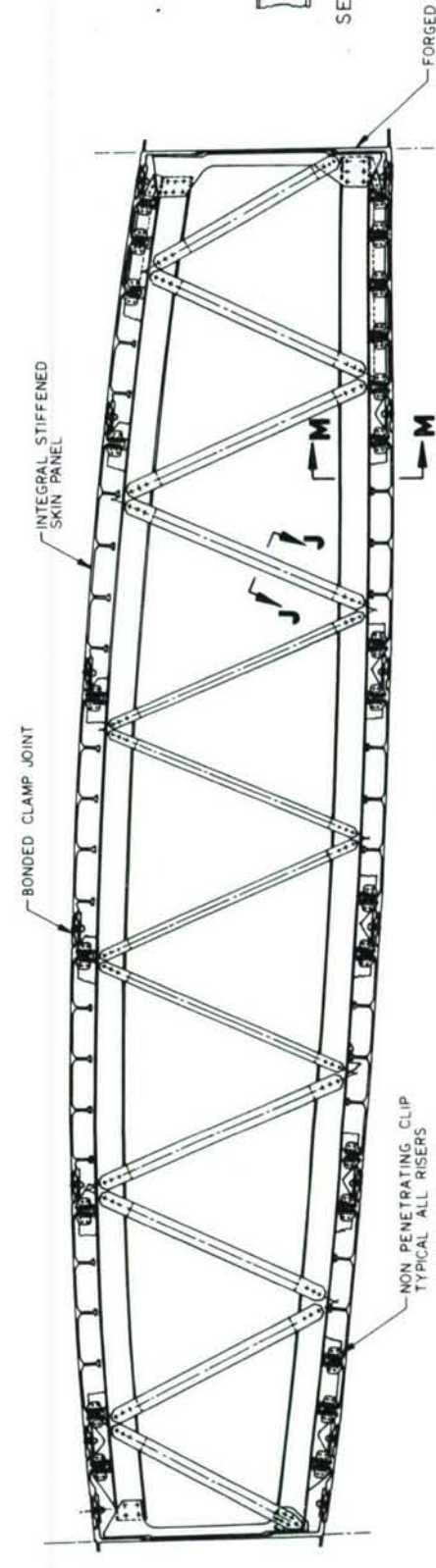
H G F E D C B A



SECTION B-B SCALE 1/2  
CHORDWISE WING JOINT

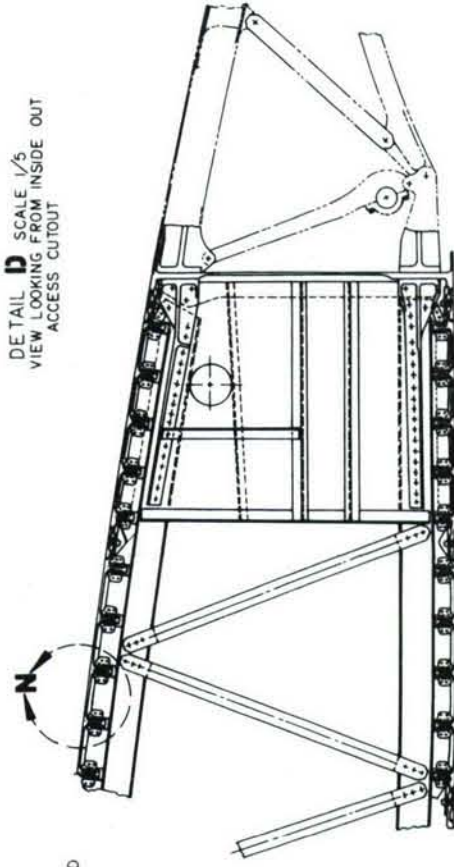
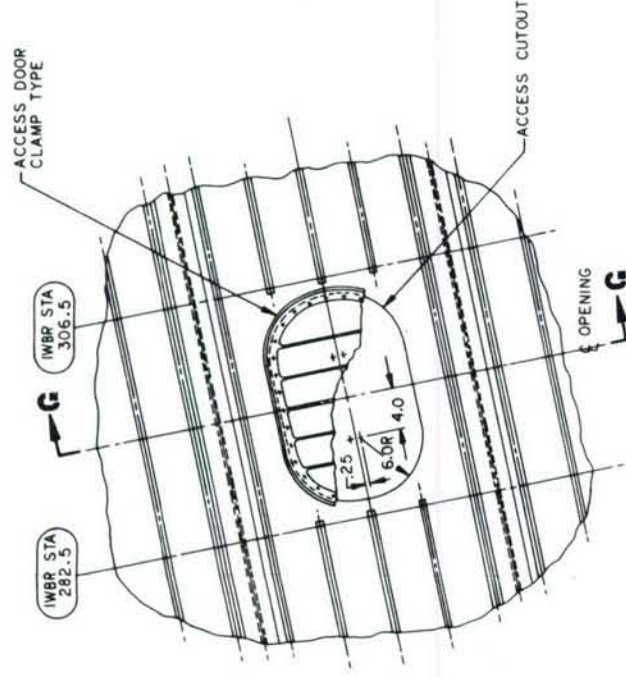
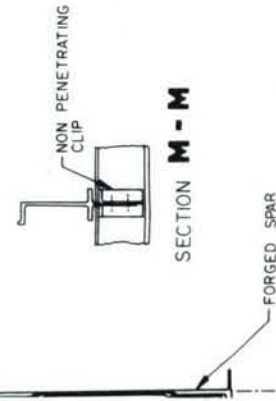
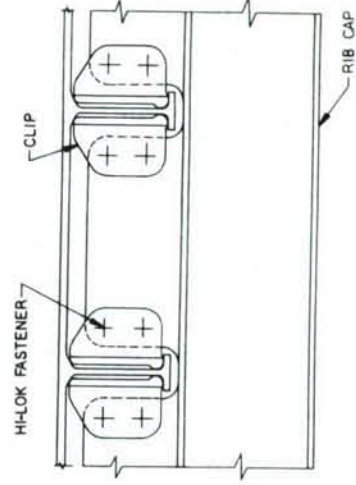
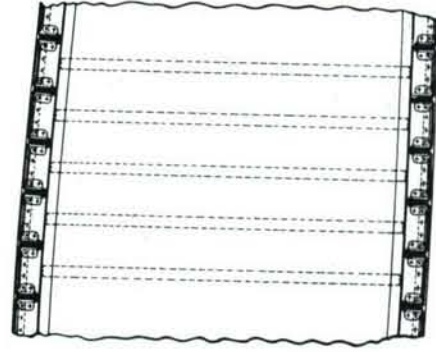
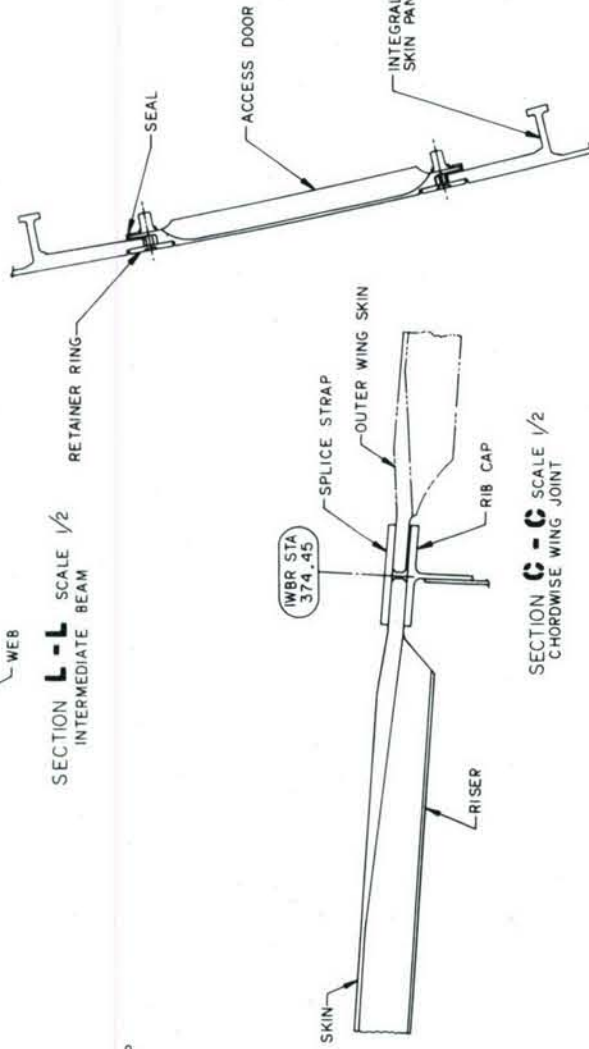
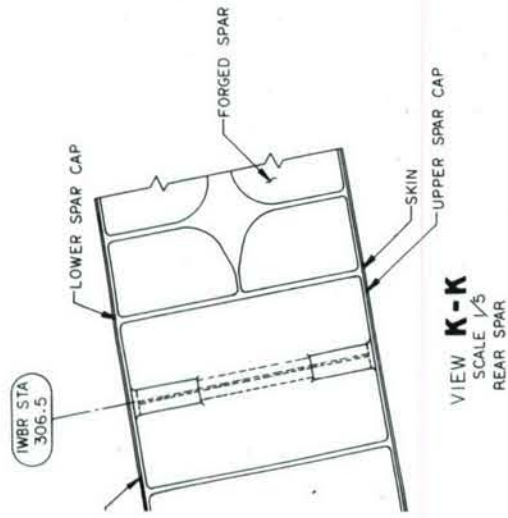
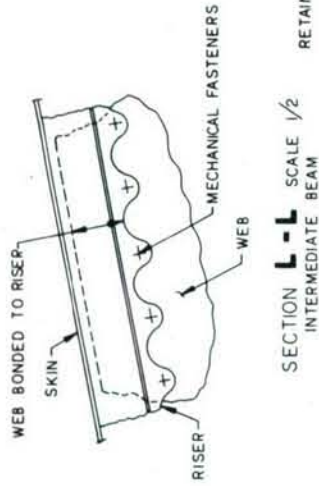
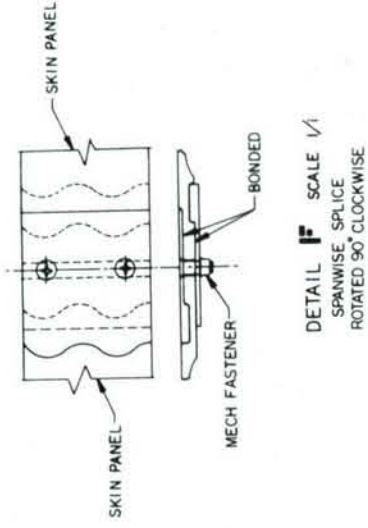


ROTATED SECTION A-A SCALE 1/5  
TYPICAL BOX RIB



ALL INFORMATION CONTAINED HEREIN IS UNCLASSIFIED EXCEPT WHERE SHOWN OTHERWISE. IT IS THE POLICY OF THE NATIONAL ARCHIVES TO MAKE ALL INFORMATION CONTAINED HEREIN AVAILABLE TO THE PUBLIC. FOR MORE INFORMATION CONTACT THE NATIONAL ARCHIVES AT COLLEGE PARK, MARYLAND 20740-6001. (201) 837-1100. WWW.NATIONALARCHIVES.GOV





SECTION G-G SCALE 1/2  
SECTION THRU ACCESS DOOR

SECTION C-C SCALE 1/2  
CHORDWISE WING JOINT

SECTION H-H SCALE 1/5  
FUEL TANK BLKD

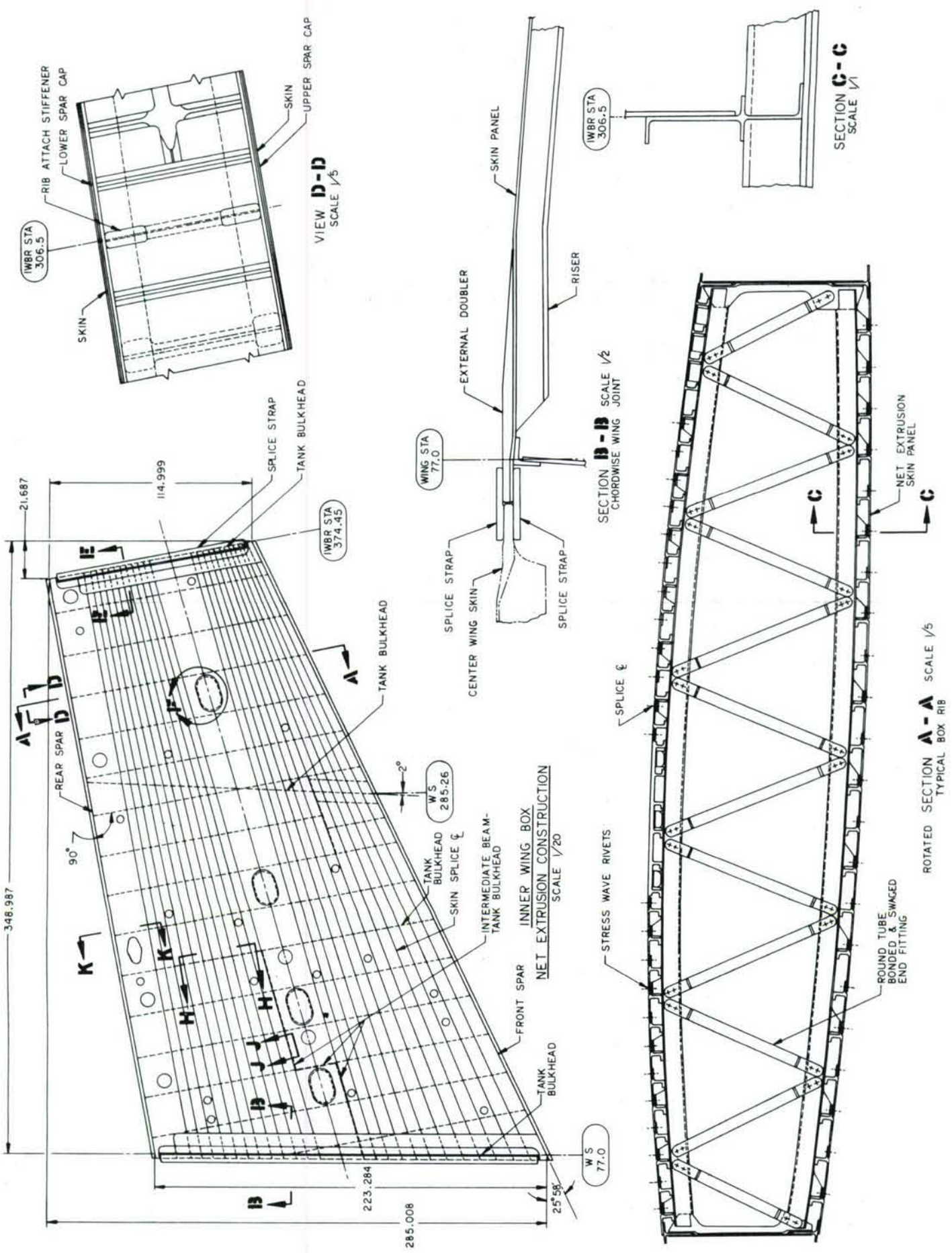
DETAIL N SCALE 1/1  
NON PENETRATING CLIP INSTALLATION

SECTION E-E SCALE 1/5  
FLAP TACK BACK UP STRUCTURE

DETAIL D SCALE 1/5  
VIEW LOOKING FROM INSIDE OUT  
ACCESS CUTOUT

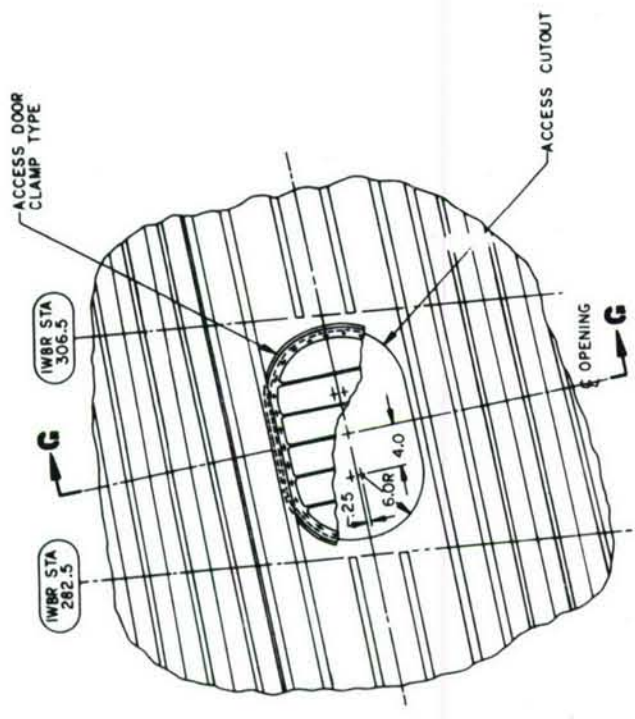
GENERAL ARRANGEMENT - INNER WING  
STRUCTURE - INTEGRAL STIFFENED SKIN PANELS  
& NON PENETRATING CLIP - CONFIGURATION 7  
**VIRGIN PLANK**

SCALE NOTED A. ROBERTSON DWG NO. 2-15-73  
ADP 1026

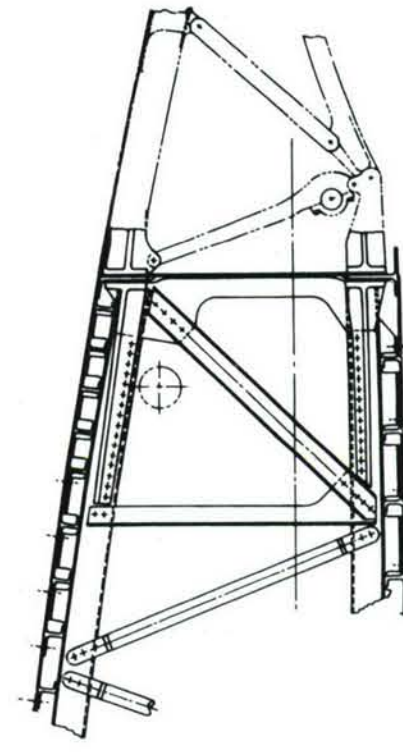


ALL DIMENSIONS ARE IN INCHES  
 UNLESS OTHERWISE SPECIFIED  
 TOLERANCES ARE AS SHOWN  
 SURFACES ARE TO BE FINISHED  
 AS SHOWN  
 MATERIALS ARE TO BE  
 AS SPECIFIED  
 FABRICATOR TO BE  
 RESPONSIBLE FOR  
 COMPLIANCE WITH  
 ALL APPLICABLE  
 SPECIFICATIONS  
 AND STANDARDS  
 GOVERNMENT PROPERTY  
 DRAWING

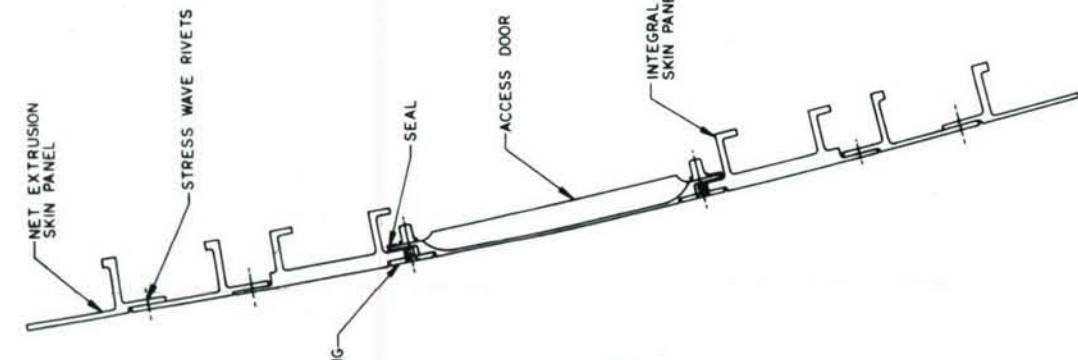




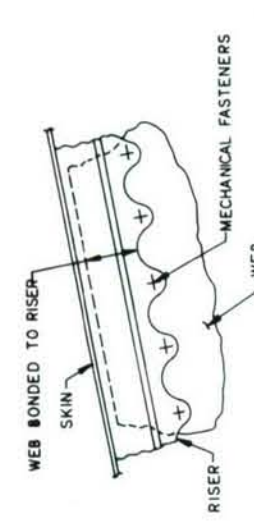
DETAIL F SCALE 1/5  
VIEW LOOKING FROM INSIDE OUT  
ACCESS CUTOUT



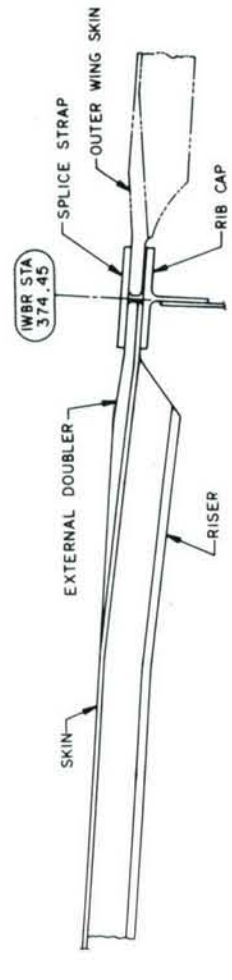
SECTION K-K SCALE 1/5  
FLAP TRACK BACK UP STRUCTURE



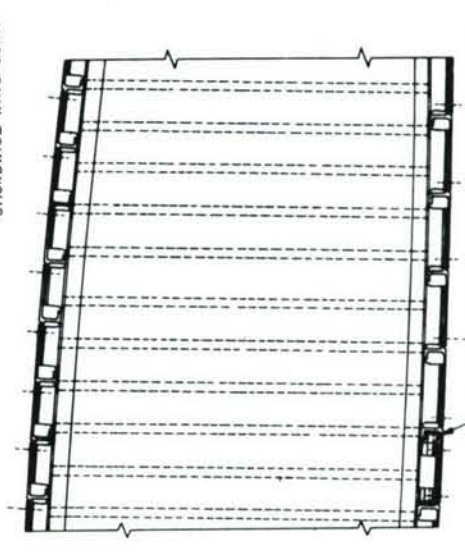
SECTION G-G SCALE 1/2  
SECTION THRU ACCESS DOOR



SECTION J-J SCALE 1/2  
INTERMEDIATE BEAM



SECTION E-E SCALE 1/2  
CHORDWISE WING JOINT



SECTION H-H SCALE 1/5  
FUEL TANK BULKHEAD

GENERAL ARRANGEMENT INNER WING STRUCTURE-NET EXTRUSION SKIN PANELS CONFIGURATION 8 - TAPERED SHINGLE			
SCALE NOTED	A. ROBERTSON	DATE 2-13-73	ADP 1027

## APPENDIX II

### SUMMARY OF TEST RESULTS

The results of materials development and component tests conducted in the Advanced Cargo/Tanker Structures Phase IA Preliminary Design Study by the Lockheed-Georgia Company are presented here. Materials development tests include tests of 7050-T73 and -T76 advanced aluminum alloy in plate and extrusion form, and tests of Ti-6Al-2Sn-2Zr-2Mo-2Cr-0.25Si and Ti-6Al-6V-2Sn plate in several tempers. The former is an advanced titanium alloy being developed under Air Force Contract F33615-72-C-1152. Component tests include static, fatigue, and damage tolerance tests of promising structural concepts developed during the study.

#### MATERIALS PROPERTIES TESTS

##### Purpose

The purpose of the material properties tests was to obtain preliminary design data for use in the Phase IA Preliminary Design of the Cargo/Tanker Structures Program.

##### Test Requirements

Requirements for the materials tests are presented in Table XXXII. Numerals opposite each type of test indicate the number of test specimens for each material alloy and temper.

Tests were performed in accordance with applicable Military Specifications, the Air Force Structural Integrity Program (ASIP), and the ASTM Standards. Data are of a form appropriate for inclusion in MIL-HDBK-5 and the Damage Tolerance Design Handbook, MCIC-HB-01.



### Material Test Parameters

Table XXXIII presents the important material test parameters, including material alloy and temper, product form and size, heat-treat and process procedures, lot designation, test temperature, and test environment.

TABLE XXXII

## MATERIALS TEST PLAN

MATERIAL FORM	Ti-6Al-2Sn-2Zr-2Mo-2Cr-0.25Si PLATE	Ti-6Al-6V-2Sn PLATE	7050			
			EXTRUSION		PLATE	
THICKNESS	5/8 INCH	5/8 INCH	7/16 INCH	T73	T76	T76 (2)
CONDITION	STA	ST	STOA	T73	T76	T76
TENSILE	5	5	3	5	5	5
COMPRESSION	2	2	1	1	2	1
SHEAR	2	2	1	1	2	1
BEARING (e/D = 2.0)	2	2	1	1	2	1
FATIGUE: ( $K_t = 3$ , $R = 0.1$ )	5	7	10	6	6	-
( $K_t = 3$ , $R = -1.0$ )	6	7	-	6	6	3
( $K_t = 5$ , $R = 0.1$ )	5	7	10	3	6	-
( $K_t = 5$ , $R = -1.0$ )	6	7	-	6	6	3
CRACK GROWTH (DA/DN): (RT AIR, 95% RH, 60* & 1200 CPM) ( $R = 0.1$ )	2	2	2	2	2	2
(RT AIR, 95% RH, SPECTRUM LOADING (3))	2	2	2	1	1	1
(RT, 3-1/2% NaCl, 60* & 1200 CPM) ( $R = 0.1$ )	2	2	2	2	2	2
FRACTURE TOUGHNESS: $K_{Ic}$	3	3	2	-	-	2
$K_c$ (1)	3	3	2	-	4	2
$K_{Isc}$ (RT, 3-1/2% NaCl)	2	3	2	-	-	-

NOTES: (1) APPROPRIATELY THIN SPECIMEN TO BE MACHINED FROM THICKER MATERIAL. TWO DIFFERENT THICKNESSES WILL BE EVALUATED UNLESS RESTRICTED BY SIZE OF AVAILABLE MATERIAL.

(2) 7050-T7351 PLATE IS 1 INCH THICK: -T7651 PLATE IS .515 INCHES THICK.

(3) CYCLIC RATE FOR THE SPECTRUM TESTS WILL BE DETERMINED FROM RESULTS OF DA/DN TESTS PERFORMED AT 95% RH.

(\*) 120 CPM FOR ALUMINUM.

TABLE XXXIII  
SUMMARY OF MATERIALS TEST PARAMETERS

MATERIAL	7050				6Al-2Sn-2Zr-2Mo-2Cr		6-6-2
FORM	PLATE		EXTRUSION		PLATE		PLATE
CONDITION	-T7351	-T7651	-T73511	-T76511	STA	ST	
PRODUCT SIZE, INCHES	1x48x18	1x48x72	Alcoa Section 191282		.625		.625x44.5x18
THICKNESS HEAT TREATED	1.0"	.515"	7/16		.625		
MATERIAL SPECIFICATION	EXPERIMENTAL						(4)
SPECIAL PROCESSING	NONE						(5)
HEAT TREATMENT PROCEDURES	UNKNOWN						(6)
LOT DESIGNATION	106-385 (Alcoa)	105-672 (Alcoa)	H31469A1 (Alcoa)	H31468A1	(1)	(3)	Heat #295226 Lot #06
TEST TEMPERATURE	ROOM TEMPERATURE						(2)
TEST ENVIRONMENT	AMBIENT AIR						

- (1) 1740°F - 1 Hr. - AC + 1000°F - 8 Hr. - AC
- (2) Made on Contract AF 33615-72-C-1152
- (3) 1740°F - 1 Hr. - AC
- (4) MIL-T-9046F, Type III, Composition E
- (5) Beta Annealed (1800°F -  $\frac{1}{2}$  Hr. - AC) before Heat Treatment
- (6) 1575°F -  $\frac{1}{2}$  Hr. - WQ + 1050°F - 8 Hr. - AC

## TEST PROCEDURES AND RESULTS

### Tensile Tests

Tensile property data for all materials were obtained using the specimen shown in Figure 106. This configuration conforms to the requirements of ASTM Method E8, "Tension Testing of Metallic Materials." Testing procedures outlined in E8 were also followed.

A constant strain rate of 0.006 inch per inch per minute was maintained until 0.2 percent offset yield stress was reached. From yield to failure, a head travel rate of 0.1 inch per minute was held. Tensile test results are presented in Table XXXIV.

### Compression Tests

The compression test specimen is shown in Figure 107. A special fixture which provided lateral support to prevent buckling was used for the compression specimens. A constant strain rate of 0.006 inch per inch per minute was maintained.

Loading at this rate was continued until a load-deformation curve was recorded from which  $F_{cy}$  and  $F_{.85}$  was obtained. Compression test results are presented in Table XXXIV.

### Shear Tests

Shear strength was determined for the various materials using the specimen shown in Figure 108. A special fixture was used to facilitate loading the specimen in double shear. The specimen was indexed to allow application of shear relative to a known grain direction. Shear test results are presented in Table XXXIV.

### Bearing Tests

Bearing tests were performed using the specimen shown in Figure 109. The test section was sandwiched between ground steel plates having bearing pin



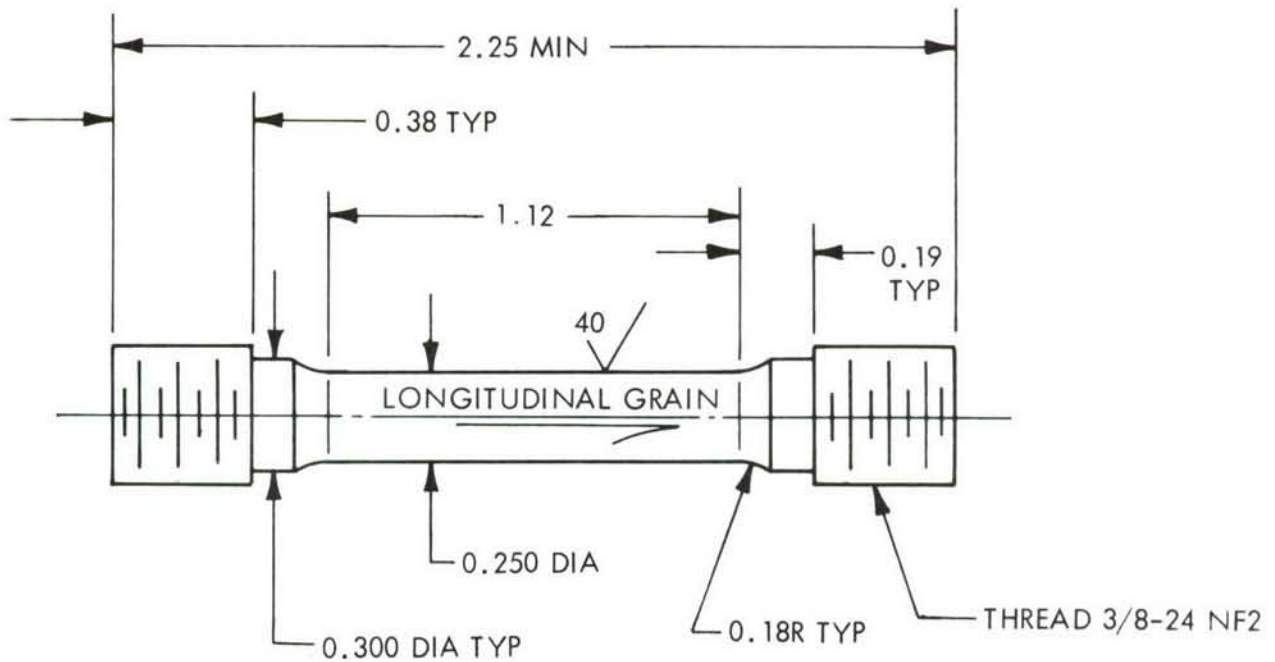
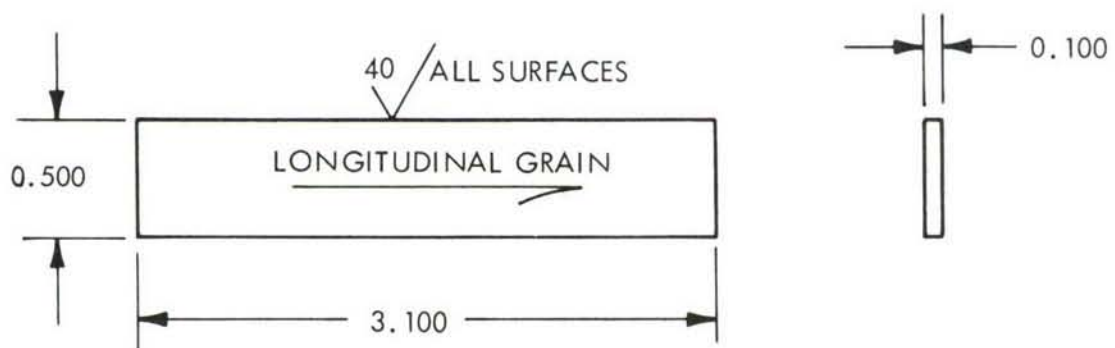


FIGURE 106 TENSILE SPECIMEN



ALL SURFACES TO BE FLAT, SQUARE AND PARALLEL

FIGURE 107 COMPRESSIVE SPECIMEN

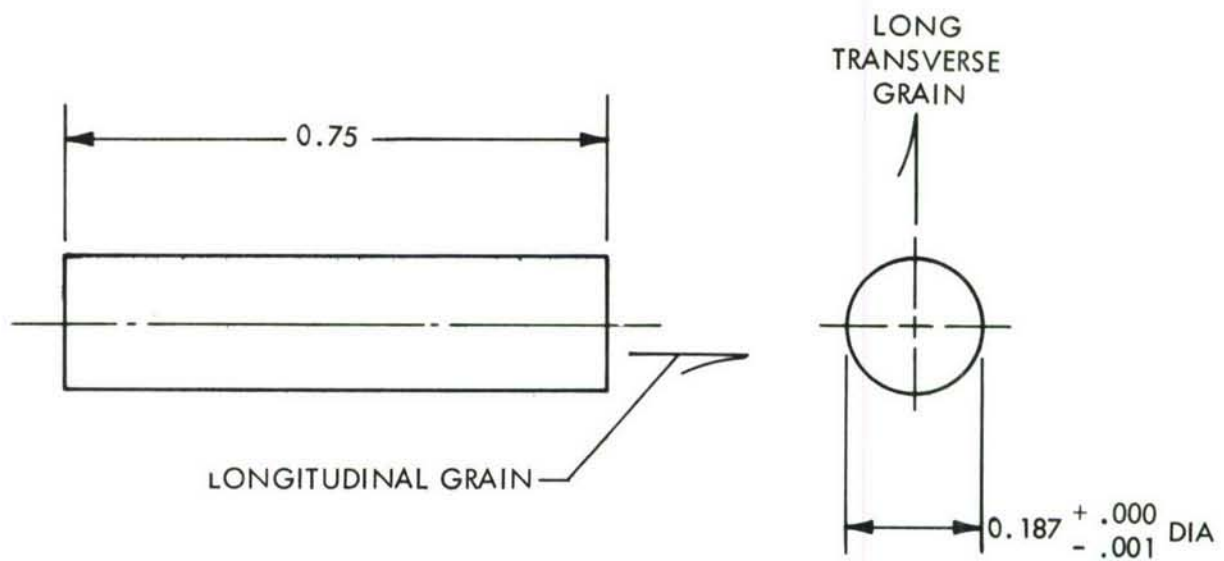
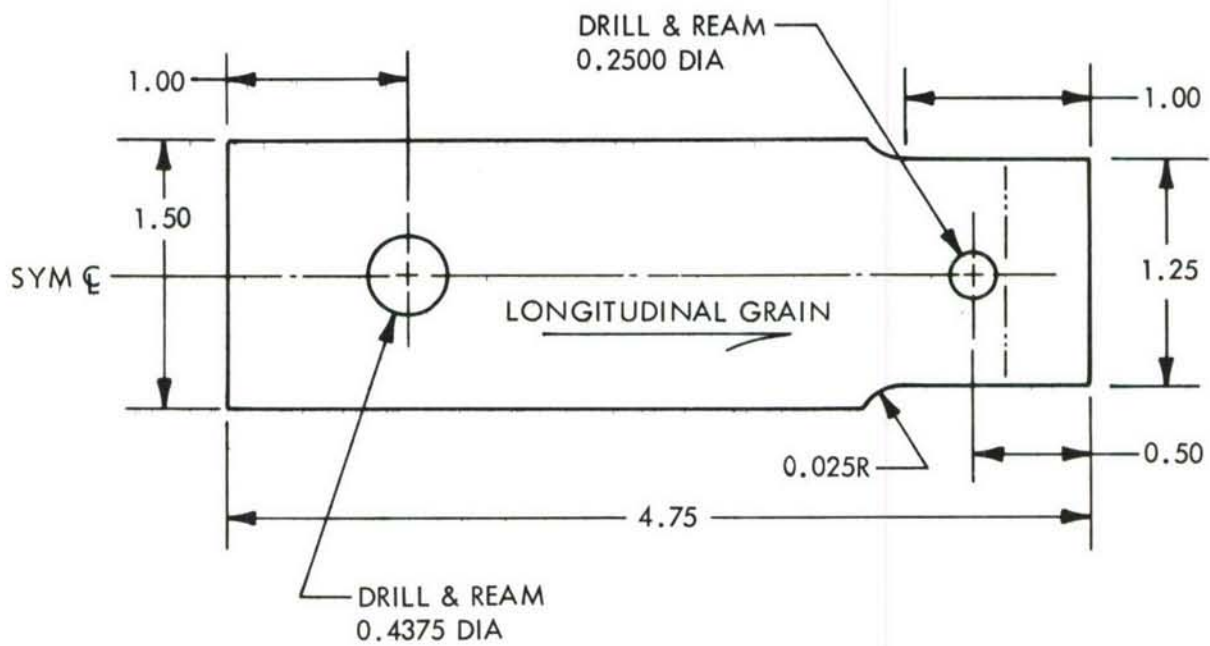


FIGURE 108 SHEAR SPECIMEN



THICKNESS = 0.125

FIGURE 109 - BEARING SPECIMEN

holes in one end and loading holes in the other. The plates also had two clamping holes to allow the specimen to be snugly sandwiched between the plates using clamping bolts. A shim, equal to the specimen thickness, was inserted between the plates to prevent excessive clamping, and the force required to withdraw the specimen did not exceed approximately five pounds. Snug fitting bearing pins of high-strength steel were used.

Bearing load was applied to give a constant deformation rate of approximately 0.008 inch per minute to yield as controlled with a strain-rate pacer driven by the extensometer. This value was selected since it generally resulted in reaching bearing yield stress in about the same lapsed time as that required to reach tensile yield stress. After bearing yield was reached, the head travel of the testing machine was adjusted to 0.1 inch per minute.  $F_{bry}$  was determined at a permanent deformation of two percent of the bearing pin diameter. Bearing test results are presented in Table XXXIV.

#### Fatigue Tests

All fatigue tests were performed under axial load conditions for theoretical stress concentration factors of 3 and 5. For the titanium alloys, round specimens as shown in Figure 110 were tested. Flat specimens as shown in Figure 111 were used for the aluminum alloys. Fatigue test results are presented in Table XXXV.

#### Crack Growth Tests

Crack growth tests for development of  $da/dN$  curves were performed at a stress ratio ( $R$ ) of 0.10 using the compact tension specimen shown in Figure 112. The stress intensity function of W. K. Wilson in Reference 11 was used, thereby allowing a complete curve to be obtained from a single specimen.

A center crack specimen, shown in Figure 113, was used for spectrum tests.

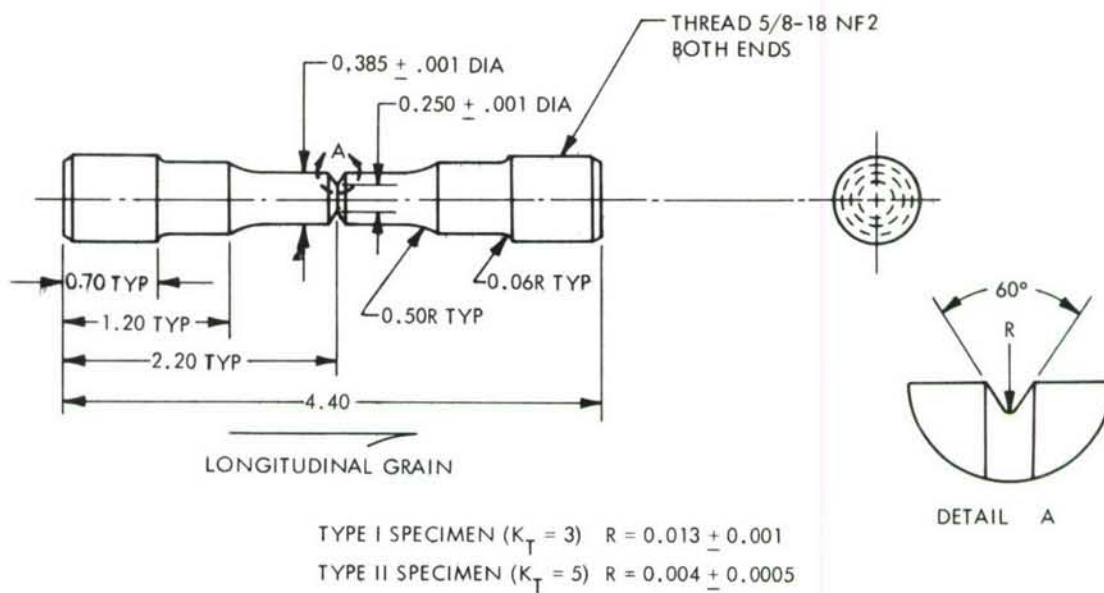


FIGURE 110 AXIAL LOAD FATIGUE SPECIMENS

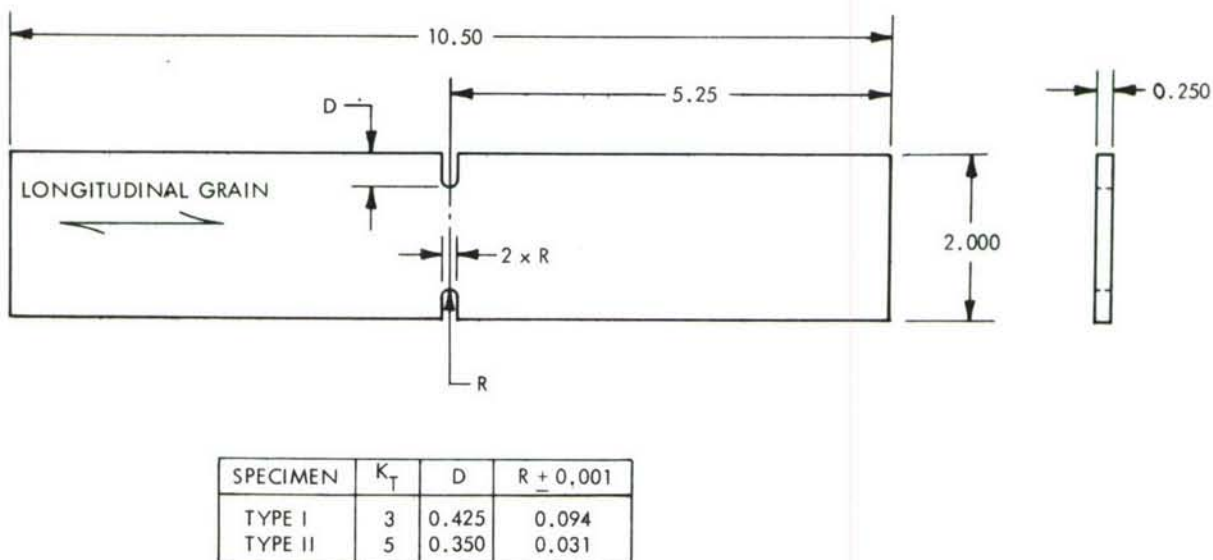


FIGURE 111 RECTANGULAR FATIGUE SPECIMEN



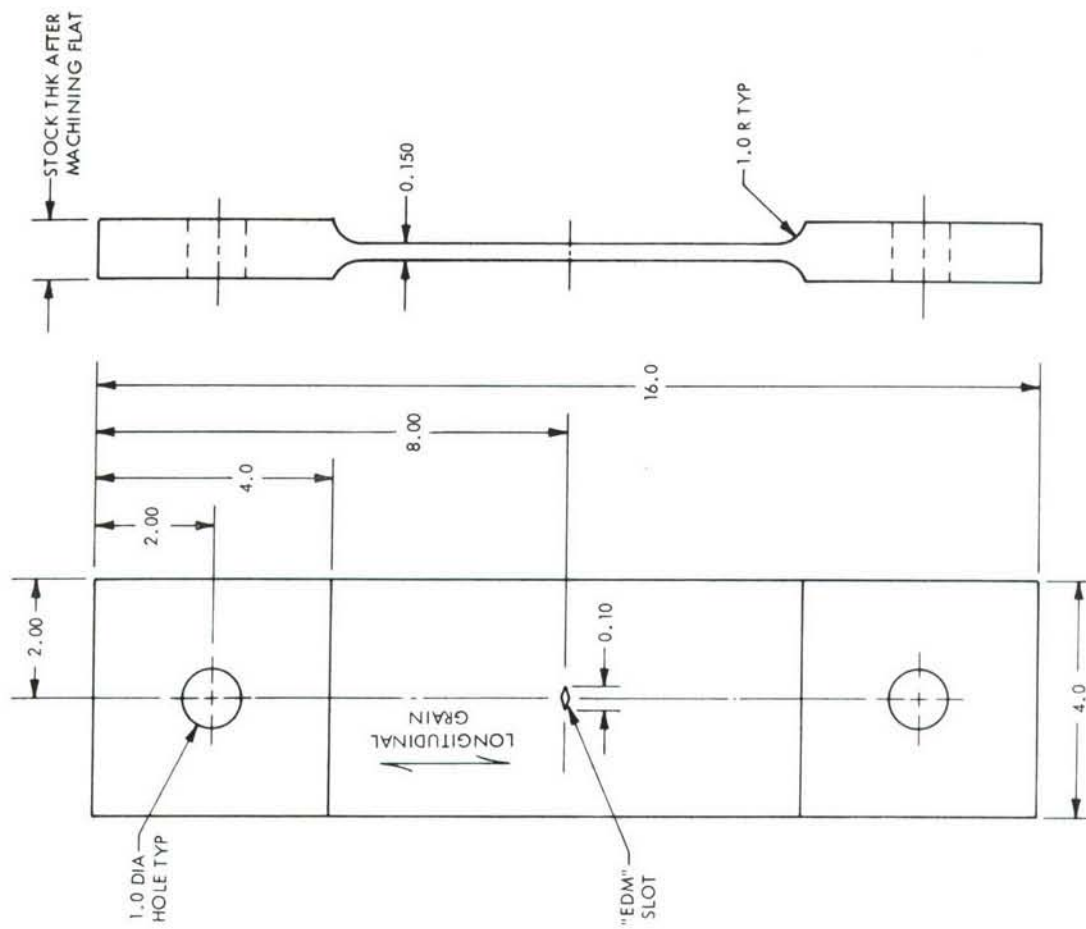


FIGURE 113 SPECTRUM CRACK GROWTH SPECIMEN

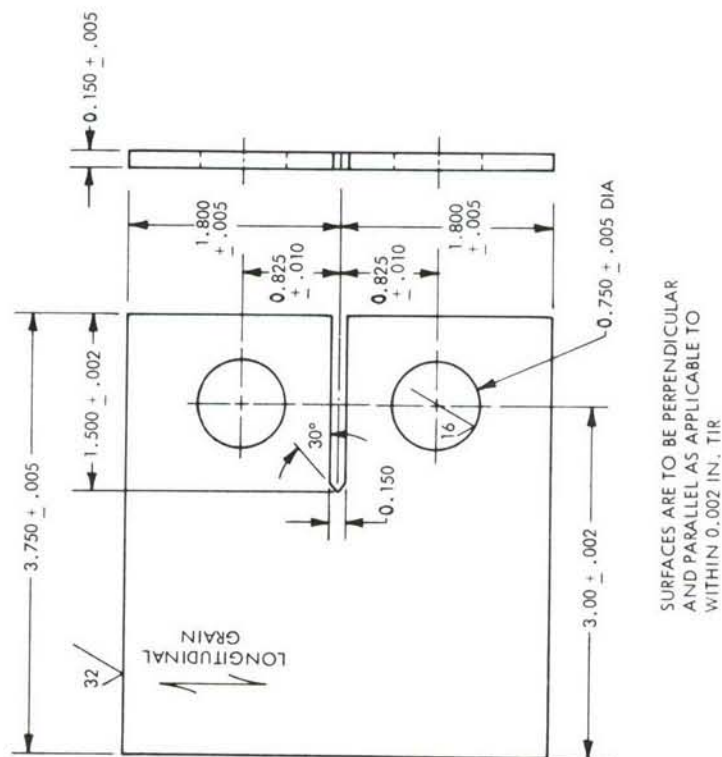


FIGURE 112 CRACK GROWTH-COMPACT TENSION SPECIMEN

The test area on all specimens was polished to enhance crack observation; reference lines were applied at a spacing of 0.010 inch to reference crack growth when observed through a variable power binocular microscope. Testing was performed in two environments: humid air (95 to 100 percent relative humidity), and an aqueous solution containing 3.5 percent NaCl by weight. Humid air was produced by bleeding ambient air through a wash bottle containing distilled water into a chamber of clear acrylic placed around the specimen. The NaCl was applied by placing a wetted wick in the chamber and attaching it to the back of the specimen.

Crack growth test results are presented in Figures 117 through 131.

#### Fracture Tests

$K_{Ic}$  - These tests were performed in accordance with ASTM 390 using the compact tension specimen configuration shown in Figure 114. The chevron starter notch option was employed, and the thickest specimen possible from the available materials was used.

$K_c$  - Plane stress tests were performed using the general specimen configuration shown in Figure 115. Two different thicknesses were tested for each material. After precracking in fatigue, the specimens were loaded to failure while crack extension was recorded on movie film to aid in calculating  $K_c$ .

$K_{Isc}$  - Bend specimens conforming to ASTM 390 were used for these evaluations. After precracking in fatigue, the specimens were loaded in four-point bending by special fixtures assembled in a creep-rupture testing machine. Environment for the tests consisted of an aqueous solution of 3 1/2 percent NaCl by weight. The specimen design is shown in Figure 116.

Fracture test results are presented in Table XXXIV.

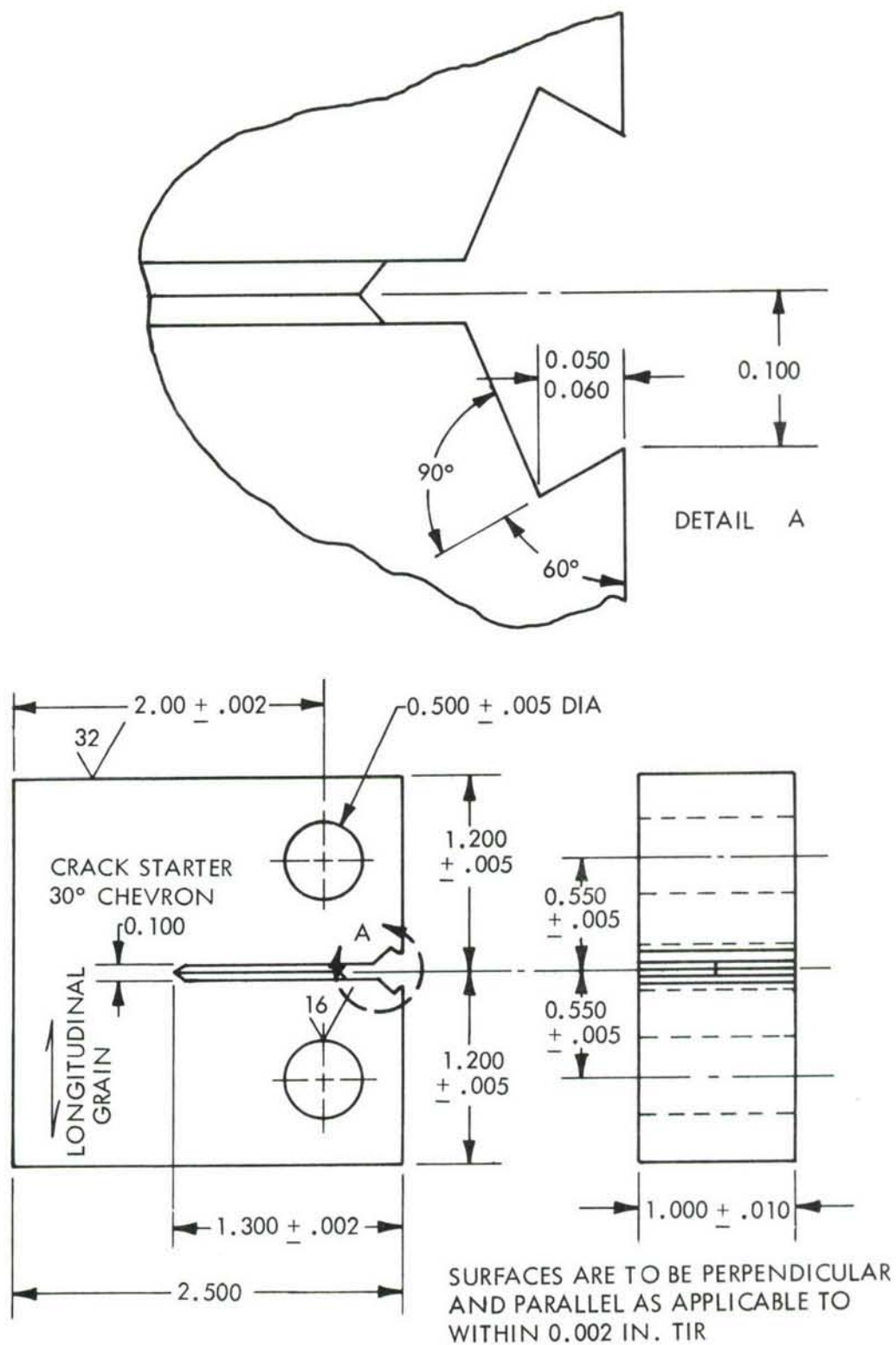


FIGURE 114 COMPACT TENSION SPECIMEN FOR  $K_{Ic}$  TESTS

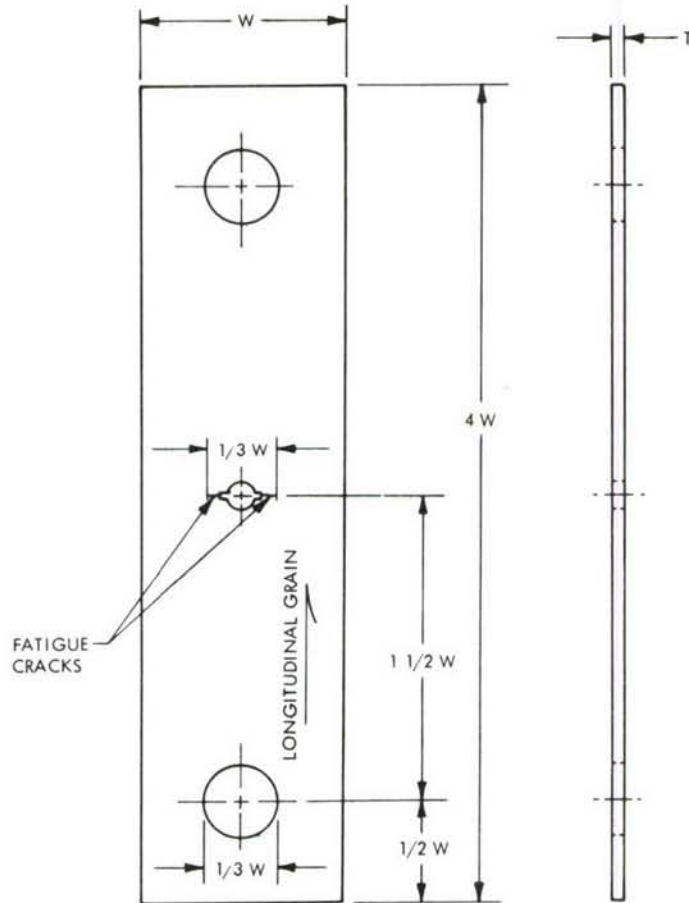


FIGURE 115 GENERAL CONFIGURATION SPECIMEN  
FOR  $K_C$  TESTS FOR  $W/T > 16 < 45$

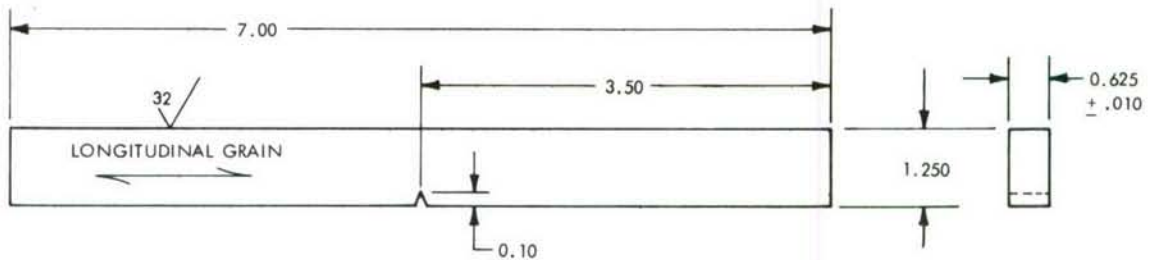


FIGURE 116 SPECIMEN CONFIGURATION FOR  $K_{ISCC}$  TESTS



TABLE XXXIV

## SUMMARY OF MATERIALS STATIC TEST RESULTS

MATERIAL		7050				6Al-2Sn-2Zr-2Mo-2Cr		6Al-6V-2Sn
FORM		PLATE		EXTRUSION		PLATE		PLATE
THICKNESS		1 INCH		7/16 INCH		5/8 INCH		5/8 INCH
CONDITION		-T7351	-T7651	-T73511	-T76511	STA	ST	STOA
MECHANICAL PROPERTIES	SPECIMEN							
$F_{tu}$ ksi L	1	79.7	85.0	82.8	84.1	176.0	165.4	167.0
	2	80.0	85.2	82.7	84.5	176.0	165.5	166.3
	3	80.0	85.3	82.8	84.8	176.7	165.0	166.1
	4	80.0	85.2	83.4	85.4	176.7	165.4	
	5	79.8	85.6	83.0	85.2	175.7	166.5	
$F_{ty}$ ksi L	1	69.7	78.3	74.3	77.2	159.3	148.7	155.4
	2	70.2	78.4	72.6	76.8	155.3	147.9	156.4
	3	69.8	78.8	74.4	77.5	157.7	147.9	155.6
	4	69.3	78.6	74.5	77.5	156.9	147.8	
	5	69.8	78.6	74.7	77.3	156.5	148.7	
$F_{cy}$ ksi L	1	67.9	78.2	74.8	78.2	170.6	148.0	169.4
	2				76.7	-	152.1	
$F_{su}$ ksi LT	1	50.5	53.9	43.4	43.4	116.9	115.1	112.9
	2				46.2	117.4	114.2	
$F_{bru}$ ksi L e/D = 2.0	1	145.0	150.0	152.6	148.7	310.0	304.0	321.0
	2				149.3	316.0	299.0	
$F_{bry}$ ksi L e/D = 2.0	1	108.0	116.0	110.4	112.5	247.0	251.0	249.0
	2				112.6	264.0	249.0	
e percent L	1	14	12	13	13	13	14	6
	2	15	12	13	12	12	14	8
	3	14	10	12	12	13	13	8
	4	14	10	12	12	14	13	
	5	14	10	13	11	13	13	
$E_t$ $10^6$ psi L	1	11.5	10.7	10.7	10.5	19.6	18.3	16.8
	2	10.8	10.5	10.8	12.0	20.0	18.3	17.7
	3	11.1	10.8	11.8	11.5	17.8	16.8	16.8
	4	10.5	10.7	11.0	12.2	18.5	17.0	
	5	10.7	10.9	11.0	10.9	18.5	-	
$E_c$ $10^6$ psi	1	10.0	10.2	10.0	9.9	17.9	16.6	16.0
	2				9.7	17.8	17.0	
$F_{.7}$ ksi L	1	69.1	79.8	76.4	79.6	185.8	157.5	174.0
	2				77.9	-	165.3	
$F_{.85}$ ksi L	1	66.3	74.3	73.6	77.2	166.2	144.5	169.4
	2				75.7	-	148.6	
$K_{Ic}$ KSI $\sqrt{IN}$ L (Note 1)	1	36.9	(2) 39.4			54.7	62.8	48.8
	2	(2) 36.9	(2) 36.8			54.3	62.0	51.3
	3	-	-			57.0	59.8	-
$K_c$ L (Note 3)	1	55.4	64.8		95.0	110.1	126.6	90.9
	2	59.5	57.3		88.3	111.1	123.5	72.1
	3				94.8	125.6	159.1	
	4				80.4			
$K_{Isc}$ (Note 4)	1					(5) 48.6	(6) 42.7	(5) 45.2
	2					(7) 32.2	(7) 41.7	(5) 36.5
	3						(7) 39.9	

For explanation of notes, see next page.

NOTES FROM TABLE XXXIV

- (1) Proposed ASTM Method, Vol. 31, 1969:

$$K_Q = K_{Ic} = \frac{P_Q}{BW^{1/2}} \left[ 29.6 \left( \frac{a}{W} \right)^{1/2} - 185.5 \left( \frac{a}{W} \right)^{3/2} + 655.7 \left( \frac{a}{W} \right)^{5/2} - 1017 \left( \frac{a}{W} \right)^{7/2} + 638.9 \left( \frac{a}{W} \right)^{9/2} \right]$$

- (2) Indicates Test did not meet Validity Check of ASTM Vol. 31, 1969.

(3) Values Computed From Formula:  $K_c = \frac{P}{BW^{1/2}} \left[ 1.77 + 0.227 \left( \frac{2a}{W} \right)^2 - 0.510 \left( \frac{2a}{W} \right)^3 + 2.7 \left( \frac{2a}{W} \right)^3 \right]$

Where P = Failing Load at Fracture, B = Specimen Thickness, W = Specimen Width,

2a = Crack Length at Fracture

- (4) Values From Notched Beam Specimens:

$$K_{Ii} = \frac{4.12 M (\alpha^{-3} - \alpha^3)^{1/2}}{BD^{3/2}} \quad \text{(From J. A. Kies, ASTM STP 381, 1965)}$$

Where  $K_{Ii}$  = Initial Stress Intensity

M = Bending Moment at Notch

B = Thickness of Specimen

D = Beam Depth of Specimen

$\alpha = 1 - \frac{a}{D}$  Where a = Average Crack Depth

- (5) Time to Fracture Less Than 5 Minutes for This Value of  $K_{Ii}$

- (6) Time to Fracture 36 Minutes at This Value of  $K_{Ii}$

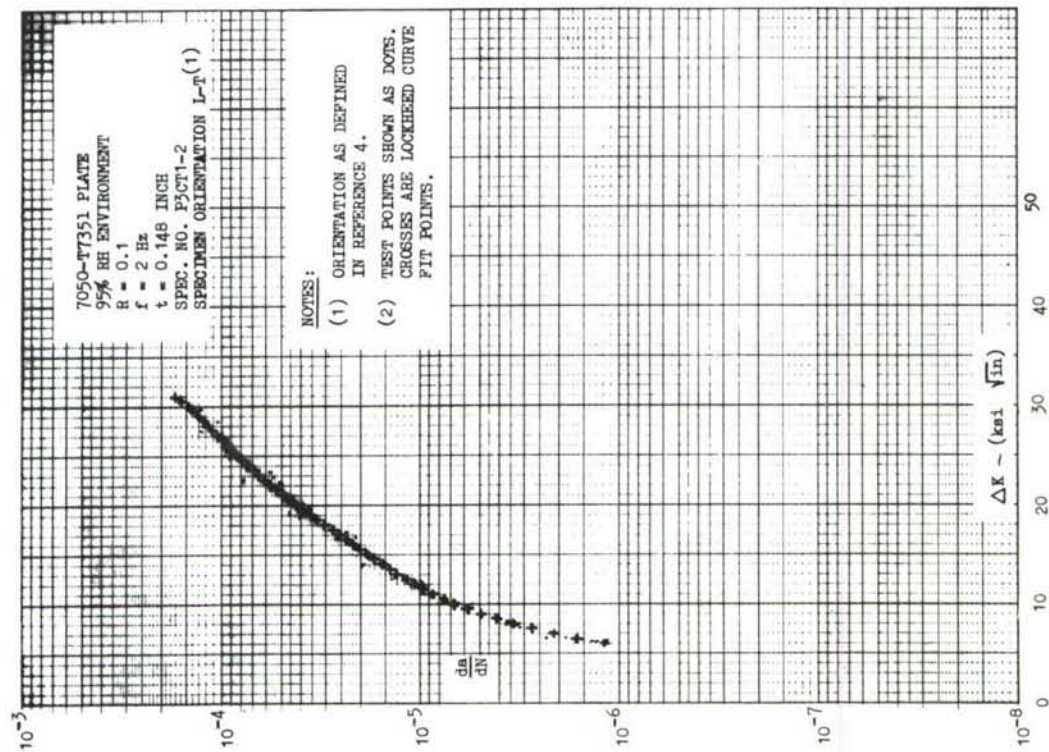
- (7) Specimen Sustained 100 Hours or More at This  $K_{Ii}$  Without Failure

TABLE XXXV

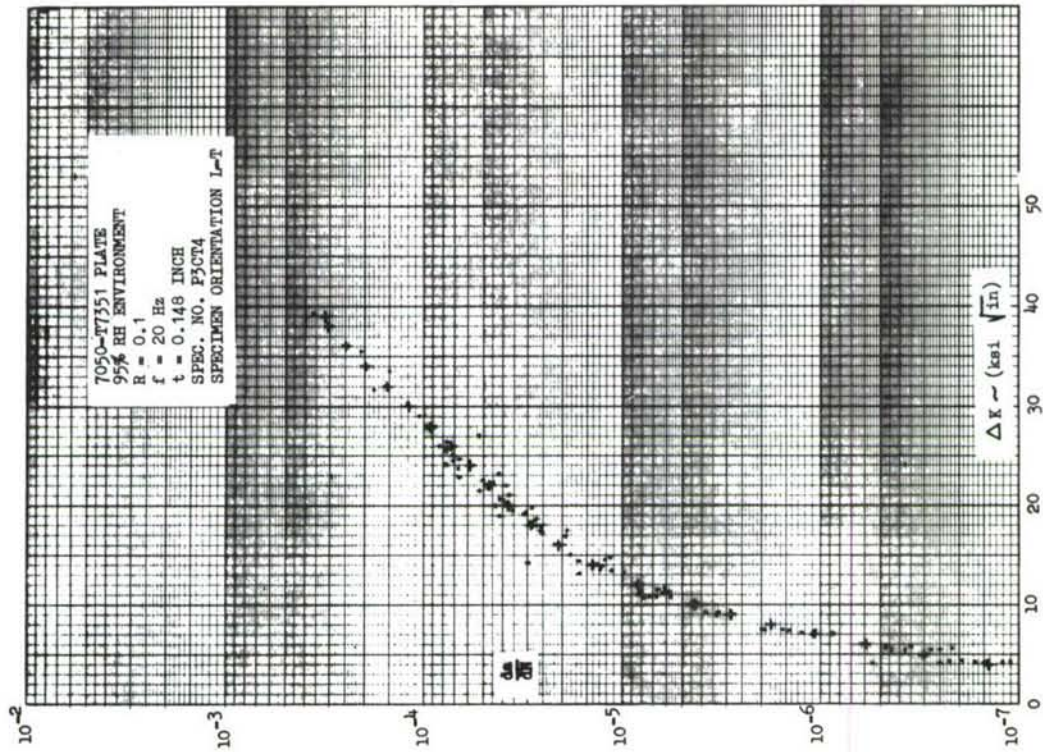
## SUMMARY OF MATERIALS FATIGUE TEST RESULTS

MATERIAL		7050				6Al-2Sn-2Zn-2Mo-2Cr				6Al-6V-2Sn			
FORM		PLATE				PLATE				PLATE			
THICKNESS		1 INCH				5/8 INCH				5/8 INCH			
CONDITION		-T7351				-T76511				STOA			
Specimen Number	Stress Ratio (R)	Max. Stress (ksi)	Cycles To Failure	Max. Stress (ksi)	Cycles To Failure	Max. Stress (ksi)	Cycles To Failure	Max. Stress (ksi)	Cycles To Failure	Max. Stress (ksi)	Cycles To Failure	Specimen Number	Cycles to Failure
1	-1.0	10.0	2,507,200	259,460	8.0	6,767,000	25.0	143,000	61,000	(1)	Initial 80,000 cycles on this specimen were at R = +0.1.		
2	-1.0	15.0	157,270(1)	73,940	10.0	63,000	34.0	53,700	58,300	(2)	Failed in grip.		
3	-1.0	25.0	6,840	8,610	11.0	327,000	34.0	37,300	18,900	(3)	No failure.		
4	-1.0				12.5	140,000	42.5	13,600	18,200	(4)	Specimen damaged prior to test.		
5	-1.0				15.0	60,000	42.5	14,500	16,900				
6	-1.0				17.5	32,000	60.0	4,090	9,600				
7	-1.0								10,100				
8	+0.1				10.0	3,610,000(2)	40.0	14,839,000(3)	11,365,000(3)	30.0	12,784,000(3)	29	80,000
9	+0.1				13.0	934,000	45.0	70,000	12,735,000	31.5	855,000	30	32,000
10	+0.1				15.0	284,000	50.0	56,000	445,000	32.5	193,000	31	32,000
11	+0.1				17.5	133,000	60.0	28,000	133,000	35.0	150,000(3)	32	20,000
12	+0.1				20.0	117,000	60.0	34,000	199,000	35.0	110,000	33	17,000
13	+0.1				23.5	27,000		(4)	99,000				
14	+0.1								35,000				
15	-1.0	10.0	163,850	62,620	6.5	3,332,000	20.0	86,300	71,000				
16	-1.0	15.0	172,200	13,390	8.0	413,000	30.0	18,600	49,000				
17	-1.0	25.0	4,760	3,690	10.0	134,000	30.0	13,400	18,300				
18	-1.0				11.0	116,000	45.0	6,900	20,600				
19	-1.0				12.0	35,000	45.0	7,100	19,100				
20	-1.0				15.0	29,000			8,340				
21	-1.0								10,200				
22	+0.1				9.0	678,000	30.0	227,000	140,000	26.0	11,378,000(3)	34	73,000
23	+0.1				10.0	136,000	31.5	195,000	369,000	27.0	482,000	35	37,000
24	+0.1				15.0	47,000	35.0	74,000	206,000	28.0	171,000	36	34,000
25	+0.1						40.0	25,000	191,000	30.0	77,000	37	26,000
26	+0.1				12.5	86,000	50.0	19,000	76,000	31.5	81,000	38	15,000
27	+0.1				15.0	23,000			50,000				
28	+0.1				16.5	21,000			22,000				





(a) 95% RH, 2 Hz



(b) 95% RH, 20 Hz

FIGURE 117 CRACK GROWTH OF 7050-T7351 ALUMINUM PLATE



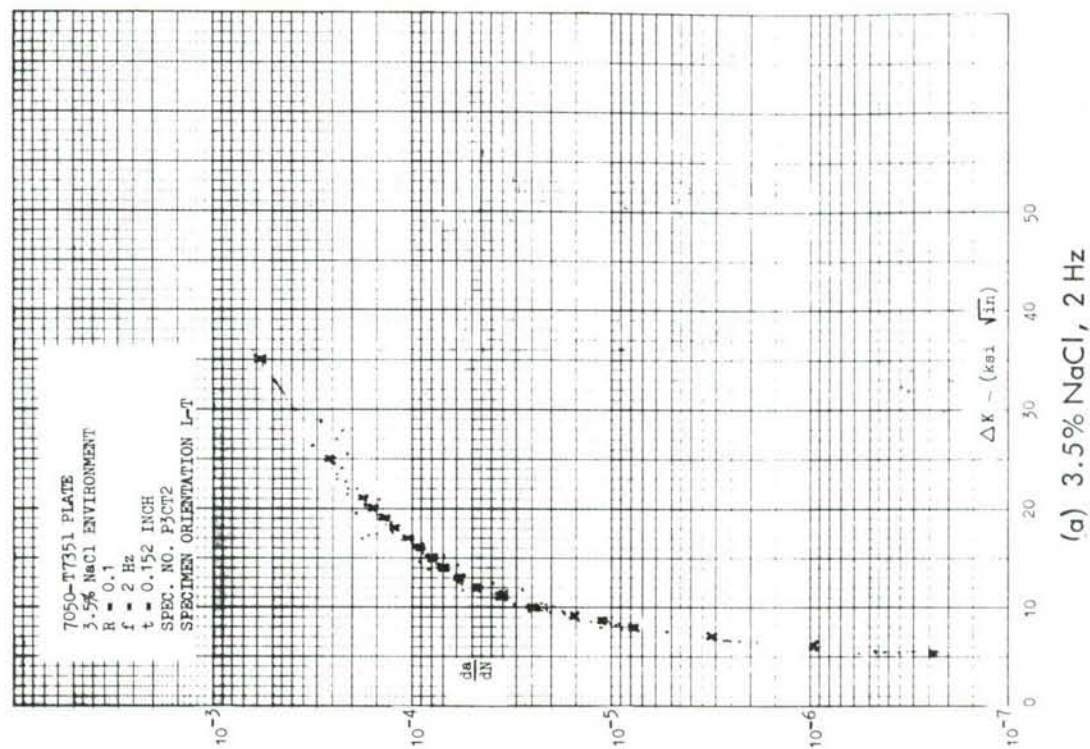
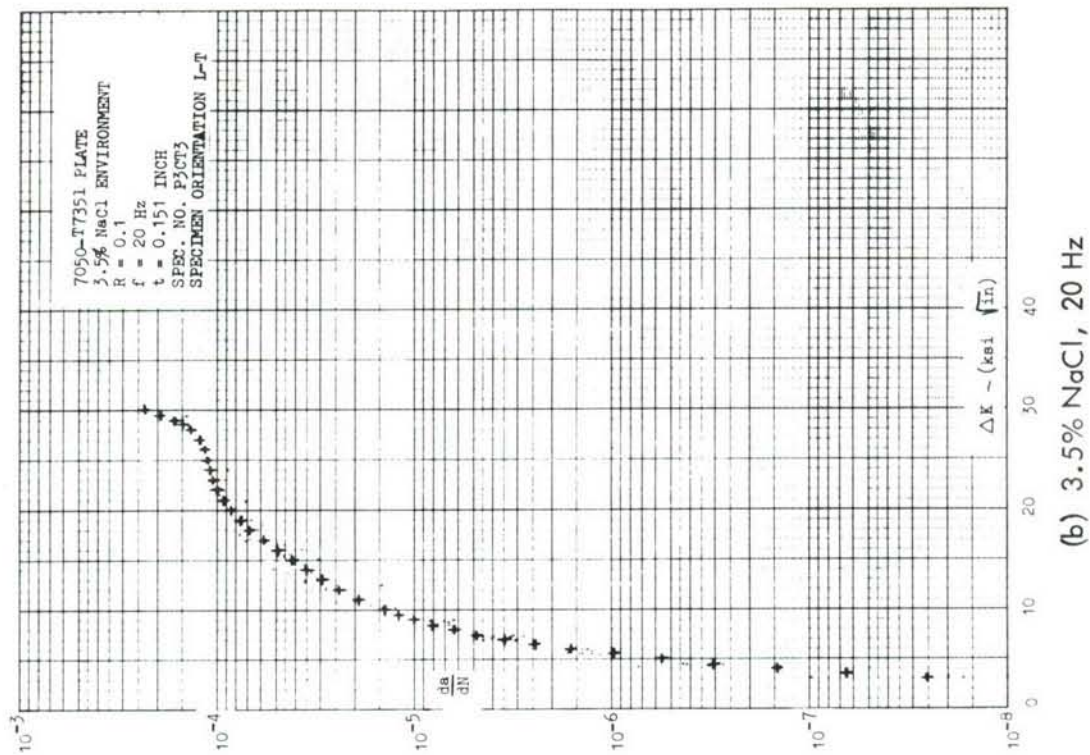


FIGURE 118 CRACK GROWTH OF 7050-T7351 ALUMINUM PLATE

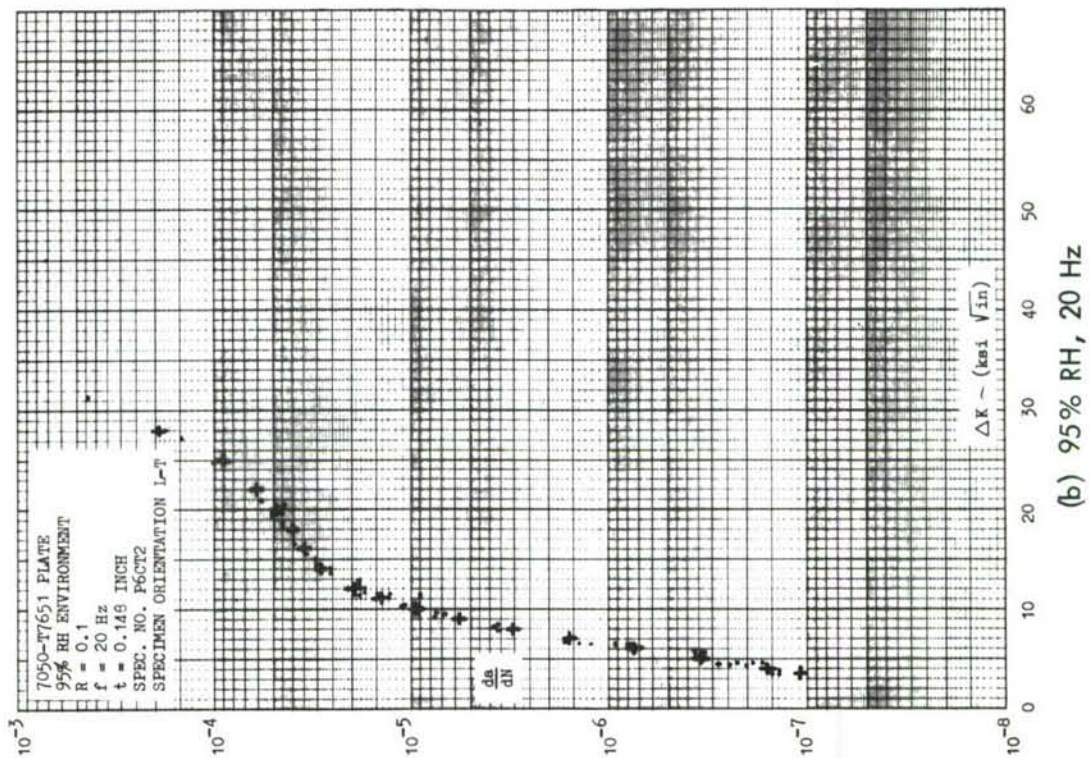
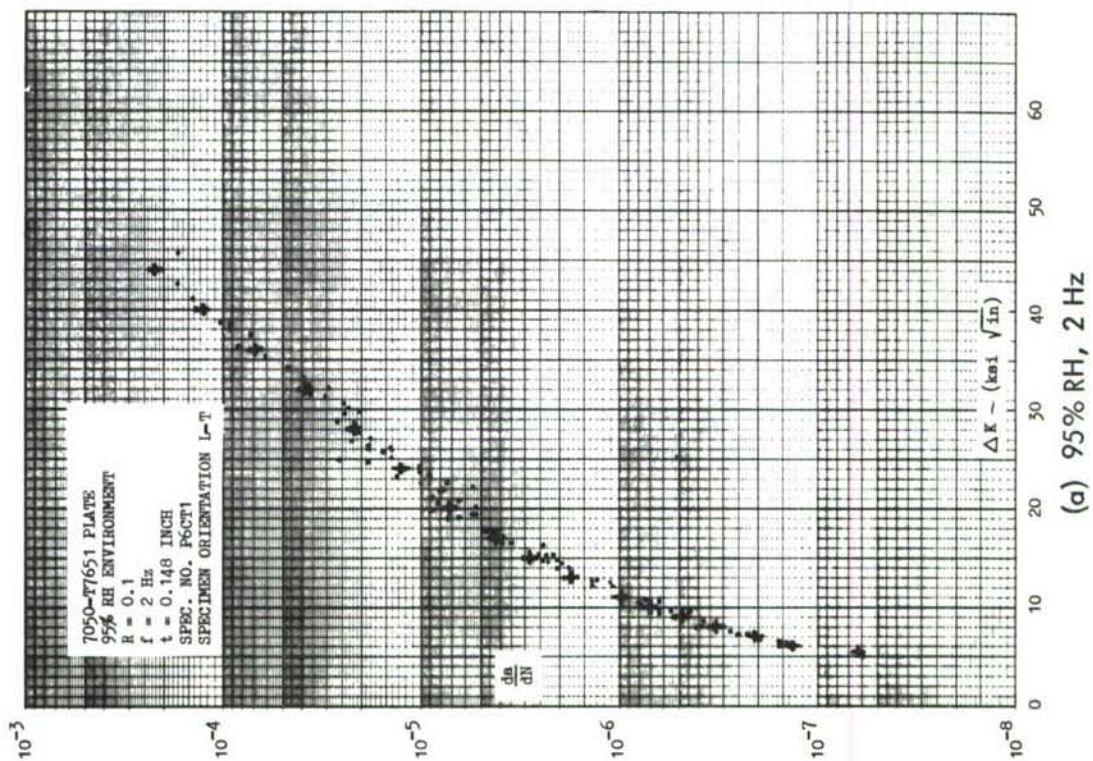


FIGURE 119 CRACK GROWTH OF 7050-T7651 ALUMINUM PLATE



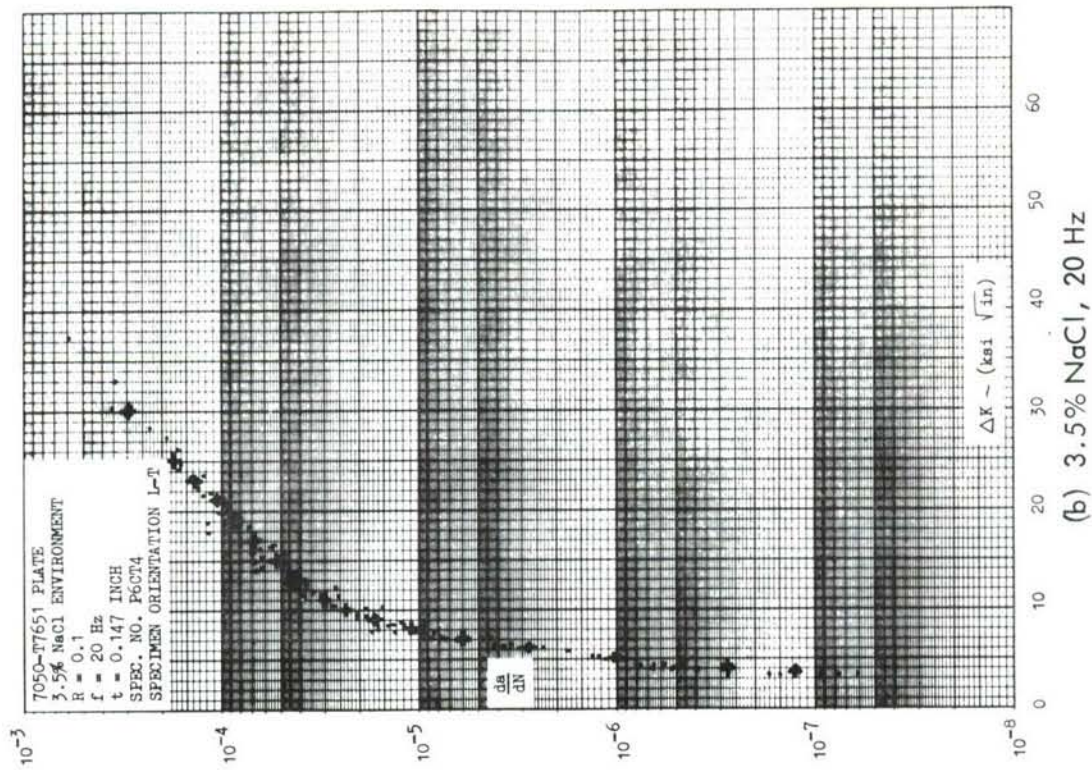
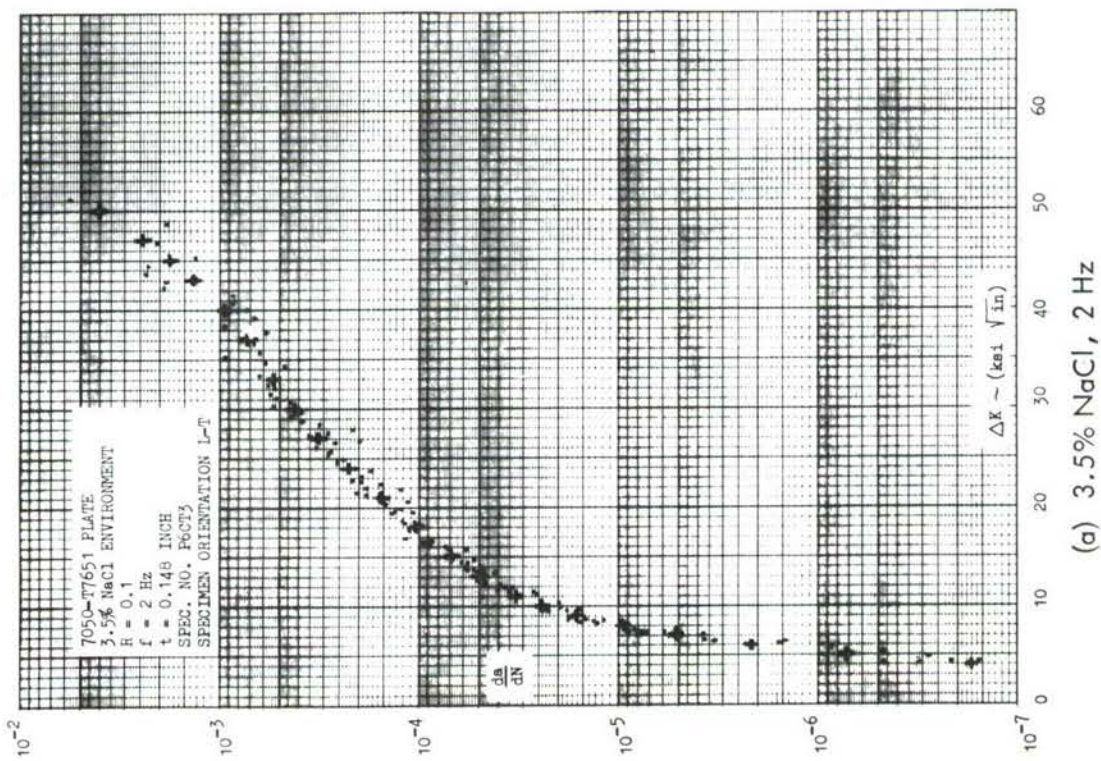


FIGURE 120 CRACK GROWTH OF 7050-T7651 ALUMINUM PLATE



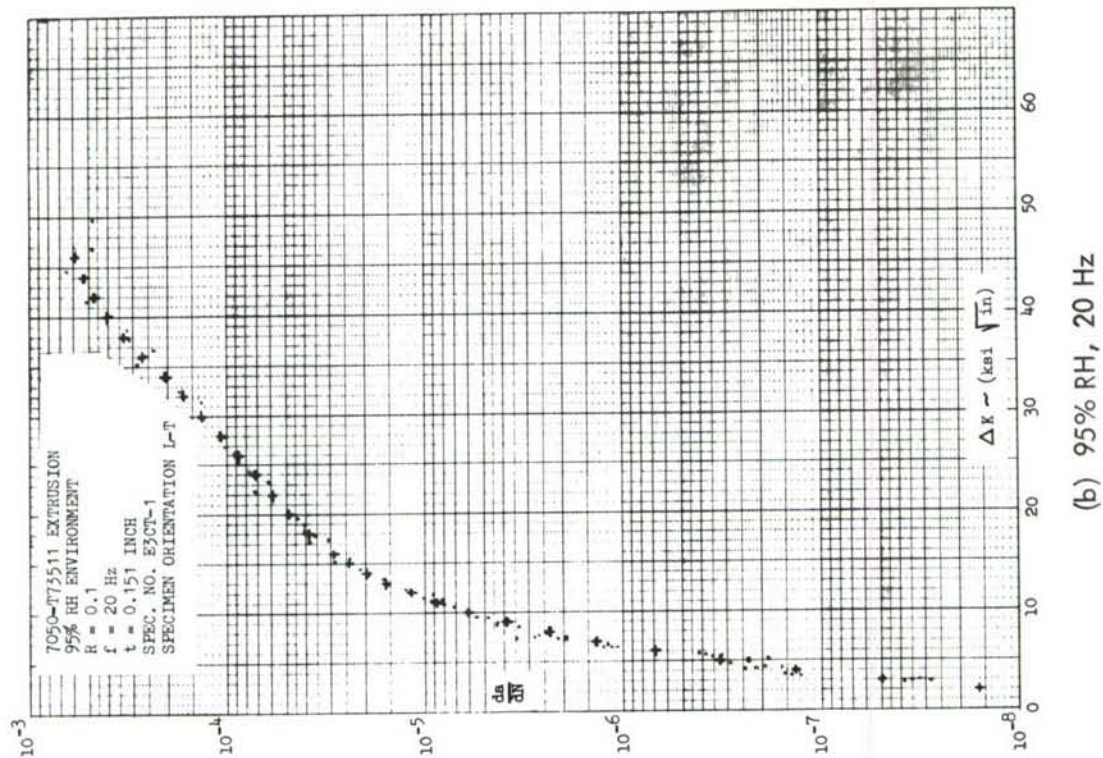
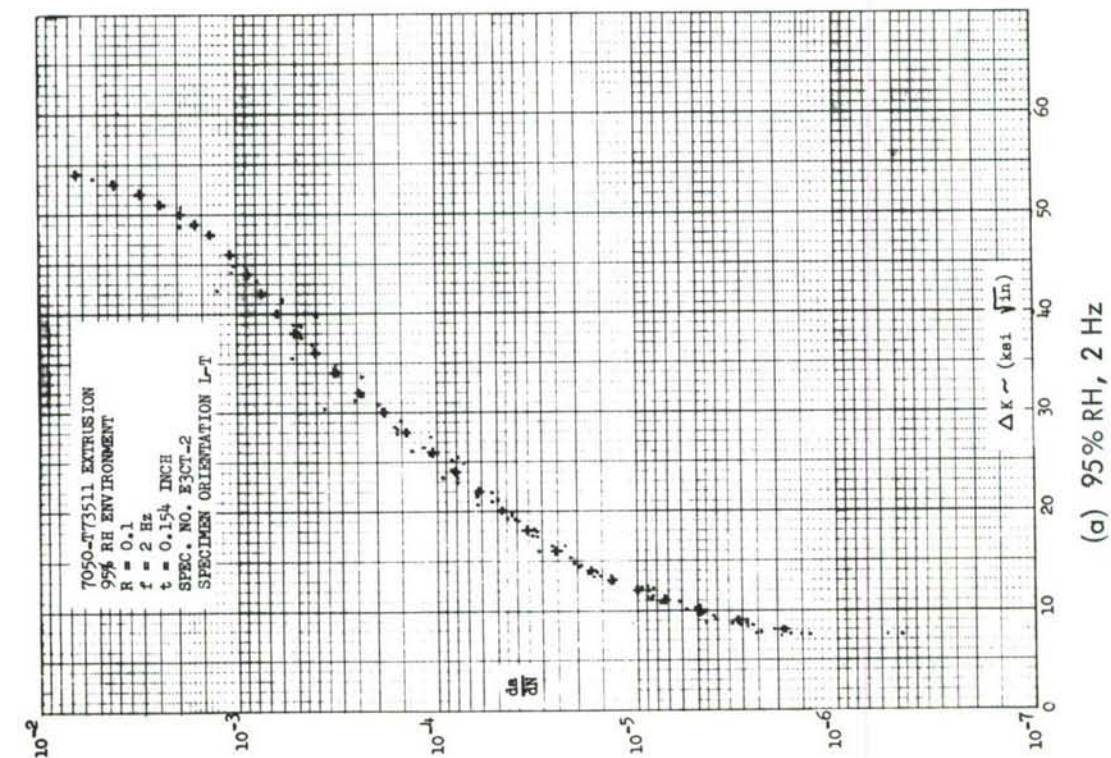


FIGURE 121 CRACK GROWTH OF 7050-T73511 ALUMINUM EXTRUSION



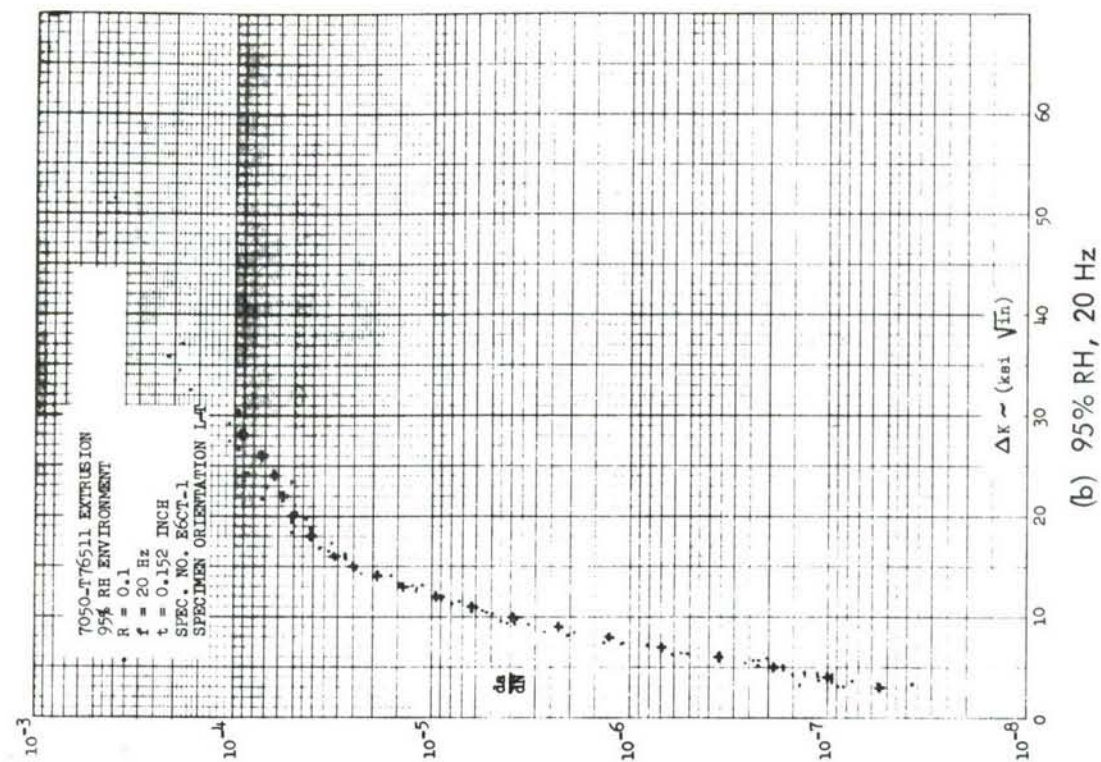
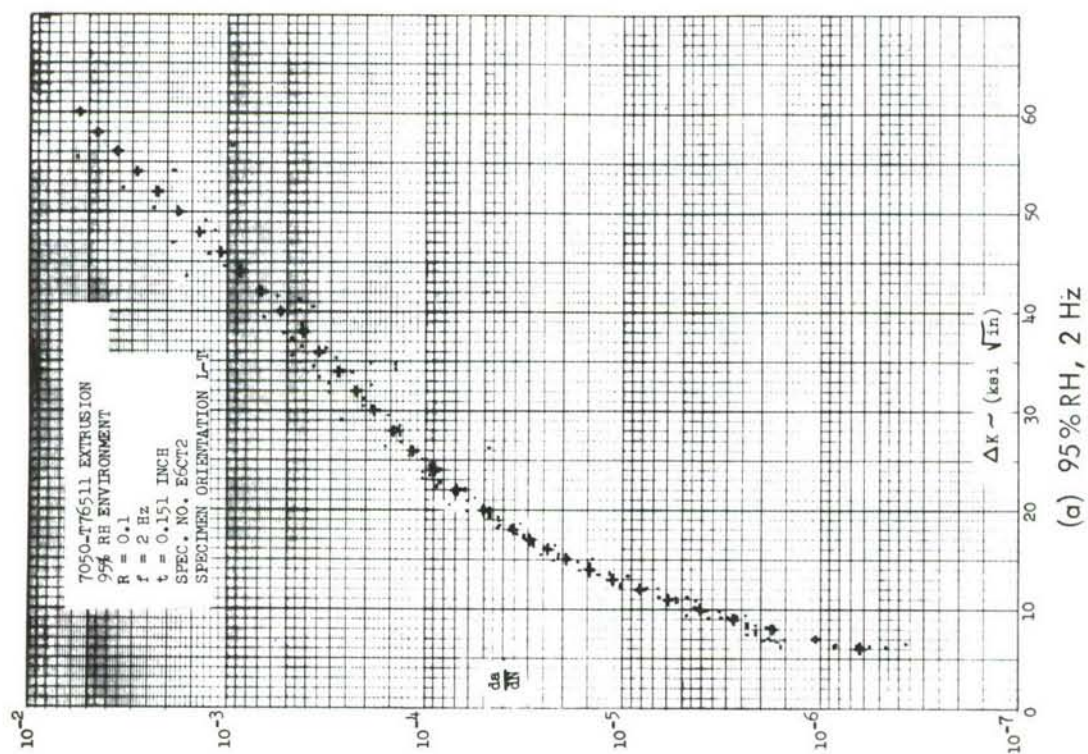


FIGURE 122 CRACK GROWTH OF 7050-T76511 ALUMINUM EXTRUSION



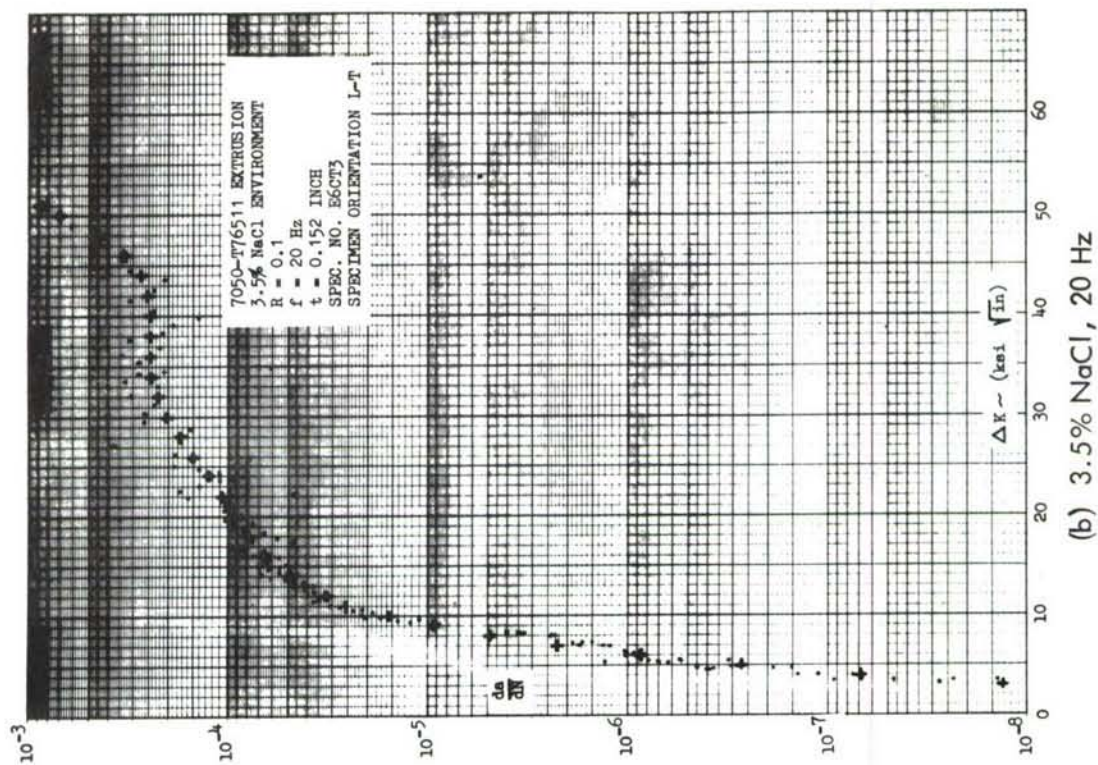
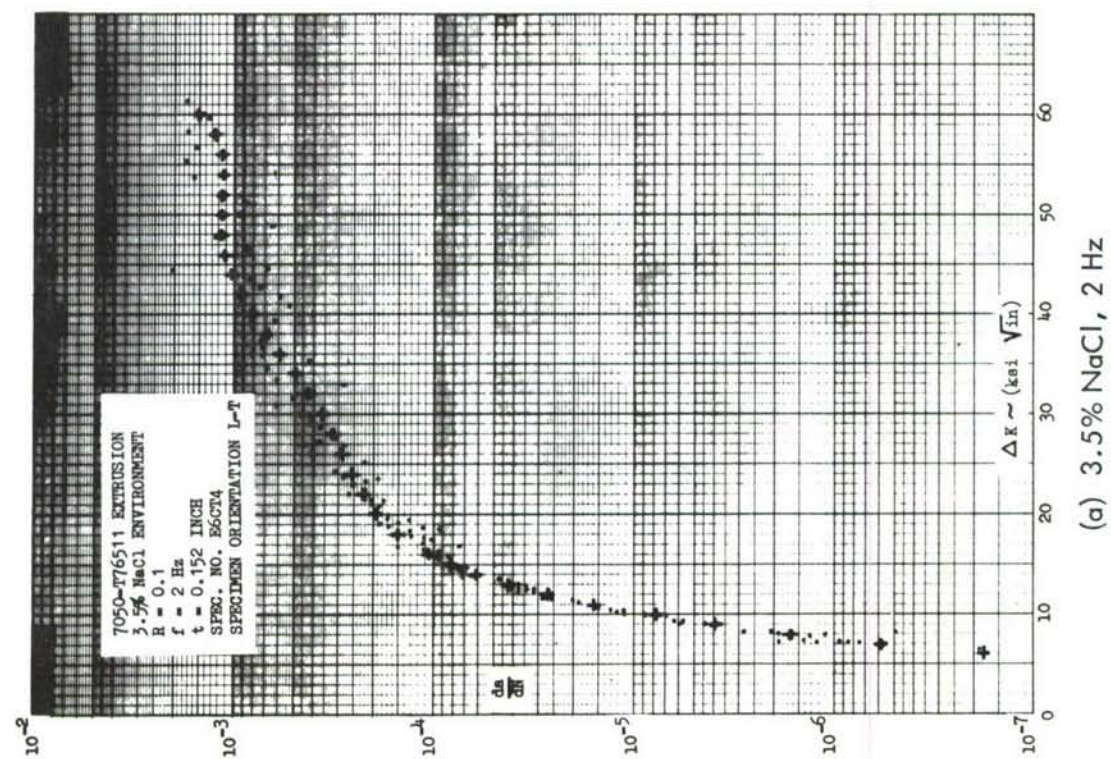


FIGURE 123 CRACK GROWTH OF 7050-T76511 ALUMINUM EXTRUSION

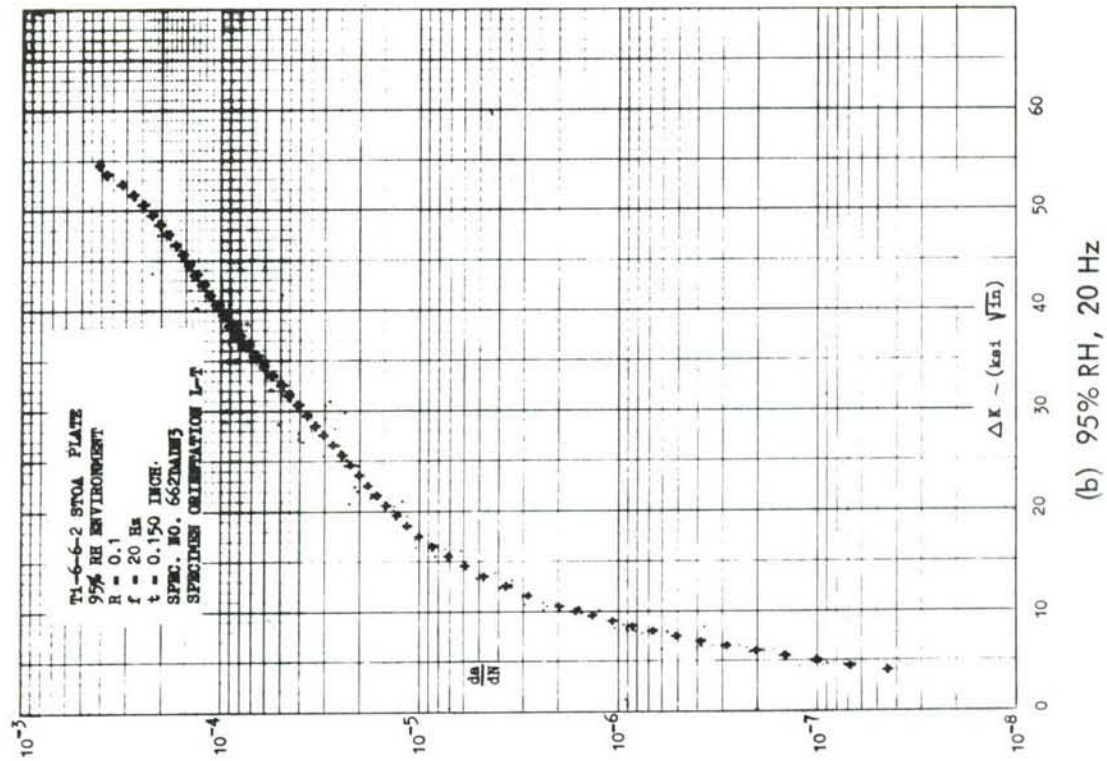
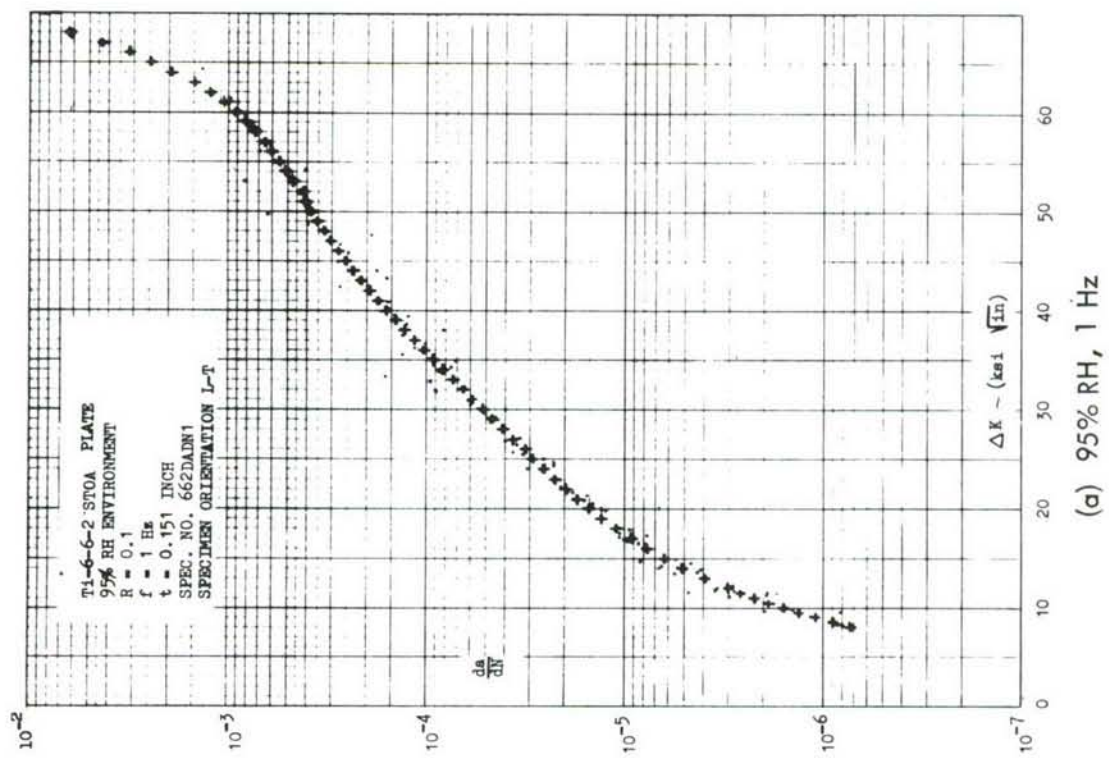


FIGURE 124 CRACK GROWTH OF TI 6-6-2 STOA PLATE



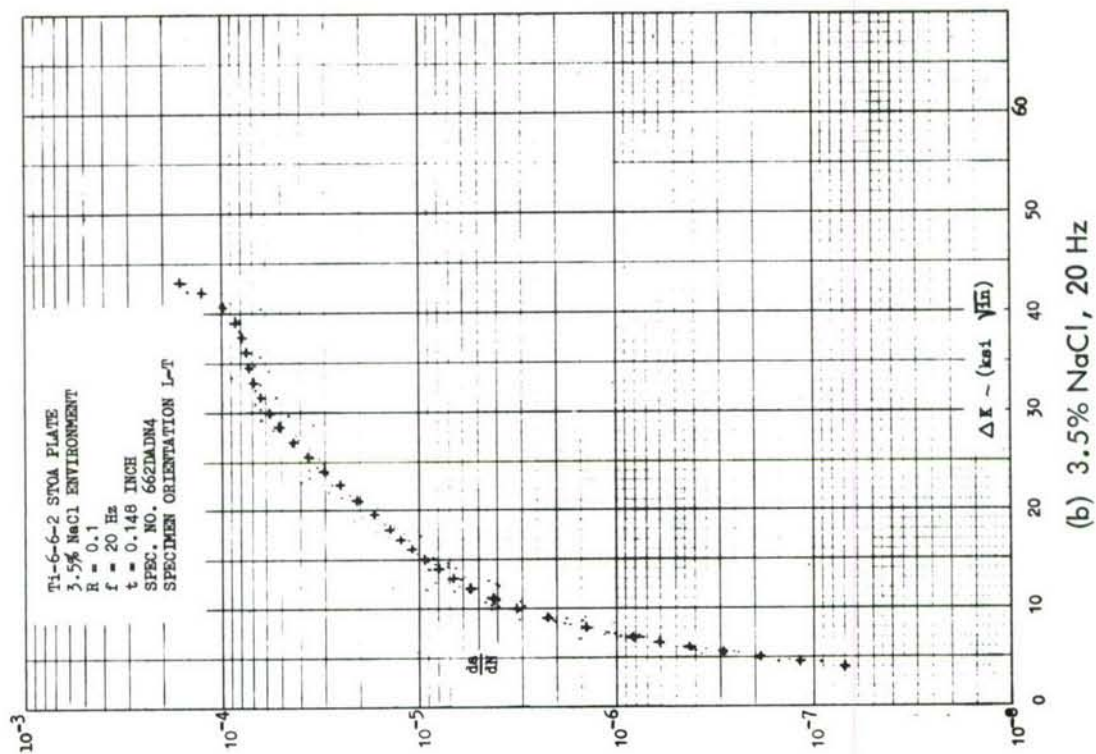
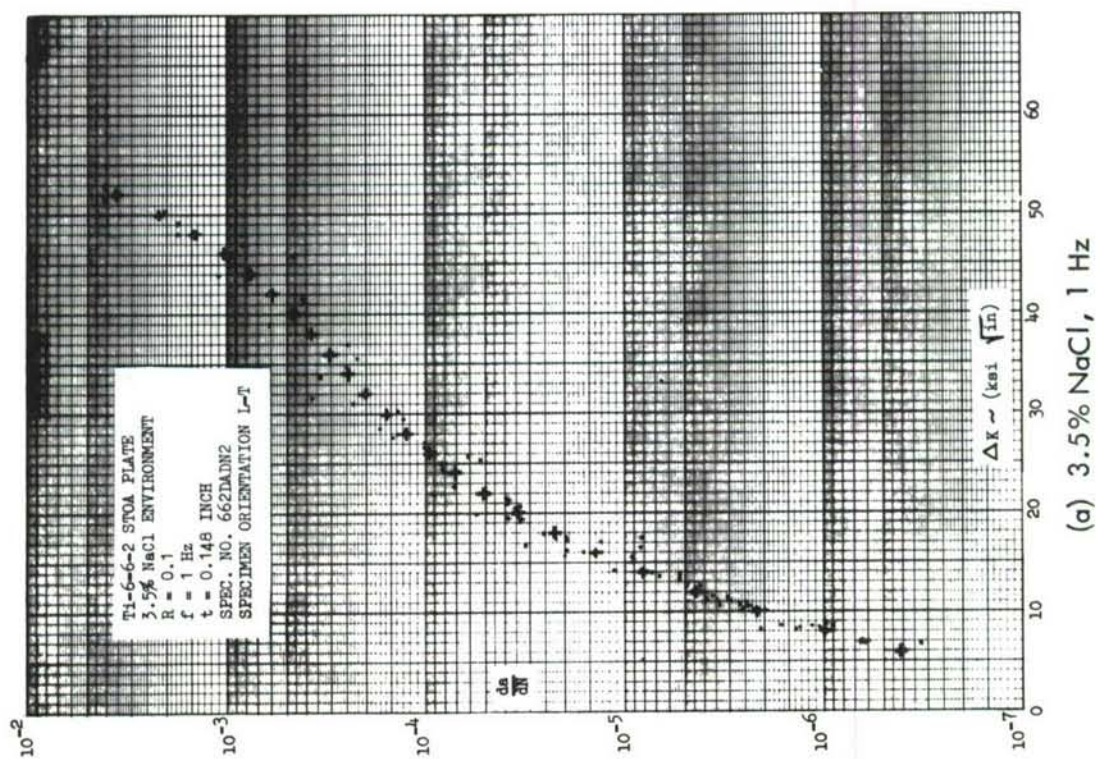


FIGURE 125 CRACK GROWTH OF TI 6-6-2 STOA PLATE



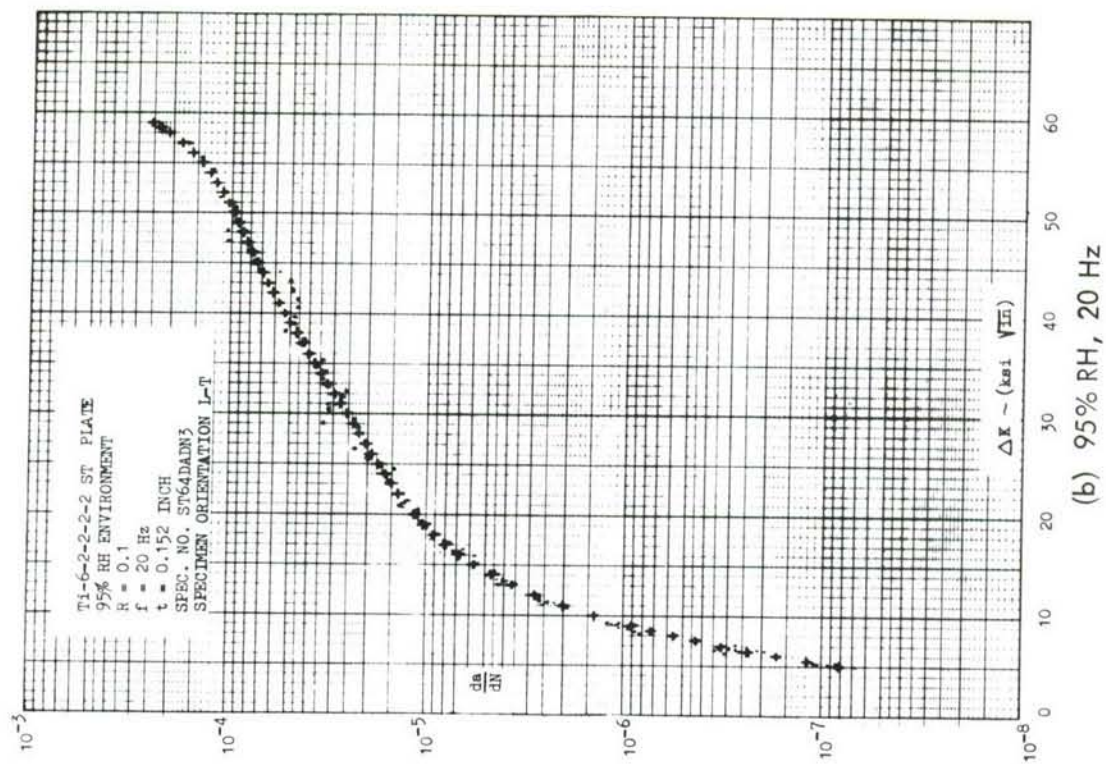
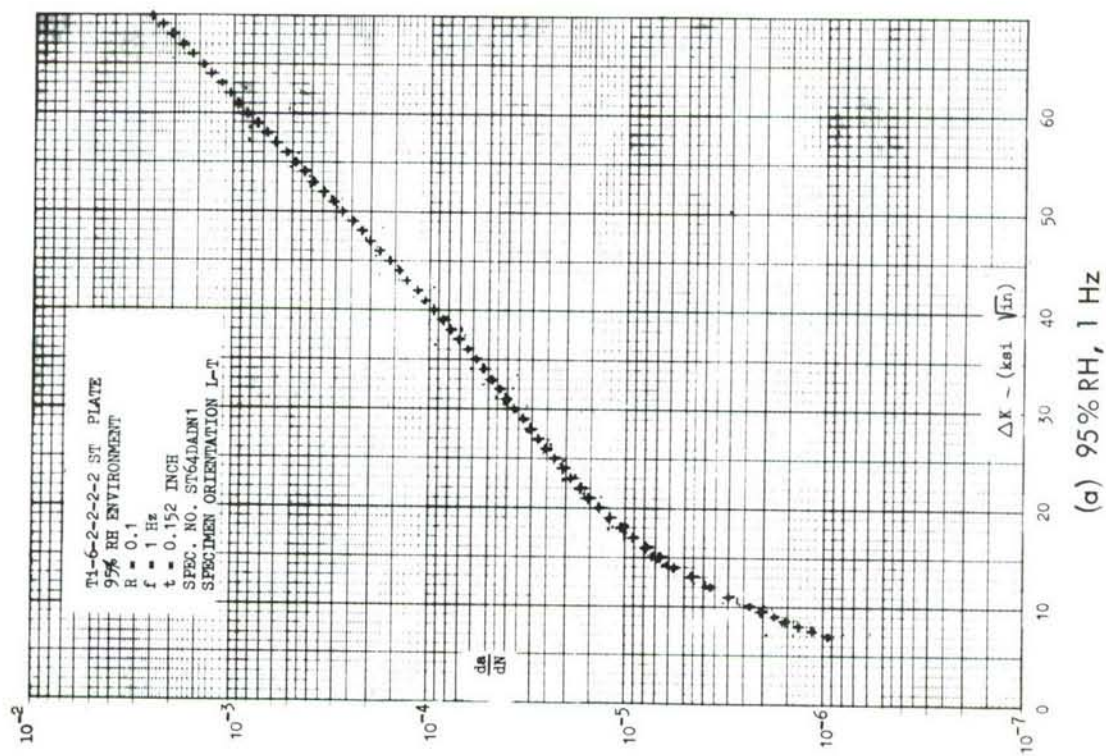


FIGURE 126 CRACK GROWTH OF TI 6-2-2-2-2 ST PLATE

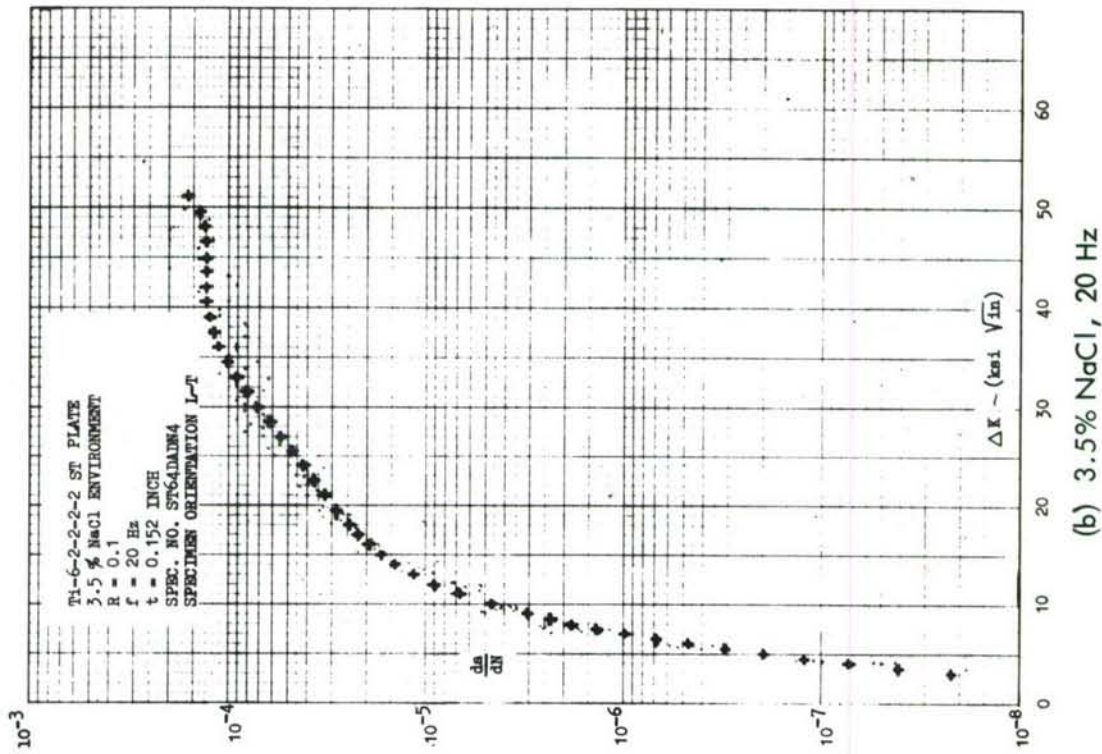
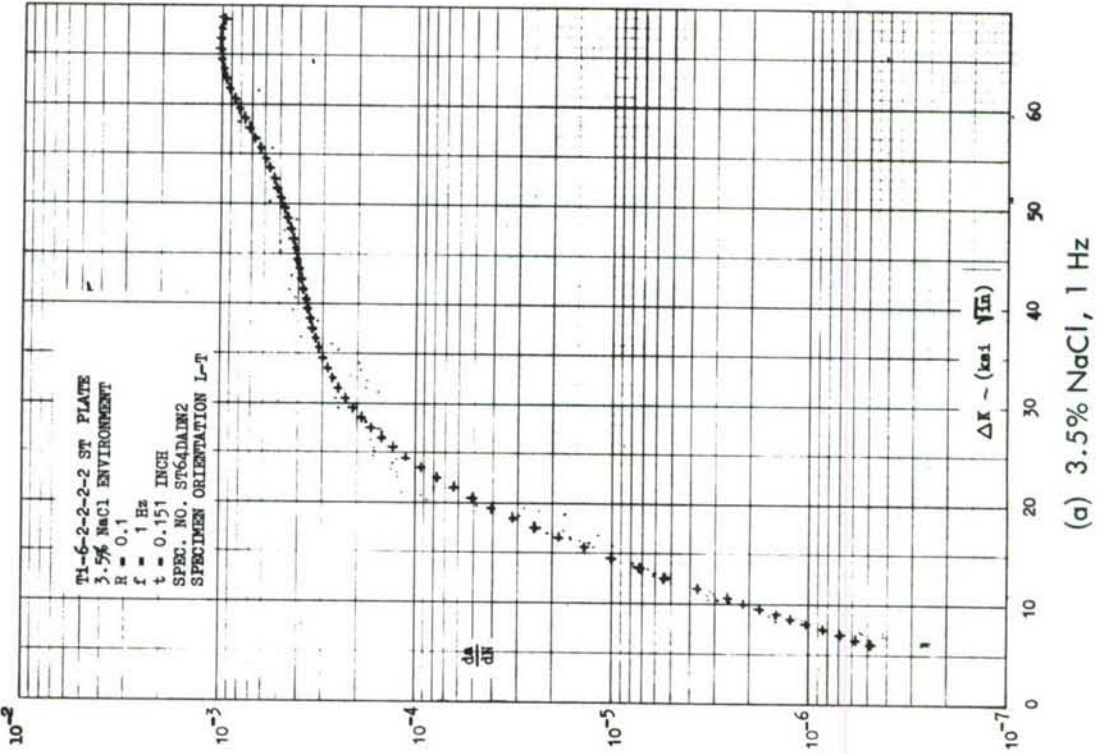


FIGURE 127 CRACK GROWTH OF TI 6-2-2-2-2 ST PLATE



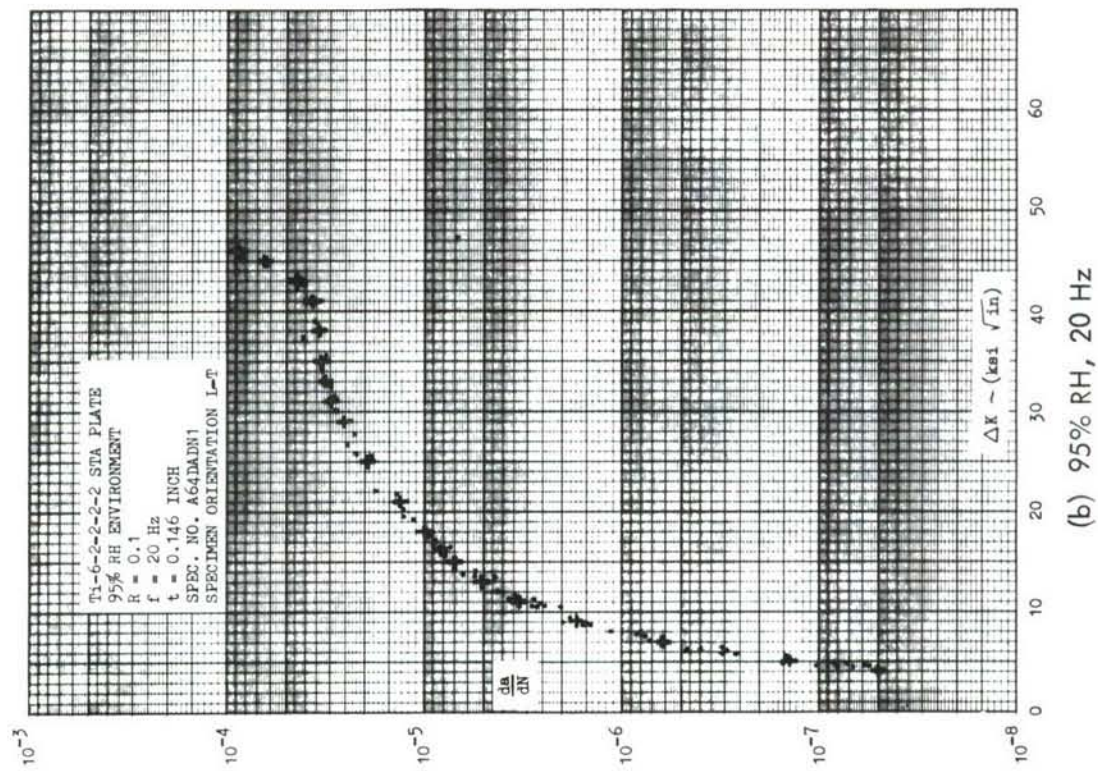
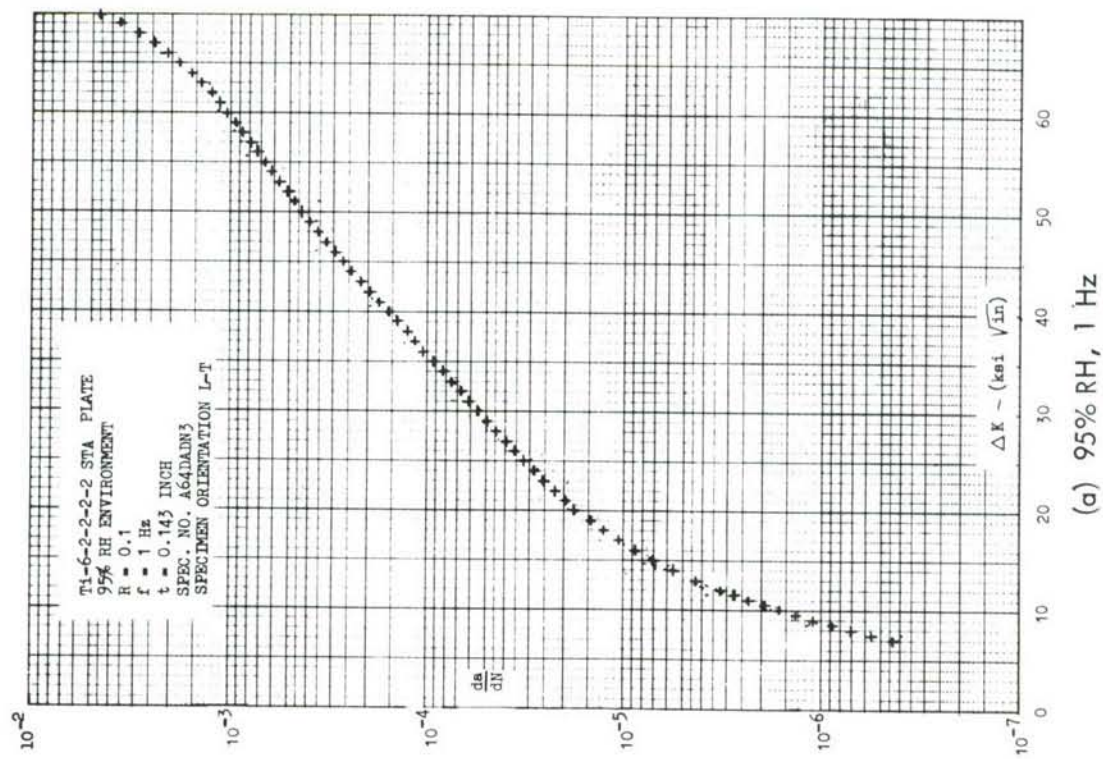


FIGURE 128 CRACK GROWTH OF TI 6-2-2-2-2 STA PLATE

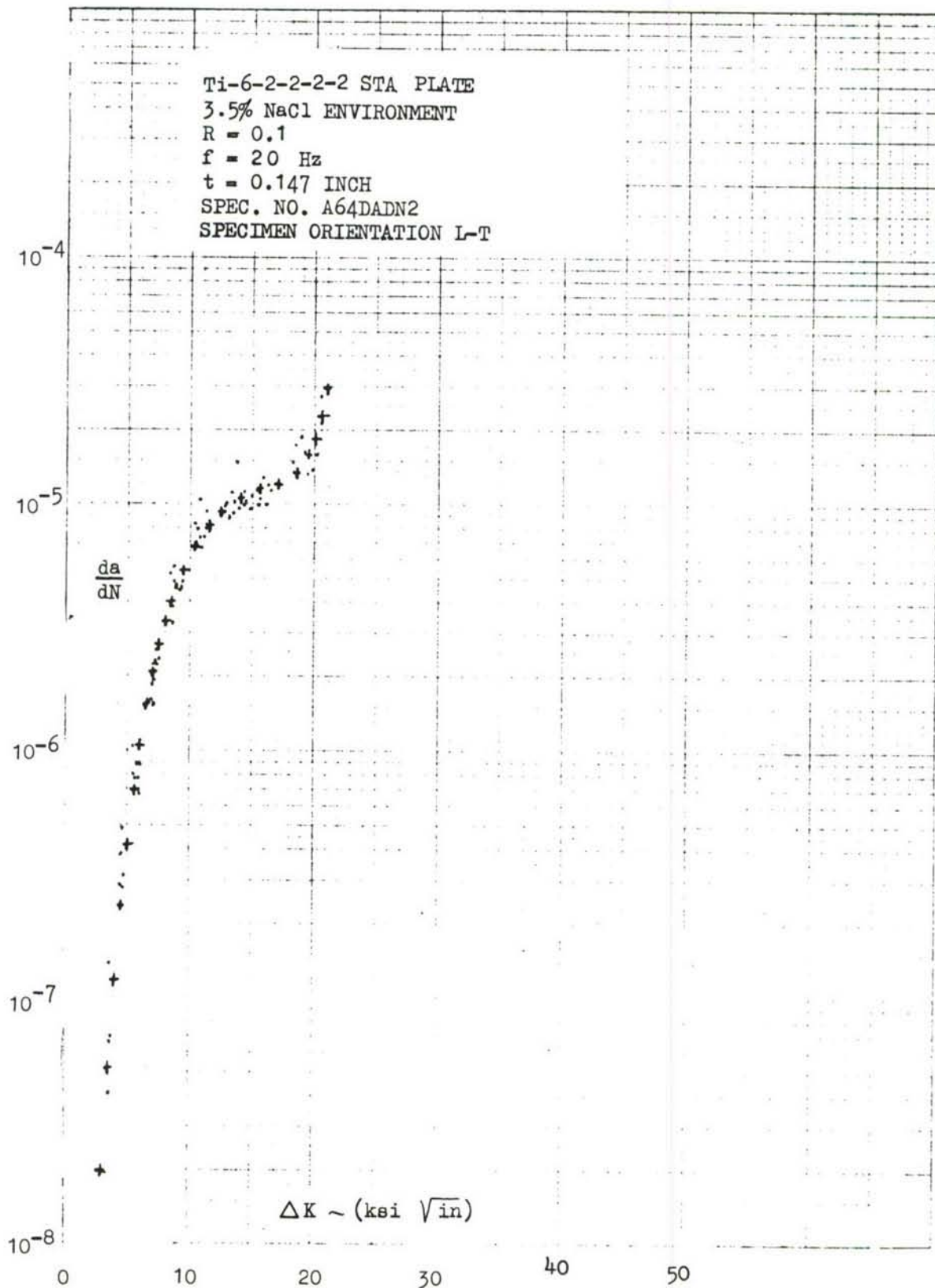


FIGURE 129 CRACK GROWTH OF T1 6-2-2-2-2 STA PLATE -  
 3.5% NaCl, 20 HZ.



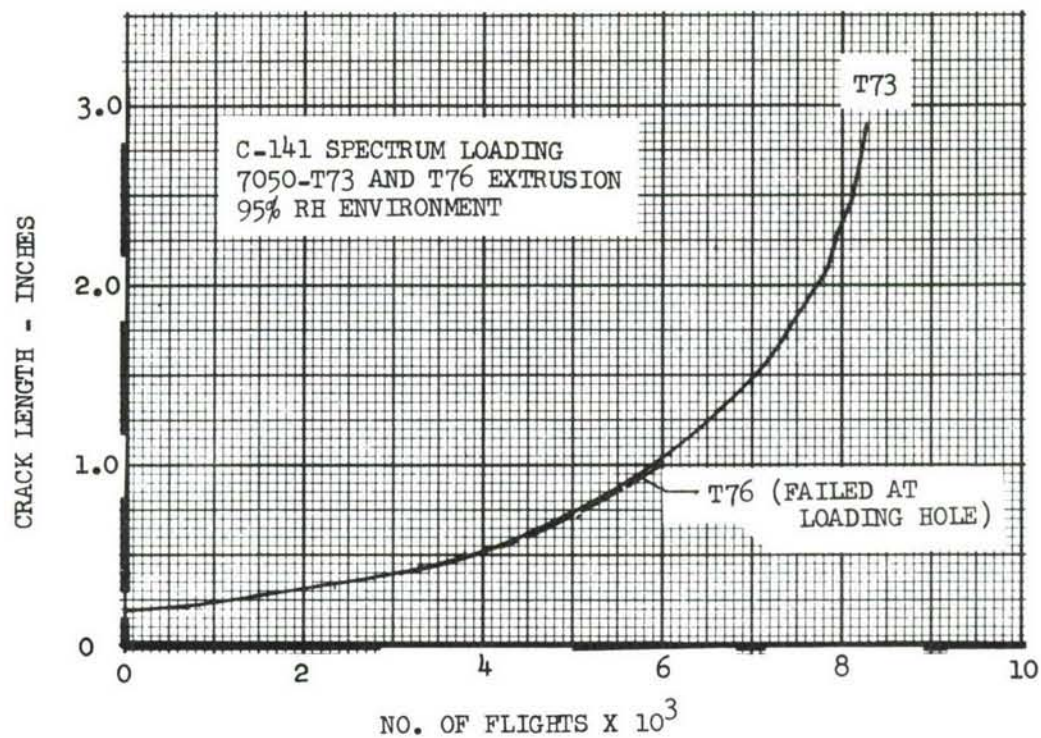


FIGURE 130 SPECTRUM CRACK GROWTH - 7050-T73 & T76  
EXT. - 95% RH

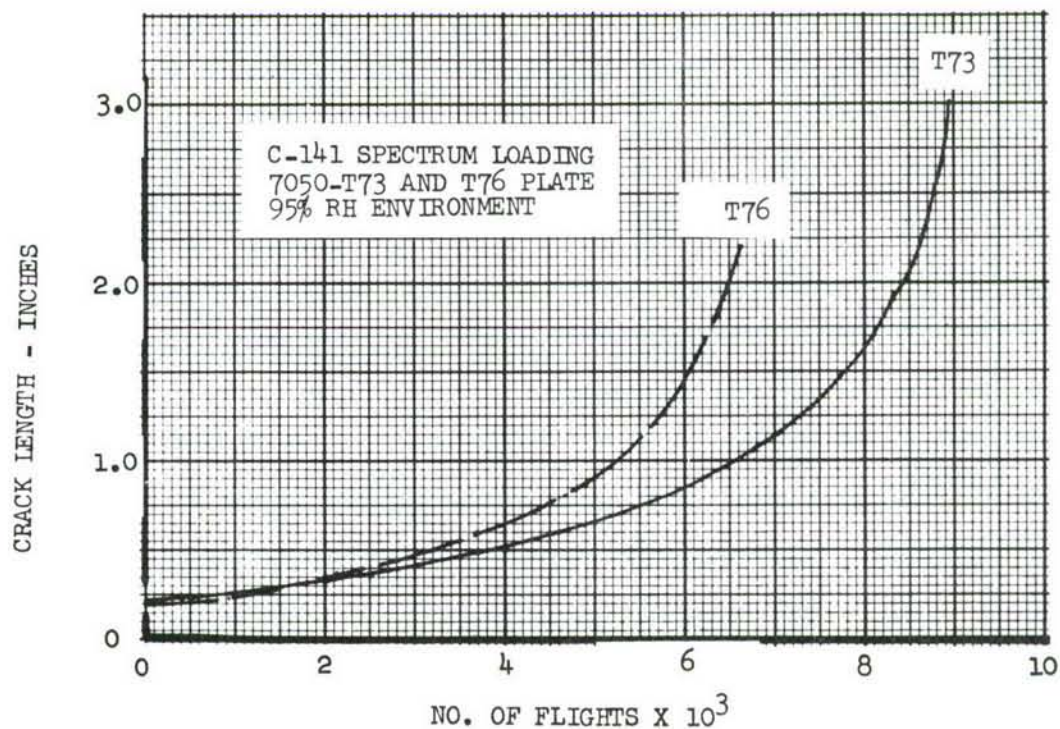


FIGURE 131 SPECTRUM CRACK GROWTH - 7050-T73 & T76  
PLATE - 95% RH

## STATIC COMPONENT TESTS

### PURPOSE

The overall purpose of the static component tests was to determine feasibility of structural configurations/concepts. The specific purpose of each test is given in Table XXXVI.

### TEST DESCRIPTIONS AND REQUIREMENTS

The descriptions and requirements of the static component tests are given in Table XXXVI and Figures 132 through 135.

### TEST RESULTS

Results of the static component tests are summarized in Table XXXVII. Figures 136 through 152 show photographs of test specimens, test set-ups and specimen failures.

TABLE XXXVI

## STATIC COMPONENT TESTS

TYPE TEST	SKETCH CONFIG. (REF)	TEST SPECIMEN NO.	FASTENER/ JOINT CONCEPT	DATA REQUIRED	INSTRUMENTATION REQUIRED	PURPOSE OF TEST
RIB CAP, SHEAR	FIG. 132	ADP1006	NON- PENETRATING CLIP	1. FAILING LOAD 2. LOAD DEFLECTION CHARACTERISTICS	NONE	DETERMINE SHEAR TRANSFER CAPA- BILITY OF A NON- PENETRATING, RIB TO COVER ATTACHMENT CLIP
RIB CAP, SHEAR	FIG. 133	ADP1003 -103	WELDBOND	1. FAILING LOAD 2. LOAD DEFLECTION CHARACTERISTICS	STRAIN GAGE - 1 REQ'D.	DETERMINE SHEAR TRANSFER CAPA- BILITY OF AN 'A' SECTION STRINGER WELDBONDED TO COVER
RIB CAP, SHEAR	FIG. 134	ADP1003 -101	WELDBOND	1. FAILING LOAD 2. LOAD DEFLECTION CHARACTERISTICS	STRAIN GAGE - 1 REQ'D.	DETERMINE SHEAR TRANSFER CAPA- BILITY OF A "TOP HAT" SECTION STRINGER WELD- BONDED TO COVER
CHORDWISE SPLICE TENSION	FIG. 135	ADP1005	CLAMPED	1. FAILING LOAD 2. LOAD DEFLECTION CHARACTERISTICS	NONE	DETERMINE TENSION AND DEFLECTION CHARACTERISTICS OF A CLAMPED CHORDWISE JOINT

NOTES: 1. ONE SPECIMEN REQUIRED FOR EACH TEST SHOWN (TOTAL OF 4).

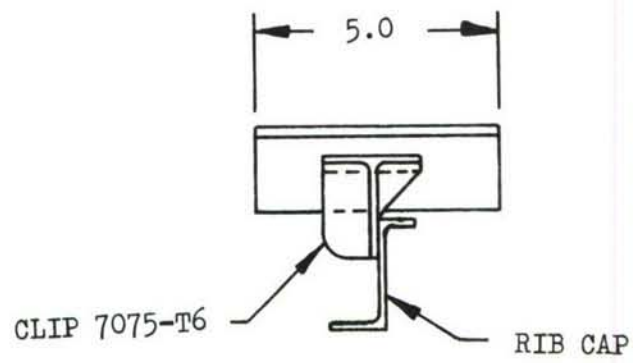
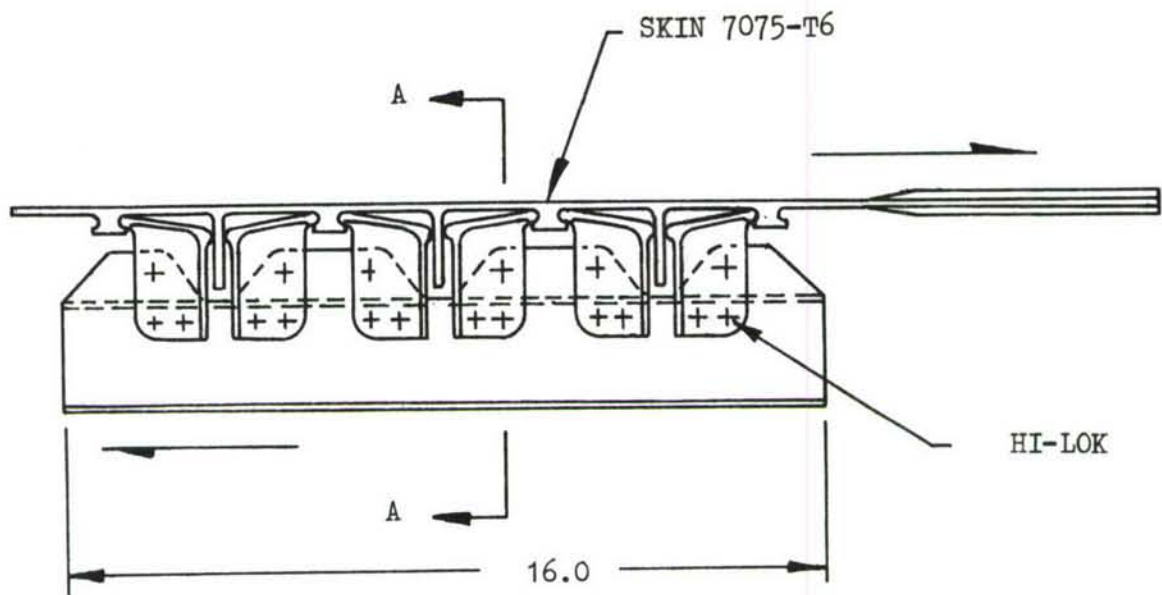
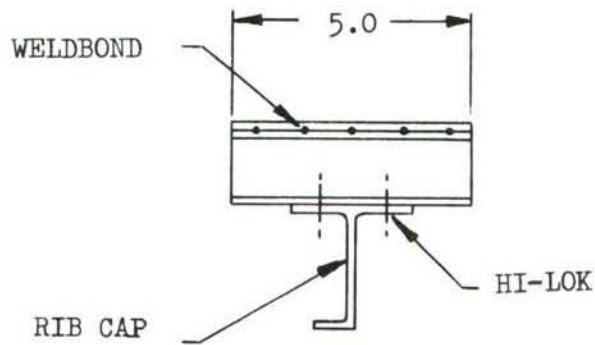
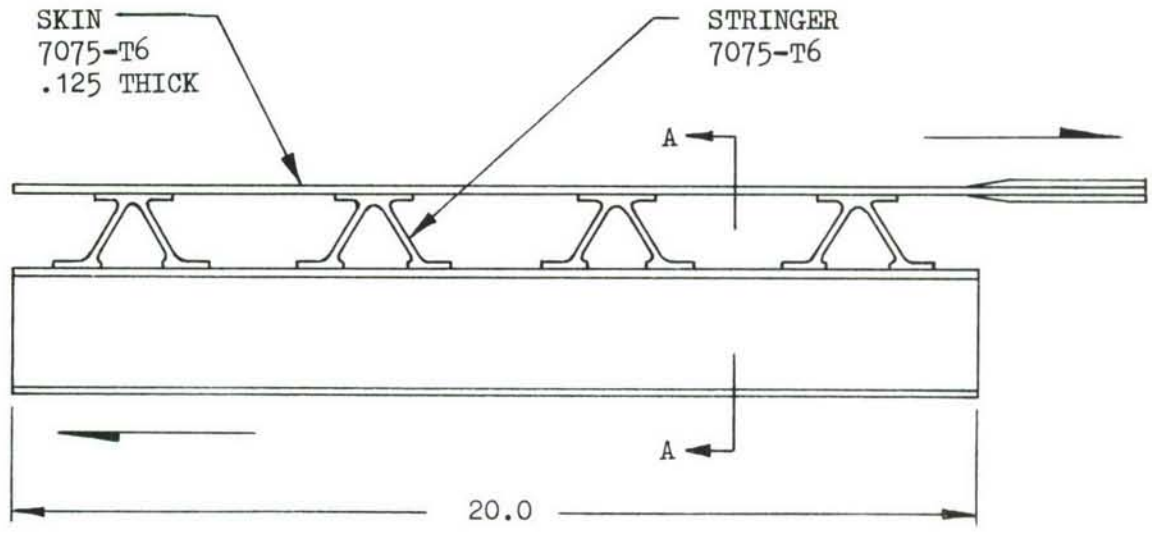


FIGURE 132 RIB CAP SHEAR SPECIMEN  
(N-P CLIPS)





SECTION A-A

FIGURE 133 RIB CAP SHEAR SPECIMEN  
(WELDBOND "A" STRINGER)

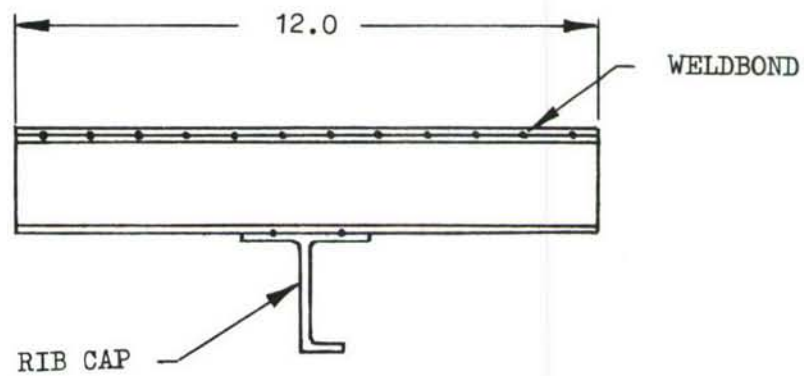
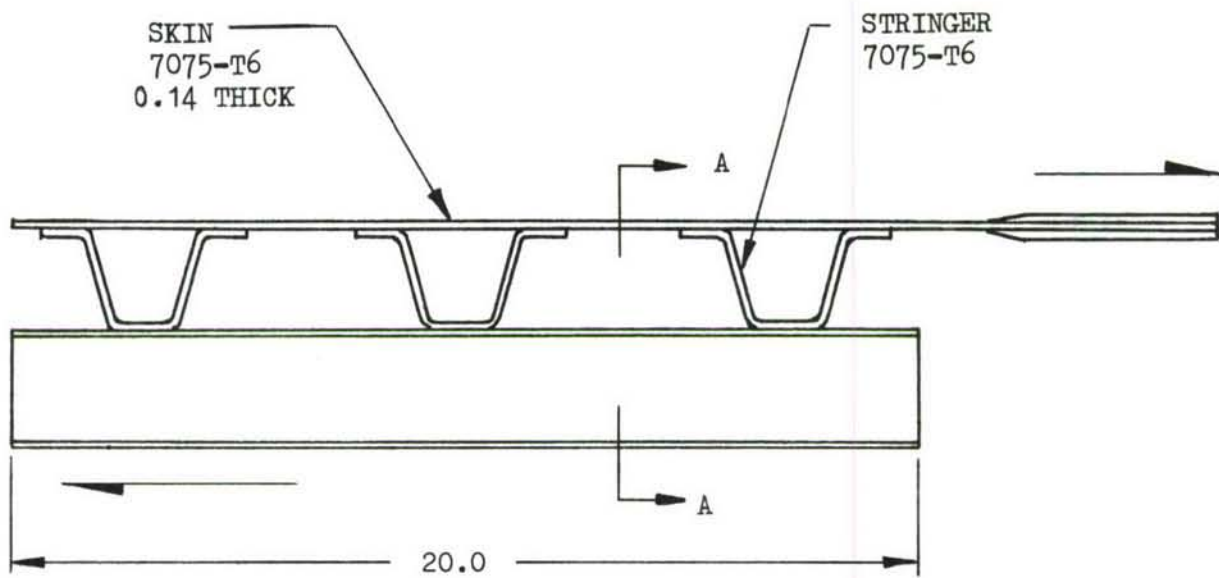
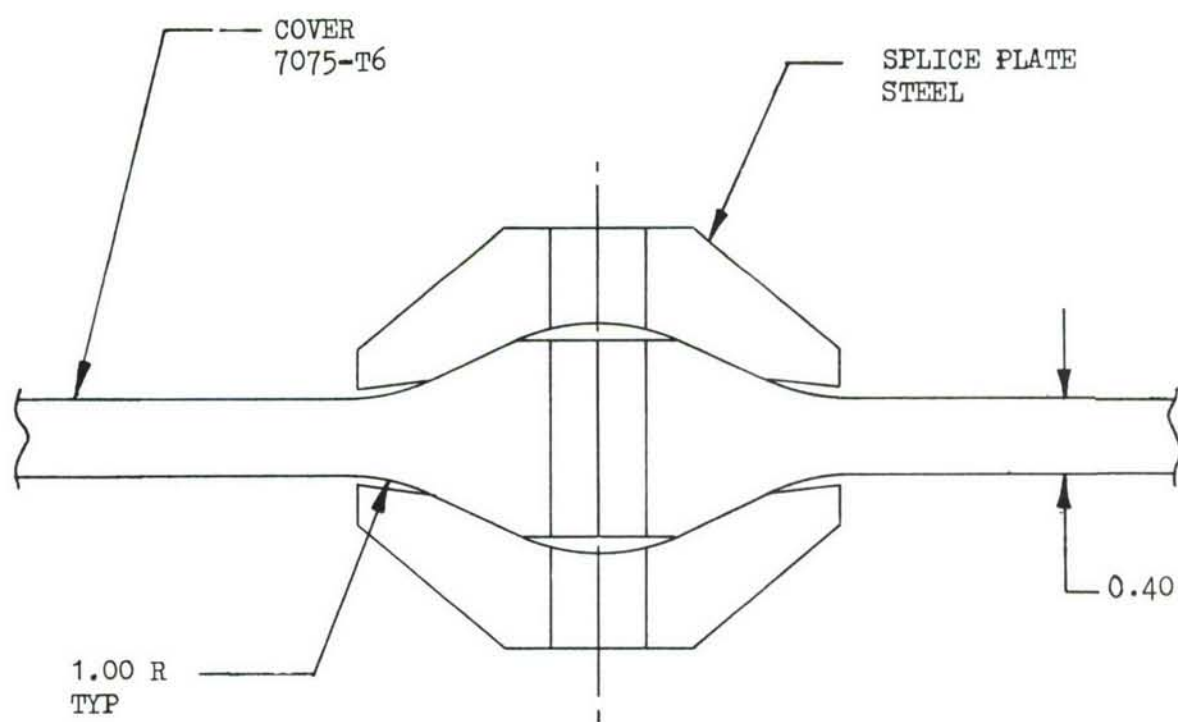
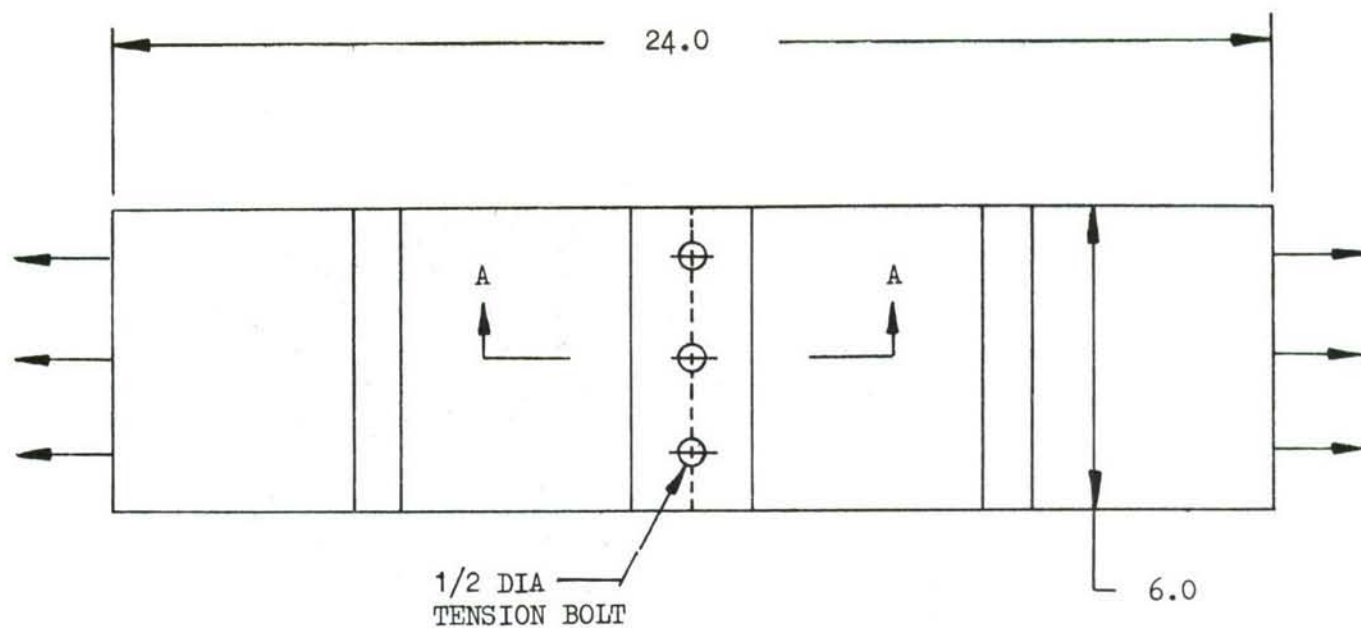


FIGURE 134 RIB CAP SHEAR SPECIMEN  
(WELDBOND "HAT" STRINGER)



SECTION A-A

FIGURE 135 CLAMPED WS 77 CHORDWISE JOINT SPECIMEN

TABLE XXXVII  
STATIC COMPONENT TEST RESULTS

TEST TITLE	TEST SPECIMEN NO.	TEST SET-UP (REF. FIG.)	FAILING LOAD	FAILURE MODE	REMARKS
Rib Cap to Surface Shear Transfer - Nonpenetrating Clip	ADP 1006	Fig. 136	17,500#	Bearing Failure of Rib Cap to Jig Support	Load/Deflection Relationships and Demonstrated Ultimate Strength Proved Feasibility of Substantial Rib/Surface Shear Transfer Thru N-P Clips ( 1170 #/in. min.)
Rib Cap to Surface Shear Transfer - "A" Stringer	ADP 1003 -103	Fig. 139 & 140	23,000#	Tension Failure of Hi-Lok Fasteners Attaching Stringer Flanges to Rib Cap (See Fig. 141)	Load/Deflection Relationship and Demonstrated Ultimate Strength Proved Feasibility of Substantial Rib/Surface Shear Transfer Without Use of Rib/Surface Clips ( 1120 #/in. min.)
Rib Cap to Surface Shear Transfer - "Hat" Stringer	ADP 1003 -101	Fig. 142	6,800#	"Hat" Stringers Pulled Away From Rib Cap After Weldbond Failed (See Fig. 143)	Tension Peel Strength of Weldbond Not Competitive with Good Mechanical Fastener. Weldbonding of Stringers to Rib Cap More Suitable For Low Load Transfer Applications
Rib Cap to Surface Shear Transfer - "Hat" Stringer	ADP 1003 -101 Rev. A (Fig. 144)	Fig. 144	17,400#	Weldbond Between "Hat" and Skin Failed in Combined Shear and Tension Peel (See Fig. 145)	Demonstrated Shear Transfer Capability Approximately 800 #/in



TABLE XXXVII (Concluded)  
STATIC COMPONENT TEST RESULTS

TEST TITLE	TEST SPEC. NO.	TEST SET-UP (REF. FIG.)	FAILING LOAD	FAILURE MODE	REMARKS
Chordwise Splice Tension - Clamped Joint	ADP 1005	Fig. 146	210,500# (28,000#/in.)	Clamping Bolts Failed in Tension at Threads (See Fig. 147)	Feasibility of Clamped Joint Concept for Major Chordwise Splices was Demonstrated
Clamped Spanwise Splice Fail Safe Shear	ADP 1008	Fig. 148	2,100#	Test Terminated Because of Excessive Shear Deformation of Splice	Separate Keys Used for Fail Safe Shear Transfer Were Not Adequately Retained Resulting in Low Load Transfer Capability. This was Corrected in Subsequent Design.
Clamped Spanwise Splice Fail Safe Tension	ADP 1009	Fig. 150	3,780#	Joint Was Pulled Apart Through Prying Deflection of Clamping Splice Plates	Feasibility of Transmitting Adequate Fail Safe Chordwise Tension Loads (After Bond Failure) Was Demonstrated.

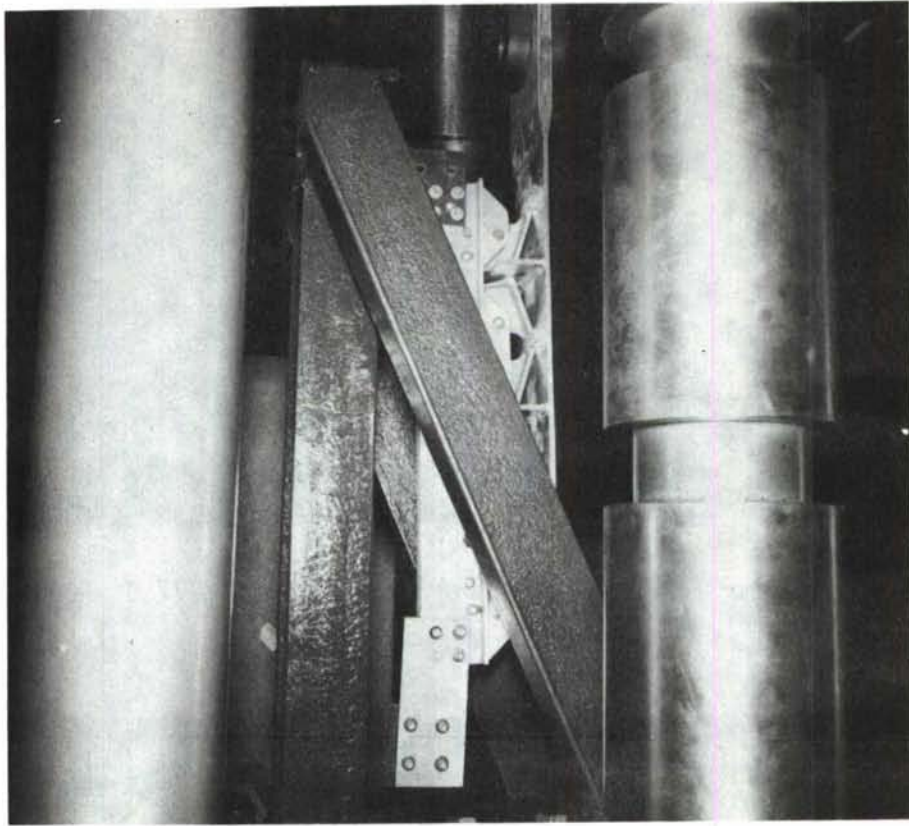


FIGURE 136 TEST ARRANGEMENT, RIB CAP TO COVER SHEAR TEST, (N-P CLIP CONFIGURATION, ADP 1006)

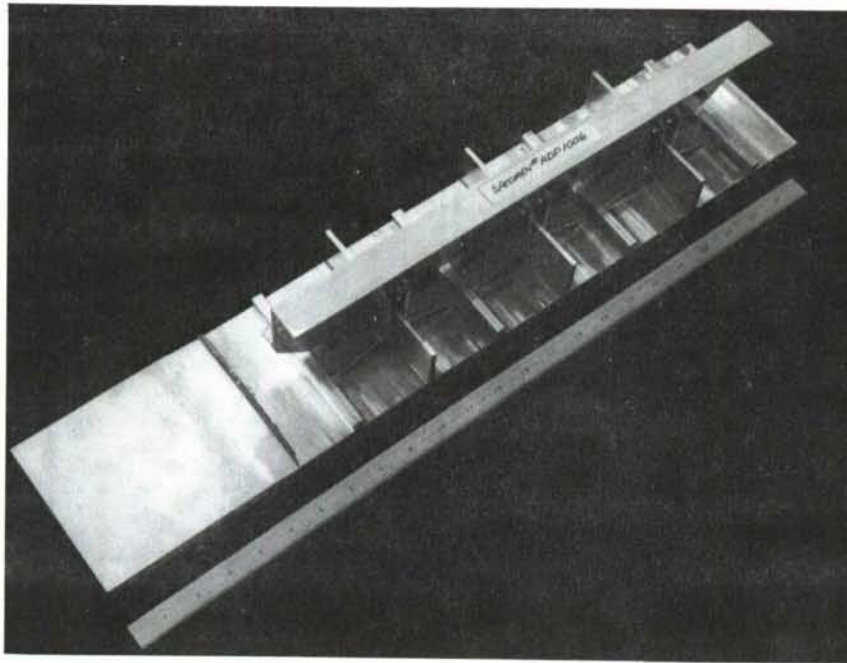


FIGURE 137 NON-PENETRATING CLIP RIB CAP/COVER TEST SPECIMEN



FIGURE 138 CLOSE-UP OF N-P CLIP ATTACHMENT BETWEEN RIB CAP AND COVER

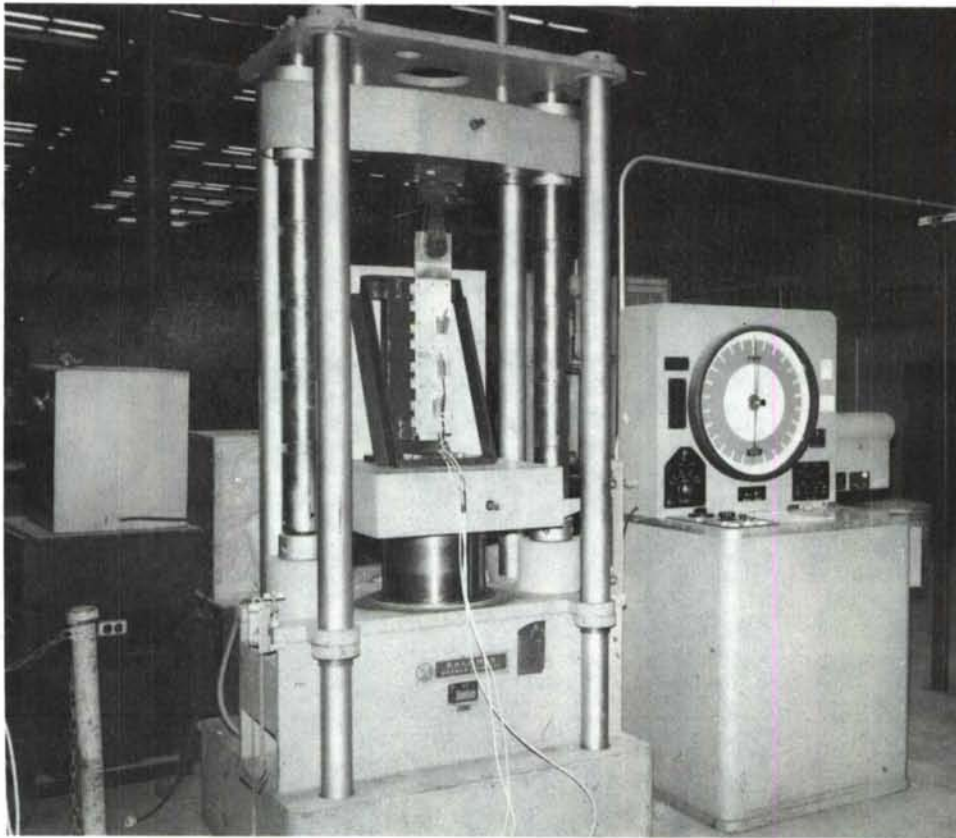
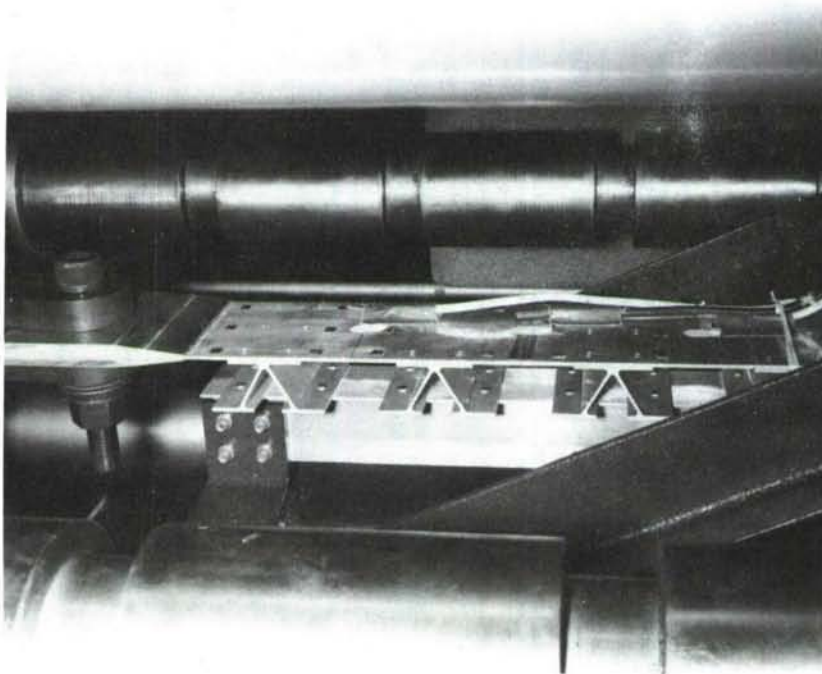
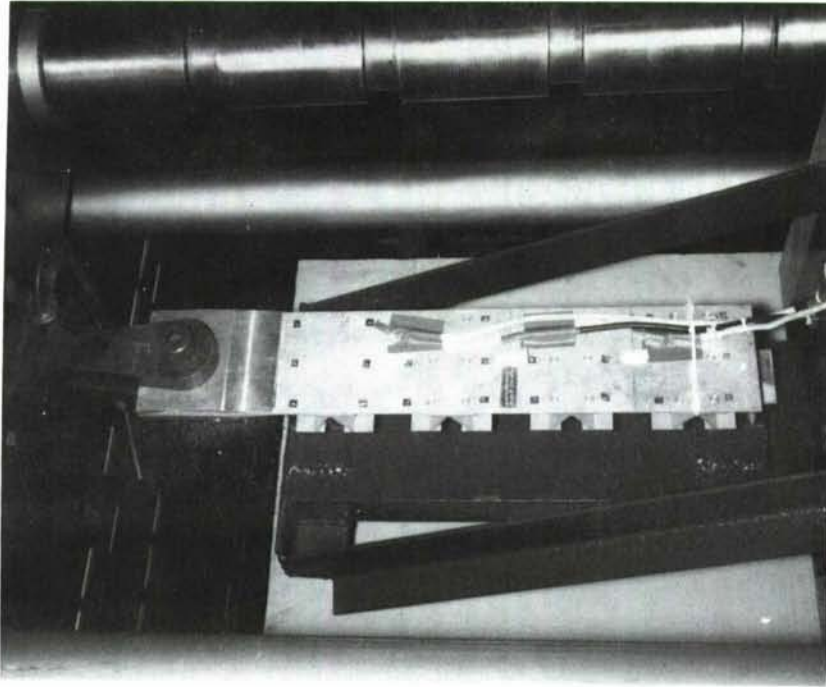


FIGURE 139 TEST ARRANGEMENT, RIB CAP TO COVER SHEAR TEST,  
(WELDBOND "A" STRINGER CONFIGURATION, ADP 1003-103)



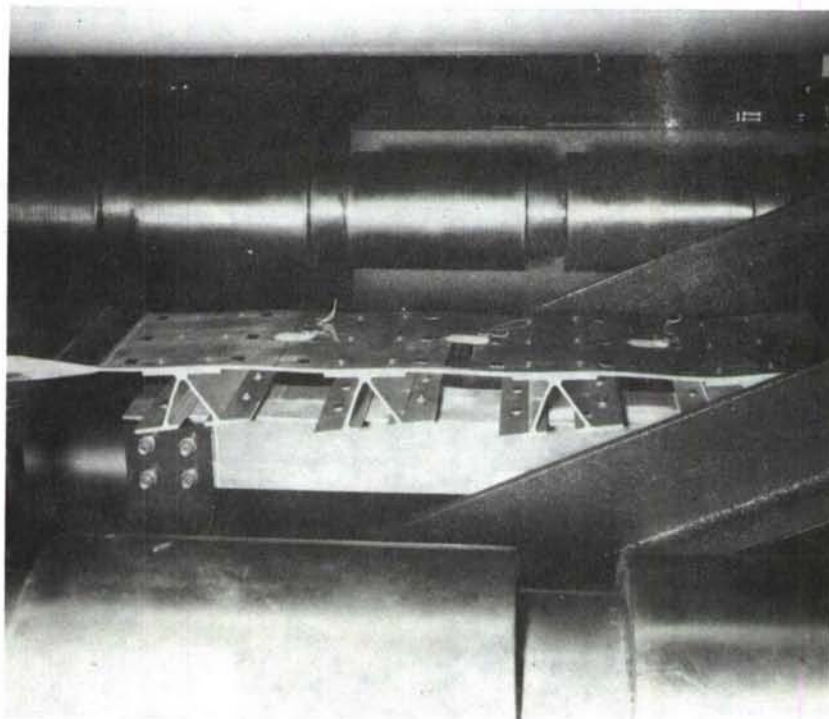


(a) Side View

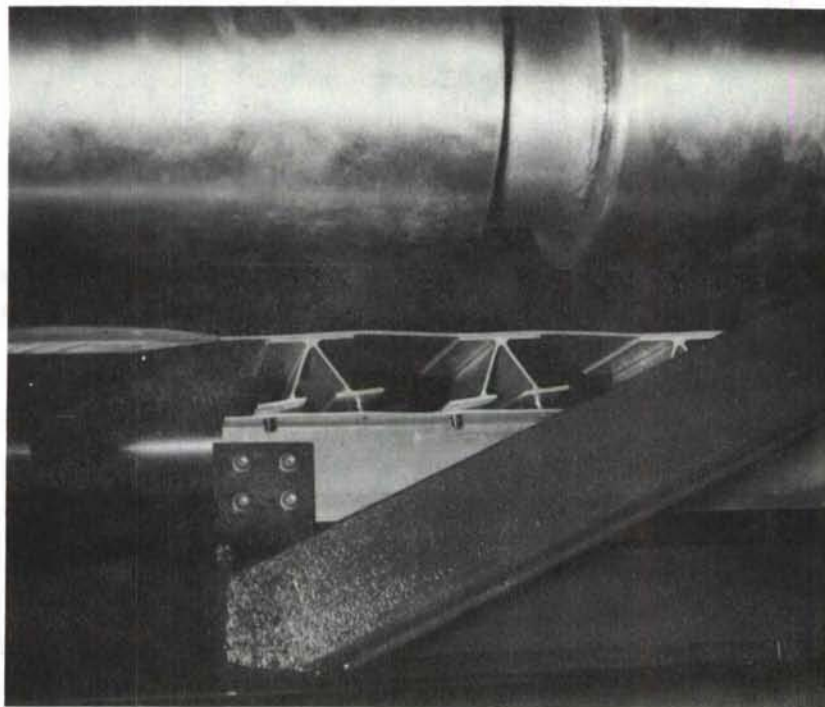


(b) Front View

FIGURE 140 FRONT AND SIDE VIEWS OF "A" STRINGER  
SHEAR TEST SPECIMEN BEFORE LOADING

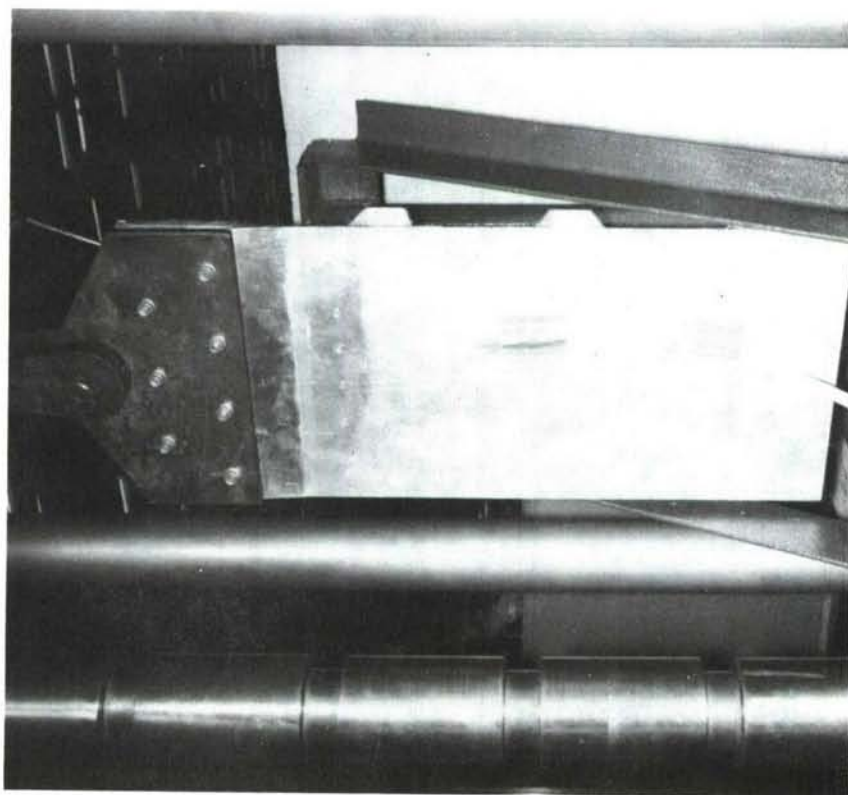


(a) Specimen Under Load

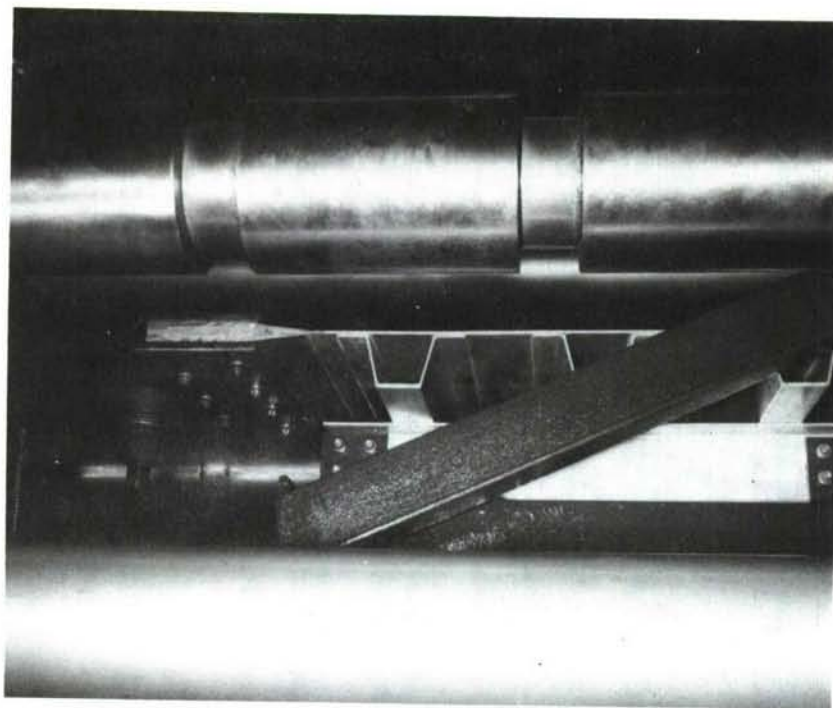


(b) Specimen Failure - Hiloks Attaching Stringer Flange to Rib Cap Failed In Tension

FIGURE 141 "A" STRINGER SHEAR TEST SPECIMEN UNDER LOAD  
AND AFTER FAILURE



(a) Front View



(b) Side View

FIGURE 142 TEST ARRANGEMENT, FRONT AND SIDE VIEWS,  
RIB CAP TO COVER SHEAR TEST (WELDBOND "HAT"  
STRINGER CONFIGURATION, ADP 1003-101)

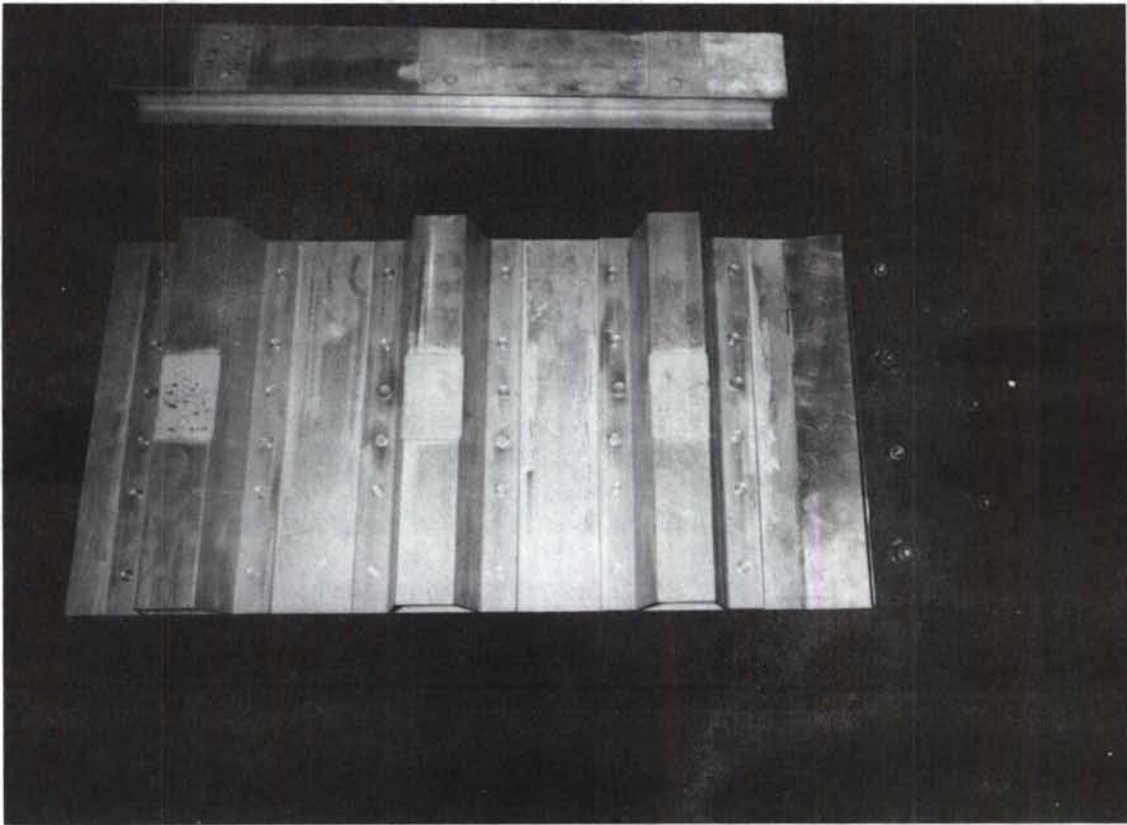


FIGURE 143 WELDBOND "HAT" TEST PANEL AFTER FAILURE (WELDBOND BETWEEN HAT CROWN AND RIB CAP PULLED APART)



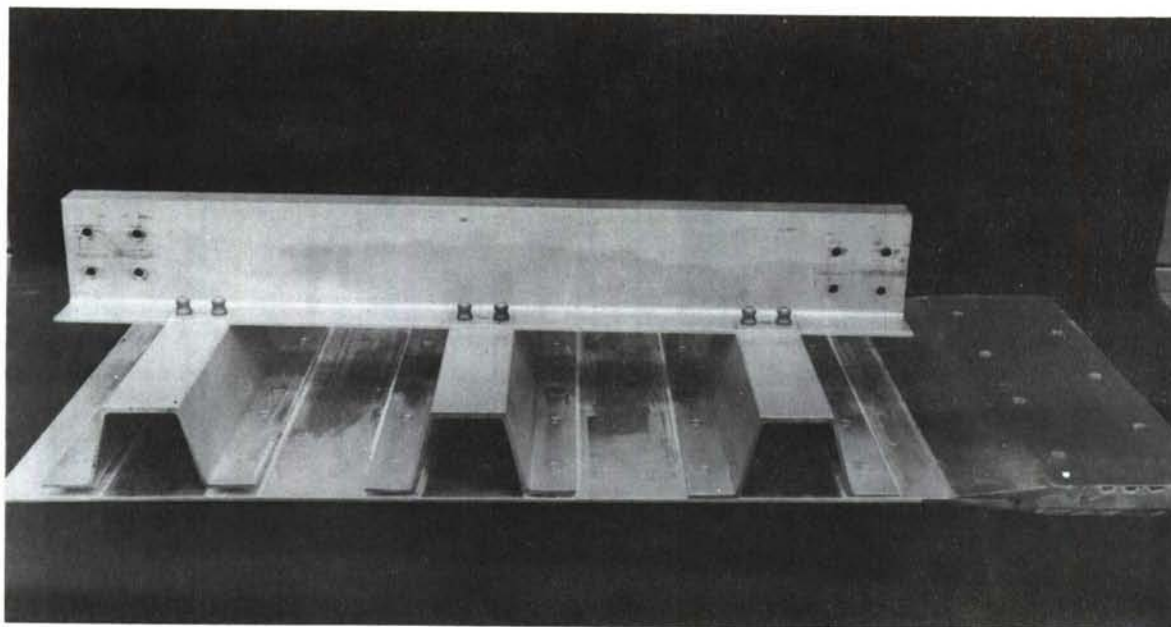


FIGURE 144 WELDBOND "HAT" SPECIMEN MODIFICATION (HILOKS  
USED FOR ATTACHING RIB CAP TO HAT CROWN)

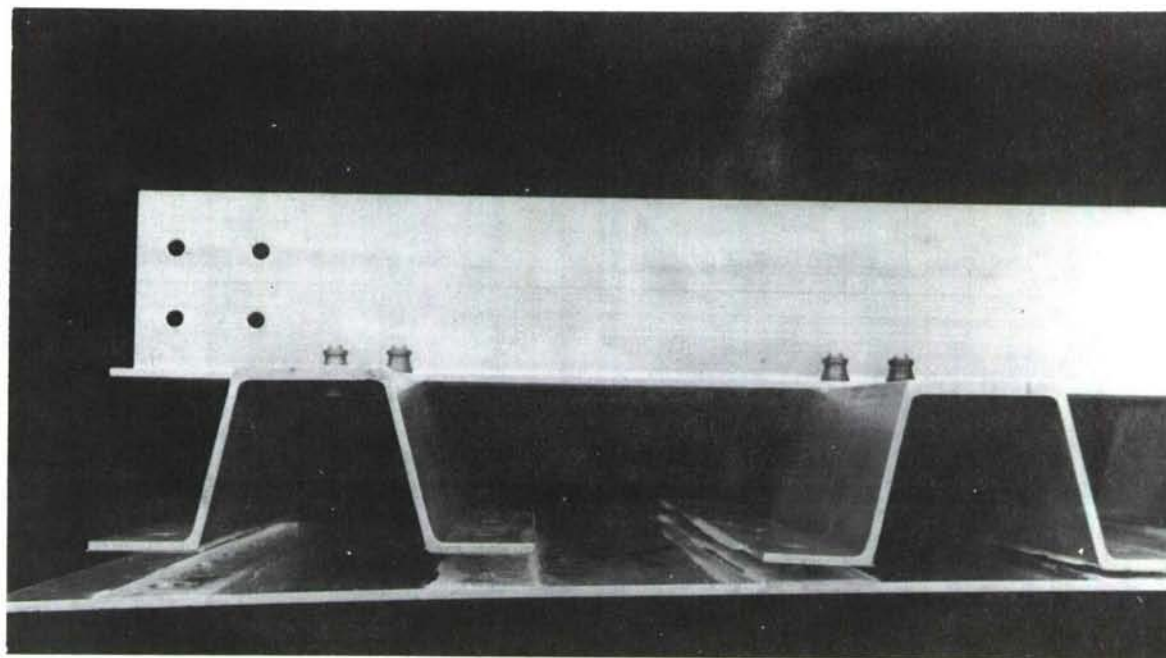


FIGURE 145 FAILURE OF MODIFIED TEST PANEL (WELDBOND  
CONNECTION AT SKIN LINE FAILED)

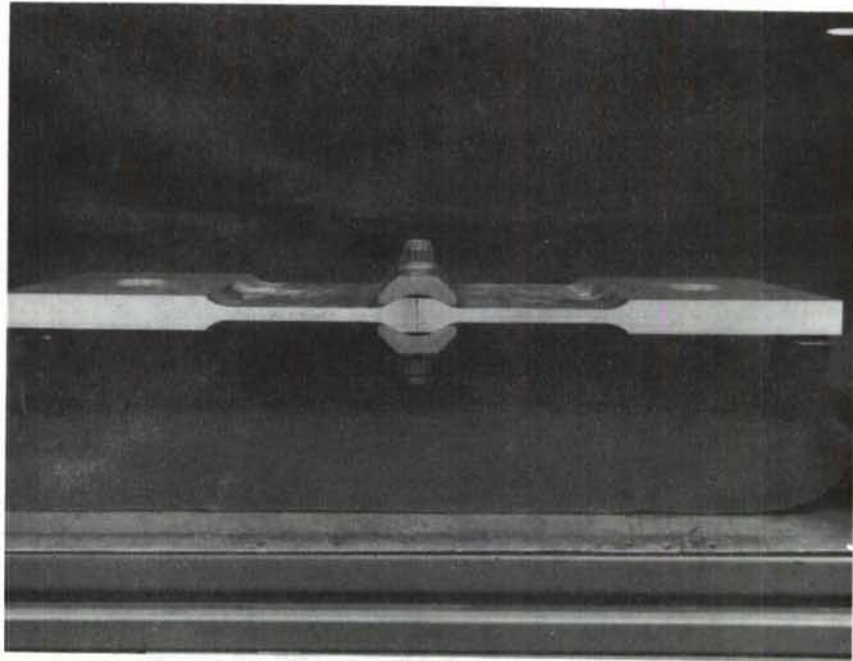


FIGURE 146 CLAMPED CHORDWISE SPLICE TENSION TEST SPECIMEN (ADP 1005)

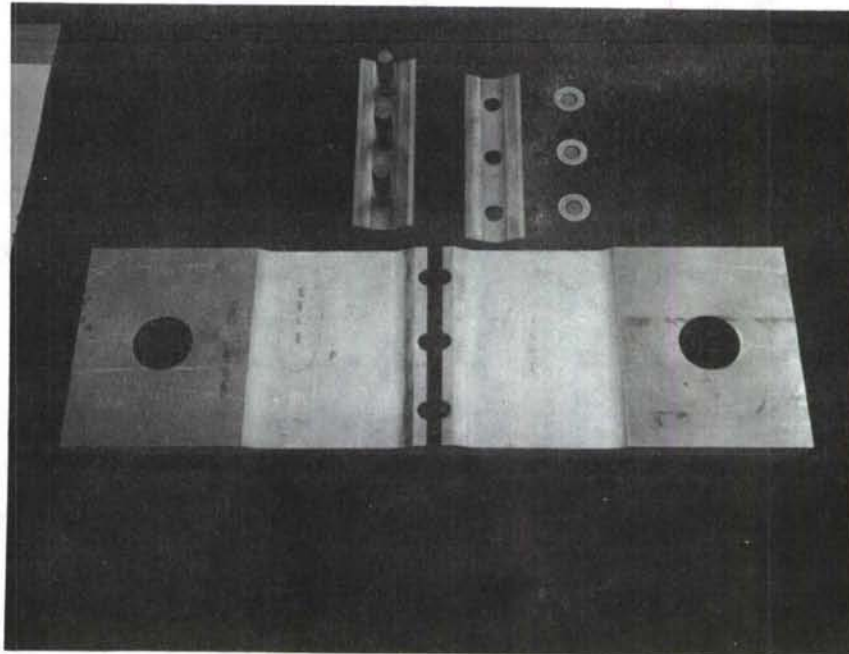


FIGURE 147 CHORDWISE SPLICE SPECIMEN AFTER FAILURE (CLAMPING BOLTS FAILED IN TENSION)

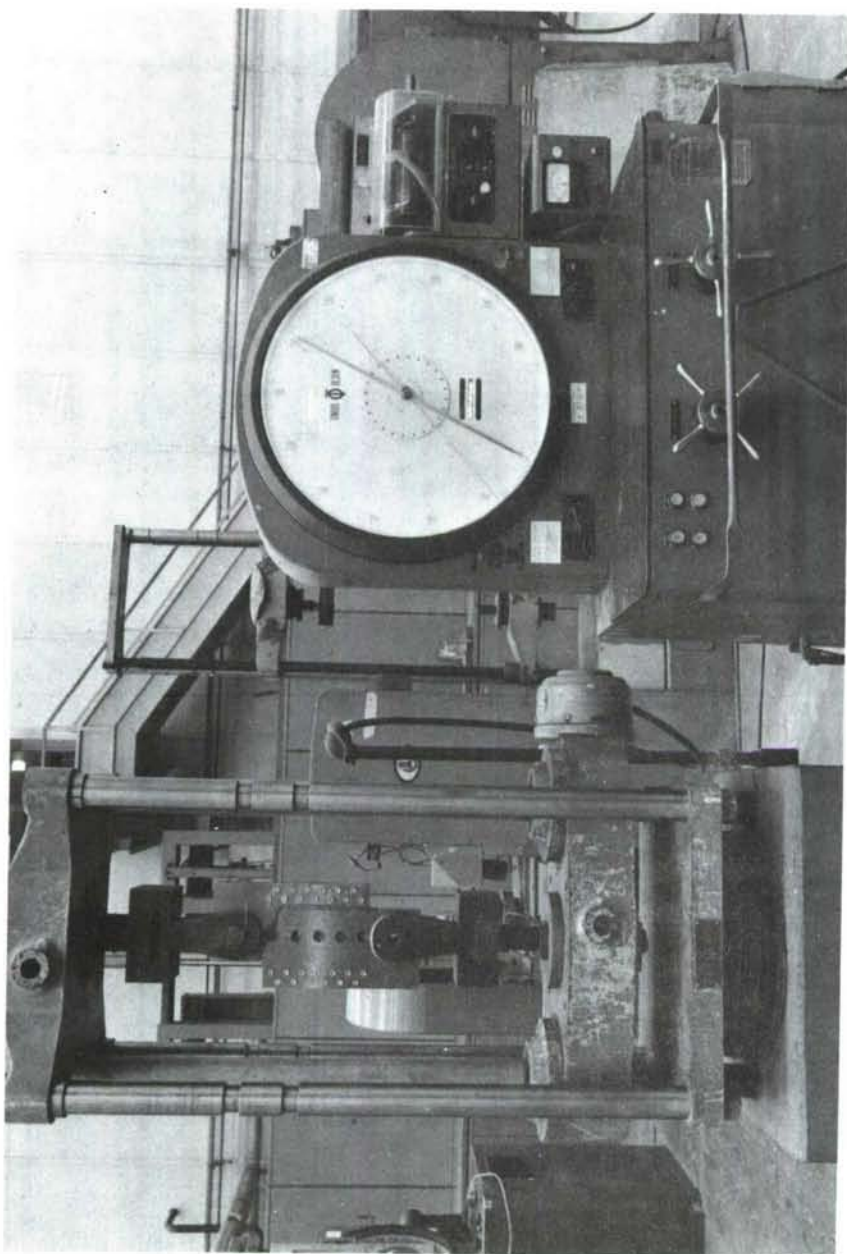
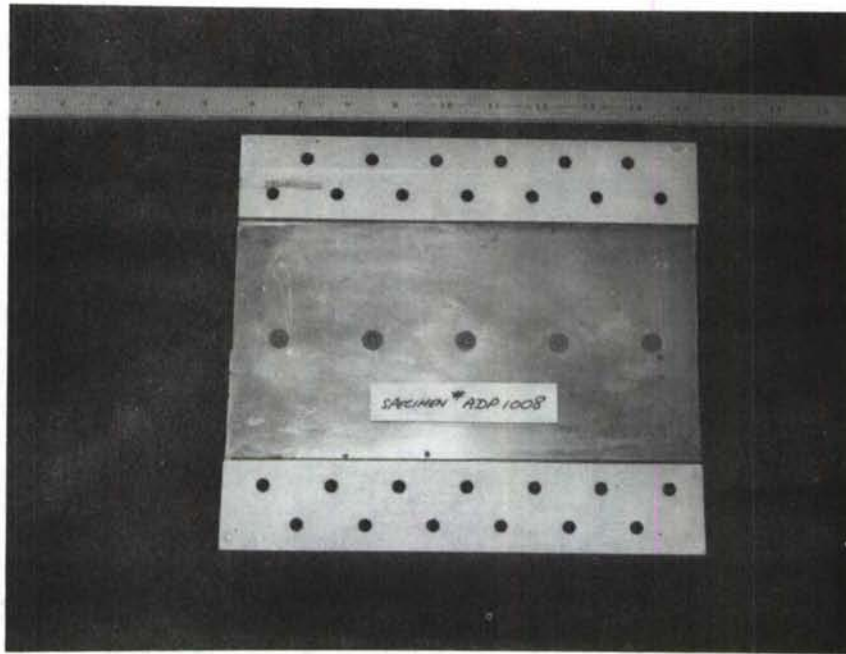
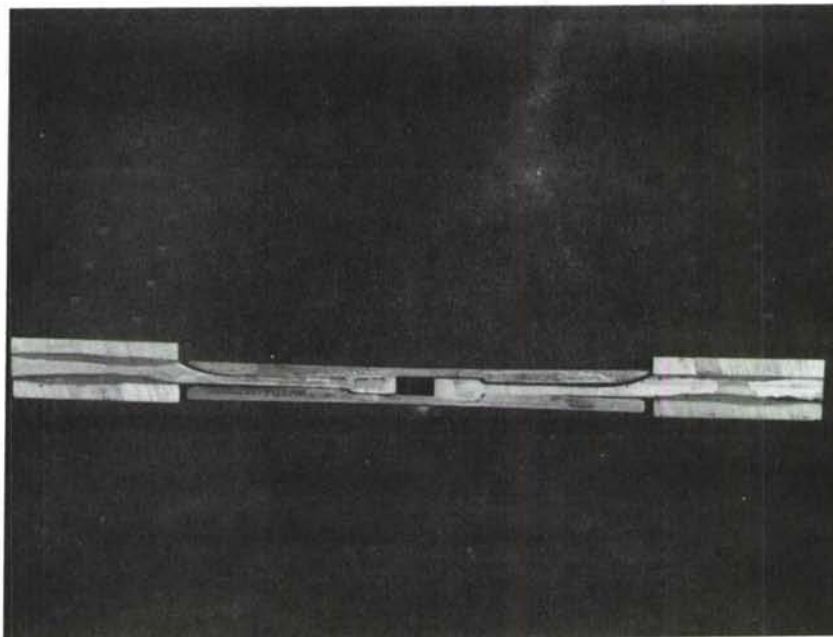


FIGURE 148 TEST ARRANGEMENT, SPANWISE SPLICE FAIL SAFE  
SHEAR TEST (ADP 1008)



(a) Plan View, Flush Side



(b) End View

FIGURE 149 PLAN AND END VIEWS OF BONDED/CLAMPED SPANWISE  
SPLICE SHEAR SPECIMEN (ADP 1008)



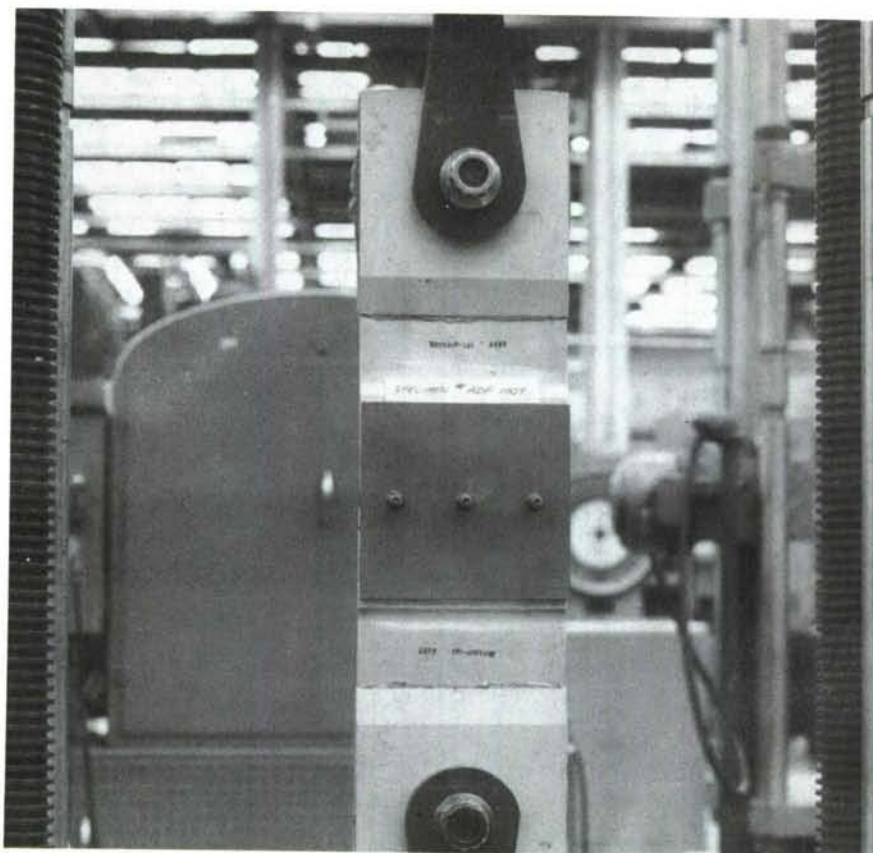


FIGURE 150 TEST ARRANGEMENT, SPANWISE SPLICE FAIL SAFE  
TENSION TEST (ADP 1009)

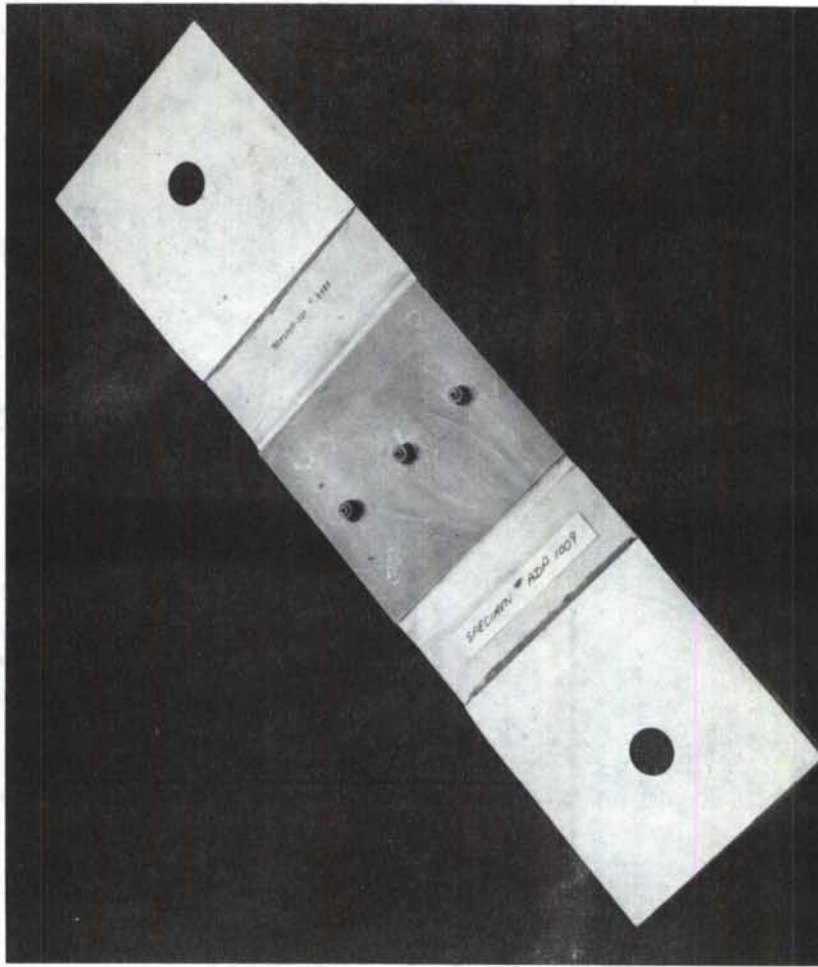


FIGURE 151 INSIDE SURFACE, SPANWISE SPLICE TENSION  
SPECIMEN (ADP 1009)

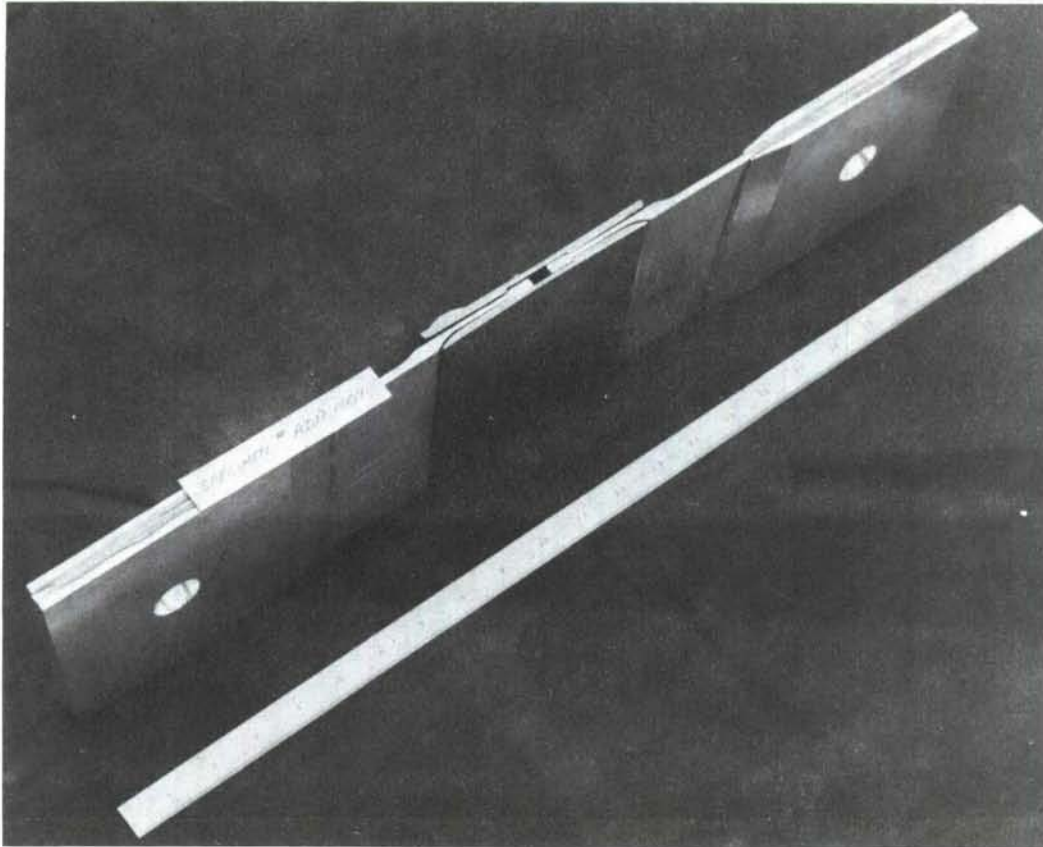


FIGURE 152 EDGE VIEW, SPANWISE SPLICE TENSION  
SPECIMEN (ADP 1009)

## FATIGUE COMPONENT TESTS

### PURPOSE

The purpose of these tests was to obtain comparative fatigue data for use in the Phase IA preliminary design study. Primary emphasis was placed on joining techniques. The specific purpose of each test is given in Table XXXVIII.

### TEST DESCRIPTIONS AND REQUIREMENTS

The descriptions and requirements of the fatigue component tests are given in Table XXXVIII and Figures 153, 154, and 155. Both constant-amplitude and spectrum fatigue loadings were applied as noted.

### TEST RESULTS

Results of fatigue component tests are summarized in Table XXXIX. Figures 156 through 164 show photographs of test specimens, test set-ups, and specimen failures.



TABLE XXXVIII

## FATIGUE COMPONENT TESTS

TYPE TEST	SKETCH CONFIG. (REF.)	TEST SPECIMEN NO.	NO. SPECI- MENS	JOINING SYSTEM	LOADING TYPE	NO. STRAIN GAGES AXIAL	DATA REQUIRED	PURPOSE OF TEST
STRINGER TO SKIN, $K_T$	FIG. 153	ADP1001 -101	3	WELDBOND	CONSTANT AMP., LOW, MID & HIGH STRESS	2	NO. OF CYCLES TO FAILURE	COMPARE $K_T$ VALUES OF A WELDBOND VS TAPER-LOK
STRINGER TO SKIN, $K_T$	FIG. 153	ADP1001 -103	3	TAPER-LOK	CONSTANT AMP., LOW, MID & HIGH STRESS	2	NO. OF CYCLES TO FAILURE	FASTENER SYSTEM IN A SKIN TO STRINGER JOINT
RIB ATTACHMENT CLIP	FIG. 154	ADP1007	1	NONE	C-141 SPECTRUM	NONE		DETERMINE EXTENT OF FRETTING AFTER CYCLING FOR 2 LIFETIMES
CHORDWISE JOINT WS 77	FIG. 155	ADP1002	3	STEEL HUCKRIMP	C-141 SPECTRUM	2	NO. OF CYCLES TO FAILURE	DETERMINE FATIGUE LIFE OF A TYPICAL BUILT-UP CHORDWISE JOINT CONFIGURATION

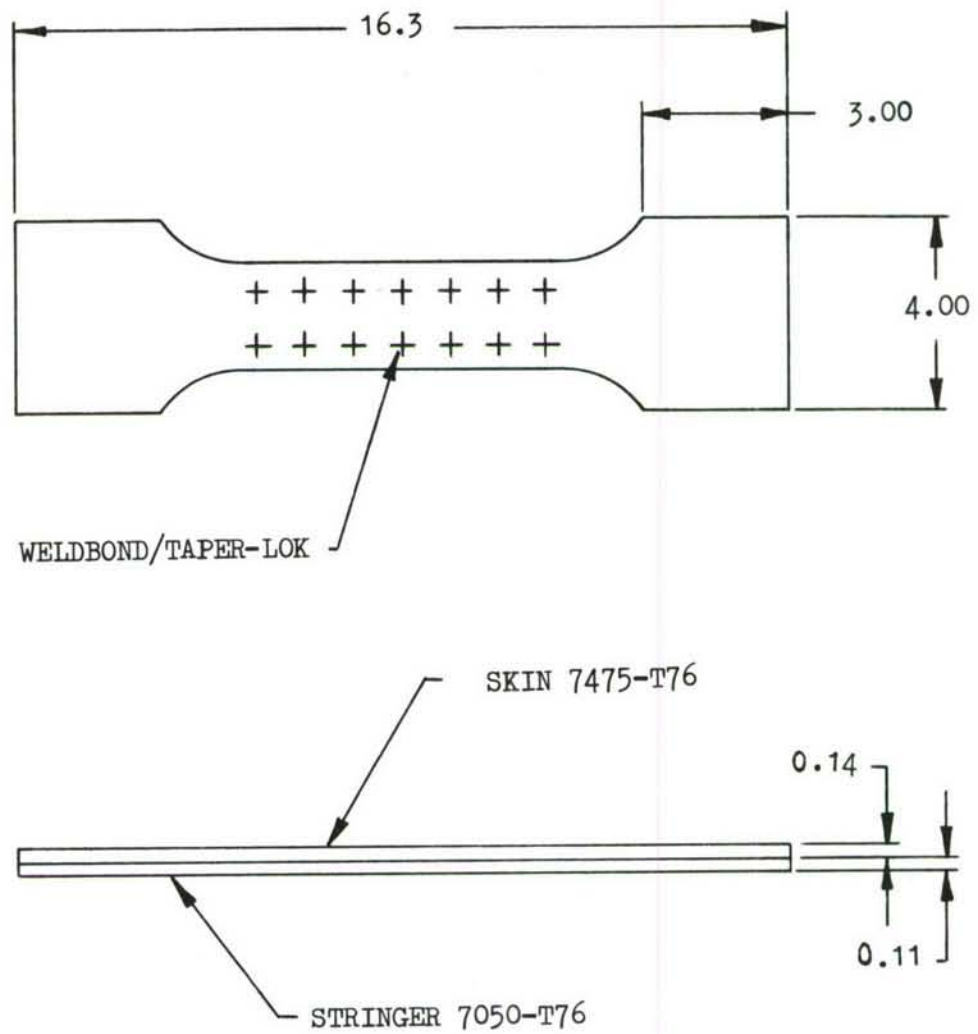
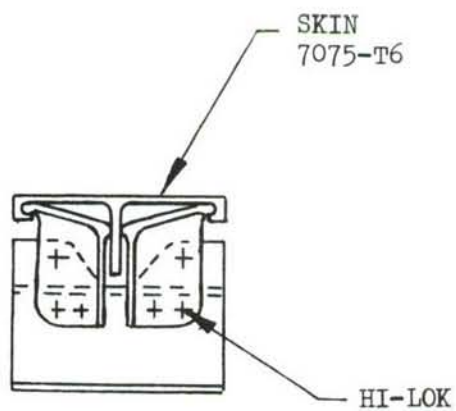
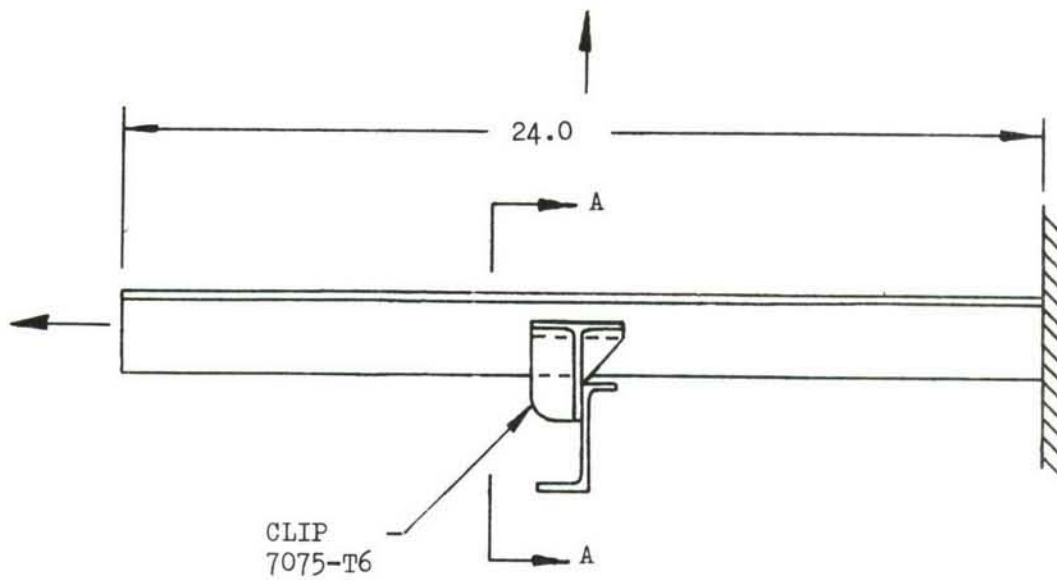


FIGURE 153 STRINGER TO SKIN  $K_T$  SPECIMEN



SECTION A-A

FIGURE 154 N-P RIB ATTACHMENT CLIP FATIGUE TEST SPECIMEN

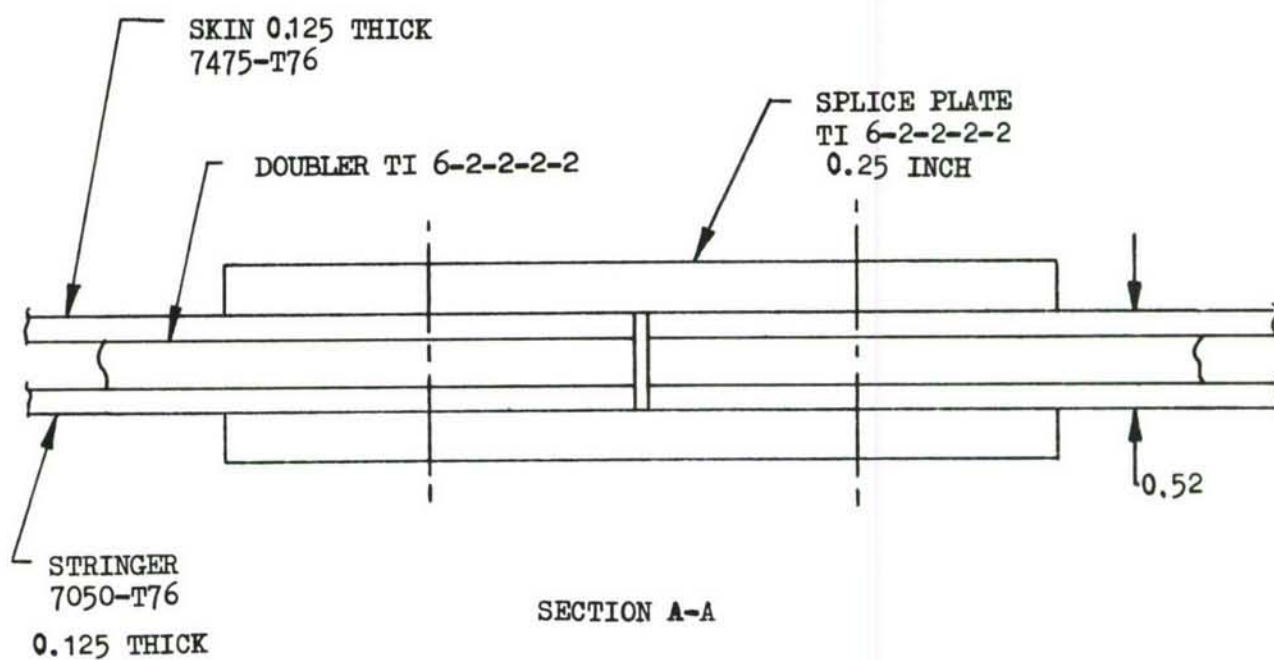
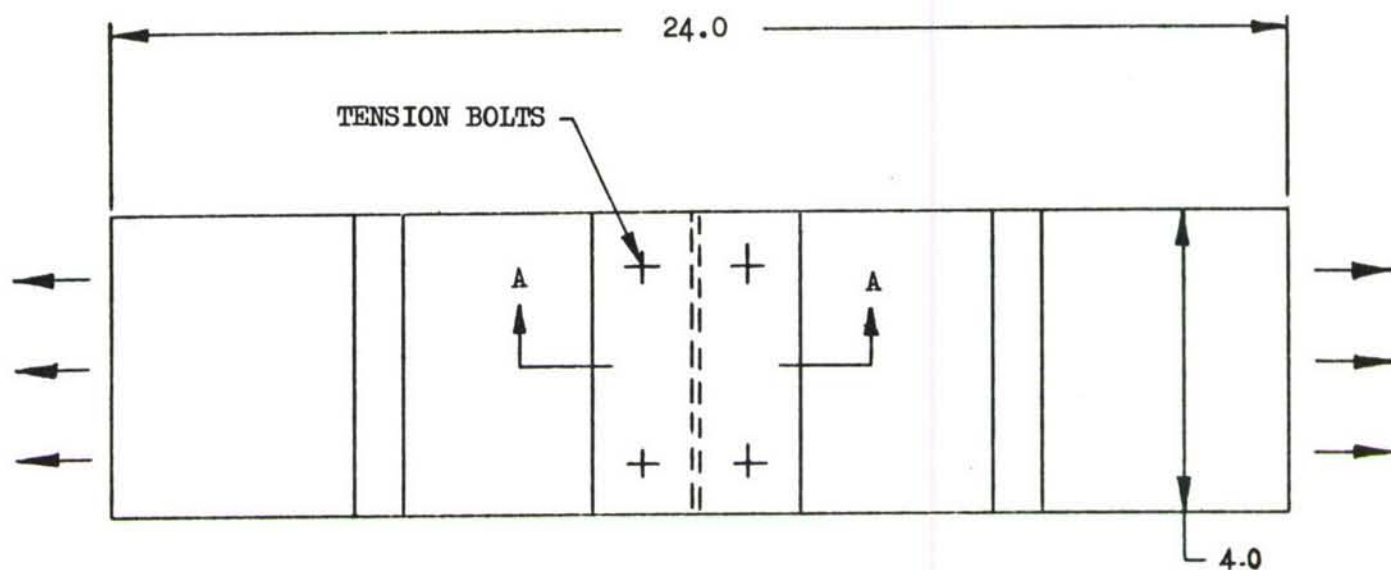


FIGURE 155 WS 77 CHORDWISE JOINT SPECIMEN



TABLE XXXIX

## FATIGUE COMPONENT TEST RESULTS

TEST TITLE	TEST SPECIMEN NO.	NO. SPECIMENS	TEST SET-UP (REF. FIG.)	TYPE OF LOADING	APPLIED STRESS (KSI)	CYCLES TO FAILURE	FAILURE MODE	REMARKS
Stringer to Skin Attachment Fatigue (Weldbond)	ADP 1001-101	3	Fig. 156 158	Constant Amplitude Fatigue	+13.5 Max. -16.9 Min.	109,690 248,160 242,210	Fatigue Progression From Nugget/HAZ	These limited data compare favorably with mechanical fasteners - $K_T \approx 3.25$ .
Stringer to Skin Attachment Fatigue (Taper-Lok)	ADP 1001-103	3	Fig. 157 158	Constant Amplitude Fatigue	+13.5 Max. -16.9 Min.	276,510 235,150 244,500	Fatigue Progression From Fastener Hole	Fatigue endurance approximately the same as weldbond. Again, $K_T \approx 3.25$ .
Rib to Surface Attachment N-P Clip Fatigue	ADP 1007	1	Fig. 159	C-141 Spectrum Fatigue (Note 1)	See Table XL	2 Life-times	None	Specimen disassembled and inspected. No evidence of fatigue damage or fretting. (See Fig. 162)
Chordwise Joint Fatigue (W.S. 77)	ADP 1002	1	Fig. 163 164	C-141 Spectrum Fatigue		4 Life-times	See Remarks	HuckRimp fasteners failures, replaced with high strength bolts and no additional problems. This configuration is not in ADP design. For information only.

NOTE: (1) Constant Normal Load of 185 Lbs. Applied Between Clips and Panel During Fatigue Cycling

TABLE XL  
C-141 SPECTRUM LOADING SCHEDULE FOR TEST ADP1007

LOAD LEVEL NO.	NO. OF CYCLES PER FLT.	PARTIAL CYCLES		LOAD - POUNDS	
		NUMBER	FLIGHTS	MAX.	MIN.
1	56	2	5	-17,320	-21,098
2	2	1	9	-15,980	-22,439
3	-	1	12	-14,420	-24,000
4	-	1	270	-12,735	-25,684
5	2	-	-	-9,567	-15,097
6	-	1	15	-8,240	-16,424
7	-	1	270	-6,556	-18,108
8	1 Ramp	-	-	17,979	
9	1 Ramp	-	-		-22,505
10	-	1 Ramp	3	8,634	
11	-	1 Ramp	3		-5,835
12	-	1 Ramp	3	8,634	
13	-	1 Ramp	3		-5,835
14	24	8	21	16,453	9,653
15	-	2	7	19,798	6,309
16	-	1	270	25,903	203
17	10	-	-	11,965	3,944
18	1	-	-	13,719	2,190
19	-	1	17	16,316	-409
20	-	1	270	19,784	-3,875

- NOTES: (1) Specimen Area (ADP 1007) = 1.325 Sq. In.  
 (2) Plus Loadings are Tension, Minus Loadings Compression  
 (3) One Lifetime Equals 8,200 Flights

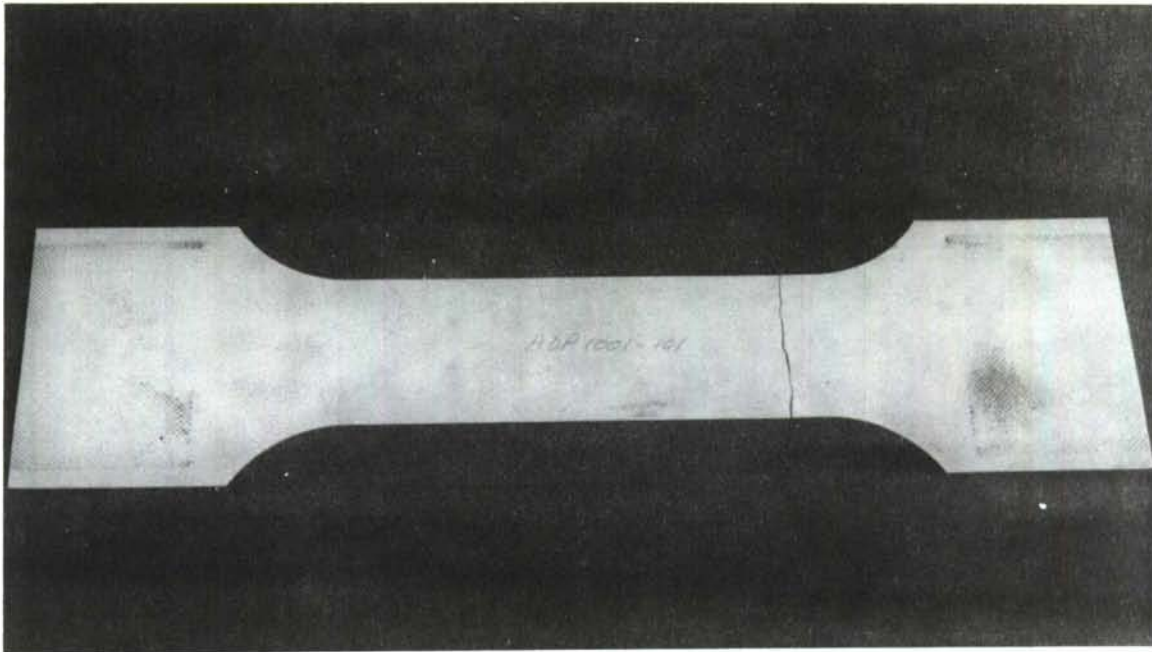


FIGURE 156 SIMULATED STRINGER/SKIN WELDBOND FATIGUE SPECIMEN (ADP 1001-101)

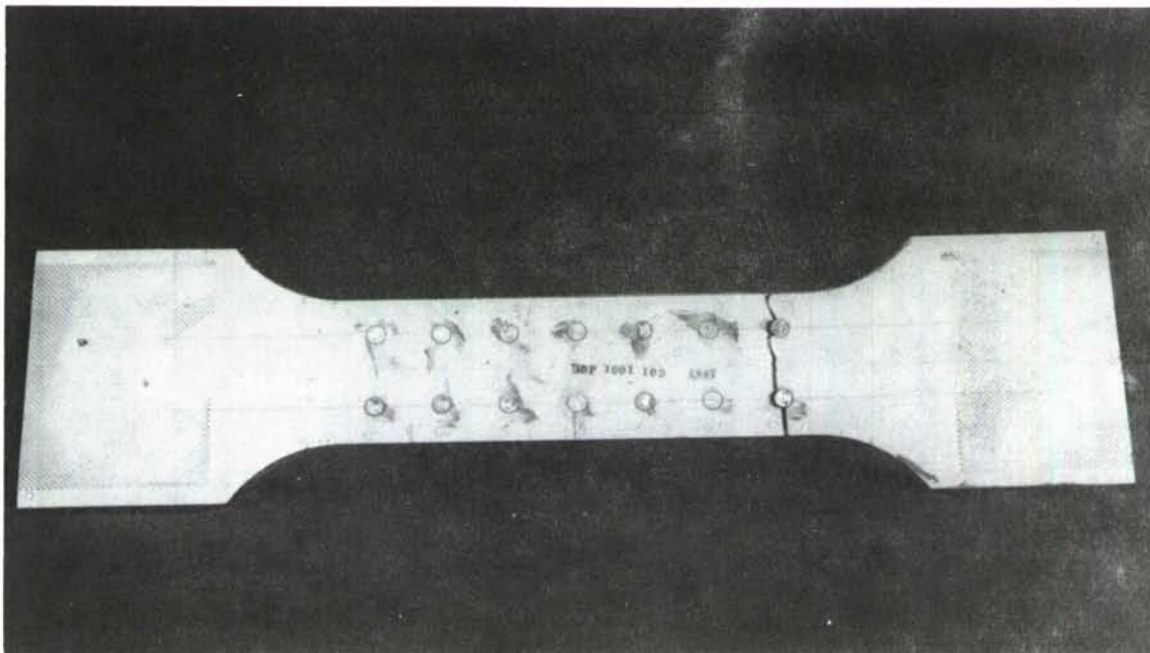
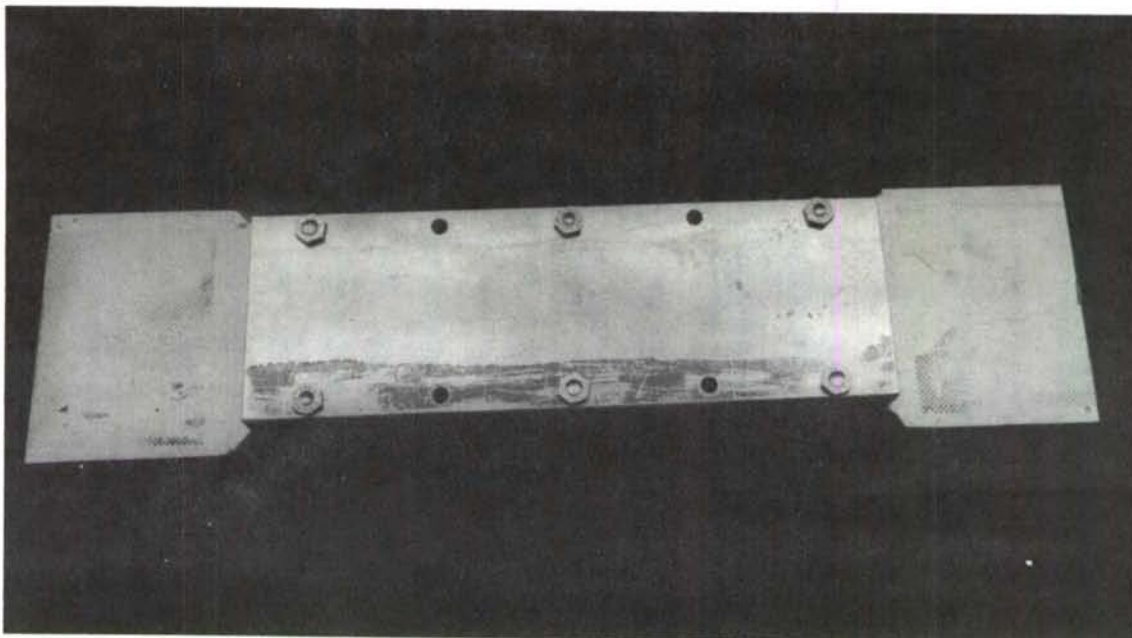
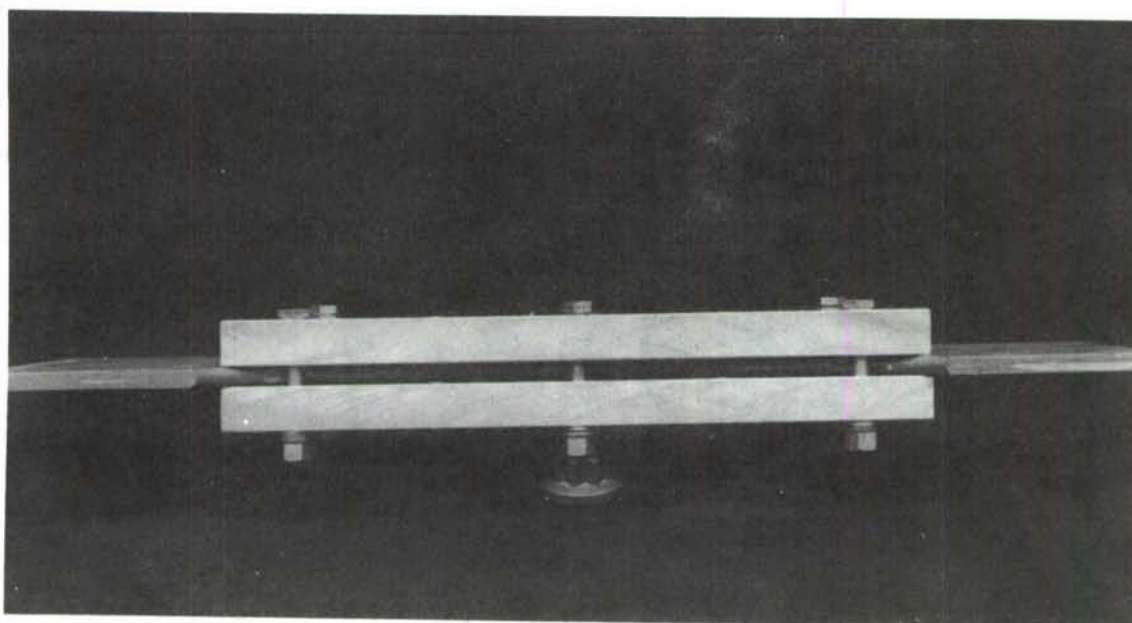


FIGURE 157 SIMULATED STRINGER/SKIN TAPERLOK FATIGUE SPECIMEN (ADP 1001-103)



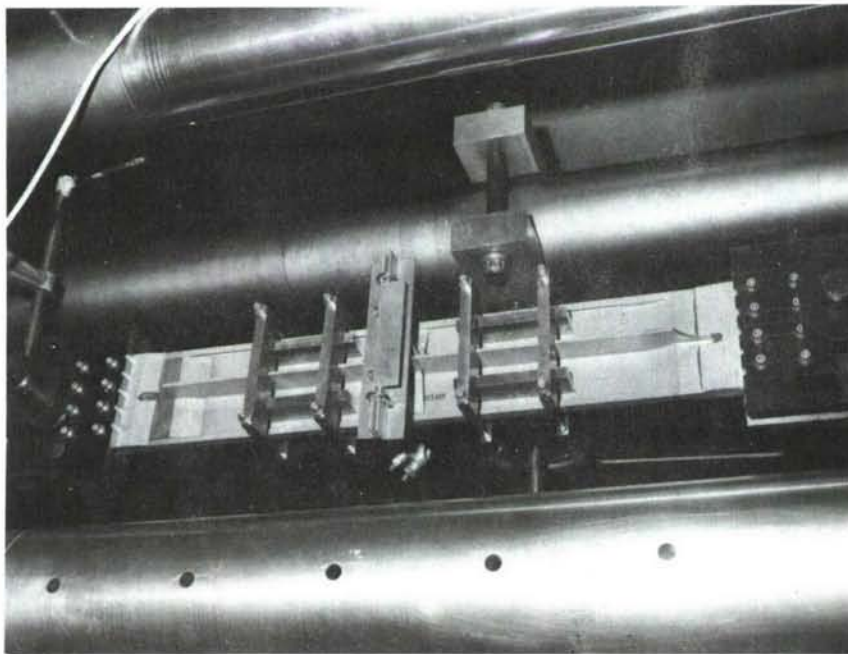
(a) Top View



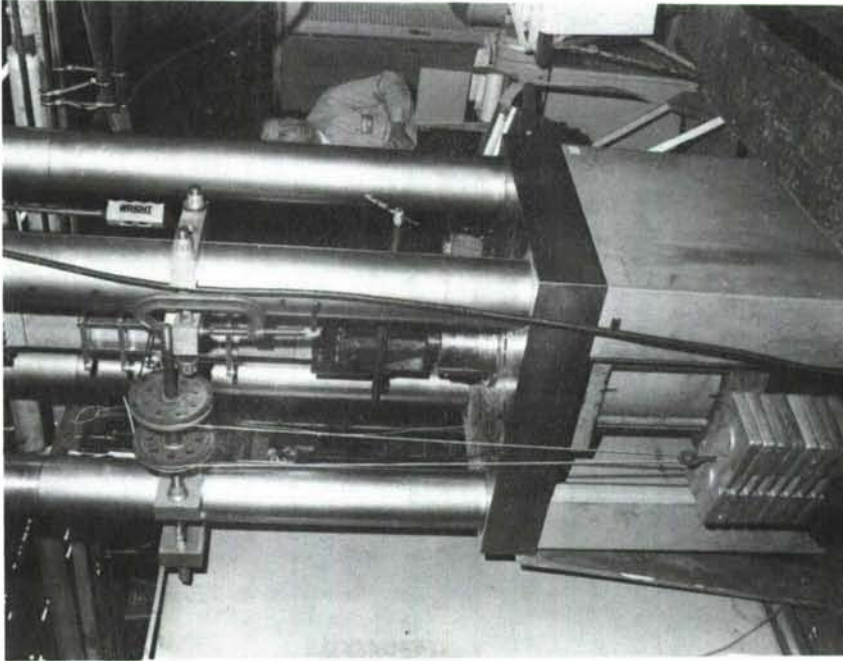
(b) Side View

FIGURE 158 COMPRESSION STABILITY PLATES USED IN STRINGER/SKIN SPECIMEN FATIGUE TESTS





(a) Inside Of Skin Panel



(b) Outside Of Skin Panel

FIGURE 159 TEST ARRANGEMENT, N-P CLIP FATIGUE TEST  
(ADP 1007)

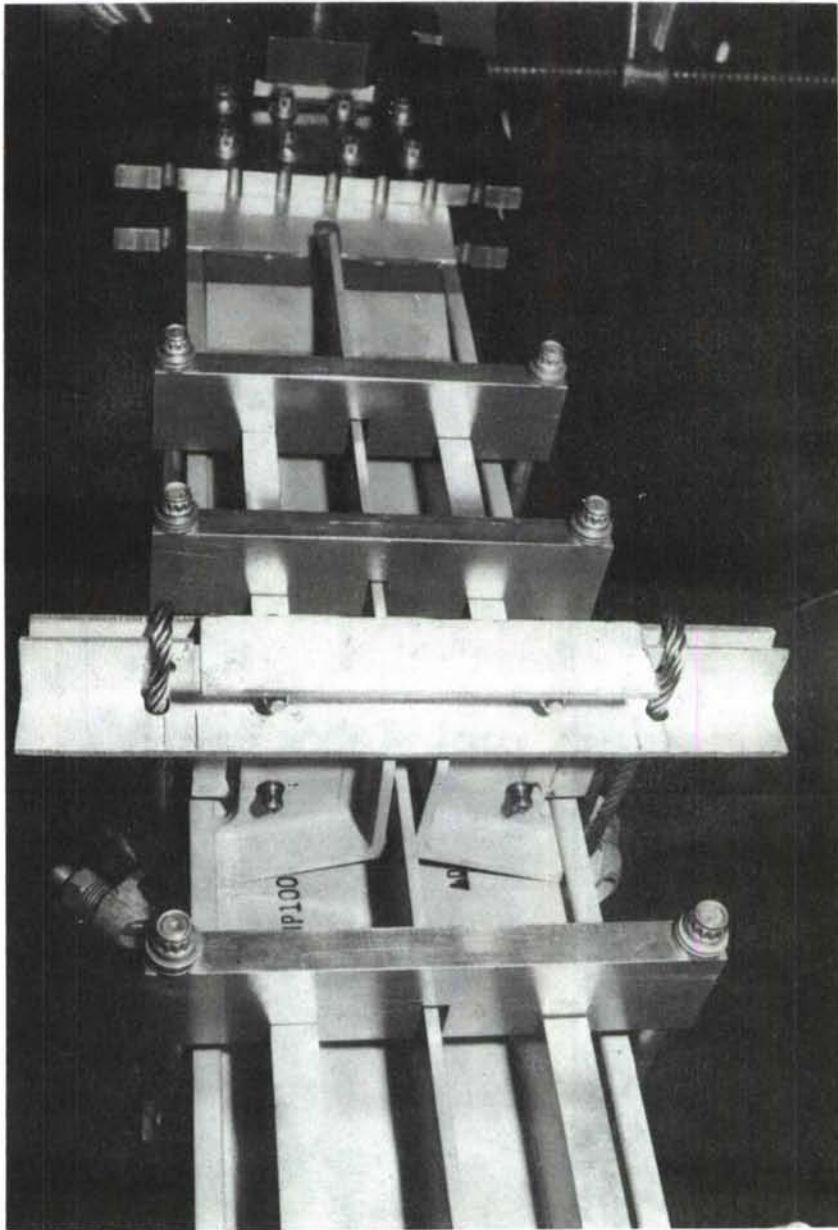


FIGURE 160 CLOSE-UP OF TEST PANEL SHOWING N-P CLIP  
ARRANGEMENT

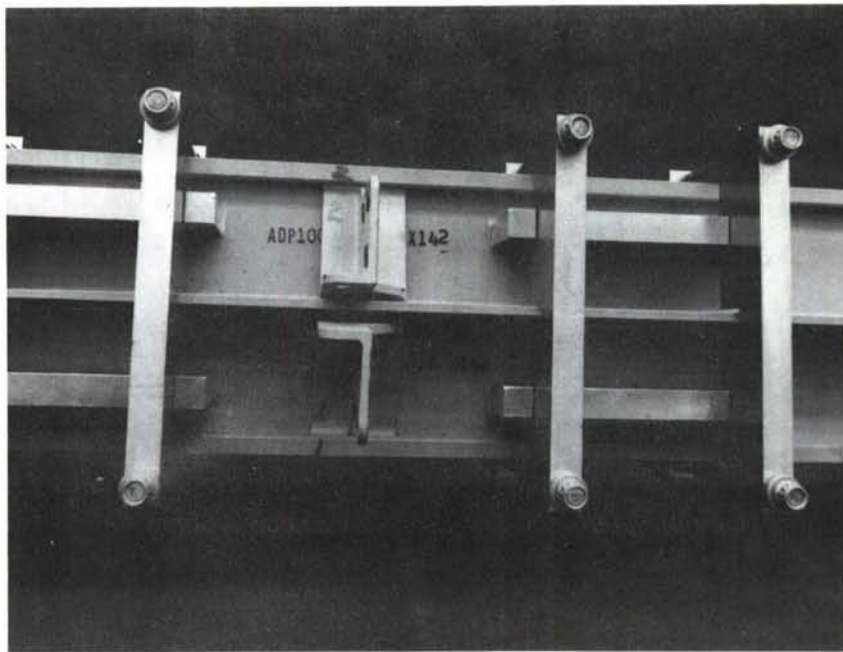


FIGURE 161 NON-PENETRATING CLIPS AND PANEL AFTER  
DISASSEMBLY

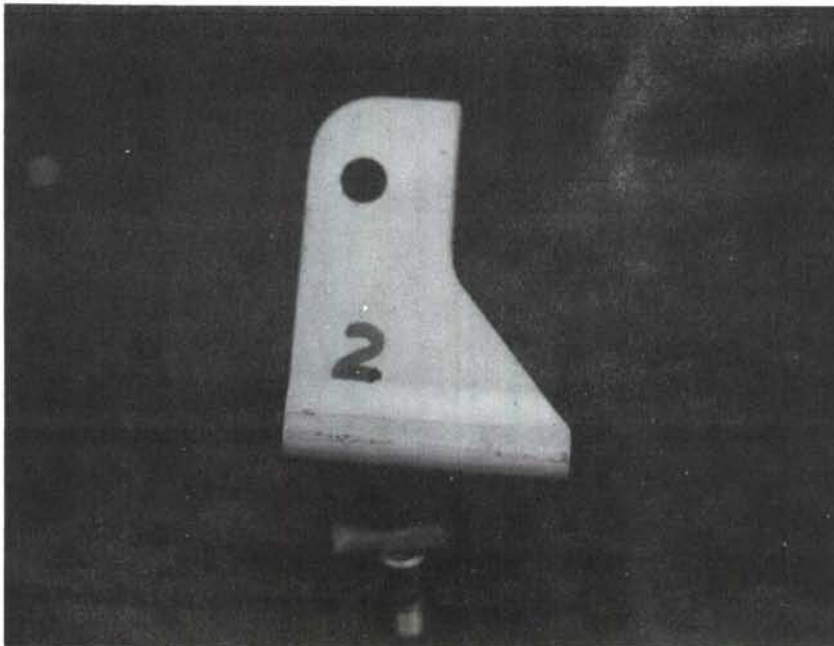


FIGURE 162 CONTACT SURFACE OF N-P CLIP INDICATING NO  
SIGNIFICANT FRETTING EFFECT

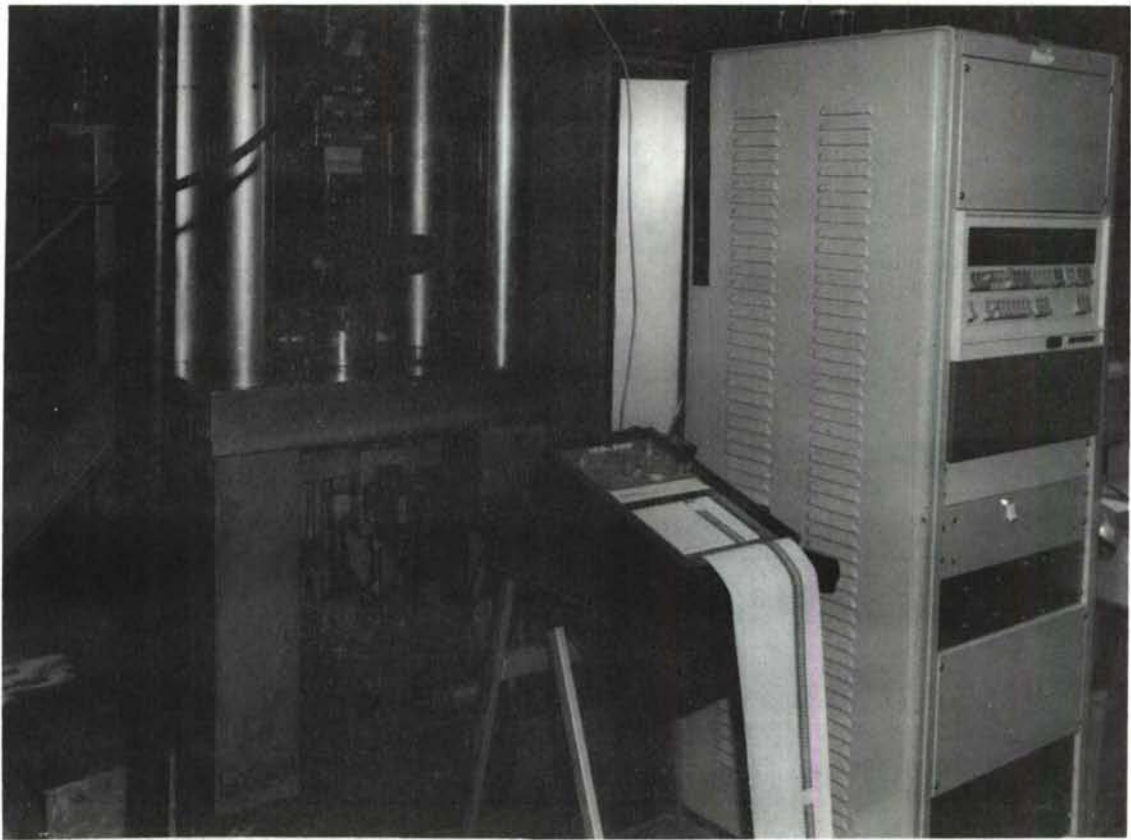
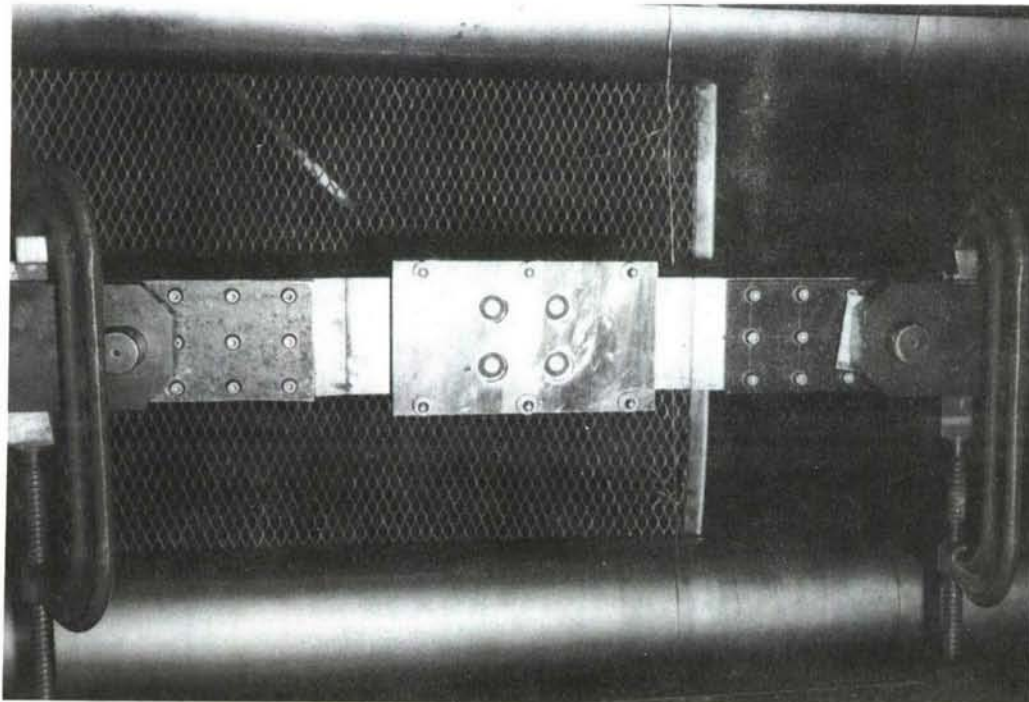
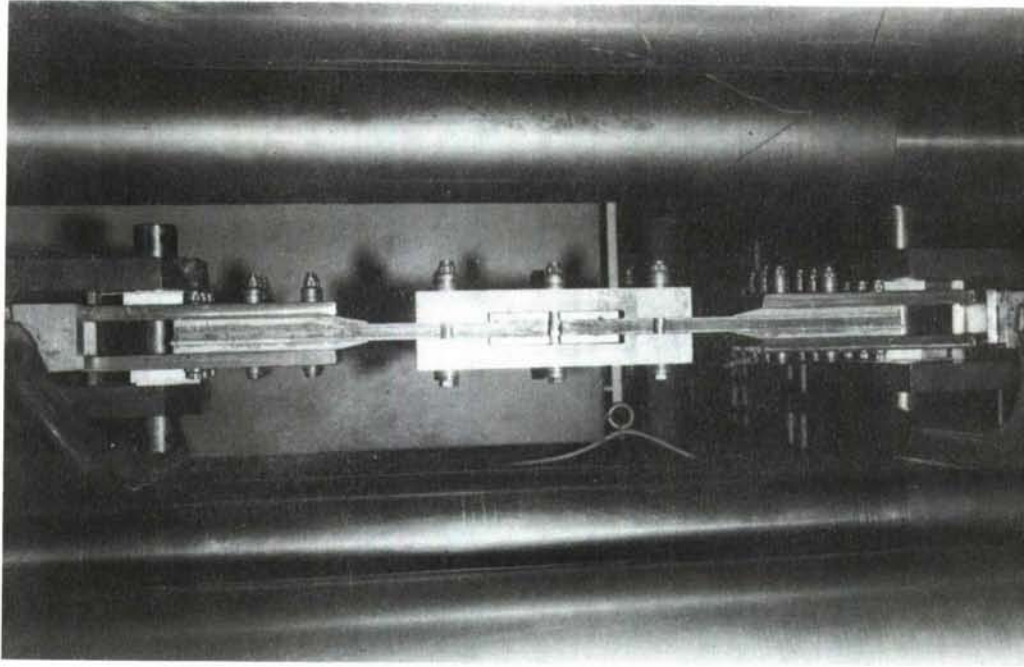


FIGURE 163 TEST ARRANGEMENT, CHORDWISE JOINT  
FATIGUE TEST (ADP 1002)





(a) Front View



(b) Side View

FIGURE 164 COMPRESSION STABILITY PLATES USED IN CHORDWISE JOINT FATIGUE TEST

## DAMAGE TOLERANCE COMPONENT TESTS

### PURPOSE

Limited damage tolerance component tests were run to obtain preliminary design data on crack growth, residual fatigue life, and/or residual strength characteristics of selected configurations. The specific purpose of each test is given in Table XLI.

### TEST DESCRIPTIONS AND REQUIREMENTS

The descriptions and requirements of the damage tolerance component tests are given in Table XLI and Figures 165 through 168.

### TEST RESULTS

Results of damage tolerance component tests are summarized in Table XLII. Figures 169 through 172 show photographs of test specimens and test set-ups.

TABLE XLI  
DAMAGE TOLERANCE COMPONENT TESTS

TYPE TEST	SKETCH CONFIG. (REF.)	TEST SPECIMEN NO.	LOADING TYPE	NUMBER STRAIN GAGES AXIAL	DATA REQUIRED	PURPOSE OF TEST
SPANWISE SPLICE SHEAR (FAIL SAFE)	FIG. 165	ADP1008	SHEAR	NONE	FAILING LOAD	DETERMINE SHEAR CAPABILITY OF JOINT AFTER BOND FAILURE
SPANWISE SPLICE TENSION (FAIL SAFE)	FIG. 166	ADP1009	TENSION	NONE	FAILING LOAD	DETERMINE TENSION CAPABILITY OF JOINT AFTER BOND FAILURE
SPANWISE SPLICE (WELDBOND)	FIG. 167	ADP1010	C-141 SPECTRUM 1 LIFE	3	CRACK GROWTH DATA RESIDUAL STRENGTH	PRELIMINARY ASSESSMENT OF DAMAGE TOLERANCE ANALYSIS
CRACK GROWTH RETARDATION	FIG. 168	ADP1015	C-141 SPECTRUM & MODIFIED SPECTRUM 1 LIFE	NONE	CRACK GROWTH DATA	VERIFY ANALYTICAL CRACK GROWTH MODEL

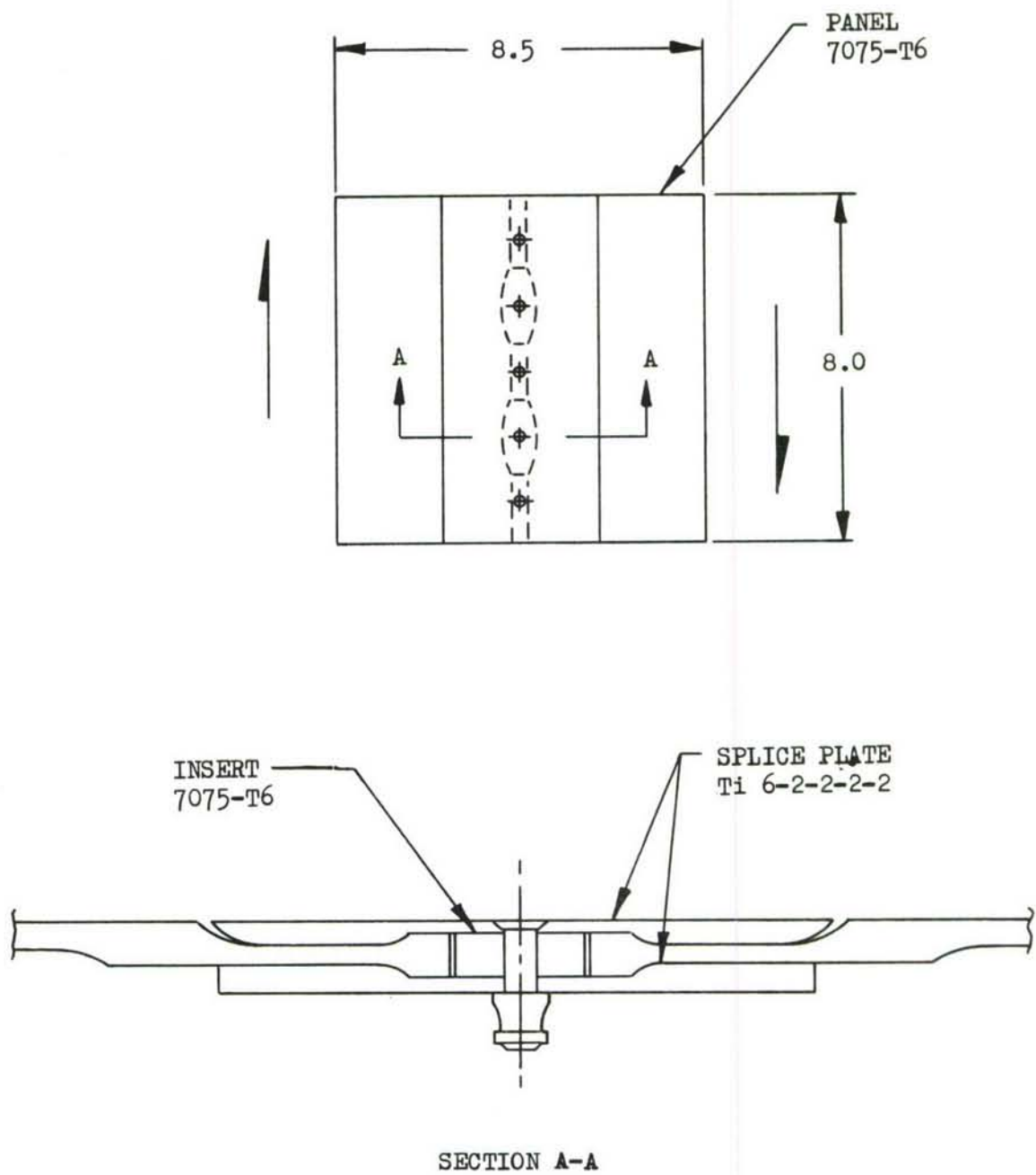
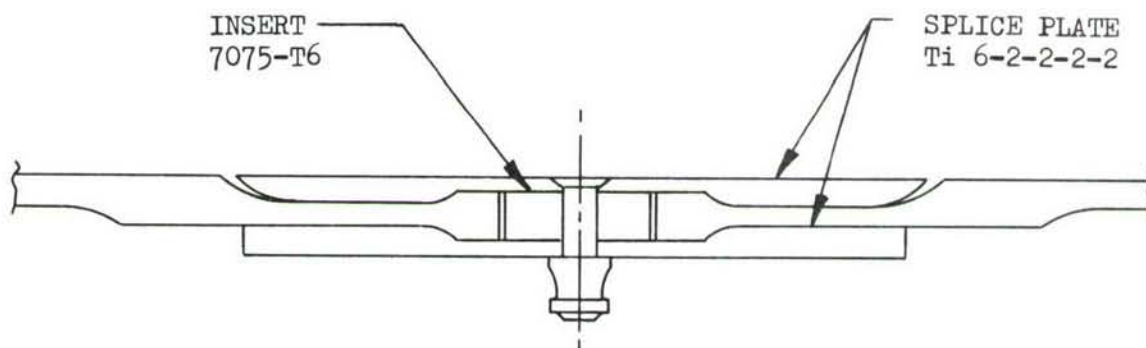
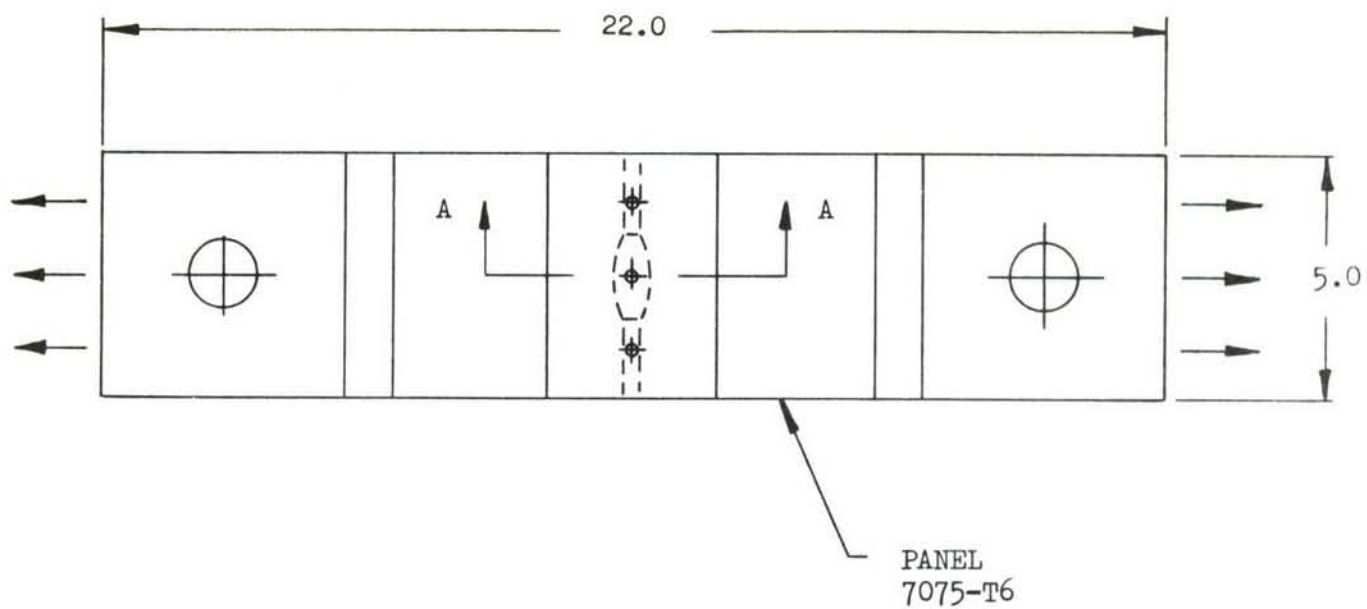


FIGURE 165 DAMAGE TOLERANCE SPANWISE SPLICE SHEAR SPECIMEN





SECTION A-A

FIGURE 166 DAMAGE TOLERANCE SPANWISE SPLICE TENSION SPECIMEN

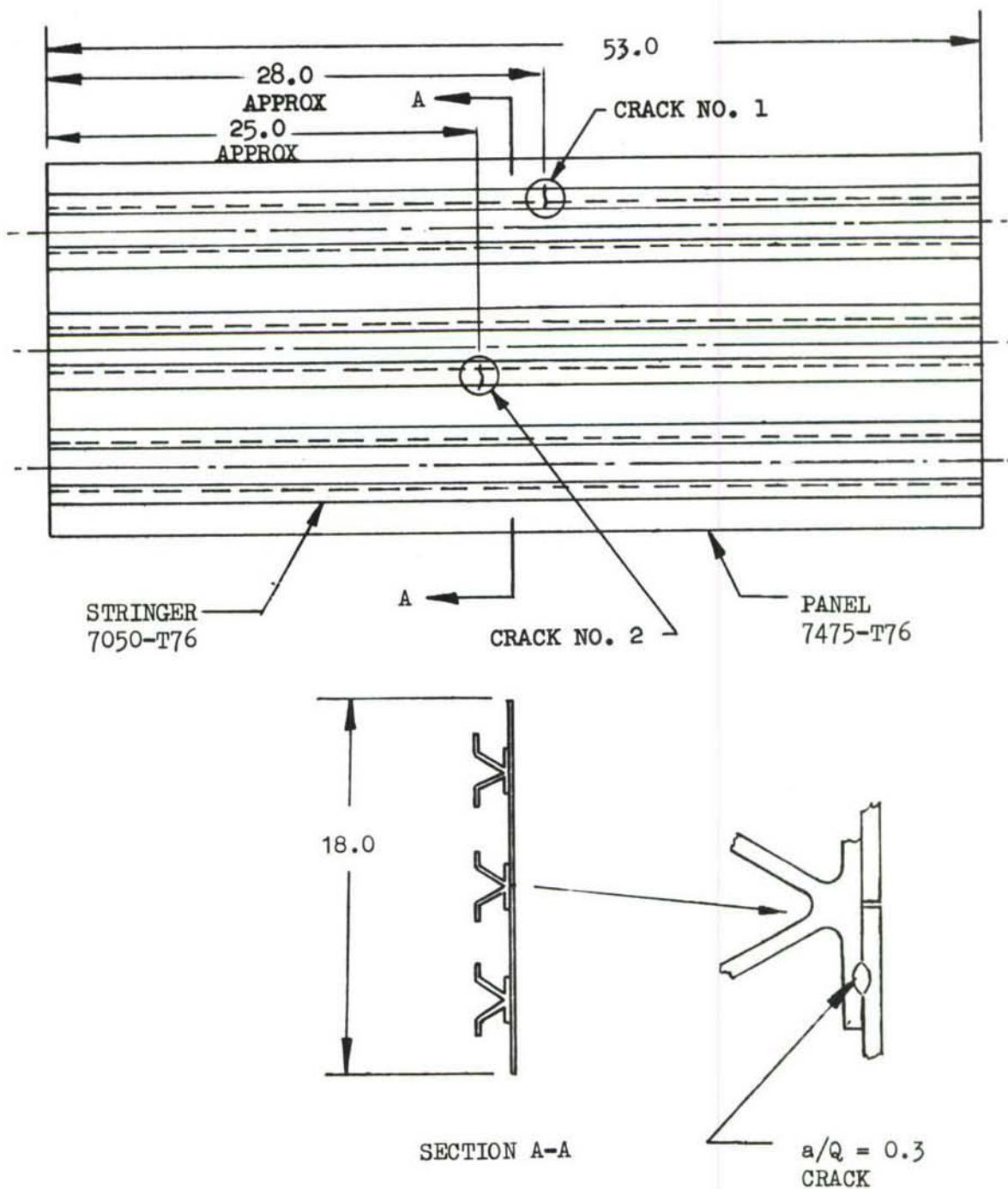
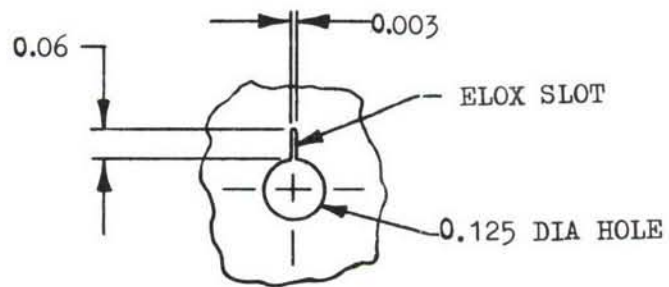
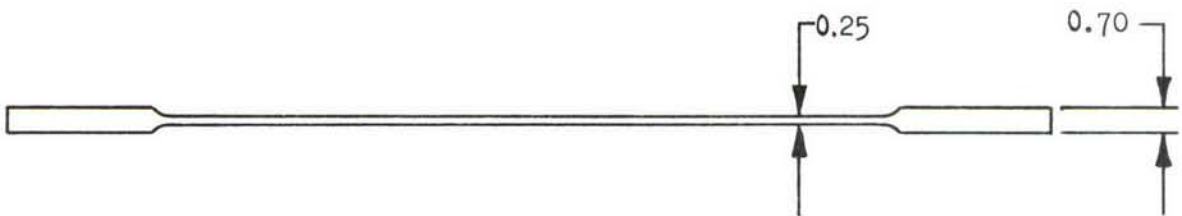
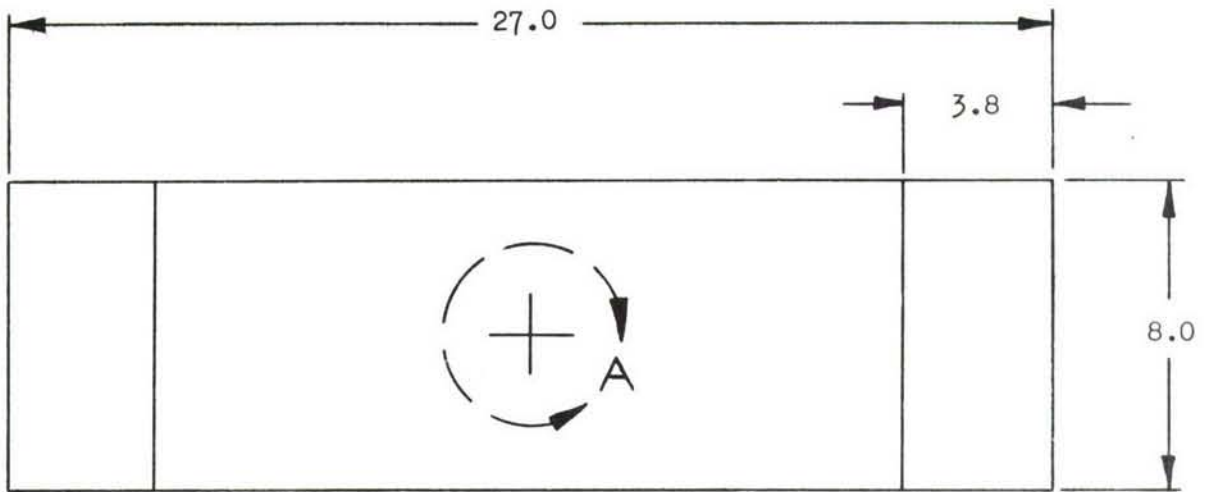


FIGURE 167 DAMAGE TOLERANCE WELDBONDED "A" STRINGER SPECIMEN



VIEW 'A'

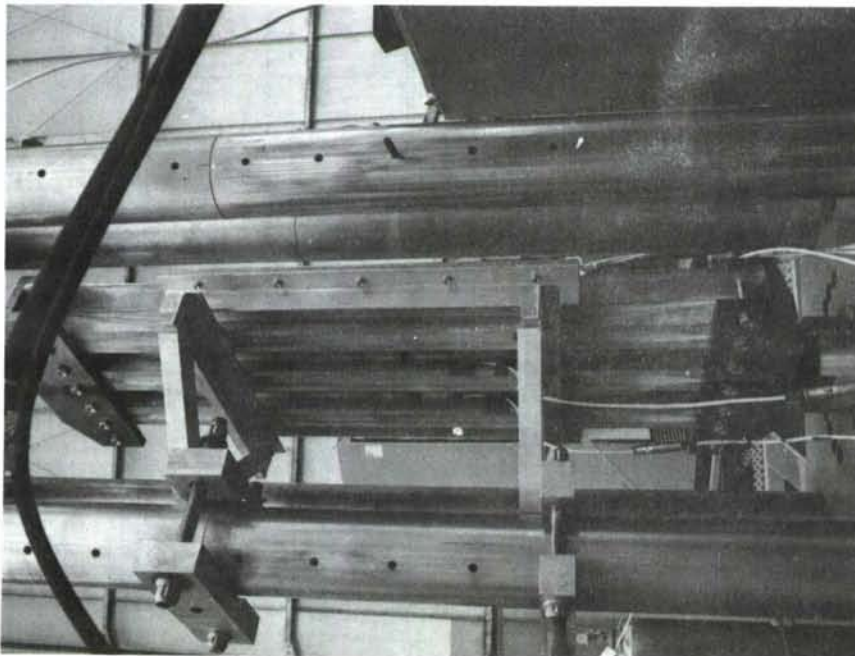
FIGURE 168 DAMAGE TOLERANCE RETARDATION TEST SPECIMEN

TABLE XLII

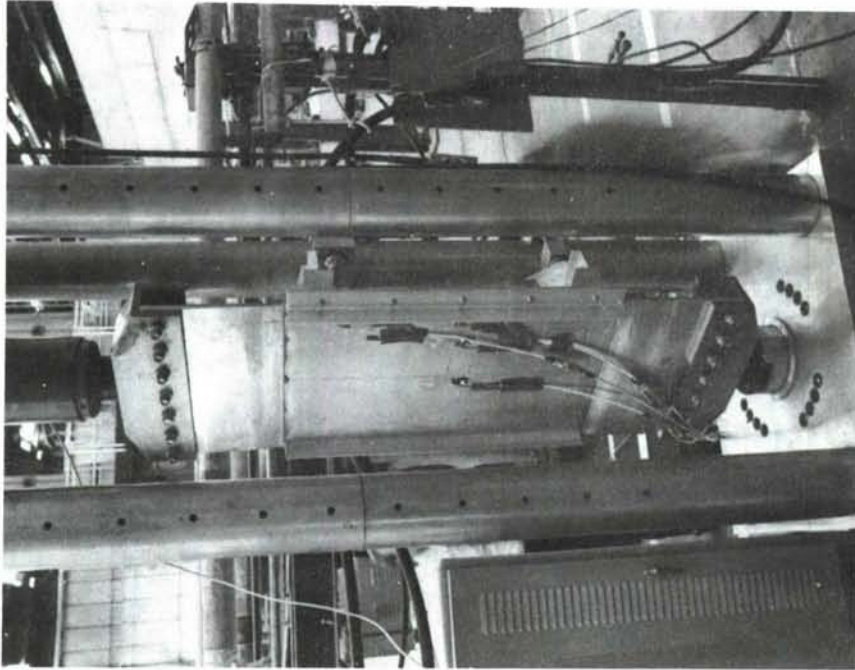
## DAMAGE TOLERANCE COMPONENT TEST RESULTS

TEST TITLE	TEST SPECIMEN NO.	TEST SET-UP (REF. FIG.)	TYPE OF LOADING	TEST RESULTS/REMARKS
Clamped Spanwise Splice Fail Safe Shear	ADP 1008	Figure 148	Shear	See Table XXXVII
Clamped Spanwise Splice Fail Safe Tension	ADP 1009	Figure 150	Tension	See Table XXXVII
Weldbond Spanwise Splice - Crack Growth and Residual Strength	ADP 1010	Figure 169	C-141 Spectrum Fatigue Plus Residual Strength Static Load	See Figures 170 and 171 for crack progression of two monitored cracks. Residual strength - 102% of limit load; see Figure 172 for residual strength test specimen
Crack Growth Retardation (7075-T6 Material) - 2 Specimens	ADP 1015		C-141 Spectrum Fatigue	1. Load spectrum - baseline design stress level 2. Safe crack growth improvement factor = 1.76
Crack Growth Retardation (7075-T6 Material) - 2 Specimens	ADP 1015		Modified C-141 Spectrum Fatigue	1. Load spectrum - 71.6% of baseline design stress level 2. Safe crack growth improvement factor = 1.50





(a) Inside of skin panel.



(b) Outside of skin panel.

FIGURE 169 TEST ARRANGEMENT, DAMAGE TOLERANCE WELDBONDED 'A' STRINGER SPECIMEN.

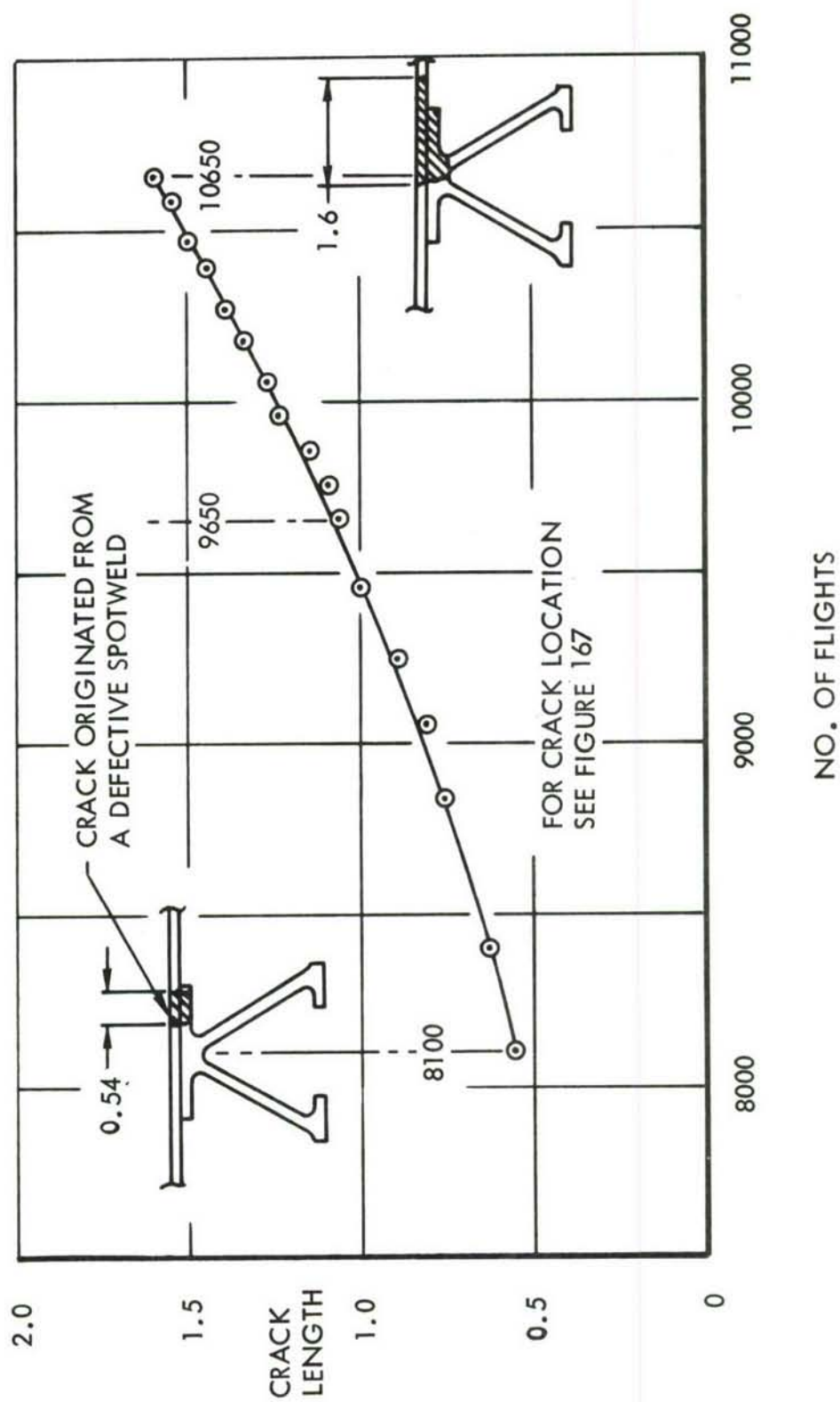


FIGURE 170 CRACK GROWTH DATA - CRACK NO. 1

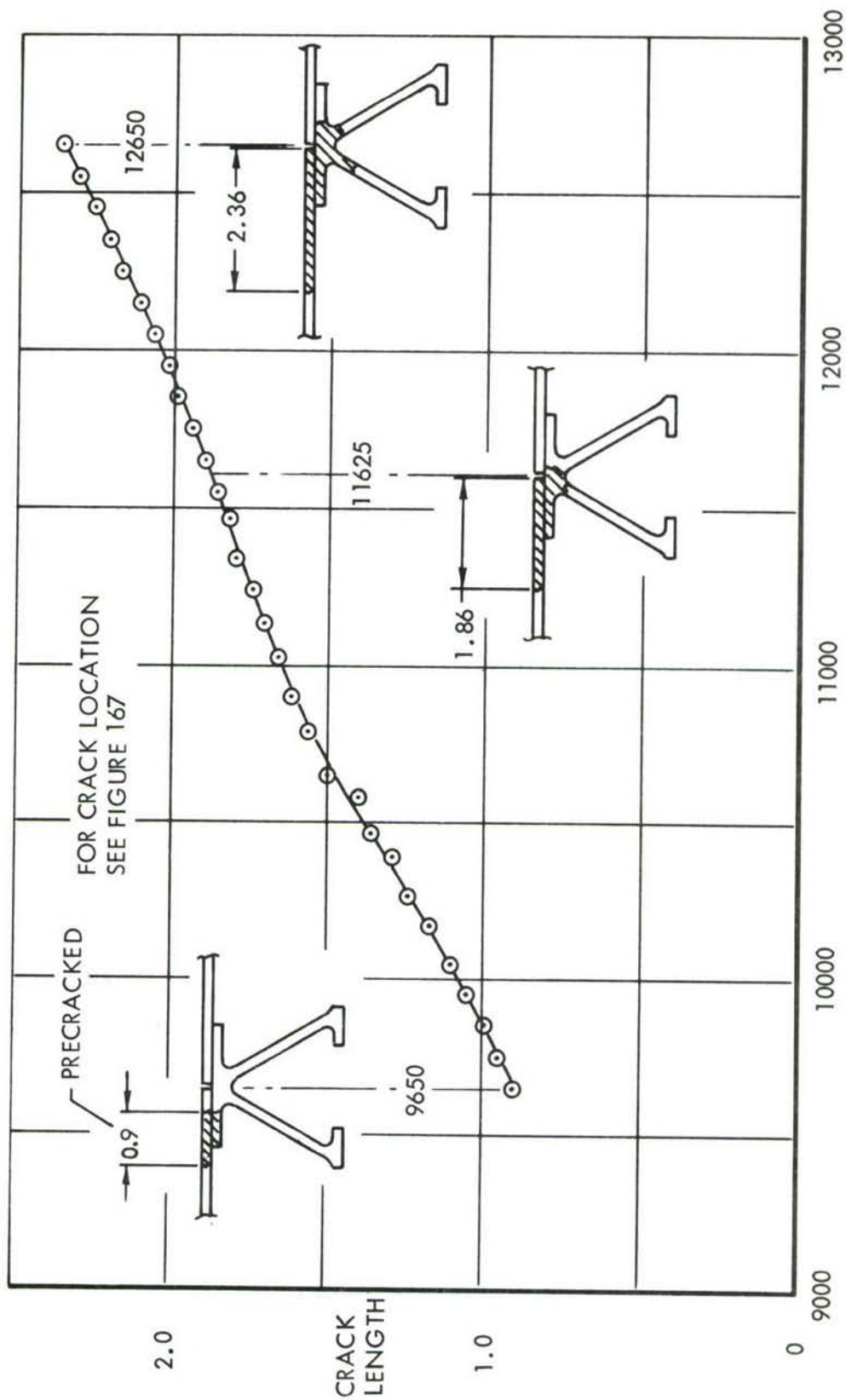


FIGURE 171 CRACK GROWTH DATA - CRACK NO. 2

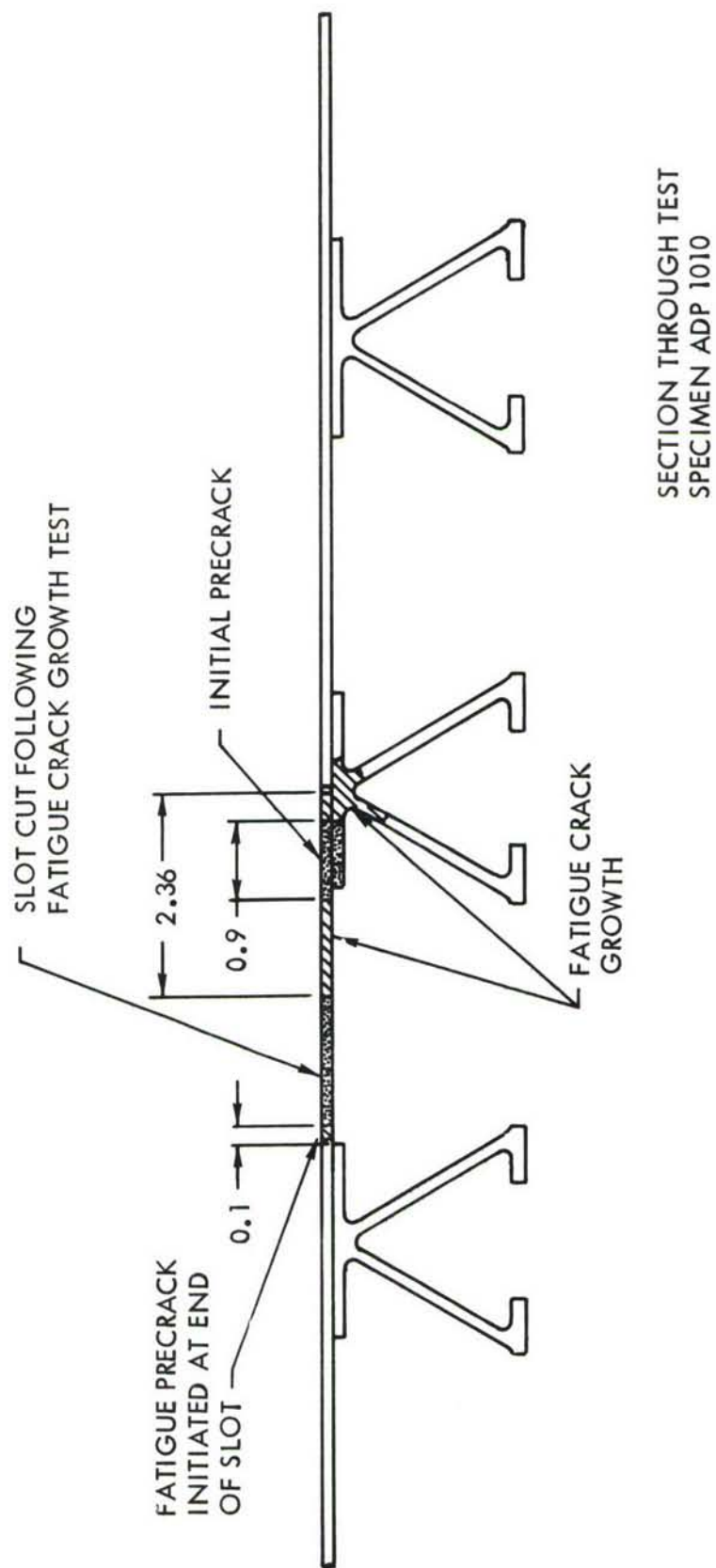


FIGURE 172 RESIDUAL STRENGTH TEST SPECIMEN



## APPENDIX III

### CRITERIA SENSITIVITY AND TRADE STUDIES

The damage tolerance criteria for the Cargo/Tanker ADP program were established early in the Phase IA program. These criteria were updated and incorporated into the basic program, and a separate study was authorized to evaluate the effects of criteria parameter variations on selected design control functions. Where possible, the influence of variations in the parameters were to be assessed as a function of crack growth life or allowable design stress. All analyses associated with the study were performed in terms of the baseline structure, materials, and load spectrum.

#### A3.1 STATISTICAL VARIATION IN FRACTURE PROPERTIES

The initial task in the sensitivity analysis included an experimental determination of crack-growth retardation effects. Four panels were fabricated to the dimensions shown in Figure 168. As indicated in Section VIII, flight-by-flight loads, based on an average mission load spectrum, were applied in the tests. Two panels were tested to a stress spectrum corresponding to the baseline loading in the lower surface wing root area. The remaining two panels were tested at a reduced spectrum severity to determine the sensitivity of crack-growth retardation as a function of design stress level. Load spectrum conversion for the less-severe stress spectrum was based on a design stress corresponding to 50 percent  $F_{TU}$ , or 71.6 percent of the baseline design stress. Figure 173 shows the test results and the calculated crack-growth curves, which assume no retardation effects. The displacement between the related experimental and analytical curves is a measure of crack-growth retardation effects. An experimentally verified analytical crack-growth model, applicable to the selected spectrum, was achieved through the development of crack-growth period extension factors derived from the integrated averages of the data in Figure 173. At the baseline design stress level, for the lower surface at W.S. 77.7, the crack-growth period with retardation was 1.76 times the calculated crack-growth period without retardation. The factor of 1.50 for the less severe stress spectrum was used in the ADP designs. Very little variation in the factor was observed in the results for the baseline

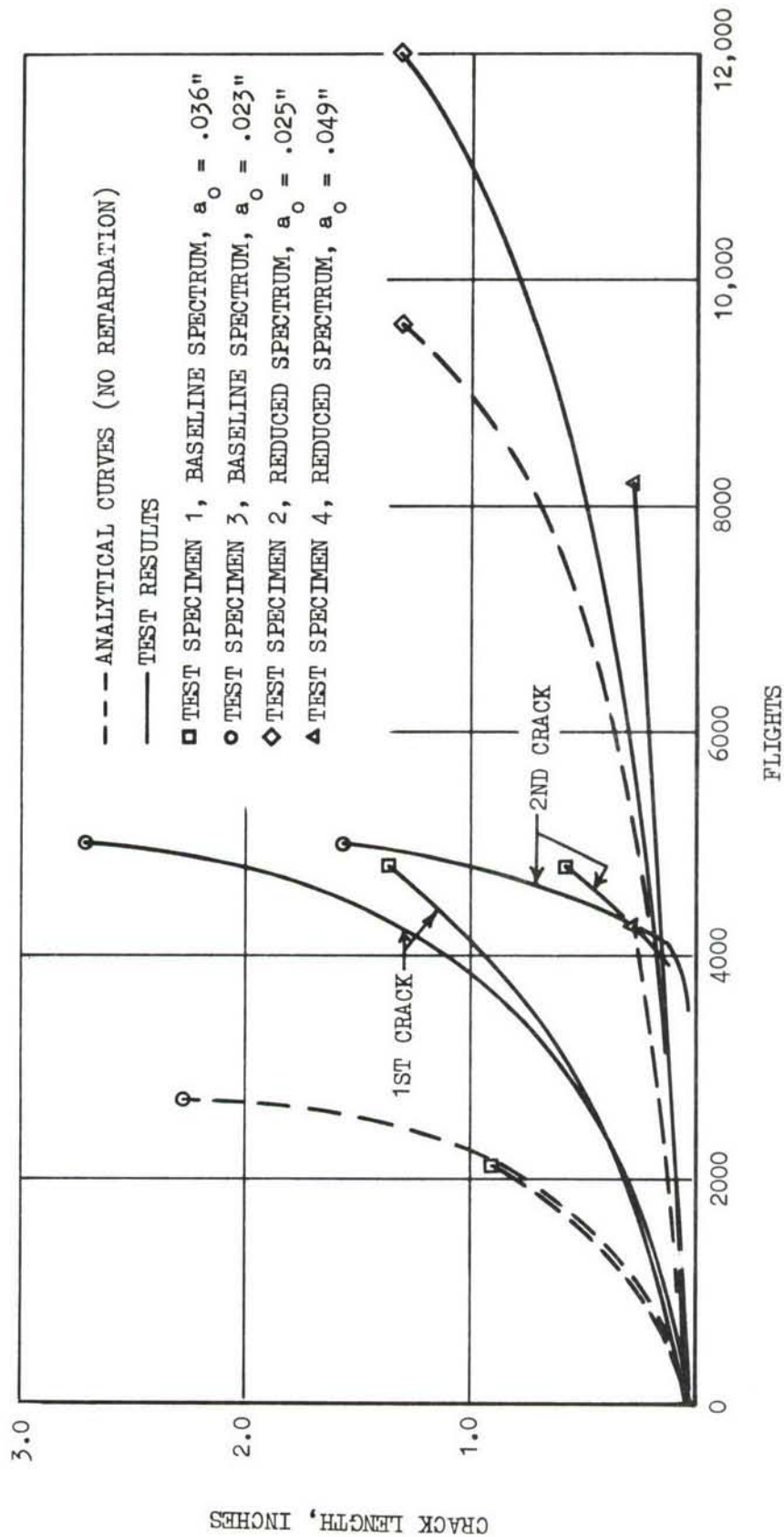


FIGURE 173 RETARDATION TEST EVALUATION  
7075-T6511 ALUMINUM

design case. However, Figure 173 shows that considerable scatter occurred in the tests at the lower design stress level. Some of the variation in these results can probably be attributed to the fact that one of the specimens tested at the lower design stress level was made from a different extrusion than that of the other specimens tested. For example, later phases of the criteria sensitivity study show a very wide variation in the safe crack-growth period based on the range of scatter reported in crack-growth rate data for the baseline material. Results of these assessments are shown in Figure 176. The influence of variations in initial flaw size was also considered later in this work with pertinent results shown in Figure 182. It can be seen that the safe crack-growth period is not greatly influenced by a change in initial flaw size from 0.025 inch to 0.050 inch. The relative position of the experimental curves for the reduced load spectrum would tend to indicate that in this case the scatter effects overshadowed the influence of variation in initial flaw size. In any case, the significant observation to be drawn from this phase of the study is that the crack-growth retardation demonstrated relatively low level and narrow range under these conditions. Since the criteria sensitivity is being assessed on the basis of conditions which pertain to the baseline lower surface in the wing root area, the directly applicable life extension factor of 1.76 was used in the determination of all safe crack-growth periods.

The results described above were used to evaluate the effects of variations in fracture properties on life and allowable design stress. Figure 174 illustrates the influence of a variation in  $K_c$  values on the design functions. Typical crack-growth rate data were used in the analysis, and crack-growth retardation effects were included. Existing data indicate an average  $K_c$  for this case of  $69 \text{ KSI-IN}^{1/2}$  with a lower bound of  $48 \text{ KSI-IN}^{1/2}$ . Assuming a symmetrical variation, the upper bound would be on the order of  $90 \text{ KSI-IN}^{1/2}$ . At a constant life equal to the depot level inspection period ( $F_{DM}$ ), the allowable design stresses corresponding to the lower bound, average, and upper bound are 38.0 KSI, 40.8 KSI, and 42.1 KSI, respectively. The influence on safe crack-growth life, based on 40.8 KSI, i.e., the design stress for an average  $K_c$ , shows that the predicted life for the lower bound  $K_c$  is 2550 flights, and 3610 flights for the upper limit  $K_c$ . At the average  $K_c$ , the safe life is, of course,  $F_{DM}$ , or 3270 flights. A separate investigation considered the effects of changes in the crack-growth rate data with an average  $K_c$  value used in the analysis. Figure 175 shows the range of the rate data considered in the study. The selection of the 6 to 1 range for the maximum



W.S. 77.7 LOWER SURFACE  
7075-T6511 ALUMINUM  
RETARDATION FACTOR = 1.76

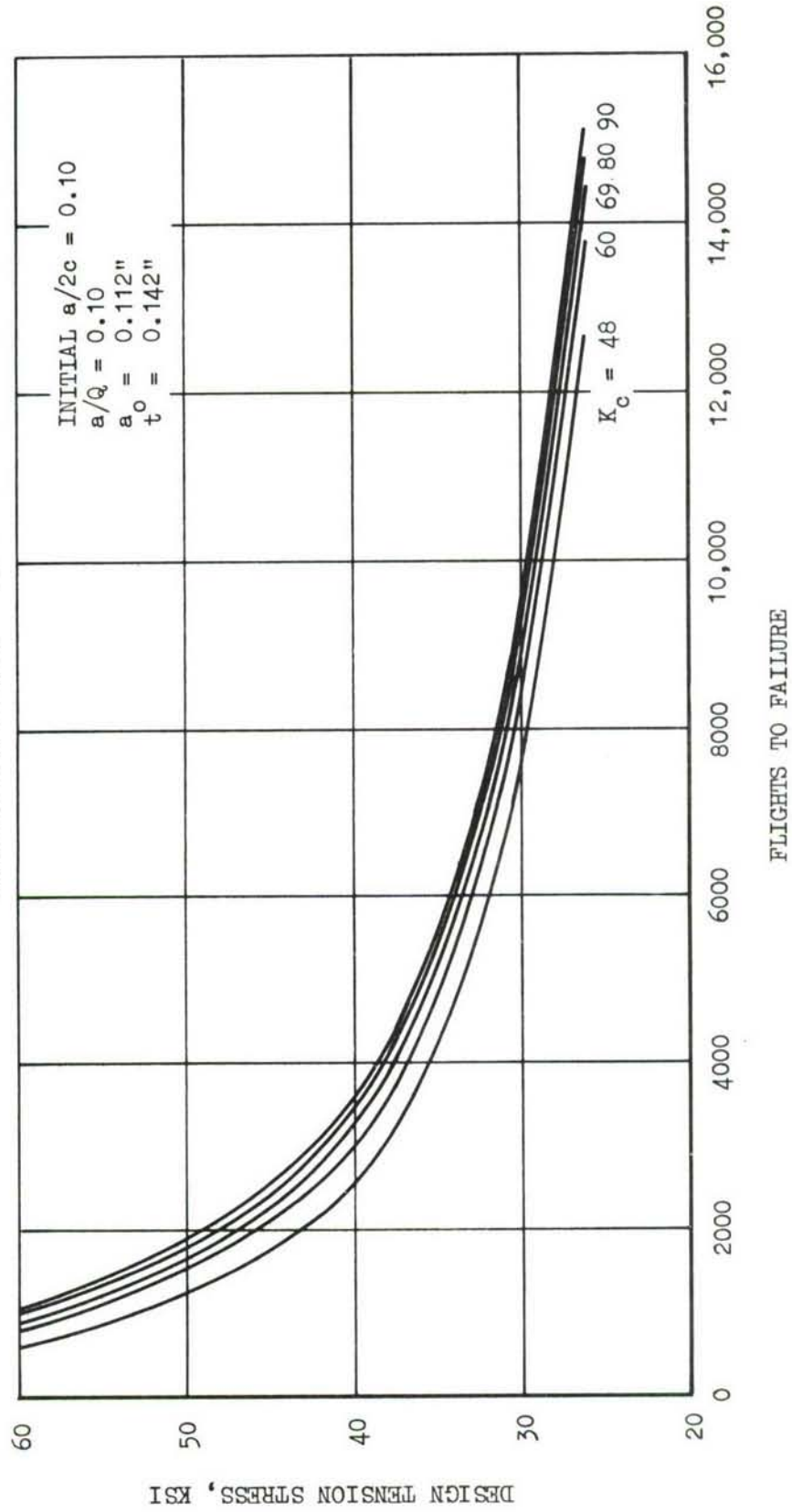


FIGURE 174  $K_c$  VARIATION EFFECT



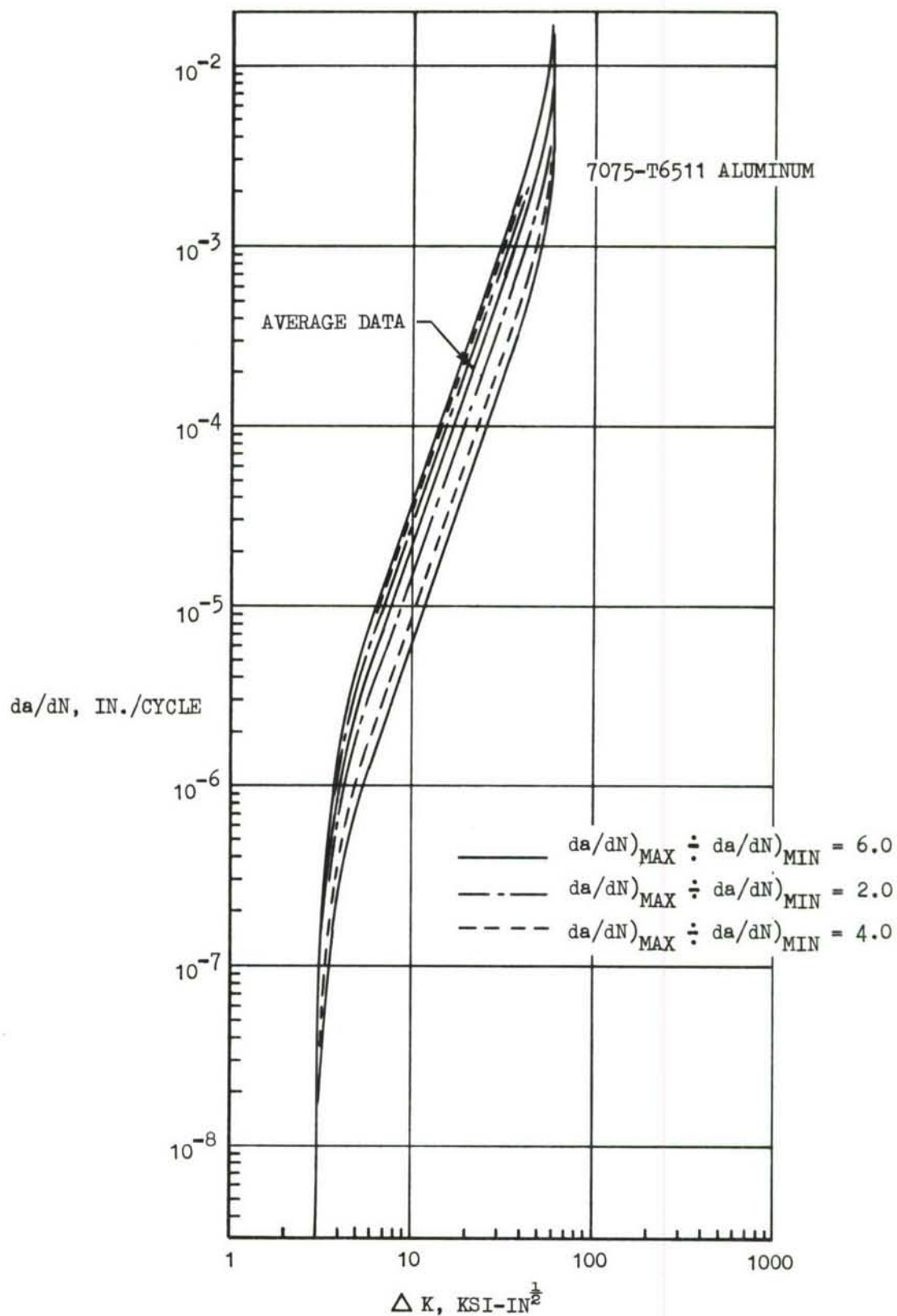
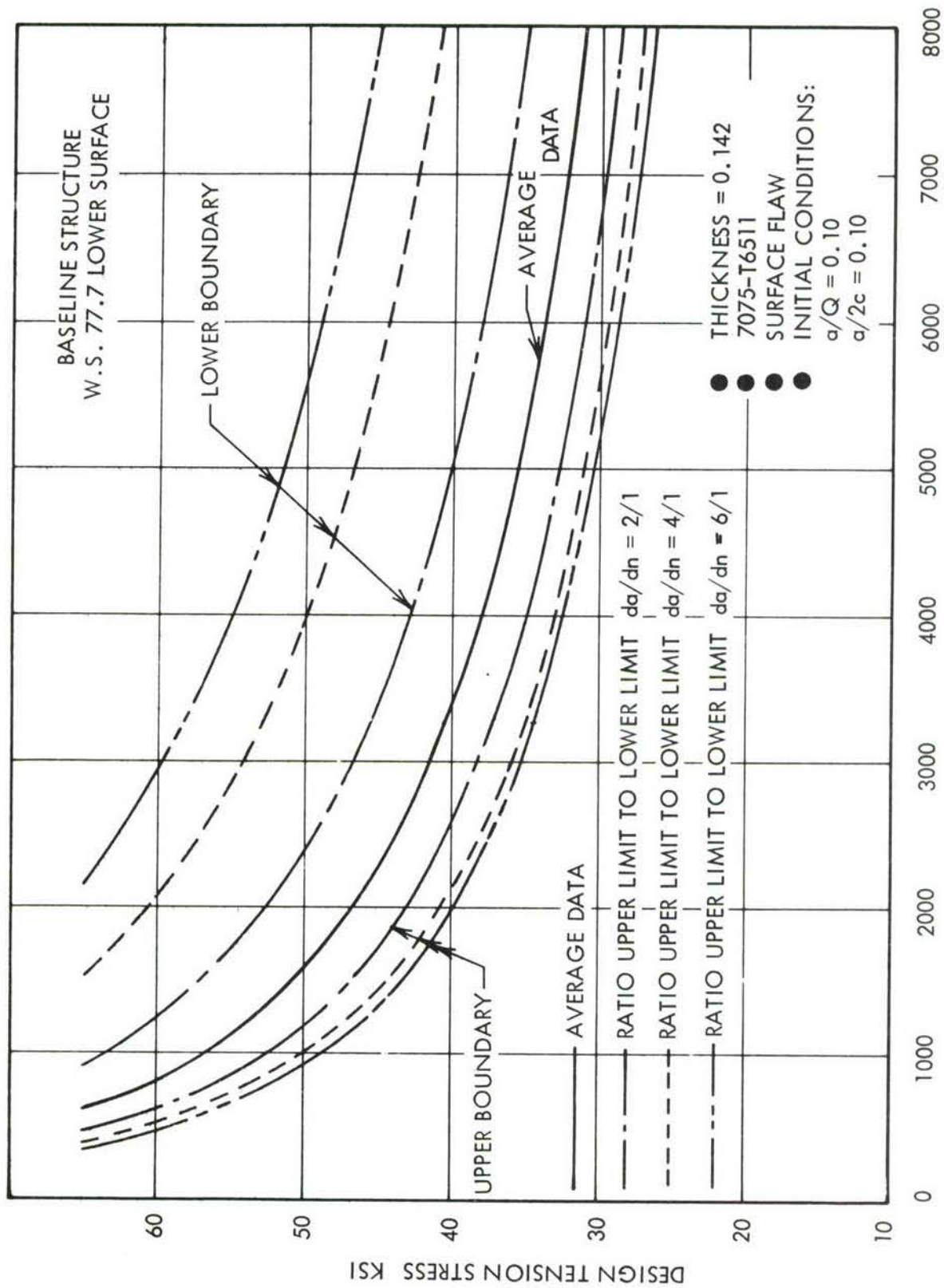


FIGURE 175  $da/dN$  VARIATION DATA

FIGURE 176 EFFECT OF SCATTER IN  $da/dN$  DATA

BASELINE STRUCTURE  
W.S. 77.7 LOWER SURFACE

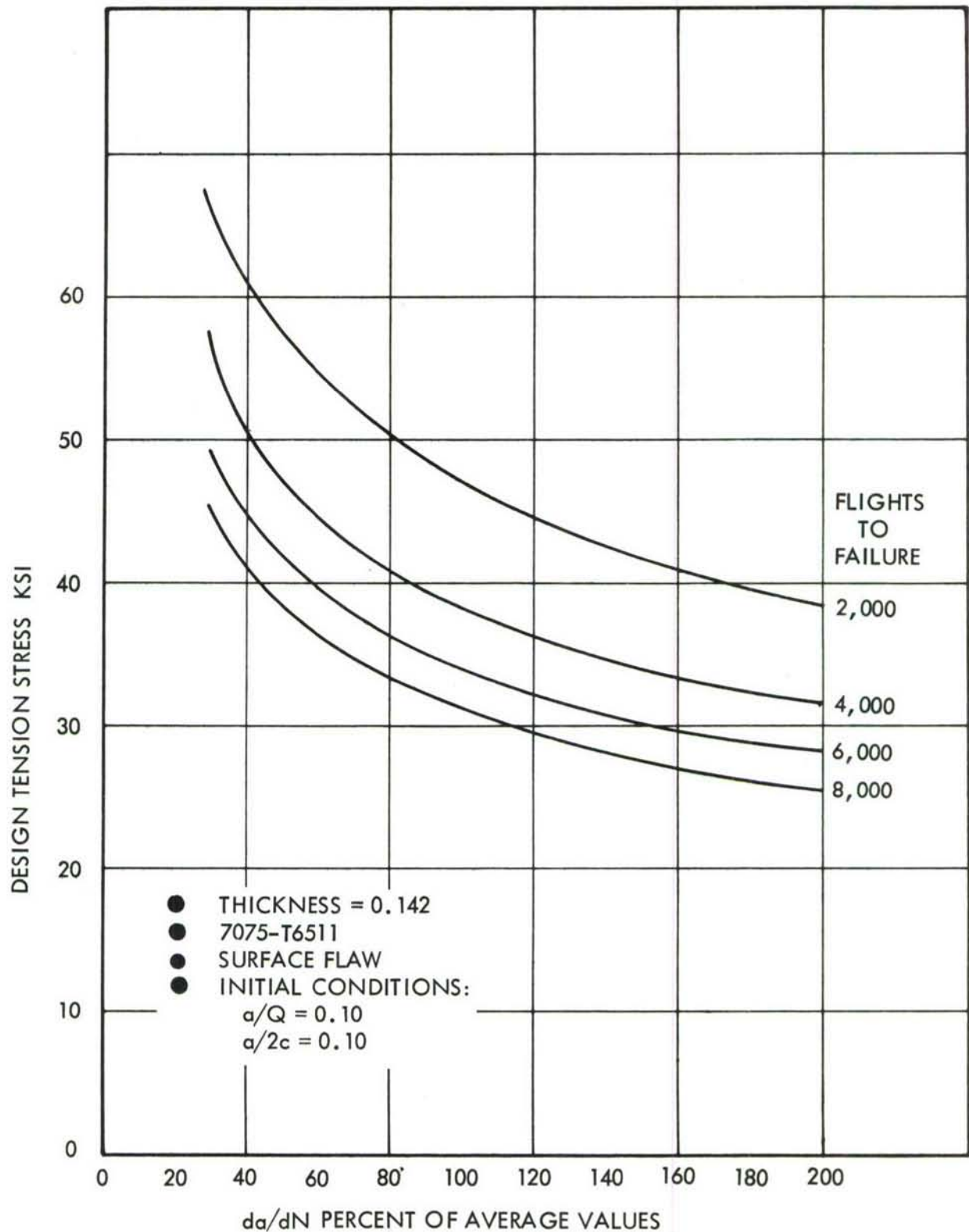


FIGURE 177 EFFECT OF SCATTER IN  $da/dN$  DATA FOR CONSTANT LIFE

variation in crack-growth rate was based on information reported in Reference 12. Results of analyses using each of the rate curves are shown in Figure 176. Again considering the  $F_{DM}$  period, the allowable design stresses associated with the upper extreme rate, average rate, and lower extreme rate data are 34.3 KSI, 40.8 KSI, and 58.0 KSI, respectively. The corresponding life variation, based on the design stress for average crack-growth rate data, indicate a life of 1880 flights for the upper extreme rate data and more than one lifetime for the lower extreme rate curve. For the average data, the safe life is  $F_{DM}$ , or 3270 flights. The results shown in Figure 176 are replotted in Figure 177 to indicate directly the influence of crack-growth rate data on allowable design stress for constant life requirements.

On the basis of the extreme limits of the variation in fracture properties considered in the above analyses, the crack growth rate variation has the greatest impact on the safe crack-growth period.

### A3.2 SPECTRUM SEVERITY

C-141 service airplane tracking program data were used to evaluate the range of severity in the usage of the baseline airplane. The tracking program provides the necessary information to monitor analytically the accumulation of fatigue damage of each airplane by tail number. These results are updated on a regular basis, and the calculated cumulative fatigue damage is tabulated in terms of the logged flight hours and full-stop landings. Plotted data, in the form of accumulated fatigue damage for individual airplanes as a function of accumulated flight hours and, separately, as a function of accumulated full-stop landings, enable the development of histograms which define the range of usage severity monitored on the basis of flight hours or full-stop landings. Histograms of this type were developed, and these are shown in Figures 178 and 179. The more critical range of the fatigue damage distribution based on flight hours was selected for the spectrum severity sensitivity analysis.

Table XLIII presents a tabulation of the average usage spectrum for the baseline airplane wing root area. From the results shown in Figure 178, it was concluded that operational C-141 airplanes experience a usage severity range extending from 25 percent more severe to 20 percent less severe than the average usage spectrum. To



W.S. 77.7 LOWER SURFACE

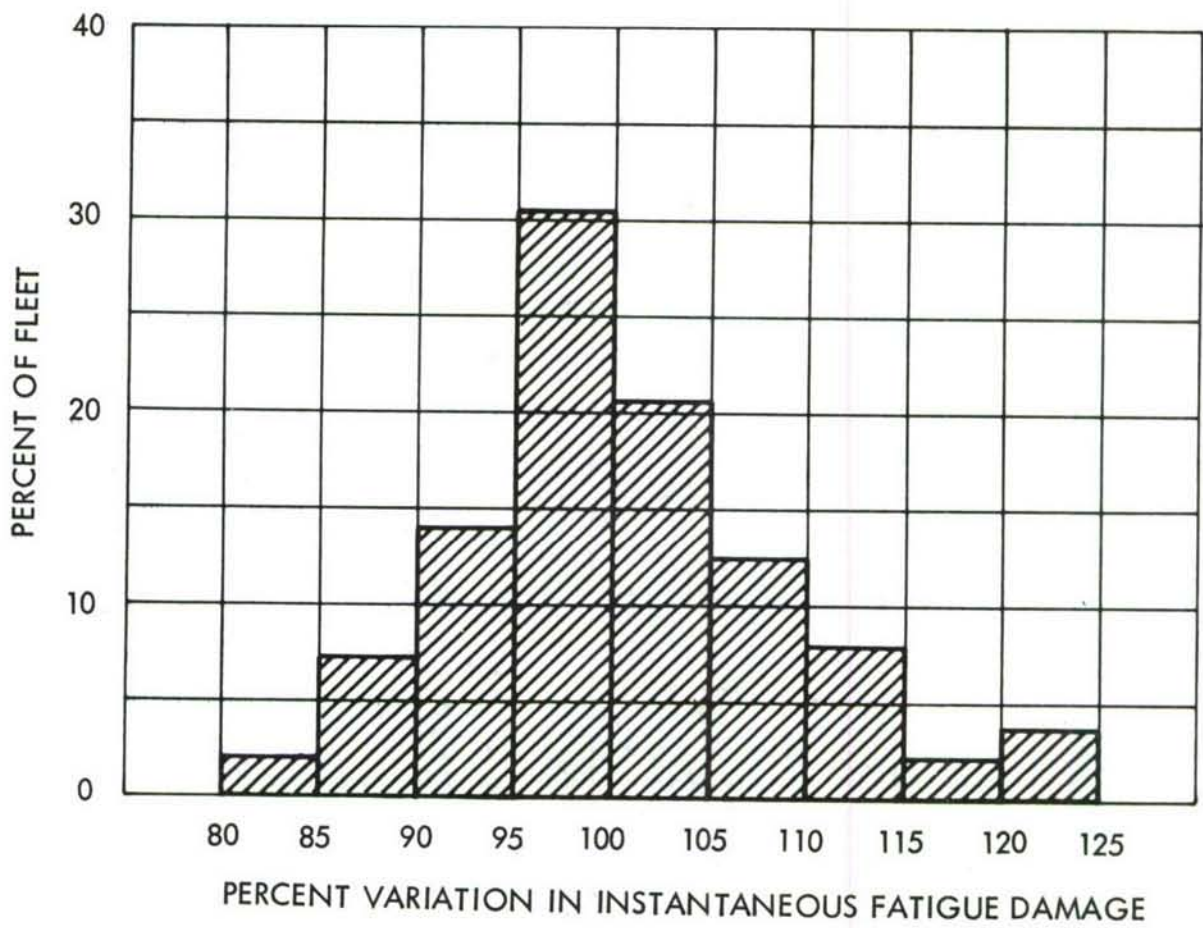


FIGURE 178 VARIATION IN FATIGUE DAMAGE BASED ON FLIGHT HOURS

W.S. 77.7 LOWER SURFACE

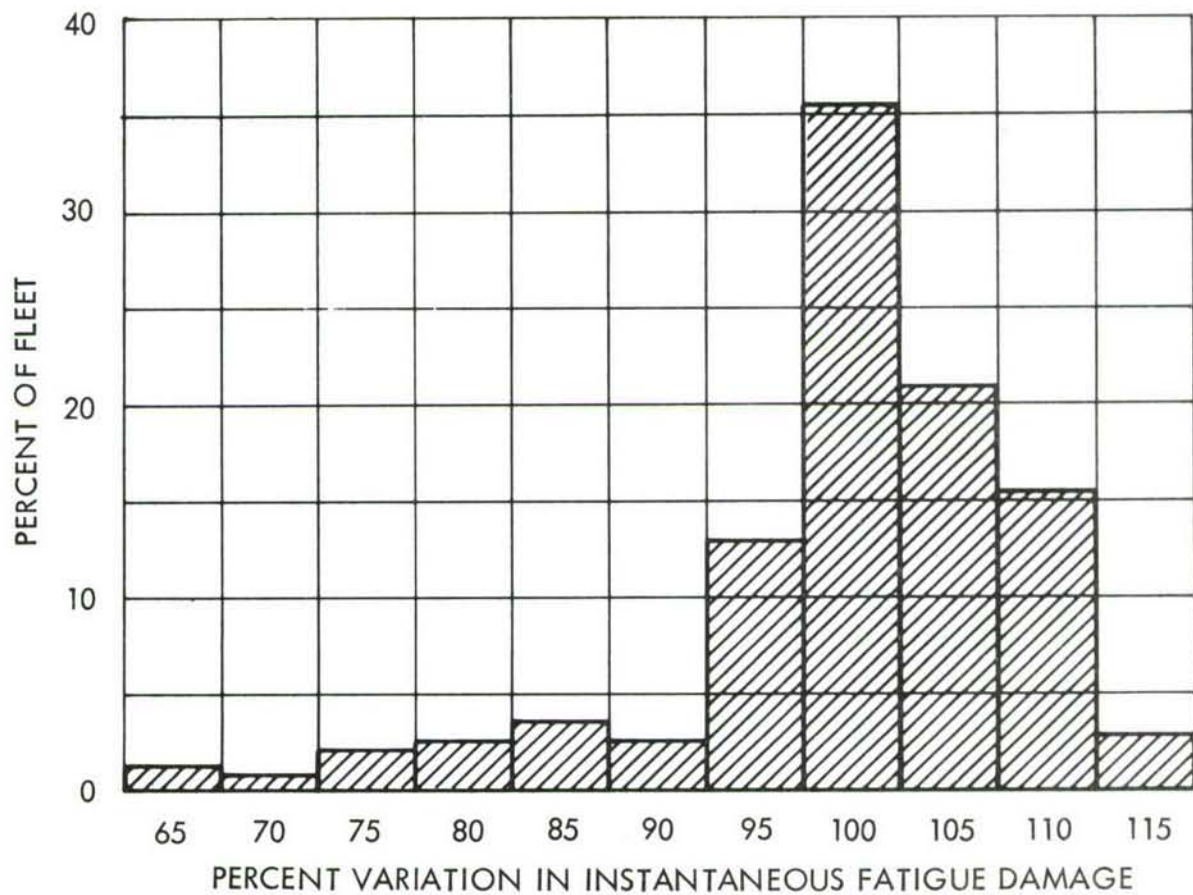


FIGURE 179 VARIATION IN FATIGUE DAMAGE  
BASED ON FULL STOP LANDINGS

TABLE XLIII  
BASELINE LOAD SPECTRUM

C-141 W.S. 77.7 (WITH PEAK-TO-PEAK GAG)  
CARGO/TANKER ADP - TEST AND ANALYSIS SPECTRA

SOURCE	CYCLES PER		*M <sub>x</sub> , In.-lbs. x 10 <sup>6</sup>	
	30,000 HRS.	FLIGHT	MAXIMUM	MINIMUM
Taxi 1A	461,800	56.4065	-33.879	-27.813
1B	17,280	2.1107	-36.033	-25.659
1C	690	.0843	-38.538	-23.154
1D	30	.0037	-41.242	-20.450
2A	15,630	1.9091	-24.241	-15.363
2B	540	.0660	-26.373	-13.231
2C	30	.0037	-29.077	-10.527
GAG	8,187	1.0000	28.872	-36.140
TAG	5,595	.6834	13.863	- 9.369
Gust 4A	199,600	24.3801	26.419	15.502
4B	2,370	.2895	31.790	10.131
4C	30	.0037	41.594	.328
5A	81,600	9.9670	19.214	6.332
5B	7,900	.9649	22.031	3.515
5C	470	.0574	26.201	- .656
5D	30	.0037	31.769	- 6.223

\*Note: To obtain baseline stress spectrum, multiply loads by  
stress/load ratio = +468 psi/in. lbs. x 10<sup>6</sup>.

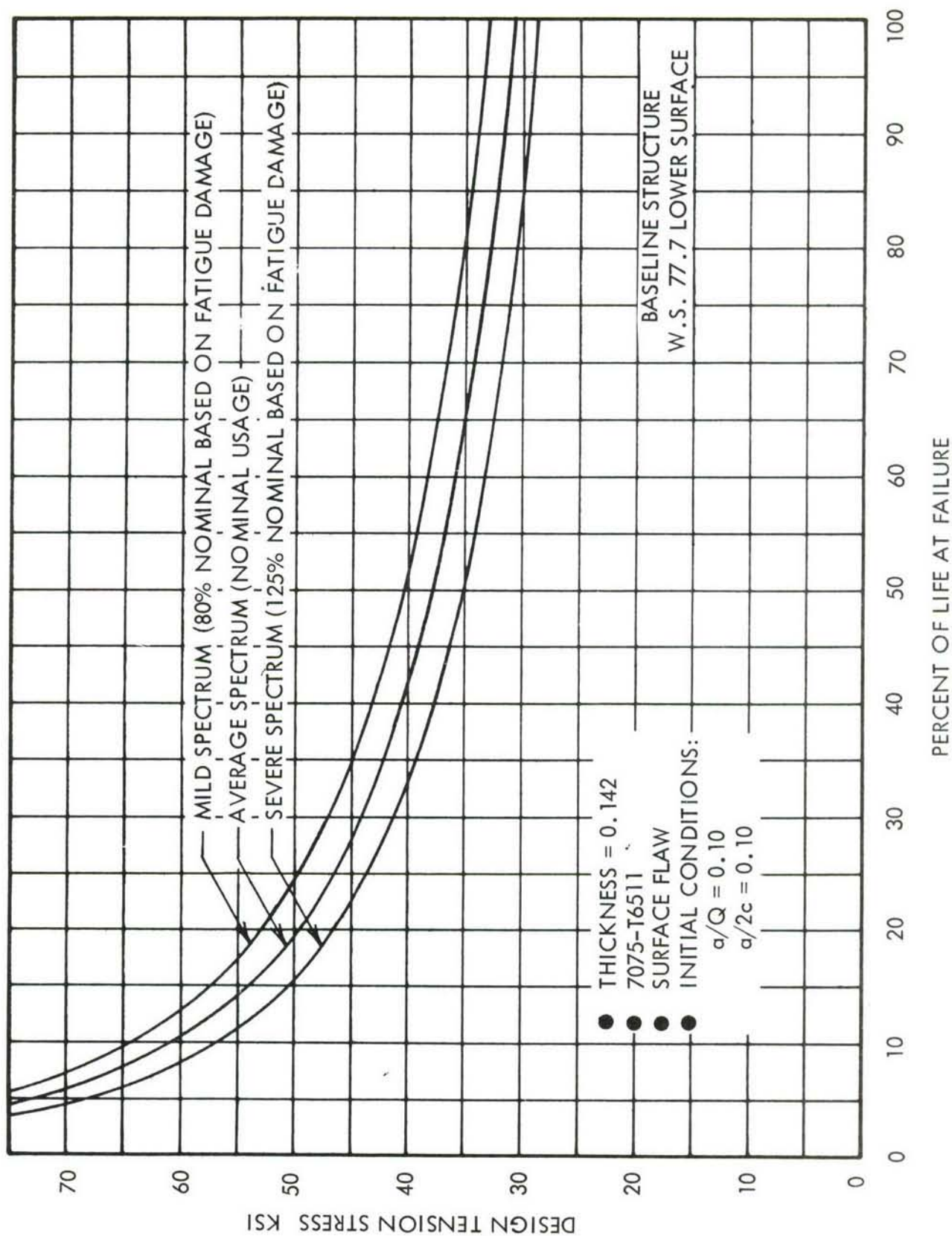


FIGURE 180 EFFECT OF SPECTRUM SEVERITY ON LIFE



reflect this variation in the sensitivity analysis, the number of cycles at each load level in the average usage spectrum was modified in direct proportion to the desired adjustment in spectrum severity. This procedure results in the preservation of the spread in the accumulated fatigue damage observed in the C-141 fleet. Table XLIV shows the modified spectra for mild and severe airplane usage. In terms of operations, the adjustment in spectrum severity can be associated with the variation in the average time per flight, which in turn affects the number of landings and the time spent at lower altitudes where gust occurrences are more prevalent.

Average material fracture properties were used in the development of the results presented in Figure 180. The data shown describe the influence of spectra severity on design stress and life. For example, at  $F_{DM}$ , which is 3270 flights, or 40 percent of 1 lifetime, the allowable design stresses for the severe, average, and mild spectrum are 37.8 KSI, 40.8 KSI, and 43.2 KSI, respectively. On the basis of the design stress level for the average spectrum, the corresponding spread in life was from 2590 flights for the severe spectrum to 4030 flights for the mild spectrum.

### A3.3 INITIAL FLAW SIZE

The influence of assumed initial flaw size on design stress and life was assessed on the basis of average data for material properties and airplane usage. Three types of flaws were considered: surface flaws, through cracks emanating from a hole, and corner cracks emanating from a hole. The latter two cases were for cracks growing out of only one side of the hole. The range of flaw sizes considered in this phase of the sensitivity study were specified by the Air Force.

Analysis results for the surface flaw are shown in Figure 181. For an initial  $a/2c$  of 0.10, the specified  $a/Q$  range is such that the fatigue crack growth originates from a part-through crack in all cases. The results reflect the period required for the crack to penetrate the panel thickness and grow as a through-the-thickness crack to an unstable crack length. Figures 182 and 183 show similar results for the cases where cracks grow from holes. Detail geometry relevant to these analyses is shown in the figures.

On the basis of the conditions analyzed, it is immediately obvious that the greatest impact on design stress and life is associated with the  $a/Q$  variation considered in the surface flaw analysis. The results for cracks emanating from holes show a much

TABLE XLIV  
MODIFIED LOAD SPECTRUM

C-141 W.S. 77.7  
(PEAK-TO-PEAK GAG)

SOURCE	CYCLES PER FLIGHT		*M <sub>x</sub> <sup>1</sup> , IN.-LBS. $\times 10^6$	
	MILD SPECTRUM	SEVERE SPECTRUM	MAXIMUM	MINIMUM
Taxi 1A	45.1252	70.5081	-33.879	-27.813
1B	1.6886	2.6384	-36.033	-25.659
1C	0.0674	0.1054	-38.538	-23.154
1D	0.0030	0.0046	-41.242	-20.450
2A	1.5273	2.3864	-24.241	-15.363
2B	0.0528	0.0825	-26.373	-13.231
2C	0.0030	0.0046	-29.077	-10.527
GAG	0.8000	1.2500	28.872	-36.140
TAG	0.5467	0.8542	13.863	-9.369
Gust 4A	19.5041	30.4751	26.419	15.502
4B	0.2316	0.3619	31.790	10.131
4C	0.0030	0.0046	41.594	0.328
5A	7.9736	12.4588	19.214	6.332
5B	0.7719	1.2061	22.031	3.515
5C	0.0459	0.0718	26.201	-0.656
5D	0.0030	0.0046	31.769	-6.223

\*Note: To obtain stress spectrum, multiply loads by stress/load ratio =  
+ 468 psi/in.-lbs.  $\times 10^6$ .

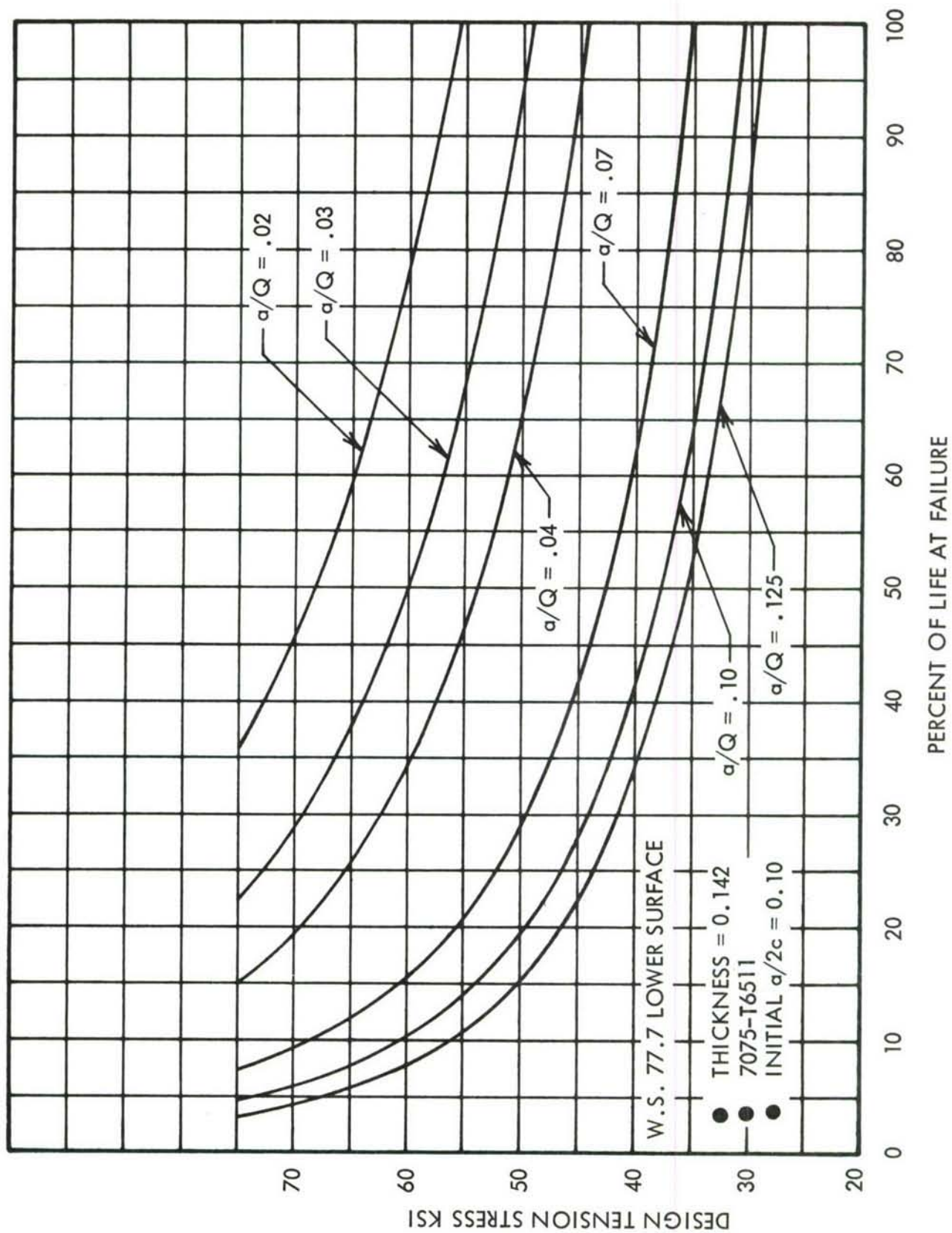


FIGURE 181 EFFECT OF INITIAL  $a/Q$  ON LIFE, SURFACE FLAW



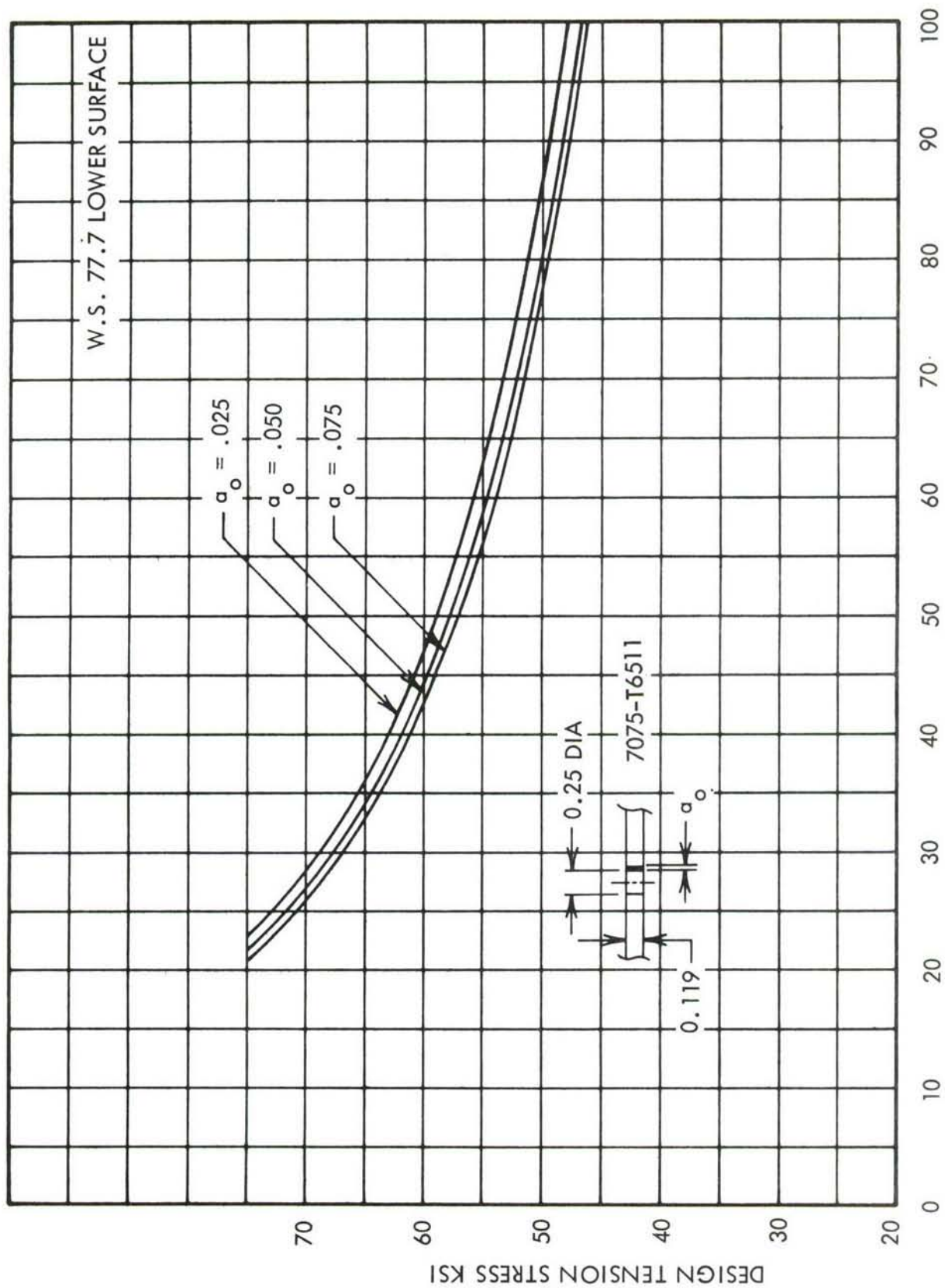


FIGURE 182 EFFECT OF INITIAL CRACK SIZE ON LIFE THROUGH CRACK EMANATING FROM A HOLE



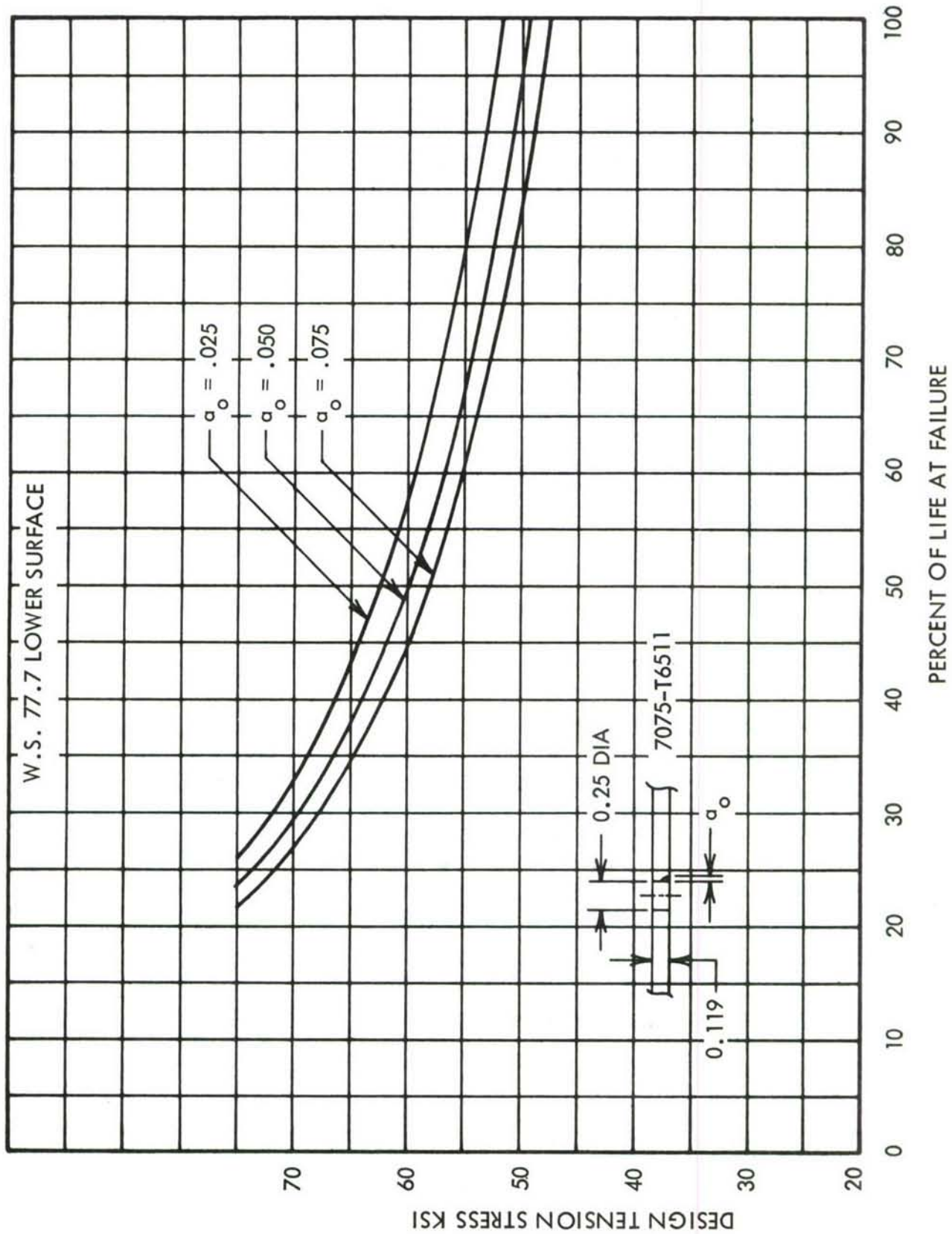


FIGURE 183 EFFECT OF INITIAL CRACK SIZE ON LIFE -  
 CORNER CRACK EMANATING FROM A HOLE

smaller effect for the range of assumed initial flaw sizes. A comparison of the results shown in Figures 182 and 183 further indicates that, in these cases, the level of influence on the design functions is of the same general order, particularly as the size of the corner flaw approaches the thickness dimension of the panel. For the smaller flaws at the edge of the hole, the corner crack is less severe than the through crack. Some of the trends shown in this study were also observed in the design analyses. For example, the  $a/Q$  of 0.10 in Figure 181 and the  $a_o$  of 0.050 in Figure 182 are the initial flaw sizes specified in the criteria for slow crack growth structure. At 40 percent of 1 lifetime,  $F_{DM}$ , the allowable design stresses are 40.8 KSI and 61.9 KSI for the respective flaw sizes. It can be seen that the surface flaw requirement governs the design in this case.

#### A3.4 THERMAL AND CHEMICAL ENVIRONMENT

The baseline airplane is subjected primarily to ambient temperature conditions ranging from  $-65^{\circ}\text{F}$  to  $160^{\circ}\text{F}$ . These conditions also apply to the inner wing structure, since high-temperature gases from the engines and APU do not impinge directly on the wing box surface. Therefore, thermal effects on the baseline structure are considered a second-order influence which can be included in a general assessment of the environmental spectra.

The predominant material used in the C-141 baseline wing structure is 7075-T6 aluminum, although limited applications of 7178-T6 aluminum occur in portions of the rib structure. Considering the use of these high strength but corrosion susceptible materials in the corrosion prone wing box structure, the design has a remarkably good corrosion resistance record; no serious corrosion problems have been reported during nine years of service. During this time the structure has been exposed to such varied chemical or corrosive environments as salt spray, salt water, engine exhaust gases, microbial contaminated fuel, sand, ultraviolet light, and full-strength cleaning chemicals called for in maintenance cleaning Technical Orders. This excellent record is attributable to several measures taken during design and manufacture to minimize corrosion problems in service. These include:

- o Optimum extrusion material utilization for minimum section thickness
- o Jogging wing joint pad areas for improving grain flow
- o Shot peening
- o Sulfuric acid anodizing
- o Use of MIL-C-27725 polyurethane integral fuel tank coating containing a biocidal additive
- o Fay surface sealing and wet installation of fasteners
- o Excellent water drainage from fuel tanks
- o Acrylic nitrocellulose lacquer exterior finish system.

Although the operational performance of the inner wing box structure has been generally satisfactory, with no overall corrosion problems of significance, fretting corrosion has occurred in local areas. These problems have been associated primarily with access door installations and with leading-edge rib caps.

The door problems involved the support flanges on upper surface panels where some fretting as well as exfoliation corrosion occurred. In some cases this caused cracks to emanate from fastener holes as a result of intergranular corrosion. Correction of this situation was accomplished in a modification program which incorporated several improvements. First, an improved tapered-sleeve dome nut was incorporated in the panel structure around the personnel access doors as a replacement for existing standard nut plates. This interference sleeve provides definite fatigue enhancement of this critical area of the structure. Second, a polyurethane finish was applied to the door support flanges in the panel, and all rivets and dome nuts were installed with corrosion-inhibitive sealant. Finally, a cast-in-place door seal was incorporated to improve sealing against moisture. With this modification, corrosion around access doors is no longer a maintenance problem.

Fretting corrosion in the leading-edge rib cap area continues to be of concern from the maintenance standpoint. These caps, which are made from extruded 2024-T6 aluminum tee sections, rub against the leading-edge assemblies made of epoxy impregnated glass cloth laminates. Rib caps were originally painted with epoxy primer, Specification MIL-P-23377; however, considerable improvement was obtained when



the finish of the fretting surface was changed to a coating of MIL-L-46147 solid-film lubricant. There has been no cracking associated with fretting in these areas, although severe pitting has occurred.

The performance of the baseline structure with respect to the thermal and chemical environmental spectra encountered by the service airplanes has been satisfactory, but even better performance can be achieved in ADP designs through the use of the overaged tempers of advanced materials, manufacturing control, and improved sealants and finishes.

### A3.5 PROOF TESTING

The strengths and limitations of proof testing can be assessed from the standpoint of production quality control or an in-service inspection function. In either case, a number of factors which are dependent on the desired objective of the test must be considered in the evaluation of the role of proof testing. The type of structure and loading characteristics also enter into these assessments. For example, proof testing of pressure vessel shells can provide useful information through leak detection. All Lockheed-Georgia transport aircraft fuselage assemblies are proof-pressure-tested on the production line to a load level corresponding to limit design pressure. The purpose of this test is to verify that maximum permissible leakage rates are not exceeded, and to substantiate that no catastrophic deficiencies are present. Proof load testing for quality control purposes is also performed on welded assemblies. Similar tests are conducted on a sampling basis on ground support equipment. In general, the assemblies selected for proof loading have single source loading or simple loading systems which permit these tests to be conducted on a cost-effective basis.

The complex loading conditions that control wing box assembly designs make proof load testing of this type of structure somewhat more difficult and more costly. However, critical subassemblies, such as forged or machined fittings, can be economically proof tested on a production basis. In the case of the baseline structure, a form of proof testing is a fallout of the material production process. The material



used in the wing cover undergoes post-extrusion stretching on the order of 1.5% to 3.0% permanent set to relieve residual stresses. This process is, in effect, a proof test of the integrally stiffened wing panels prior to machining and assembly. On the basis of the yield stress level, surface flaws with an  $a/Q$  as low as 0.036 are "proofed out" under these conditions.

As indicated in the above discussion, the underlying purpose of these tests has been a general quality-control measure. The assessment of results under these conditions is on a go-no go basis. However, experience gained in this area is directly applicable to one aspect of proof testing within the broader context of damage tolerance technology. On the basis of fracture analyses, proof-test load levels can be selected to determine theoretical thresholds of maximum flaw sizes in specific areas upon successfully sustaining the proof-test load. Flaws that exceed the threshold size in a local area would theoretically result in unstable crack growth during proof test.

An expansion of the proof-test concept involves additional fracture analyses where safe crack-growth periods, subsequent to proof tests, are determined on the basis of the threshold flaw sizes. The role of proof testing on the broader scale of the damage tolerance criteria is highly analytical and is very dependent on the detail design and operating stress levels in the structure. Figure 184 presents the results of analysis for proof-test considerations in a local area of the baseline structure. The analysis is concerned with potential surface flaw occurrences in the lower surface wing root area. Flaws are assumed to have an initial  $a/2c$  of 0.10, and baseline design stress levels are used in the parametric assessment.

The tabulated values in the figure are the proof load levels considered in the study, and the corresponding critical flaw sizes for the statically applied loads. Proof load levels are listed as a percent of design limit load. If flaw sizes in excess of the calculated critical size are present, unstable crack growth will occur during the proof load test. The successful completion of the proof test is considered a substantiation that flaw sizes in excess of the calculated critical size do not exist in the area of the structure in question. Safe crack-growth periods can, therefore, be

W.S. 77.7 LOWER SURFACE  
7075-T6511 ALUMINUM  
RETARDATION FACTOR = 1.76

DESIGN STRESS = 52.4 KSI  
LIMIT STRESS = 34.6 KSI  
 $t = .142$   $F_{ty} = 71.0$  KSI  
INITIAL  $a/2c = .10$

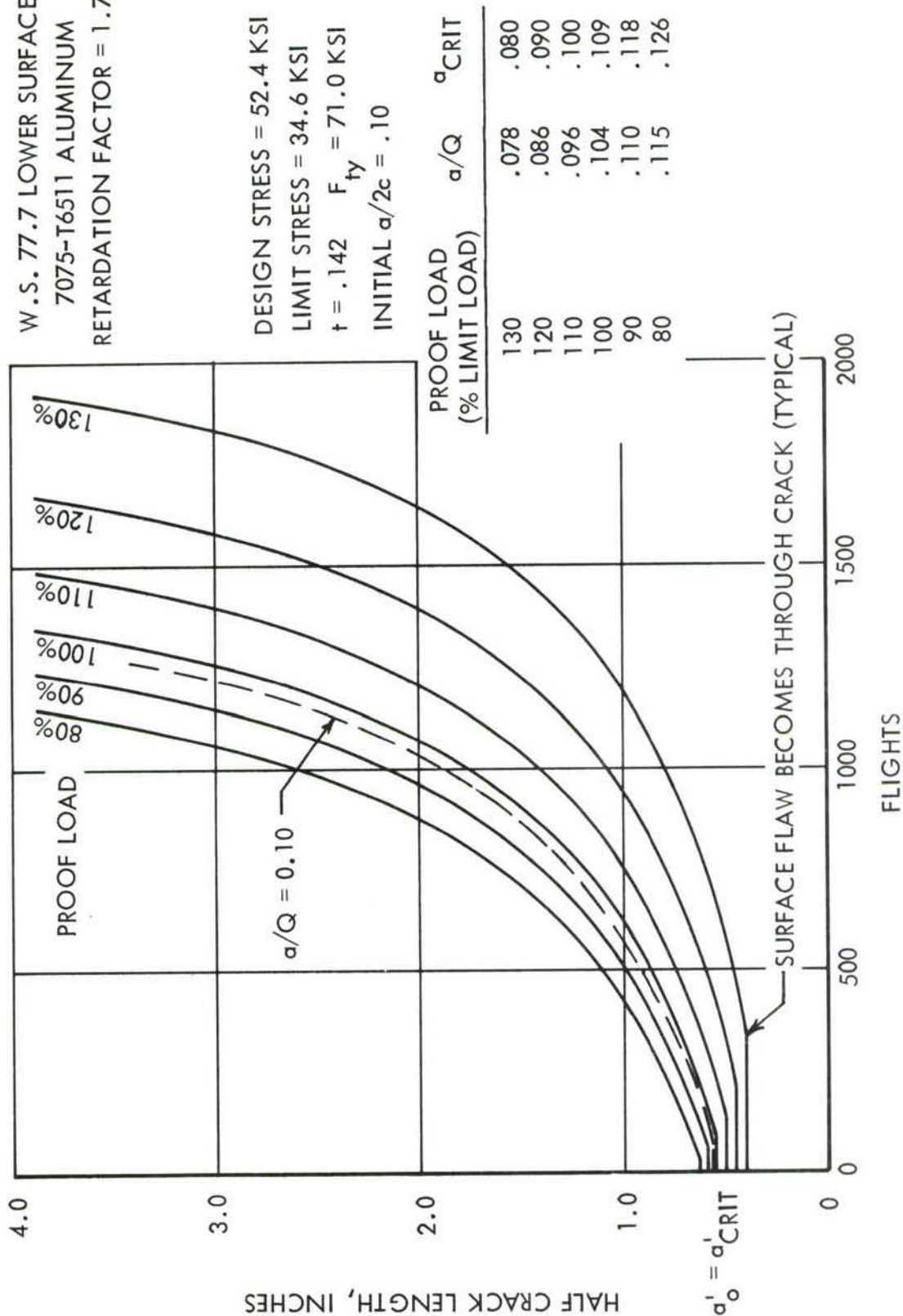


FIGURE 184 PROOF LOAD VARIATION

based on the maximum flaw size that could have been present in the structure during proof test without causing failure. Crack-growth analyses were performed using initial flaw sizes based on the proof load level. These results are also shown in Figure 184. In addition, the crack-growth curve based on the flaw size data in the fracture criteria is shown for reference purposes.

Inspection of the results show that a proof load on the order of 96 percent of design limit load would be required to verify that flaw sizes in excess of the criteria value are not present in the structure. At the actual design stress level, the safe life, based on an  $a/Q$  of 0.10 and an initial  $a/2c$  of 0.10, is 1316 flights. Proof testing to 80 percent of design limit load would provide assurance of a remaining safe crack-growth life of 1155 flights. Proof loads of 100 percent and 120 percent of limit load would substantiate residual safe crack-growth lives of 1351 flights and 1674 flights, respectively. Although proof load tests at load levels in excess of design limit load are not being recommended, it should be noted that, even at 130 percent of limit load, the yield stress of the material is not exceeded in the area under analysis.

In conclusion, proof testing may be considered a supplement to NDT and not a replacement. The complex loading system of wing structure and design strength envelopes make proof testing of a wing box a costly inspection procedure. The downtime required to perform the proof test on operational aircraft would also adversely affect the performance of the operating force.



## A3.6 NDT DEMONSTRATION PROGRAM

### A3.6.1 Needs for an NDT Demonstration Program

When structural design philosophies are predicated on fracture and fatigue considerations, quantitative evaluations must be made of maximum defect sizes which could escape detection. A properly designed NDT demonstration program which measures the degree of success attainable in detecting flaws, based on sufficient statistical data, will provide these quantitative values.

Alternatively, an NDT Demonstration Program would be less important if the detection of small defects has no significance; i.e., detection of a 0.25" long fatigue crack would not require immediate repair, for example. Such may be the case for properly designed multiple-load-path structure.

### A3.6.2 Methods for Conducting an NDT Demonstration Program

A demonstration of NDT capabilities requires consideration of production inspection of detailed parts and in-service inspection of built-up structure. The number of data samples should be large enough to yield statistically significant results to attain a desired level of confidence. The program should also aim toward the measurement of detection probabilities and not the resolution or size assessment capabilities of various NDT techniques. Consideration should be given to the fact that some NDT methods are more responsive to total flaw area, while some are predominantly sensitive to depth or length. The probability of detection is generally influenced by a number of factors, including: (i) access to the area to be inspected; (ii) inspection time/area; (iii) inspection method; (iv) standards and calibration techniques; (v) defect character and size, i.e., surface crack, inclusion, etc.; (vi) surface shape and condition; (vii) stress at the flaw site; (viii) defect density; (ix) human factors; and (x) material differences.

### A3.6.3 NDI Reliability Demonstration Procedures

#### Specimens and Procedures

Specimen configurations should be representative of production parts but should not be complex. Experience with developing nondestructive inspection techniques for



complex shapes, such as in landing gear yokes or hydraulic shuttle valve bodies where compound curvature is involved, has shown that these shapes are extremely difficult or impossible to inspect with a reasonable degree of confidence. Flat and moderately complex configurations for specimens are recommended where a statistical treatment of data is to be used. If complex shapes were used in specimen design, costs would be high, and the results would be applicable only to a narrow range of configurations. The quantitative translation of results on flat to moderately complex specimens to actual parts of complex shape is not feasible within the existing state of the art. However, an empirical evaluation of inspectability based on the 10 factors listed above should promote the development of quantitative assessments of flaw detection probabilities for a variety of part shapes. For example, inspectability could be established by assigning indices to each of the 10 contributing factors. The composite inspectability index for the specific part in question would be determined as the product of the 10 indices. This index product approach takes advantage of the fact that all factors but one may rule out inspection, thus yielding a very low or zero inspectability. For example, all factors except access to the area to be inspected may be favorable, but inspection is impossible, and the composite inspectability index is zero. A hypothetical three-dimensional plot of detection probability relative to flaw size and inspectability is shown in Figure 185.

The number and types of defects recommended are:

- (i) approximately 30 each in six 0.05" length increments from 0.05" to 0.30" (this is a basic group size);
- (ii) one group of through fatigue cracks and one group of part-through fatigue cracks with  $a/2c = 0.25$ ;
- (iii) through cracks in 0.25" thick specimens, and part-through cracks in 0.50" thick plate or extrusion.

Defects should be adjacent to 1/4-inch diameter holes to allow for simulation of cracks around fasteners.

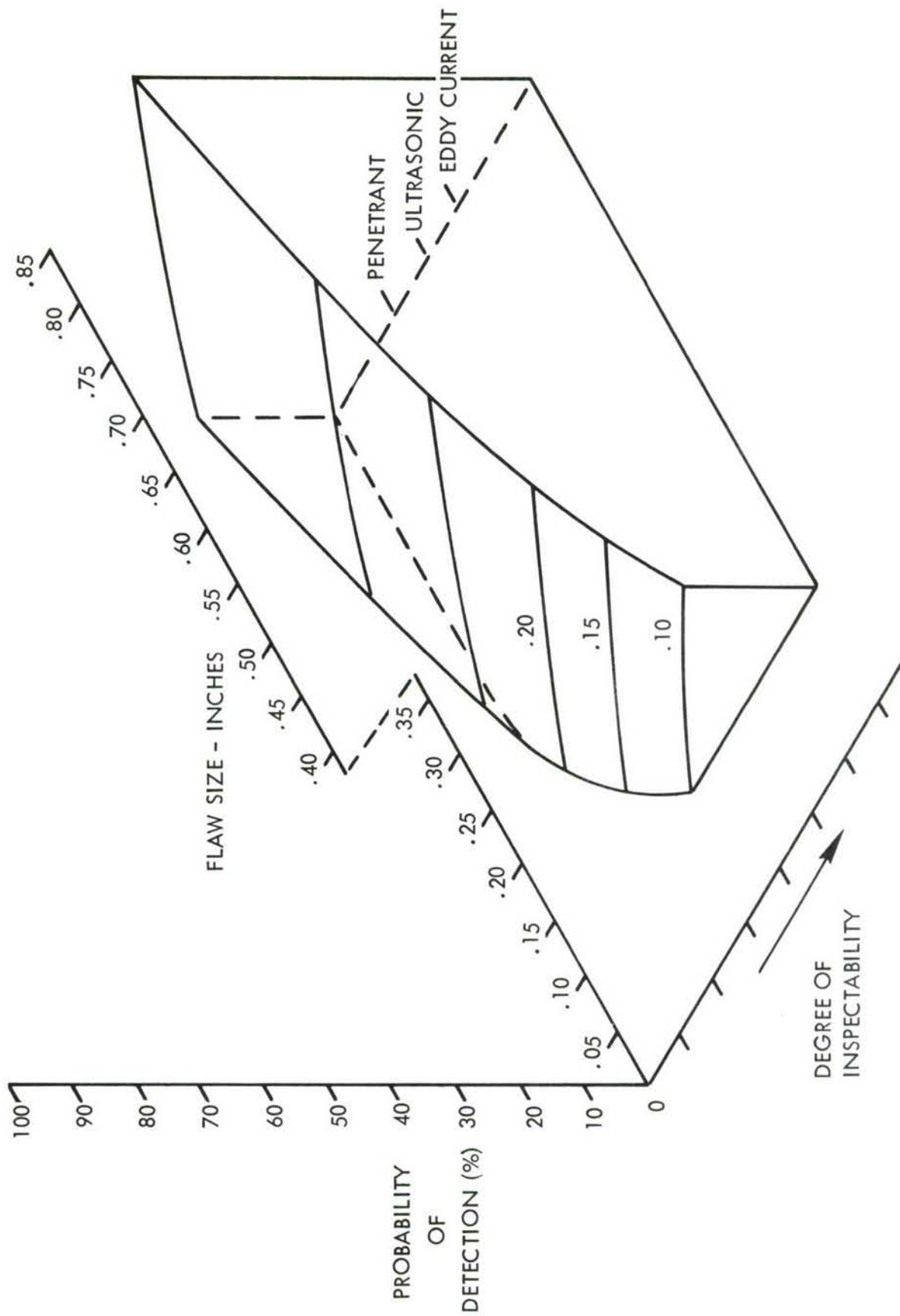


FIGURE 185 HYPOTHETICAL DETECTION PROBABILITY SURFACE

The size increments and total size range in (i) are based on experience in acquiring detection probabilities for fatigue cracks around fasteners in simulated extrusions with an ultrasonic shear-wave technique. The increments were small enough to be practical for optical monitoring during fatigue growth. The choice of through and part-through cracks with  $a/2c = 0.25$  is based on attaining two representative conditions for actual flaws, and attendant conditions for NDT detection. This means that some techniques are predominantly flaw-area-dependent, while others are dependent on flaw length or depth. Table XLV lists NDT techniques and the associated flaw geometry dependence. The choice of the fatigue crack as a flaw type is made because it represents a severe form of defect which is difficult to detect and relatively easy to generate in controlled sizes.

Minimizing operator awareness of the demonstration is best accomplished by assigning the inspection task on a routine work order basis, with dummy part numbers assigned to the demonstration specimens. There is a risk that the specimens may not resemble production parts and, therefore, will attract special attention. This problem can be largely averted if the assignment is made by a test engineering organization which routinely works with experimental component designs.

The problem of assuring representative data with regard to duplicating production conditions, equipment, personnel, and procedures may be handled best by the appropriate NDT request document and procedure in conjunction with explicit instructions for performing the inspection. The mechanism for implementing this type of activity is outlined in the following sequence:

- (i) Critical areas or parts are defined by the engineering stress groups, and the information is transmitted to a fracture control group.
- (ii) The fracture control group determines the size of defects to be found along with the required time of inspection, and transmits this information to a quality assurance group on a nondestructive inspection request document. This document calls out defect size, orientation, location and required NDI time. This procedure is applicable to the inspection of detailed parts and built-up structure.

TABLE XLV  
NDT TECHNIQUE/FLAW GEOMETRY DEPENDENCE

NDT TECHNIQUE	PREDOMINANT FLAW DETECTION FACTOR
X-ray Radiography	Flaw depth, depth percentage of part thickness
Ultrasonic	Flaw area, plane normal to the incident wave propagation
Eddy Current	Flaw length
Penetrant	Flaw length
Magnetic Particle	Flaw length



- (iii) The quality assurance group reviews the NDI requirements and determines the most suitable techniques for detecting the flaw. A procedure is written, and a calibration standard is designed to simulate the flaw.
- (iv) The NDI requirements are transmitted to the inspection group by job assignment with the appropriate NDI procedures document.

It is proposed that the same approach be used in a demonstration program with dummy parts carrying typical part numbers.

#### Defect Character Specification

It has been noted in the previous section and Table XLV that specific NDI techniques are flaw length, depth, or area responsive. The most direct approach to the specification of defect character is to define its aspect ratio,  $a/2c$ . This form is convenient for both the fracture analysis and the NDI applications engineer who makes the decision on what technique is best. Since each case in designing NDI techniques is unique, other parameters to specify flaw character must be at least as general as the  $a/2c$  designation. No alternatives to the aspect ratio show promise for useful application to NDI.

#### Efficient Demonstrations

The objective in a demonstration is to acquire a sufficient quantity of data samples to establish statistically valid results under real-world inspection conditions. There is no need to produce a large number of specimens if they are recycled through inspection. The tradeoff is between the numbers of specimens to expedite results and the cost of producing the specimens. A configuration with fatigue cracks generated at holes is a multi-purpose article which can function as a simulated detailed part or which can be fastened in groups to simulate structure with cracks around fasteners.

Care must be taken in recycling specimens so that they will not be identified by inspectors. A time lapse between the inspection cycles helps in this respect, since the exact nature of the specimen is forgotten. Experience has shown that a time lapse of 2 to 3 weeks is sufficient to forget the location of fatigue cracks on C-130 wing box specimens used in independent NDI research at Lockheed. Fatigue-damaged

structures from component or full-scale test articles and in-service damaged items are valuable for NDI demonstration purposes. Damaged C-130 center wing boxes have yielded a number of surface fatigue cracks for inspection reliability tests.

Cost and complexity may be minimized through the use of a probability surface such as that shown in Figure 185. Three detection probability curves at different inspectability levels could be developed experimentally to establish the surface. This could then be applied generally to a wide spectrum of inspectability cases. The goal is to avert the extremely high cost and complexity of establishing NDI reliability values for a variety of part configurations. The probability surface approach has the drawback that inspectabilities must be subjectively assigned to a part in question. It is anticipated that refinement of inspectability rating systems through experience will lead to an acceptable method for assessing flaw detection reliabilities.

### A3.7 FRACTURE AND FATIGUE CONTROL PLAN

The purpose of this fracture and fatigue control plan is to identify and specifically define all of the tasks necessary to ensure compliance with the design service-life criteria and the damage tolerance and fatigue requirements of MIL-STD-1530 and MIL-A-008866. The plan assures that materials used for fabrication of fracture- and fatigue-critical structure are controlled by a system of procedures and specifications that precludes the use of parts whose properties are inferior to those assumed in the design.

The objectives of the fracture and fatigue control program are to minimize the service maintenance problems due to fatigue and other crack initiation mechanisms and to prevent the failure of safety-of-flight structure. Damage-tolerant design will be implemented for primary structure to ensure structural safety against undetected flaws or damage.

The material selections and manufacturing and processing of all parts fabricated from fracture- and fatigue-controlled material will be monitored by a Fracture and Fatigue Control Board. This Board consists of Engineering, Quality Assurance, and Manufacturing Operations Specialists in fatigue, fracture mechanics, processing, and inspection. This Board will report directly to the Program Manager.

The Control Board will oversee all aspects of fracture- and fatigue-critical structure. Their principal task will be to coordinate with Engineering, Manufacturing, and Quality Assurance organizations to see that the following tasks are accomplished:

- 1) Define the fracture- and fatigue-critical parts to be controlled. Engineering will designate these parts on the drawings.
- 2) Define critical operations in manufacturing and processing. Applicable specifications will be called out on engineering drawings, and special inspections and tests will be required by the shop-planning paper work.
- 3) Review applicable material and process specifications. Review basic specifications and their revisions to ensure compliance with the fracture



and fatigue control plan.

- 4) Control documentation and material traceability. Maintain records that will provide complete part and material traceability of all fracture- and fatigue-critical parts.
- 5) Control material receiving, handling, processing, storing, and fabrication of fracture- and fatigue-critical parts. Audit material flow for compliance with applicable processes and specifications.
- 6) Control costs; regulate schedule, engineering release, and drawing control. The Board will coordinate with all departments to control costs and maintain schedule during the program.
- 7) Establish process control and inspection procedures, including complete requirements for nondestructive inspection, quality control, and corrosion control. Use the initial lot of parts to firm-up and check out the complete quality control procedures for the program. Review and revise specifications as required.
- 8) Perform on-site reviews of manufacturing operations and verification tests during production. The Board will periodically review operations during manufacturing and witness verification tests to ensure compliance with specifications.
- 9) Monitor subcontractor, supplier, and vendor fracture and fatigue control of critical parts during processing. Periodically review subcontractors', suppliers', and vendors' operations with on-site inspections to ensure compliance with specifications.
- 10) Maintain adherence to MIL-STD-1530, MIL-A-008866, and MIL-A-008867. The Control Board will monitor all phases of the program periodically to assure compliance with these specifications.
- 11) Obtain Air Force approvals for compliance with MIL-STD-1530. The Control Board will act under the directions of the Program Manager and coordinate with the Air Force by providing reports of pertinent tests,



procedures, and specifications; conduct on-site reviews with Air Force representatives, and thereby obtain the required approvals for compliance with MIL-STD-1530.

- 12) Establish field maintenance, inspection, and repair techniques. The Control Board will work with engineering personnel to establish periodic inspection requirements, that include nondestructive inspection techniques, and field maintenance and repair techniques for fracture- and fatigue-critical parts.

Figure 186 gives the breakdown of the program organization, showing the position of the Fracture and Fatigue Control Board.

To implement this fracture and fatigue control plan, close coordination among Engineering, Quality Assurance, and Manufacturing organizations will exist from the outset of the program until completion. Trade studies and damage tolerance tests will be conducted to facilitate material selections and the basic design to obtain a low-weight, cost-effective design. Tight control will be imposed through specifications and inspections commensurate with structural analysis, load analysis, fracture mechanics, fatigue, and quality control to ensure compliance with the service-life design criteria of MIL-STD-1530.

Table XLVI lists the fracture and fatigue critical parts for the ADP Cargo/Tanker inner-wing box structure. Parts listed were selected on the basis of high operating stress, high stress concentration, environmental factors, and the risk associated with the potential failure of a part or component in terms of safety-in-flight. These parts will be defined on the Engineering drawing with a "C" suffix to the part number, for example: ADP 1017-101C, which will alert Manufacturing, Inspection, and Liaison Engineering to the special requirements in processing, handling, testing, and inspection of these parts. This system will also facilitate the documentation and traceability of these critical parts.

A procedure for establishing verification of this control plan will be incorporated at the outset of the manufacturing processing. Critical processes, such as heat-treatment, stress relieving, stretch forming, and welding will be subjected to rigid

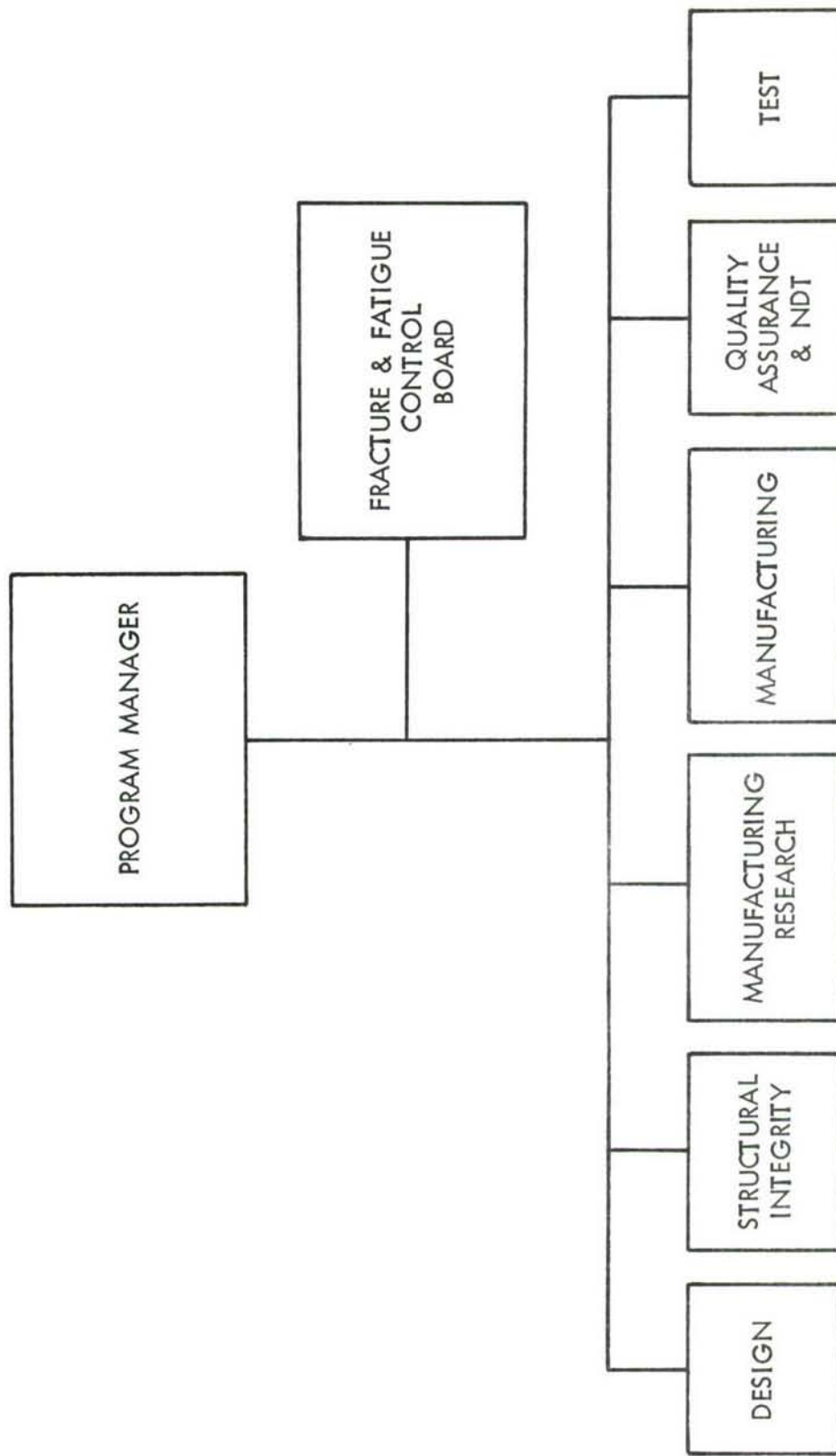


FIGURE 186 PROGRAM ORGANIZATION

detailed inspection and documentation on the first lot of parts. This initial lot of parts will establish critical points for inspection and detailed planning which will be followed during each subsequent lot of parts to be manufactured. Verification tests will be performed at specified intervals to prove the system. Use of this close process and quality control will result in repeated high-quality parts.

TABLE XLVI  
FRACTURE & FATIGUE CRITICAL PARTS - INNER WING BOX

<u>NO. PARTS PER A/C</u>	<u>DESCRIPTION</u>
6	*Skin Panel - Upper Surface
6	*Skin Panel - Wing Lower Surface
132	*Stringer - Wing Box Surface
4	Cap - Front Spar
2	*Web - Front Spar
4	Cap - Rear Spar
2	*Web - Rear Spar
10	Pylon Attach Fitting
6	Pylon Support Fitting
4	W.S. 77 Chordwise Rib Cap
24	W.S. 77 Chordwise Splice Plate
24	W.S. 77 Chordwise Splice Fitting
6	W.S. 77 Tension Fitting (2 ea. at Front Spar, 1 ea. at Rear Spar)
4	W.S. 374 Chordwise Rib Cap
4	W.S. 374 Chordwise Splice Plate
16	W.S. 374 Chordwise Splice Fittings
4	W.S. 374 Front Spar Cap Splice
2	W.S. 374 Rear Spar Splice Fitting/Jack Pad

\*Fracture Critical

### A3.7.1 Cost Impact

To determine the cost impact of establishing this fracture and fatigue control plan, it was assumed that 200 left- and right-hand units of the ADP Cargo/Tanker inner-wing box structure would be fabricated at a scheduled rate equivalent to that of the C-141 production program. Therefore, a span of 72 months from go-ahead to the delivery of 200 L/R production units is assumed for the pricing impact. Pertinent milestones which have been established for the plan are presented in Figure 187. No cost consideration has been given to the monitoring, documentation, and technical support that would be required during in-service life of the airplane for a complete program. This is assumed to be accomplished under a separate contract.

A summary of the total cost to implement this fracture and fatigue control plan is presented in Table XLVII, followed by a detailed breakdown of manhour and material costs for the four major categories listed.



<u>ENGINEERING</u>	<u>Months After Go-Ahead</u>
Define Critical Parts	2
Basic Fracture Data	6
Material Selection	6
Material Specifications	10
Vendor Material Test Approvals	12
Complete Material Tests & Specification Requirements	12
Final Design - Dwg. Release 90%	16
Complete Fatigue & Fracture Structural Analysis	21
Full-scale Components/Major Assemblies Test Complete	26
Repair Techniques and Inspection Procedures	30
<u>QUALITY ASSURANCE</u>	
Documentation and Material Traceability Procedures	3
Material Control Procedures	4
Test Procedures Approved	8
Complete NDI Techniques & Requirements	24
<u>MANUFACTURING OPERATIONS</u>	
Standard Format for Process Control Work Authorization	3
Detailed Shop Orders & PJS for Critical Parts	12
Start Assembly - 1st Production Unit	14
Complete Assembly - 1st Production Unit	28
1st Flight	33
1st Delivery	38

FIGURE 187 FRACTURE & FATIGUE CONTROL PLAN MILESTONES

TABLE XLVII  
SUMMARY OF TOTAL COST  
FRACTURE AND FATIGUE CONTROL PLAN

<u>ORGANIZATION</u>	<u>MANHOURS</u>	<u>MATERIAL COSTS 1972 DOLLARS</u>
I. ENGINEERING	104,262	\$ 31,450
II. QUALITY ASSURANCE	24,220	-
III. MANUFACTURING	2,000	168,000
IV. OTHERS	<u>27,300</u>	<u>16,000</u>
SUM TOTAL:	157,782	\$215,450

# 1. ENGINEERING COST SUMMARY

<u>ORGANIZATION</u>	<u>MANHOURS</u>	<u>MATERIAL COSTS 1972 DOLLARS</u>
A. Design	5,200	
B. Stress	900	
C. Fatigue	4,500	
D. Fracture	25,300	
E. Specifications	420	
F. Material	1,200	
G. Loads	200	
H. Weights	200	
I. Lifeson	6,000	
J. Manuals	860	
K. Testing	58,282	\$31,450
L. Administration	<u>1,200</u>	
Total (Engineering)	104,262	<u>\$31,450</u>

## Explanation of Significant Engineering Costs

- Assumptions:
1. Standard Program of 72 months.
  2. Coverage is provided through fabrication of last unit and through completion of fracture and fatigue testing.
  3. Costs applies to additional work over-and-above the current airplane development requirements.

<u>ITEM A - DESIGN</u>	<u>MANHOURS</u>
1. Phase I(b) Preliminary Design (12 months) -----	416
2. Phase II Detail Design (15 months) -----	1840
3. Phase III Fabrication (45 months) -----	1944
4. Phase IV Testing -----	<u>1000</u>
Sub-Total: -----	5200

ITEM C - FATIGUE	<u>MANHOURS</u>
1. Analysis & Design Support -----	1000
2. Engr. Liaison Support -----	500
3. Material and Process Control Support -----	500
4. Reporting & Documentation -----	500
5. Test Program Support -----	2000
Sub-Total: -----	<u>4500</u>

ITEM D - FRACTURE	<u>MANHOURS</u>
1. Analysis & Design Support -----	18000
2. Engr. Liaison Support -----	3000
3. Material and Process Control Support -----	800
4. Reporting & Documentation -----	500
5. Test Program Support -----	3000
Sub-Total: -----	<u>25300</u>

ITEM I - LIAISON	<u>MANHOURS</u>
Direct Engineering Liaison support to Manufacturing and Quality Assurance through all stages of fabrication and assembly -----	6000



ITEM K - TESTING

TESTING REQUIREMENTS	
FATIGUE	FRACTURE
<u>Materials -</u> No Additional	<u>Materials -</u> <ul style="list-style-type: none"> <li>o Upgrade data to MIL-HDBK-5 Standards</li> <li>o <math>K_c</math>, <math>da/dN</math>, environment</li> </ul>
<u>Design Development -</u> No Additional	<u>Design Development -</u> <ul style="list-style-type: none"> <li>o Retardation effects.</li> <li>o Redistribution effects.</li> <li>o Design eval. &amp; trade studies.               <ul style="list-style-type: none"> <li>- crack growth</li> <li>- residual strength</li> </ul> </li> </ul>
<u>Design Verification -</u> No Additional	<u>Design Verification -</u> <ul style="list-style-type: none"> <li>o Add crack growth monitoring to fatigue test.</li> <li>o Induce flaws &amp; measure crack growth rates.</li> <li>o Residual strength.</li> <li>o Airplane inspection data.</li> </ul>
<u>Airplane Tests -</u> No Additional	<u>Airplane Tests -</u> <ul style="list-style-type: none"> <li>o Full scale inner wing box damage tol. &amp; residual strength.</li> </ul>

# ITEM K - TESTING - CONTINUED:

1. Basic Fracture Data to support trade studies, final design, and fabrication processes (i.e.

$K_{IC}$ , $K_C$ , $da/dN$ , etc.).	<u>MANHOURS</u>
a) 100 tests at 10 M/H -----	1000
b) 40 tests at 40 M/H -----	1600
c) 10 tests at 100 M/H -----	1000
Sub-Total: -----	3600

2. Design Development Tests - Retardation, load re-distribution, crack growth, residual strength, damage-tolerance evaluation, and inspectability requirements.

a) 10 tests at 160 M/H -----	1600
b) 5 tests at 1200 M/H -----	6000
c) 3 tests at 3000 M/H -----	9000
Sub-Total: -----	16,600

3. Pre-production Design-Verification-Tests - Full-scale components and portions of major assemblies - damage tolerance, residual strength, and inspection data.

a) 3 tests at 1360 M/H -----	4080
b) 2 tests at 4000 M/H -----	8000
Sub-Total: -----	12,080

## ITEM K - TESTING - CONTINUED:

### 4. Full-scale Inner Wing Box Damage Tolerance and Residual Strength Test.

#### MANHOURS

#### a) Test set-up Materials

Lab Shop	--	4920
Instrumentation Data	\$ 850	984
Lab Engineering	27,900	1476
Sub-Total:	<u>\$28,750</u>	<u>7380</u>

#### b) Test run

Lab Shop	--	7564
Instrumentation Data	\$ 800	2657
Lab Engineering	1,900	8401
Sub-Total:	<u>\$ 2,700</u>	<u>18,622</u>
Total:	\$31,450	26,002

## II. QUALITY ASSURANCE

24,220 M/H

### TASKS:

- A) Control special documentation and material traceability.
- B) Control special material receiving, handling, processing, storing, and fabrication of fracture and fatigue critical parts.
- C) Nondestructive inspection added requirements and techniques.
- D) Closely monitor vendor fracture and fatigue critical parts during processing operations.
- E) Establish special inspection requirements and techniques for fracture- and fatigue-critical operations in manufacturing and processing.
- F) In-service inspection and maintenance control (technique and requirements).
- G) Testing/verification.
- H) Fastener and adhesive (Weldbond) increased installation control.

COSTS: Receipt, Test, and Material Control.		<u>MANHOURS</u>
A) Receiving Inspection (Four year program) -----		4000
B) Receipt tests: 18 lots; 30 coupons/lot: 30 tests/ lot x 18 x 8 M/H -----		4320
C) Processing/Fabrication:		
1) Control & Traceability - 160 tests at 10 M/H ---		1600
2) Inspection & Documentation - (52000 parts, 1300 shop orders) -----		3900
D) Assembly Inspection Traceability:		
1) Traceability & Documentation (10 M/H per A/C) -		2000
2) Inspection and Maintenance (Eddy Current - 40 Hrs./Week) -----		8000
E) Serial Number Control and Traceability -----		400
	TOTAL: ----	<u>24,220</u>

III. MANUFACTURING                      \$168,000                      2000 M/H

A) TASKS:

- 1) Additional planning paperwork (logs, records, etc.).
- 2) Detailed planning for critical manufacturing and processing operations, including verification.
- 3) Plan and provide time for additional inspection and quality assurance checks of fracture and fatigue critical parts.
- 4) Initial on-site reviews of in-plant and vendor manufacturing operations.
- 5) Verification procedures requiring additional time of manufacturing personnel.

Sub-Total:                      2000 M/H

- B) Cost of separate test article for damage tolerance  
and residual strength tests                      \$168,000



IV. OTHERS	\$16,000	27,300 M/H
A) Required material testing by vendor (material to be purchased in 18 lots for production of 200 airplanes)		
1) 7050-T76 Plate: 8 tests at 10 M/H x 18 -----		1,440
2) 7050-T76 Extrusion: 40 tests at 10 M/H x 18 -----		7,200
3) 7050-T76 Forging: 9 tests at 10 M/H x 18 -----		1,620
4) 7475-T76 Sheet: 8 tests at 10 M/H x 18 -----		1,440
5) Steel Forgings: 12 tests at 10 M/H x 18 -----		2,160
	Sub-Total: -----	13,860
B) Purchasing Specifications -----		240
C) Fracture and Fatigue Control Board -----		12,000
D) Administration -----		1,200
E) Travel: \$16,000 (Assumes 17 trips, 3 people at 2 days)		
	Sub-Total: -----	13,400
	Total: -----	27,300

### A3.7.2 Suggested Modifications for Potential Cost Reduction

With a view to reducing the overall cost of the program several modifications to the basic plan were considered. Three of the more significant items investigated together with potential cost savings are listed below.

1. Use simple, notched tensile testing for most of vendor material qualification tests (fracture test).  
SAVINGS: Approx. 75% of Item IV.  $A = .75 \times 13860 = 10,395 \text{ M/H}$
2. Use full-scale fatigue test article for dual test purposes. Perform damage tolerance and residual strength tests upon completion of the fatigue test in lieu of having an additional full-scale test article. This involves some added risks of not attaining all of the desired results, but it will substantially lower the cost.

Even though 100% of desired results may not be attained by this suggested modification, structural integrity and safety will not be jeopardized. For example, if the fatigue test article wears out prior to completion of all damage-tolerance tests, meaningful crack-growth data will have been obtained. These data may be slightly different and/or at different locations; however, the data will be just as useful in assessing structural integrity. Data will also be available from the development and verification component test programs. If deemed necessary, additional components tests could be performed at the conclusion of the full-scale article test program.

On the positive side, there are several advantages other than reduced costs in using one in lieu of two test articles for these tests. Test results will be based on all instrumentation being at exact locations and on common structure; and, interpretation of test results cannot be misunderstood due to different thicknesses, load paths, tolerances, or instrumentation variations between specimens; and the damage tolerance and residual strength tests will be applied to "fatigued" structure rather than new "virgin" structure, which is more likely to be the condition encountered in service.

	<u>MANHOURS</u>	<u>MATERIALS</u>
SAVINGS: Item I. K. 4.	5,340	\$ 28,750
Item III. B.	<u>      </u>	<u>168,000</u>
Total:	5,340	\$196,750

3. Schedule full-scale box damage-tolerance tests after fatigue tests. If, for some reason, suggestion 2 above is not implemented, some of the cost reductions are still possible by scheduling the damage-tolerance tests in a time span after the completion of the fatigue tests. In this manner, the cost of an additional test setup and the associated facilities are saved. This also has the added technical advantage of having all the fatigue test results and knowledge prior to the start of the damage-tolerance tests.

SAVINGS: Item I. K. 4.	Materials -----	\$ 27,950
	Manhours -----	4,034

## A3.8 IN-SERVICE INSPECTABILITY FACTORS

### A3.8.1 Background Data

A3.8.1.1 Analysis and Test: Analysis and test data for the inner-wing baseline structure are contained in several C-141A reports which make up a portion of the technical data file. These are identified by Lockheed "ER" report numbers which are further described below.

Baseline design external loads are presented in ER 5058, C-141 Wing Loads. These loads were used to develop the internal loads in the structure which, in turn, formed the basis for the stress analysis presented in ER 4992, C-141 Wing Stress Analysis. Both of these documents were updated to reflect changes in loads resulting from the flight test program and new mission requirements.

Mission profiles used to develop fatigue analysis spectra are contained in ER 9502, C-141 Fatigue Loads Criteria for Updated Fatigue Program. Included in these profiles are information gained from various C-141 flight test programs, including the VGH/GLS data recorded during the C-141 Aircraft Flight Loads Data Program. Also reflected is an updated aircraft utilization schedule derived from actual service experience. These mission profiles were used to develop the analytical design fatigue spectra contained in ER 9506, C-141 Basic and Dynamic Loads. The latter forms the basis for the wing fatigue analysis presented in ER 5030, Volume I - C-141 Wing Safe Life Analysis, and the full-scale airplane test spectra developed for the Wing/Fuselage Fatigue Specimen "A" as contained in ER 6802, Volume V.

The fatigue and crack growth analyses conducted in the course of this sensitivity study are based on the test loads spectra developed for Specimen "A", except that the following changes were made:

- (1) A peak-to-peak description of the ground-air-ground cycle was substituted for the mean-to-mean cycle used in the baseline.
- (2) The number of full-stop landings was increased from 6405 to 8187 to reflect the latest fleet usage information.

Table XLIII shows the test loads spectra which incorporate the above changes.



A3.8.1.2 In-Service Inspection Information: Data on the frequency and type of structural inspections, accessibility factors, NDI techniques used, and assumed damage size detection capabilities have been previously listed in Table XXV and its accompanying T.O. 1C-141A-36 abstract. The damage size detection capability presented in this table is based largely on estimates obtained from experience in full-scale fatigue testing, since meaningful data from in-service inspections are virtually nonexistent.

A3.8.1.2.1 Full-Scale Fatigue Test Inspection: The absence of defect detection information from service records necessitated that other sources of information be exploited. Considerable data exist in damage reports covering the full-scale C-141 Wing/Fuselage Specimen "B" fatigue test. These are reported in ER 4950, Volume IV, and results summarized in Table XLVIII. Included is a listing of number of occurrences of cracking by location category and the minimum-size cracks detected as well as assumed maximum crack sizes which could be missed as a function of NDI technique used. These data represent two simulated lifetimes of fatigue testing and include effects of all critical flight and ground landings. Inspections were performed at the end of each fatigue block spectrum pass, an increment equivalent to 1/10 lifetime (3,000 flight hours).

One of the inner-wing areas affording the most crack-growth information during the fatigue test was the area surrounding the fuel probe holes (Figure 188). This area was subjected to additional analysis in an attempt to work backwards from known crack observations and determine the size of these cracks at the previous inspection interval. Three crack-growth models were used to obtain the results shown in Figure 189. One model was the Walker Panel Analysis with an assumed initial damage of a crack 0.30" long from a 0.22" hole through to the edge of the probe hole flange. The total initial length was 0.52", including the hole. A second model also used Walker's Analysis, but the initial length was 0.37", including the hole. The remaining model used Forman's Equation with an initial length of 0.37", including the hole. No crack retardation factors were used in the calculations. Stress/moment ratios used in the calculations were derived from design data for the Inner Wing Box Rib Station (IWBRs) 65 location. Eight of the 28

TABLE XLVIII

## SUMMARY OF C-141 INNER WING FATIGUE SPECIMEN "B" INSPECTION &amp; DAMAGE

LOCATION CATEGORY	NUMBER OF OCCURRENCES	THROUGH CRACKS		INCIDENCE OF SINGLE OR MULTIPLE CRACKING
		MINIMUM CRACK LENGTH DETECTED (IN.) TECHNIQUE	ASSUMED MAX. CRACK LENGTH THAT COULD BE MISSED (IN.) TECHNIQUE	
1. Upper Skin Panel at Cutouts	28	0.2 VIS.	VIS, 2.0, E/C, 0.10", U/S, 0.25, E/C, Bolt Hole Probe .08	57 Single  8 Multiple (3 In Skin Panels)
2. Crack Extension Upper Skin Panel at Cutouts	6	See 1.	See 1.	
3. Access Door Areas	12	2.3 VIS.	VIS, 2.0, P, 0.10	
4. Beam Web	7	0.3 VIS.	E/S, 0.20, VIS, 2.0	
5. Beam Splice	2	2.0	E/C, 0.20, VIS, 2.0	
6. Splice Plate	5	3.0	E/C, 0.20, VIS, 2.0	
7. Fittings	5	0.5	E/C, 0.20, VIS, 2.0	

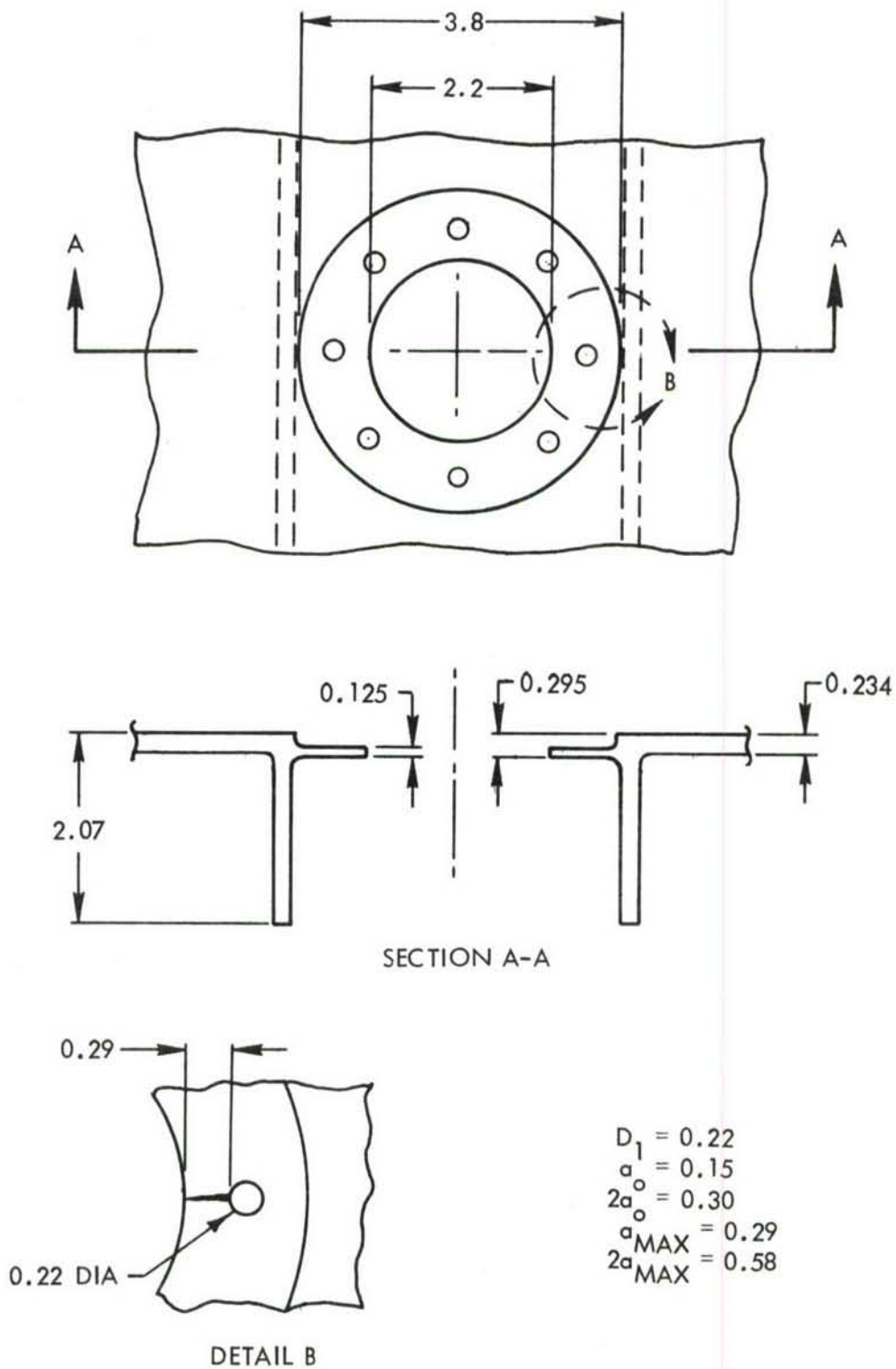


FIGURE 188 FUEL PROBE HOLE CONFIGURATION

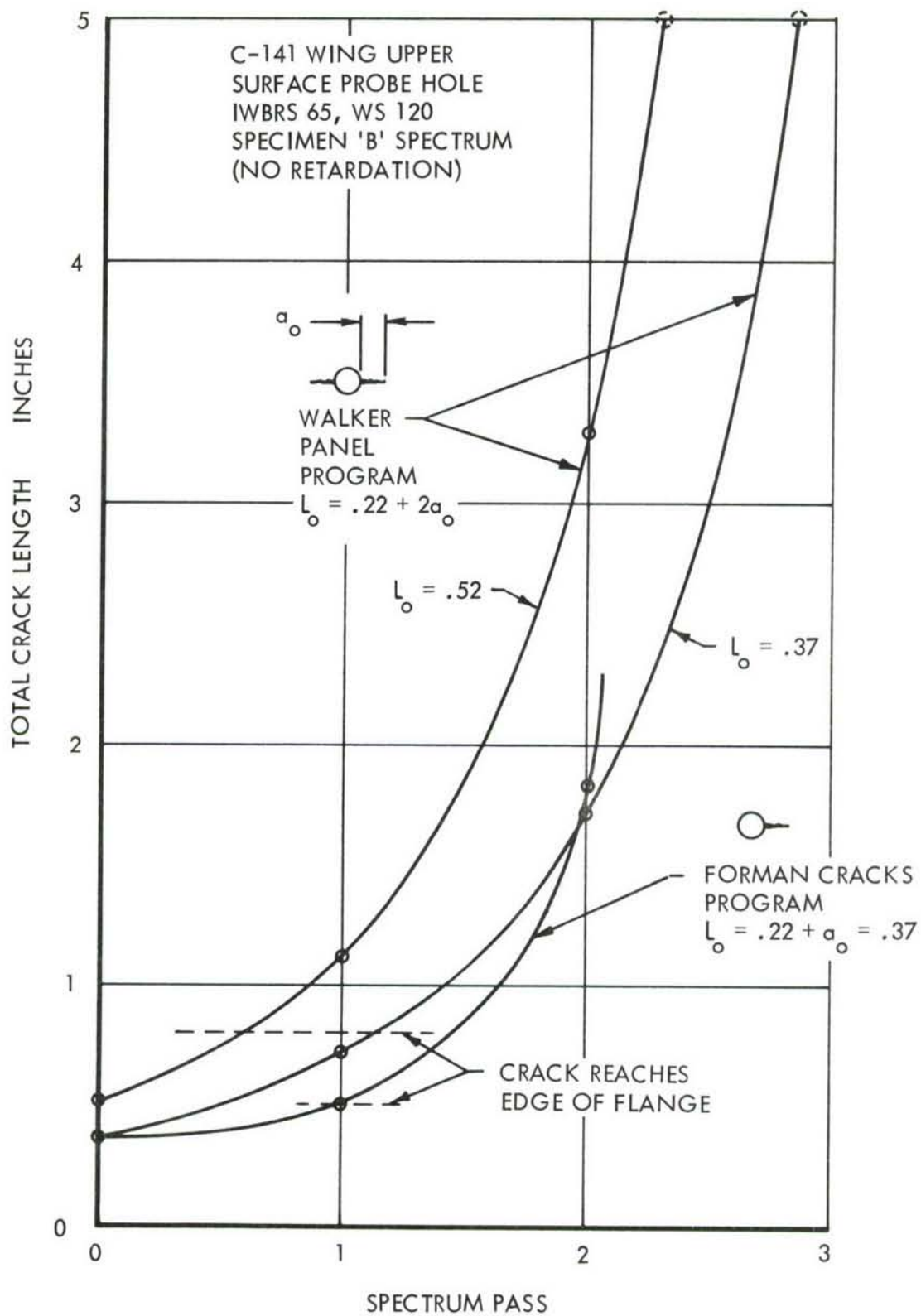


FIGURE 189 CRACK GROWTH ANALYSIS



observations were made at IWBR5 55, and the remainder at various locations outboard to IWBR5 361.

Points on the curves were established with known lengths and projected back one pass increment to yield the flaw size that existed, but was previously missed by visual inspection. For example, tabulated observations show a 1.5-inch crack at IWBR5 56.7 (right) recorded at the completion of pass number 16, yet no previous record of a crack at this location was noted. Projection back one pass from the 1.5" point on each of the 3 curves yielded crack length values of 0.65", 0.65" and 0.48" for the two Walker curves and the Forman equation, respectively. Results of the projections are given in Table XLIX. Histograms of the observed flaws and projected values are presented by size range in Figures 190 through 193. For cases where back-projected values were less than 0.40", flaw lengths were grouped into the 0.20" to 0.40" range. No values less than 0.20" were considered, since no cracks that small were recorded in the inspections of fuel probe hole areas. The smallest recorded values were 0.30".

A comparison of directly observed "finds" with projected values of flaws missed in the previous inspection shows how data are transformed by crack growth models. The two applications of the Walker Program yield approximately the same results. The Forman equations produces a highly skewed grouping of "misses" to the small size ranges, 0.20" to 0.40" and 0.40" to 0.60". The data presented are only indicative of the following:

- (a) The "find" size distribution shows trends but does not actually indicate all possible flaws.
- (b) The "missed" size distributions depict only flaws which were overlooked and subsequently found in the next inspection.

It should be noted that the analytical flaw growth curves predict higher growth rates than those observed experimentally, and this indicates that all "missed" flaw lengths determined by this study are too small. Analytically predicted rates ranged from 0.30" per pass to 2.8" per pass. Experimentally observed rates ranged from 0.16" per pass to 0.30" per pass. The absence of a retardation model, however, is not considered to be an influencing factor, since "missed" values were derived by projection on the

TABLE XLIX  
ANALYTIC VALUES FOR FLAWS VISUALLY MISSED

ITEM NO. FATIGUE SPECIMEN "B"	INITIAL LENGTH VISUALLY DETECTED (IN.)	CALCULATED LENGTH, PREVIOUS PASS (IN.)		
		WALKER, $L_0 = .52$	WALKER, $L_0 = .37$	FORMAN, $L_0 = .37$
162	1.9	0.80	0.80	0.50
163	1.5	0.65	0.65	0.48
142	4.5	1.45	1.45	--
182	3.8 (2 ea.)	1.10	1.25	--
182	2.0 (2 ea.)	0.82	0.82	0.52
33	1.0	<.52	0.52	0.40
34	0.5	"	<.37	<.37
35	0.5 (3 ea.)	"	"	"
36	0.3	"	"	"
64	0.25	"	"	"
65	0.40 (2 ea.)	"	"	"
79	0.35	"	"	"
79	0.50	"	"	"
25	2.6	1.95	1.90	--
27	0.3	<.52	<.37	<.37
28	0.3	"	"	"
29	1.0	"	0.52	0.40
30	1.6 (2 ea.)	0.65	0.65	0.45
31	0.8 (2 ea.)	<.52	0.32	0.38
32	0.3 (2 ea.)	"	<.37	<.37

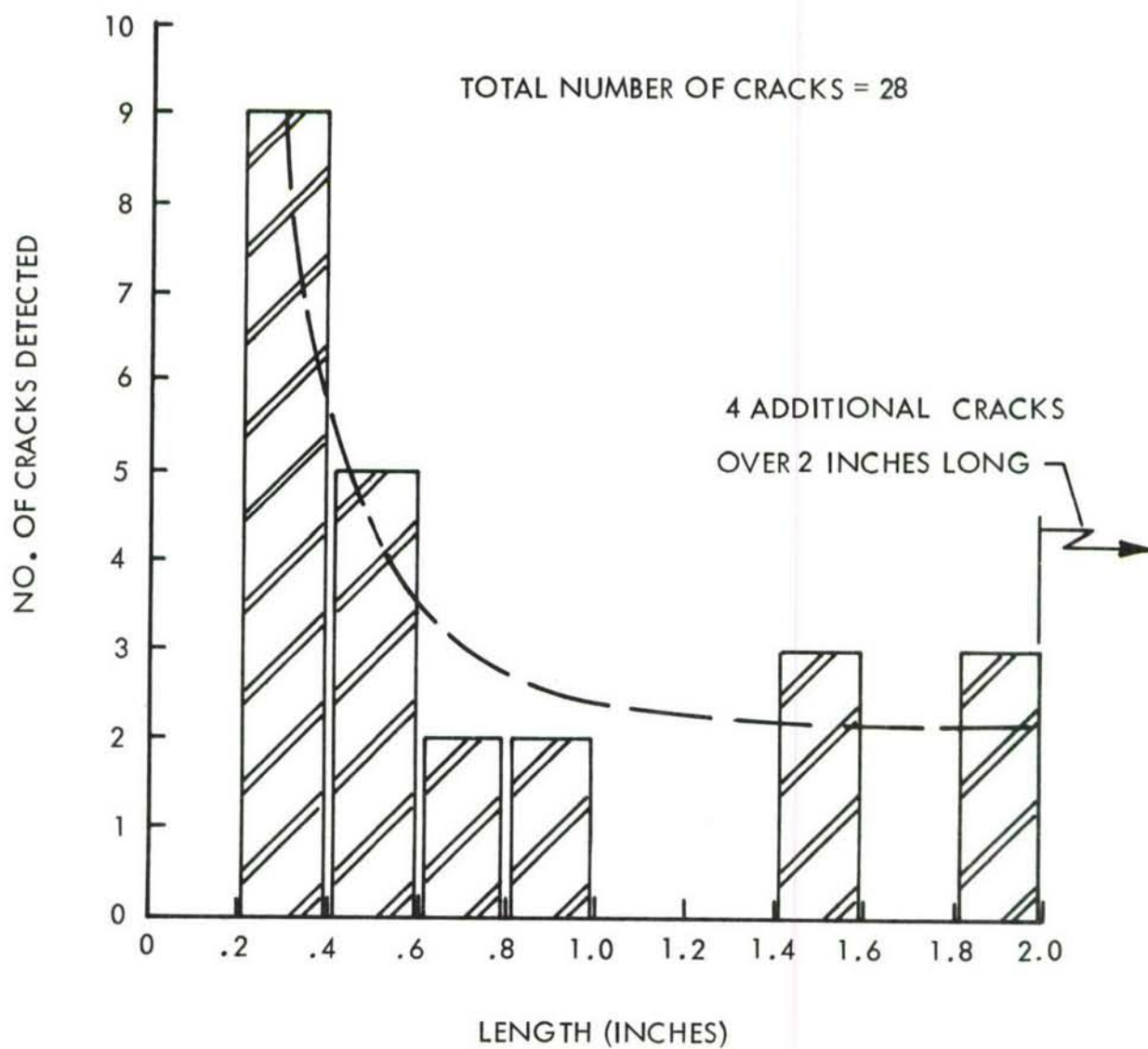


FIGURE 190 VISUALLY DETECTED CRACK LENGTH DISTRIBUTION  
FUEL PROBE HOLE, INNER WING, C-141  
FATIGUE SPECIMEN 'B'

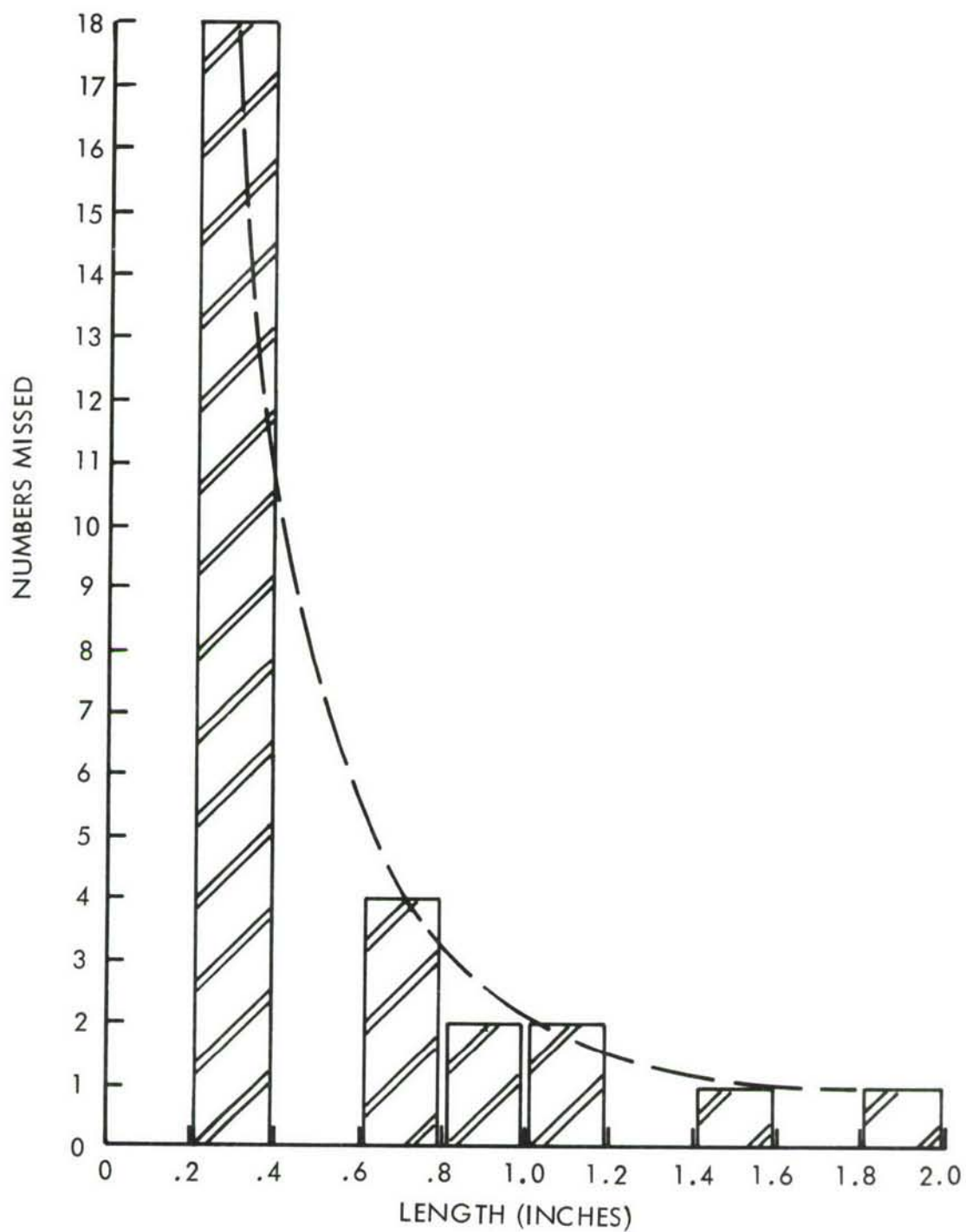


FIGURE 191 VISUALLY "MISSED" CRACK LENGTH DISTRIBUTION  
USING WALKER ANALYSIS, INITIAL FLAW LENGTH  $L_0 = .52$



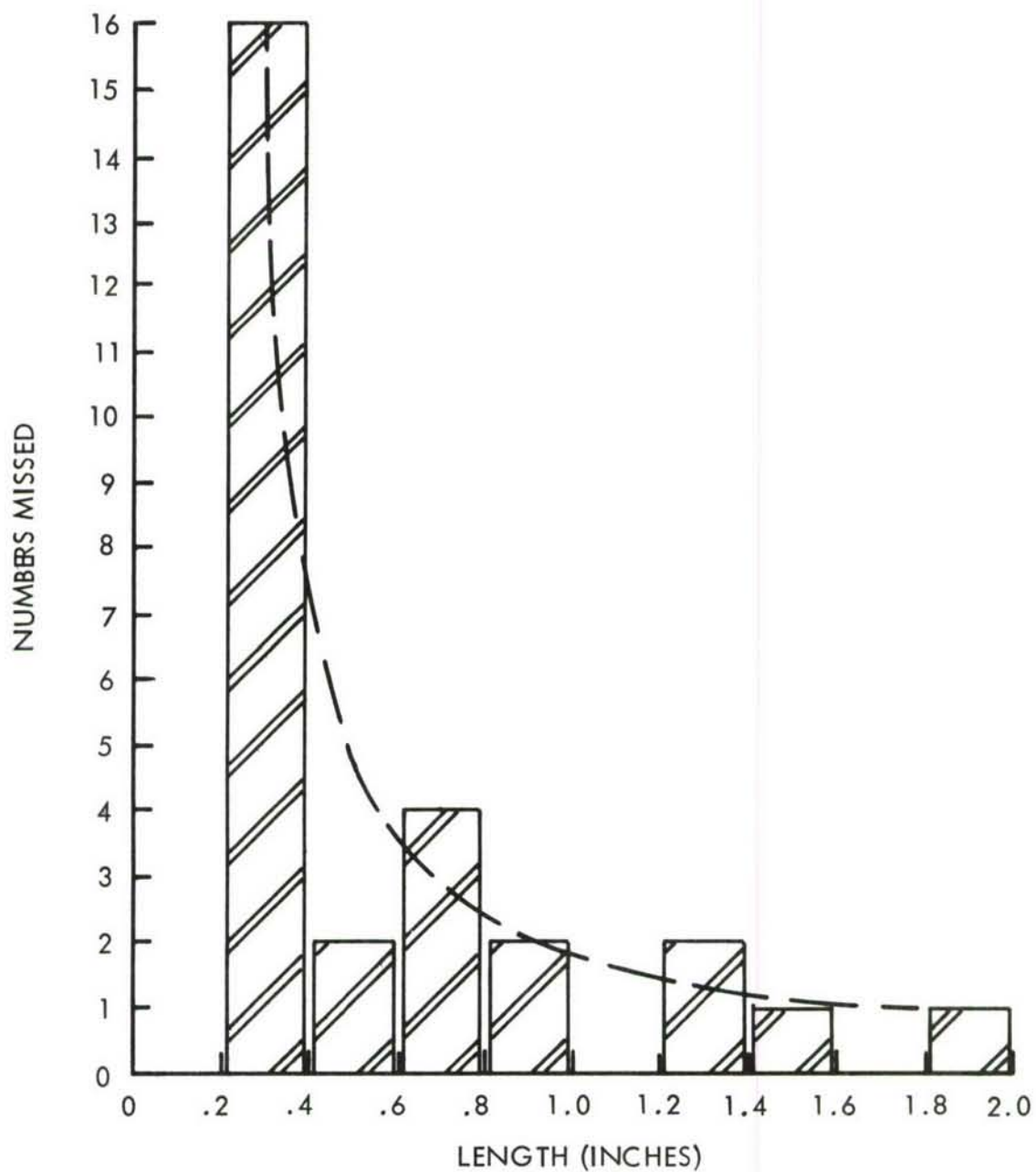


FIGURE 192 VISUALLY "MISSED" CRACK LENGTH DISTRIBUTION  
USING WALKER ANALYSIS, INITIAL FLAW LENGTH  $L_0 = .37$

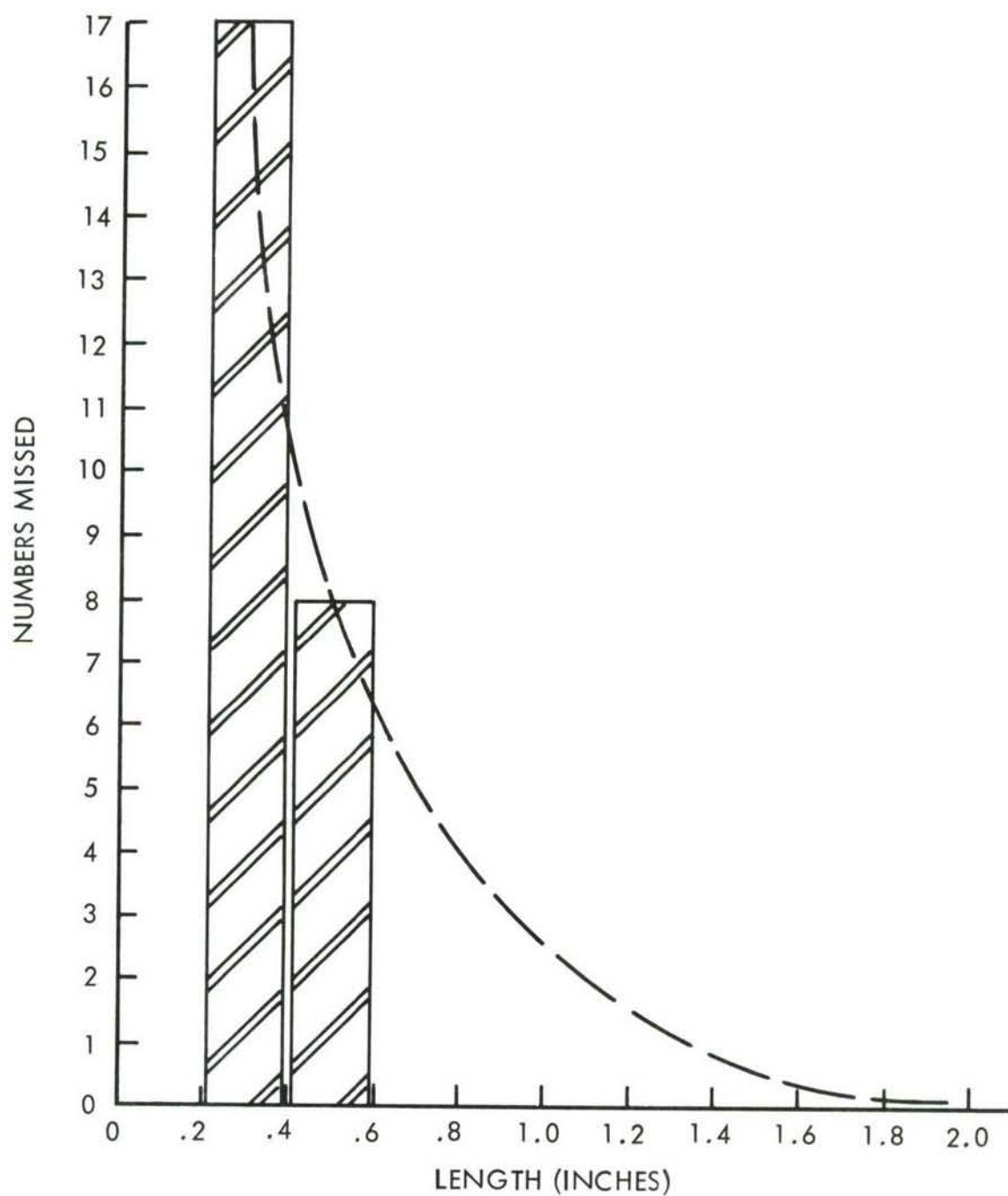


FIGURE 193 VISUALLY "MISSED" CRACK LENGTH DISTRIBUTION  
USING FORMAN ANALYSIS, INITIAL FLAW LENGTH  $L_0 = .37$

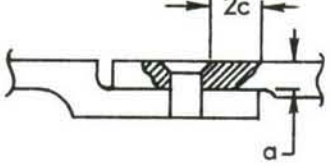
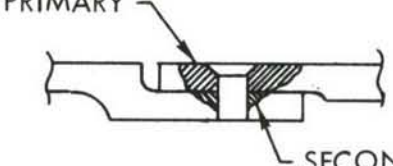
curves using a fixed increment; i.e., only the curve slope is significant, and a retardation factor does not change the shape.

Results further indicate that there is a low probability that cracks less than 0.20" in length can be visually detected in structure of this type. If the results are literally interpreted by adding the number of cracks "missed" to the number "detected" to give an assumed total number of flaws, approximately 30% are detectable in the 0.20" to 0.40" length range. Such an interpretation is based on the gross assumption that no other defects existed beyond those accounted for, i.e., when they became large enough they would certainly be detected. Experience has shown that this is not the case, but there remains a high probability of detection if the flaw is large. Fatigue cracks 2" long are large enough for visual detection with high probability. Therefore, a literal interpretation of results should be applicable for crack lengths near 2". The two Walker-derived curves yield a 75% detection level for cracks in the 1.80" to 2.00" range. The Forman-derived curve indicates that nearly a 100% detection level is possible for this same range. It is plausible from these observations to state that there is less than a 30% chance of visual detection for cracks less than 0.20" to 0.40" length, and a 75% chance of visual detection for crack lengths 1.80" to 2.00".

It must be emphasized that these were close visual inspections in known suspect areas. Personnel conducting the inspections were engineers in charge of the C-141 fatigue test. Their proficiency for visual detection is considered average to above average for this structure. Comparable performance could be expected from a special visual inspection of aircraft in service.

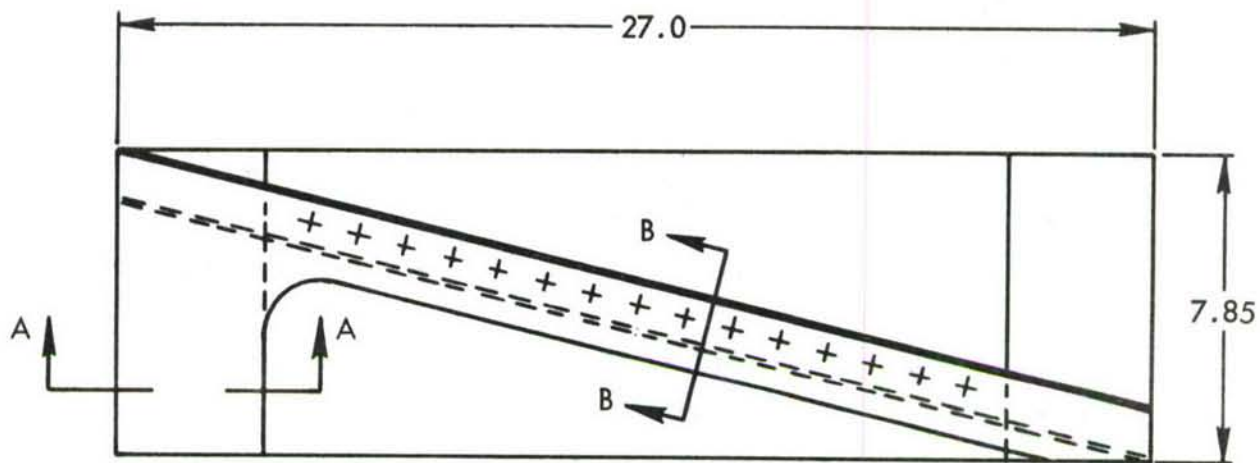
A3.8.1.2.2 Component Fatigue Tests: A source of data exists on fatigue crack commonality in adjacent members from component tests run to evaluate spanwise splices for cargo/transport-type aircraft. This information is presented in Table L . The dimensions given in this table denote the extent of fatigue crack growth immediately prior to failure. Precracked specimens were prepared by notching on undersized fastener hole, cycling to initiate a fatigue crack, drilling a full-sized hole at the crack site, and subsequent fatigue cycling to failure. These commonality data are not conclusive with respect to predominance of either single or multiple cracking in a two-component splice. Further, it is questionable that the degree of commonality of cracking in these specimens is representative of experience in full-scale structures.

TABLE L  
COMPONENT SPANWISE SPLICE CRACK MORPHOLOGY

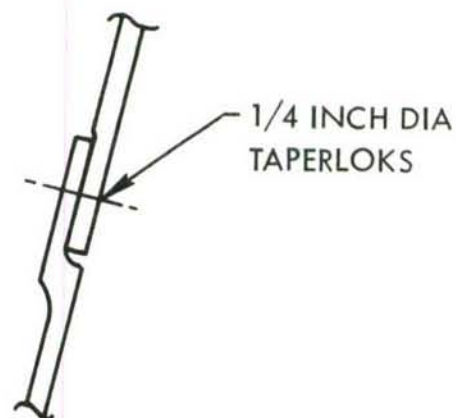
SINGLE	MULTIPLE		CONDITION
	PRIMARY	SECONDARY	
			
$a/2c$	$a/2c$	$a/2c$	
<div>.17/1.3</div> <div>.22/0.4 (1)</div> <hr/> <div>.25/1.5</div> <div>.20/0.4</div> <hr/> <div>.25/1.3</div> <div>.23/.35</div> <hr/> <div>.03/.03</div> <div>.10/.10</div> <hr/> <div>.03/.03 (2)</div>	<div>.25/.05</div> <div>.15/.17</div> <hr/> <div>.10/.10</div>	<div>.04/.04</div> <div>.04/.04</div> <hr/> <div>.015/.015</div>	Specimens Without Precrack
<div>.04/.05</div> <div>.04/.06</div> <hr/> <div>.08/.09</div> <div>.03/.03</div> <hr/> <div>.05/.10</div> <div>.02/.05</div> <hr/> <div>.06/.05</div> <hr/> <div>.02/.03</div> <hr/> <div>.03/.05</div>	<div>.12/.10</div> <hr/> <div>.02/.03</div> <div>.03/.04</div> <hr/> <div>.02/.03</div> <div>.05/.05</div> <hr/> <div>.03/.04</div> <div>.03/.03</div> <hr/> <div>.03/.04</div> <hr/> <div>.06/.03</div> <div>.03/.04</div>	<div>.01/.02</div> <hr/> <div>.05/.09</div> <div>.03/.10</div> <hr/> <div>.01/.01</div> <div>.04/.20</div> <hr/> <div>.05/.08</div> <div>.03/.07</div> <hr/> <div>.02/.02</div> <hr/> <div>.02/.03</div>	Specimens With Precrack

- NOTES: (1) Double entry indicates cracks from both sides of fastener.  
 (2) Single entry indicates crack from one side of fastener only.  
 (3) For general arrangement of typical test specimen, see Figure 194.





SECTION A-A



SECTION B-B

FIGURE 194 SPANWISE SPLICE JOINT SPECIMEN

### A3.8.2 Service Inspection Functions

Three basic functions were considered with respect to inspections. They included the inspection interval, the size of the initial damage present at the beginning of the inspection interval, and the required period of safe crack growth following the failure of a principal element in multiple-load-path structure. The assessment of the impact of in-service inspection functions in the damage-tolerance criteria, as they apply to the baseline structure, is presented in the following subsections:

A3.8.2.1 Inspection Interval: Although the objective in this subtask was to study the influence of in-service inspection functions, the effect of the allowable crack-growth period for intact structure was also considered. This was included since, in the implementation of the criteria on the baseline structure, it was often found that the allowable design stress was limited by requirements pertaining to assumed initial flaws in new structure and the specified period of unrepaired service usage.

Figure 195 shows the results of analyses for the various types of inspections. Airplane operational inspections are plotted in addition to the criteria in-service inspections to evaluate the potential influence of upgrading these inspections to criteria standards. It is evident that the additional operational inspections occur at the mid-interval of the inspections used to establish design allowable stresses. These inspections provide a ready means for reducing the inspection interval to 50 percent of current requirements. The allowable design stresses, based on the fracture criteria, would be improved by approximately 10 KSI. It is important to observe that this order of improvement holds for both the in-service inspection and the minimum period of unrepaired service usage.

A3.8.2.2 Initial Damage Subsequent to Inspection: Another important parameter in the criteria which influences design stress level control is the assumed size of undetected flaws in the structure subsequent to inspection. This parameter was also treated in terms of a percentage of the values listed in the criteria. As in the case of the inspection-interval study, the additional airplane operational inspections were included here to assess separately the effects of the flaw size assumption and the inspection interval.

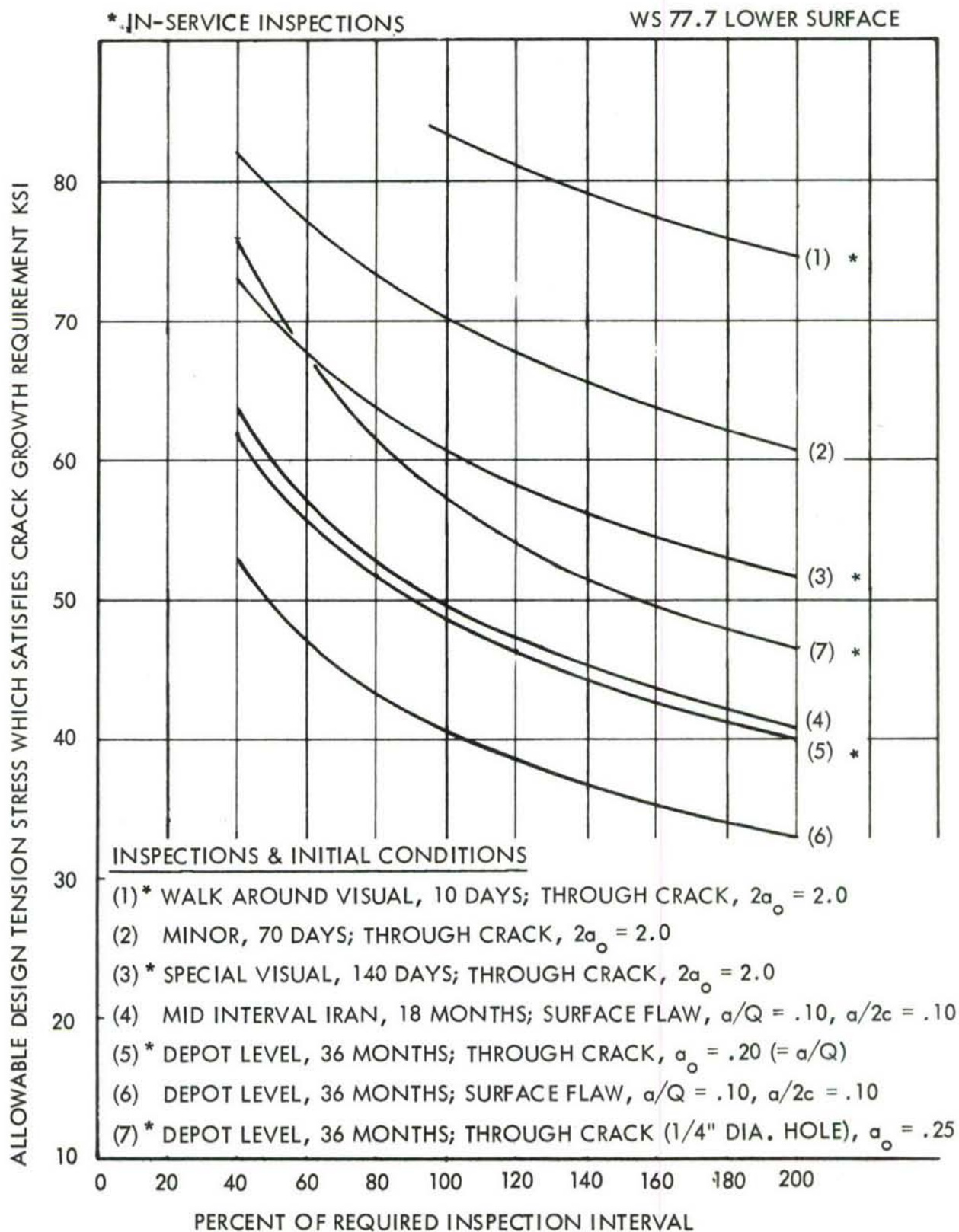


FIGURE 195 EFFECT OF INSPECTION INTERVAL -  
DESIGN TENSION STRESS



Figure 196 shows the results derived on the basis of the surface flaw requirement. The discontinuity in the curves for a given inspection interval is caused by an anomaly which arises in the implementation of the criteria. The problem is that the thickness of the structural element under analysis can be less than the depth specified in the criteria for the surface flaw. By direction of the ADPO, whenever an  $a/Q$  condition in the criteria exceeded the thickness limit of a structural element, a through-the-thickness crack, with a half crack length equal to the  $a/Q$  specified, was to be substituted. This resolution of the problem is based on the selection of equivalent crack geometries in terms of developing equal stress intensity levels. However, it should be observed that this interpretation has a significant influence on the size of the initial crack length used to determine the safe crack-growth period.

The above results are very useful in studying the effects of intact structure and in-service flaw criteria on allowable design stress. The detailed nature of the fracture criteria is such that, for a particular area, there can be a close interaction between the detail design of the structure and various elements of the criteria. For example, referring to Figure 196, the  $a/Q$  of 100 percent corresponds to the specified assumed initial damage present at the beginning of the in-service inspection interval. At 50 percent, the  $a/Q$  is 0.10, which is the initial flaw size assumed to be present in new structure. The fracture criteria for slow-crack-growth structure specifies that, in each of these cases, the flaw shall not grow and cause failure in less than  $F_{DM}$  for depot level inspectable structure. To comply with this requirement on the lower wing surface root area, the figure shows that the allowable design stress would be controlled by the part of the criteria which applies to the intact structure. Specifically, the allowable stresses for the  $a/Q$ 's of 0.10 and 0.20 are 40.8 KSI and 48.7 KSI, respectively. The discontinuous nature of the curve is significant in this case. It should also be noted that the position of the discontinuity is dependent on the thickness of the structural element under investigation. Figure 197 shows the remainder of the conditions considered in this phase of the sensitivity study.

Table LI provides a summary of design stress variation for 50, 100, and 150 percent of the criteria in-service inspection interval and in-service inspection flaw size. A



TABLE LI  
SUMMARY - INFLUENCE OF IN-SERVICE INSPECTION INTERVAL  
AND FLAW SIZE VARIATION ON ALLOWABLE DESIGN STRESS

INSPECTION	INSPECTION INTERVAL (100%)	FLAW SIZE (100%)	DESIGN TENSION STRESS (KSI)					
			PERCENT OF REQUIRED INSPECTION INTERVAL			PERCENT OF REQUIRED FLAW SIZE		
			50%	100%	150%	50%	100%	150%
			$F_{tu}$	83.3	78.3	$F_{tu}$	83.3	71.7
Walk Around Visual	10 Days	$2a_o = 2.0"$	$F_{tu}$	83.3	78.3	$F_{tu}$	83.3	71.7
Special Visual	140 Days	$2a_o = 2.0"$	70.2	60.6	55.4	73.0	60.6	54.1
Depot Level	36 Months	$a/Q = 0.20$	58.5	48.8	43.5	40.9	48.8	45.1
Depot Level	36 Months	Hole Through- Crack, $a_o = 0.25"$	71.4	57.4	50.5	60.0	57.4	55.5

\* IN-SERVICE INSPECTION

W.S. 77.7 LOWER SURFACE

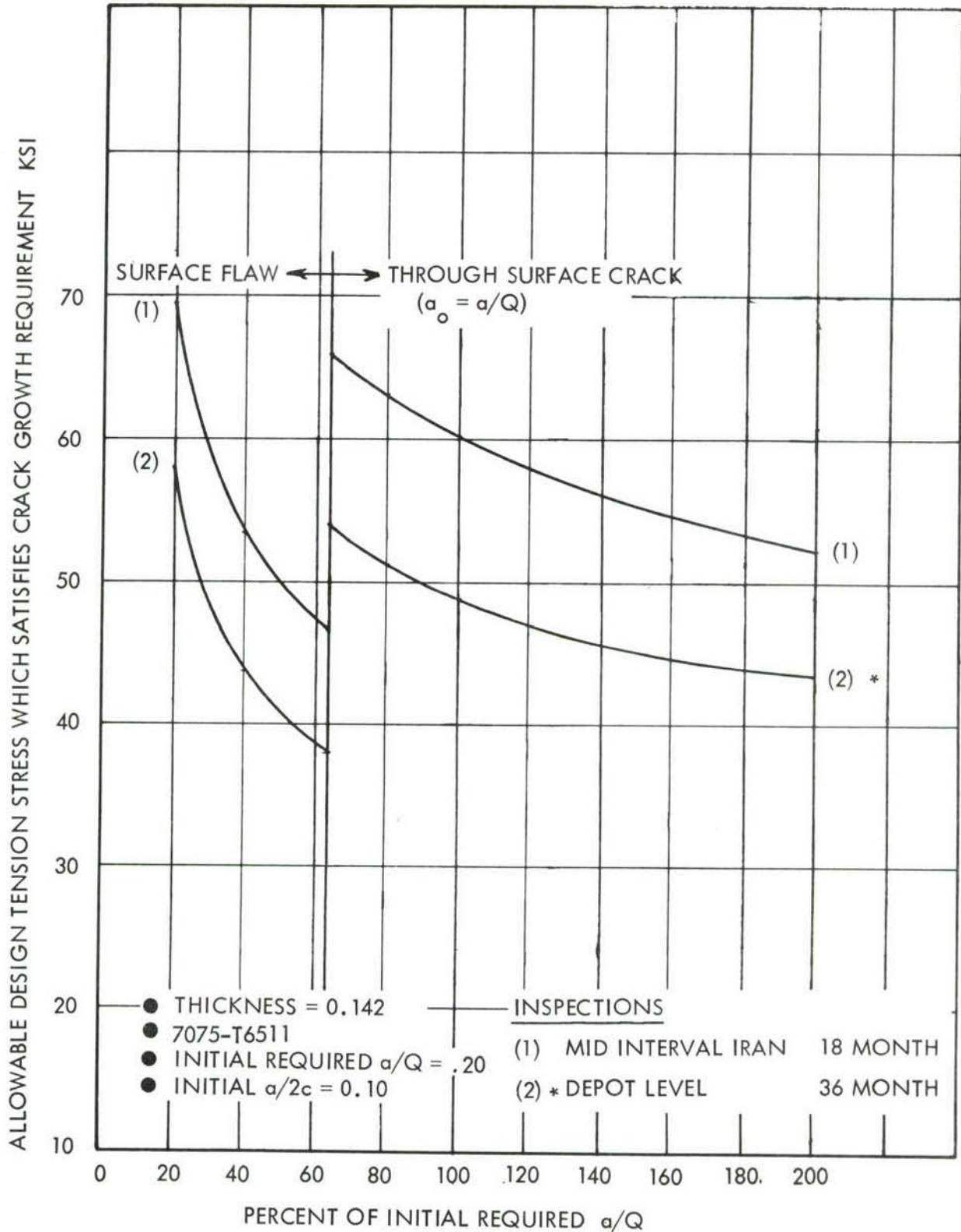


FIGURE 196 SURFACE FLAW - EFFECT OF INITIAL  $a/Q$  ON DESIGN TENSION STRESS

\* IN-SERVICE INSPECTIONS

W.S. 77.7 LOWER SURFACE

ALLOWABLE DESIGN TENSION STRESS WHICH SATISFIES CRACK GROWTH REQUIREMENT KSI

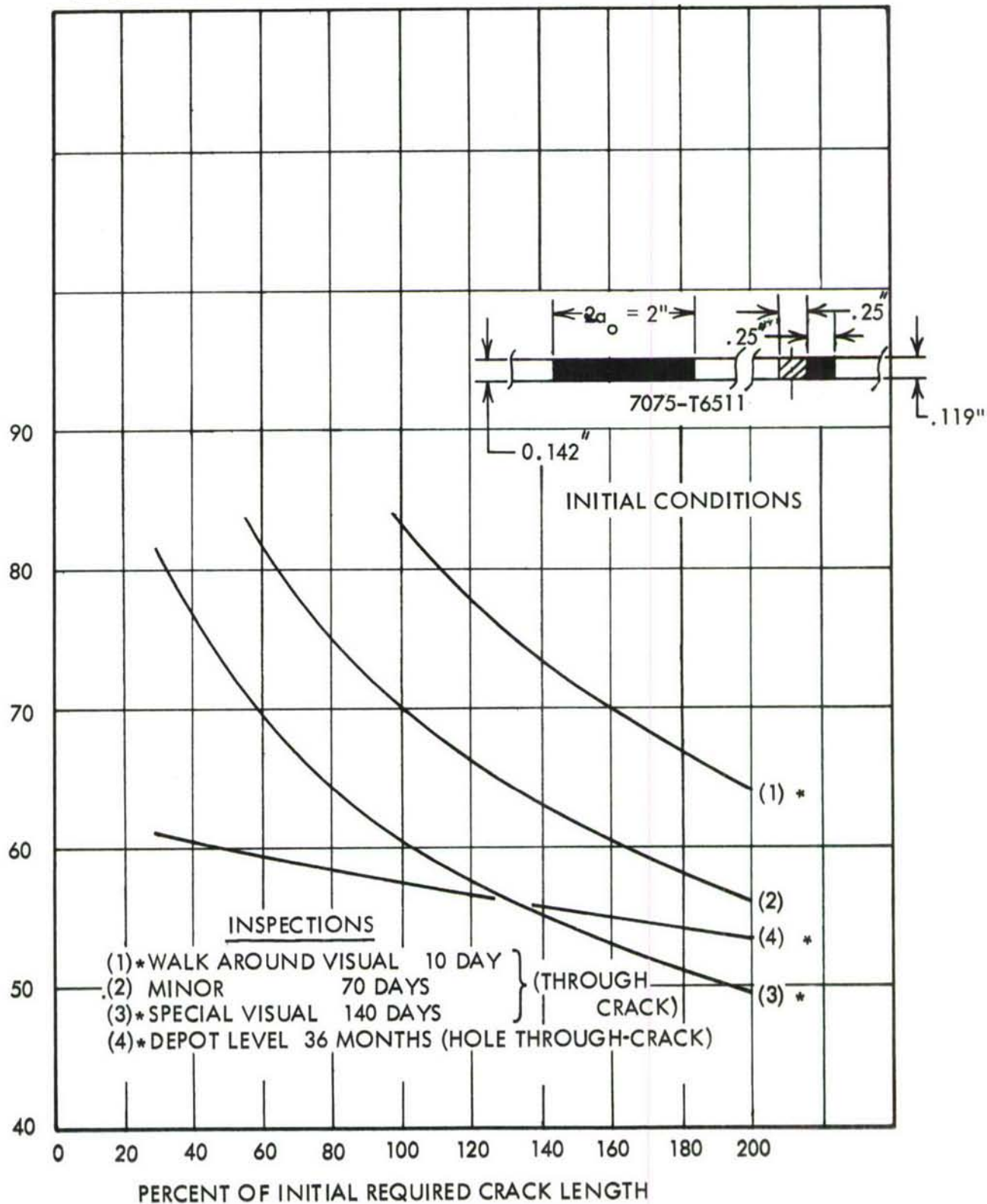


FIGURE 197 THROUGH THE THICKNESS CRACK - EFFECT OF INITIAL CRACK SIZE ON DESIGN TENSION STRESS

comparison of results shows that, on a percentage basis, a variation in flaw size has a greater influence on the allowable design stress than does a variation in the safe crack-growth period for both the walk-around visual and special visual in-service inspection conditions. As indicated previously, the discontinuity in the curves shown in Figure 196 is thickness dependent; however, as in this case, the design stress can be unexpectedly influenced by a variation in the assumed surface flaw size. Apart from the effects of the discontinuity in the curve, it can be further observed that, for the depot level in-service inspection conditions, steeper curves are generated as a result of changes in inspection interval size than for changes in flaw size. The observation on the relative slopes of the curves applies to both regions of the data shown in Figure 196. On this basis, it is quite evident that, for the through-the-thickness crack emanating from a hole, the design stress is more significantly influenced by a change in the inspection interval than by a similar percentage change in the flaw size.

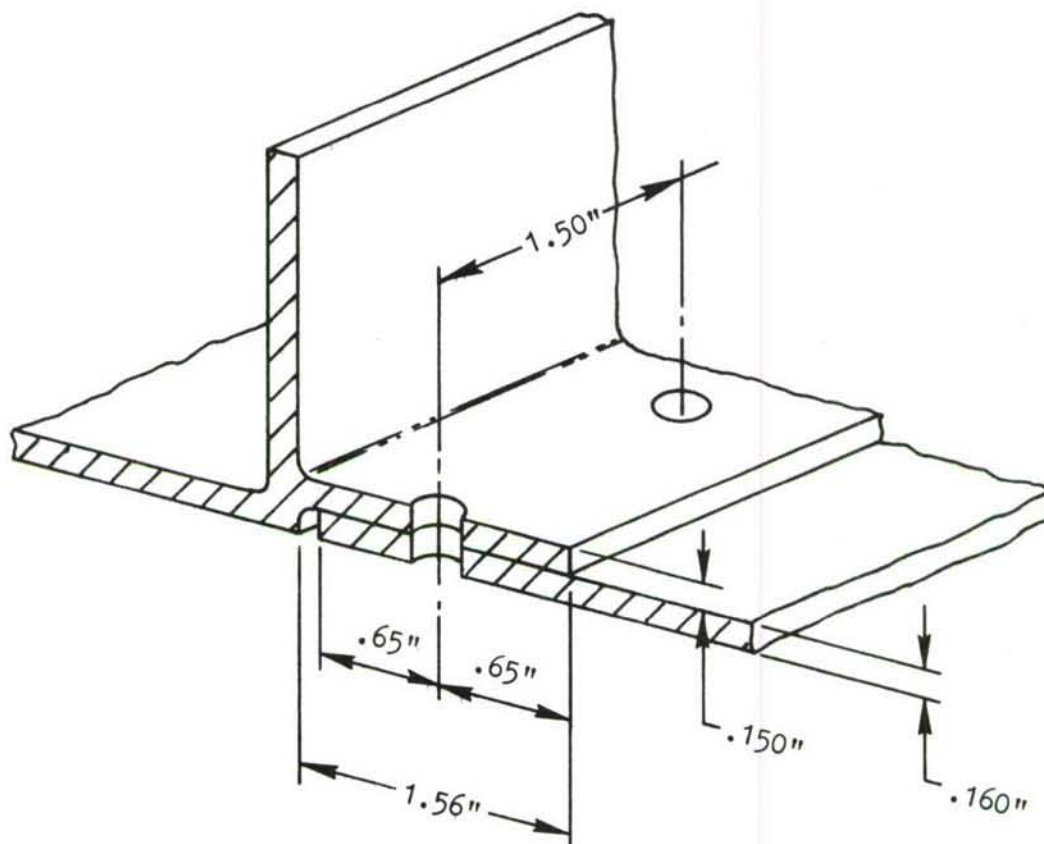
A3.8.2.3 Period Subsequent to Load Path Failure: This portion of the study is a parametric analysis showing the effect on the design tension stress of multiple-load-path structure by varying the safe crack-growth period after failure of a single principal element. For this analysis, three safe crack periods were selected for use from actual C-141 in-service inspection periods:

- o Twice IRAN Inspection Period - 3274 Flights  
(IRAN period = 3 years = 1637 Flights)
- o Twice Mid-IRAN Inspection Period - 1637 Flights
- o Twice Major Inspection Period - 418 Flights  
(Major inspection = 140 days = 209 Flights)

A cross-section of the typical baseline spanwise splice is shown in Figure 198. The multiple plank structure, providing multiple load paths, is shown in the sketch in Figure 199.

Criteria: The damage assumed to exist adjacent to the primary failure (center panel failure) in the remaining multiple-load-path dependent structure at the time of and





FASTENER - 5/16" STEEL TAPERLOKS

$$t/d = .497$$

$$s/d = 4.80$$

FIGURE 198 TYPICAL C-141 BASELINE SPANWISE SPLICE

following the failure of a load path shall be (1) equal to an 0.020" long through-the-thickness crack emanating from one side of a hole, or (2) damage equal to  $a/Q = 0.030$ " at locations other than holes, plus the amount of growth  $\Delta a$  which occurs prior to load path failure.

It has been determined from the baseline update and ADP design analyses that the 0.020" single hole crack is more critical than the 0.030"  $a/Q$  part-through crack condition. The amount of  $\Delta a$  crack growth in the dependent load path structure prior to failure of the center panel must be determined by analysis. No damage is assumed in the independent structure adjacent to the center panel.

Method of Analysis: To determine the  $\Delta a$  crack growth in the dependent load path, the following assumptions were necessary relative to the initial crack size and time to failure of the center panel:

- (1) Time to failure of the center panel is one period of unrepaired service usage ( $F_{XX}$ ), which is the safe crack-growth period defined previously.
- (2) The primary failure occurs when the crack reaches the length which is critical under application of the failsafe load ( $P_{XX}$ ).
- (3) For any design stress, the initial crack length in the center panel is that length necessary for the crack to reach critical length for  $P_{XX}$  during  $F_{XX}$ .

Load redistribution from the center panel occurs across the spanwise splice into the dependent load path during the crack growth in the center panel. This load redistribution is a function of the crack size in the center panel. Upon complete loss of the center panel, half of its load is distributed to the adjacent dependent load path. (It is assumed that, in panelized multiple load path structure, there are two panels available to take the load from the failed panel.) This load redistribution varies across the panel width of the dependent load path.

Determination of the stress environment across the dependent load path due to a growing crack in the center panel requires a complex analysis. Adequate description of this variable stress environment requires the use of a finite-element model.

The basic approach used in this analysis is described in a paper entitled "Application of Damage Tolerance Criteria To Multi-Plank Wing Cover Design," Reference 13, which was presented to the American Society for Metals 1972 WESTEC Conference. A similar finite-element model was used to determine the stress variation in the dependent load path due to a failed center panel. Results of this analysis are presented in Figure 199 as stress redistribution curves. These curves depict the varying stress factors across the dependent load-path panel for various crack lengths in the center panel.

The above mentioned curves are for an intact dependent load path. However, as the initial crack of 0.020" in the dependent load path grows, the spanwise splice becomes locally ineffective for transmitting load from the center panel to the dependent load path, and the two load paths essentially act as one. The crack length at which this occurs was calculated assuming a triangular shear lag at the spanwise splice, using actual splice geometry as shown in Figure 198. At this point, the crack in the dependent load path combines with the center panel crack to form a center crack of length  $2a$  equal to the combined crack lengths minus the overlap of the splice. Since the splice is ineffective for transmitting load, the stress redistribution factor becomes 1.0 at this point.

Knowing the crack growth in the center panel and the stress redistribution factors in the dependent load path, the stress environment at the tip of the crack in the dependent load path can be determined by modifying the field stress used in the calculation of stress intensity levels. This was accomplished by multiplying all analysis spectrum stresses by the redistribution factors obtained from Figure 199. The redistribution factors were input into the crack-growth computer program, and all multiplications were made internally prior to the calculations of stress intensities at the crack tip.

The crack growth  $\Delta a$  in the dependent load path during crack growth in the center panel is dependent upon the crack geometry. It is evident from Figure 199 and the previous discussion that the growing crack in the dependent load path can be analyzed in three crack segments:

# FIELD STRESS IN WING PANEL DUE TO CRACK IN CENTER PANEL

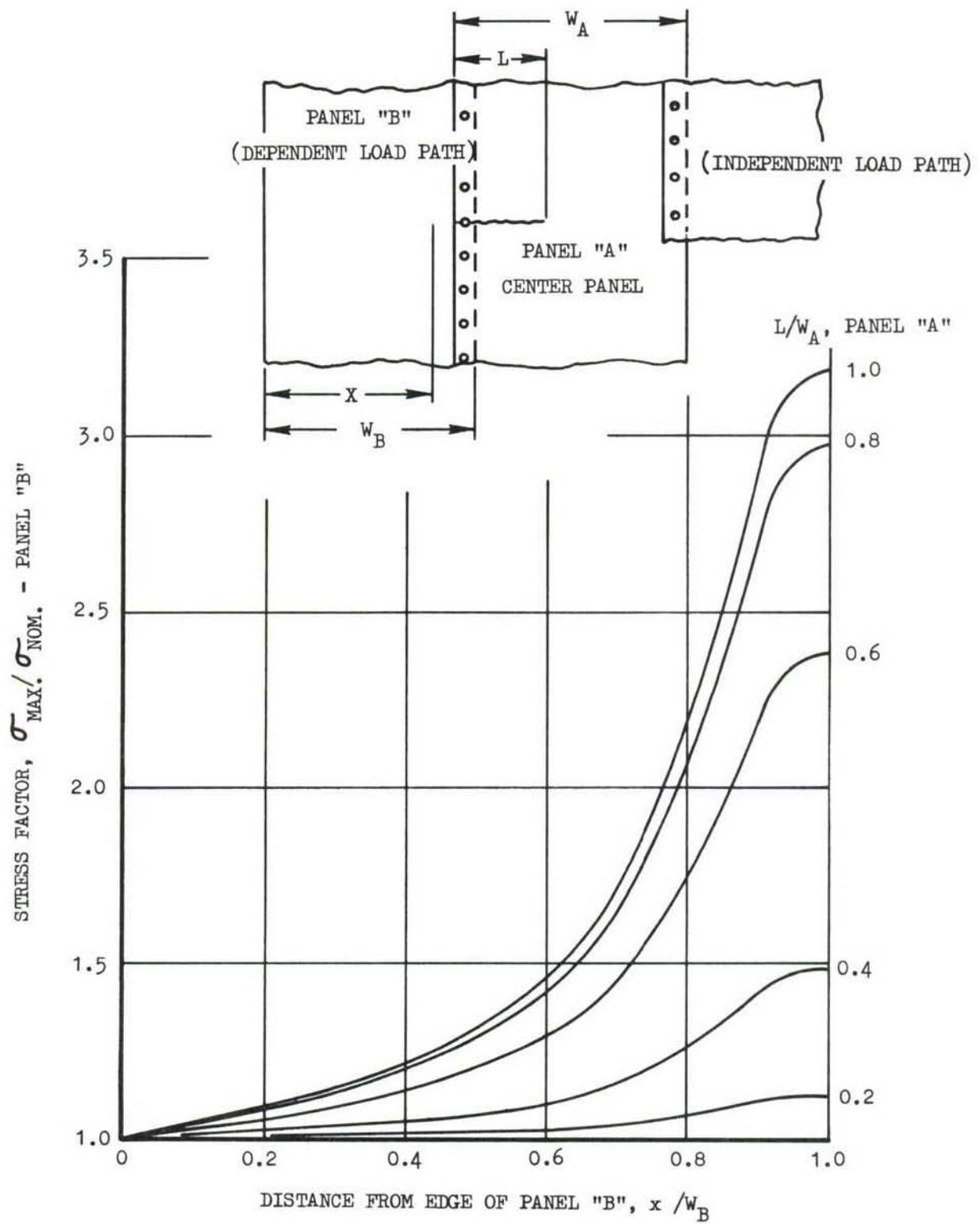


FIGURE 199 STRESS REDISTRIBUTION CURVES



- (1) The crack begins as a through crack (.020") at a spanwise splice hole at the side nearest the panel edge. The crack grows as a hole crack until it reaches the edge of the panel.
- (2) The next load cycle (conservatively assumed), after the crack has reached the panel edge, initiates a crack at the opposite side of the hole. This crack begins as an edge crack of initial length equal to the crack length to the panel edge plus the hole diameter. It grows as an edge crack until the splice becomes locally ineffective for transmitting load to the dependent panel as discussed previously.
- (3) Once the splice becomes ineffective, the cracks in the center panel and dependent load-path panel combine to form a center crack.

The crack in the dependent panel was analyzed for each applicable segment above. The solution was terminated at failure of the dependent load path under fail-safe load, completion of the safe crack-growth period, or the point at which the dependent load path is unable to take the dynamic fail-safe load from the failed center panel. Once the initial crack size and load redistribution have been established for the dependent load path, the final step is to calculate the time to failure. If the critical crack length under application of fail-safe load has been reached, or the dependent load path is unable to take the fail-safe load from the failed center panel, then the time to failure of the dependent load path after failure of the center load path is obviously zero. However, if the damage condition of the dependent load path at the time of failure of the center panel is such as to allow additional crack growth, then the solution is reinitialized, beginning at a crack length equal to  $0.02" + \Delta a$  and carried through the applicable crack growth segment(s) previously described. The time to failure of the dependent load path then becomes:

- (1) The time to critical crack length under application of fail-safe load,
- (2) The time at which the dependent load path is unable to support the fail-safe load from the failed center panel, or
- (3) The time required for the crack to grow completely across the dependent load path.

Analysis Results: The entire process, from the determination of initial crack size to calculation of time to failure of the dependent load path, was repeated for several design stresses for each of the three selected safe crack-growth periods. The results are plotted in Figure 200. By entering the appropriate curve at the safe crack-growth period, the design stress required for failure of the dependent load path at the end of this period can be determined. Similar curves and required design stresses can be developed for other safe crack-growth periods by repeating the entire analysis.

The results of Figure 200, the required design stresses at the selected safe crack-growth periods, are cross-plotted in Figure 201. This curve thus presents the allowable design stresses versus the safe crack growth period. By cross plotting in this manner, the safe crack-growth period to the center panel failure and the dependent load-path failure are equated, with the center panel failure occurring at the end of one safe crack-growth period, and the dependent load-path failure occurring at the end of the next period.

It is evident that a small change in design stress has a marked effect on the safe crack-growth period. However, it should be noted that, for the range of safe crack growth periods selected, the allowable design stresses are quite low, indicating the overall severity of the fail-safe structure damage tolerance criteria.

#### A3.8.3 NDI Considerations

The manner in which inspection criteria are being evolved during the service life management program for a current cargo aircraft has pertinence to NDI considerations in this parametric study. The inspection plan for the current aircraft program involves the identification of structurally critical areas from test and in-service data, analytical predictions of flaw growth, and specification of required inspection intervals based on both safe flaw-growth periods and inspection capabilities. It is being proposed that each aircraft be treated individually for flaw growth analysis using flight log data, i.e., actual loading history rather than elapsed time, to establish inspection intervals. This approach should yield greater economy by eliminating superfluous inspections and concentrating on items with the greatest need.

MULTIPLE LOAD PATH STRUCTURE  
 C-141 INNER WING COVER PANELS  
 RETARDATION FACTOR = 1.76

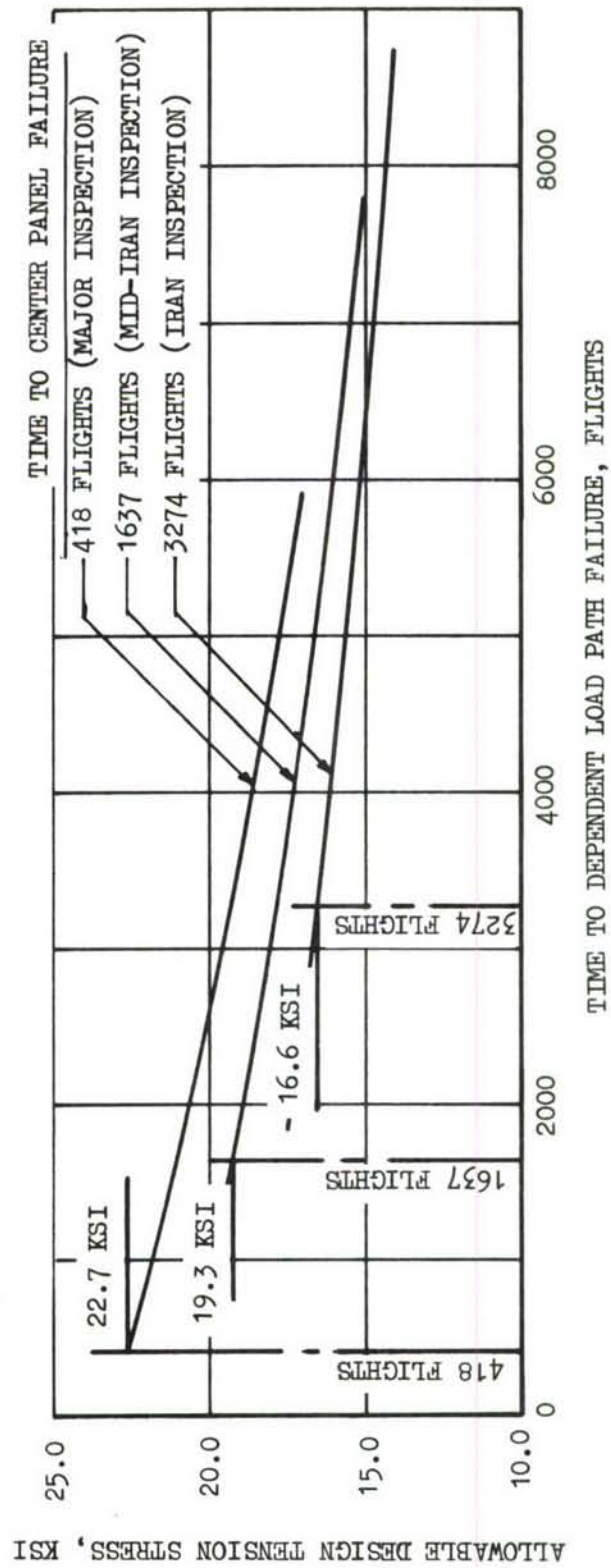


FIGURE 200 SAFE CRACK GROWTH PERIOD VARIATION  
 DESIGN STRESS VS. TIME TO LOAD PATH FAILURE

MULTIPLE LOAD PATH STRUCTURE  
 C-141 INNER WING COVER PANELS  
 RETARDATION FACTOR = 1.76

NOTE: CENTER PANEL FAILURE OCCURS AT END OF ONE  
 SAFE CRACK GROWTH PERIOD, AND DEPENDENT LOAD  
 PATH FAILURE OCCURS AT END OF NEXT PERIOD.

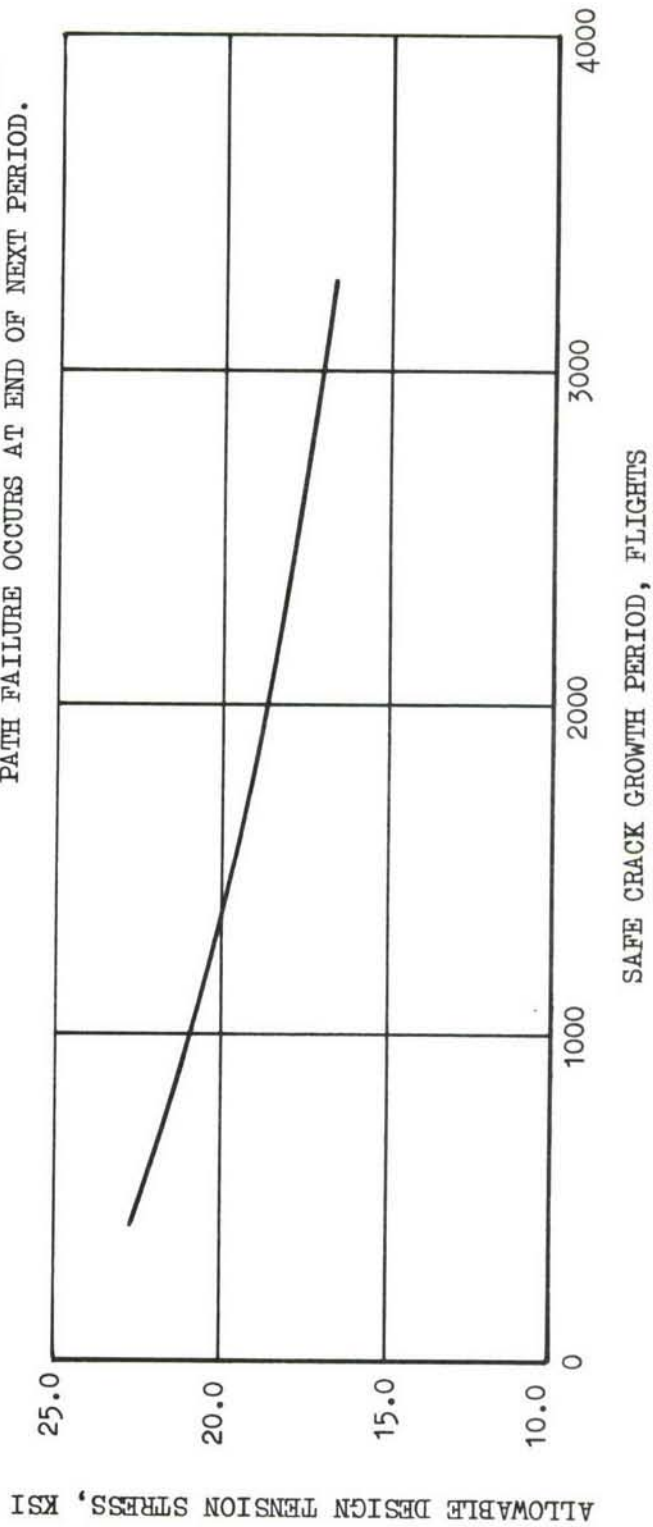


FIGURE 201 SAFE CRACK GROWTH PERIOD VARIATION  
 DESIGN STRESS VS. SAFE CRACK GROWTH PERIOD



This rationale, however, is effective only with prior knowledge of critical areas and accurate flaw-growth rate predictions. At the present time, most of this information is based on empirical data.

The range of variation for inspection interval, damage size, and safe crack-growth period will be discussed with this aircraft program experience in mind. Furthermore, the capability for NDI and visual inspection to detect flaws reliably will strongly influence the length of inspection intervals for given periods of crack growth. The following comments are listed in the sequence given in the statement of work.

A3.8.3.1 Effect of Inspection Interval on Ultimate Design Stress: The required inspection intervals about which time ranges are projected, i.e., the 100% values, are based on current C-141 requirements. The types of inspection dictate the minimum defect size that can be detected with a high degree of probability. The flaw-length inspection capability in Section X give walk-around visual detection at 10", special visual at 2", and depot level ranging from 0.20" to 1.25". (A typical value for depot level capabilities is 0.40", but no general length limits can be authoritatively stated.) The depot level inspection at 18- and 36-month intervals is the predominant deciding factor in this study. The special visuals serve as backups to inspections keyed to design stress levels from 30 to 40 KSI. The depot level inspection intervals are based on an average utilization rate and in-service load history. With this scheme, there are four opportunities to detect flaws grown to 2" within the time elapsed between adjacent depot level inspections. This is considered adequate as a backup to the depot level activity.

A3.8.3.2 Effects of Changing Initial Crack Length or Ultimate Design Stress: A 2-inch crack length, which is both a value specified as an initial size for growth assumptions and the size considered detectable in a special visual inspection, is consistent with visual inspection data presented in Section A3.8.1. However, if one must select design stress on reliable detection of 10-inch cracks during a 10-day walk-around visual inspection, then the selected stress range is not conservative.

A3.8.3.3 Effects of Changing  $a/Q$  on Ultimate Design Stress: A discussion of flaw shape with reference to NDI requires a consideration of the NDI methods in common use. Penetrant and eddy-current methods, along with magnetic particle, are primarily flaw length dependent. Ultrasonic and radiographic methods are primarily flaw area responsive. Therefore, the latter two methods are applicable to  $a/Q$  considerations. Ultrasonic methods are assumed capable of routinely detecting surface flaws in the length range from 0.2" to 0.4" if the depth is in excess of 10% of the material thickness or 0.2", whichever is least. Radiography is assumed to be responsive to defects near 1.25" if the depth is in excess of 3% of the material thickness.

In the case for this study, mean values of  $a/Q$  are 0.10 and 0.20 and  $a/2c_{\text{initial}}$  is 0.1. This yields an initial "a" of 0.112" and 0.224" and "2c" of 1.12" and 2.24" for an operating to yield stress ratio of zero. The material thickness is 0.142"; therefore, "a" is sufficiently large for both ultrasonic and radiographic techniques. The length "2c<sub>initial</sub>" of 1.12" and 2.24" is marginal for radiographic detection but is adequate for an ultrasonic response. Therefore, the total range of  $a/Q$  presented is compatible with all methods but radiography. The  $a/Q$  values less than 0.10 mean are inadequate for radiographic flaw detection.

A3.8.3.4 Safe Crack Growth Period: Inspection intervals and flaw length considerations for safe crack growth period analyses are consistent with both visual inspection and NDI currently in practice on the baseline structure. A critical review of the inspection policies, however, should be made. If the objective is to monitor the progression of slow crack growth, high-resolution NDI applied at frequent intervals should be considered. If the objective is to detect flaws before they become critical, low-resolution visual techniques applied at frequent intervals may be used. Tradeoffs among frequency of inspection, resolution capabilities, and cost should be examined with regard to the purpose of the inspection.

#### A3.8.4 Multiple Cracking

The assumed location of multiple flaws will influence the crack growth pattern as well as the safe crack growth period at a given design stress level. Several



combinations of flaw locations in the spanwise splice were assumed to determine the sensitivity of these variables on safe life and design stress.

The first series of cases considered in the study are shown in Figure 202. Initial crack sizes were the same at all locations, including the corner crack in Case B. Furthermore, all initial flaws shown were assumed to be present at the beginning of the safe crack growth period. In the analysis of Cases B and C, cracks were assumed to initiate on the other side of the hole immediately following the propagation of the initial crack across the edge ligament of the panel. For further clarification, the crack growth pattern for each case is coded on the figure. In addition, relative crack growth characteristics for cyclic loadings based on a design stress of 45.8 KSI are shown in Figure 203. These results are presented to illustrate the typical incremental crack growth patterns for each of the cases considered. Similar analyses were performed at other design stress levels to fully develop the parametric results shown in Figure 202.

A separate case, Case D, was considered where the flaw growth assumptions are somewhat related to the fracture criteria applicable to fail-safe structural concepts. The general structural arrangement analyzed is shown in Figure 204. In this case, the initial flaws shown in Panels B and C are secondary flaws that are not assumed to develop until after Panel A has completely failed. As shown in the figure, the crack growth pattern consists of stable crack growth in the center panel until the safe crack growth life of the panel is reached. The undamaged adjacent panels sustain the residual strength requirement specified in the criteria, including the 1.15 dynamic factor. At this point, it is assumed that fatigue crack growth immediately initiates at the attachment holes in Panels B and C. Stable crack growth may again occur until the safe crack growth life of the adjacent panels is expended and final failure is precipitated. Load redistribution effects were considered in the analysis. Figure 205 shows the incremental crack growth pattern for this case at the same design stress level used in the similar presentation for the other three cases. The relationship between design tension stress and flights to failure for Case D is shown in Figure 204.

W.S. 77.7 LOWER SURFACE  
7075-T6511 ALUMINUM

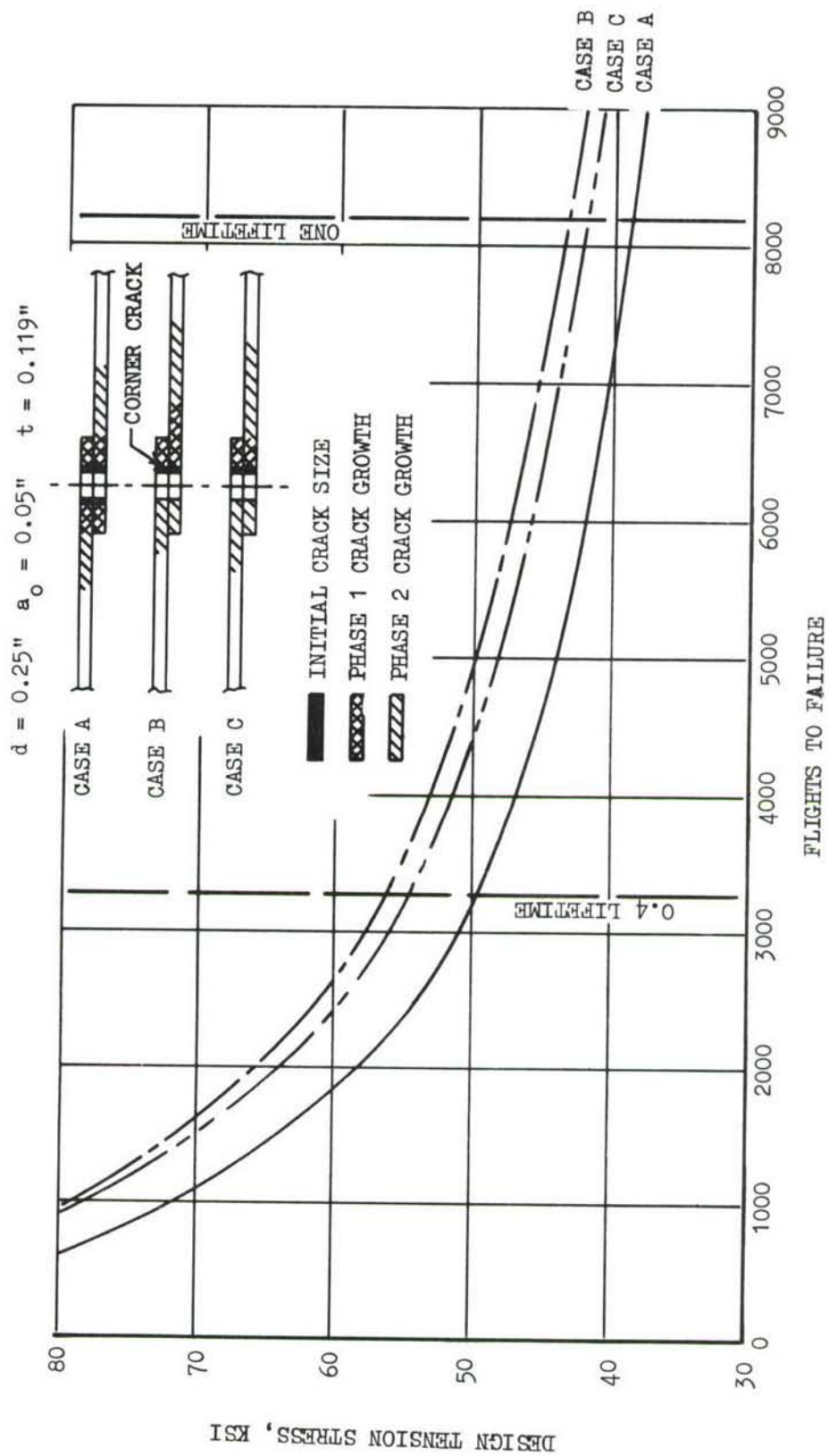


FIGURE 202 MULTIPLE CRACK STUDY, TWO PANELS  
ALLOWABLE DESIGN STRESS



W.S. 77.7 LOWER SURFACE  
 DESIGN STRESS = 45.8 KSI  
 7075-T6511 ALUMINUM

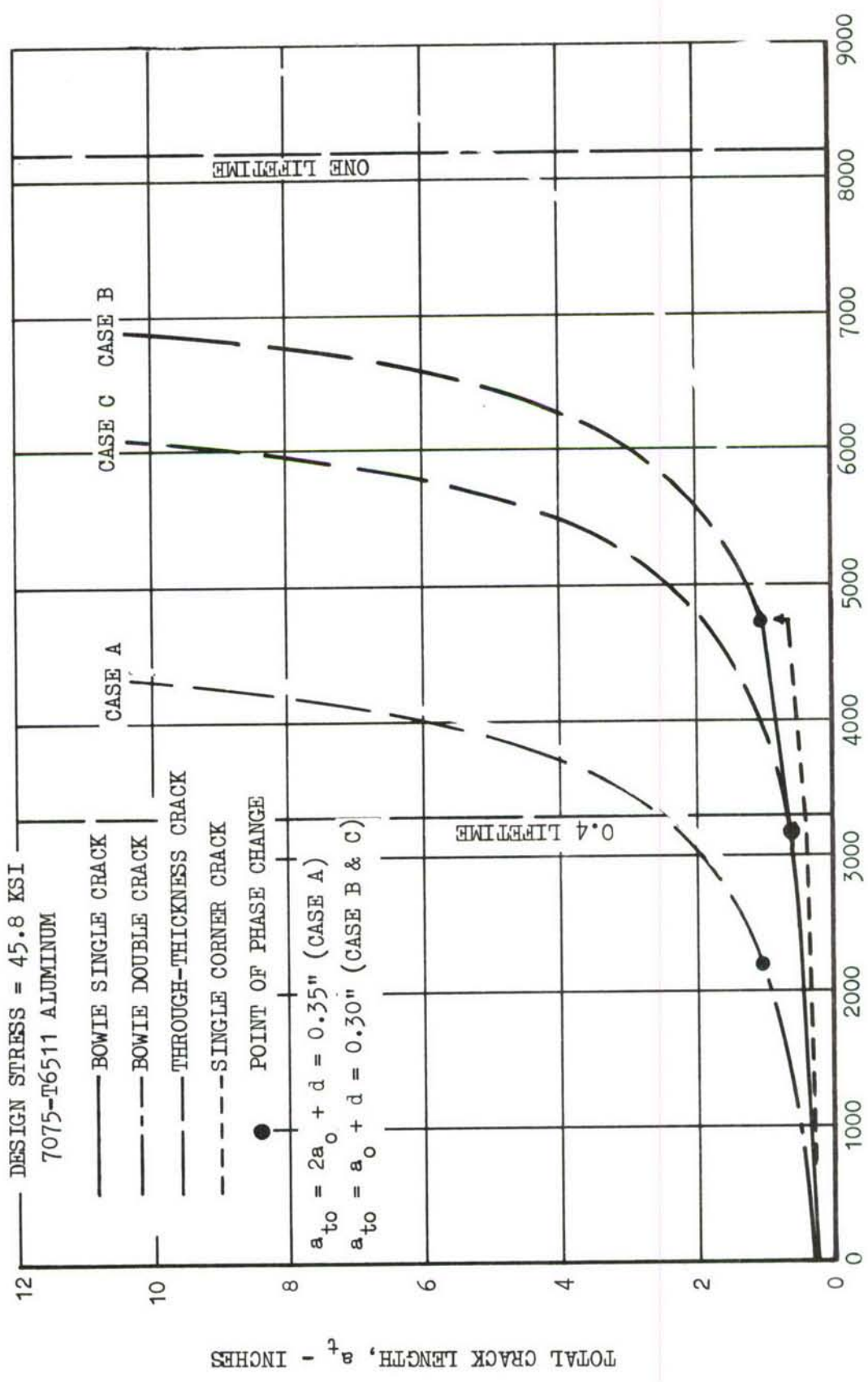


FIGURE 203 MULTIPLE CRACK STUDY, TWO PANELS  
 CRACK GROWTH CURVES

W.S. 77.7 LOWER SURFACE  
7075-T6511 ALUMINUM

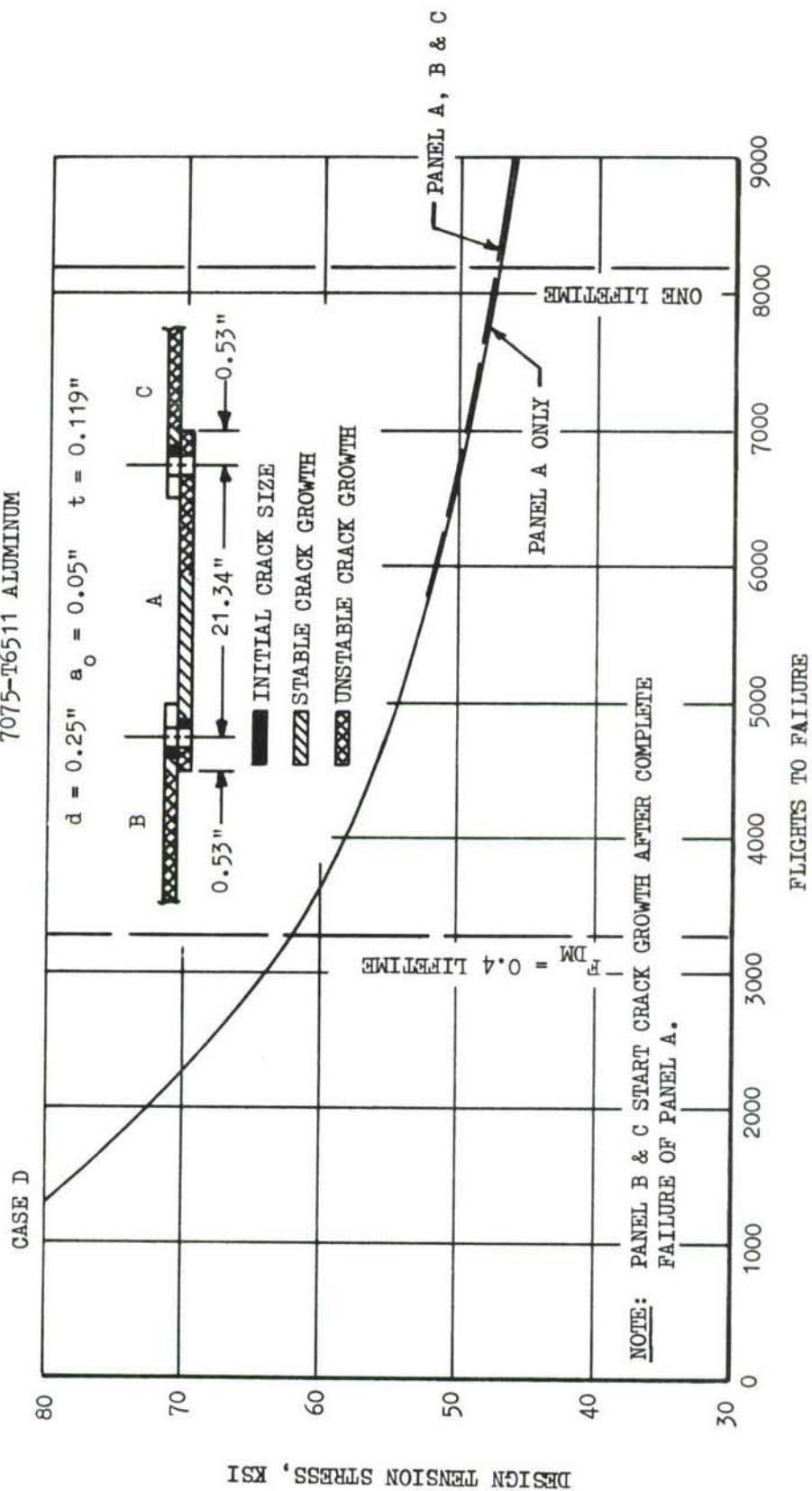


FIGURE 204 MULTIPLE CRACK STUDY, THREE PANELS  
ALLOWABLE DESIGN STRESS

W.S. 77.7 LOWER SURFACE

7075-T6511 ALUMINUM

DESIGN STRESS = 45.8 KSI

CASE D

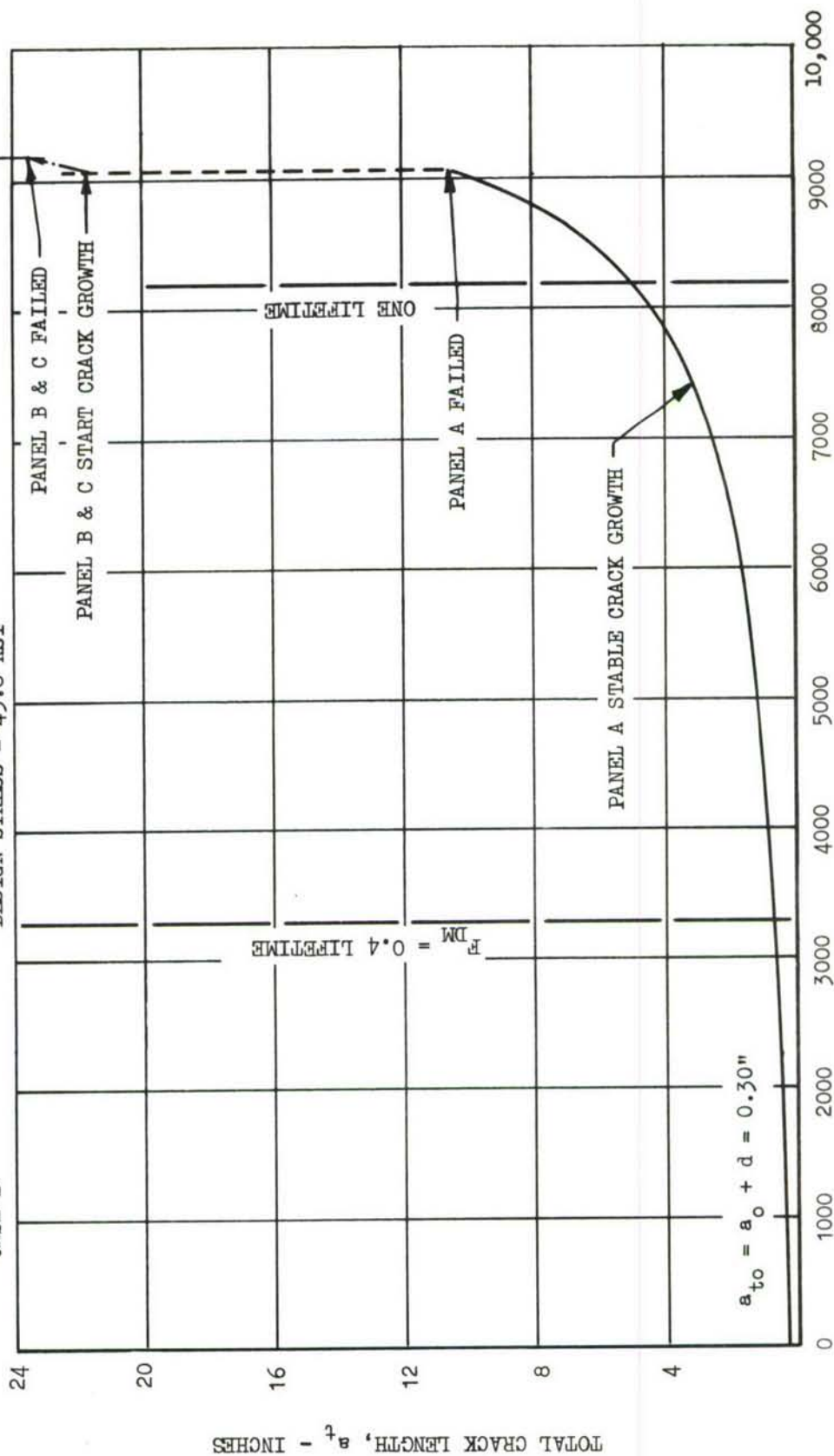


FIGURE 205 MULTIPLE CRACK STUDY, THREE PANELS  
CRACK GROWTH CURVE

A comparison of the results presented in Figures 202 and 204 provide an indication of the sensitivity of multiple flaw assumptions on design stress and life. It can be seen that the most severe condition considered was the case of through-the-thickness cracks on both sides of a fastener hole in the spanwise splice. The results for Case D indicate that it was the least severe of the conditions evaluated. Case C, a through-the-thickness crack at one edge of a fastener hole, is representative of the assumed condition in the implementation of the fracture criteria. Allowable design stresses based on this multiple flaw assumption are approximately 10 percent higher than for Case A.

### A3.9 RESIDUAL STRENGTH LOAD REQUIREMENT

The residual strength load requirement in the fracture criteria is specified in terms of the maximum load that can be expected to occur within a given period of service experience. Exposure periods are specified in terms of a multiple of the inspection intervals. Currently, the criteria requires that the residual strength load be determined on the basis of 100 inspection intervals. The purpose of this phase of the study was to evaluate the sensitivity of variations in exposure periods in terms of allowable design stress and life.

Residual strength loads were determined from cumulative load occurrence data derived from the service load spectrum. The mean and variable loads of the fatigue spectrum were converted to cumulative cycles of minimum and maximum load excursion schedules. These schedules were developed to include load occurrence frequencies on the order of one cycle in 600,000 flight hours. Residual strength load requirements can be selected from these schedules for periods ranging up to 100 times 2 lifetimes.

Table LII lists the inspections and inspection intervals used as a basis for the parametric analysis. The "inspection factor" shown in the table was used to determine the minimum period of unrepaired service usage for the evaluation of the safe crack growth life, excluding the residual strength load requirement. Allowable design stresses in compliance with the safe crack growth requirements in the criteria



TABLE LII  
ALLOWABLE DESIGN STRESS FOR RESIDUAL STRENGTH VARIATION

BASELINE STRUCTURE  
W.S. 77.7 LOWER SURFACE

INSPECTION	FREQUENCY OF INSPECTION	INSPECTION FACTOR	UNREPAIRED SERVICE PERIOD (FLIGHTS)	INITIAL DAMAGE		100 INSPECTION INTERVALS				10 INSPECTION INTERVALS				1 INSPECTION INTERVAL			
				TYPE	INITIAL SIZE	DESIGN STRESS - CRACK GROWTH (KSI)	RESID. STRENGTH (% LIMIT LOAD)	DESIGN STRESS - INCL. RESID. STRENGTH (KSI)	RESID. STRENGTH (KSI)	RESID. STRENGTH (% LIMIT LOAD)	DESIGN STRESS - INCL. RESID. STRENGTH (KSI)	RESID. STRENGTH (KSI)	RESID. STRENGTH (% LIMIT LOAD)	DESIGN STRESS - INCL. RESID. STRENGTH (KSI)	RESID. STRENGTH (KSI)	RESID. STRENGTH (% LIMIT LOAD)	DESIGN STRESS - INCL. RESID. STRENGTH (KSI)
C-141																	
HOME STATION	WALK AROUND VISUAL (1)	5	75	THRU CRACK	2a = 2"	83.0	61.7	79.0	32.5	52.7	83.0	29.2	44.6	83.0	24.7		
MINOR	SPECIAL VISUAL	2	209	THRU CRACK	2a = 2"	70.0	68.2	64.5	29.3	60.4	67.8	27.3	51.2	70.0	23.9		
MAJOR	SPECIAL VISUAL (1)	2	418	THRU CRACK	2a = 2"	60.6	70.6	55.8	26.2	62.9	58.5	24.5	54.0	60.6	21.8		
MID INTERVAL DEPOT OR IRAN	DEPOT OR BASE LEVEL	2	1,637	SURF. FLAW	a/Q = .10 a/2C = .10	49.5	75.3	47.1	23.6	67.1	48.1	21.5	59.5	49.0	19.4		
IRAN	DEPOT OR BASE LEVEL (1)	2	3,274	SURF. FLAW	a/Q = .10 a/2C = .10	40.5	77.7	38.5	19.9	69.9	39.4	18.4	62.1	40.0	16.6		
—	NON-INSPECTABLE (1)	—	16,374 <sup>(2)</sup>	SURF. FLAW	a/Q = .10 a/2C = .10	25.4	83.5	25.1	13.9	75.3	25.2	12.6	67.1	25.3	11.3		

NOTES:  
(1) USAF DAMAGE TOLERANCE CRITERIA INSPECTIONS  
(2) 2 LIFETIMES

were determined for later use in evaluating the influence of the residual strength loads.

Residual strength load effects are introduced by determining the residual load level requirement on the basis of the maximum load expected to occur in 100, 10, and 1 inspection intervals. The exposure periods corresponding to these intervals were used with the cumulative load occurrence data to determine the maximum expected load within each period. Loads derived in this manner are the residual strength loads applicable to each type of inspection and multiple of the inspection interval. These loads are listed in the table in terms of percent of limit load. The allowable design stress, including the residual strength load requirement, was determined for each case and the results are shown in the table. Stress levels corresponding to the residual strength loads are also shown. The analytical methods used to establish the allowable design stresses are discussed in detail in Section 8.2.2.

As can be seen from Table LII, the amount of stress reduction for residual strength requirements from the basic crack growth allowable is dependent upon the inspection period as well as the number of inspection intervals. For 1 inspection interval the stress reduction varies from 0.0 to 0.5 KSI, while for 100 inspection intervals the reduction is from 0.3 to 5.5 KSI. Additionally, the difference in stress reduction between the 100 inspection and 1 inspection intervals within a given inspection period category is a minimum of 0.2 KSI for the noninspectable and a maximum of 5.5 KSI for the 70-day Special Visual category. For the critical ADP analysis inspection category, the 36-month Depot Level, the difference in stress reduction is 1.5 KSI.

Generally the residual strength requirements have not imposed large stress reductions in the Cargo/Tanker ADP program. However, some noticeable weight savings could be realized by reducing the present 100 inspection interval residual strength load requirement.

## REFERENCES

1. MIL-A-8860 (ASG) Series Specifications, 18 May 1960.
2. "Civil Aeronautics Regulations 4b: Airplane Airworthiness; Transport Categories," through Amendment 4b-11, effective October 1, 1959.
3. Staff, Engineering Structural Life-Assurance Manual, Lockheed-California Company.
4. Campbell, J. E., Berry, W. E., and Feddersen, C. E., Damage Tolerant Design Handbook, MCIC-HB-01, Metals and Ceramics Information Center, Battelle, December 1972.
5. Unpublished Data, Phase IA Program of Contract No. F33615-72-C-2165, Lockheed-Georgia Company.
6. Babilon, C. F., Wygonika, R. H., et al., Progress Reports, Mechanical Properties, Fracture Toughness, Fatigue, Environmental Fatigue Crack Growth Rates and Corrosion Characteristics of High-Toughness Aluminum Alloy Forgings, Sheet and Plate, Contract No. F33615-71-C-1571, ALCOA.
7. Forman, R. G., et al., Computer Analysis of Two-Dimensional Fatigue Flaw Growth Problems, NASA-TM-X-58086 (NASA N72-24937), February 1972.
8. Anderson, J. M., Aberson, J. A., and Hardy, R. H., "A High-Order Cracked Finite Element," Presented at the ASME, ASM, and University of New Mexico 13th Annual Symposium: Fracture and Flaws, Albuquerque, N.M., March 1973.
9. Aberson, J. A., "The Application of a Cracked Finite Element in a Realistic Aircraft Structural Component Analysis," Presented to the ASTM E24.06 Sub-Committee on Fracture Mechanics Application, Williamsburg, Va., March 1973.
10. C-141 Nondestructive Inspection Procedures, T.O. 1C-141A-36, AFLC Robbins Air Force Base, June 1971.

## REFERENCES (concluded)

11. Wilson, W. K., "Stress Intensity Factors for Deep Cracks in Bending and Compact Tension Specimens," Engineering Fracture Mechanics, Volume 2, pp. 169-171, 1970.
12. Danielson, G. R., Deneff, G. V., et al, Advanced Military Tanker, Wing/Fuselage Structural Concept Study, AFFDL-TR-72-89, July 1972.
13. Caustin, Edward L., "NDT Production and In-Service Inspection," Presented at Materials Design Forum on Prevention of Structure Failure Using NDT/Fracture Mechanics at Port St. Lucie, Florida, April 1973.
14. Wood, H. A., Engle, R. M., and Bader, R. M., Prediction of Spectrum Crack Growth For C-5A Wing Locations Using CRACKS and the Willenborg Retardation Model, AFFDL-TM-72-3-FBR, November 1972.
15. Freyre, O. L., Lassiter, L. W., Aberson, J. A., McKinney, J. M., "Application of Damage Tolerance Criteria to Multi-Plank Wing Cover Design," Presented at the 1972 WESTEC Conference, Los Angeles, California, March 1972 (To Be Published).



UNCLASSIFIED

Security Classification

## DOCUMENT CONTROL DATA - R &amp; D

(Security classification of title, body of abstract and indexing annotation must be entered when the overall report is classified)

1. ORIGINATING ACTIVITY (Corporate author) Lockheed-Georgia Company A Division of Lockheed Aircraft Corporation Marietta, Georgia 30063		2a. REPORT SECURITY CLASSIFICATION Unclassified	
		2b. GROUP	
3. REPORT TITLE ADVANCED METALLIC STRUCTURES: CARGO WING DESIGN FOR IMPROVED COST, WEIGHT, AND INTEGRITY			
4. DESCRIPTIVE NOTES (Type of report and inclusive dates) Final Technical Report July, 1972 through June, 1973			
5. AUTHOR(S) (First name, middle initial, last name) C. R. Bigham, et al			
6. REPORT DATE June, 1973		7a. TOTAL NO. OF PAGES 390	7b. NO. OF REFS 15
8a. CONTRACT OR GRANT NO. F33615-72-C-2165		9a. ORIGINATOR'S REPORT NUMBER(S) LG73ER0126	
b. PROJECT NO. 486U			
c.		9b. OTHER REPORT NO(S) (Any other numbers that may be assigned this report)	
d.		AFFDL-TR-73-51	
10. DISTRIBUTION STATEMENT Distribution limited to U. S. Government agencies only; test and evaluation; statement applied June, 1973. Other requests for this document must be referred to AF Flight Dynamics Laboratory (FBA), Wright-Patterson AFB, Ohio 45433.			
11. SUPPLEMENTARY NOTES		12. SPONSORING MILITARY ACTIVITY Air Force Flight Dynamics Laboratory Air Force Materials Laboratory Air Force Systems Command Wright-Patterson AFB, Ohio 45433	
13. ABSTRACT With the current Air Force medium transport and tanker fleets rapidly approaching the end of their useful life, a requirement for their replacement is inevitable. Demonstration of innovative advanced structures concepts is required prior to production design decisions in order to qualify these advances for new system acceptance. The long lead times required for the development and demonstration of advanced structures dictates that advanced development programs be initiated now to insure the availability of the various technologies when needed for anticipated future systems. This requirement has led to this advanced development program to develop improved aircraft structural designs for a cargo/tanker category aircraft. The C-141 inner wing box was used as the baseline for the preliminary design study phase of this development program. The major objective of this study was to develop advanced designs which would double the fatigue life endurance of the baseline, and which could be produced at lower cost and weight. The objective was achieved through an iterative process of integrating, evaluating, and exploiting new and improved technology in design concepts, fracture mechanics, analysis methods, design criteria, materials, tests, manufacturing methods, and nondestructive inspection methods. From the study of a comprehensive matrix of cover and substructure concepts, eight configurations were formulated for analysis. Upon completion of the analysis, the configurations were evaluated using a merit rating system which recognized the important performance characteristics of a structural design. This evaluation resulted in the selection of three recommended configurations which met the objective for further study in the planned follow-on program. Also, a comprehensive damage tolerance criteria sensitivity analysis was performed as a part of this study to evaluate the effects of variations in critical criteria parameters on selected design control functions.			

DD FORM 1 NOV 65 1473

UNCLASSIFIED

Security Classification

UNCLASSIFIED

Security Classification

14. KEY WORDS	LINK A		LINK B		LINK C	
	ROLE	WT	ROLE	WT	ROLE	WT
Wing structure						
Cargo aircraft wing						
Advanced materials						
Structural concepts						
Fatigue						
Damage tolerance						
Fracture						
Aluminum						
Titanium						
Advanced composites						
Structural tests						
Material tests						
Nondestructive Inspection						
Weldbond						
Finite element analysis						
Adhesive bonding						
Advanced manufacturing methods						
Weight reduction						
Structure costs						
Advanced structures technology						